UNIVERSITY OF SOUTHAMPTON

FACULTY OF ENGINEERING AND PHYSICAL SCIENCES

School of Chemistry

Consequences of the Mechanical Bond in Rotaxanes;

Novel Reactivity and Unusual Chirality

by

Ellen M. G. Jamieson

Thesis for the degree of Doctor of Philosophy

January 2020

UNIVERSITY OF SOUTHAMPTON

ABSTRACT

FACULTY OF ENGINEERING AND PHYSICAL SCIENCES

Chemistry

Thesis for the degree of Doctor of Philosophy

CONSEQUENCES OF THE MECHANICAL BOND IN ROTAXANES;

NOVEL REACTIVITY AND UNUSUAL CHIRALITY

Ellen M. G. Jamieson

Reports of mechanically interlocked molecules (MIMs) have grown in recent years, aided by the relative synthetic ease by which they can now be obtained in comparison to the challenging syntheses reported originally. With this influx of research into the area, boosted even more by the 2016 Nobel Prize in the field for 'the design and production of molecular machines' there have been a lot of recent developments, showing the potential of MIMs for different applications such as switches, sensors or in catalysis due to the unique environment of the mechanical bond.

The introductory chapter provides a detailed overview of chirality in the context of MIMs. In addition to discussing the properties and applications of MIMs containing covalent stereogenic units, the different forms of chirality that arise as a *consequence* of the mechanical bond, and the influence this can have on the properties of molecules will be outlined.

Chapter two details the design and synthesis of a dynamic co-conformationally mechanically planar chiral rotaxane which exists as a pair of rapidly exchanging enantiomers. This novel rotaxane binds diastereoselectively to chiral anions. The biasing of the co-conformations of the rotaxane host through guest binding leads to an induced circular dichroism (CD) signal even when the chiral anionic guest does not display a CD signal on its own. Our results demonstrate the long-term potential of such stereodynamic rotaxanes in determining the enantiopurity of chiral analytes.

Chapter three describes the unexpected discovery of a novel acrylamide rotaxane, formed as an unintended consequence of the mechanical bond stabilizing a Cu^{I}-triazolide intermediate. This novel reactivity was investigated in depth, firstly by exploring the scope of the reaction and then *via* experiments designed to gain insight into key reaction intermediates. Using our results, a possible a mechanism of the reaction was proposed.

Table of Contents

DECLARATION OF AUTHORSHIP

I, ELLEN M. G. JAMIESON

declare that this thesis and the work presented in it are my own and has been generated by me as the result of my own original research.

Consequences of the Mechanical Bond in Rotaxanes; Novel Reactivity and Unusual Chirality

I confirm that:

1. This work was done wholly or mainly while in candidature for a research degree at this University;
2. Where any part of this thesis has previously been submitted for a degree or any other qualification at this University or any other institution, this has been clearly stated;
3. Where I have consulted the published work of others, this is always clearly attributed;
4. Where I have quoted from the work of others, the source is always given. With the exception of such quotations, this thesis is entirely my own work;
5. I have acknowledged all main sources of help;
6. Where the thesis is based on work done by myself jointly with others, I have made clear exactly what was done by others and what I have contributed myself;
7. Parts of this work have been published as: E. M. G. Jamieson, F. Modicom and S. M. Goldup, "*Chirality in Rotaxanes and Catenanes*", *Chem. Soc. Rev.*, **2018**, *42*, 5266. doi:10.1039/C8CS00097B and F. Modicom, E. M. G. Jamieson, E. Rochette and S. M. Goldup, "*Chemical consequences of mechanical bonding in catenanes and rotaxanes: isomerism, modification, catalysis and molecular machines for synthesis*", *Angew. Chem. Int. Ed.*, 2019, **58**, 3875–3879.

Signed: Ellen M. G. Jamieson.....

Date:.....

Acknowledgements

‘With the oversight of my main supervisor, editorial advice has been sought. No changes of intellectual content were made as a result of this advice.’

First and foremost, I would like to thank Steve; I could not have asked for a better or more supportive supervisor for the last few years. I cannot thank you enough for not only the opportunities afforded to me during my PhD but also for giving me the chance to join the group.

Secondly I have to thank everyone who has been a part of the group during the last three years, making the lab what it is, it has been an exceptional experience to work with you all.

To some of the members of times gone past: Marzia, thank you for dragging me climbing and your endless enthusiasm; to Jamie for all of the excellent beer recommendations over the years; Mathieu, for being such an excellent desk mate and keeping me in a supply of fresh green bananas and Peggy, for just being… Peggy.

Florian, thank you for your endless drive especially on our joint projects, it has been excellent to work with you.

To Andrew for your excellent humour, company and for proofreading a lot of this thesis; and Jack, for your music around the lab. Mike, thank you for all of your excellent meals over the years; Amanda, thanks for all of the help, particularly with the growing garden that’s been taking over my desk, and to Shu Shu Bao Bao, Poom Poom Poom, Dr. Lasange, Albertowl, and Jorge; you have all been fantastic.

Matt, Arnau and Fede, it has been great getting to know you guys over the last year and getting to argue over games of Catan with you all.

And thirdly, on a personal note, I’d like to extend a thanks to Claire, I could not ask for a better friend over the past few years and especially the last few months while writing.

To Robert, I couldn’t have done this without you, thank you for everything.

And finally to Mum and Dave, thank you for always believing in me.

Definitions and Abbreviations

δ ..... Chemical shift

Ac ..... Acetyl

AT ..... Active template

AT-CuAAC .....Active-template Cu-catalysed azide-alkyne cycloaddition

Aq. ..... Aqueous

BINOL .....1,1'-binaphthyl-2,2'-diyl

Boc .....*t*-Butyloxycarbonyl

CD .....Circular dichroism

CDI .....1,1'-carbonyldiimidazole

CIP ..... Cahn-Ingold-Prelog

COSY ..... Correlation spectroscopy

Cy.....Cyclohexyl

DBU ..... 1,8-Diazabicyclo[5.4.0]undec-7-ene

DIPEA ..... *N,N*-diisopropylethylamine

DMAP 4-Dimethylaminopyridine

DMF .....*N,N*-Dimethylformamide

DMSO .....Dimethylsulfoxide

EDTA .....*N,N,N',N'*-ethylenediamine tetraacetate

e.e. ..... Enantiomeric excess

EI .....Electron Ionisation

Equiv. .....Equivalent

EtOAc .....Ethyl acetate

EtOH ..... Ethanol

h .....Hours

HMBC .....Heteronuclear multiple-bond correlation

HPLC .....High performance liquid chromatography

HRMS .....High resolution mass spectrometry

HSQC .....Heteronuclear single quantum correlation

J ..... Coupling constant

J-MOD .....J-modulation spin-echo

LR MS .....Low resolution mass spectrometry

M ..... Molar

(co-)MAC ..... (co-conformational) Mechanical Axial Chirality

MeOH ..... Methanol

MIMs ..... Mechanically Interlocked Molecules

min ..... Minute

MLCT ..... Metal-to-ligand charge transfer

m.p. ..... Melting point

(co-)MPC ..... (co-conformational) Mechanical Planar Chirality

Ms ..... Methanesulfonyl

MS ..... Mass spectrometry

(co-)MTC ..... (co-conformational) Mechanical Topological Chirality

NMR ..... Nuclear magnetic resonance

OTf ..... Trifluoromethanosulfonate

ppm ..... Parts per million

quant. ..... Quantitative

$R_{co\text{-}c}$ ..... *R* isomer (co-conformationally covalently chiral)

$R_{(co\text{-})ma}$ ..... *R* isomer ((co-conformationally) mechanically axially chiral)

$R_{(co\text{-})mp}$ ..... *R* isomer ((co-conformationally) mechanically planar chiral)

$R_{(co\text{-})mt}$ ..... *R* isomer ((co-conformationally) mechanically topologically chiral)

rt ..... Room temperature

$S_{co\text{-}c}$ ..... *S* isomer (co-conformationally covalently chiral)

$S_{(co\text{-})ma}$ ..... *S* isomer ((co-conformationally) mechanically axially chiral)

$S_{(co\text{-})mp}$ ..... *S* isomer ((co-conformationally)mechanically planar chiral)

$S_{(co\text{-})mt}$ ..... *S* isomer ((co-conformationally) mechanically topologically chiral)

TBA ..... Tetrabutylammonium

TBDMS ..... *Tert*-butyldimethylsilyl

THF ..... Tetrahydrofuran

TLC ..... Thin layer chromatography

Ts 4-Toluenesulfonyl

UV-Vis ..... Ultraviolet-visible radiation

VT ..... Variable temperature

Chapter 1: Introduction

Abstract: The study of interlocked molecules is an emerging field, bolstered by the recent 2016 Nobel Prize to Stoddart and Sauvage "For the Design and Synthesis of Molecular Machines". With this newfound interest, it is important to consider the implications of the mechanical bond and the unusual properties that it can engender. The ways in which chirality can be expressed not only in addition to the mechanical bond but as a *consequence* of the mechanical bond will be discussed here. Novel forms of chirality that arise from the mechanical bond will be described, and we will highlight some unreported mechanical stereogenic units for future investigation.

Prior publication: The majority of this chapter (sections 1.2 to 1.4) was prepared in collaboration with F. Modicom and previously published as part of:

E. M. G. Jamieson, F. Modicom and S. M. Goldup, "*Chirality in Rotaxanes and Catenanes*", *Chem. Soc. Rev.*, **2018**, *42*, 5266. doi:10.1039/C8CS00097B.

1.1. Introduction to Mechanically Interlocked Molecules

'Traditional' forms of bonding; ionic, covalent and metallic, are defined by attractive forces holding two or more atoms together, either through shared electrons, or through coulombic attraction. Mechanical bonding, however, does not fit into these definitions; the mechanical bond is a link between two or more molecules due to the fact that atoms cannot pass through one another in space, rather than any attraction between the components.[1]

Mechanically Interlocked Molecules, (MIMs) are typically separated into catenanes, rotaxanes and knots; a catenane is two or more macrocycles interlocked to form links in a chain (**Figure 1.1a**), a rotaxane is at least one 'axle' with large end groups that prevent the slippage of the macrocycle wrapped around it (**Figure 1.1b**), while molecular knots resemble macroscopic knots. (**Figure 1.1c**). Rotaxanes and catenanes are held together by a mechanical bond, and while no covalent or ionic link holds them in place, they cannot be separated without breaking one or more covalent bonds (**Figure 1.1**).[1]

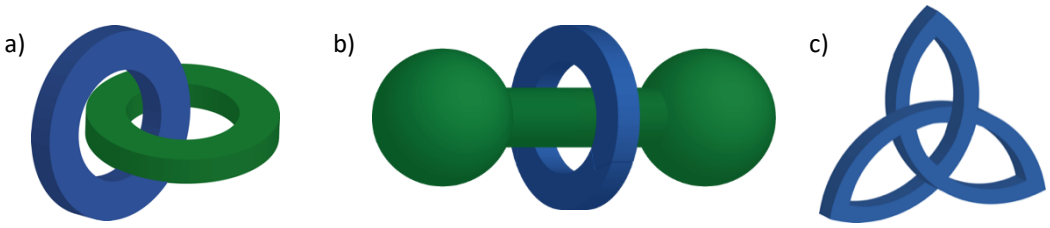

Figure 1.1 Schematic of a) a [2]catenane, b) a [2]rotaxane and c) a trefoil knot.

1.1.1. Early Syntheses of MIMs

The first synthesis of a MIM was in 1960 by Wasserman using a 'statistical' synthesis method. He synthesized a [2]catenane,[2] with an approximate 1% yield, becoming the first to demonstrate that mechanically interlocked molecules could exist and be isolated, albeit in very low quantities. Following from this discovery, in 1983 Sauvage and co-workers published the synthesis of **4**, a [2]catenane using a copper 'template' directed synthesis in two steps (**Scheme 1.1**).[3]

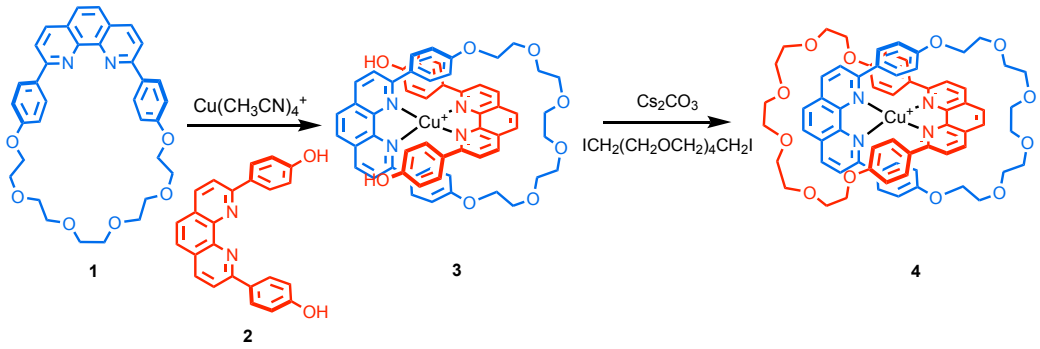

Scheme 1.1 First example of a metal templated synthesis of a catenane, counter ions were omitted for clarity.[3]

This method, now referred to as 'passive templation' relied on the tetrahedral geometry of Cu^{I} to pre-organise the macrocycle precursors. Once the components are 'arranged' the reaction can proceed to yield the catenane in a 27% yield; much higher yield than previously achieved. After this first publication Sauvage and co-workers de-metalated the system to give the interlocked ligand that was then termed a 'catenand', in recognition of its ability to act as a ligand.[4]

Sauvage's work demonstrated the first 'templated' synthesis of a catenane, leading to a re-vitalisation of the field and pathing the way for other methods for the synthesis of MIMs exploiting this new passive template concept. Early examples of this can be seen from Stoddart and co-workers, who relied on π-π stacking between electron-rich/electron-poor systems in many of his MIMs, rather than the metal templates of Sauvage (**Scheme 1.2**).[5,6,7]

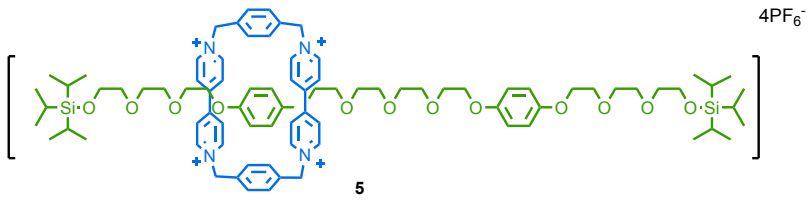

Scheme 1.2 Stoddart and co-workers early example of a passive-templated rotaxane **5** using electron-rich/electron-poor π-stacking.[5]

Both Sauvage and Stoddart's contributions to the field were deemed so important that they received the 2016 Nobel prize, alongside Ben Feringa who developed molecular switches and motors using covalently bonded systems, for 'The Design and Synthesis of Molecular Machines'.[8]

1.1.2. The Active Template Approach to MIMs

Following on from this passive template approach, in 2006 Leigh and co-workers reported the first example of an 'active' template approach.[9] They reported using the copper-catalyzed azide alkyne cycloaddition (CuAAC) "click" reaction for the synthesis of **9**, where

the copper acts as both a catalyst for the axle formation, and is also the template, pre-organising the macrocycle in during the reaction (**Scheme 1.3**). This breakthrough laid the groundwork for the development of many different active templated (AT) rotaxane syntheses, such as an AT-Glaser coupling,[10] or an AT sp^3-sp^3 homo bromide coupling[11] to mention just a few.[12] This has allowed the development of many new MIMs, and facilitated access to new functional molecules.

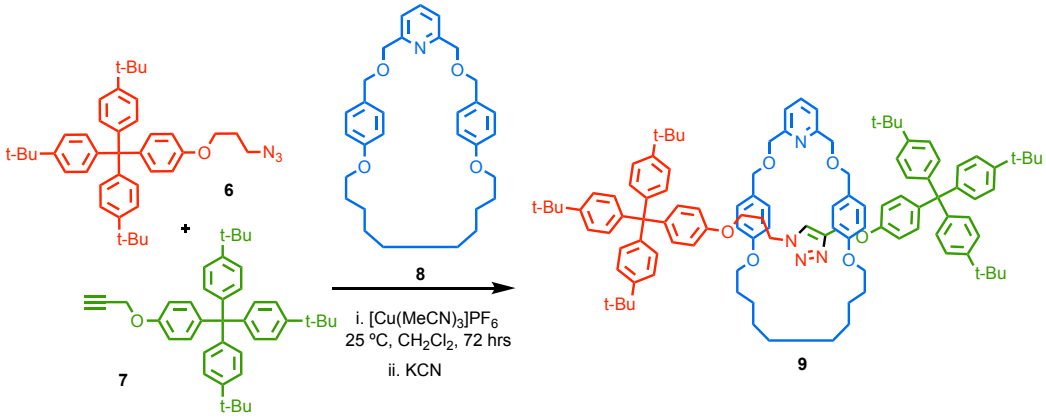

Scheme 1.3 Leigh's first AT-CuAAC synthesis of a rotaxane **9**.[9]

In 2011, Goldup and co-workers published a family of 'small' functionalised rotaxane using the AT-CuAAC approach. They demonstrated that it was not only possible to decrease the cavity size, but in their example it was shown that using a smaller macrocycle, and therefore increasing the steric hindrance in the system, *increased* the overall isolated yield (**Scheme 1.4**).[13] In Leigh's earlier examples, five equivalents of half-axle components to one equivalent of macrocycle were required to achieve high yields. Goldup and co-workers only required one equivalent of the azide and alkyne to give rotaxane **13** with a yield of 99%.

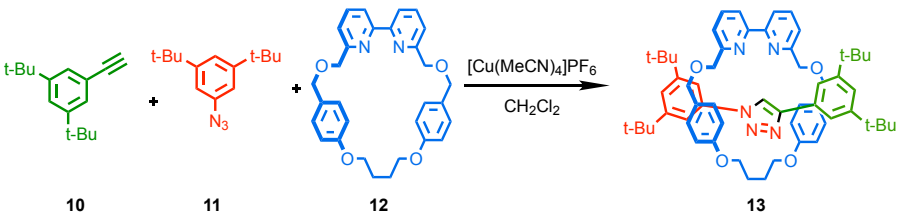

Scheme 1.4 Goldup's synthesis of a crowded rotaxane **13** using a small bipyiridne macrocycle.[13]

This high yield of rotaxane is due in part to the smaller macrocycle cavity size disfavouring reactions on the same macrocyclic face through sterics, an unproductive pathway that produces non-interlocked axle. Also, the use of a bipyridine macrocycle means that two of the copper's tetrahedral binding sites are occupied, leaving only two remaining coordination sites of the copper, on either face of the macrocycle (**Figure 1.2**).[12]

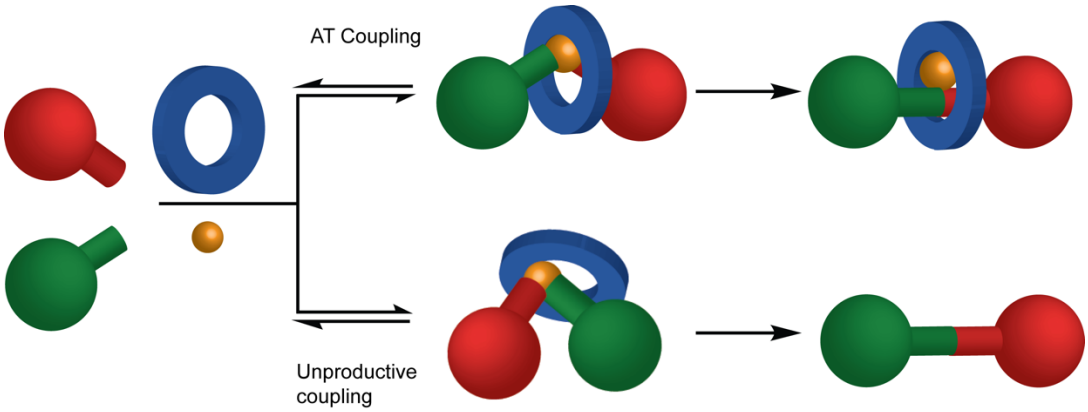

Figure 1.2 Cartoon representation of productive and unproductive AT pathways.

By using macrocycles with reduced cavity sizes, Goldup and co-workers were able to use smaller 'stoppers', meaning the half-axle components can be synthesized from simple, commercially available starting materials without requiring modification to include very 'bulky' groups, such as trityl groups which were used in past like compounds **6** and **7**. The introduction of 'small' macrocycles for the AT-CuAAC reaction has allowed the development of novel rotaxanes for use in areas such as catalysis,[14] ion binding,[15,16] and the development of an efficient approach to mechanically planar chiral rotaxanes.[17]

The AT-CuAAC has been shown to proceed *via* a Cu-triazolide intermediate. Goldup and co-workers serendipitously isolated an example of this in a 82% yield (**Scheme 1.5**).[18]

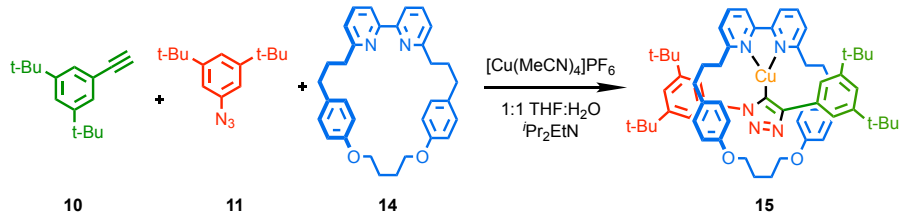

Scheme 1.5 Goldup and co-workers' synthesis of stable Cu-triazolide **5**.[18]

Triazolide **15** is remarkably stable under aqueous conditions, in contrast to a previous report by Straub,[19] the only published example of such a system prior to **19** (**Scheme 1.6**). Straub reported triazolide **19** to be incredibly sensitive to moisture and air and require careful handling under an inert atmosphere.

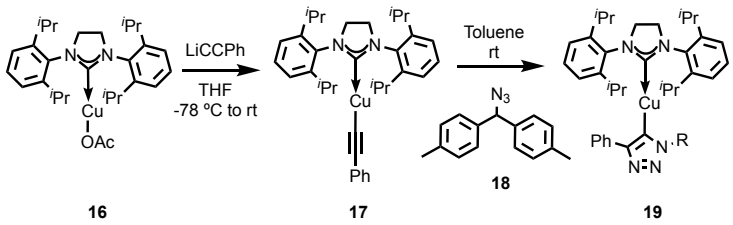

Scheme 1.6 Straub and co-workers synthesis of a Cu^{I} triazolide **19**. [19]

The higher stability of **15** in comparison to **19** is thought to be due to the steric constraints of the rotaxane, which kinetically prevents the protonolysis of the Cu-C bond. In keeping with this, when the experiment was repeated with a less sterically hindered azide **20** (**Scheme 1.7**), although Goldup and co-workers were able to observe triazolide **21a**, upon aqueous work-up the corresponding triazole **21b** was the only product observed.

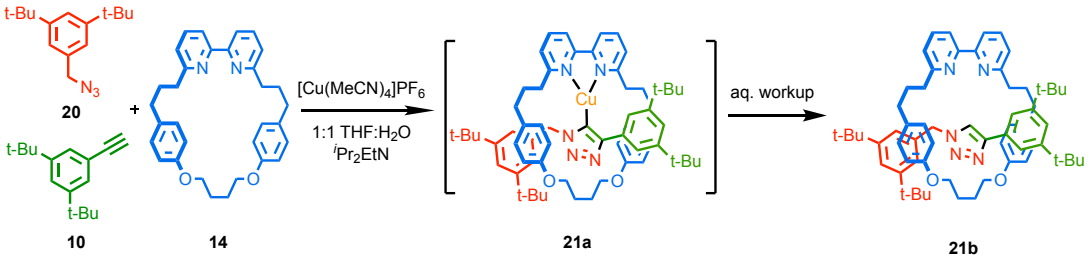

Scheme 1.7 Goldup and co-workers' synthesis of unstable Cu-triazolide **21a** and its transformation to rotaxane **21b** during aqueous workup.[18]

1.2. MIMs Containing Covalent Stereogenic Units

When considering the stereochemistry of MIMs it is important to first consider the simplest, and most familiar form of chirality; covalent chirality. Covalent chirality is chirality that arises from a covalent bond, i.e. point chirality, (the chirality that can arise around a tetrahedral carbon), axial chirality (along an axis, exemplified in binol), planar chirality (desymmetrisation of a plane, like in ferrocene compounds) and helical chirality (in helical molecules, for example in [n]helicenes). Covalent stereogenic units occur in a lot of MIMs, perhaps most notably in structures utilising cyclodextrin. Cyclodextrin, being a sugar derived macrocycle is one of the most common commercially available macrocycles and is derived from 6, 7 or 8 D-glucose units, and inherently possess chirality as a consequence of this. In a lot of these publications however, the chirality is a side consequence of the chemistry used to achieve the end structure, rather than something intentionally designed or utilised. There have been some reports however of MIMs that use covalent stereogenic units for a range of applications.

1.2.1. MIMs Containing Covalent Stereogenic Units as Enantioselective Hosts

Due to the steric environment imposed by the mechanical bond, MIMs usually present different properties compared to their non-interlocked components. In particular, the threading of one molecule through another creates a sterically crowded 'pocket'.

Extrapolating this to MIMs containing covalent stereogenic centres, this interlocked 'pocket' can result in a well-expressed chirotopic region for guest binding. This concept has been exploited for selective binding of chiral guests. Niemeyer and co-workers reported chiral phosphate [2]catenane (*S,*S)-**22**,[20] that displayed enantioselective binding (**Figure 1.3**).

a)

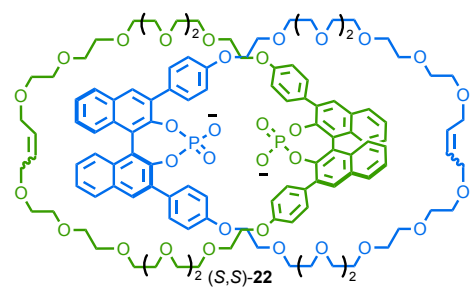

b)

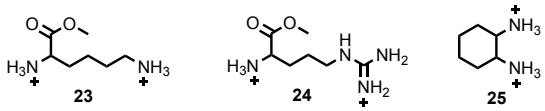

	macrocycle		(*S*,*S*)-**22**	
Cation*	K_a [M^{-1}]	K_{fav}/K_{disfav}	K_a [M^{-1}]	K_{fav}/K_{disfav}
(*S*)-**23**	630 ± 20	1.1	4100 ± 610	1.4
(*R*)-**23**	700 ± 30		5700 ± 730	
(*S*)-**24**	570 ± 25	1.3	5550 ± 320	1.5
(*R*)-**24**	770 ± 35		8200 ± 610	
(*S*,*S*)-**25**	870 ± 170	1.0	15800 ± 2900	1.6
(*R*,*R*)-**25**	840 ± 100		10050 ± 1300	

Figure 1.3 a) Structure of catenane (*S,S*)-**22** and b) assosiation constants for guests **23**, **24**, and **25**. Counter ions omited for clarity.[20]

(*S,S*)-**22** showed a marked increase in association constants for one enantiomer over the other for different dicationic salts when compared with the non-interlocked macrocycle. This enantioselective binding was the first demonstration of such a feature. Particularly for guest **25**, which showed no signification differentiation in binding constants for the macrocycle alone but the rate of K_{fav}/K_{disfav} increased to 1.6 for (*S,S*)-**22**. Also remarkable was the increase in the magnitude of binding constants across all guests with the [2]catenane host when compared with the lone macrocycle, although this is probably, at least in part due to the higher charge of the interlocked compound.

Recently Beer and co-workers have developed a series rotaxanes for the enantioselective binding of anionic guests.[21] Rotaxanes (S,S,*S)*-**26**, (*S,S)*-**27**, and (*S*)-**28** were synthesised using Beer's iodo-triazole modification of the AT-CuAAC reaction. Rotaxane (*S,S,S*)-**26** showed remarkable enantioselectivity for different anions, with a maximum of selectivity of ~3:1 for proline derived salt **31** (**Figure 1.4**). [21]

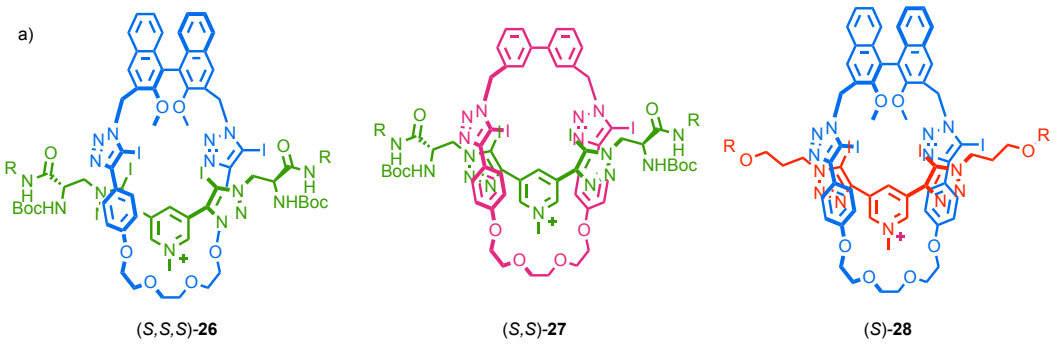

Enantioselectivity for (*S*)

Anion	(*S,S,S*)-**26**	(*S,S*)-**27**	(*S*)-**28**	macrocycle from **26**/**28**	axle of **26**/**27**
29	1.62 ± 0.17	0.94 ± 0.08	0.29 ± 0.03	0.67 ±0.03	1.30 ± 0.07
30	1.73 ± 0.14	0.85 ± 0.07	0.62 ± 0.06	0.66 ± 0.03	1.41 ± 0.10
31	2.93 ± 0.13	0.90 ± 0.03	0.66 ±0.04	0.70 ±0.01	1.22 ± 0.04
32	0.47 ± 0.04	1.19 ± 0.06	0.56 ± 0.06	1.58 ± 0.11	0.82 ± 0.04

Figure 1.4 a) Struture of rotaxanes (*S,S,S*)-**26**, (*S,S*)-**27** and (*S*)-**28,** and b) chiral anions tested for selective binding and their observed selectivty. Counter ions removed for clarity. R = -(C_6H_4)-C(4-(C_6H_4)-^{t}Bu)$_3$.[21]

Rotaxane (*S,S,S*)-**26** possesses chirotopic units on both the axle and the macrocycle, and shows strong enantioselectivity for all guests shown above, but particularly the proline salt. Rotaxanes (*S,S*)-**27** and (*S*)-**28** were also synthesised to contrast the difference between

rotaxanes with chirotopic units centred only on the axle and the macrocycle respectively. While the selectivity for (*S*)-**28** is reversed relative to (*S,S,S*)-**26** in most cases (other than **32**), (*S*)-**28** still showed a relatively strong selectivity, particularly for anion **29**.[21] Interestingly, rotaxane (*S*)-**27** displays much lower selectivity, even in comparison to the axle or macrocycle.[21] Thus, the macrocycle structure was shown to have a large influence on the stereoselectivity observed from each of the rotaxanes. Beer and co-workers reported DFT calculations that helped to rationalise the observed selectivity for rotaxane by showing the multiple possible interactions between the anion and host.[21]

Although reports on chiral guest binding with MIMs is still limited, these early studies show the promise in the field.

1.2.2. MIMs Containing Covalent Stereogenic Units as Catalysts

Leigh and co-workers reported rotaxane (*R,R*)-**33** as a ligand for enantioselective transition metal couplings[22] (**Scheme 1.8**). For comparison they used an acyclic analogue of the macrocycle, compound (*R,R*)-**34**. Rotaxane (*R,R*)-**33** showed a significant increase in the enantioselectivity (86% e.e.) compared with (*R,R*)-**34** (33% e.e.).[22] The authors propose that this increase comes from the more sterically congested catalytic centre, helping to increase the chiral information transfer from (*R,R*)-**33** to the product. This also unfortunately is what likely leads to the large decrease in catalytic activity, from 2 days for acyclic (*R,R*)-**34**, to 27 days for rotaxane (*R,R*)-**33**. [22]

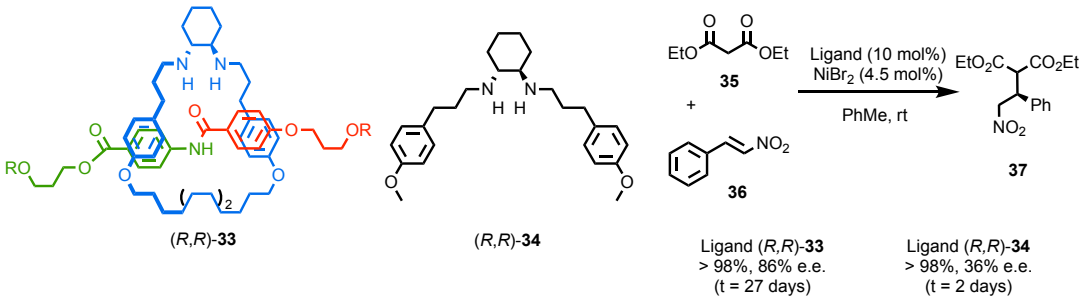

Scheme 1.8 Rotaxanes (*R,R*)-**33** and acyclic ligand (*R,R*)-**34** and their performance in an enantioselective Ni-catalysed michael addition. R = 4-(C_6H_4)-C(4-(C_6H_4)-tBu)$_3$.[22]

Takata and co-workers have also investigated the use of MIMs for enantioselective catalysis.[23,24] They reported an enantioselective acyl transfer reaction using rotaxane (*R*)-**38** (**Scheme 1.8**).[24] In the presence of rotaxane (*R*)-**38**, the de-symmetrisation of *meso* compound **39** yielded **40** in 98% e.e. at –80 °C, whereas the non-interlocked components gave the product in much lower selectivity (8% e.e. at rt compared with 78% e.e. for (*R*)-**38** at r.t.).[22] This a very impressive example that shows the ability of rotaxanes to aid in

enantioselective catalysis, including reactions that are usually difficult to complete enantioselectively, and how chirality can be transferred to an achiral reaction site *via* the mechanical bond. Interestingly this system actually results in a dramatic *increase* in the reaction rate when compared with just the axle or the axle and macrocycle, although the reason for this is uncertain.[22]

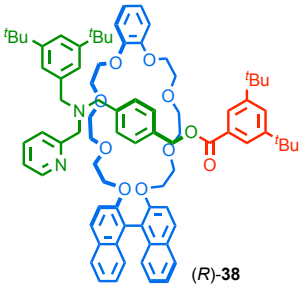

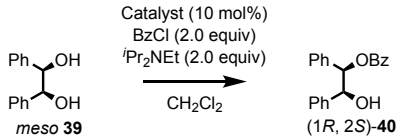

Catalyst	Temperature (°C)	Time (h)	Yield (%)	ee (%)
(*R*)-**38**	rt	12	> 99	78
(*R*)-**38**	-80	24	> 99	98
axle	rt	48	47	-
axle + macrocycle	rt	48	46	8

Scheme 1.9 Structure of (*R*)-**38** and reaction scheme for acyl transfer by Takata and co-workers.[24]

Leigh and co-workers have previously worked on the development of 'switchable' catalysts[25] using rotaxanes as a 'molecular machines', more recently they have expanded this approach to molecular shuttle (*S*)-**41**, which performs an enantioselective Michael addition (**Scheme 1.9**).[26]

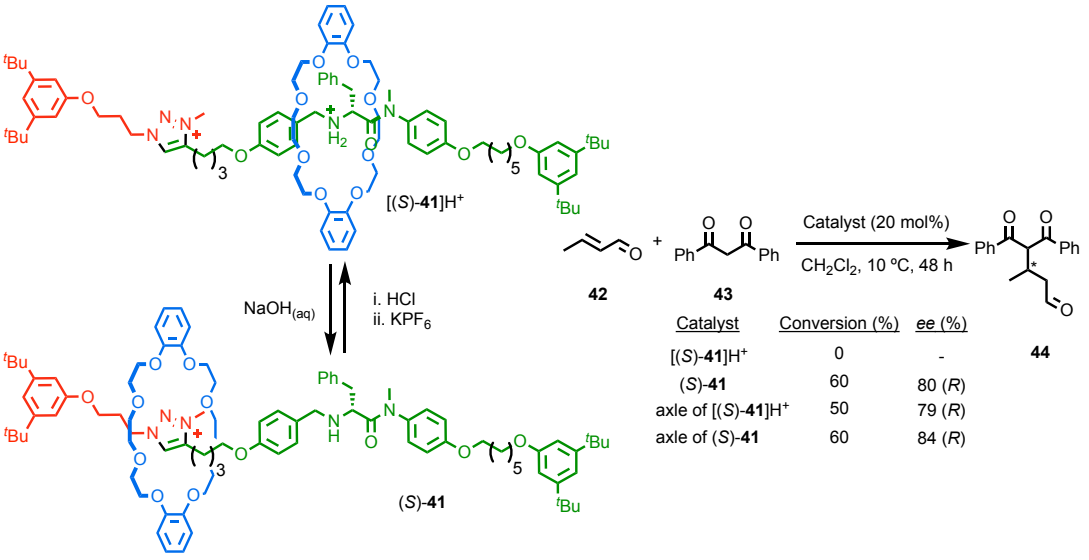

Catalyst	Conversion (%)	ee (%)
[(*S*)-**41**]H$^+$	0	-
(*S*)-**41**	60	80 (*R*)
axle of [(*S*)-**41**]H$^+$	50	79 (*R*)
axle of (*S*)-**41**	60	84 (*R*)

Scheme 1.10 Structure of switchable rotaxane-based catalyst (*S*)-**41** and reaction scheme for asymmetric Michael addition performed. Counter ions omitted for clarity.[26]

When rotaxane (*S*)-**41** is protonated to give [(*S*)-**41**]H$^+$, the macrocycle occupies the ammonium station, inhibiting its catalytic activity both sterically and by increasing its pK_a. Deprotonation results in shuttling of the crown ether macrocycle onto the triazolium functionality, enabling catalytic turnover from the vacant secondary amine station.[26] The e.e

of the product and the conversion of the starting material both remain comparable between the free axle and (*S*)-**41**. This is not unsurprising in this system that the enantiomeric excess is not affected by the mechanical bond dramatically; the triazolium motif is relatively far removed from the catalytic site so the steric influence of the crown ether would be negligible in the case of (*S*)-**41**.

1.2.3. Chiroptical Properties of MIMs Containing Covalent Stereogenic Units

MIMs that contain covalent stereogenic units which render them therefore chiral will display optical rotation and related chiroptical properties as expected. However, like with the previous examples of amplification of catalytic and/or binding properties of chiral MIMs, the optical properties of these molecules can be augmented by their inclusion into a MIM scaffold.

Saito and co-workers reported rotaxane **45**,[27] which displayed a strong CD signal (**Figure 1.5**). Similarly, to the earlier acyl transfer catalyst, (*R*)-**38** which, in which chiral information from the covalent stereogenic unit, located on the macrocycle, is transferred to the achiral axle resulting in enantioselective catalysis, rotaxane **45** also displayed a chirality transfer to its achiral axle. This is displayed in the CD spectra by the bands at 320 nm and 348 nm which are attributed to the axle, rather than the macrocycle. [27]

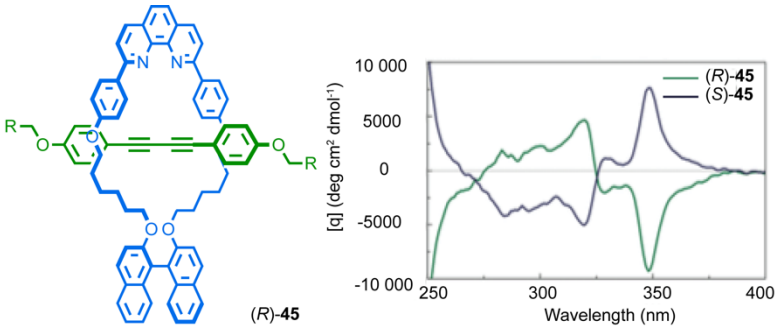

Figure 1.5 Structure of (*R*)-**45**, and the CD spectra for both enantiomers. R = C(4-(C_6H_4)-(4-(C_6H_4)-cyclohexyl))$_3$. CD spectra reprinted with permission from ref. 27 copyright 2015 The Chemical Society of Japan. [27]

Leigh and co-workers reported rotaxane (*S*)-**46**,[28] which they used to investigate the influence of the mechanical bond on the chiral structure *via* its CD signal (**Figure 1.6**). The rotaxane showed a significant, strong CD signals in comparison to the non-interlocked axle. Interestingly the CD response varied dramatically depending on the solvent used. When the CD spectra were collected in a less polar, aprotic solvent, the signal was much higher in intensity than in a polar, protic solvent. Most strikingly, the sign of the CD was inverted at

~245 nm in chloroform compared with methanol. The temperature dependence of the CD response of (*S*)-**46** was also investigated and displayed large changes in methanol, while chloroform did not show changes with changes with varied temperature. X-ray crystallography and computational analysis suggest that the diphenylmethane units contribute to the observed chiroptical response, due to an indirect transfer of chiral information from the peptide moiety *via* the achiral macrocycle. This helps to explain the dramatic influence of solvent on the CD signal, as methanol can act as a competing hydrogen bond (HB) donor and so strongly influence the (co)conformation of the system. [28]

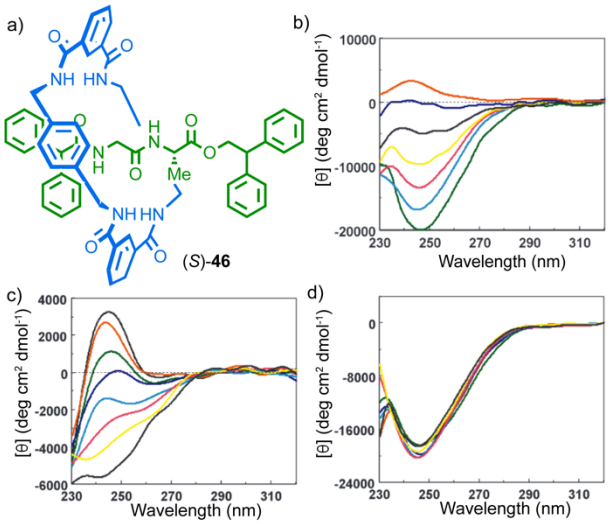

Figure 1.6 a) structure of rotaxane (*S*)-**46**, b) solvent dependent CD spectra (0.1 mM) of rotaxane (*S*)-**46** in $CHCl_3$ (green), 1:1 $CHCl_3$/MeOH (cyan), 2 : 3 $CHCl_3$/MeOH (yellow), 1 : 5 $CHCl_3$/MeOH (black), 1 : 10 $CHCl_3$/MeOH (blue) and 100% MeOH (red). Temperature-dependent CD spectra (0.1 mM) of rotaxane (*S*)-**46** in (c) MeOH and (d) CHCl3 : 263 K (black), 273 K (red), 283 K (green), 293 K (blue), 303 K (cyan), 313 K (magenta), 323 K (yellow) and 333 K (black) Reprinted with permission from ref. 28. Copyright 2002 American Chemical Society. [28]

1.3. Chirotopic Mechanical Stereogenic Units

While it is important to consider how mechanically bonded molecules can be affected by covalent stereogenic units, perhaps more interestingly, from a theoretical point of view are systems which can be considered 'mechanically chiral'. MIMs can possess chirality that arises as a function of the mechanical bond, rather than any covalent stereogenic unit. The term 'mechanically chiral' is a broad term to describe this phenomenon. However, mechanical chirality can arise due to a number of distinct stereogenic units. Below I will outline the key members of this family based on their underlying structural features.[29]

1.3.1. Mechanical Planar Chirality

Mechanical planar chirality (MPC), a term coined in 2014,[17] was first recognised as a possibility by Schill 1971[30] and is the only fixed form of mechanical chirality to apply to rotaxanes. Mechanically planar chirality can be observed in rotaxanes that possess C_{nh} symmetrical macrocycle (principal axis aligned *perpendicular* to the macrocyclic plane) which encircle a C_{nv} axle (principal axis and mirror planes aligned to the 'length' of the axis). C_{nh} macrocycles are typically referred to as 'orientated' particularly in the context of MPC (**Figure 1.7**).

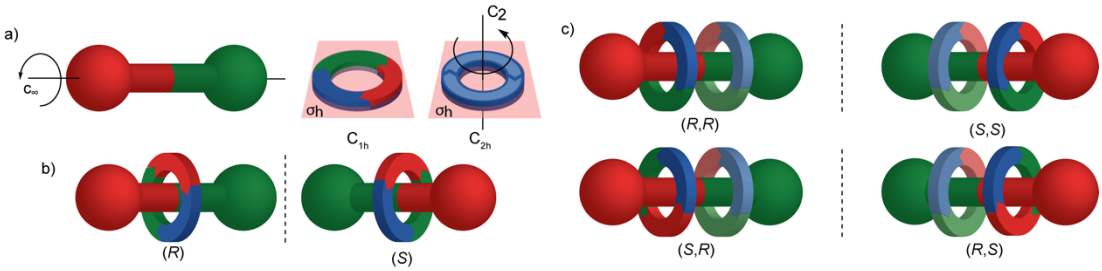

Figure 1.7 a) Axle (C_{nv}) and macrocycle (C_{1h}, C_{2h}) components suitable for inclusion in mechanically planar chiral rotaxanes, b) A MPC chiral [2]rotaxane enantiomers, c) A mechanically planar chiral hetero[3]rotaxane and the stereoisomers possible. [29]

MPC occurs due to the decrease in symmetry upon forming the mechanical bond, and the subsequent loss of planes of symmetry present in the macrocycle and axle. Assignment of chirality for these structures, while not simple, can still be rationalised using basic Cahn–Ingold–Prelog (CIP) rules.

Step 1: Assign the highest priority atom of the axle, this is now **A**

Step 2: Determine the highest priority atom attached to A that allows directionality to be assigned, this is now **B**

Step 3: Repeat steps 1 & 2 for the macrocycle to determine it's 'orientation', labelling the corresponding atoms **C** and **D**.

Step 4. View the rotaxane down the vector of **A** to **B**. Determine if **C** and **D** are disposed 'clockwise' (R_{mp}), or anti-clockwise (S_{mp}) in this orientation.

This procedure is demonstrated below on rotaxane **47** (**Figure 1.8**).[31]

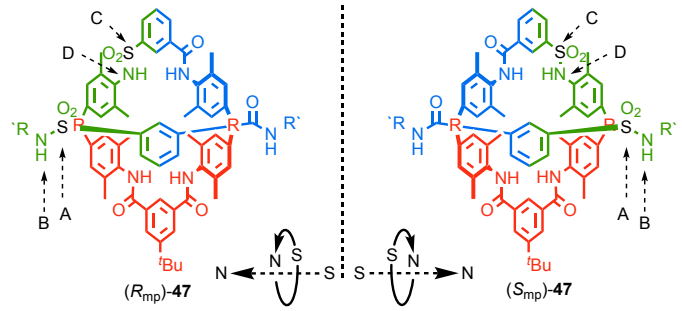

Figure 1.8 Structure of Vögtle's MPC rotaxanes **47** and the assignment of their stereochemistry. R = 1,1-cyclohexyl, R' = $-C_6H_4-$Tr.[31]

Rotaxane **47** was the first reported example of an enantiopure mechanically planar chiral rotaxane, and was synthesised by Vögtle, in 1997.[31] The enantiomers were resolved using preparative chiral stationary phase HPLC, yielding the enantiomerically pure rotaxanes. However their absolute stereochemistry could not be determined, only their optical rotations, which were found to be approximately equal and opposite. This method of separation is unfortunately limited in scale due to the technical limitations of chiral preparative HPLC.

Following from this Takata and co-workers reported the first catalytic asymmetric synthesis of a MPC rotaxane (**Scheme 1.11**).[32] Rotaxane **49** was produced using a dynamic kinetic resolution strategy mediated by a chiral phosphine reagent. Acylation of a racemic mixture of pseudo-rotaxane **48** gave **49** in up to 4.4% e.e. [32] Unfortunately 4.4% e.e. is not enough to be a useful scalable method of enantioselective rotaxane synthesis, and in order to obtain pure samples of each enantiomer, chiral preparative HPLC was also required for this system.[32]

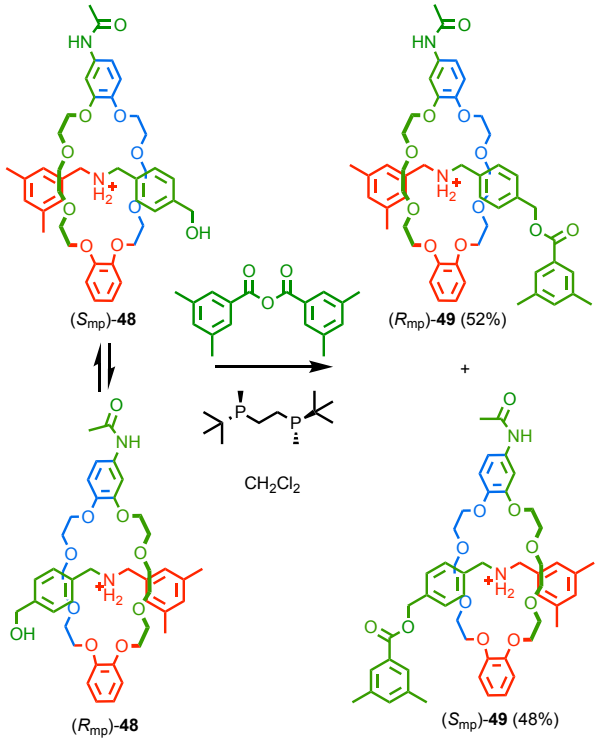

Scheme 1.11 Takata's enantioselective dynamic kinetic resolution of pseudo-rotaxane **48** to give rotaxane **49.**[32]

Goldup and co-workers then reported a scalable route to MPC rotaxanes by utilising a method commonly used for enantiopure organic synthesis: a chiral auxiliary strategy.[17] Rotaxane **52** was synthesised with a sugar-based azide **50**. The point chirality from the covalent stereogenic unit combined with the MPC stereogenic unit resulted in a pair of diastereoisomeric rotaxanes which were separable by normal phase column chromatography. They could then exchange the sugar stopper by aminolysis to remove the source of covalent chirality, yielding rotaxanes **54** in excellent enantiopurity (**Scheme 1.11**).[17] This chiral auxiliary concept means that enantiomerically pure MPC rotaxanes can be synthesised readily.[17] It is also worth noting that the MPC stereodescriptor 'switches' in the conversion of **52** to **54** as a consequence of the change in the identify of atom "A".

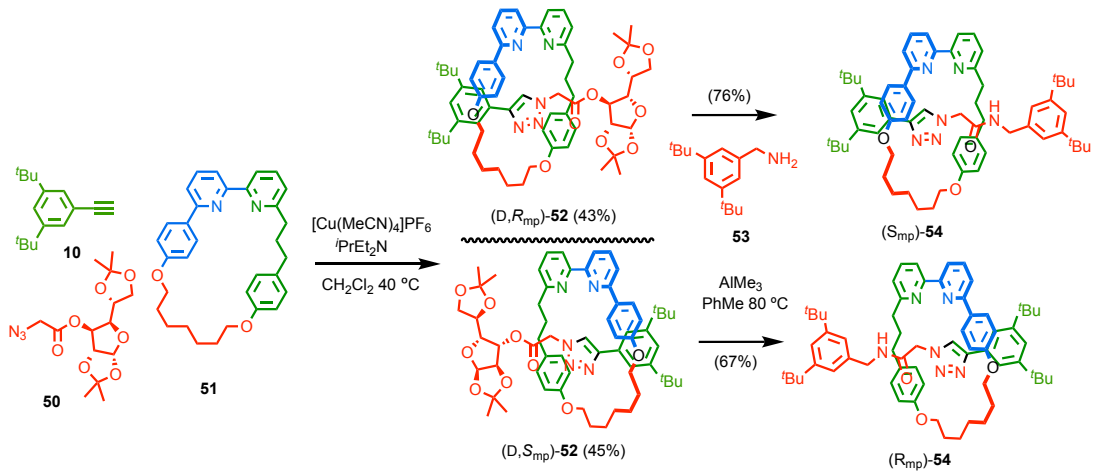

Scheme 1.12 Goldup's chiral auxiliary route to enantiopure rotaxanes (R_{mp})-**54** and (S_{mp})-**54**.[17]

Building on this result, Goldup and co-workers have developed stereoselective procedures to access MPC rotaxanes (**Scheme 1.12**).[33] Rotaxane **56** was produced in excellent diastereoselectivity (98:2). In contrast to their previous report in which stopper exchange was used to remove the covalent stereochemistry, in the case of **56** the covalent stereogenic unit was removed by the *addition* of another benzyl group to the covalent stereogenic centre; alkylation yielded rotaxane **57** in which the mechanical bond is the only stereogenic unit.

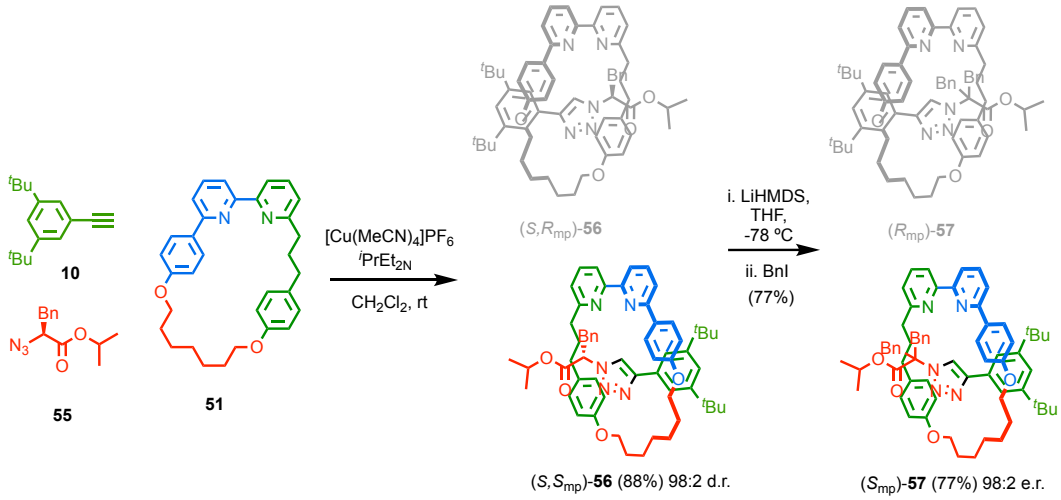

Scheme 1.13 Goldup and co-workers' stereoselective synthesis of rotaxane (S,S_{mp})-**56**. Alkylation removes the covalent stereogenic unit to yield rotaxane (S_{mp})-**57.** [33]

Due to the inherent challenge of synthesising MPC rotaxanes in high enantiopurity, reports regarding these chiral molecules are limited and often make use of racemic samples. One example of this was published by Evans and co-workers where they influenced the expression of MPC in ^{1}H NMR. (**Figure 1.9**).[34] Rotaxane **58** was synthesised using a hydrogen

bond template approach.[34] ^{1}H NMR analysis of **58** in various solvents was used to probe how the position of the macrocycle affected the expression of the MPC stereogenic element on the axle. All methylene units in a chiral molecule are nominally diastereotopic but this is typically not expressed in their ^{1}H NMR spectra unless they are located near to the stereogenic unit. In chloroform which is non-polar and aprotic, the methylene protons next to the amide unit (**Figure 1.9**) are clearly resolved into a diastereoisotopic pair. However, in solvents such as dimethyl sulfoxide that present competing H-bond donors/acceptors, this diastereotopicity is poorly expressed in the ^{1}H NMR spectrum of **58**. Similarly, treatment of **58** with TFA, which causes the macrocycle to shuttle away from the amide unit to encircle the protonated triazole, results in the signals corresponding to H and H` becoming coincident. The authors rationalise these observations by suggesting that the MPC stereogenic unit is well expressed in the region around the amide when the macrocycle occupies this position. In protic solvents or upon protonation, the macrocycle moves away from the amide.

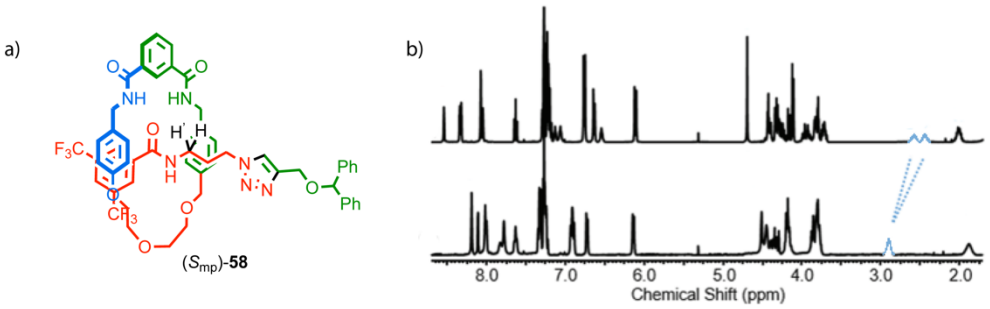

Figure 1.9 Evans and co-workers MPC rotaxane, a) (S_{mp})-**58**. A single enantiomer (arbitrarily chosen) is shown for clarity and b) partial ^{1}H NMR of **58** (top) and **58** after treatment with TFA (bottom), protons labeled H' and H are highlighted in blue. ^{1}H NMR spectra reprinted with permission from ref. 34 copyright 2019 from The Royal Society of Chemistry.[34]

Recently Goldup and co-workers published the first report of a MPC rotaxane acting as an enantioselective catalysts.[35] The first step for this was the synthesis of diastereoisomeric rotaxanes **60** using chiral azide **55** as a stereo-differentiating unit (**Scheme 1.13, 1.14**). After separation of diastereoisomeric rotaxanes **60**, they were then alkylated with benzyl iodide to remove the covalent stereogenic unit, yielding rotaxane **61** (**Scheme 1.14**). Reduction and coordination to gold(I) chloride gave pre-catalyst [Au((R_{mp})-**62**)(Cl)]. Rotaxane [Au((R_{mp})-**62**)(Cl)] mediated an enantioselective cyclopropanation reaction with selectivities that were comparable to those achieved with more conventional covalent catalysts.[36] This report marks an important step forward for the real-world applications of MPC rotaxanes.

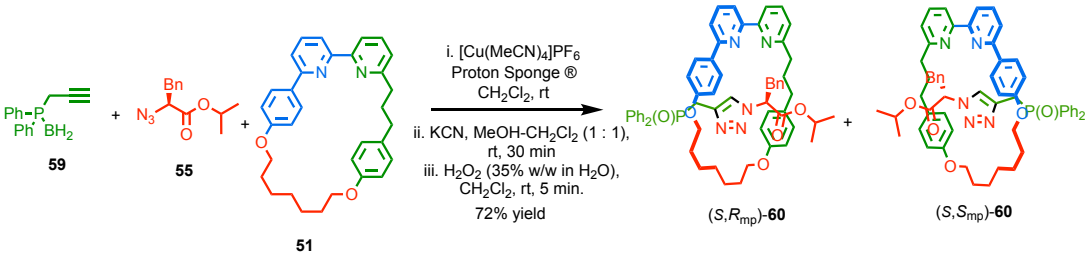

Scheme 1.14 Synthesis of diasterioisomeric rotaxanes (*S*,R_{mp})-**60** and (*S*,S_{mp})-**60** in a 1:1.2 diasteriosomeric ratio. [35]

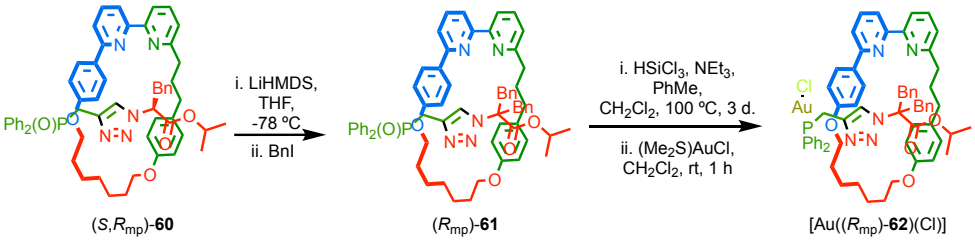

Scheme 1.15 Goldup and co-workers' synthesis of an enantiopure gold(I) complex [Au((*R*$_{mp}$)-**62**)(Cl)].[35]

MPC is a growing topic of interest, particularly with respect to how this stereogenic unit can influence a rotaxane's behaviour and deliver unique properties and applications. To date, progress has been hindered due to limitations of the synthesis of such molecules. Hopefully recent developments, both in terms of synthetic methodology and the applications of MPC rotaxanes, bode well for the future.

1.3.2. Mechanical Topological Chirality

Mechanical topological chirality (MTC) is specific to catenanes and can be considered the catenane 'analogue' of MPC. If you were to take a MPC rotaxane and 'tie' the ends of the axle together (an approach called 'clipping'), converting it to catenane, then it would become mechanically topologically chiral. It should be noted that topological chirality is not solely a property of catenanes and can also be observed in covalent molecules. Generally, molecules are topologically chiral when any bond can be stretched, any angle changed, so long as the bonds do not pass through each other, and it remains distinct from their mirror image.[30,37,38]

In systems possessing two or more adjacent C_{nh} symmetric, macrocycles i.e. 'orientated', MTC will always be observed (**Figure 1.10**). Increasing the number of macrocycles, provided they are all orientated, does not alter the existence of chirality, and each additional ring will add one additional MTC descriptor.

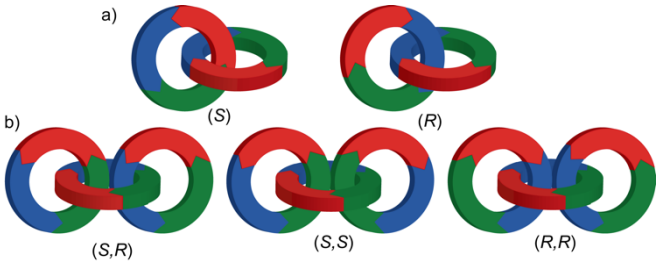

Figure 1.10 Mechanically topologically chiral a) homo[2]catenane and b) homo[3]catenanes.[29]

However when considering a hetero[n>2]catenanes containing a mixture of orientated and non-orientated rings the situation becomes more complex. For linear [n]catenanes containing two orientated macrocycles, if the orientated rings are separated by an 'odd' number of macrocycles, they will not express MTC, whereas they will if there are an even number of intervening rings (**Figure 1.11**). In the former case, although the system is achiral, they will instead exist as a pair of diastereoisomers that can be described as *syn* or *anti* to one another.

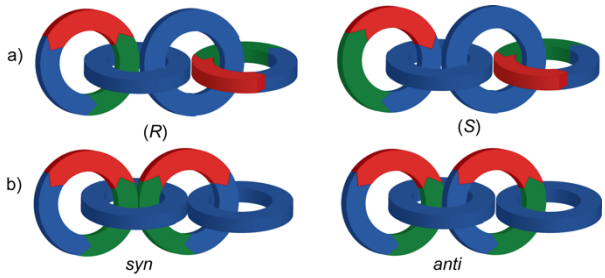

Figure 1.11 Linear oligomeric catenanes displaying (a) MTC, and (b) *syn*/*anti* diastereoisomerisim. [29]

For the assignment of (R_{mt}) or (S_{mt}) for MTC, the first step is to assign the priority atoms of each ring, labelling each pair **A**/**B** in the same manner as detailed in section **1.3.1.** Using this assignment, the structure is viewed with one A->B vector passing away from the observer through the cavity of the other ring. The stereodescriptor is that assigned by identifying if the A/B vector of the second ring is oriented clockwise (*R*), or anti-clockwise (*S*). This approach is exemplified for catenane **63**, the first example of an enantiopure MTC catenane reported. Sauvage and co-workers first synthesised **63** and proved the chirality of the complex by using Pirkle's reagent to induce diastereomeric splitting of key peaks.[39] It took another five years before they were able to produce an enantiopure sample of **63**, using chiral preparative HPLC and at the time they were unable to unambiguously assign the chirality of the catenane, instead having to assign it as + or – according to its optical rotation.[40]

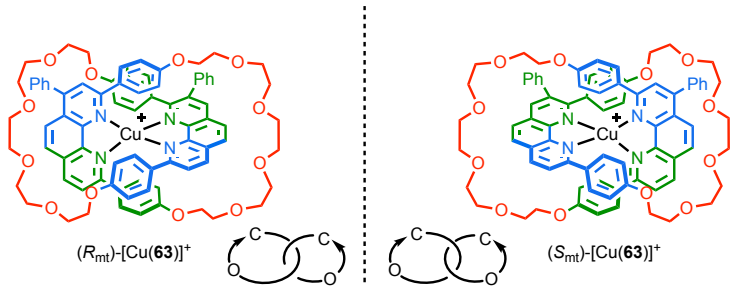

Figure 1.12 Sauvage and co-workers MTC catenane **63**, counter ions omitted for clarity.[39]

Much like MPC rotaxanes, MTC catenanes research has been limited by the difficult enantiomer separation and reliance on preparative HPLC. For this reason, very little is known regarding their properties. One potential solution to this problem is to synthesise catenanes containing a covalent stereogenic unit, which raises the possibility of stereoselectivity or separation using standard techniques.

Any macrocycle that contains a chiral centre is, by definition orientated, provide it is not a *meso* form. In 2005 Sanders and co-workers reported catenane **65** which was isolated from a dynamic covalent self-assembly of enantiopure peptide building blocks in the presence of acetylcholine (**Scheme 1.16**).[41] On a preparative scale catenane ($(S,S)_8S_{mt}$)-**65** was synthesised in a 68% yield. ^{1}H NMR analysis suggested that **65** was formed as a single diastereoisomer, meaning that the covalent chirality directs the MTC stereogenic unit, although the absolute topological stereochemistry of the product was not determined in this case.[41]

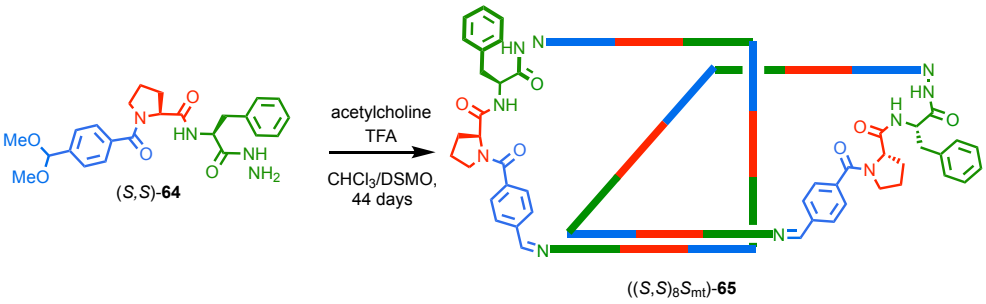

Scheme 1.16 Sanders and co-workers catenane **65** with covalent and MTC stereogenic units.[41]

Building on their high yielding AT-CuAAC catenane synthesis,[42] Goldup and co-workers have recently disclosed a scalable approach to MTC catenanes, by utilising a chiral auxiliary,[43] in a similar manner to their early MPC rotaxane synthesis (**Scheme 1.16**).[17] Separation of the diastereoisomers of catenane **68**, followed by removal of the chiral auxiliary gave enantiomerically pure catenane **69**. While previous work by Sanders,[41] (**Scheme 1.16**) and also Gagné,[44] and Trabolsi,[45] have yielded serendipitous stereoselective synthesis of MTC

catenanes, these approaches leave the covalent stereochemistry in the final product. This work shows the first example of a selective route to enantiomerically pure MTC catenanes in which the mechanical bond provides the only stereogenic unit without the requirement of chiral preparative HPLC (**Scheme 1.17**).

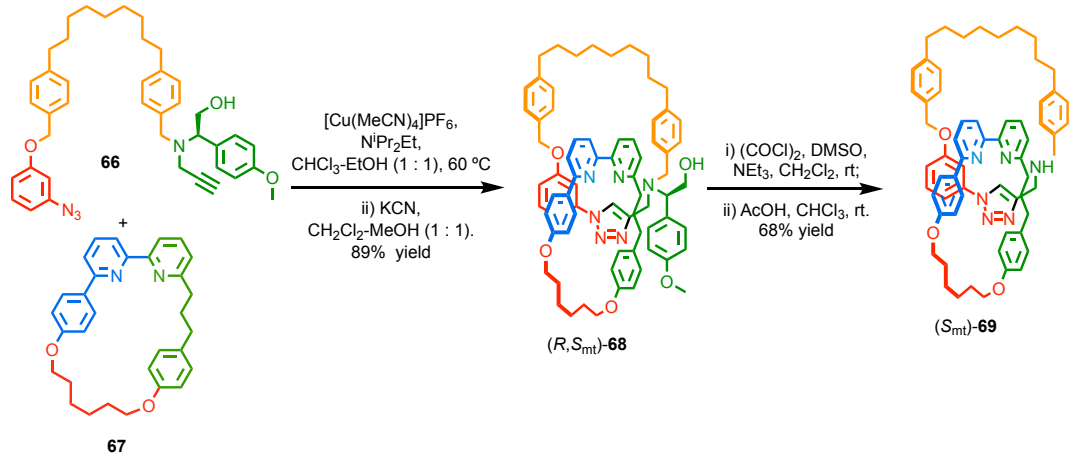

Scheme 1.17 Synthesis of MTC catenanes **68** and **69**. Catenane **68** is formed as a 2:1 diastereoisomeric mixture that is seperated by normal phase chromatography (major diastereoisomer is shown for clarity).

1.3.3. Mechanical Axial Chirality

Even more rare than MTC, is mechanically axially chiral (MAC) catenanes. Mechanical axial chirality occurs with two macrocycles of C_{nv} symmetry are interlocked, and can be considered Euclidean in origin rather than topological, as enantiomers can be interchanged if the Euclidean properties of the molecule are relaxed (**Figure 1.13**). In a similar vein to MTC catenanes, a linear hetero[n]catenane where n >2 and the facially desymmetrised rings are not directly linked, the catenane can exist as diastereoisomers (*syn/anti*) when the number of rings separating them is odd, or 2 enantiomers (R_{ma}/S_{ma}) when the number of rings separating them is even.

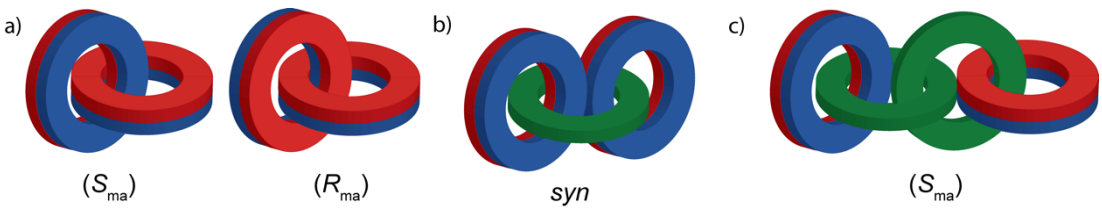

Figure 1.13 Cartoon representations of mechanically (a) axial chiral catenanes, (b) the *syn* diasterioisomer of a hetero[3]catenane and (c) one enantiomer of a hetero[4]catenane. [29]

To assign the absolute stereochemistry, the approach used for covalent axial chirality can be extended to these mechanically bonded structures.

Step 1: Assign the highest priority atom using CIP rules that does not lie within the macrocyclic plane, then define a vector from A to the macrocycle plane. Do this for both macrocycles.

Step 2. View the relative orientation of the vectors to one another, and consider the rotation from the head of the 'front' vector to the tail of the rear' vector as either clockwise (R_{ma}) or anticlockwise (S_{ma}).

Whereas there is a strong conceptual link between MPC rotaxanes and MTC catenanes, it is difficult to hypothesise an equivalent rotaxane structure. A rotaxane with a C_{nv} symmetrical macrocycle (principal axis aligned *perpendicular* to the macrocyclic plane) encircling a C_{nv} axle (principal axis and mirror planes aligned to the 'length' of the axis) is achiral. This arrangement is still stereogenic but in this case the stereoisomers are diastereoisomers. (**Figure 1.14**). The nomenclature of these would likely be *syn/anti*, to follow precedent, but to our best knowledge a rotaxane with this stereo descriptor has not been published and this stereoisomerism has not been discussed.

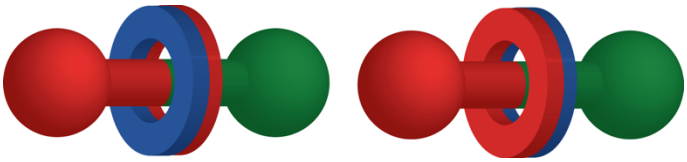

Figure 1.14 Cartoon representation of mechanically diastereoisomeric rotaxanes.

Much like the prior examples of MTC catenanes, MAC catenanes are also not well researched, due partially to the difficulties in synthesis and separation of such species. The first example of such a molecule was by Puddephat and co-workers in 2002 (**Figure 1.15**).[46] Puddephat and co-workers originally described this stereochemistry as 'topological' in nature, however, as explained earlier, mechanically axially chiral catenanes do not fit the definition of topological chirality as the enantiomers can be interchanged by assuming the Euclidean properties of atoms and bonds are relaxed. In this case (R_{ma})-**70** and (S_{ma})-**70** can be exchanged by 'switching' aryl group and the hydrogen atom as they are the off-ring plane atoms which determine priority.

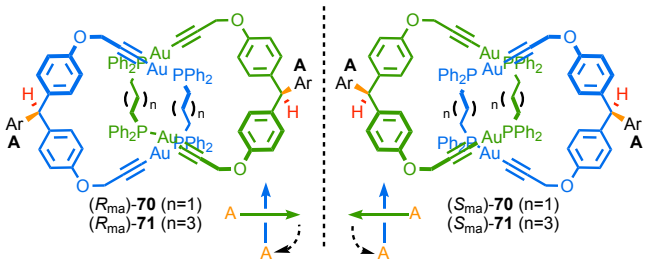

Figure 1.15 Structure and assignment for Puddephat and co-workers MAC catenanes-**70** and **71**. [46]

The catenanes **70** and **71** were both formed as racemic mixtures, with the absence of any chiral directing group. By ^{31}P NMR, **70** displayed an AB quartet when is consistent with the symmetry expected for the chiral catenane, while for **71** displayed only a singlet, suggesting the added flexibility results in poorly expressed facial asymmetry. There was no diastereotopicity exhibited in the signals present in the ^{1}H NMR, and even the addition of chiral shift reagents failed to give rise to diastereoisomeric signals, suggesting that the chirality is very poorly expressed in such a system.

Marinetti and co-workers also synthesised a MAC catenane in 2006 (**Figure 1.16**).[47] The mixture of diastereoisomeric catenanes was separated by HPLC. While the lone macrocycle does not display a significant de-symmetrisation of the phenanthroline moiety by ^{1}H NMR, both diastereoisomers of **72** show distinct separate signals for many of the phenanthroline resonances, which shows that the MAC is expressed through the entire molecule, unlike the earlier example by Puddephat.

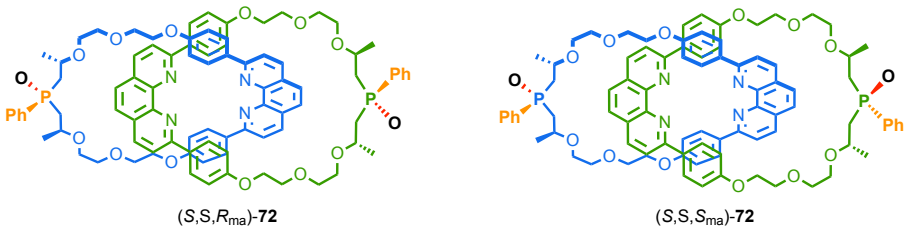

Figure 1.16 Structure of Marinetti's MAC catenanes (*S,S,S*$_{ma}$)-42 and (*S,S,R*$_{ma}$)-**42**.

1.4. Co-conformational Stereogenic Units

Chirality is usually discussed as a static, unchangeable property of a molecule. However, achiral molecules can adopt chiral conformations. Developing on this idea, achirotopic interlocked molecules can display chirality, depending on the co-conformation adopted, which can lead to de-symmetrisation of otherwise symmetrical sub-units. By analogy with non-interlocked molecules this family of stereogenic units are termed 'co-conformational chiral'. This term has been relatively recently suggested as a way to distinguish between MIMs composed of achiral units that display chirality but do not meet the symmetry requirements detailed in section 1.3. Co-conformational chirality can be either a static or dynamic property of the molecule, depending on the barrier to co-conformational motion.

1.4.1. Co-conformational Covalent Chirality

When considering a prochiral carbon centre either in a rotaxane, or a catenane, this centre can be desymmetrised by the addition of a mechanical bond. When the macrocycle is perfectly aligned with the mirror plane of the prochiral the system is achiral, whereas in any other relative arrangement it will display co-conformational covalent point chirality (**Figure 1.17**). This has previously been termed by Leigh and co-workers as mechanical point chiral to highlight the role the mechanical bond plays.[48] However the term 'covalent co-conformational' was designed to emphasise the role played by the covalent stereochemistry in combination with co-conformation and to emphasise the potential for dynamic behaviour.

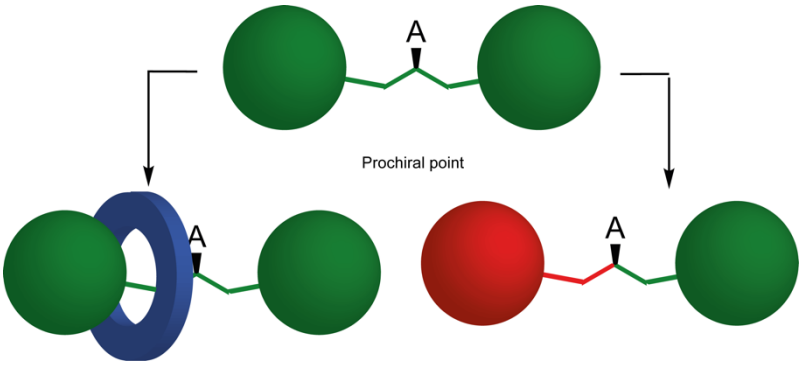

Figure 1.17 Cartoon representations of a prochiral molecule and the stereogenic units arising either by covalent modification (shown in red) to yield a covalent point chiral molecule, or by mechanical bond formation to yield a co-conformationally covalent point chiral molecule.

Leigh and co-workers studied co-conformational covalent point chirality in the context of molecular motors and catalysis. In their first report,[49] dynamically co-conformationally point chiral rotaxane **73** was benzoylated, using DMAP as an achiral catalyst, to produce a static racemic mixture of ($R_{co\text{-}c}$)-**74** and ($S_{co\text{-}c}$)-**74** as judged by analytical chiral HPLC. (**Scheme 1.18**).

When the reaction was performed with a chiral catalyst, (*R*)-**75**, in the place of DMAP, an excess of ($R_{co\text{-}c}$)-**74** was formed, making this an enantioselective synthesis. The opposite selectivity could be achieved with (*S*)-**75**. In terms of molecular machines, the conversion of rotaxane **73** to **74** is achieved by an 'information ratchet' mechanism as the position of the macrocycle affects the rate of the reaction that selectively traps it in one mechanical state.

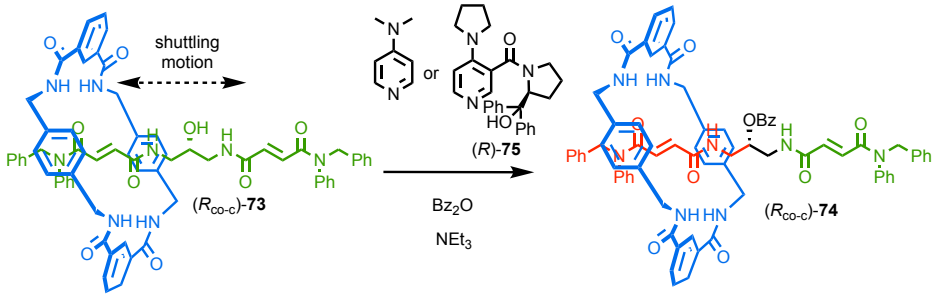

Scheme 1.18 Benzoylation of Leigh's dynamically co-conformationally point chiral rotaxane **73** to give co-conformationally locked chiral rotaxane **74**. Only one enantiomer of each is shown for clarity. When DMAP is used a racemic mixture of **74** is produced, whereas catalyst **75** gives a 2:1 mixture of stereoisomers. [49]

In a similar fashion, co-conformational forms of any covalent stereogenic unit can be imagined, such as co-conformational covalent planar chirality or co-conformational covalent axial chirality (**Figure 1.18**). These forms of chirality in a similar method to the co-conformational covalent point chirality, can be either dynamic or static depending on the freedom of the macrocycle to shuttle along the axle.

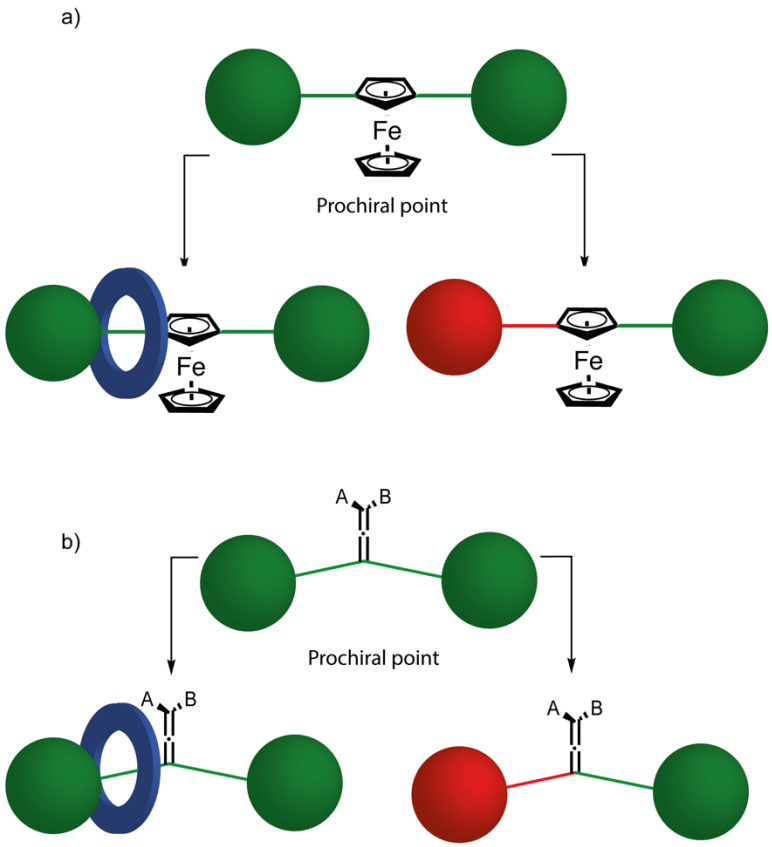

Figure 1.18 Cartoon representations of (a) co-conformational covalent planar chirality and (b) co-conformational axial stereogenic units and their relationship to 'regular' covalent planar or covalent axial stereochemistry.

1.4.2. Co-conformational Mechanical Chirality

Co-conformational chirality is not limited to prochiral covalent stereogenic units. Mechanical stereogenic units also have their co-conformational analogues.

1.4.2.1. Co-conformational Mechanical Topological Chirality

Following from the principles already laid out in sections 1.3.2 and 1.4.1, it is possible to observe co-conformational mechanical topological chirality (co-MTC) in catenanes which do not have an 'orientated' ring. When a catenane is formed from an orientated ring, and a C_{2v} symmetric macrocycle, the catenane will display chirality whenever the symmetry plane of the C_{2v} macrocycle is not aligned with the vertical mirror plane of the oriented ring (**Figure 1.19**). As with covalent conformational stereogenic units, co-conformational mechanical stereogenic units can either be dynamic or static in nature. A co-conformational mechanically topologically chiral catenane can also exist as a static system if there is a large 'blocking' group that prevents the oriented macrocycle from occupying the symmetry plane of the C_{2v} ring. While co-conformationally topologically chiral is somewhat of a self-

contradictory term, - topologically chiral objects by definition cannot be exchanged by relative motion of the sub-components - due to its obvious link to MTC it seems troubling to propose a unique term.

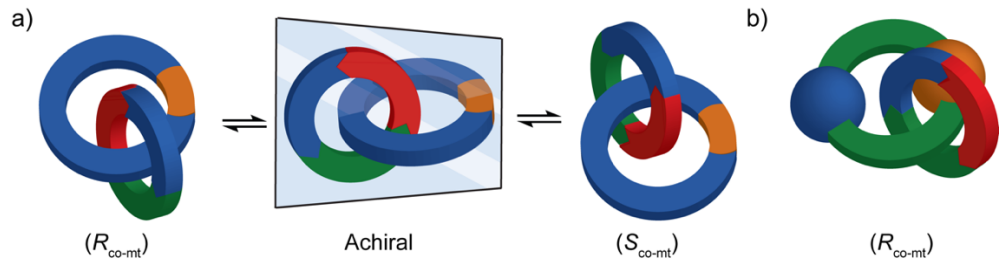

Figure 1.19 Cartoon representation of co-conformational topological chirality in a) a dynamic system and b) a static system.

Although co-MTC has not been discussed previously, Goldup and co-workers recently reported a modification of the AT-CuAAC where they synthesised a series of different catenanes.[42] In this publication it was noted that several of the structures display MTC conformations in the solid state (**Figure 1.20**). This methodology allowed them to access hetero[2]catenanes, either with C_{1h} macrocycles present or a C_{3h} macrocycle (via multicomponent AT-CuAAC). (*S/R*$_{co\text{-}mt}$)-**76** and (*S/R*$_{co\text{-}mt}$)-**77** crystallised as an enantiomeric pair of co-conformations and can both be observed in their X-ray crystal structures. Catenane **77** is a relatively 'tight' catenane. However, despite this only one triazole resonance is observed by ^{1}H NMR, showing that it remains in fast exchange upon the NMR timescale.

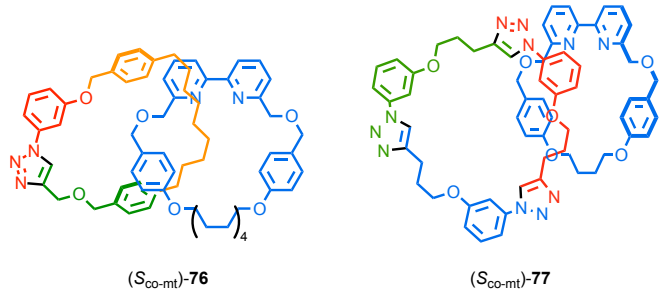

Figure 1.20 Structures of selected catenanes from Goldup and co-workers AT-CuAAC catenane synthesis that display co-conformational topological chirality. Stereochemistry shown is arbitrary. [42]

1.4.2.2. Co-Conformational Mechanical Axial Chirality

As discussed above, mechanical axial chirality relies on a combination of two C_{nv} macrocycles. If we consider a catenane composed of one C_{nv} macrocycle and one C_{2h} macrocycle, analysis similar to that above reveals a molecule which will display two diastereoisomeric limiting co-conformations that themselves exist as pairs of enantiomers (**Figure 1.21**). Unusually, unlike the previous examples, there is no relative positioning of the two rings that render the

structure superimposable upon its mirror image. Thus, the stereoisomers of such a catenane can exchange by pirouetting of the C_{2h} macrocycle relative to the C_{nv} ring without ever passing through an achiral co-conformation.

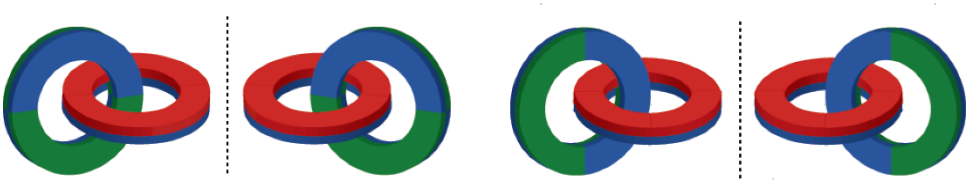

Figure 1.21 Cartoon representations of different enantiomers/diasterioisomers of a co-MAC chiral catenane.

Similar homo[2]catenanes consisting of only C_{2h} or D_{nd} macrocycles display interesting stereochemical properties. A homo[2]catenane composed of two C_{2h} macrocycles will have four diastereomeric limiting co-conformations related to one another by 90° rotations, only one of which is achiral (**Figure 1.22**). Although it is possible to exchange the co conformers via the achiral S_4 symmetric diastereomer, the shortest path between enantiomers is via chiral co-conformations for two of the three diastereomers. Similar behaviour appears with D_{nd} symmetrical macrocycles.

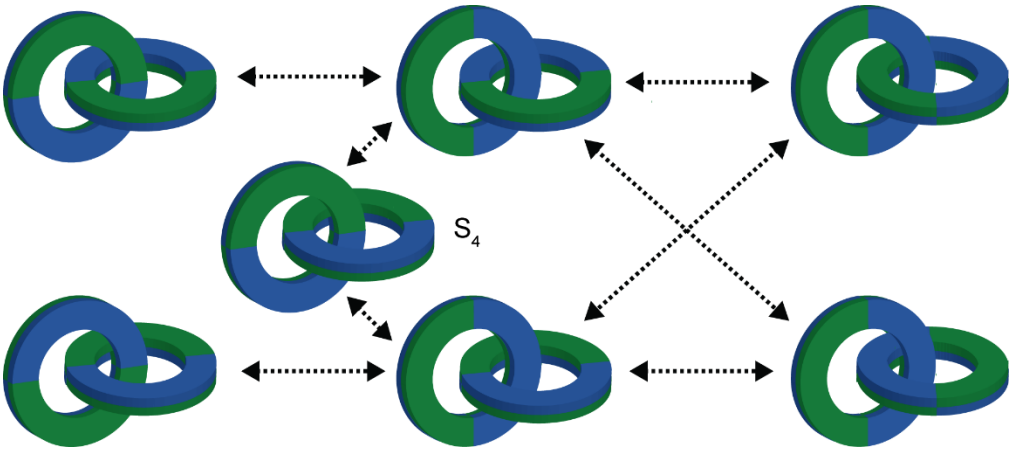

Figure 1.22 Cartoon representation of the network of stereoisomers formed by a [2]catenane based on two C_{2h} macrocycles (each arrow corresponds to a 90° rotation of one ring; vertical pairs of structures are related as enantiomers; achiral diastereomer is indicated as S4 symmetric).

While this form of stereochemistry has not been formally reported in literature, an example of a catenane that appears to conform to this type of symmetry was identified during the preparation of our recent review.[29] Catenane **79**, reported by Puddephatt and co-workers, is formed through the assembly of four equivalents of racemic chiral building block **78** in the presence of Pd^{II} (**Scheme 1.19**).[50] X-ray analysis of **79** reveals that, although three stereoisomeric macrocycles can be formed from (*rac*)-**78**, in the solid-state catenane **79** is composed exclusively of *meso* macrocycles with (*R,S*) absolute stereochemistry that

individually have C_{2h} symmetry and are thus achiral when not interlocked. However, catenane **79** adopts an axially chiral co-conformation in the solid-state and both enantiomers were present in equal amounts in the unit cell.

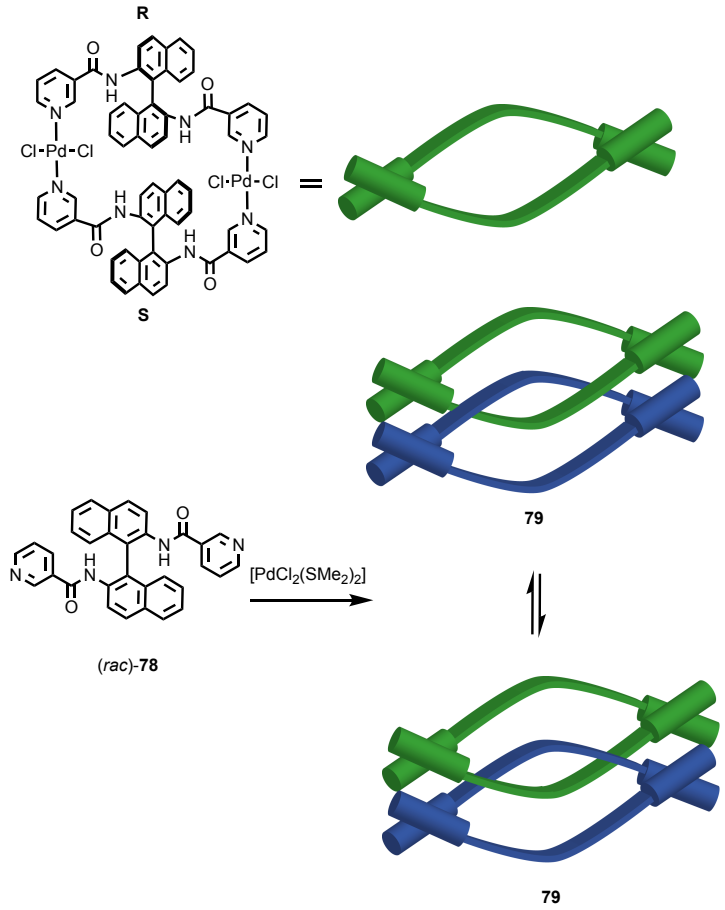

Scheme 1.19 Puddephatt and co-workers co-conformationally axially chiral catenane **79**, which is composed of two *meso* macrocycles. [50]

^{1}H NMR analysis of catenane **79** revealed four distinct NH resonances, consistent with the C_2 symmetry of the solid-state chiral co-conformation. However, at 298 K, cross peaks were observed between pairs of NH environments by COSY NMR analysis which are absent at 273 K, suggesting that a dynamic process exchanges these positions. This pairwise exchange process is consistent with the pirouetting of the rings which exchanges pairs of enantiotopic protons.

The method of assigning of co-MAC is not intuitive, particularly due to the different diastereoisomers that can arise. Given the dearth of examples and unusual nature of this chirality a method of stereochemical assignment has not been proposed to date.

1.4.2.3. Co-Conformational Mechanical Planar Chirality

The last form of co-conformational mechanical chirality to describe is the most widely researched; co-conformationally mechanically planar chiral rotaxanes (co-MPC). Systems containing an orientated macrocycle encircling an axle in which the two 'ends' are identical (C_{2v} or $D_{\infty h}$), will, like the previous examples of co-MTC, be achiral when the macrocycle occupies the central mirror plane of the axle. If the macrocycle shuttles either side of this position, then chiral co-conformations are produced. Such molecules can be dynamic if shuttling is relatively unhindered. However, if a blocking group is present to limit co-conformational motion, a statically chiral system is produced. (**Figure 1.23**).

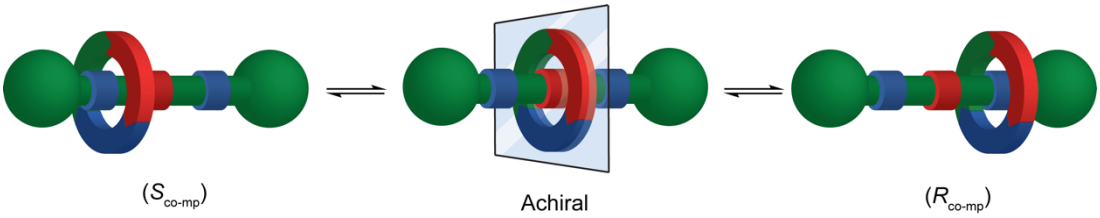

Figure 1.23 Dynamic co-MPC chiral rotaxane in ($R_{co\text{-}mp}$), ($S_{co\text{-}mp}$) and achrial conformations.

Similar stereoisomerism can manifest in [n]rotaxanes where n>2 and at least one of the macrocycles is orientated, if macrocycles are assumed to be unable to pass over one another on the axle (a rare feature in rotaxanes but not unreported).[51] Thus, this form of co-MPC is almost always a static stereochemical feature (**Figure 1.24**). In systems that possess one orientated and one non-orientated ring feature, this resulting rotaxane will exist as a pair of enantiomers, while if both macrocycles are orientated, they will exist as two diastereoisomers; one of which is achiral, and one of which exists as an achiral *meso* form.

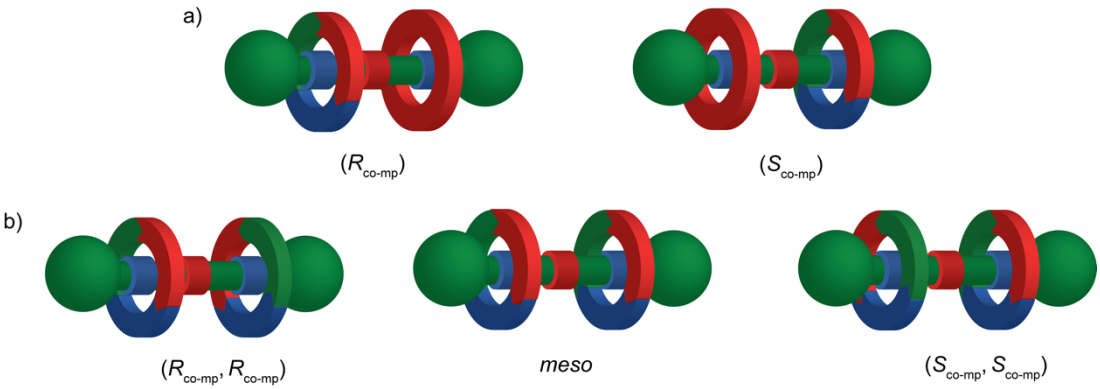

Figure 1.24 Stereoisomeric forms for [3]rotaxanes possesing a) 1 orientated and 1 non-orientated ring, and b) two orientated rings.

While rotaxanes which conform to these stereogenic descriptors have been reported previously in literature, Saito and co-workers have disclosed the first application of this form

of stereochemistry (**Figure 1.25**).[52] In this report, they synthesised a racemic mixture of rotaxane **80**. As the shuttling rate was slow enough, they purified this mixture using chiral HPLC. The shuttling rate of the rotaxane **80** too slow to monitor by ^{1}H NMR but could be obtained readily by monitoring the rate of racemisation using chiral HPLC. The absolute configuration of the molecule was not determined.[52]

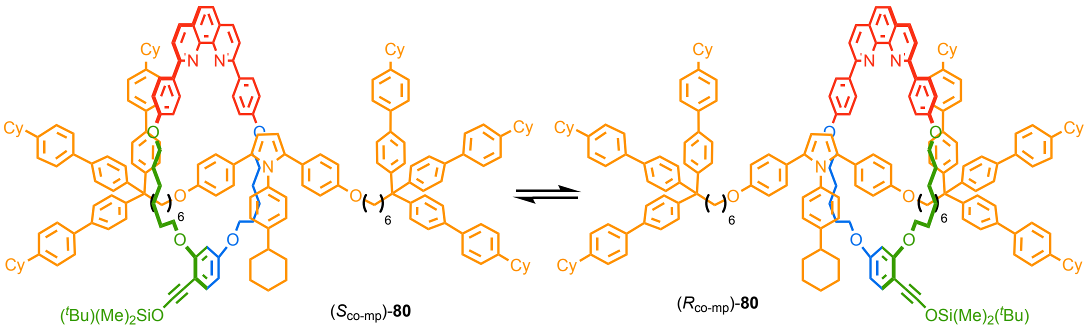

Figure 1.25 Saito and co-workers co-MPC rotaxane **80.**[52]

Vögtle and co-workers investigated the stereochemistry of a [3]rotaxane, with a centro-symmetric axle, and two orientated macrocycles (**Figure 1.26**).[53] Rotaxanes **81** were separated using chiral HPLC. CD spectroscopy was used to confirm that two of the separated diastereomers, ($R_{co\text{-}mp}$, $R_{co\text{-}mp}$)-**81** and ($S_{co\text{-}mp}$, $S_{co\text{-}mp}$)-**81** displayed oposite cotton effects while the third, *meso* compound ($R_{co\text{-}mp}$, $S_{co\text{-}mp}$)-**81**, was CD silent.

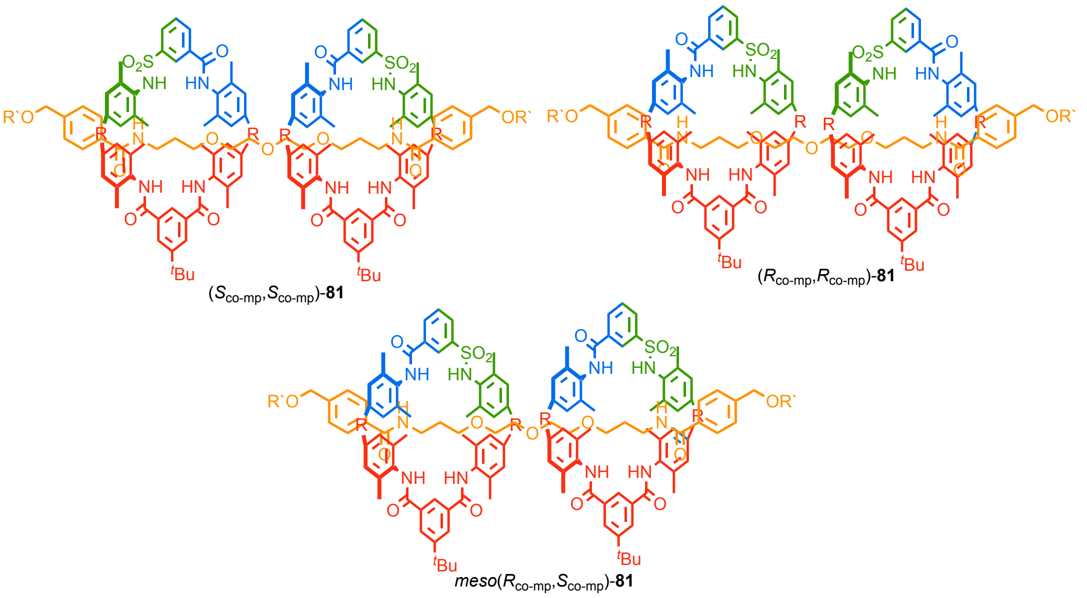

Figure 1.26 Vögtle's co-MPC [3]rotaxanes, showing the two enantiomers, and one *meso* achiral diastereoisomer. [53]

Recently Credi and co-workers have published a detailed study of a dynamic Co-MPC rotaxane (**Scheme 1.20**).[54] Rotaxane **82** was synthesised using a passive template approach.

In the protonated state, the major co-conformation of **82**, in which the macrocycle occupies the central ammonium unit, is achiral. Treating **82** with base to deprotonate the central ammonium unit yielded dynamic Co-MPC rotaxane **83** as a racemic mixture of co-conformations in which the macrocycle occupies the two triazolium stations.

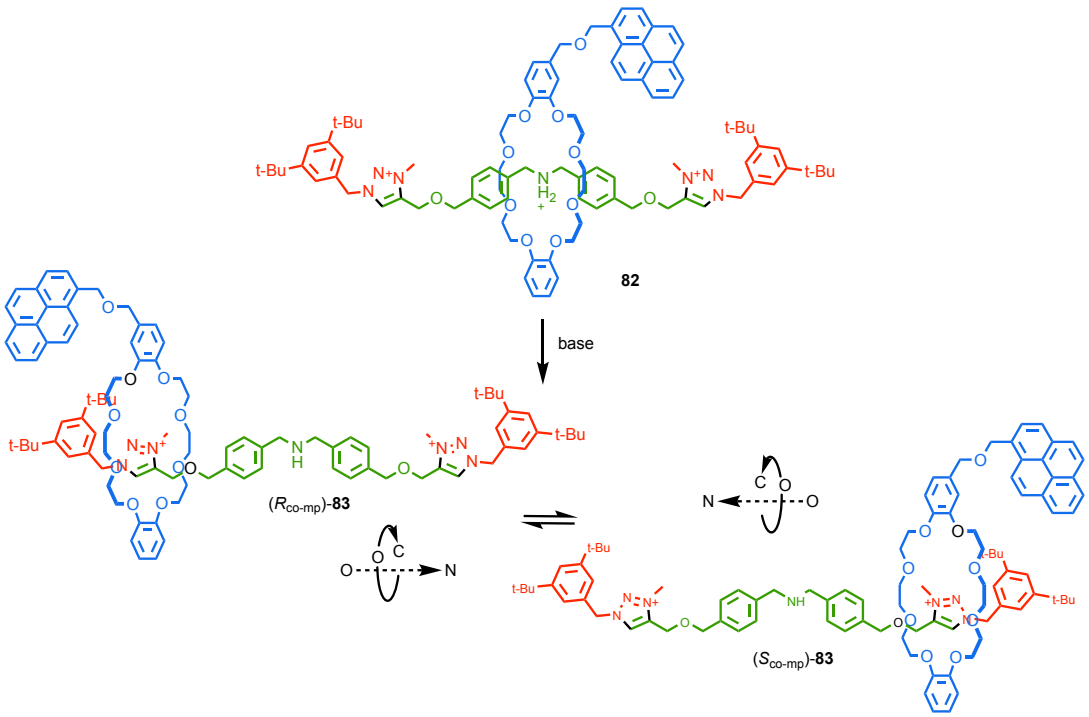

Scheme 1.20 Credi and co-workers 'achiral' rotaxane, **82**, and dynamically co-MPC chiral rotaxane **83**. Counter ions excluded for clarity.

In the presence of an excess of (+)–camphor sulfonate as its tetrabutylammonium salt, two diastereomeric complexes were observed by ^{1}H NMR in a ratio of 85:15. This result demonstrates that binding of the chiral anion leads to a biasing of the enantiomeric co-conformations of rotaxane **83**. An equal mixture of diastereomers were observed with Δ-TRISPHAT tetrabutylammonium salt, presumably due to the lack of strong interactions between the rotaxane and the chiral anion.

1.5. Conclusions

Mechanically Interlocked Molecules, their synthesis and their properties while perhaps initial thought of as an intellectual curiosity, has grown in the past few decades into a promising field of research regarding applications, as well as an opportunity to study the fundamental properties of molecules and how they can interact in confined spaces. Chirality, and how it relates to interlocked molecules is under-researched perhaps in comparison to the breadth

of the topic in general chemistry,[55,56] but recent research in the area has shown promising results, particularly from an applications perspective.

Perhaps one of the most interesting aspects of chirality in interlocked molecules is the *range* of stereogenic units that can arise as a function of how the molecule is interlocked, rather than being dependent on any chirotopic covalent stereogenic unit. How this sort of 'mechanical chirality' can be expressed or used is still under development but recent publications have been making great strides in this, particularly for MPC and MTC interlocked systems.

1.6. Bibliography

1 J. F. Stoddart and C. J. Bruns, *The Nature of the Mechanical Bond*, Wiley, 2016.

2 E. Wasserman, *J. Am. Chem. Soc.*, 1960, **82**, 4433–4434.

3 C. O. Dietrich-Buchecker, J. P. Sauvage and J. P. Kintzinger, *Tetrahedron Lett.*, 1983, **24**, 5095–5098.

4 C. O. Dietrich-Buchecker, J. P. Sauvage and J. M. Kern, *J. Am. Chem. Soc.*, 1984, **106**, 3043–3045.

5 P. R. Ashton, M. Grognuz, A. M. Z. Slawin, J. Fraser Stoddart and D. J. Williams, *Tetrahedron Lett.*, 1991, **32**, 6235–6238.

6 P. R. Ashton, I. W. Parsons, F. M. Raymo, J. F. Stoddart, A. J. P. White and D. J. Williams, *Angew. Chem. Int. Ed.*, 1998, **37**, 1294–1297.

7 P. L. Anelli, N. Spencer and J. F. Stoddart, *J. Am. Chem. Soc.*, 1991, **113**, 5131–5133.

8 The Novel Prize in Chemistry 2016, https://www.nobelprize.org/nobel_prizes/chemistry/laureates/2016/, (accessed 20 January 2017).

9 V. Aucagne, K. D. Hänni, D. A. Leigh, P. J. Lusby and D. B. Walker, *J. Am. Chem. Soc.*, 2006, **128**, 2186–2187.

10 S. Saito, E. Takahashi and K. Nakazono, *Org. Lett.*, 2006, **8**, 5133–5136.

11 J. J. Danon, D. A. Leigh, P. R. McGonigal, J. W. Ward and J. Wu, *J. Am. Chem. Soc.*, 2016, **138**, 12643–12647.

12 M. Denis and S. M. Goldup, *Nat. Rev. Chem.*, 2017, **1**, 1–18.

13 H. Lahlali, K. Jobe, M. Watkinson and S. M. Goldup, *Angew. Chem. Int. Ed.*, 2011, **50**, 4151–4155.

14 M. Galli, J. E. M. Lewis and S. M. Goldup, *Angew. Chem. Int. Ed.*, 2015, **54**, 13545–13549.

15 M. Denis, L. Qin, P. Turner, K. A. Jolliffe and S. M. Goldup, *Angew. Chem. Int. Ed.*, 2018, 2–7.

16 M. Denis, J. Pancholi, K. Jobe, M. Watkinson and S. M. Goldup, *Angew. Chem. Int. Ed.*, 2018, **2**, 1–6.

17 R. J. Bordoli and S. M. Goldup, *J. Am. Chem. Soc.*, 2014, **136**, 4817–4820.

18 J. Winn, A. Pinczewska and S. M. Goldup, *J. Am. Chem. Soc.*, 2013, **135**, 13318–13321.

19 C. Nolte, P. Mayer and B. F. Straub, *Angew. Chem. Int. Ed.*, 2007, **46**, 2101–2103.

20 R. Mitra, M. Thiele, F. Octa-Smolin, M. C. Letzel and J. Niemeyer, *Chem. Commun.*, 2016, **52**, 5977–5980.

21 J. Y. C. Lim, I. Marques, V. Félix and P. D. Beer, *J. Am. Chem. Soc.*, 2017, **139**, 12228–12239.

22 S. Hoekman, M. O. Kitching, D. A. Leigh, M. Papmeyer and D. Roke, *J. Am. Chem. Soc.*,

2015, **137**, 7656–7659.

23 Y. Tachibana, N. Kihara and T. Takata, *J. Am. Chem. Soc.*, 2004, **126**, 3438–3439.

24 Y. Tachibana, N. Kihara, K. Nakazono and T. Takata, *Phosphorus, Sulfur, Silicon Relat. Elem.*, 2010, **185**, 1182–1205.

25 V. Blanco, D. A. Leigh and V. Marcos, *Chem. Soc. Rev.*, 2015, **44**, 5341–5370.

26 V. Blanco, D. A. Leigh, V. Marcos, J. A. Morales-Serna and A. L. Nussbaumer, *J. Am. Chem. Soc.*, 2014, **136**, 4905–4908.

27 S. Saito, Y. Hirano, Y. Mutoh and T. Kasama, *Chem. Lett.*, 2015, **44**, 1509–1511.

28 M. Asakawa, G. Brancato, M. Fanti, D. A. Leigh, T. Shimizu, A. M. Z. Slawin, J. K. Y. Wong, F. Zerbetto and S. Zhang, *J. Am. Chem. Soc.*, 2002, **124**, 2939–2950.

29 E. M. G. Jamieson, F. Modicom and S. M. Goldup, *Chem. Soc. Rev.*, 2018, **47**, 5266–5311.

30 G. Schill, *Catenanes, Rotaxanes and Knots*, Academic Press, New York, 71st edn., 1971.

31 C. Yamamoto, Y. Okamoto, T. Schmidt, R. Jäger and F. Vögtle, *J. Am. Chem. Soc.*, 1997, **119**, 10547–10548.

32 Y. Makita, N. Kihara, N. Nakakoji, T. Takata, S. Inagaki, C. Yamamoto and Y. Okamoto, *Chem. Lett.*, 2007, **36**, 162–163.

33 M. A. Jinks, A. de Juan, M. Denis, C. J. Fletcher, M. Galli, E. M. G. Jamieson, F. Modicom, Z. Zhang and S. M. Goldup, *Angew. Chem. Int. Ed.*, 2018, **57**, 14806–14810.

34 C. E. Gell, T. A. McArdle-Ismaguilov and N. H. Evans, *Chem. Commun.*, 2019, **55**, 1576–1579.

35 A. Heard and S. Goldup, *A Mechanically Planar Chiral Rotaxane Ligand for Enantioselective Catalysis,* Preprint, *ChemRxiv*, 2019, 1–7, DOI: https://doi.org/10.26434/chemrxiv.9701789.v1

36 E. Gross, J. H. Liu, S. Alayoglu, M. A. Marcus, S. C. Fakra, F. D. Toste and G. A. Somorjai, *J. Am. Chem. Soc.*, 2013, **135**, 3881–3886.

37 M. Hisatome, N. Watanabe, T. Sakamoto and K. Yamakawa, *J. Organomet. Chem.*, 1977, **125**, 79–93.

38 C. W. Carter, G. Bartsch, T. Freer and A. Alden, *J. Biol. Chem.*, 1974, **249**, 4212–4225.

39 D. Mitchell and J. Sauvage, *Angew. Chem. Int. Ed.*, 1988, **27**, 27–28.

40 Y. Kaida, Y. Okamoto, J. C. Chambron, D. K. Mitchell and J. P. Sauvage, *Tetrahedron Lett.*, 1993, **34**, 1019–1022.

41 R. T. S. Lam, A. Belenguer, S. L. Roberts, C. Naumann, T. Jarrosson, S. Otto and J. K. M. Sanders, *Science (80)*, 2005, **308**, 2003–2005.

42 J. E. M. Lewis, F. Modicom and S. M. Goldup, *J. Am. Chem. Soc.*, 2018, **140**, 4787–4791.

43 M. Denis, J. E. M. Lewis, F. Modicom and S. M. Goldup, *Chem*, 2019, **5**, 1512–1520.

44 M. K. Chung, P. S. White, S. J. Lee and M. R. Gagné, *Angew. Chem. Int. Ed.*, 2009, **48**, 8683–8686.

45 T. Prakasam, M. Lusi, E. Nauha, J.-C. Olsen, M. Sy, C. Platas-Iglesias, L. J. Charbonnière and A. Trabolsi, *Chem. Commun.*, 2015, **51**, 5840–5843.

46 C. P. Mcardle, S. Van, M. C. Jennings and R. J. Puddephatt, *J. Am. Chem. Soc.*, 2002, **124**, 3959–3965.

47 A. Theil, C. Mauve, M. T. Adeline, A. Marinetti and J. P. Sauvage, *Angew. Chem. Int. Ed.*, 2006, **45**, 2104–2107.

48 M. Alvarez-Pérez, S. M. Goldup, D. A. Leigh and A. M. Z. Slawin, *J. Am. Chem. Soc.*, 2008, **15**, 1836–1838.

49 A. Carlone, S. M. Goldup, N. Lebrasseur, D. A. Leigh and A. Wilson, *J. Am. Chem. Soc.*, 2012, **134**, 8321–8323.

50 T. J. Burchell, D. J. Eisler and R. J. Puddephatt, *Dalt. Trans.*, 2005, 268–272.

51 K. Zhu, G. Baggi and S. J. Loeb, *Nat. Chem.*, 2018, **10**, 625–630.

52 Y. Mochizuki, K. Ikeyatsu, Y. Mutoh, S. Hosoya and S. Saito, *Org. Lett.*, 2017, **19**, 4347–4350.

53 R. Schmieder, G. Hübner, C. Seel and F. Vögtle, *Angew. Chem. Int. Ed.*, 1999, **38**, 3528–3530.

54 S. Corra, C. De Vet, J. Groppi, M. La Rosa, S. Silvi, M. Baroncini and A. Credi, *J. Am. Chem. Soc.*, 2019, **141**, 9129–9133.

55 A Scopus search for articles with ‘“*rotax* OR *catenan*”’ in the title, abstract or keywords returns 3402 hits between 2007 and 2017. The same search with ‘“*chiral* OR enantio*”’ in the title, abstract or keywords returns 119 hits.

56 A Scopus search for all articles published in J. Am. Chem. Soc., Angew. Chem., Int. Ed., Chem. Sci., Chem. Commun. or Chem. Eur. J. in 2016 returns 11 638 hits. The same search with ‘“*chiral* OR enantio*”’ in the title, abstract or keywords returns 111.

Chapter 2. Co-Conformationally Mechanically Planar Chiral Urea Rotaxane for Chiral Guest Sensing

Abstract: This chapter reports the synthesis of an achiral rotaxane, functionalised with a urea moiety, which can display dynamic co-conformational mechanical planar chirality. Its binding properties were then investigated with a series of salts, mostly derived from amino acids. VT NMR studies showed the rotaxane to display diastereoselective binding in response to the chiral guest. Further to this, CD analysis of mixtures of the rotaxane with chiral guests revealed positive or negative signals that correspond to the enantiomer of the guest used, although the guest was not itself CD active. This allows the achiral rotaxane to act as a sensor to determine the enantiomeric excess of a scalemic sample of a proline derived salt.

Acknowledgements: I would like to thank M. Denis for providing salts **93**, **94**, **95** and **98.**

Prior publication: None of this work has been previously published.

2.1. Introduction

2.1.1. Rotaxane Anion Binding

The study of rotaxanes in host guest complexation is a broad and varied topic. In general, rotaxanes bind guests in the unique 'pocket' formed by the mechanical bond, in the area between the macrocycle(s) and the axle(s), which can provide unique selectivity or increased binding strength. Beer and co-workers have reported many examples of anion binding MIMs.[1,2,3] An early example of this which clearly showed the potential of this field used a rotaxane, **84**, which had been synthesised using chloride ion template.[4] The use of passive templation requires that the pseudorotaxane precursor be held together by strong interactions to ensure a reasonable yield of the interlocked structure. After successful synthesis of **84** the authors determined binding constants for the rotaxane **84** for various anions and compared them to those of the free axle. Rotaxane showed a 10 fold stronger binding strength for Cl^- compared with the axle, while it showed an order of magnitude *weaker* binding of acetate anions due to the larger steric demand of the latter (**Figure 2.1**).[4]

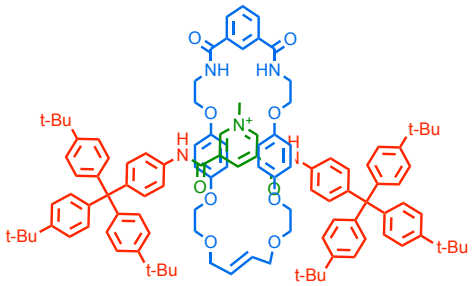

84

	Axle	**84**
	K_a [M^{-1}]	K_a [M^{-1}]
Cl^-	125	1130
AcO^-	22000	100

Figure 2.1 Structure of Beer and co-workers anion binding rotaxane **84** and a comparison of its binding constants with those of the corresponding axle.

Since these early reports, there have been several papers published investigating the properties of MIMs as hosts, and specifically as anion sensors. However, in the majority of cases the interlocked molecules were synthesised by anion passive templation, which limits the scope of the molecule.[5,6,2] Recently, Goldup and co-workers reported a new rotaxane with a urea functionalised binding pocket, synthesised using the AT-CuAAC reaction.[7] Anion binding studies revealed that no binding occurred, apparently due to the macrocycle occupying the urea binding motif.[7] Transformation of the rotaxane into the salt **85**.HBF_4 however pleasingly led to the macrocycle occupying the positively charged triazole station, freeing the urea for anion binding.[7] **85**.HBF_4 showed selectivity for chloride over stronger, more basic anions such as fluoride or acetate, which lead to deprotonation of the host. This

system also displayed a fluorescence switch-on upon binding that was not observed for the free axle (**Figure 2.2**).[7]

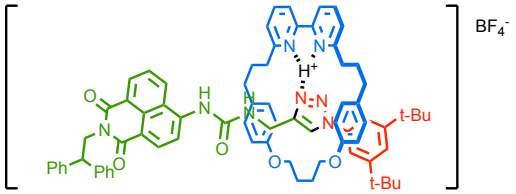

85.HBF_4

Figure 2.2 Structure of Goldup and co-workers urea functionalised rotaxane anion sensor **85**.HBF_4.[7]

2.1.2. Aims and Objectives

Building on the results with **85**.HBF_4,[7] a new rotaxane, **86**, was designed. **86** is formally achiral, but will display co-conformational mechanical planar chirality, a relatively unexplored form of stereochemistry, if the macrocycle is displaced either side of the mirror plane that bisects the axle (**Figure 2.3**).[8] The intention was to investigate the binding behaviour of **86** with chiral anions. If this structure displayed the same 'reluctance' of the macrocycle to vacate the urea position as observed for **85**,[7] the triazoles of the axle could be methylated to yield charged triazolium functionalised rotaxane **86**. This would yield a more competitive station for the bipyridine macrocycle to occupy, freeing the urea to bind to anionic guests.

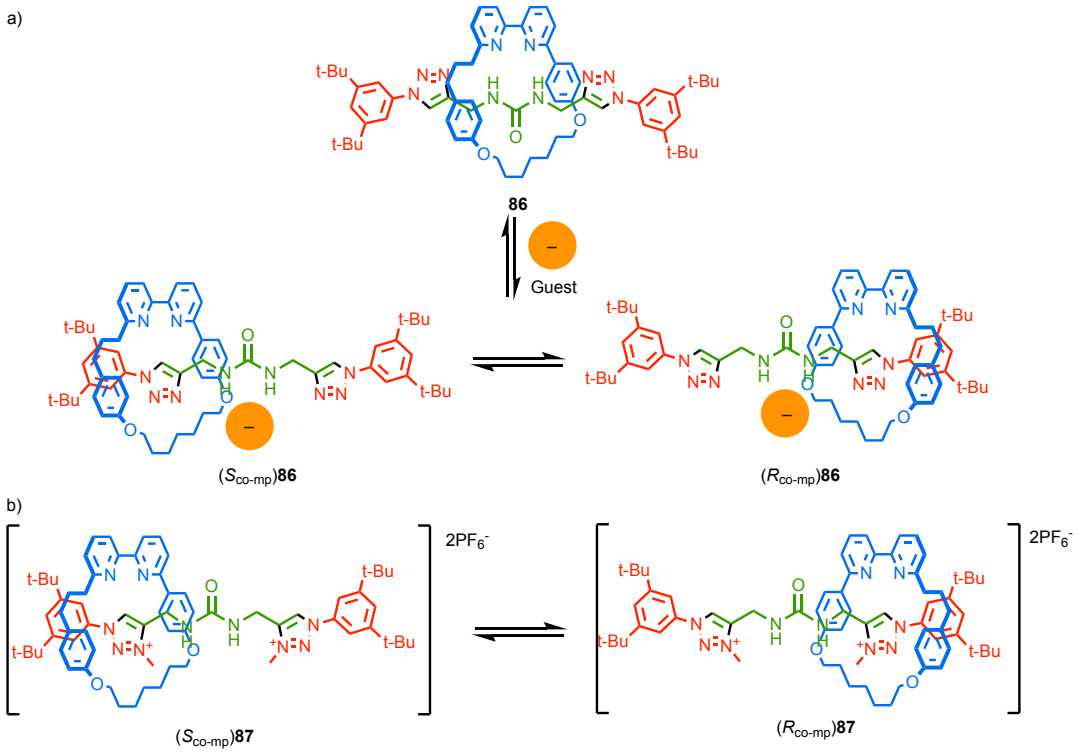

Figure 2.3 Proposed structure of dynamically co-conformationally mechanicaly planar chiral rotaxanes a) **86** with anion bound co-conformations, and b) **87**.

The binding of chiral guests to rotaxanes **86** and **87** will be studied by ^{1}H NMR, including variable temperature (VT) ^{1}H NMR if required, and circular dichroism (CD) to determine if the binding of chiral anionic guests leads to stereoselective shuttling. By complexing these small chiral guests with our rotaxane it was hoped that a CD signal could be induced even for CD silent guests. This would allow determination of the enantiopurity a guest using the rotaxane as a sensor.

2.2. Results and Discussion

2.2.1. Neutral Urea Rotaxane Host

2.2.1.1. Design and Synthesis

The design of **86** was intentionally simple. Key features are i) a C_{2v} symmetrical axle, ii) a central urea unit to bind to anions, iii) enough space for the macrocycle to 'shuttle' from the central position, iv) two triazole units to provide alternative binding sites for the macrocycle.

88 was prepared according to a literature procedure[9] in a 55% yield (**Scheme 2.1**). The other precursors to **86**, macrocycle **51**[10] and azide **11**[11] were synthesised previously in the group.

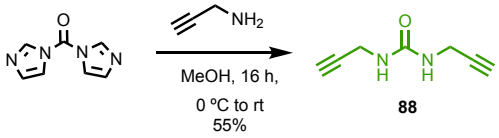

Scheme 2.1 Synthesis of **88**.

Synthesis of [2]rotaxane **86** was performed using the AT-CuAAC reaction. After the first triazole formation the pseudo rotaxane complex was expected to dissociate. The second triazole formation was expected to trap the macrocycle in as a [2]rotaxane. In keeping with this, no [3]rotaxane was observed in the crude reaction product. (**Scheme 2.2**)

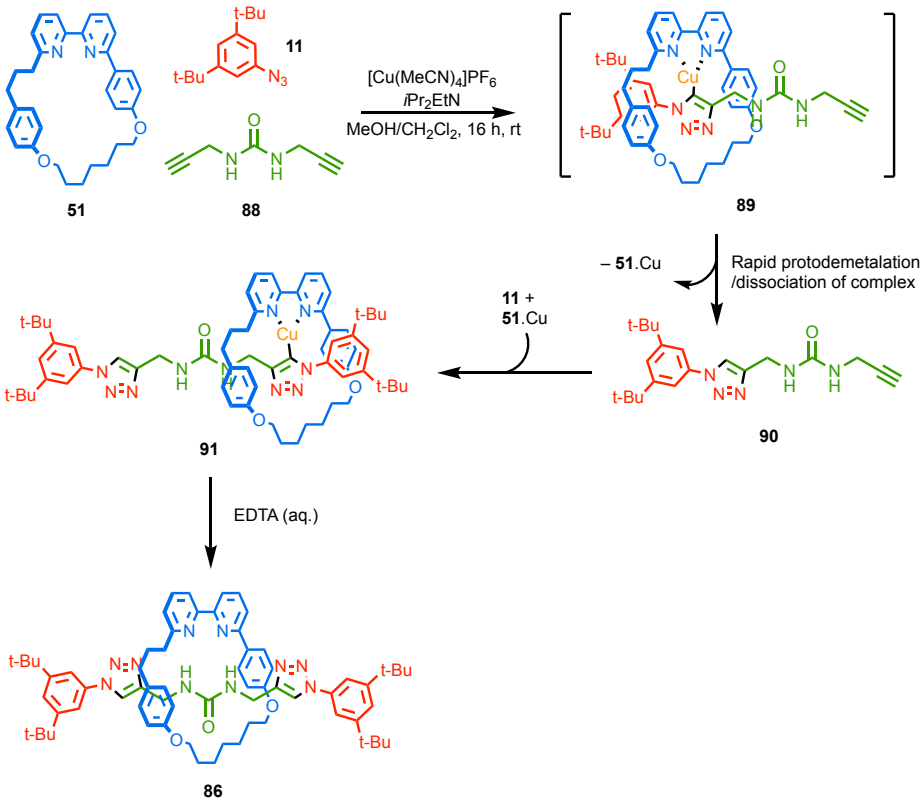

Scheme 2.2 Synthesis of rotaxane **86**.

Although the synthesis of **86** was relatively simple, purification turned out to be slightly more complex. If any macrocycle **51** remained in the product mixture it was impossible to separate from **86** by using simple column chromatography. Thus, in order to ensure full conversion of the macrocycle, 1.2 equivalents of alkyne **88**, and 2.4 equivalents of azide **11** respectively were used. However, this caused its own purification problems. Rotaxane **86** is initially formed as a Cu^{I}-triazolide, and the Cu ion remains coordinated until an EDTA solution is added to remove the copper. This means that once all the macrocycle is consumed there is no more catalyst and so half axle **90**, produced after the first round of triazole formation, remains in the product mixture confirmed via LCMS *m/z* =757.7 which is consistent with **90** $[2M+Na]^{+}$ (calc. for $C_{42}H_{58}N_{10}O_2Na$ = 757.5). Attempts to separate this from **86** was met with varied success. **86** could be purified, but the yield was diminished due to fractions contaminated with half-axle **90.**

In order to overcome this, after the AT-CuAAC reaction was complete, the reaction was treated with another equivalent of Cu^{I} catalyst to complete the conversion of **90** to the axle. This was very successful and allowed the yield of **86** in up to 81% (**Scheme 2.3**).

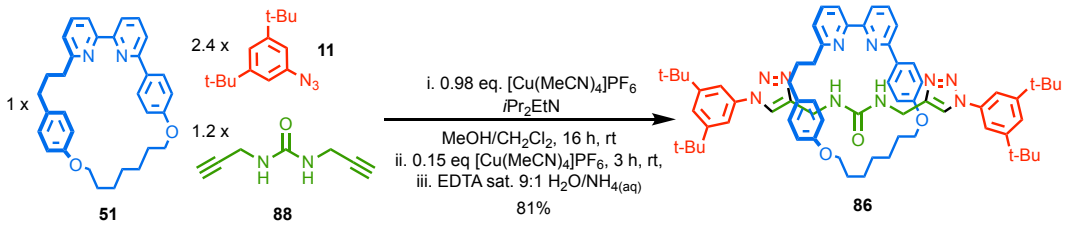

Scheme 2.3 Optimised reaction conditions for synthesis of **86.**

^{1}H NMR analysis of rotaxane **86** did not show the characteristic triazole C-H resonance at high ppm usually seen in rotaxanes based on **51**. Given that deshielding of the triazole resonance in such systems arises due to hydrogen bonding between the triazole proton and the bipyridine of the macrocycle, this observation suggested that the macrocycle was not located on the triazole stations but was instead localised predominantly over the urea station. In keeping with this, the ^{1}H NMR spectrum of **86** also does not show any sort of desymmetrisation of the axle by the macrocycle as would be expected if the macrocycle was not centred on the urea. When the spectrum was collected at -50 °C, the most significant change was that the urea protons shifted to higher ppm, consistent with a bipyridine-urea hydrogen bonding interaction that becomes even more favourable as the temperature is lowered. Overall, ^{1}H NMR analysis suggests that the macrocycle is predominantly localised over the urea moiety through hydrogen bonding and that there is not a significant interaction between the macrocycle and the triazole protons (**Figure 2.4**).

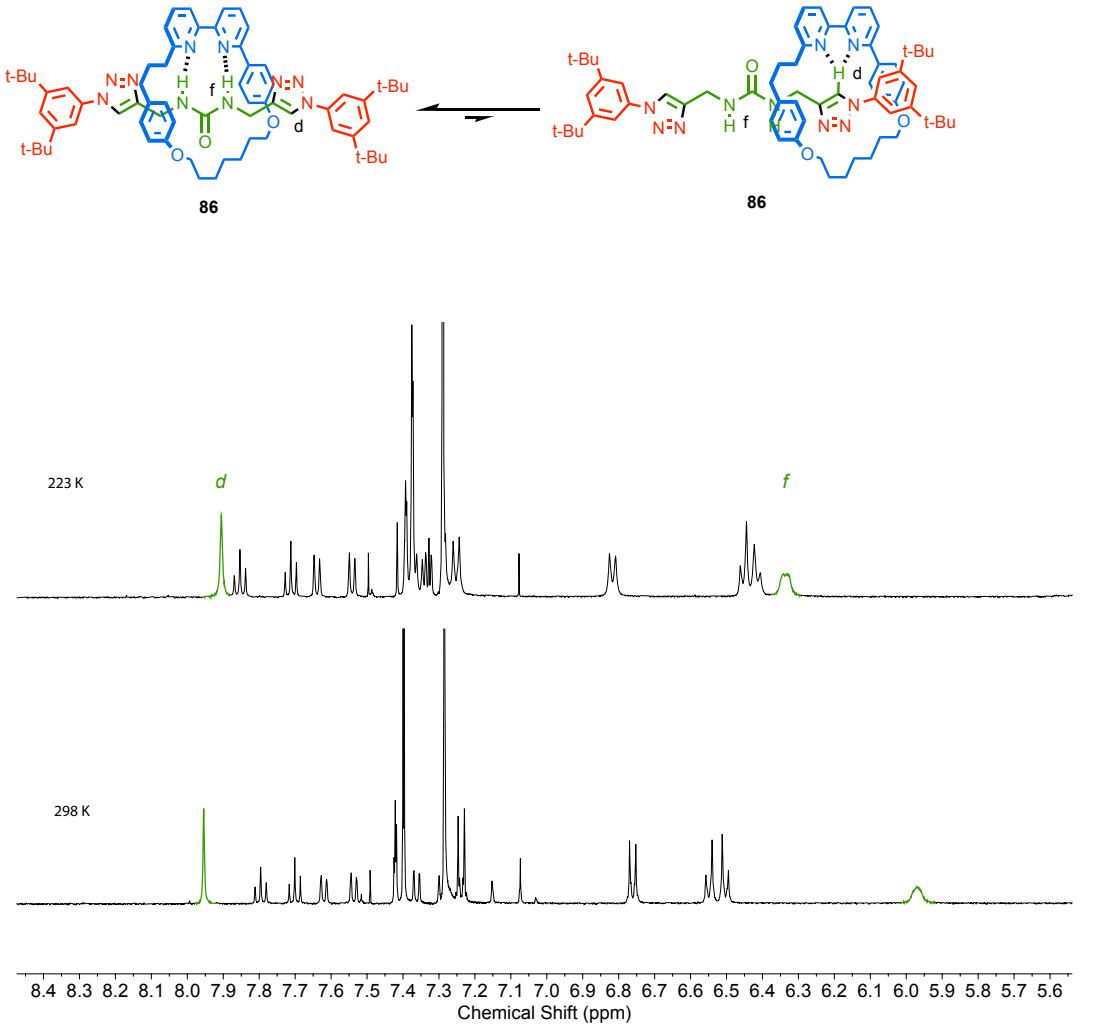

Figure 2.4 Different co-conformations of **86** (arbitrary chirality shown), and partial ^{1}H NMR stack plot ($CDCl_3$, 500 MHz, 298 K and 223 K) of **86**, Triazole protons H_d and urea protons H_f are in green..

2.2.1.2. NMR titration

A ^{1}H NMR titration was performed ($CDCl_3$, 400 MHz, 298 K) by incremental additions of binol phosphoric acid salt, **92**, (0-10 equiv.) to a solution of **86** (c = 2.5 mM). **92** was chosen due to it's strong anionic character, and the size of the molecule. It was hoped that using a large bulky chiral anion would help to bias the diastereoselective binding further as it would have a larger steric clash with **86**.

A binding constant was calculated by plotting the variation in chemical shift of resonances that underwent significant changes on addition of the guest by applying a nonlinear least-squares curve fitting procedure using the website http://supramolecular.org/ with a 1:1 global fitting model (Nelder-Mead method).[12] This indicated a very weak binding between **86** and **92** with K_a = 44. M^{-1} (**Figure 2.5**).

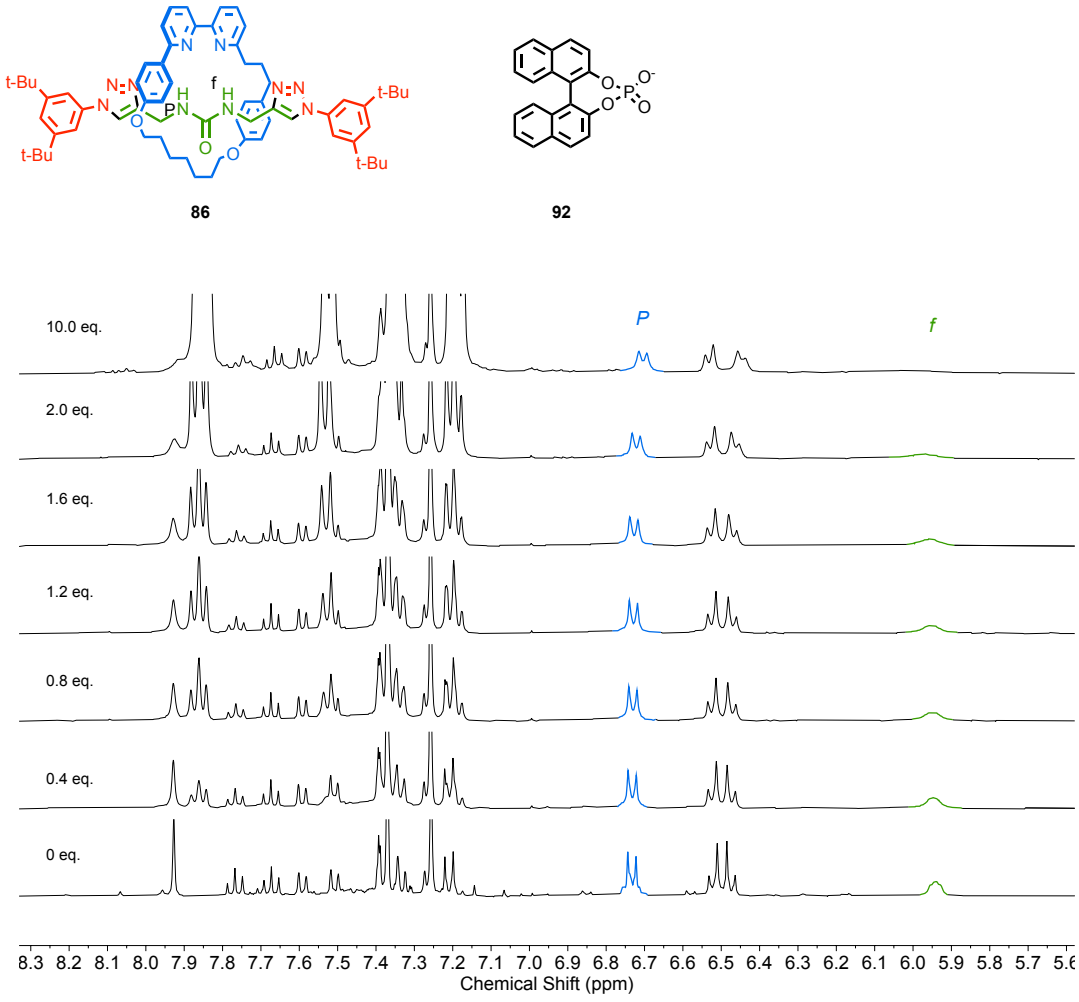

Figure 2.5 Partial ^{1}H NMR stack plot ($CDCl_3$, 400 MHz, 298 K) of **86** with 0-10 eq of **92** and plot. Macrocyclic protons H_P are highlighted in blue and Urea protons H_f are in green.

Considering the relatively weak binding between **86** and **92**, and the earlier evidence of the localisation of the macrocycle around the urea component (**figure 2.4**), **86** was not

considered to be a good host for further investigation. This is presumably due to the same issues observed with rotaxane **85**, in which protonation of the triazole unit was required to 'free' the urea for binding to anionic guests.[7]

2.2.2. Dicationic Rotaxane Host

2.2.2.1. Design, Synthesis and Characterisation

Although protonation was sufficient to activate **85** to anion binding, its use was limited as more basic anions deprotonated the rotaxane salt. With this in mind, rather than protonation, we decided to convert the triazole units to methyl triazoliums, which can act as more competitive stations for the bipyridine ring.

86 was treated with two equivalents of methyl triflate. Strictly anhydrous conditions were required, as if water was not excluded, methyl triflate was degraded to triflic acid and methanol. This led to protonation of the triazole motif, which then prevented methylation, even in the presence of excess methyl triflate (**Scheme 2.4, Figure 2.6**).

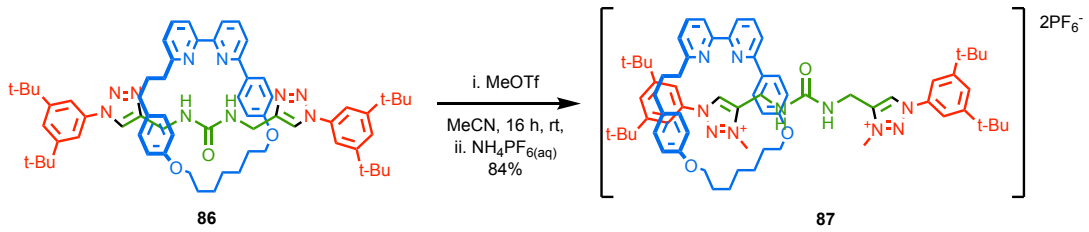

Scheme 2.4 Synthesis of rotaxane **87** (arbitrary enatiomer shown).

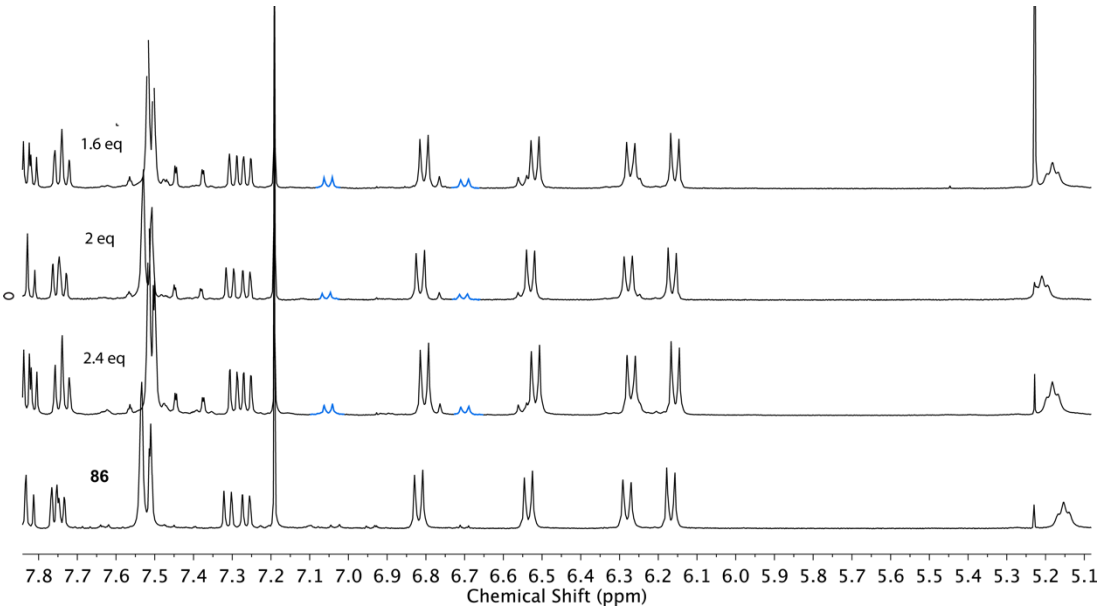

Figure 2.6 Partial ^{1}H NMR stack plot ($CHCl_3$, 400 MHz, 298 K) of crude reactions of **86** with various equivalents of methyl triflate. Impurity protons are highlighted in blue.

87 was readily purified by column chromatography with subsequent filtration over potassium carbonate and anion exchange with $NH_4PF_{6(aq)}$ to ensure only the $^-PF_6$ anion was present. ^{1}H NMR analysis ($CDCl_3$, 500 MHz) of **87** (**Figure 2.7**) showed that many of the signals were broadened, presumably due to co-conformational motion, making the unambiguous assignment of signals challenging.

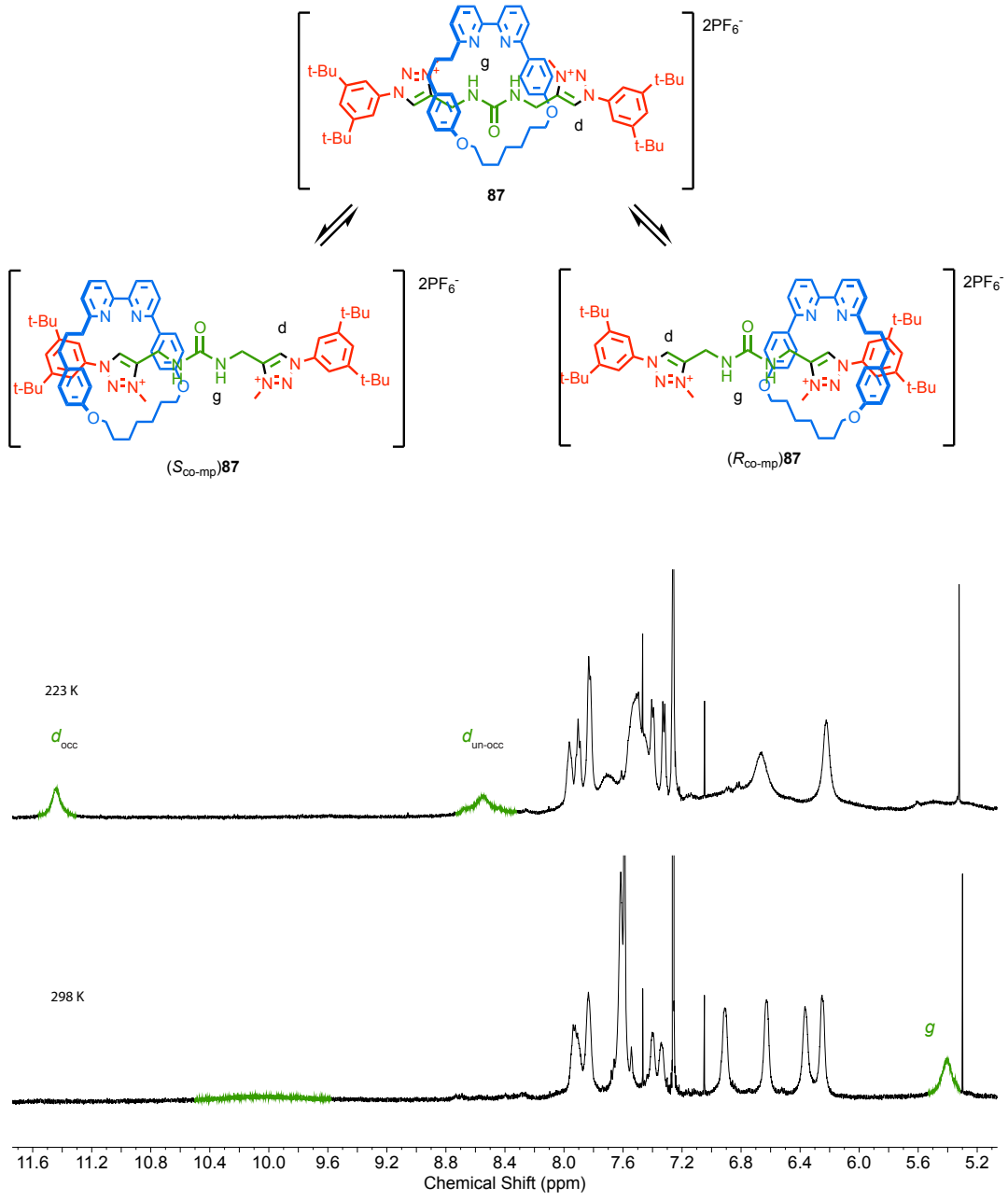

Figure 2.7 Partial ^{1}H NMR stack plot ($CDCl_3$, 500 MHz, 298 K and 223 K) of **87**. Labels d_{occ} and $d_{un\text{-}occ}$ refer to the occupied and unoccupied triazolium protons and and H_d and H_g are shown in green.

At 400 MHz, and after treatment with potassium carbonate, the urea protons were shown by COSY analysis to be at 5.15 ppm, which is lower than in rotaxane **86**. This is consistent with the urea-bipyridine interaction being disfavoured in rotaxane **87** due to the competitive triazolium-bipyridine interaction. At 298 K, no sharp signal for triazole protons H_d could be identified. However, a broad signal at approximately 10 ppm which we considered could be due to protons H_d if the rate of exchange between the enantiomeric co-conformations were comparable to the NMR timescale. In order to resolve this, the sample was cooled to -50 °C, which led to the appearance of two new resonances at high ppm, approximately equidistant from the original broad resonance, both of which were assigned as protons H_d. The higher ppm signal is thought to correspond to the "occupied" station, in which the bipyridine unit is hydrogen bonded to the triazolium C-H, while the lower ppm signal is consistent with the "unoccupied" station. Based on these results, it appears that the urea unit is not the only occupied station for the macrocycle in the case of **87**. Instead the triazoliums act as alternative binding sites, meaning that **87** displays co-MPC co-conformations and will exist in a dynamic racemic mixture of ($R_{co\text{-}mp}$)-**87** and ($S_{co\text{-}mp}$)-**87**

*2.2.2.2. NMR Titrations of **87** with Chiral Anions*

With **87** in hand, we examined its binding with binol phosphate **92**. A ^{1}H NMR titration was performed ($CDCl_3$, 400 MHz, 298 K) by incremental addition of **92** (0-10 equiv. added in 0.2 equiv. increments between 0 and 2 eq) to a solution of **87** (c = 2.5 mM) (**Figure 2.8**).

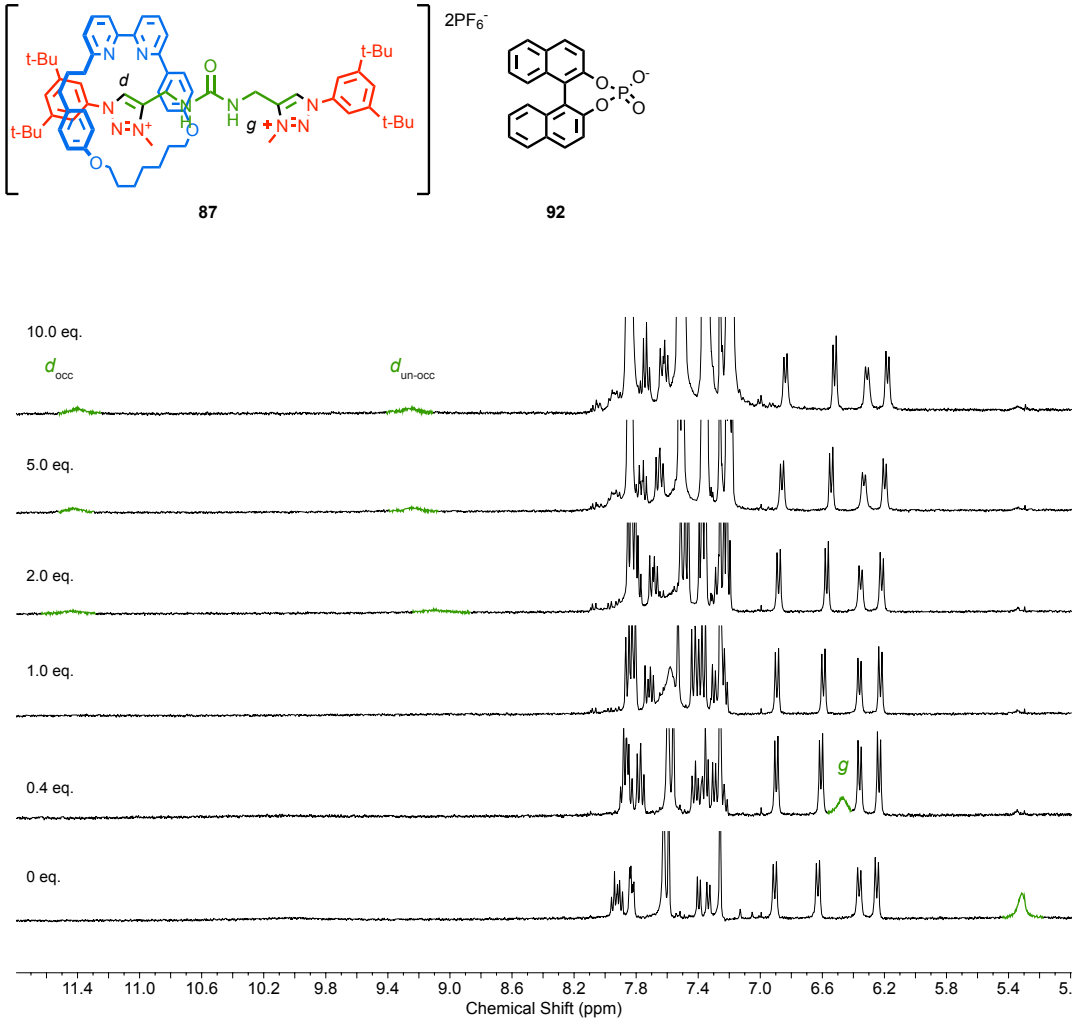

Figure 2.8 Partial ^{1}H NMR stack plot ($CDCl_3$, 400 MHz, 298 K) of **87** (c = 2.5 mM) with 0 - 10 eq of **92** (selected spectra shown). H_d and H_g are shown in green. A reduced number of spectra have been shown.

Pleasingly these results showed that **87** interacted strongly with the anionic guest. Urea protons H_g shifted to higher ppm on addition of **92**. However, before even one full equivalent of guest was added, they were 'lost' under the aromatic signals of **87** and **92**. Incremental addition of **92** also caused the broad signal corresponding to the occupied and unoccupied states of triazolium protons H_d to initially broaden further and essentially disappear, before individual signals for the occupied and unoccupied triazolium protons resolved into two distinct, if still broad, peaks, one at higher ppm which was assigned to H_d(occ) and the other at lower ppm assigned to H_d(un-occ).

These results suggest that **92** binds to the urea unit and, in doing so, slows the shuttling of the macrocycle between the triazolium binding sites. However, although increasing equivalents of guest **92** did not cause significant changes in the chemical shift of H_d(occ) the signal for H_d(un-occ) shifts to higher ppm with increasing equivalents of **92**. Similarly, the

changes observed in signals due to the macrocycle do not fit any discernible 1:1 or 1:2 binding model. Thus, it appears that more than one binding process is taking place, with the first equivalent of **92** binding to the urea unit as intended, but further equivalents of **92** potentially engaging in a secondary charge-charge/H-bonding interaction with the cationic unoccupied triazolium station.

Due to the disappearance of the urea protons under the aromatic signals and the complex binding behaviour apparent for other signals, we were unable to determine binding constants for the interaction of **87** and **92**. However, it is clear that the rotaxane is acting as a host species for the anion and this strongly effects its co-conformational behaviour.

Building on these results, **87** was then investigated with a series of different amino acid derived guests (**93**, **94**, **95, 96** and **97**) and camphor sulfonate, **98**, all as their TBA salts (**Figure 2.9**), which were chosen partially due to their ready commercial availability, and biological importance, and were used as the TBA salt as TBA is weakly co-ordinating and would not interfere with the binding. Differentiation of these small point chiral molecules is difficult by CD spectroscopy and it was hoped that provided they participated in binding, they could display a CD signal for the complex formation.

The chirality of the compound is irrelevant for NMR studies as the NMR is looking at the diastereoselectivity of the binding from the achiral **87**. Binding of all these guests all showed similar behaviour to **92** (full details can be found in **section 2.4**).

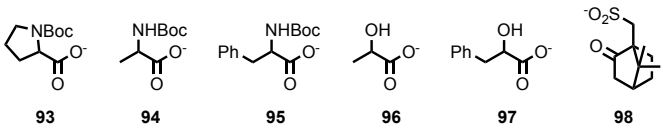

Figure 2.9 Structures of anionic guests tested with **87**. All were used as the corresponding TBA salt.

The only significant difference between the results obtained with guests **93**-**98** and those discussed above for **92** was that, in all cases, the change in chemical shift of the urea protons H_g to higher ppm was more significant suggesting that the HB bonds are more polarized than in **87•92**. Indeed, as shown for **93**, protons H_g overlap with those corresponding to H_d(un-occ), which leads to some ambiguity of which peak is which (**Figure 2.10**).

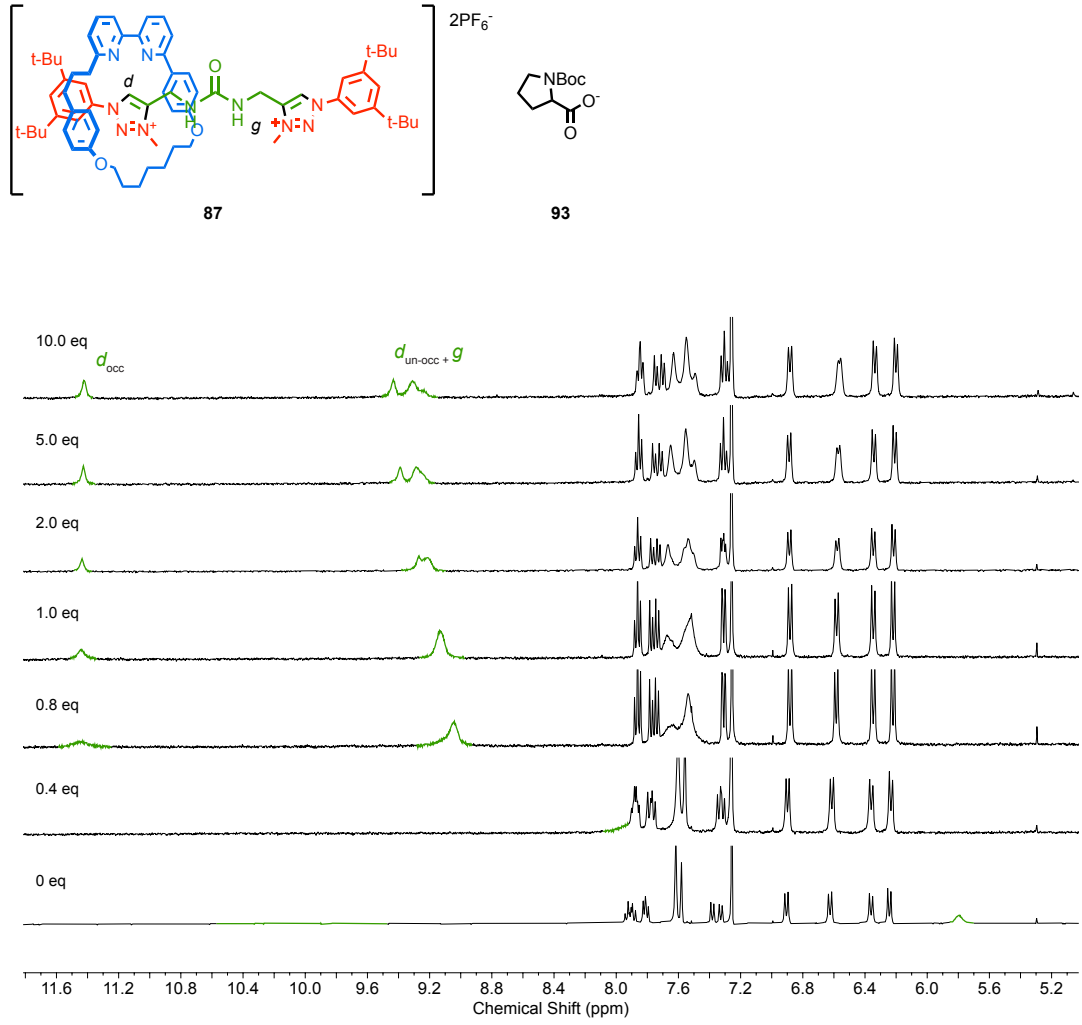

Figure 2.10 Partial ^{1}H NMR stack plot ($CDCl_3$, 400 MHz, 298 K) of **87** with 0-10 eq of **93**. H_d and H_g are shown in green. A reduced number of spectra have been shown.

*2.2.2.3. Variable Temperature ^{1}H NMR Analysis of **87** with Chiral Anions*

The results above clearly demonstrate that rotaxane **87** interacts with chiral phosphate, carboxylate, and sulfonate guests. Given that two enantiomeric co-conformations of **87** are possible, two diastereomeric host-guest complexes are likely to be present. However, the results above do not shed any light on this stereochemical detail. As VT ^{1}H NMR had proven successful in resolving the broad signals of H_d in rotaxane **87**, we decided to investigate the different **87**-chiral anion complexes at –50 °C.

^{1}H NMR analysis of mixtures of **87** and **92** at lower temperature revealed two sets of signals corresponding to H_d which were assigned as due to the two possible diastereomeric host-guest complexes. Integration of these signals suggested a diatereomeric ratio of 6:4 that was unaffected by the equivalents of **92** (**Figure 2.11**). This was a very pleasing result that showed that the chiral anion is able to bias the stereodynamic co-MPC stereogenic unit.

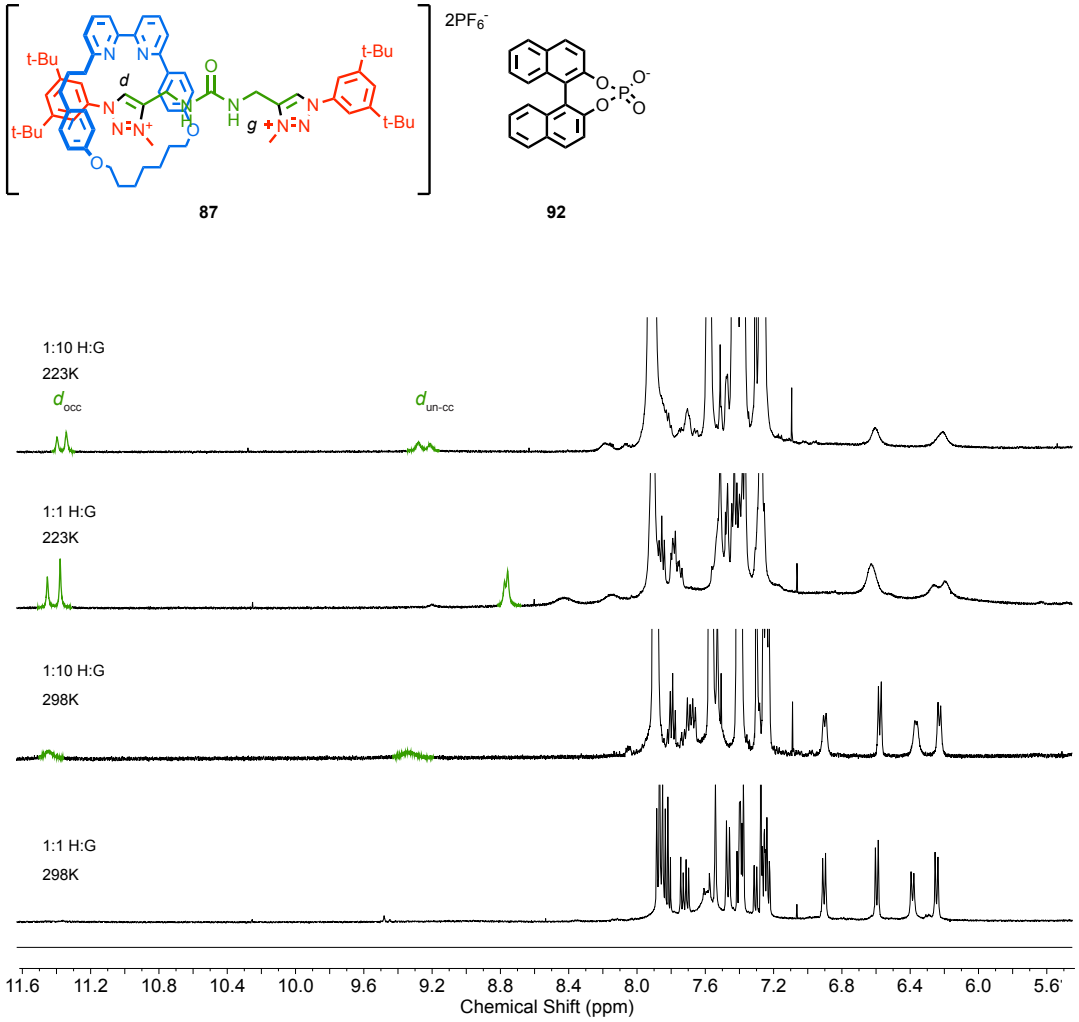

Figure 2.11 Partial ^{1}H NMR spectra ($CDCl_3$, 500 MHz, 298 K and 223 K) of **87•92**. Labels d_{occ} and $d_{un\text{-}occ}$ refer to the occupied and unoccupied triazolium protons and H_g are labeled in green.

Similarly, **93** showed a 6:4 ratio of diastereomeric complexes, as judged by integration of the two signals corresponding to H_d(occ) in the presence of 10 equivalents of the guest. However, in the presence of 1 equivalent of **93** the signals were unresolved even at –50 °C (**Figure 2.12**). The analysis was also complicated by splitting of the signals corresponding to H_g into four resonances.

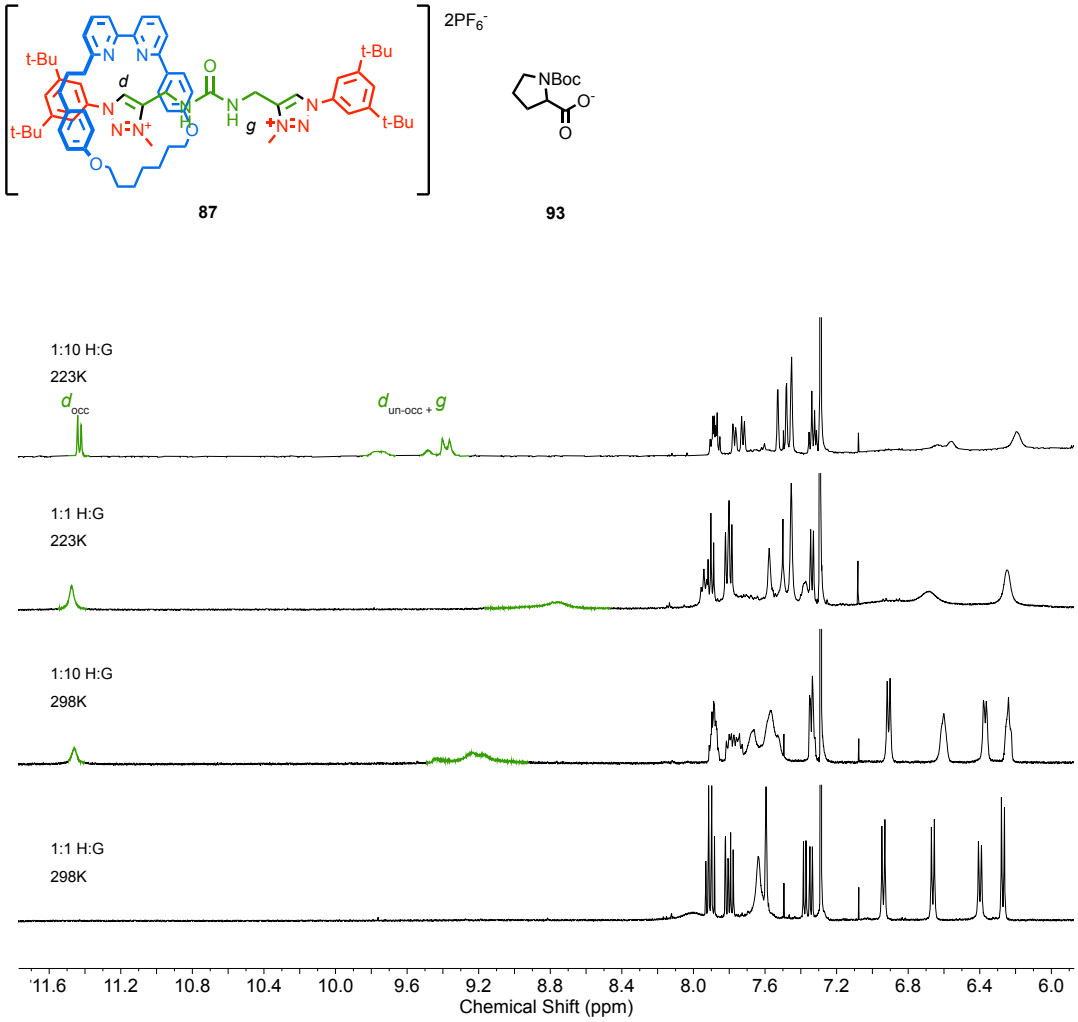

Figure 2.12 Partial ^{1}H NMR spectra ($CDCl_3$, 500 MHz, 298 K and 223 K) of mixtures of **87** and **93**. Labels d_{occ} and $d_{un\text{-}occ}$ refer to the occupied and unoccupied triazolium protons, and H_d and H_g are shown in green.

The same experiments with guests **94-98** revealed similar results to those obtained with **93**. Separate H_d(occ) signals were observed for the diastereomeric complexes at low temperature, alongside splitting of H_g. However, in these cases no measurable diastereoselectivity was observed (e.g. **Figure 2.13**, see **Section 2.4** for details).

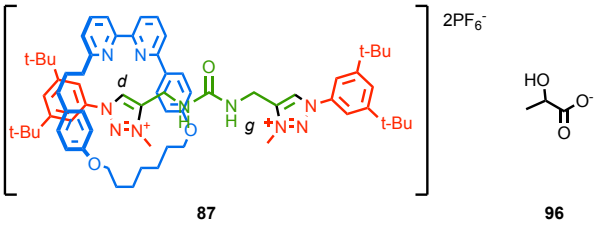

87 **96**

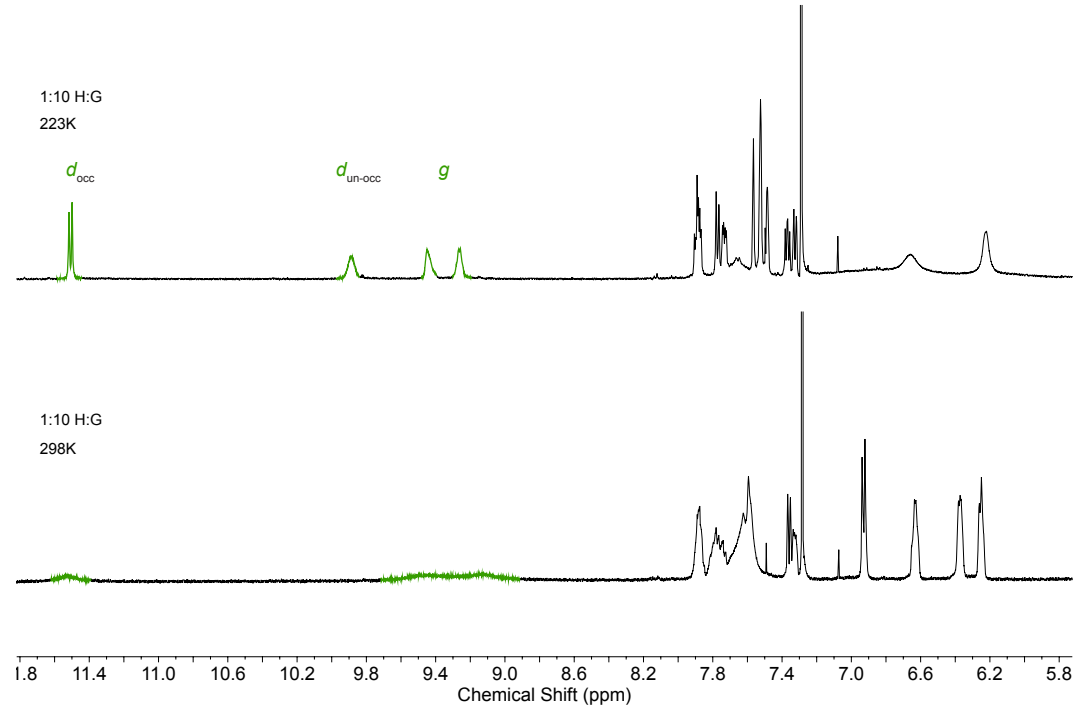

Figure 2.13 Partial ^{1}H NMR spectra ($CDCl_3$, 500 MHz, 298 K and 223 K) of **87•96**. Labels d_{occ} and $d_{un\text{-}occ}$ refer to the occupied and unoccupied triazolium protons and H_d and H_g are shown in green..

*2.2.2.4. Circular Dichroism Analysis of Mixtures of **87** and Chiral Anions*

CD spectroscopy is often used in the characterisation of chiral molecules. Previous work in the group has shown that MPC rotaxanes[7] and MTC catenanes[8] can show strong Cotton effects due to the mechanical stereogenic unit. As **87** is on average achiral due to rapid exchange between two enantiomeric co-conformation, it displays no discernible CD signal in the absence of a chiral stimulus. It was hoped that the complexes of **87** and chiral anions would display a CD signal due to the co-MPC stereogenic unit if diastereoselectivity was observed in complex formation. If this could be achieved**, 87** would be able to act as a sensor

to determine the hand and enantiopurity of chiral guests that are themselves CD silent using a calibration curve that would need to be determined prior to use with a known sample.

Initial attempts to study the complex formed by **87** and **92** by CD spectroscopy failed as **92** alone produces a very strong CD signal (**Section 2.4**). Thus **92** was unsuitable for these experiments. The mixture of **93** and **87** displayed a CD signal with a maximum at ~305 nm that was absent in solutions of the host or guest alone. When the enantiomer of **93** was used the sign of the CD response at 310 nm was inverted (**Figure 2.14**). This is a very pleasing result, as CD analysis of **93** or **87** alone under identical conditions gave no measurable CD response, meaning that the observed signal arises due to diastereoselective complex formation. Addition of further equivalents of **93** to **87** only slightly increased the intensity of the CD signal at 310 nm (See **Section 2.4** for more details).

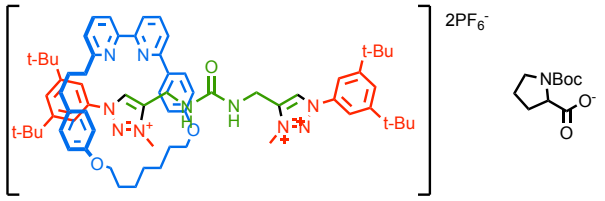

87 **93**

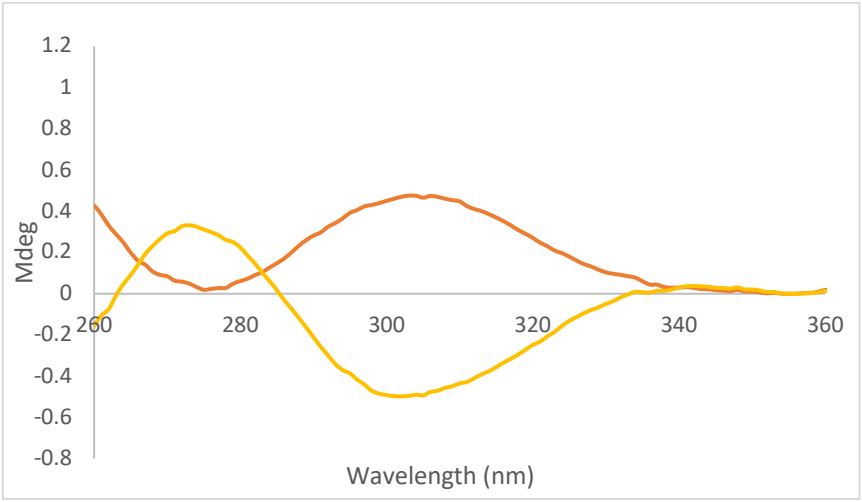

Figure 2.14 CD spectra ($CHCl_3$, 293 K) of a 1:1 mixture of **87** and **93** (c = 2.5 x 10^{-5} M); **87**•(*R*)**93** (orange), and **87**•(*S*)**93** (yellow). Spectra are normalised to 0 at λ = 355 nm and data smoothing has been applied.

It should be noted that we are currently experiencing technical issues with the CD spectrometer used in these experiments that include significant baseline drift. This is responsible for the poor shape of the curves obtained, particularly at lower wavelengths. However, the key feature of the data presented, the maxima/minima at ~305 nm, was reproducible and is thus unaffected by these technical concerns.

Even though no diastereoselectivity could be observed by ^{1}H NMR in the formation of complexes between **87** and guests **94**-**98**, it was hoped that any bias that was present could be observed by CD given that this technique can be extremely sensitive to chiral species. CD analysis of a 1:1 mixture of **87** and **94** revealed signal at ~300 nm that was not present in solutions of **94** alone under identical conditions (**Figure 2.15**). The similarity between the CD spectrum of **87** in the presence of **93** and **94** suggests that in both cases the induced signals are due to biasing of the co-MPC stereogenic unit by binding of the chiral anion. It is important to consider the lack of a CD spectra for **87** is due to the destructive interference of the two enantiomers: **87**-($R_{co\text{-}mp}$) and **87**-($S_{co\text{-}mp}$). Biasing the spectra so you have **87**-($R_{co\text{-}mp}$)•**G** ≠ **87**-($S_{co\text{-}mp}$)•**G** induces the signal, so therefore it follows that the degree of bias will influence the intensity of the complex signal.

The lower intensity of the signal in the case of **94** is therefore consistent with lower diastereoselectivity in the formation of the host-guest complex, which is in turn consistent with the results obtained by ^{1}H NMR.

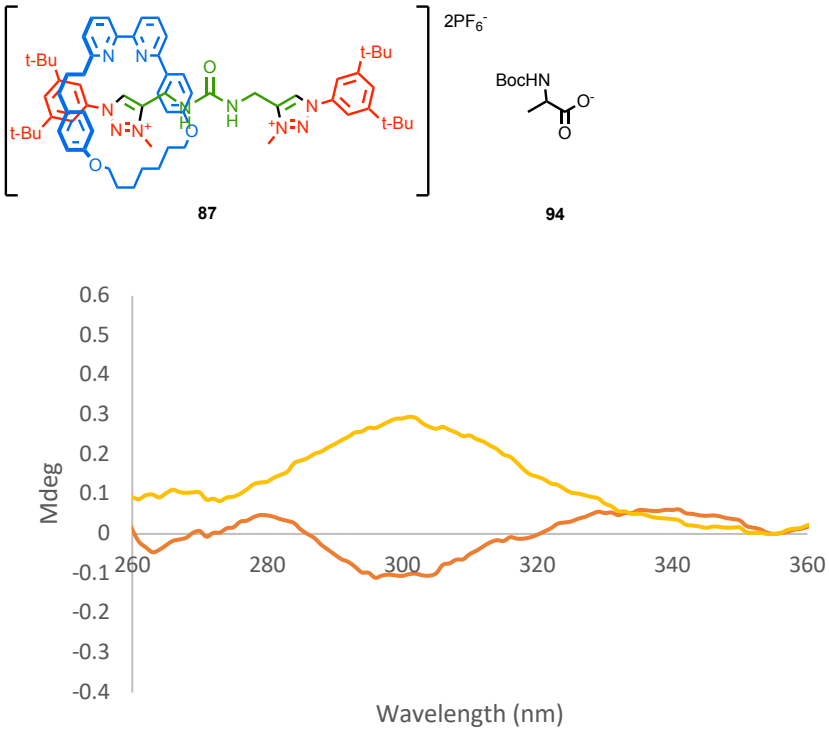

Figure 2.15 CD spectra ($CHCl_3$, 293 K) of a 1:1 mixture of **87** and **94** (c = 2.5 x 10^{-5} M);), **87**•(*R*)**94** (orange), and **87**•(*S*)**94** (yellow). Spectra are normalised to 0 at λ = 355 nm and data smoothing has been applied.

Analysis of a 1:1 mixture of **87** and **95** revealed an extremely weak CD response around 300 nm that could not be reliably distinguished from the baseline. When 10 equivalents of **95** were used the intensity of the CD signal increased (**Figure 2.16**).

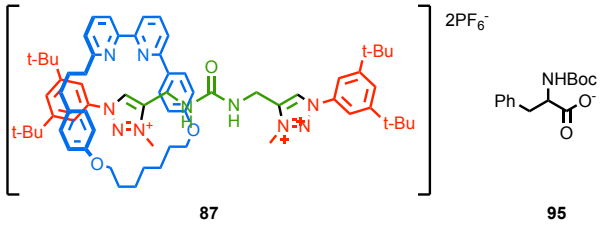

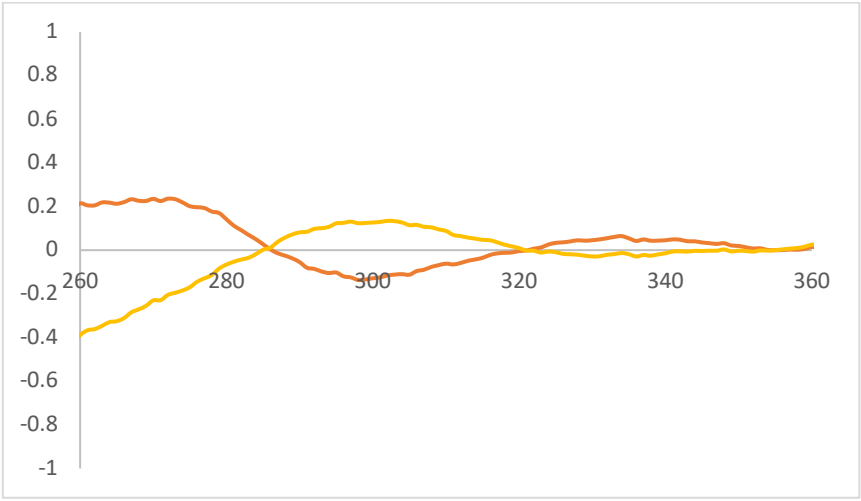

Figure 2.16 CD spectra ($CHCl_3$, 293 K) of **87•95 1:10**, **87** C = 2.5 x10^{-5} M, **95** C = 2.5 x10^{-4}, **87•**(*R*)**94** (orange), and **87•**(*S*)**94** (yellow). Spectra are normalised to 0 at λ = 355 nm and Chirascan data smoothing has been applied.

Mixtures of **87** with anion **96** gave no discernible CD signal regardless of the equivalents (1:1 and 1:10) of the chiral guest used. It was hoped that a signal could be induced by cooling the solution to 273 K but it did not remedy this (**Section 2.4**). In contrast, mixtures of **87** and **97** showed a clear and intense cotton effect in the same region as previous complexes, although in the 1:10 **87**:**97** experiment the higher concentration means signals related to **97** alone can be observed as well (**Figure 2.17**). Anion **98** showed a strong CD signal in the 300 nm region of interest and so was not suitable for this experiment.

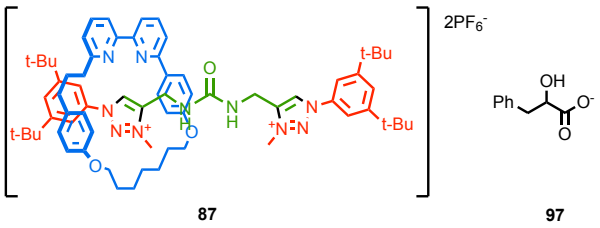

87 **97**

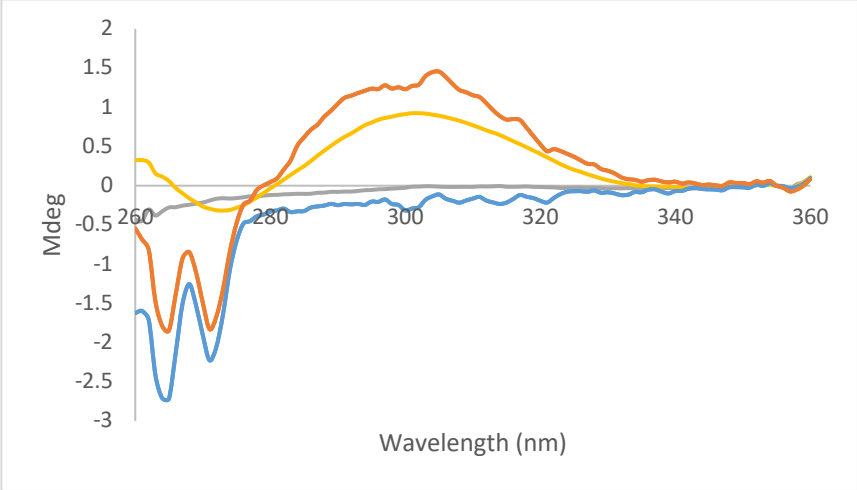

Figure 2.17 CD spectra ($CHCl_3$, 273 K, **87** C = 2.5 x10^{-5} M and **97** C = 2.5 x10^{-5} M and 2.5 x10^{-4} M) of **87•**(*R*)**97 1:1** (yellow), **87•**(*R*)**97 1:10**, (orange), (*R*)**97** C = 2.5 x10^{-5} (grey) and C = 2.5 x10^{-4} (blue). Chirascan data smoothing has been applied, to a lesser extent with **87•97 1:10** and **97** C = 2.5 x10^{-4} as it resulted in heavy alteration of the feature at 270 nm.

The experiments above demonstrate that the addition of chiral anions to a solution of **87** results in a CD signal at around 300 nm. The remarkable consistency of this result, the only major difference between different guests is the intensity of this signal rather than its position, supports the idea that this band is due to the diastereoselective biasing of rotaxane **87** between the two available co-MPC states through binding of the chiral anion to the urea moiety. Although the lactic acid salt **96** did not show this amplification, the remaining salts all showed this feature, suggesting that the co-conformational biasing of **87** by binding of anionic guests is relatively general.

*2.2.2.5. CD Analysis of **87** in the Presence Scalemic Guest **93***

With these results in hand, we investigated whether **87** could, in principle, be used to determine the *e.e.* of a chiral anionic guest. Salt **93** was chosen for this experiment as it displayed the strongest CD signal when combined with **87** and does not itself display a CD signal in the region of interest. During experiments with **97**, we found that lowering the temperature increased the intensity of the CD signal and so these experiments were carried out at 273 K. We also increased the concentration of **87** to maximise signal to noise in the 300 nm region of the spectrum.

Addition of 10 equiv. of scalemic samples of **93** of different, known *e.e.*, to rotaxane **87** resulted in a CD response at ~300 nm that varied depending on the *e.e.* of the sample. Plotting sample *e.e.* vs the intensity of the CD signal at 305 nm resulted in a straight line. This demonstrates that the CD response in this system is directly proportionate to the *e.e.* of the sample and suggests that the general principle of biasing a stereodynamic co-MPC unit using guest binding can be used to develop sensors capable of determining the enantiomeric excess of small chiral guests (**Figure 2.18**).

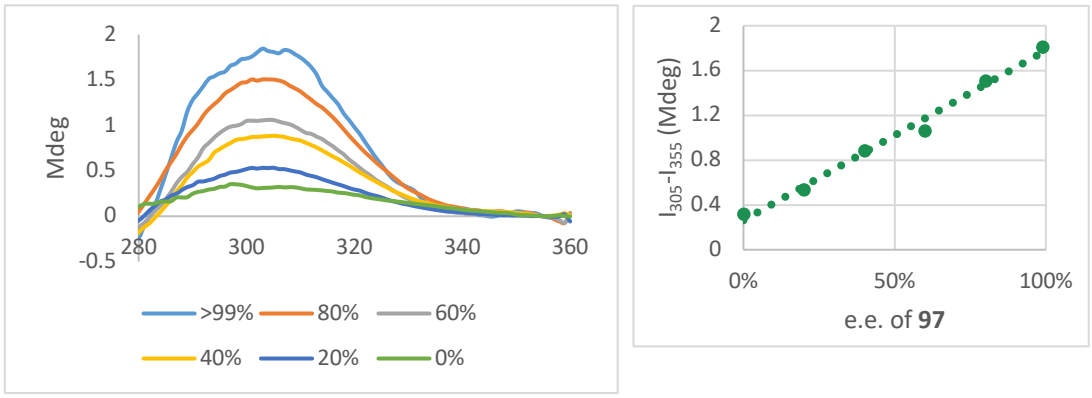

Figure 2.18 Calibration of **97** using CD spectra of [**87**•(*S**)**97**] 1:10 eq. Spectrum collected at 278 K, and **87** C = 5.0 x 10^{-5} and **97** C = 5.0 x10^{-4}. I

2.3. Conclusions and Future Work

This chapter details the successful synthesis of two formally achiral urea functionalised rotaxanes, **86** and **87** that can display co-conformational mechanical planar chirality. Whereas **86** exists predominantly in an achiral co-conformation in which the macrocycle is bound to the urea moiety, ^{1}H NMR analysis of **87** revealed that chiral co-conformations, in which the macrocycle is bound to one of two identical triazolium stations, are significantly populated.

87 was then tested for its binding properties with chiral anions. Although ^{1}H NMR analysis demonstrated that the rotaxane host bound anionic guests, we were unable to obtain binding constants from this data due to secondary processes that we attributed to charge/charge or H-bonding interactions between excess anion and the unbound triazolium station which complicated the observed spectral changes. However, from the data, it could be deduced that the first guest equivalent appeared to bind to the urea unit as expected as signals assigned to this unit shifted significantly between 0 and 1 equiv. of the guest and were relatively unaffected addition equivalents of the salt. In contrast, the signal assigned to the unoccupied triazolium station continued to change as additional equivalents of guest was added.

Cooling a mixture of **87** and the chiral guest anions led to doubling of many signals, most notably the signal corresponding to the C-H of the occupied triazolium moiety. The two sets of signals were attributed to the formation of diastereomeric host-guest complexes that differ in their co-MPC stereochemistry. Although diastereomeric complexes were observed in all cases, only in the cases of guests **92** and **93** was a measurable diastereoselectivity (6:4) observed by ^{1}H NMR.

Using CD spectroscopy allowed us to investigate the potential of hosts such as **87** to report on the stereochemistry and enantiopurity of CD-silent chiral small molecules. With the exception of guest **96**, binding of the chiral anion to **87** induced a CD signal at ~300 nm that depended on the stereochemistry of the guest. This suggests that the CD signal induced by binding of the anion to **87** must originate in the rotaxane as it remains constant across the series of guests. Pleasingly even guest complexes that did show a measurable diastereoselectivity by ^{1}H NMR still displayed an induced CD signal, suggesting that even weak co-conformational diastereoselectivity can be detected in this manner. Finally, we demonstrated that **87** can, in principle, be used to determine the *e.e.* of a scalemic guest by

showing that the intensity of the induced CD signal depends linearly on the e.e. of the sample.

Looking to the future, a number of challenges remain to be overcome. Firstly, although the data described in this chapter is compelling, technical issues with the CD spectrometer used in the experiments will require most of the data to be re-collected prior to publication to ensure that accurate baselines are obtained. There is also a need to repeat experiments with different guests under identical conditions. Some data was collected at 293 K but better results were obtained at 273 K later in the study.

Secondly, although ^{1}H NMR demonstrated that diastereoselective shuttling occurred in the presence of two of the guests, this data cannot be used directly to determine the absolute configuration of the preferred co-conformation. X-ray crystallography of a precipitated complex would not provide an answer as the minor diastereomer could preferentially crystallise from solution. One possible solution though, albeit a synthetically complex one, would be the synthesis of enantiopure 'chiral' shuttle **99**, in which the stations are differentiated by deuteration of the triazolium position (**Figure 2.19**). ^{1}H NMR analysis of **99** in the presence of chiral guests would allow the position of the macrocycle in the preferred co-conformation to be deduced directly by integration as the deutero-triazolium would have (to a good approximation) have the same binding properties as the proto-triazolium .

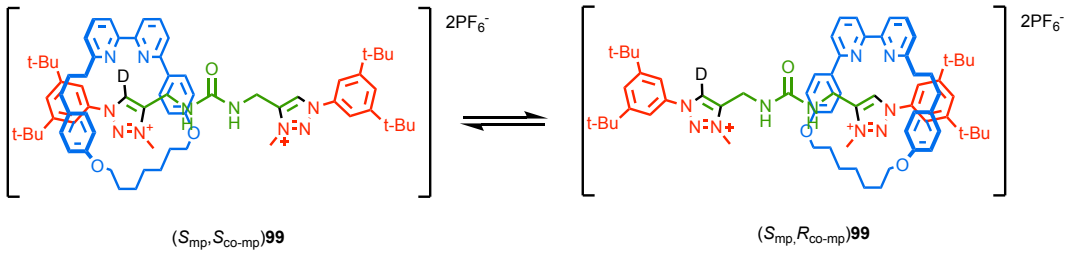

(S_{mp},$S_{co\text{-}mp}$)**99** (S_{mp},$R_{co\text{-}mp}$)**99**

Figure 2.19 Hypothetical rotaxane **99** which could be used to determine absolute conformation of H•G complex.

2.4. Experimental

General Experimental

Synthesis: Unless otherwise stated, all reagents, including anhydrous solvents, were purchased from commercial sources and used without further purification. All reactions were carried out under an atmosphere of N_2 using anhydrous solvents, unless otherwise stated. Petrol refers to the fraction of petroleum ether boiling in the range 40–60 °C. EDTA-NH_3 solution refers to an aqueous solution of NH_3 (17% w/w) with 0.1 M sodium-ethylenediaminetetraacetate. Flash column chromatography was performed using Biotage Isolera-4 or Biotage Isolera-1 automated chromatography system, employing Biotage ZIP cartridges. Analytical TLC was performed on pre-coated silica gel plates (0.25 mm thick, 60F254, Merck, Darmstadt, Germany) and observed under UV light.

Analysis: NMR spectra were recorded on Bruker AV400, AV3-400 or AV500 instrument, at a constant temperature of 298 K unless stated otherwise. Chemical shifts are reported in parts per million (ppm) from low to high field and referenced to residual solvent. Coupling constants (*J*) are reported in Hertz (Hz). Standard abbreviations indicating multiplicity were used as follows: m = multiplet, quint = quintet, q = quartet, t = triplet, d = doublet, s = singlet, app. = apparent, br = broad. Signal assignment was carried out using 2D NMR methods (HSQC, HMBC, COSY) where necessary. All melting points were determined using a Griffin apparatus and are uncorrected. Low resolution mass spectrometry was carried out by the mass spectrometry services at the University of Southampton (Waters TQD mass spectrometer equipped with a triple quadrupole analyser with UHPLC injection [BEH C18 column; MeCN-hexane gradient {0.2% formic acid}]). High resolution mass spectrometry was carried out by the mass spectrometry services at the University of Southampton (MaXis, Bruker Daltonics, with a Time of Flight (TOF) analyser; samples were introduced to the mass spectrometer via a Dionex Ultimate 3000 autosampler and uHPLC pump in a gradient of 20% acetonitrile in hexane to 100% acetonitrile (0.2% formic acid) over 5 min at 0.6 mL min; column: Acquity UPLC BEH C18 (Waters) 1.7 micron 50 × 2.1mm). The following compounds were synthesised according to literature procedures: 1-azido-3,5-di-*tert*-butylbenzene **11**, macrocycle **51**.[15]

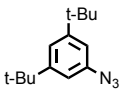

11

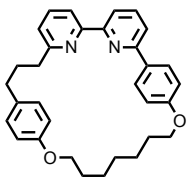

51

Preparation of chiral tetrabutylammonium (TBA) salts of anions

96 was purchased as a 30% aqueous solution, dried under high vac. and used without further purification.

Using Beer and co-workers procedure,[16] the appropriate commercial available *N*-Boc-amino acid, mandelic acid or BinolPO_4H derivative (1 mmol) was mixed with MeOH and cooled to 0 °C. To this solution was added a 1.0 M solution of Bu_4NOH (1 eq) in MeOH dropwise. The resulting solution was stirred at rt for 30 min. The solvent was then removed *in vacuo* and the product dried under high vacuum for one day before usage. The salts were stored in a vacuum desiccator over P_2O_5 between usage.

Experimental Data

*Compound **88***

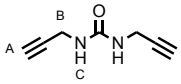

Carbonyldiimidazole (1.0 g, 6.2 mmol) was dissolved in CH_2Cl_2 (25 mL) under N_2 at 0 °C. Propargyl amine (0.82 mL, 13 mmol) in CH_2Cl_2 (10 mL) was added slowly. The mixture was allowed to warm slowly to room temperature, and stirred for 3 days. The reaction was concentrated *in vacuo*, then dissolved in a minimum amount of boiling ethanol. It was left over night at 0-5 °C, then the filtered to yield **88** as white needle crystals (0.46 g, 55%). ^{1}H NMR (400 MHz, d_6-DMSO) δ 6.21 (t, J = 4.8, 2H, H_C), 3.79 (dd, J = 5.6, 4.8, 4H, H_B), 3.05 (t, J = 5.6, 2H, H_A). ^{13}C NMR (101 MHz, d_6-DMSO) δ 157.4, 82.8, 73.1, 29.3.

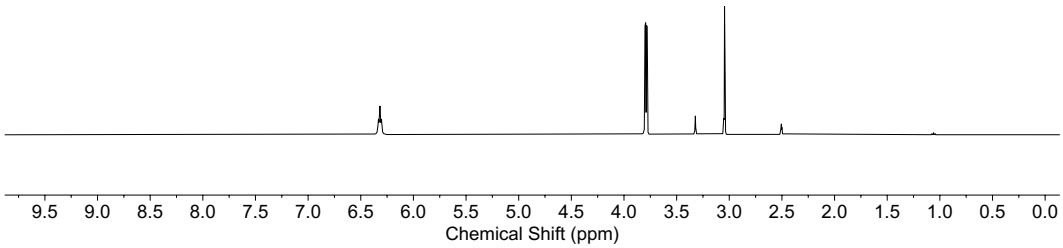

Figure 2.20 ^{1}H NMR (400 MHz, d_6-DMSO) of **88**.

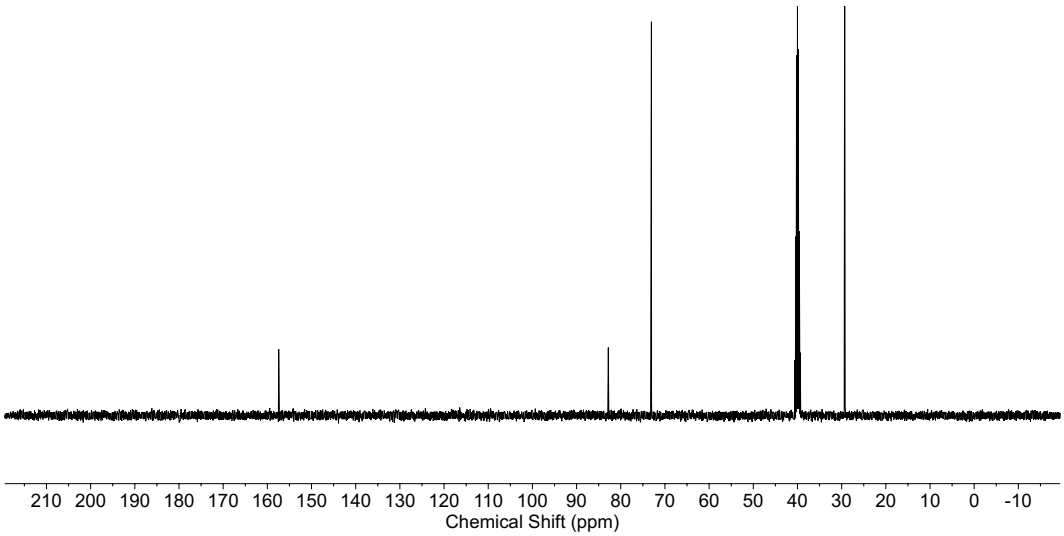

Figure 2.21 DEPT-135 ^{13}C NMR (400 MHz, d_6-DMSO) of **88**.*

*Unexpected phasing matches literature.[17]

*Rotaxane **83***

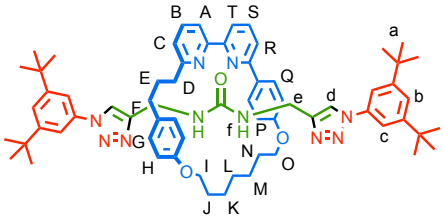

88 (27.1 mg, 0.199 mmol), **11** (95.7 mg, 0.414 mmol), **51** (79.4 mg, 0.166 mmol), $^{i}Pr_2EtN$ (140 µL, 0.80 mmol) and $[Cu(MeCN)_4]PF_6$ (61.1 mg, 0.165 mmol) in CH_2Cl_2 (5 mL) and MeOH (4 mL) in a sealed microwave vial (CEM Ltd.) under N_2. The deep red mixture was stirred at rt for 16 hours. The vial was then opened to air and additional $[Cu(MeCN)_4]PF_6$ (10 mg, 0.027 mmol) was added, and stirred for a further three hours. The reaction mixture was diluted with CH_2Cl_2 (30 mL) and stirred over EDTA-NH_3 solution (50 mL) for two hours. The aqueous layer was extracted with CH_2Cl_2 (2 × 100 mL). Combined organic extracts were washed with brine (100 mL), dried ($MgSO_4$), filtered and the solvent removed *in vacuo*. Chromatography (petrol:CH_2Cl_2 1:1, with a gradient of 0 to 20% acetonitrile) gave **83** as a white foam (188 7mg, 81%). ^{1}H NMR (400 MHz, $CDCl_3$) δ 7.95 (s, 2H, H_d), 7.77 (app. t, *J* = 8.0, 1H, H_B) 7.67 (app. t, *J* = 7.6, 1H, H_S), 7.59 (d, *J* = 8.0, 1H, H_A), 7.51 (d, *J* = 7.6, 1H, H_T), 7.40 (t, *J* = 2.0, 2H, H_b), 7.38 (d, *J* = 2.0, 4H, H_c), 7.33 (d, *J* = 7.6, 1H, H_R), 7.27 (d, *J* = 8.0, 1H, H_C), 7.21 (d, *J* = 8.8, 2H, H_Q), 6.74 (d, *J* = 8.4, 2H, H_P), 6.52 (d, *J* = 8.8, 2H, H_G), 6.48 (d, *J* = 8.8, 2H, H_H), 5.96 (br. dd, *J* = 4.0, 7.2, 2H, H_f), 4.18 (t, *J* = 6.4, 2H, H_O), 4.09 (dd, *J* = 6.5, 14.8, 1H, H_e), 3.97 (t, *J* = 5.5, 2H, H_I), 3.66, (dd, *J* = 3.9, 15.2, 1H, H_e), 2.63-2.59 (m, 2H, H_D), 2.43 (app. t, *J* = 6.0, 2H, H_F), 1.87-1.72 (m, 6H, H_E, H_J, H_N) 1.72-1.48 (m, 6H, H_K, H_L, H_M), 1.29 (s, 36 H, H_a).^{13}C NMR (101 MHz, $CHCl_3$) δ 163.8, 160.0, 158.9, 157.9, 157.3, 156.9, 156.8, 152.6, 147.2, 137.9, 137.5, 137.0, 132.0, 131.9, 129.0, 128.9, 123.0, 122.3, 121.3, 120.6, 120.3, 120.2, 115.7, 114.8, 114.2, 68.0, 66.8, 36.6, 35.9, 35.2, 35.1, 32.9, 31.4, 29.8, 29.0, 28.3, 26.3, 26.0. LR-ESI MS m/z = 1077.7 $[M+H]^+$ (calc. $C_{67}H_{85}N_{10}O_3$ = 1077.7)

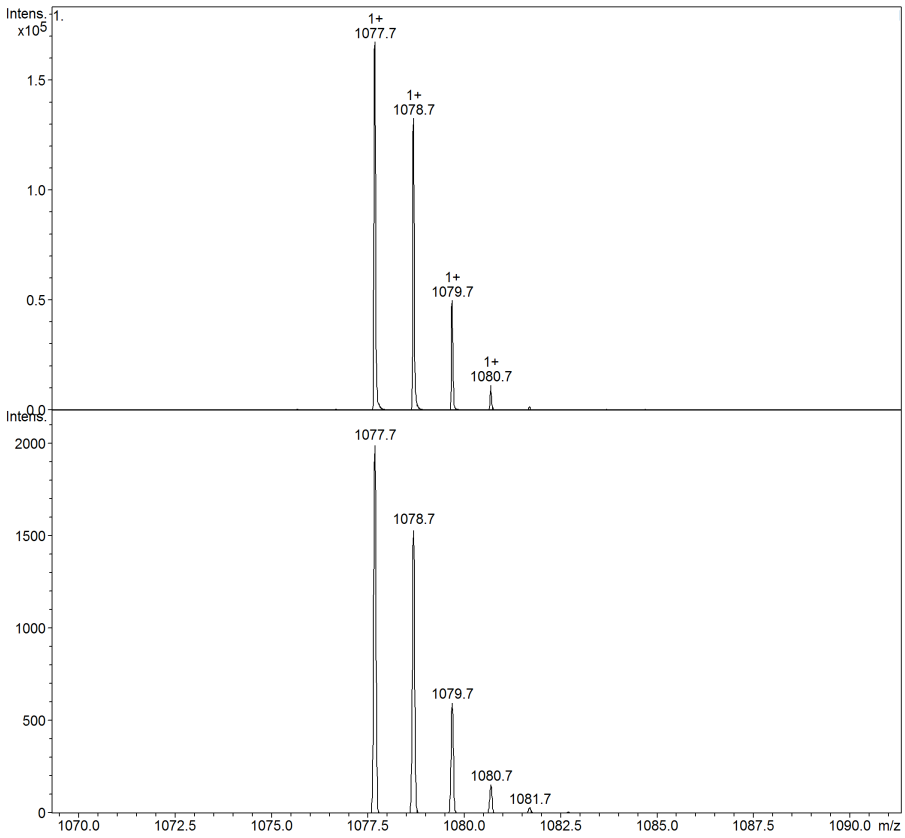

Figure 2. 22 Observed (top) and calculated (bottom) isotope patterns for $[M+H]^+$ for **83**.

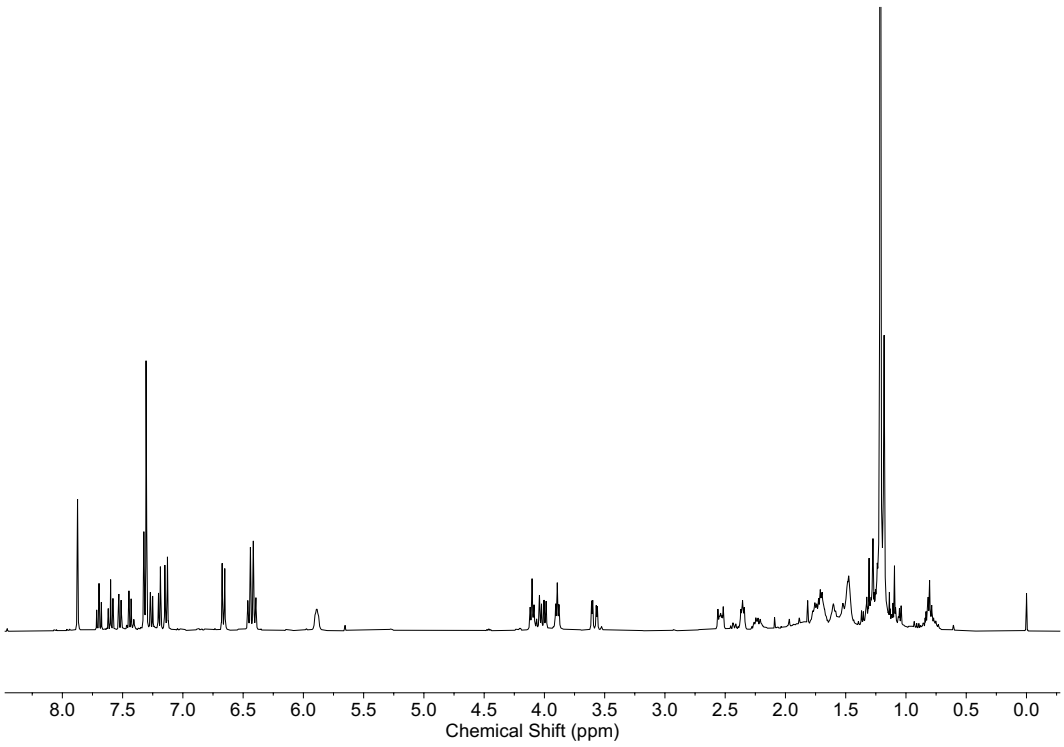

Figure 2.23 ^1H NMR ($CDCl_3$, 400 MHz) of **83**.

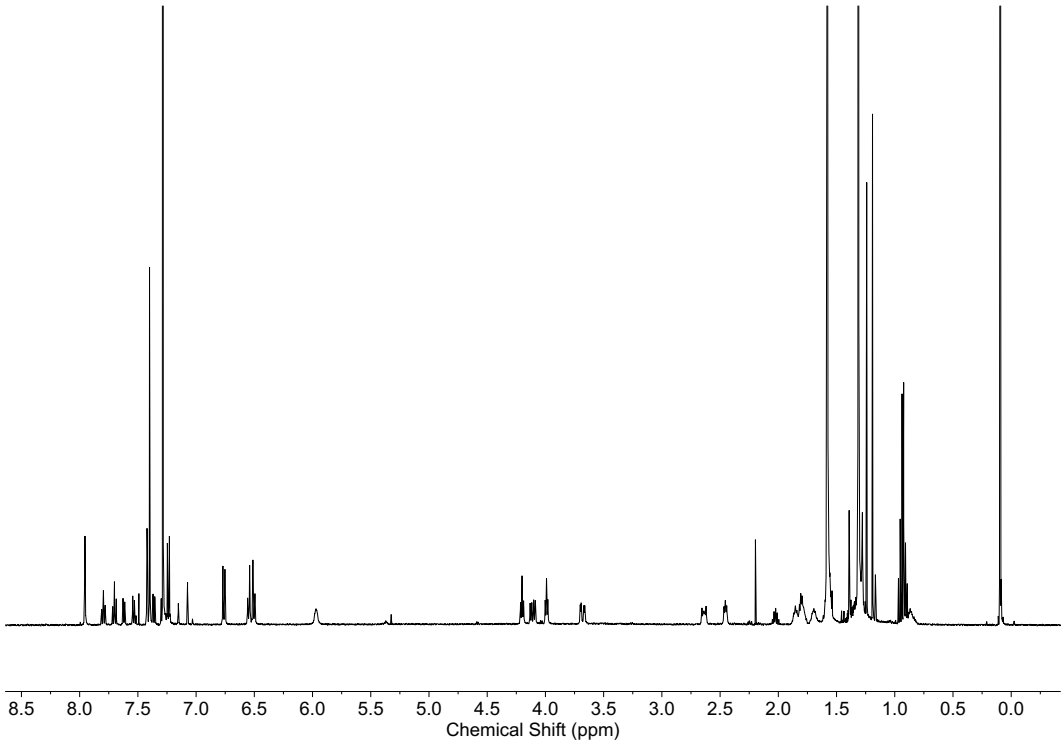

Figure 2.24 ^{1}H NMR ($CDCl_3$, 500 MHz) of **83.**

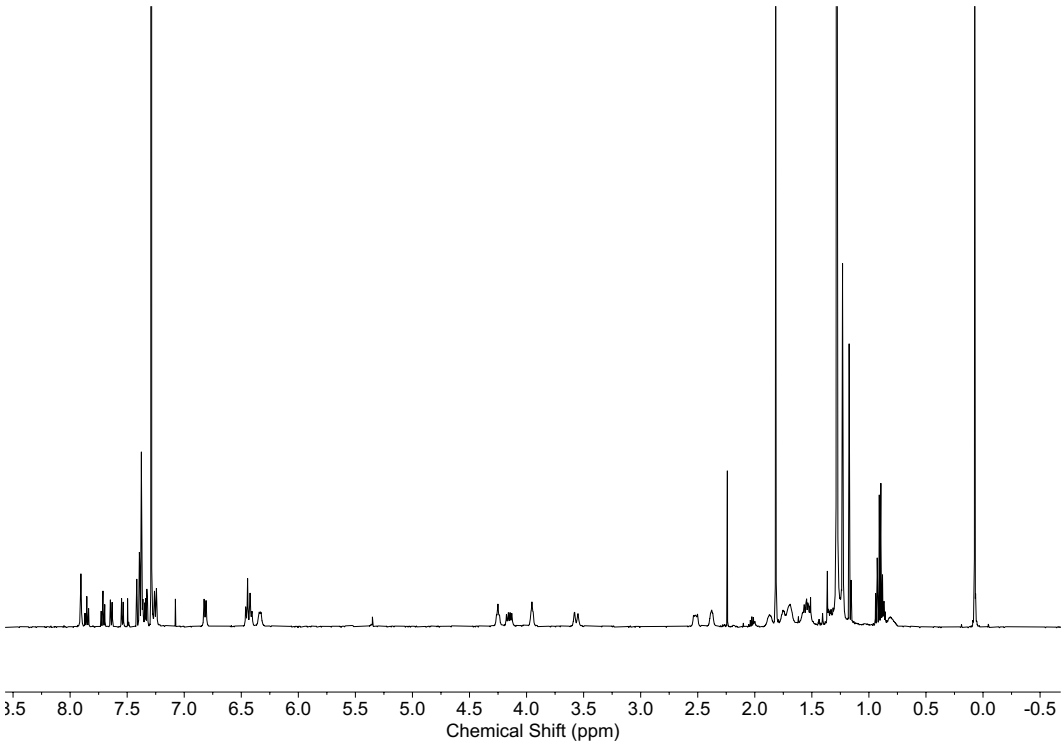

Figure 2.25 ^{1}H NMR ($CDCl_3$, 500 MHz) of **83** at 223 K.

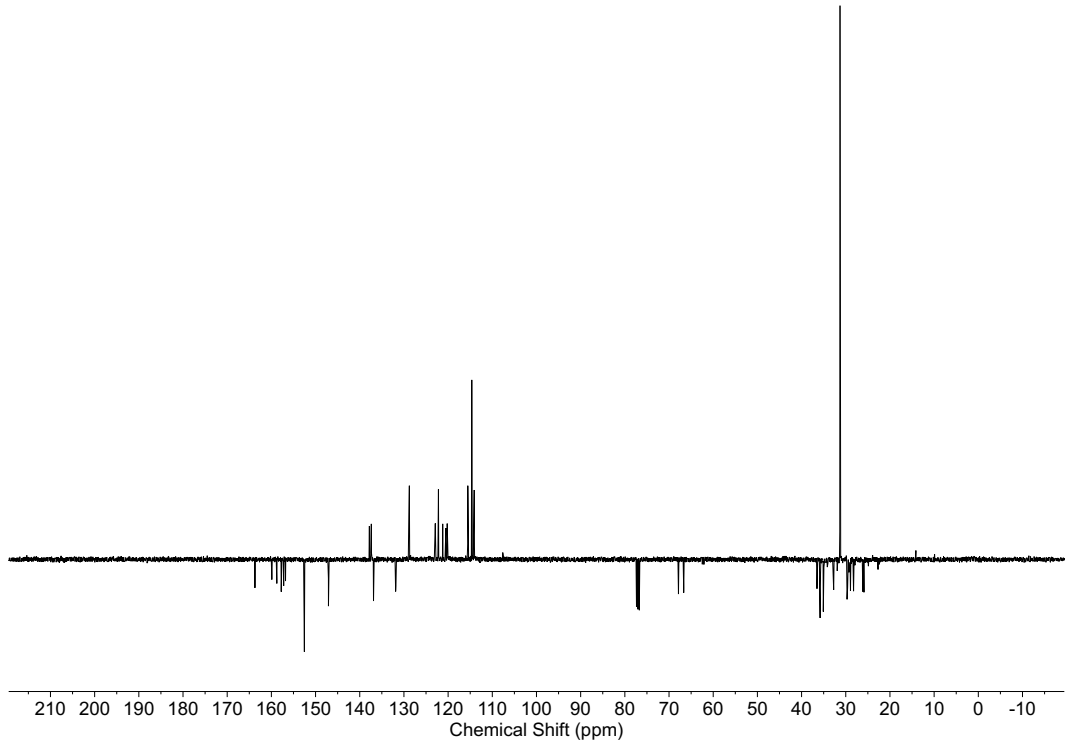

Figure 2.26 JMOD NMR ($CDCl_3$, 101 MHz) of **83**.

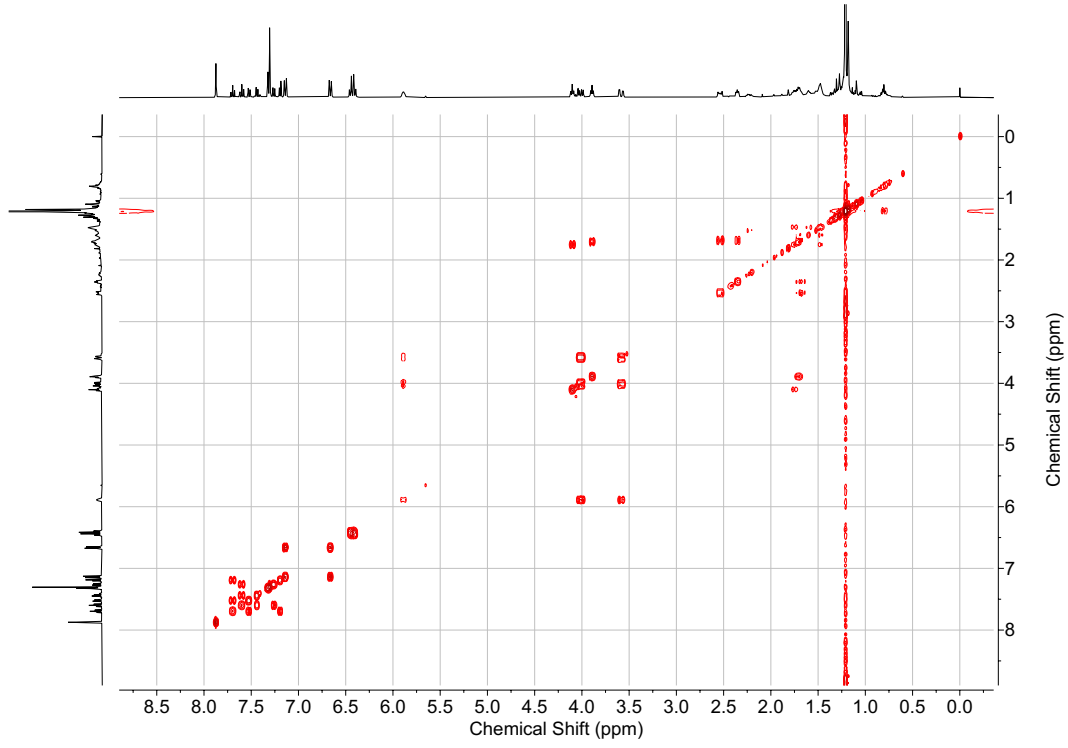

Figure 2.27 COSY NMR ($CDCl_3$) of **83**.

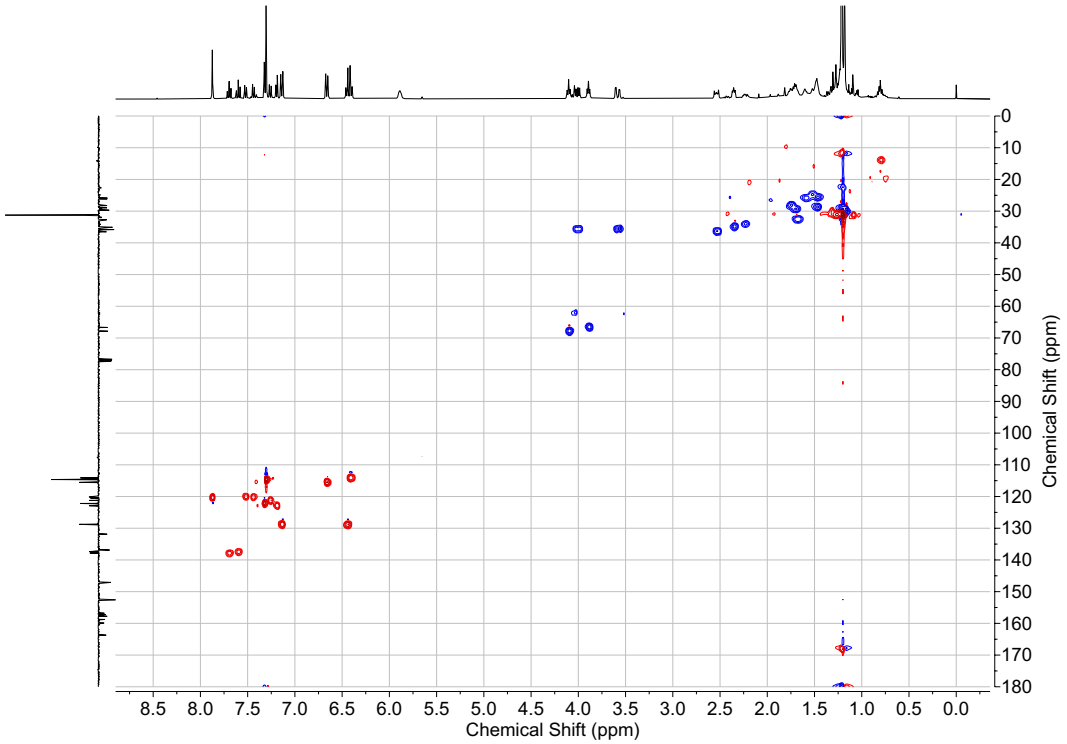

Figure 2.28 HSQC NMR ($CDCl_3$) of **83**.

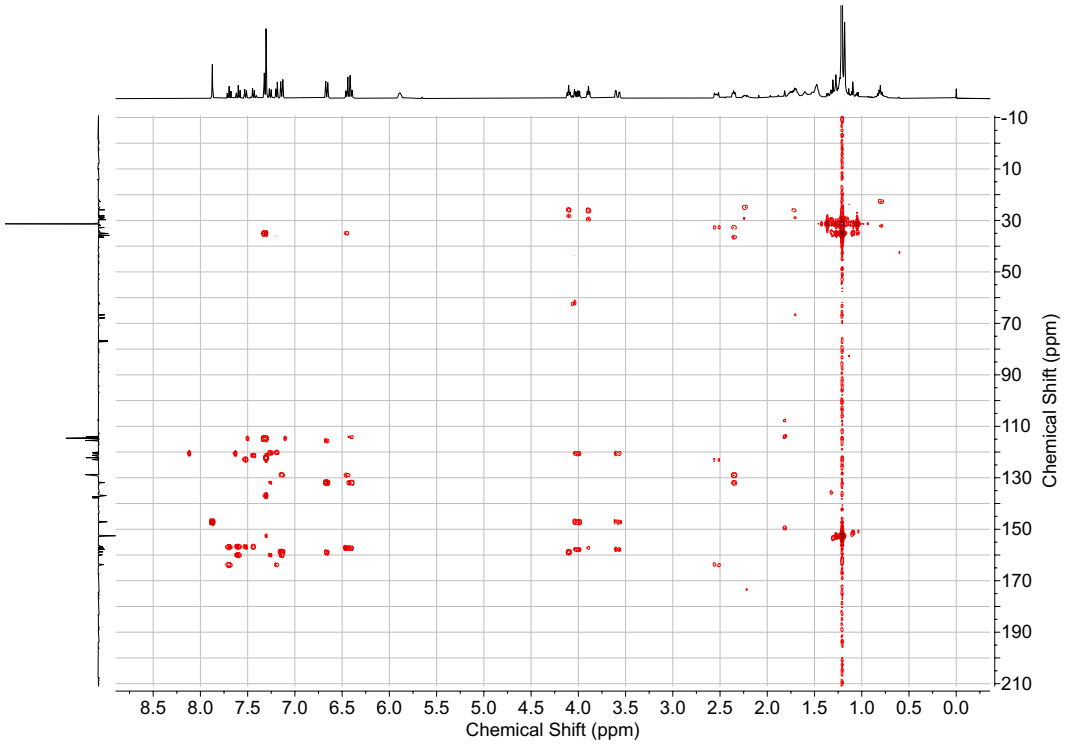

Figure 2.29 HMBC NMR ($CDCl_3$) of **83**.

Rotaxane ***87***

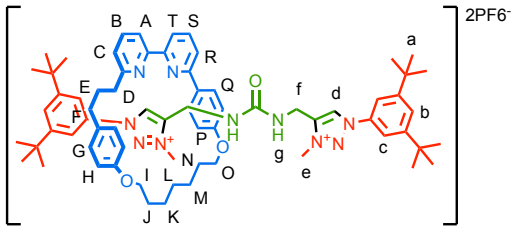

83 (51.5 mg, 0.047 mmol) was dissolved in MeCN (1 mL) under N_2 in an oven dried microwave vial (CEM ltd.). MeOTf (100 µL, 0.94 M in MeCN) was prepared in a stock under N_2 also in an oven dried microwave vial, then added to the mixture, which was then stirred for 16 hrs at rt. The reaction mixture was diluted in CH_2Cl_2 (20 mL), and an aqueous solution of NH_4PF_6 (1 M, 20 mL). The aqueous layer was then extracted with CH_2Cl_2 (2 x 10 mL), and the combined organic layers were then washed with NH_4PF_6 (3 x 10 mL), dried ($MgSO_4$), filtered and concentrated *in vacuo*. The crude was purified with chromatography (petrol:CH_2Cl_2 1:1, with a gradient of 0 to 10% MeOH), then, stirred over K_2CO_3, filtered, and washed with NH_4PF_6 (2 x 10 mL), dried($MgSO_4$), and concentrated *in vacuo*, to afford **87** as a pale white solid, (55 mg, 84%)* (mp. 85 - 86 °C. ^{1}H NMR (400 MHz, $CDCl_3$) δ 9.96 (br. s, 2H, H_d), 7.69 (app. q, *J* = 8.8, 2H, H_B, H_S), 7.76 (d, *J* = 5.3, 1H, H_A), 7.74 (d, *J* = 5.5, 1H, H_T), 7.53 (app. s, 4H, H_c), 7.51 (t, *J* = 1.6, 2H, H_b), 7.31 (d, *J* = 8.6, 1H, H_R), 7.27 (d, *J* = 6.7, 1H, H_C), 6.82 (d, *J* = 8.3, 1H, H_Q), 6.54 (d, *J* = 8.5, 1H, H_G), 6.28 (d, *J* = 8.3, 1H, H_P), 6.17 (d, *J* = 8.5, 1H, H_H), 5.15 (br. t, *J* = 6.6, 2H, H_g), 4.20- 4.07 (m, 10H, H_f, H_e), 3.87 (t, *J* = 5.5, 2H, H_O), 3.83 (t, *J* = 5.5, 2H, H_I), 2.61-2.52, (m, 2H, H_D), 2.42-2.34 (m, 2H, H_F), 1.90-1.44 (m, 12H, H_J H_K, H_L, H_M, H_N, H_E), 1.20 (s, 36H, H_a).^{13}C NMR (101 MHz, $CHCl_3$) δ 163.3, 158.8, 156.9, 156.8, 156.8, 156.3, 153.5, 139.3, 137.5, 134.6, 134.0, 131.7, 130.5, 128.4, 125.5, 123.9, 122.2, 121.1, 120.4, 115.4, 113.4, 112.6, 66.4, 64.5, 38.9, 36.9, 35.3, 34.6, 33.5, 33.0, 31.1, 29.7, 28.9, 28.8, 26.9, 25.9, 25.5. Signal for C_d is not observed due to coalescence between occupied and unoccupied conformations. LR-ESI MS *m/z* = 553.4 $[1/2M]^{2+}$ (calc. m/z for $C_{69}H_{90}N_{10}O_3^{2+}$ = 553.4)

*Yield could vary from 31% - 84 % depending on quality of MeOTf reagent.

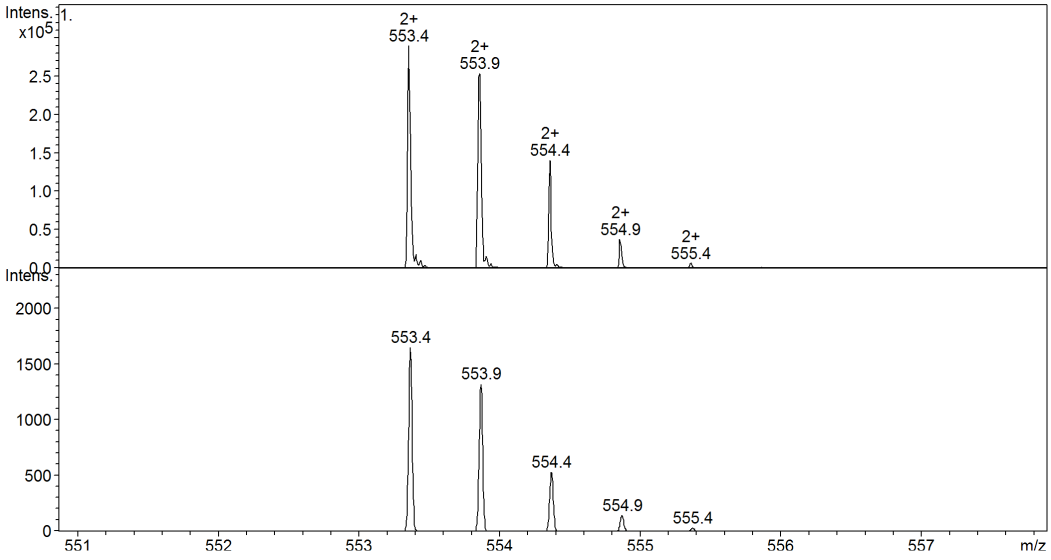

Figure 2.30 Observed (top) and calculated (bottom) isotope patterns for $[1/2M]^{2+}$ for **87.**

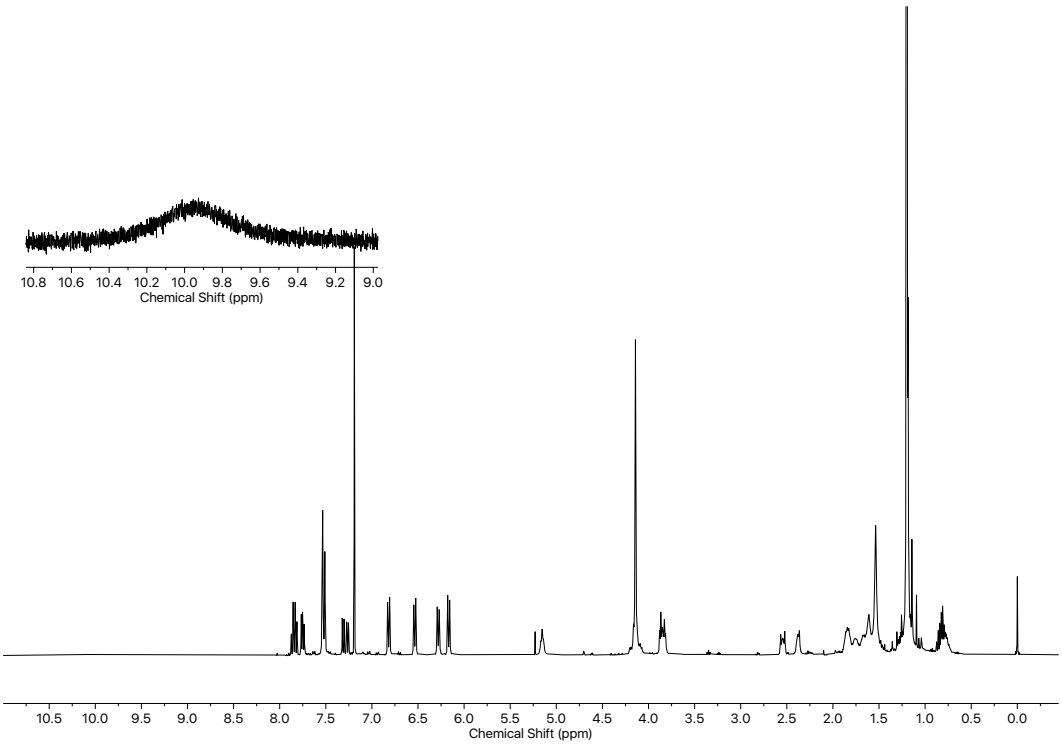

Figure 2. 31 ^{1}H NMR ($CDCl_3$, 400 MHz) of **87.**

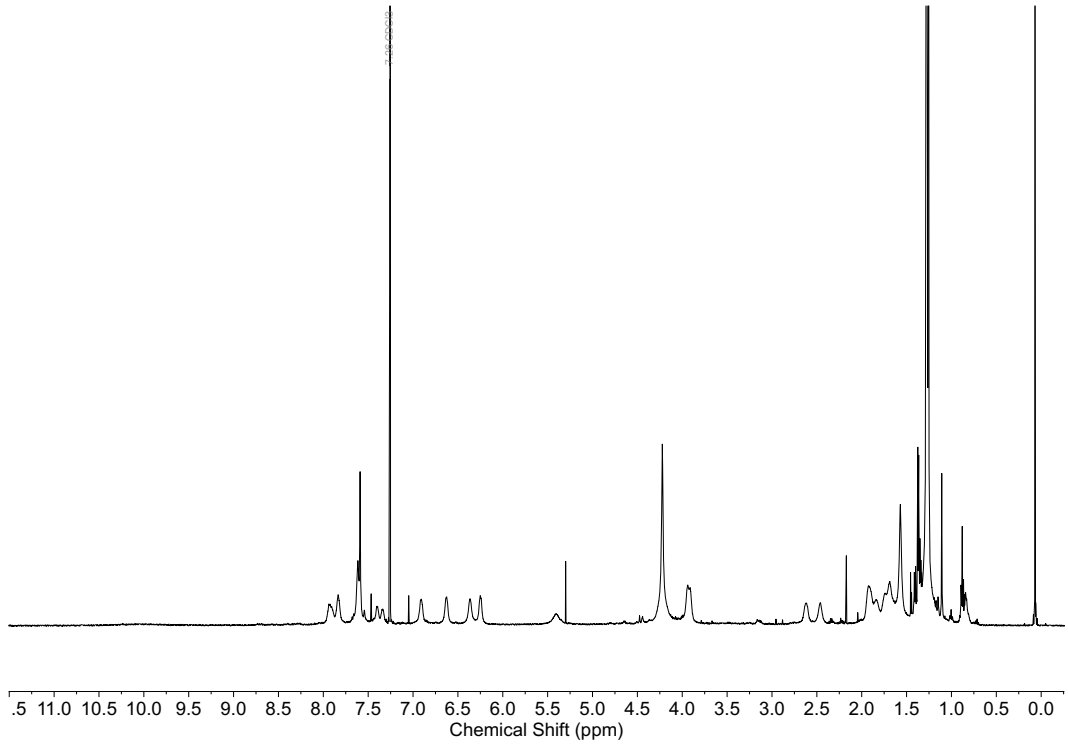

Figure 2. 32 ^{1}H NMR ($CDCl_3$, 500 MHz) of **87.**

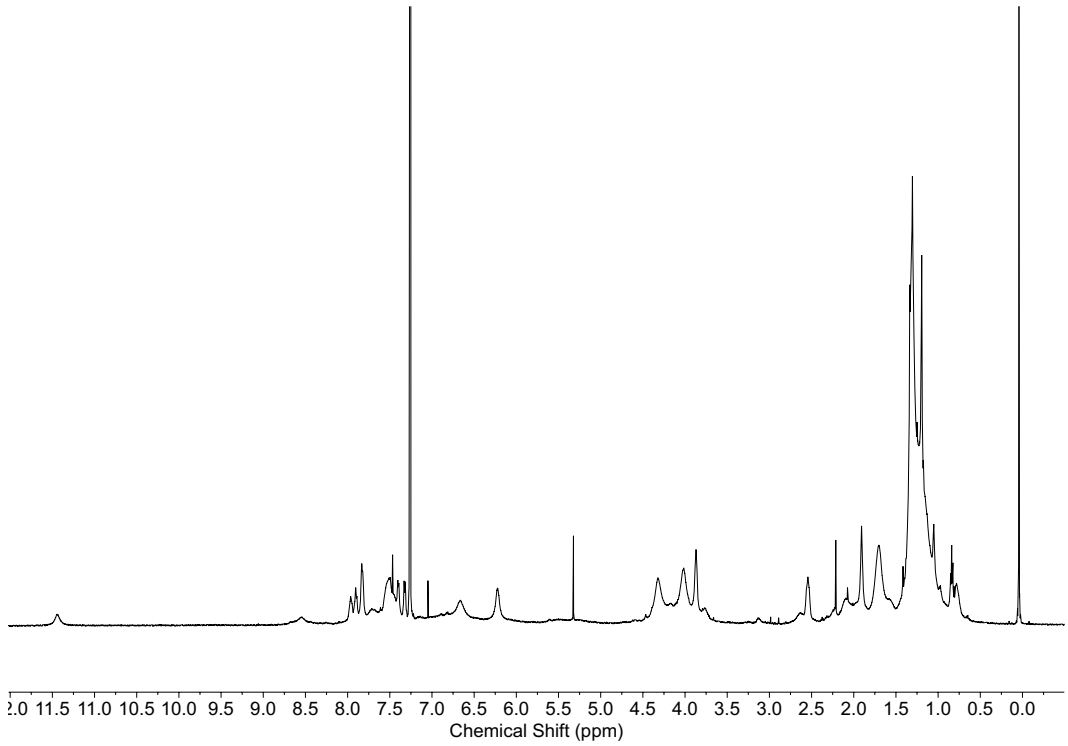

Figure 2. 33 ^{1}H NMR ($CDCl_3$, 500 MHz) of **87** at 223 K.

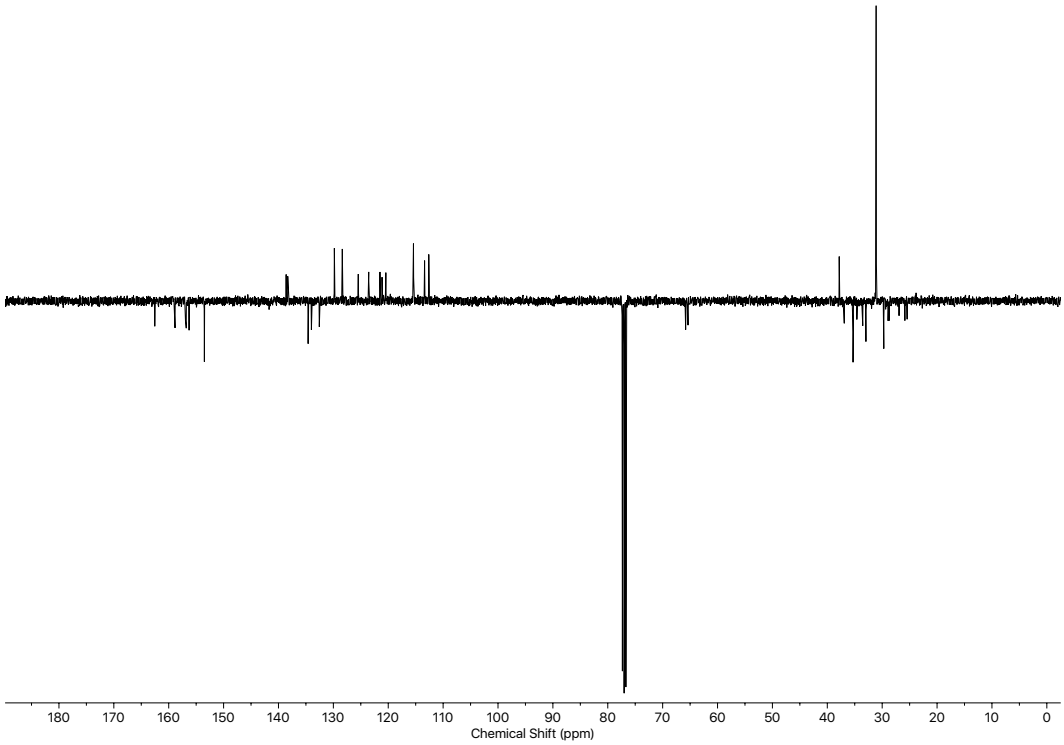

Figure 2.34 JMOD NMR ($CDCl_3$, 101 MHz) of **87**.

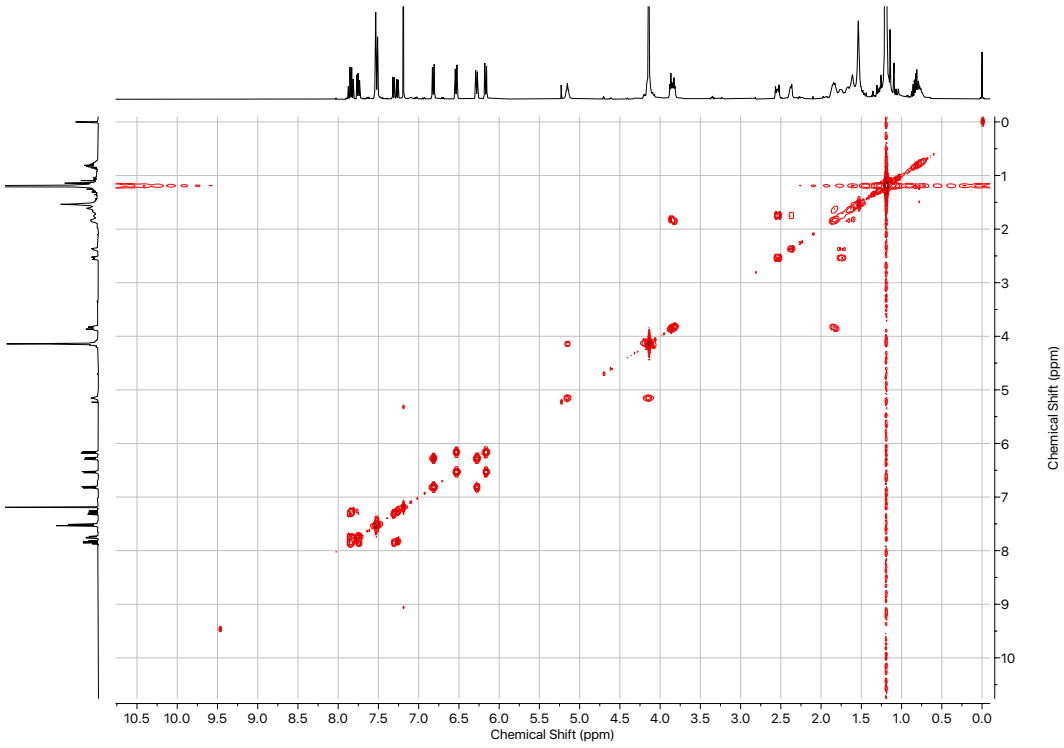

Figure 2.35 COSY NMR ($CDCl_3$) of **87**.

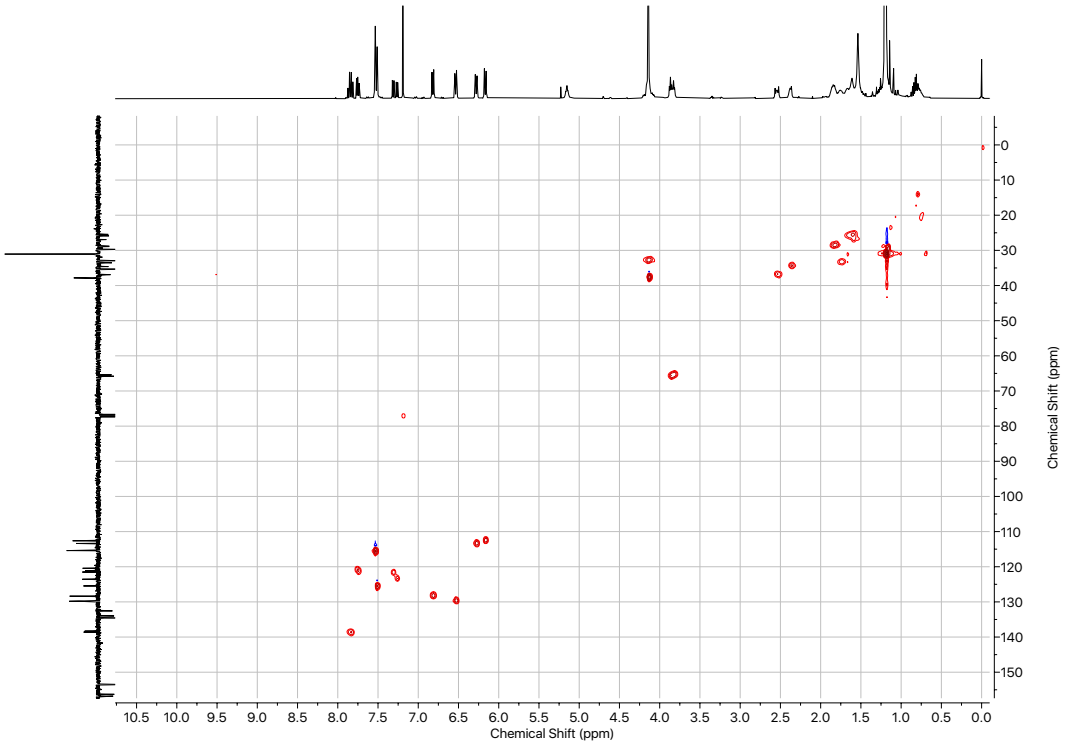

Figure 2.36 HSQC NMR ($CDCl_3$) of **87**.

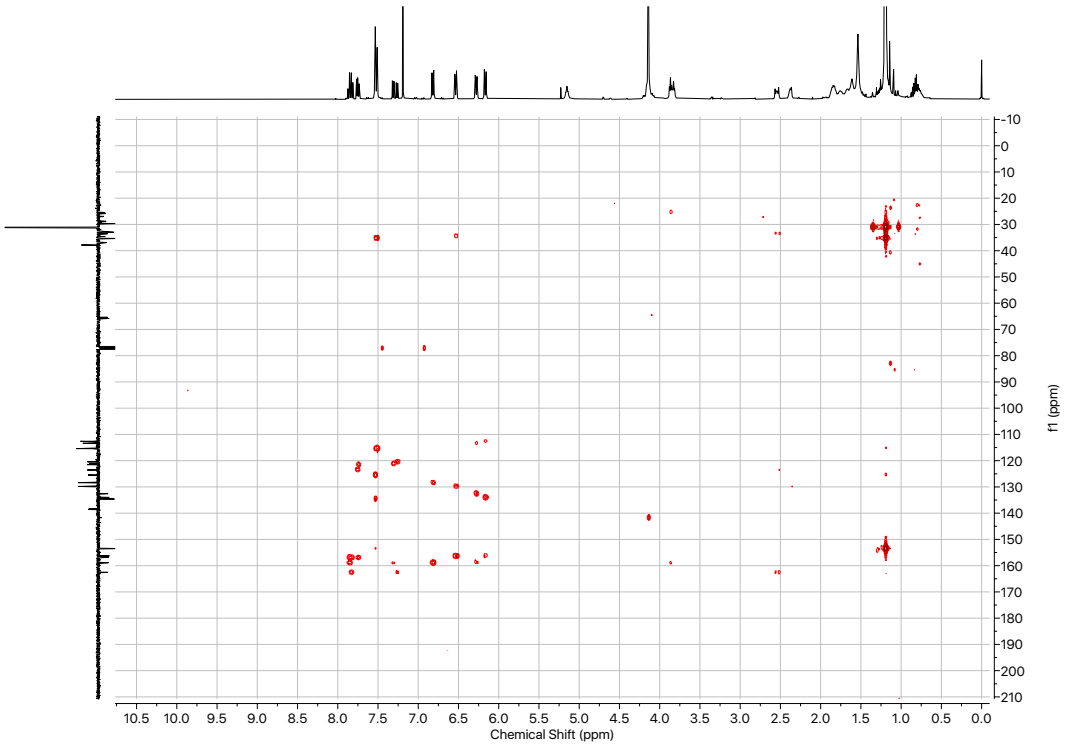

Figure 2.37 HMBC NMR ($CDCl_3$) of **87**.

NMR Titrations, VT experiements and CD data

^{1}H NMR binding studies procedure

A 2.5 mM stock of the receptor was prepared in deuterated $CDCl_3$ which had been passed over K_2CO_3 prior to sample preparation. Solutions of guest at 250 mM were prepared in the 2.5 mM stock of the receptor. A 500 µL sample of the host solution in an NMR tube was titrated with increasing equivalents of the guest solution. After each addition a 1H NMR spectrum was recorded on a Brucker Avance 400 spectrometer at 298 K. Where applicable global analysis of the data was carried out using a nonlinear least squares curve fitting procedure using the online softwear http://supramolecular.org with a 1:1 global fitting model using the Nelder-Mead method.

Assosiation constants can theoretically be related to NMR shifts using the basic formula: $\Delta\delta = \delta_{\Delta \mathrm{HG}}(\frac{[\mathrm{HG}]}{[\mathrm{H}]_0})$, however practically it is not as quite as simple as this; see ref. 12 for futher information.

VT NMR binding studies procedure

A 5 mM stock of the receptor and solutions of guest at 5 mM and 50 mM were prepared in deuterated $CDCl_3$ which had been passed over $K2CO_3$ prior to sample preparation. Solutions of guest at 5 mM and 50 mM were prepared. A 250 µL sample of the host solution and 250 µL of the guest were mixed in an NMR tube and a ^{1}H NMR spectrum was recorded on a Brucker Avance III 500 spectrometer at 223 K and 298 K.

CD binding studies prodcedure

A 5 mM stock of the receptor and solutions of guest at 5 mM and 50 mM were prepared in HPLC grade $CHCl_3$. A 1500 µL sample of the host solution and 1500 µL of the guest were mixed (or for non complexed spectrum a 1500 µL sample was diluted by a factor of 2) in an quartz cuvette. A CD spectrum was recorded at either 273 K or 293 K using a Chirascan spectropolarimeter, and recorded using Applied Photophysics software Ver. 4.2.0. The CD absorbance was recorded from 260-360 nm, and each spectra is an average of 10 scans.

NMR Titrations

*^{1}H NMR titration of **83***

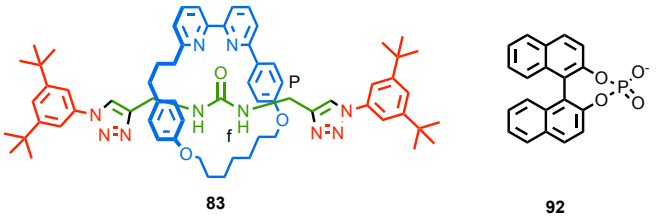

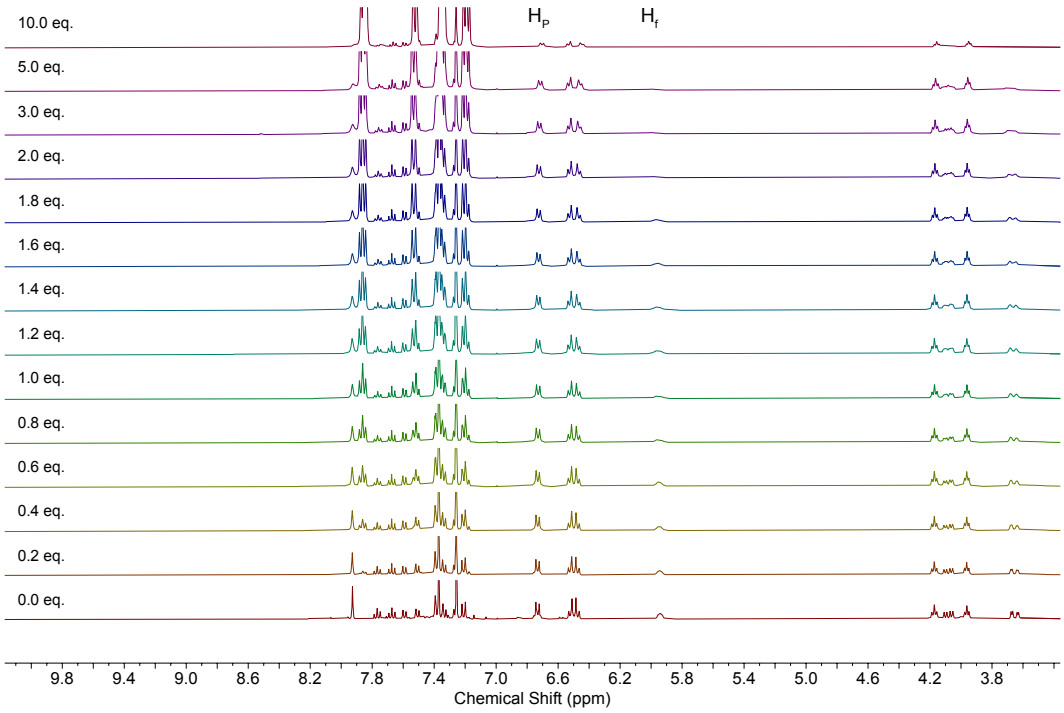

Figure 2.38 Partial ^{1}H NMR titration of **83** with **92** (0→10 eq.) in $CDCl_3$ at 298 K.

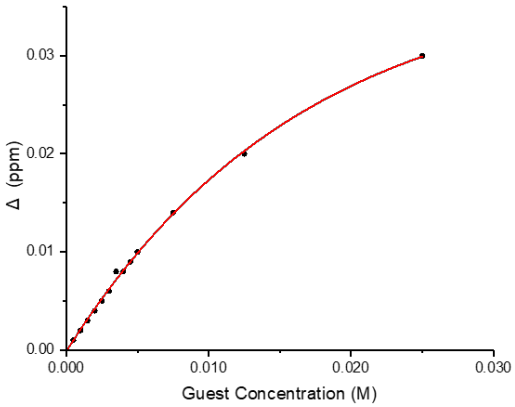

Figure 2.39 Binding plot for **83** with **92**. K_a = 44 M^{-1}.

^{1}H NMR titrations of ***87***

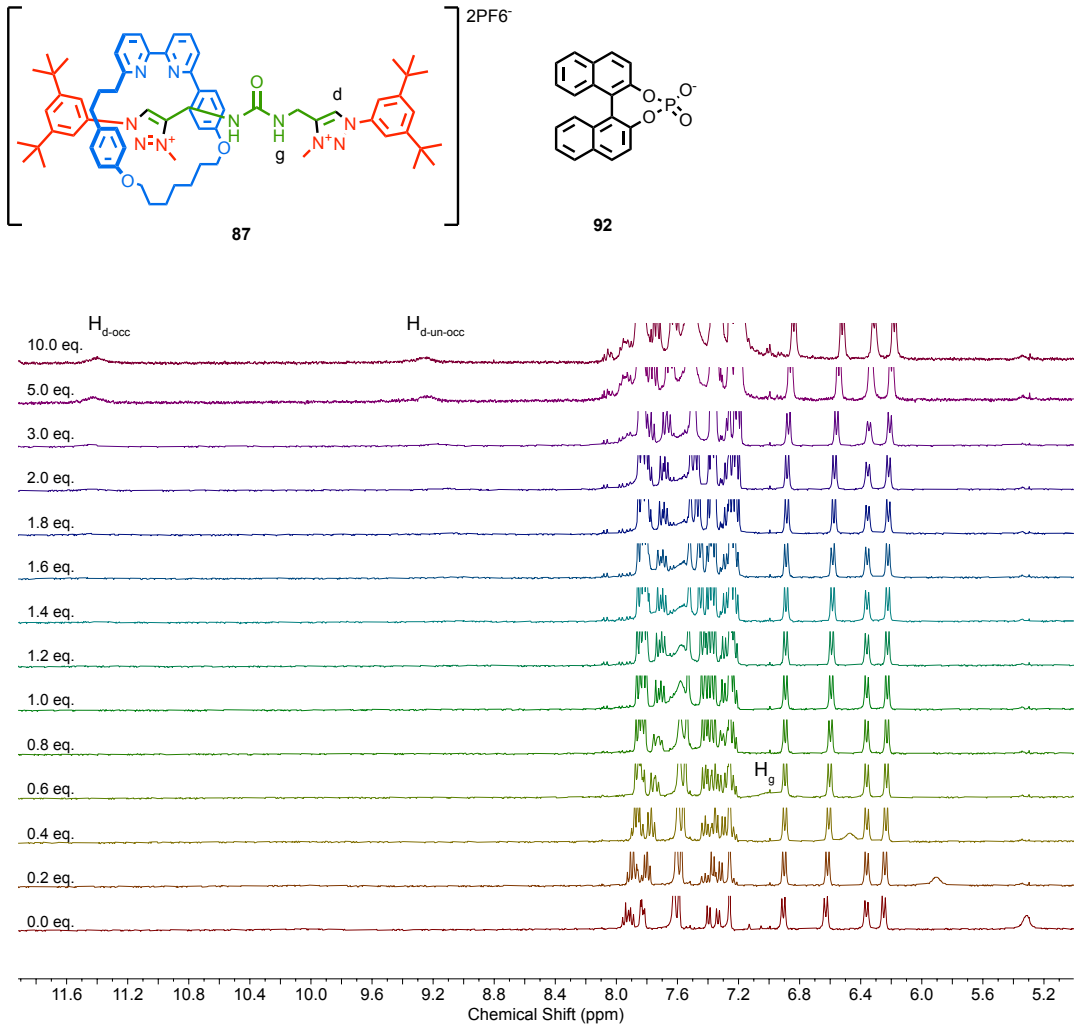

Figure 2.40 Partial ^{1}H NMR titration of **87** with **92** (0→10 eq.) in $CDCl_3$ at 298 K.

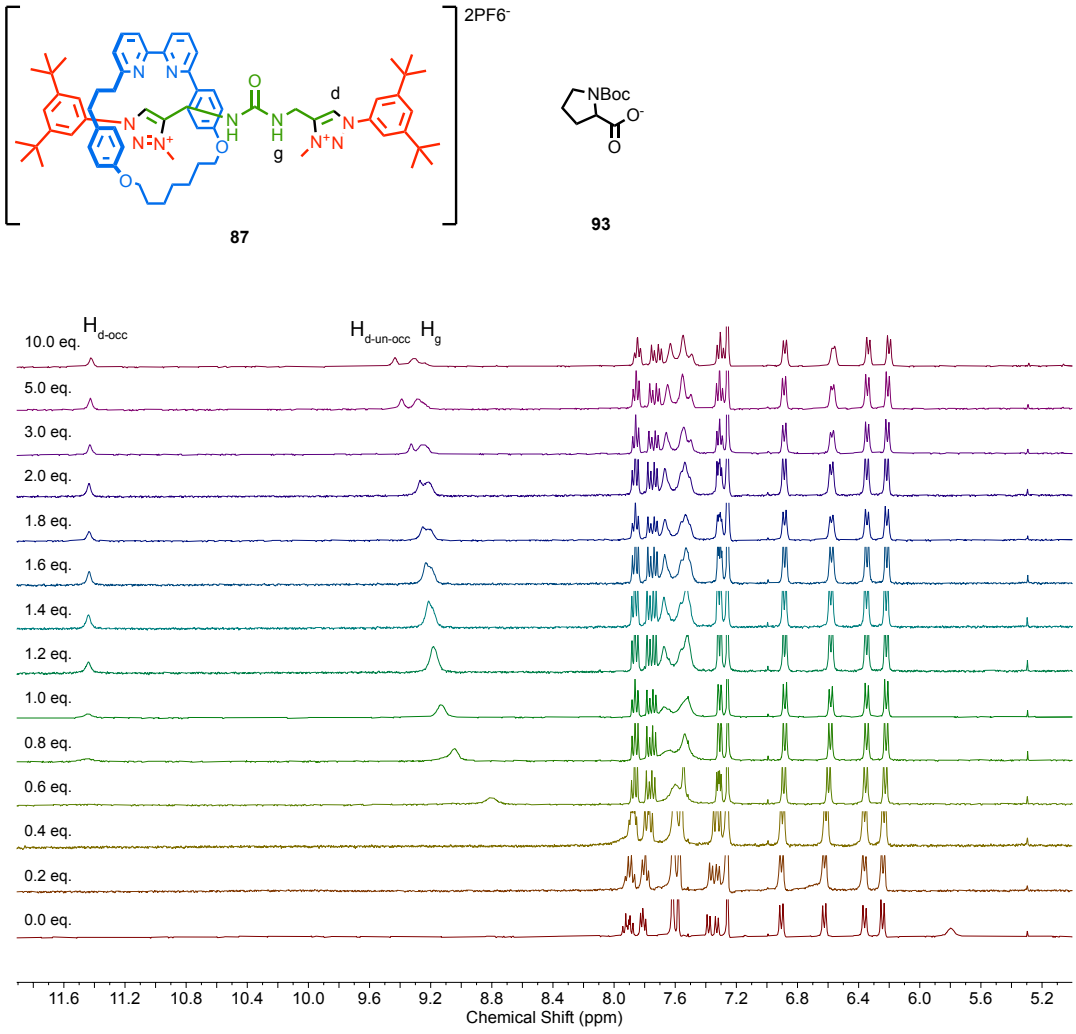

Figure 2.41 Partial ^{1}H NMR titration of **87** with **93** (0→10 eq.) in $CDCl_3$ at 298 K.

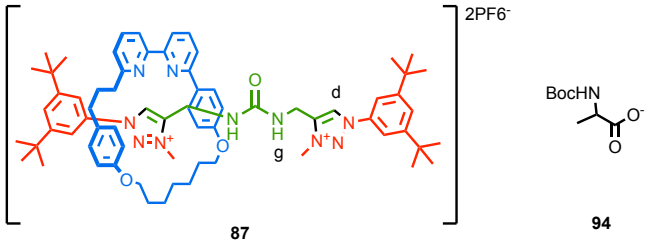

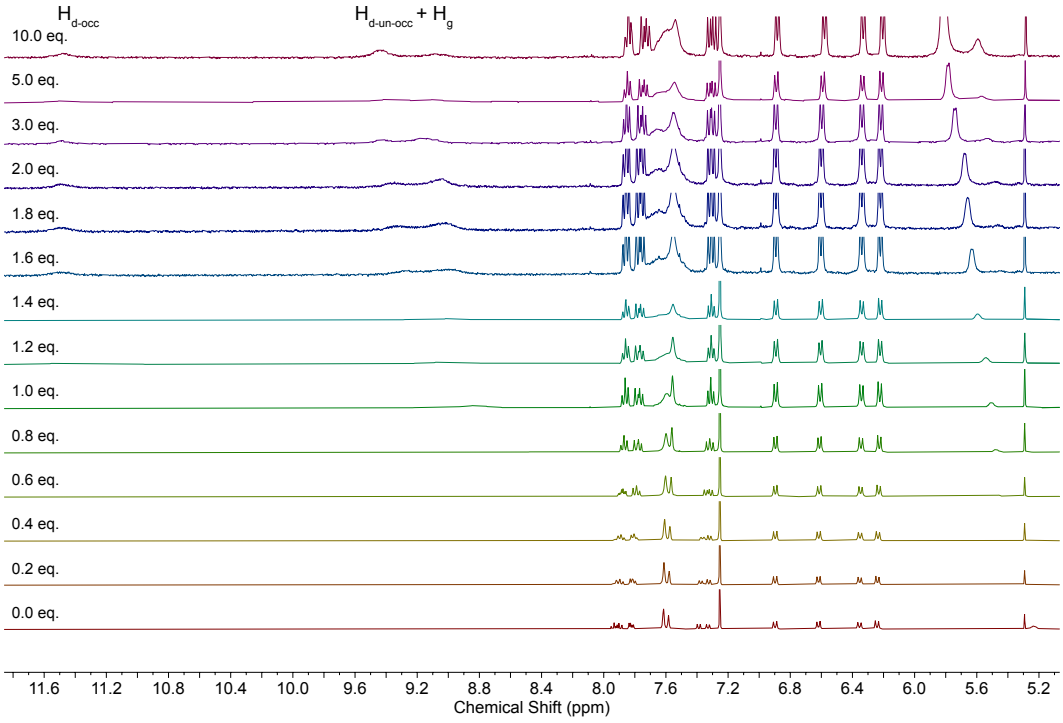

Figure 2.42 Partial ^{1}H NMR titration of **87** with **94** (0→10 eq.) in $CDCl_3$ at 298 K. Unable to unabigiously determine which is $H_{d\text{-}un\text{-}occ}$ and which peak is H_g.

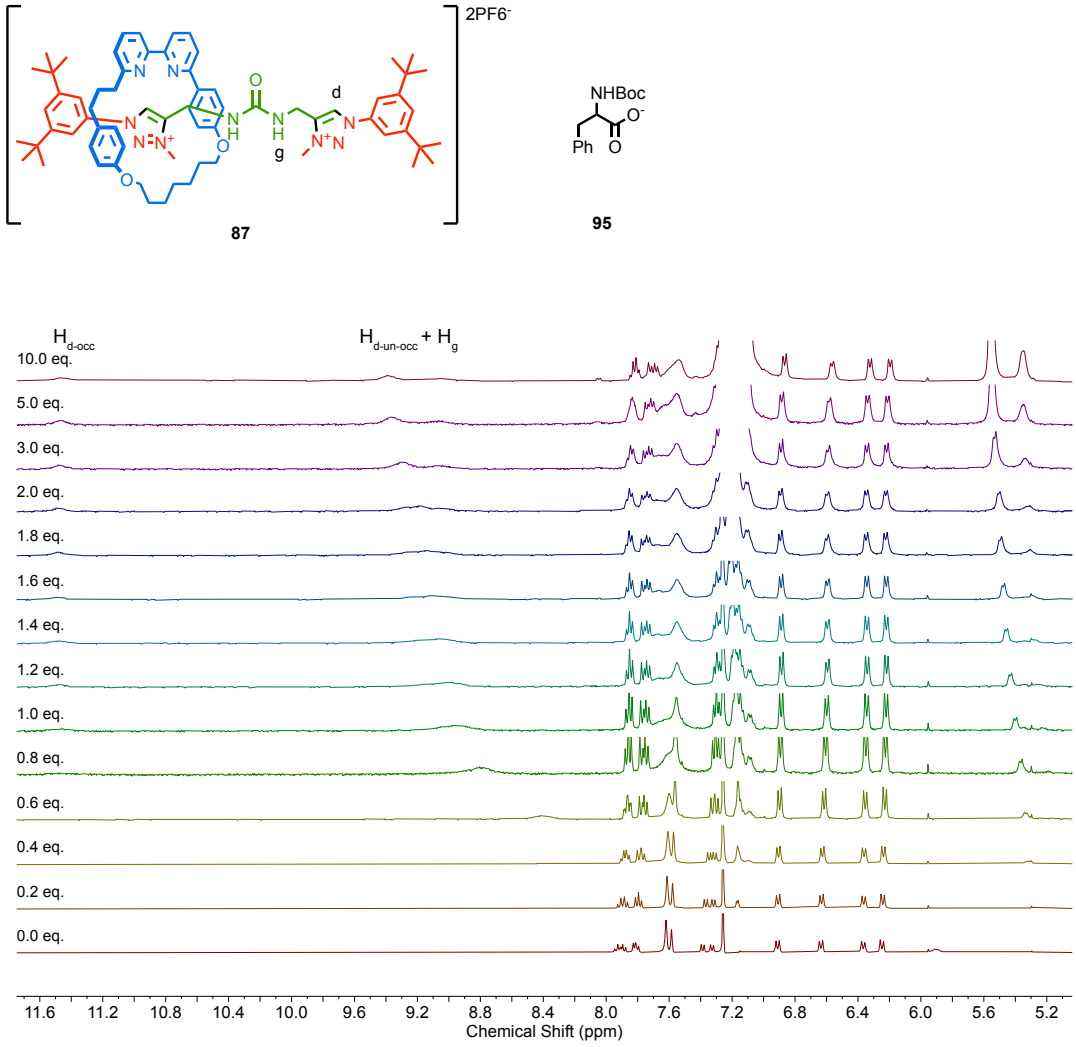

Figure 2.43 Partial ^{1}H NMR titration of **87** with **95** (0→10 eq.) in $CDCl_3$ at 298 K. Unable to unabigiously determine which is $H_{d\text{-}un\text{-}occ}$ and which peak is H_g.

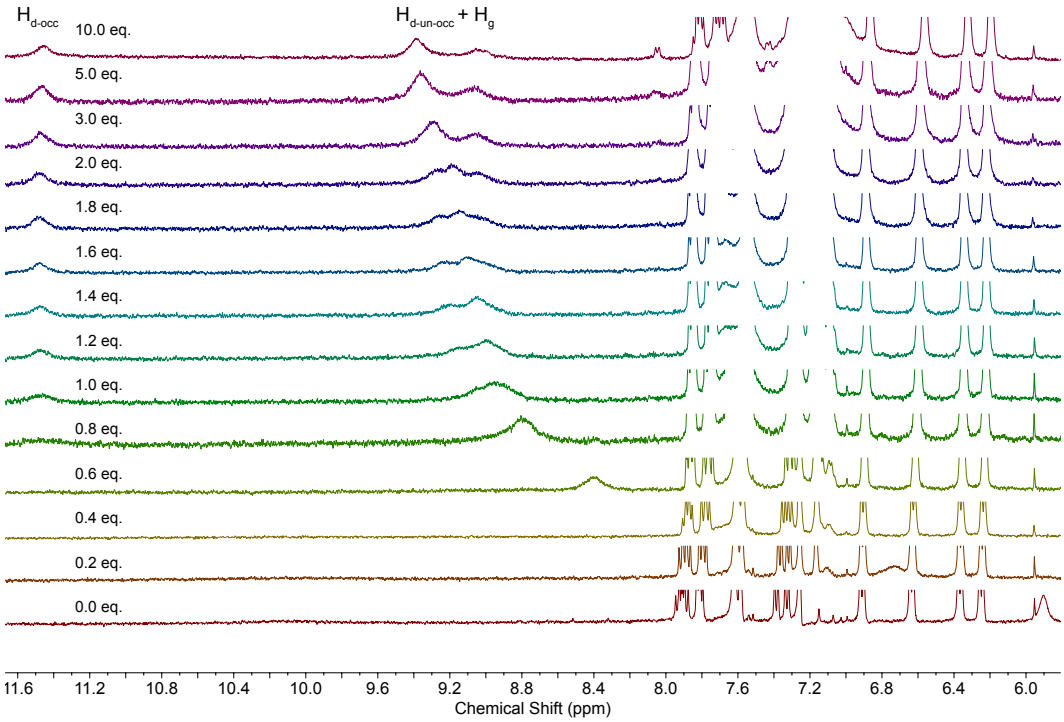

Figure 2.44 Increased intensity of the same partial ^{1}H NMR titration of **87** with **95** (0→10 eq.) in $CDCl_3$ at 298 K.

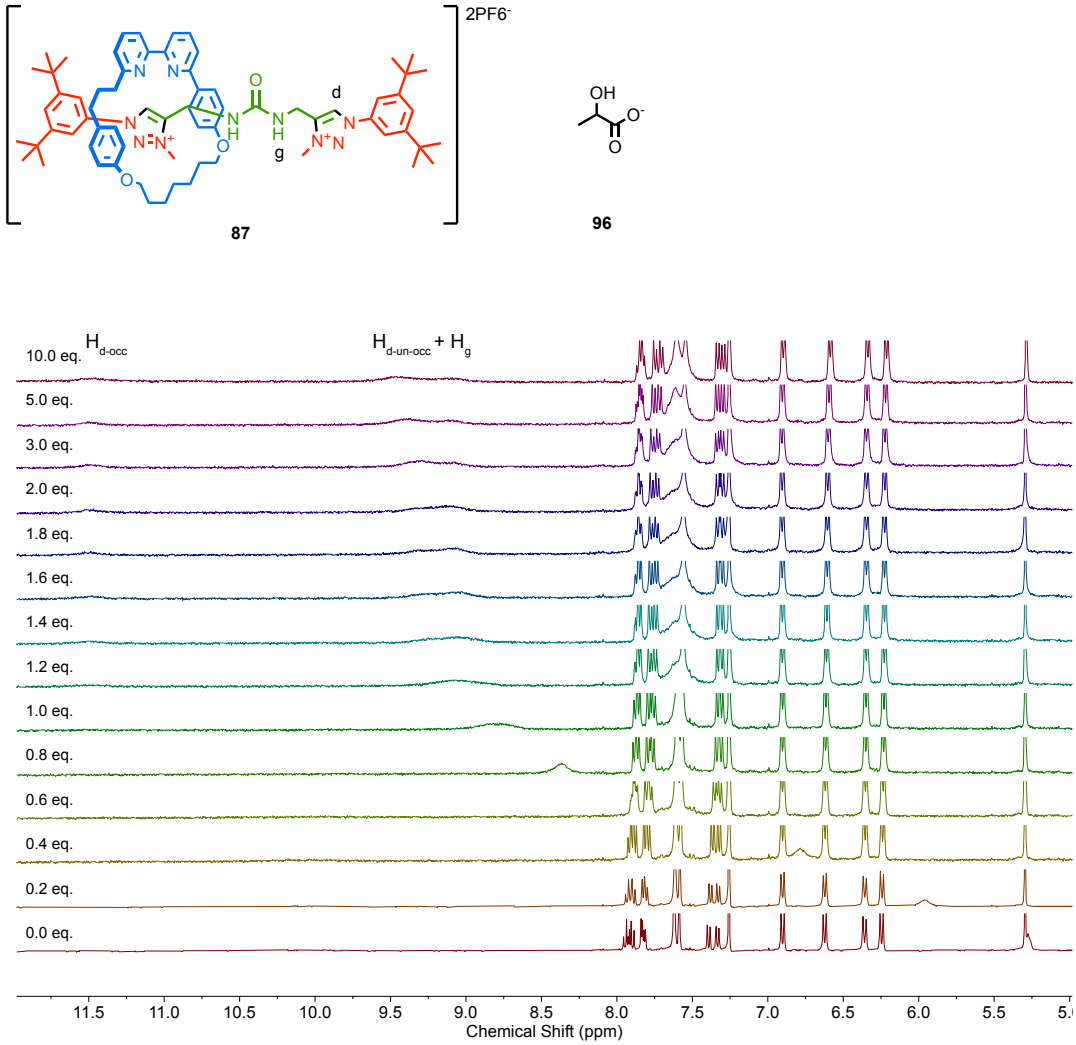

Figure 2.45 Partial ^{1}H NMR titration of **87** with **96** (0→10 eq.) in $CDCl_3$ at 298 K. Unable to unabigiously determine which is $H_{d\text{-}un\text{-}occ}$ and which peak is H_g.

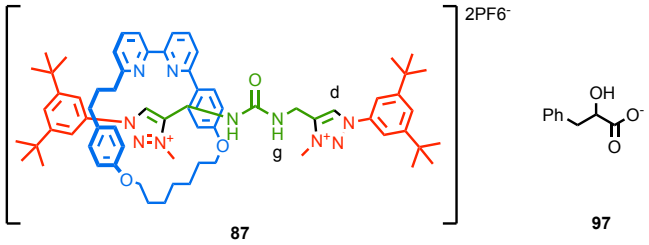

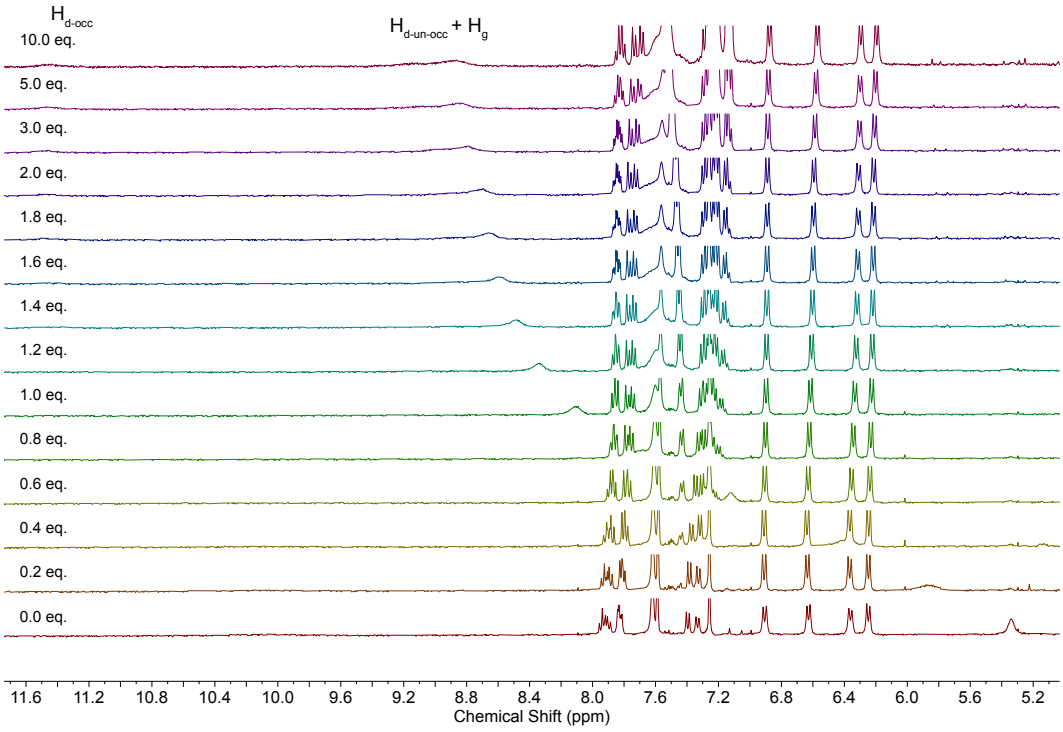

Figure 2.46 Partial ^{1}H NMR titration of **87** with **97** (0→10 eq.) in $CDCl_3$ at 298 K. Unable to unabigiously determine which is $H_{d\text{-}un\text{-}occ}$ and which peak is H_g.

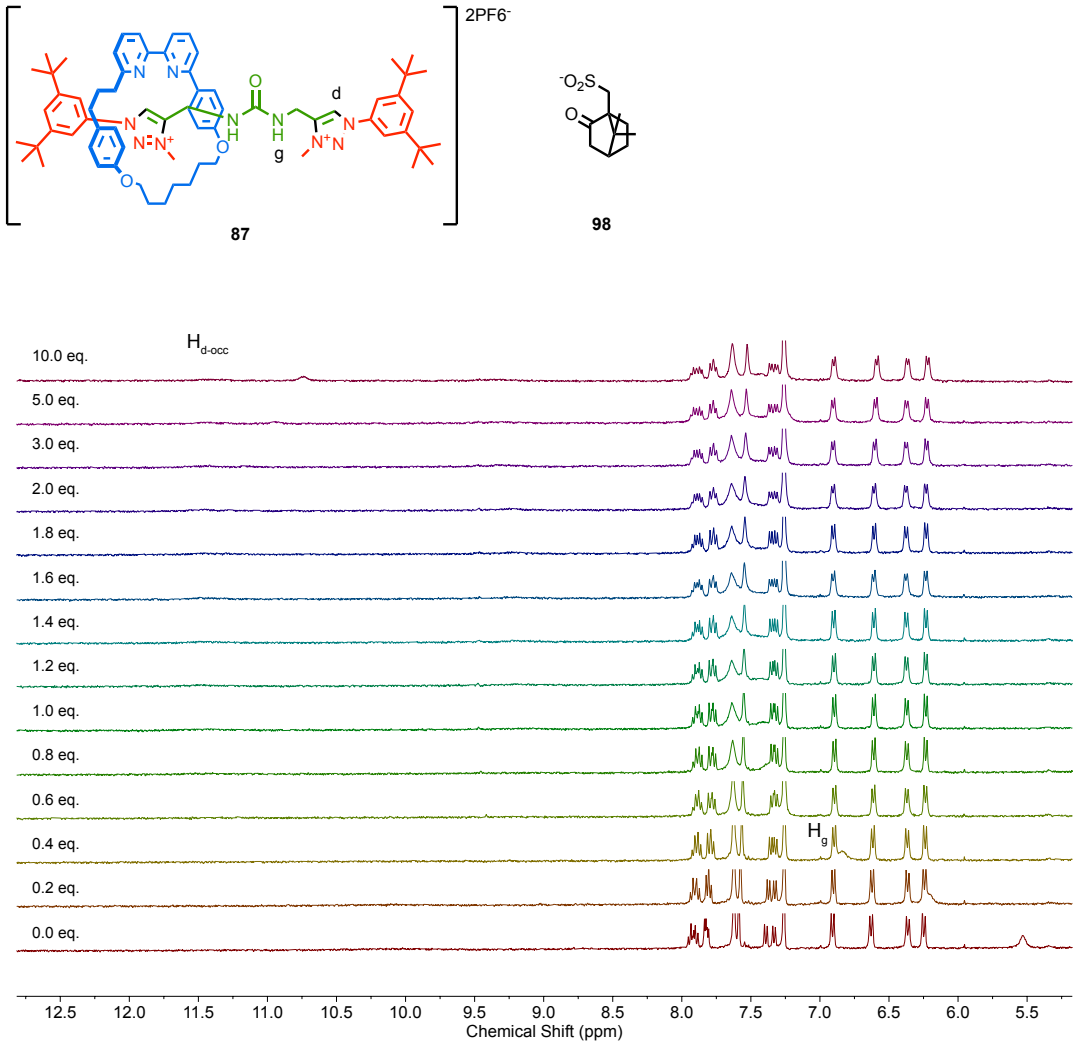

Figure 2.47 Partial ^{1}H NMR titration of **87** with **98** (0→10 eq.) in $CDCl_3$ at 298 K.

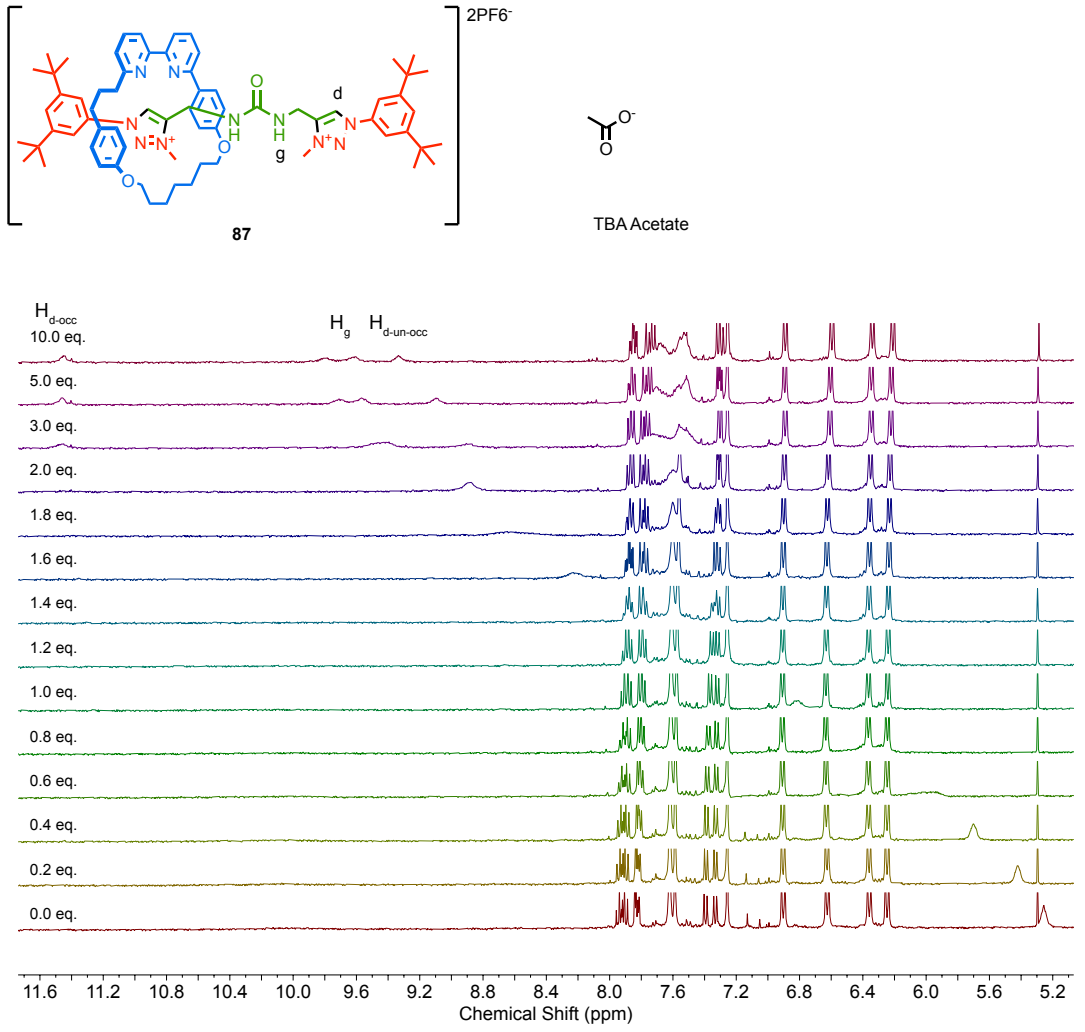

Figure 2. 48 Partial ^{1}H NMR titration of **87** with TBA Acetate (0→10 eq.) in $CDCl_3$ at 298 K.

VT NMR Studies

*VT ^{1}H NMR of **87** and Guests*

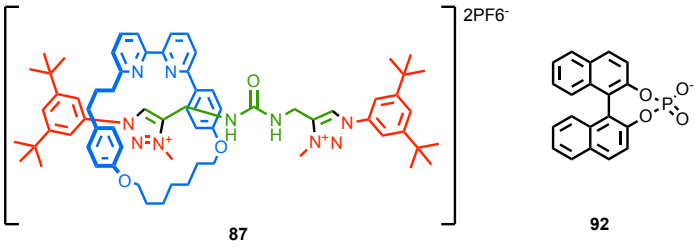

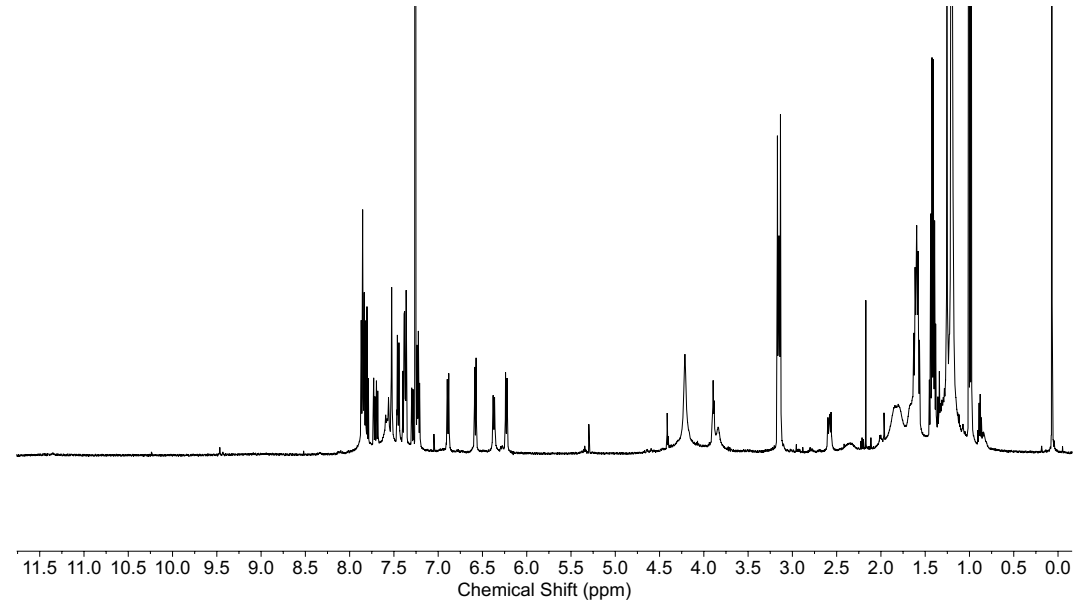

Figure 2.49 ^{1}H NMR (500 MHz, $CDCl_3$) of 1:1 **87**:**92** at 293 K.

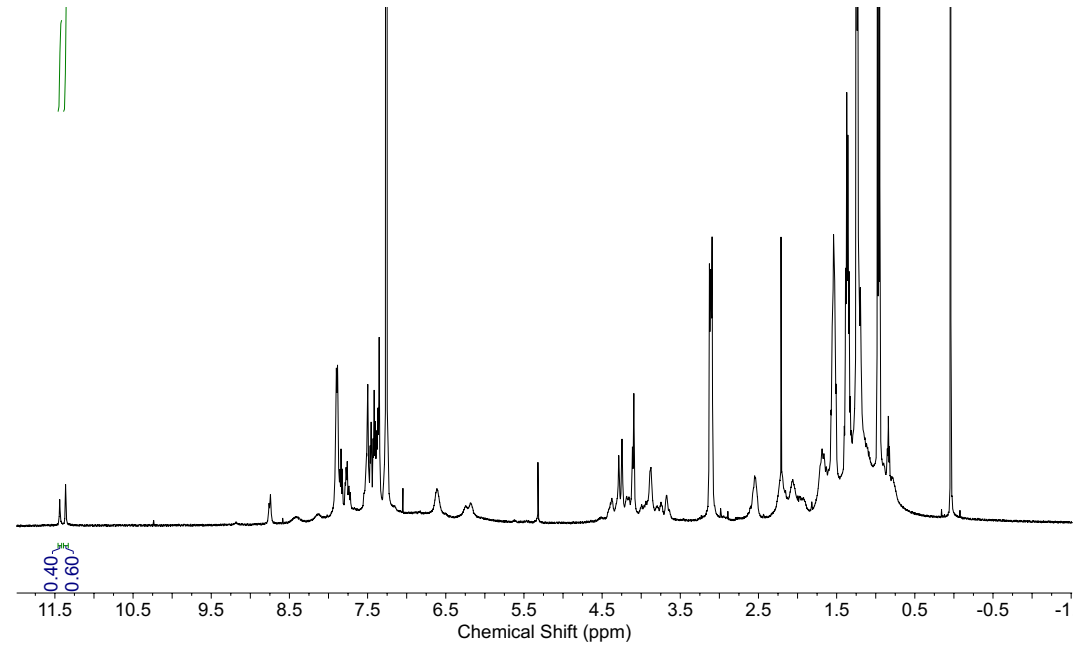

Figure 2.50 ^{1}H NMR (500 MHz, $CDCl_3$) of 1:1 **87**:**92** at 223 K.

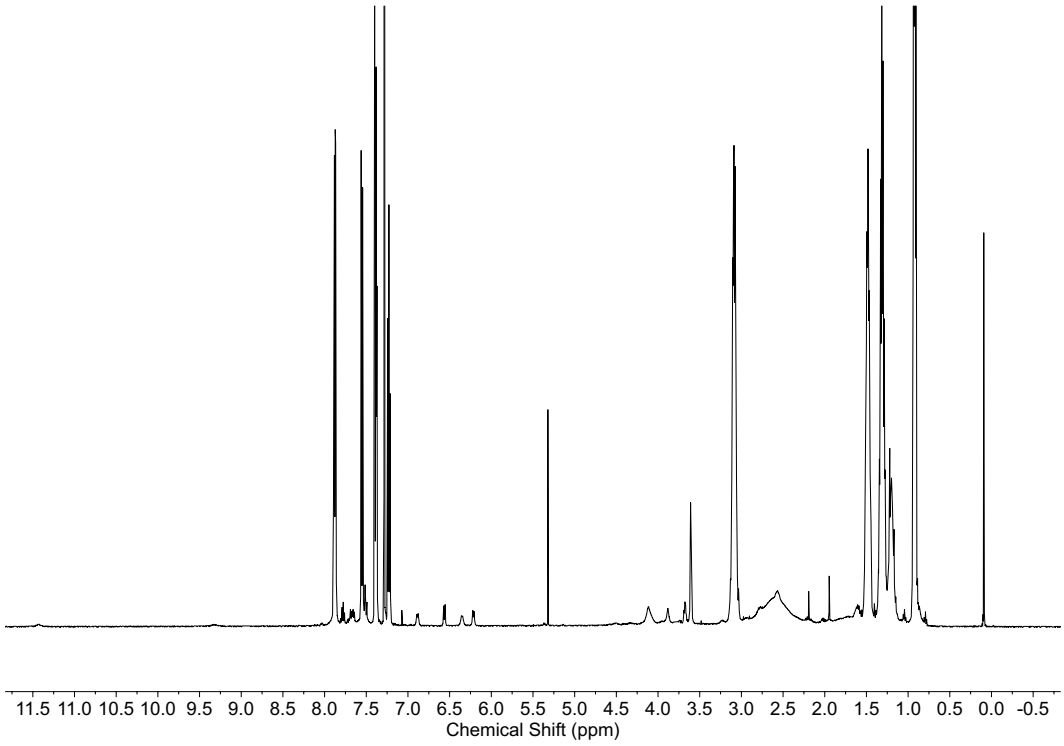

Figure 2. 51 ^{1}H NMR (500 MHz, $CDCl_3$) of 1:10 **87**:**92** at 293 K.

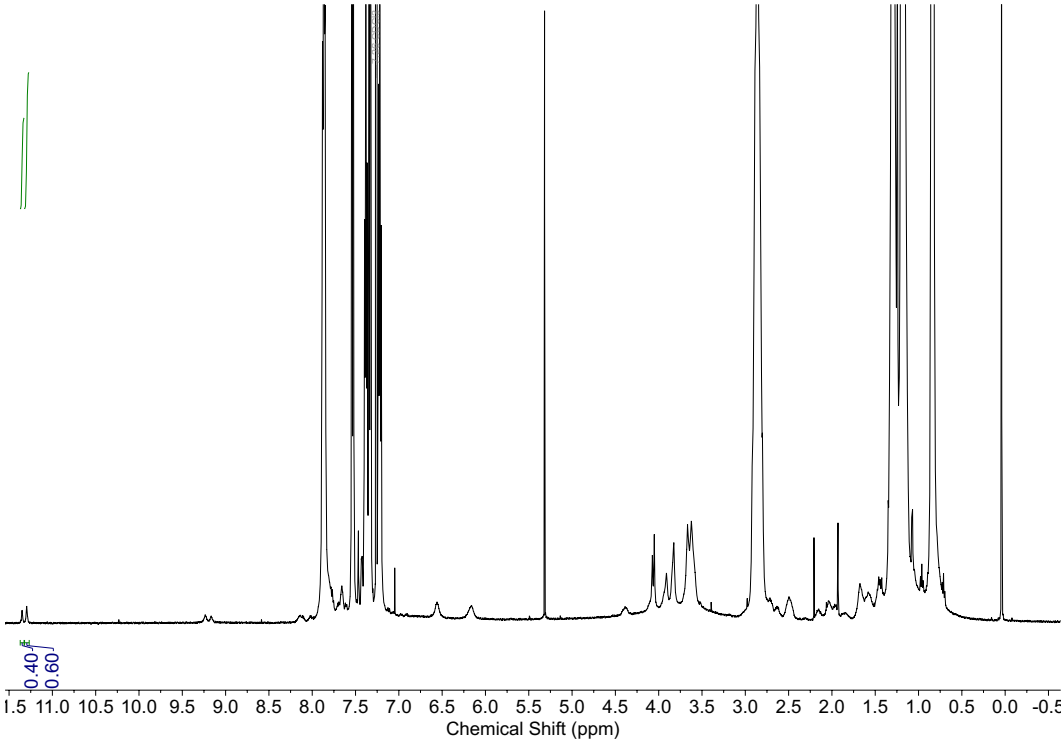

Figure 2. 52 ^{1}H NMR (500 MHz, $CDCl_3$) of 1:10 **87**:**92** at 223 K

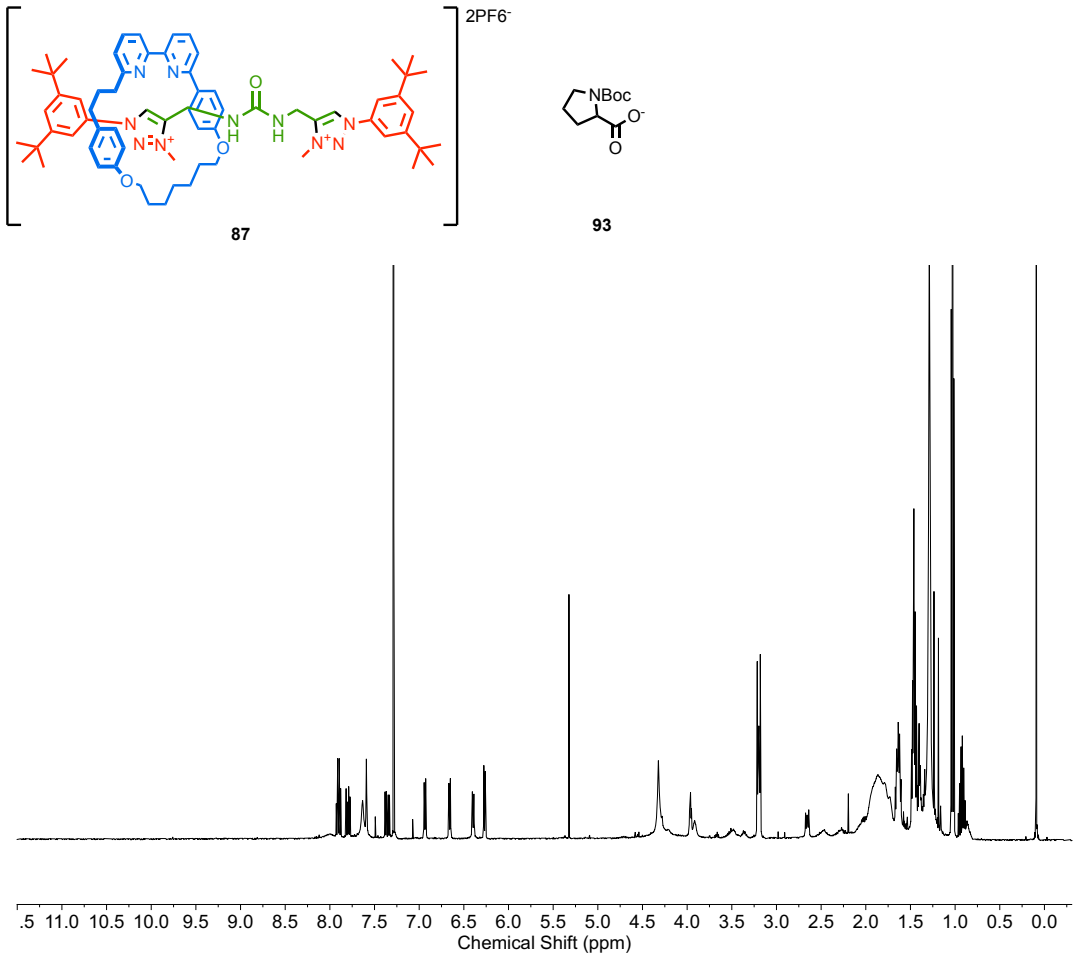

Figure 2.53 ^{1}H NMR (500 MHz, $CDCl_3$) of 1:1 **87**:**93** at 293 K

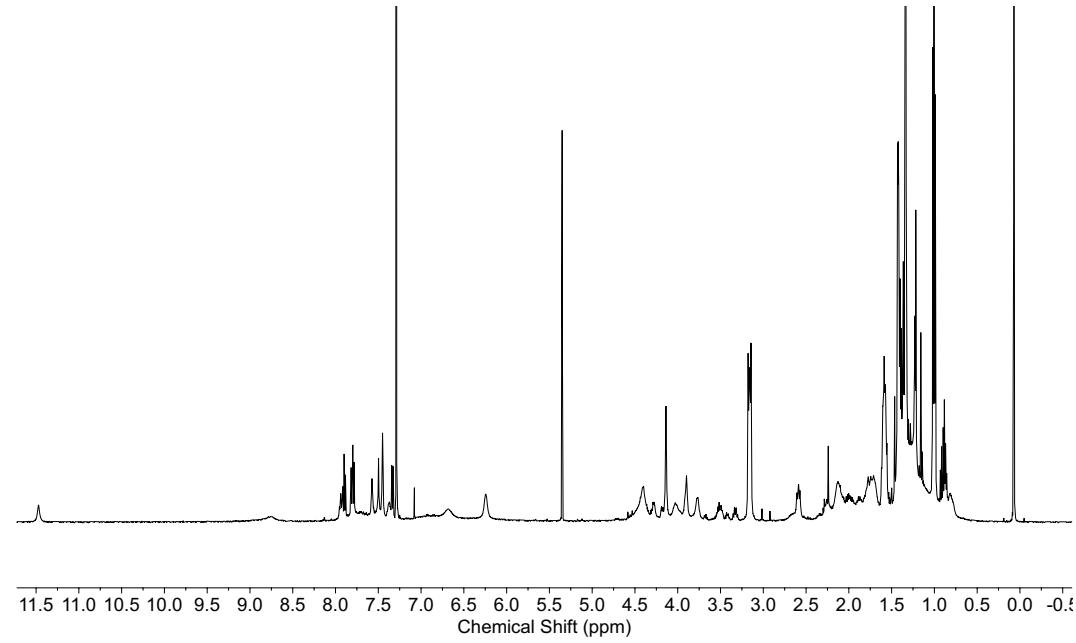

Figure 2.54 ^{1}H NMR (500 MHz, $CDCl_3$) of 1:1 **87**:**93** at 223 K.

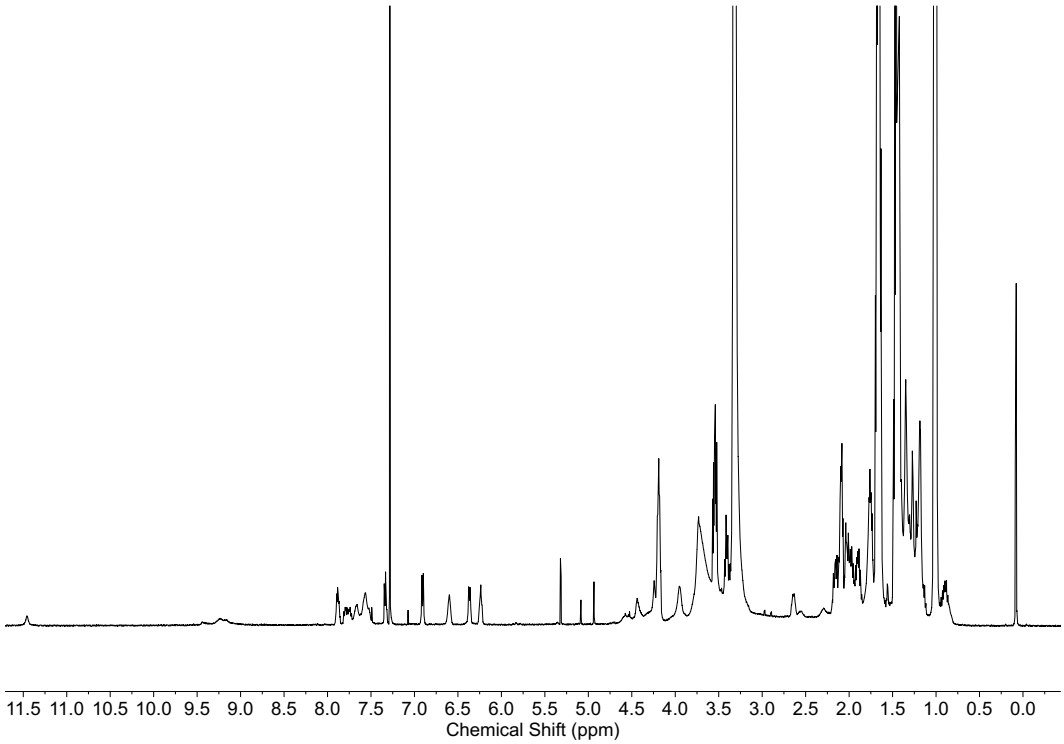

Figure 2. 55 ^{1}H NMR (500 MHz, $CDCl_3$) of 1:10 **87**:**93** at 293 K.

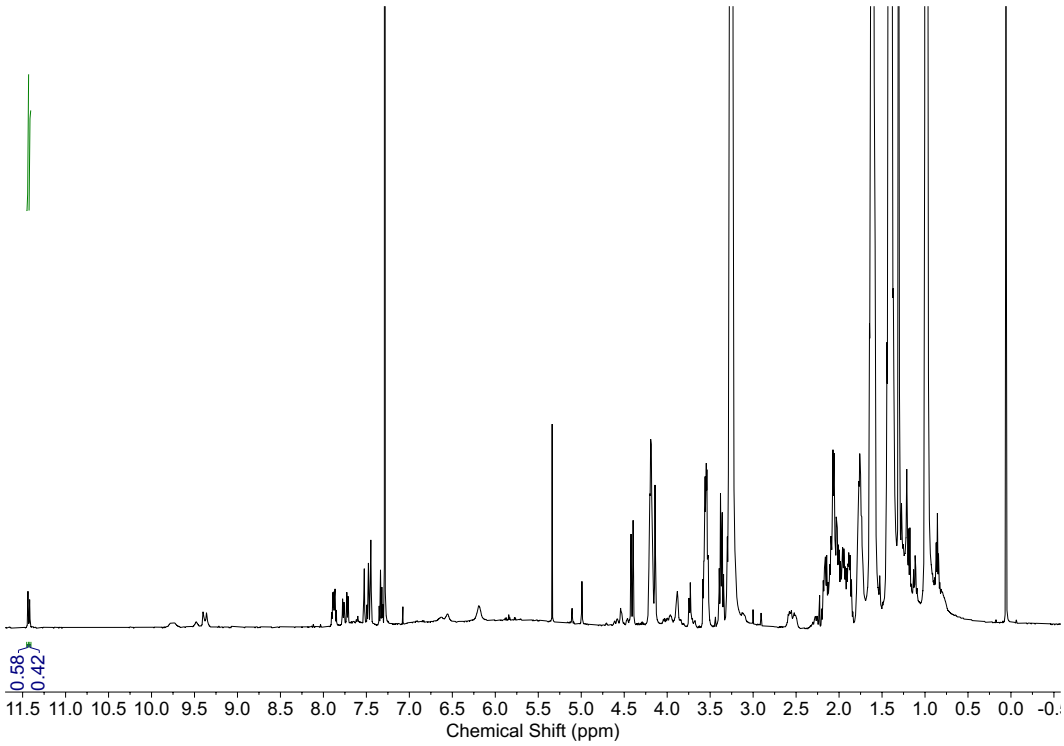

Figure 2. 56 ^{1}H NMR (500 MHz, $CDCl_3$) of 1:10 **87**:**93** at 223 K

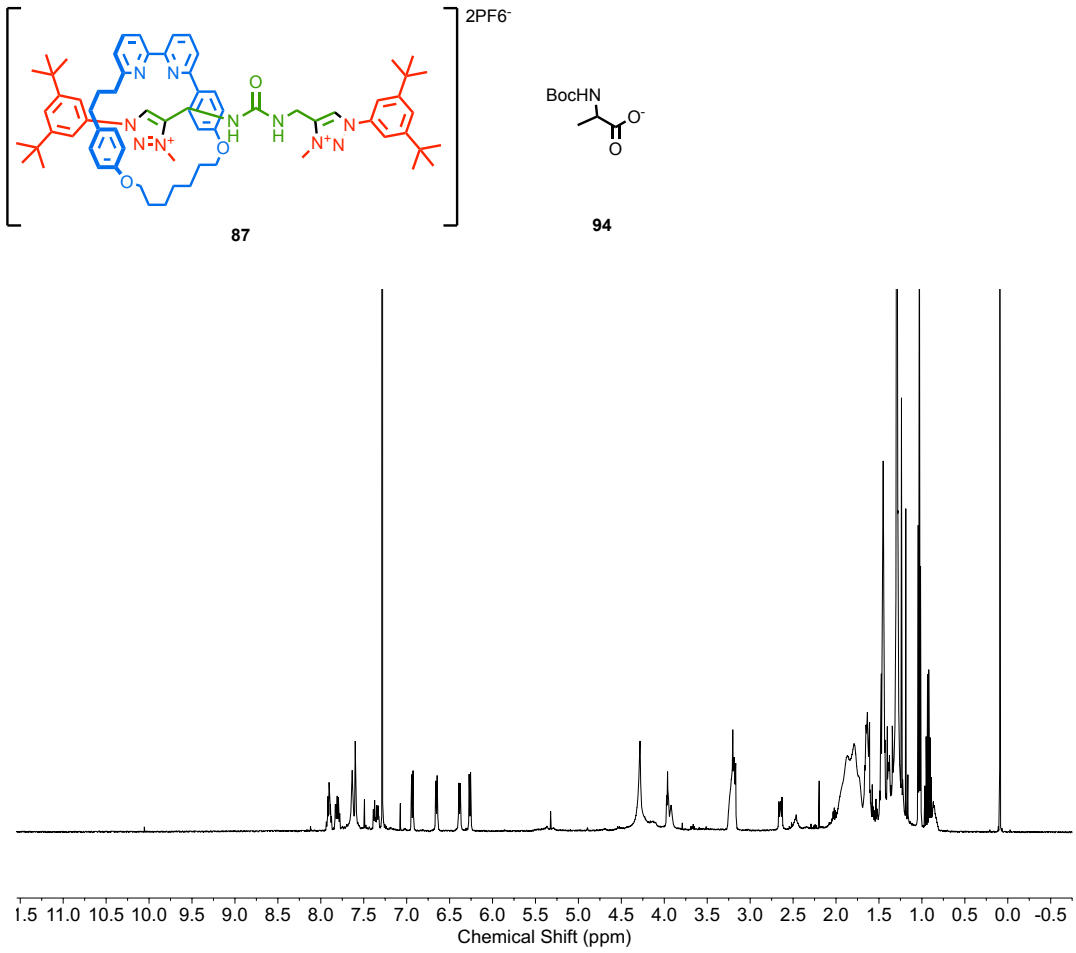

Figure 2.57 ^{1}H NMR (500 MHz, $CDCl_3$) of 1:1 **87**:**94** at 293 K.

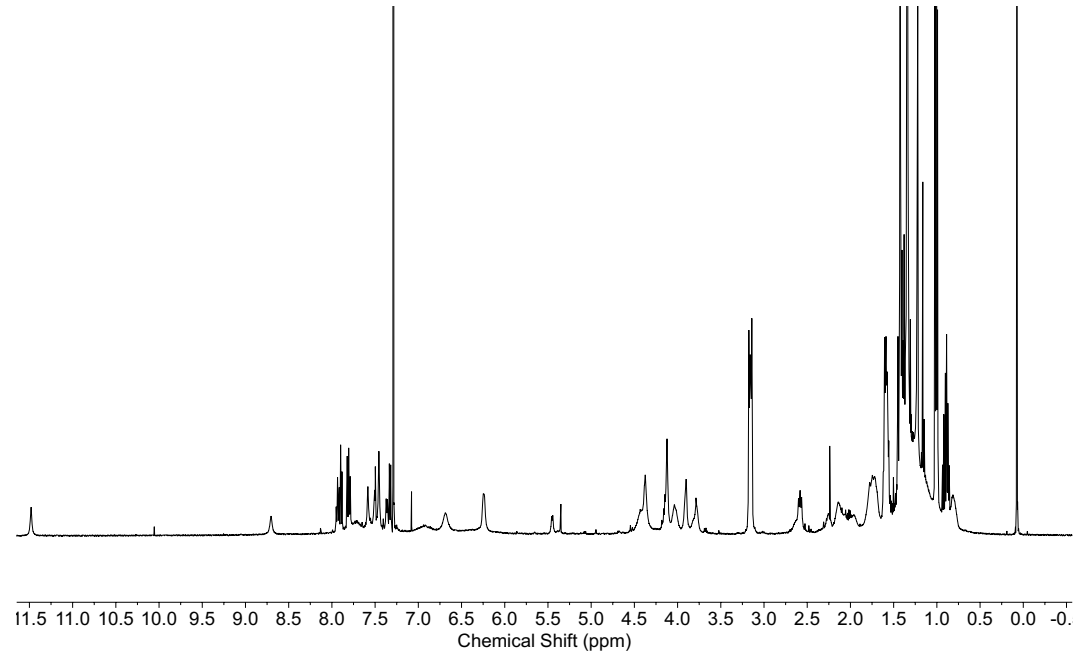

Figure 2.58 ^{1}H NMR (500 MHz, $CDCl_3$) of 1:1 **87**:**94** at 223 K.

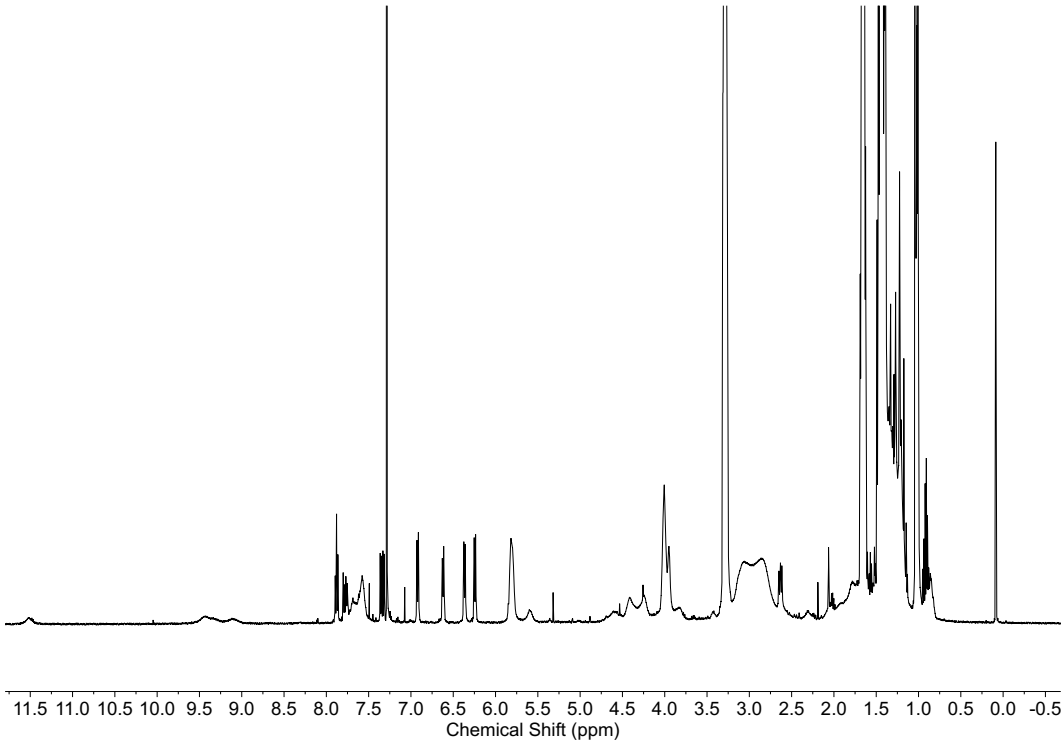

Figure 2.59 ^{1}H NMR (500 MHz, $CDCl_3$) of 1:10 **87**:**94** at 293 K.

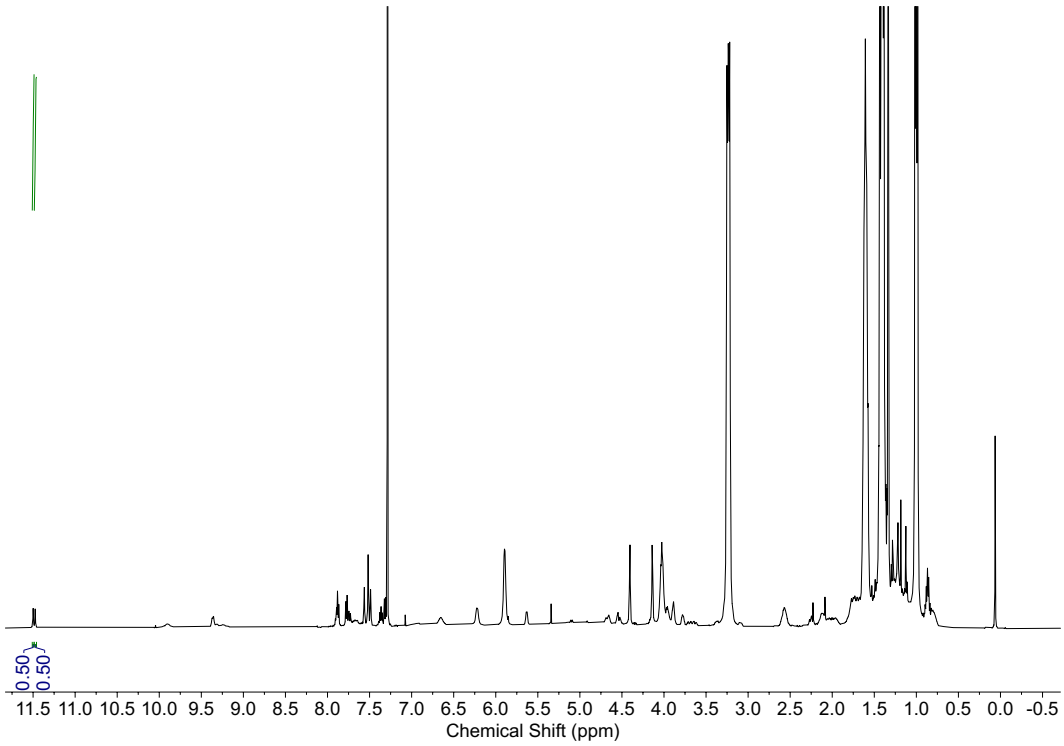

Figure 2.60 ^{1}H NMR (500 MHz, $CDCl_3$) of 1:10 **87:94** at 223 K.

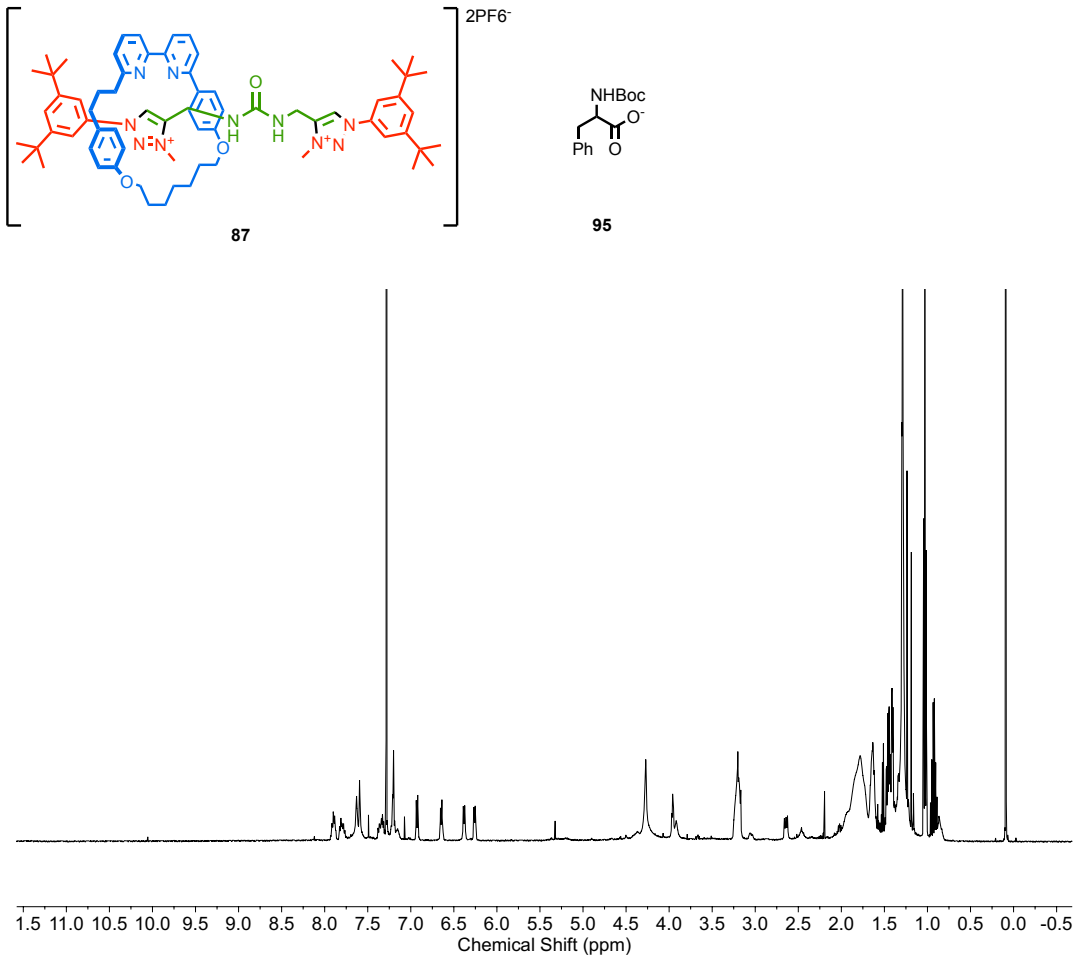

Figure 2.61 ^{1}H NMR (500 MHz, $CDCl_3$) of 1:1 **87**:**95** at 293 K.

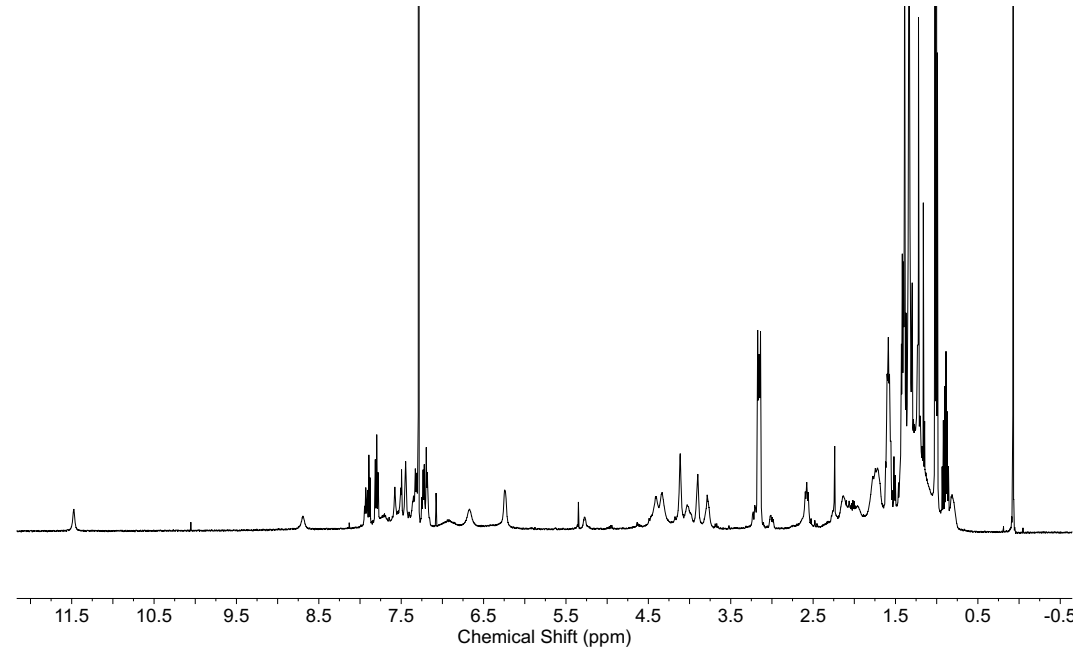

Figure 2.62 ^{1}H NMR (500 MHz, $CDCl_3$) of 1:1 **87**:**95** at 223 K.

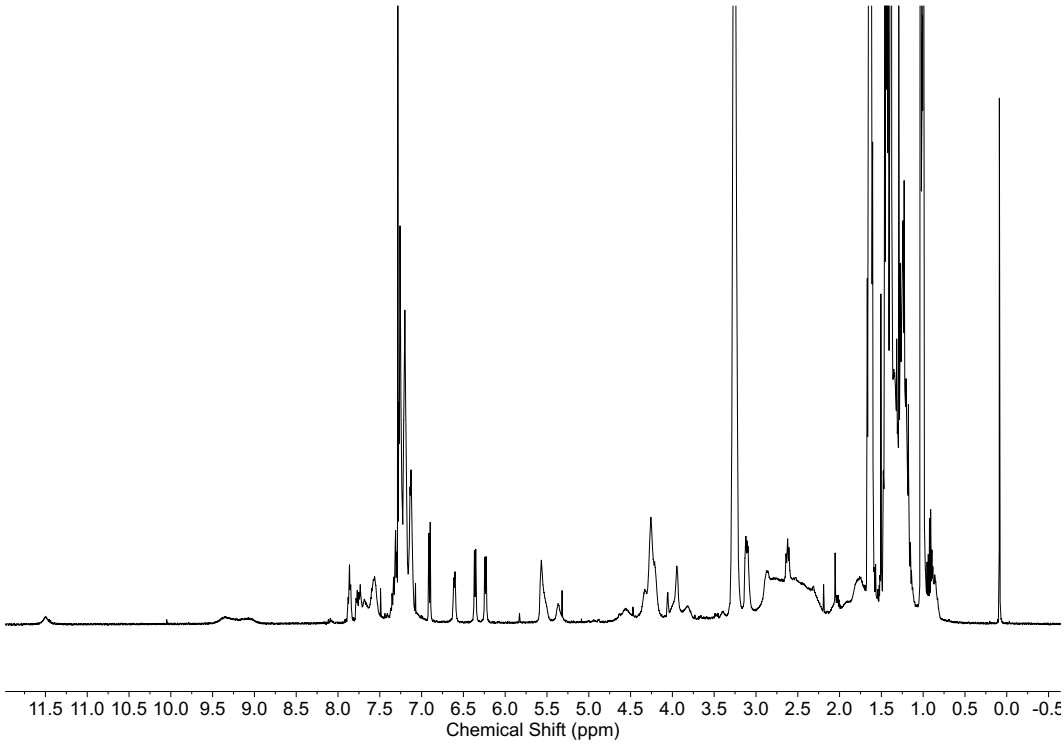

Figure 2.63 ^{1}H NMR (500 MHz, $CDCl_3$) of 1:10 **87**:**95** at 293 K.

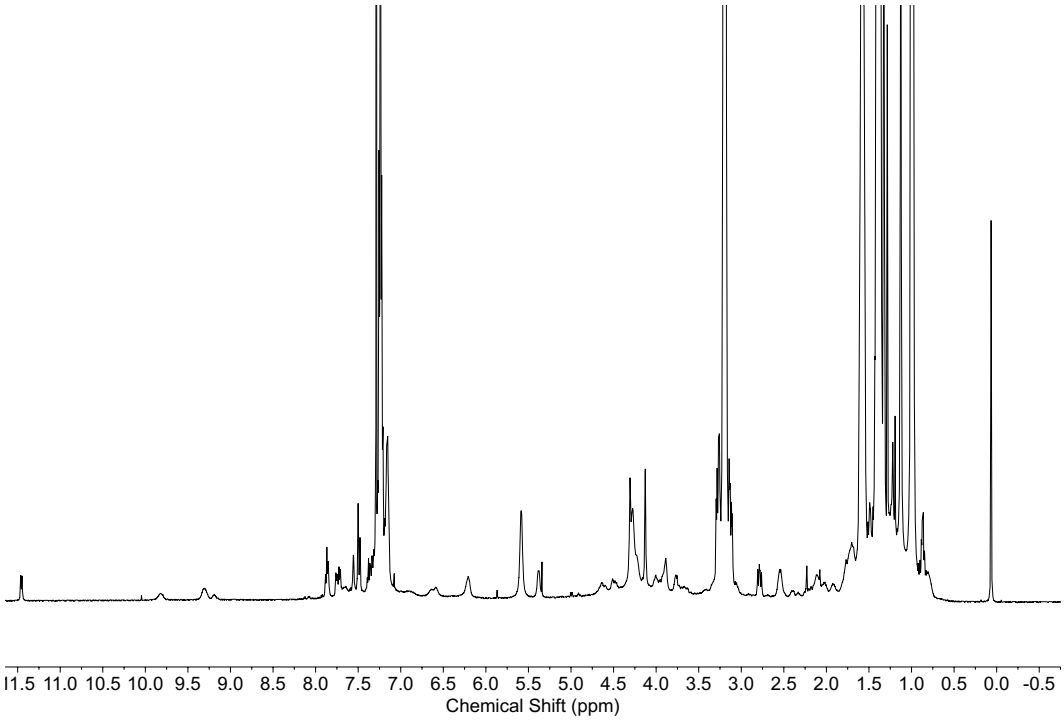

Figure 2.64 ^{1}H NMR (500 MHz, $CDCl_3$) of 1:10 **87**:**95** at 223 K.

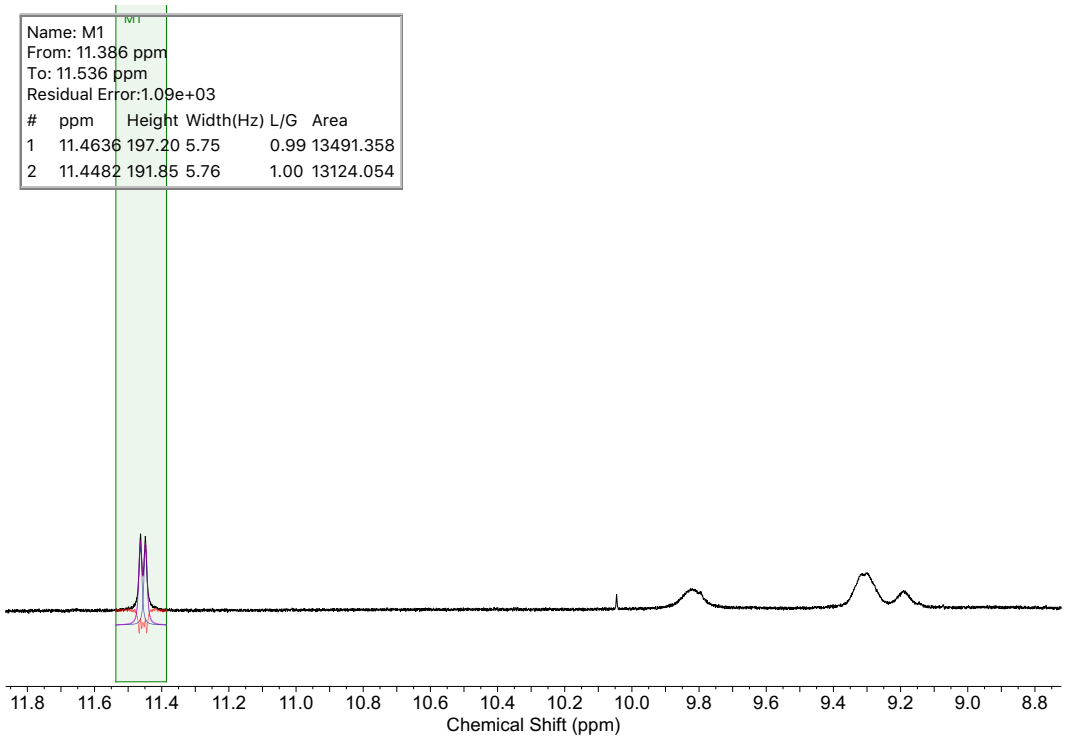

Figure 2.65 Partial ^{1}H NMR (500 MHz, $CDCl_3$) of 1:10 **87**:**95** at 223 K with deconvolution of peaks.

Due to overlap between occupied triazolium protons, the peaks were deconvoluted using MestReNova's line fitting tool. The peak area was used to calculate the diastereoisomeric ratio of 1:1.

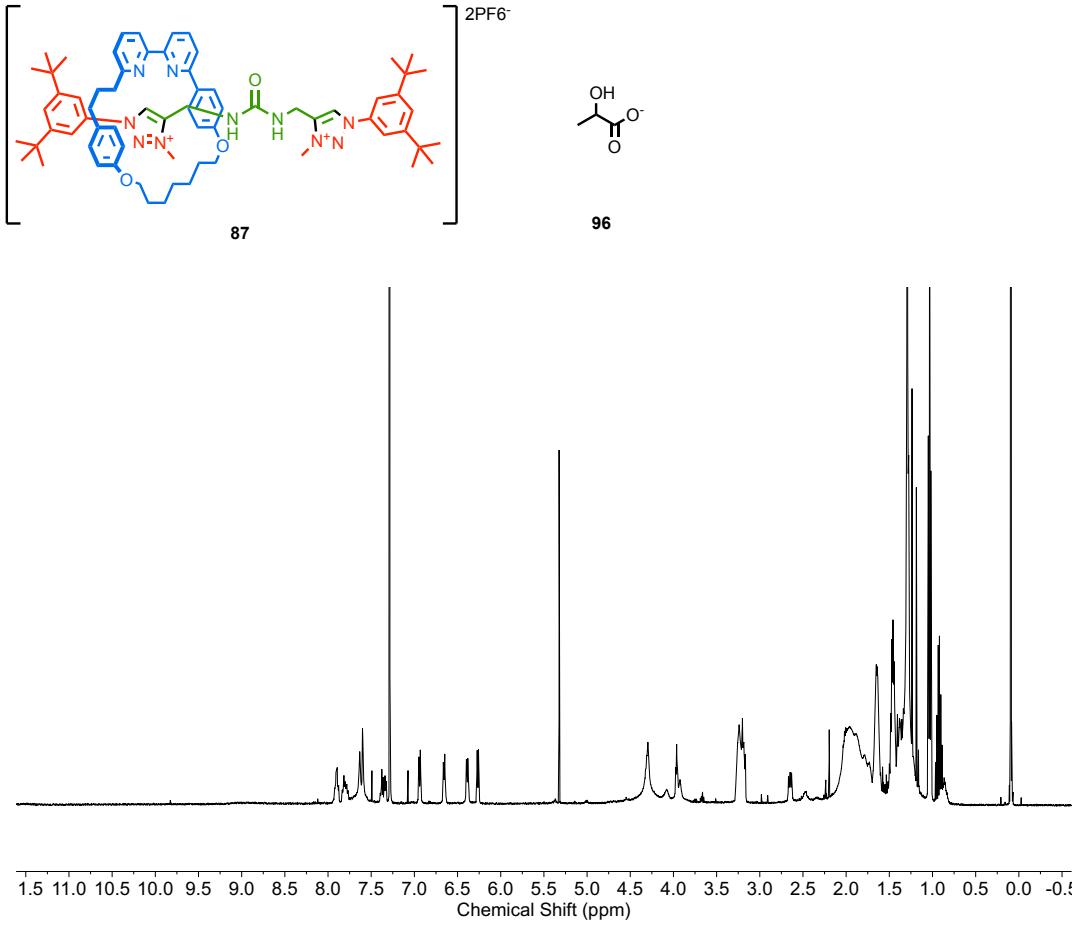

Figure 2.66 ^{1}H NMR (500 MHz, $CDCl_3$) of 1:1 **87**:**96** at 293 K.

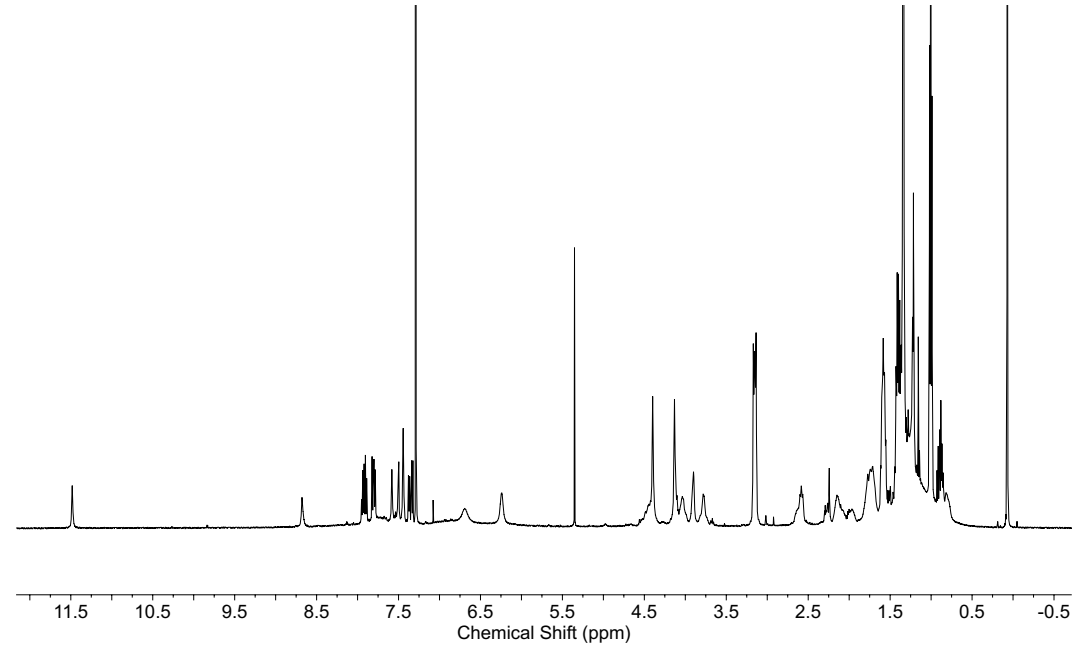

Figure 2.67 ^{1}H NMR (500 MHz, $CDCl_3$) of 1:1 **87**:**96** at 223 K.

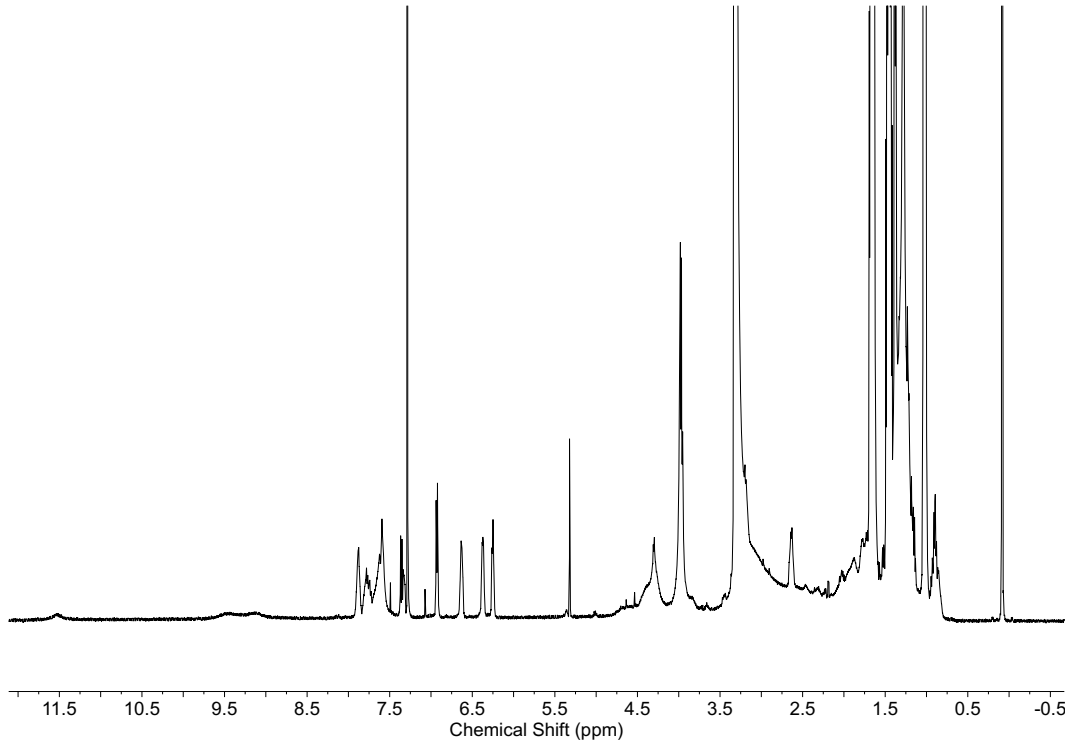

Figure 2.68 ^{1}H NMR (500 MHz, $CDCl_3$) of 1:10 **87**:**96** at 293 K.

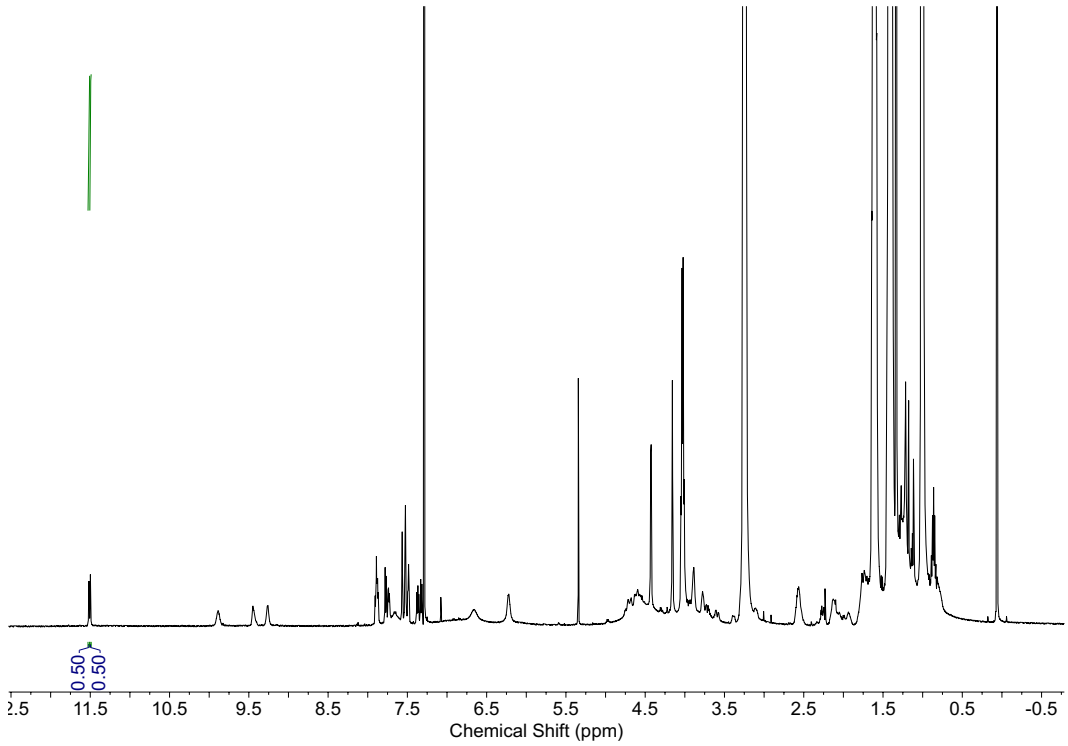

Figure 2.69 ^{1}H NMR (500 MHz, $CDCl_3$) of 1:10 **87**:**96** at 223 K.

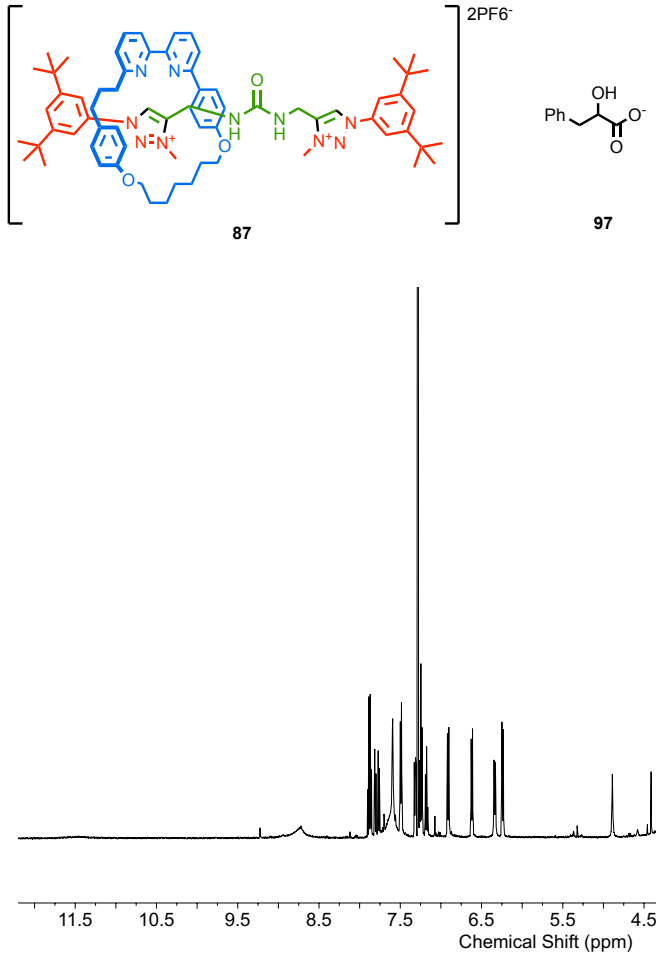

Figure 2.70 ^{1}H NMR (500 MHz, $CDCl_3$) of 1:1 **87**:**97** at 293 K.

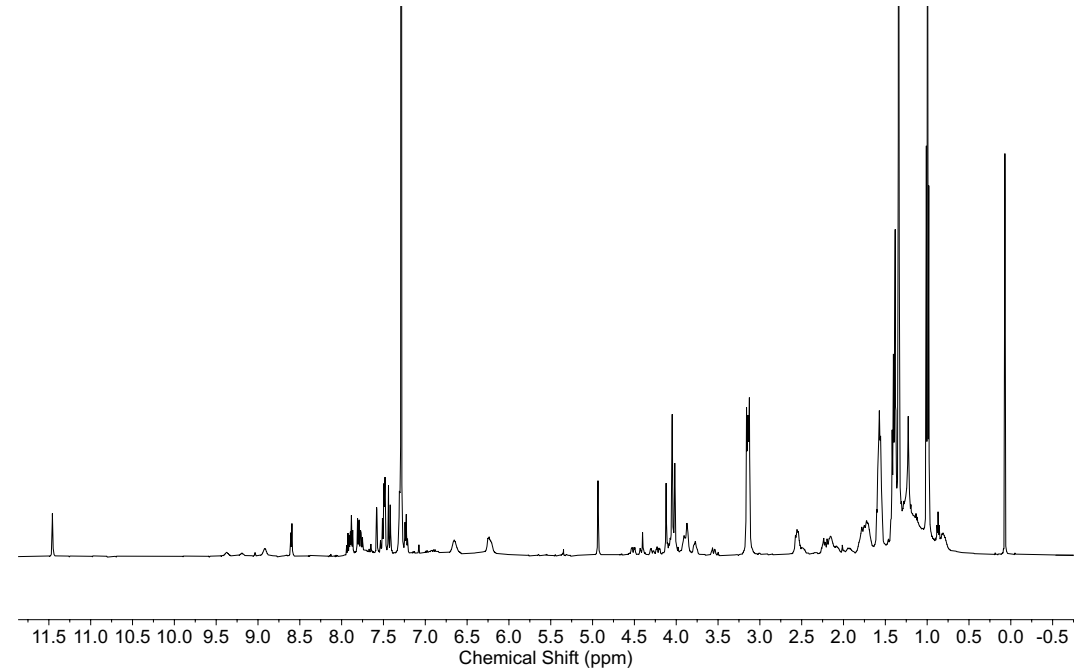

Figure 2.71 ^{1}H NMR (500 MHz, $CDCl_3$) of 1:1 **87**:**97** at 223 K.

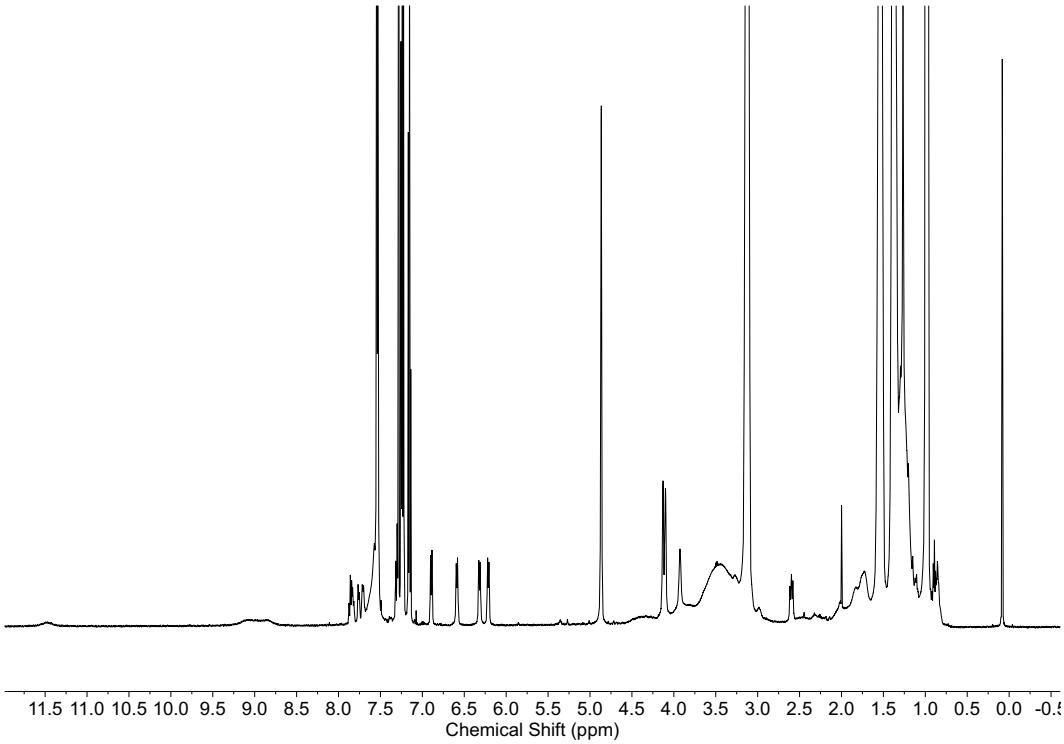

Figure 2.72 ^{1}H NMR (500 MHz, $CDCl_3$) of 1:10 **87**:**97** at 293 K.

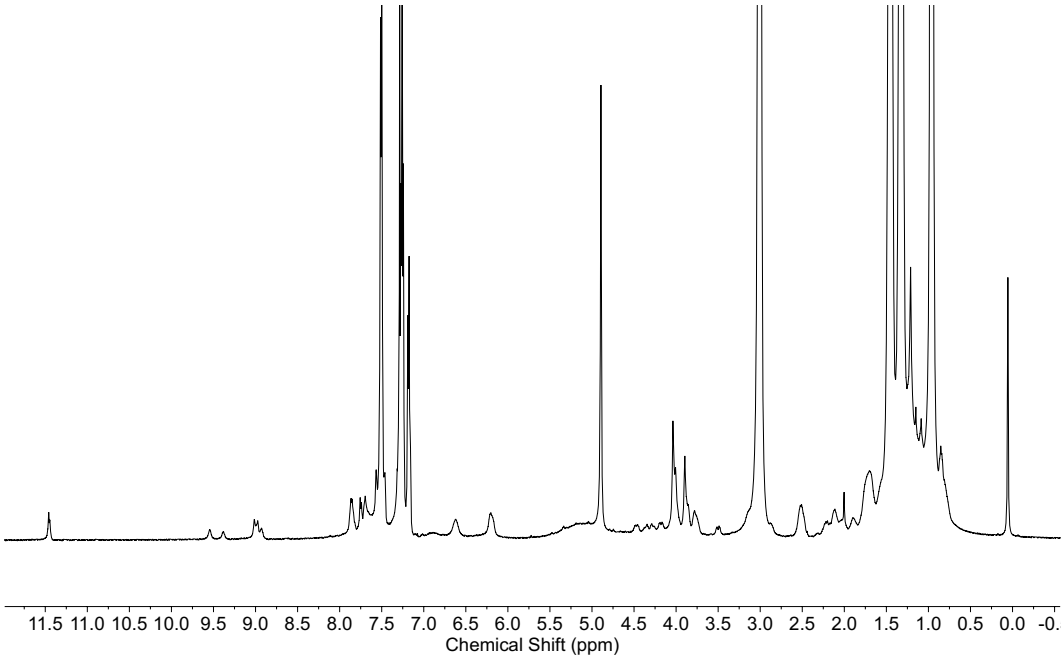

Figure 2.73 ^{1}H NMR (500 MHz, $CDCl_3$) of 1:10 **87**:**97** at 223 K.

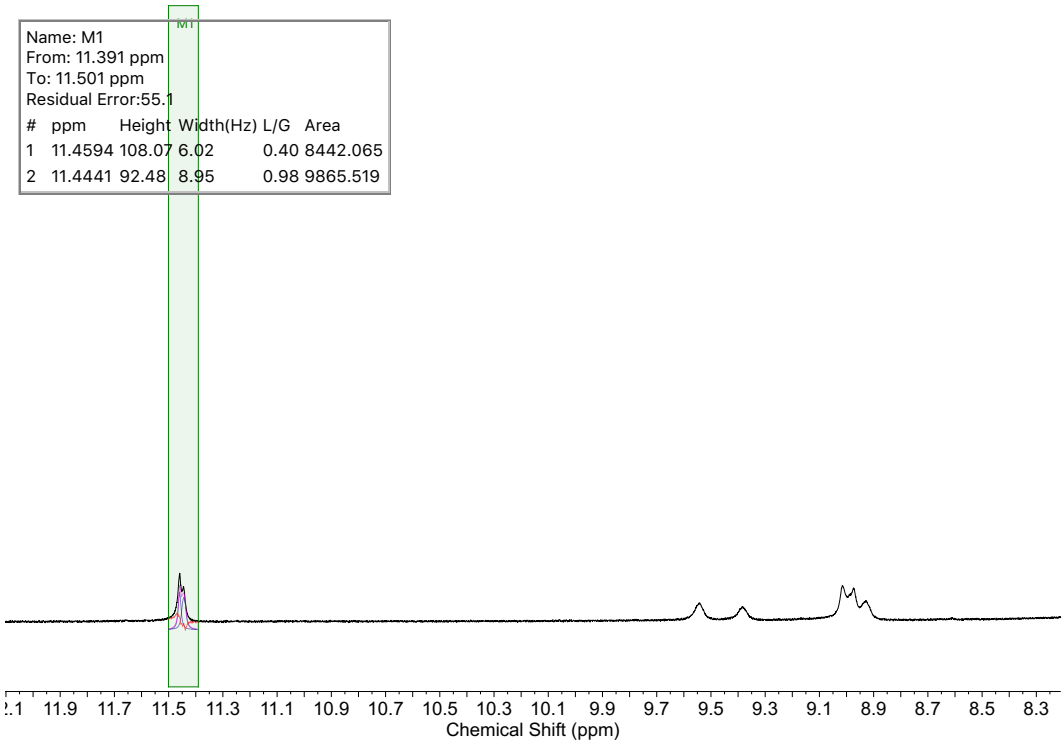

Figure 2. 74 Partial ^{1}H NMR (500 MHz, $CDCl_3$) of 1:10 **87**:**97** at 223 K with deconvolution of peaks.

Due to overlap between occupied triazolium protons, the peaks were deconvoluted using MestReNova's line fitting tool. The peak area was used to calculate the diastereoisomeric ratio of 1:1.

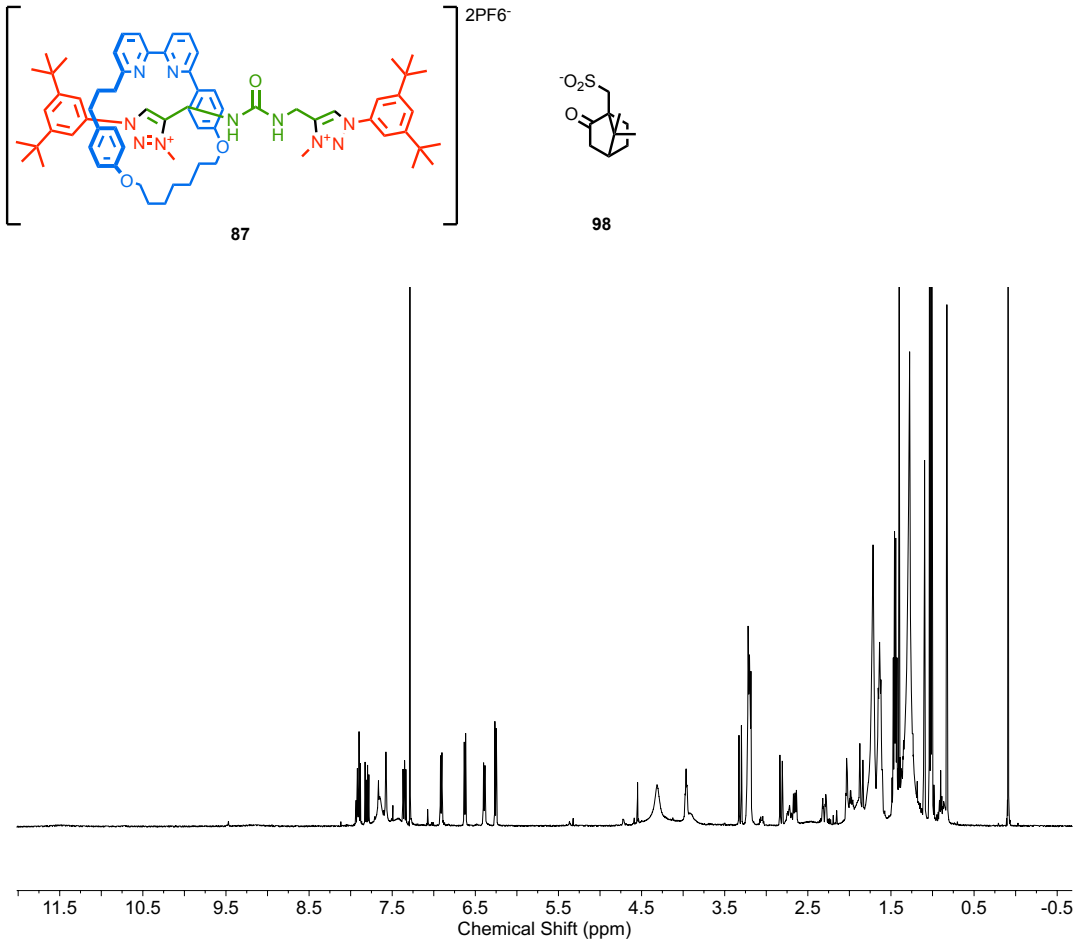

Figure 2.75 ^{1}H NMR (500 MHz, $CDCl_3$) of 1:1 **87**:**98** at 293 K.

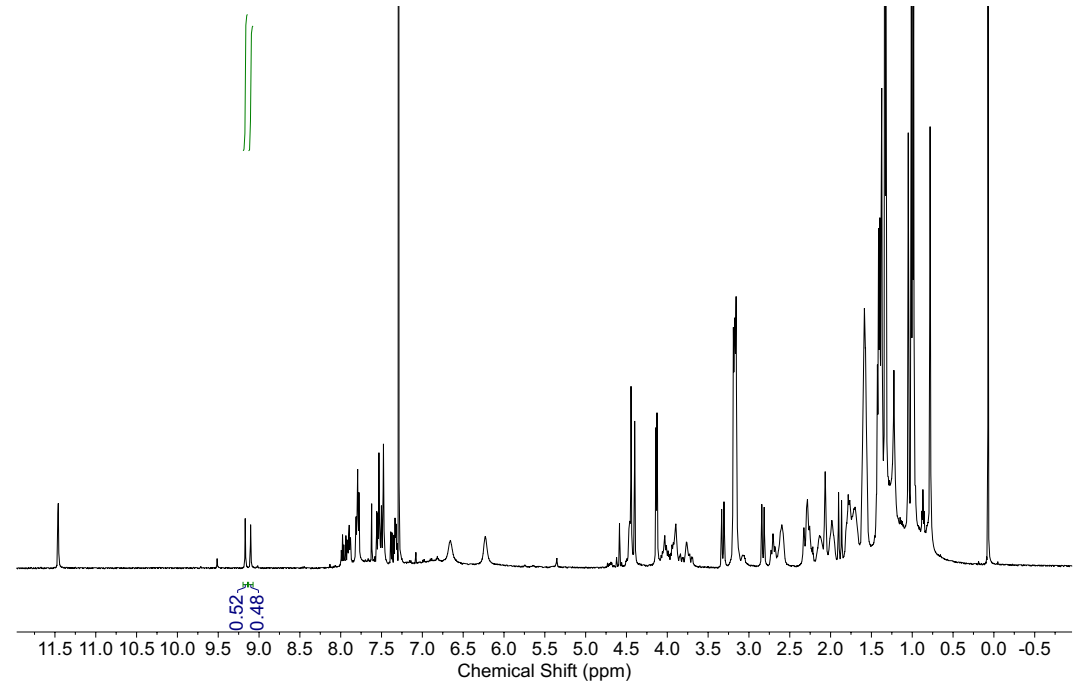

Figure 2.76 ^{1}H NMR (500 MHz, $CDCl_3$) of 1:1 **87**:**98** at 223 K.

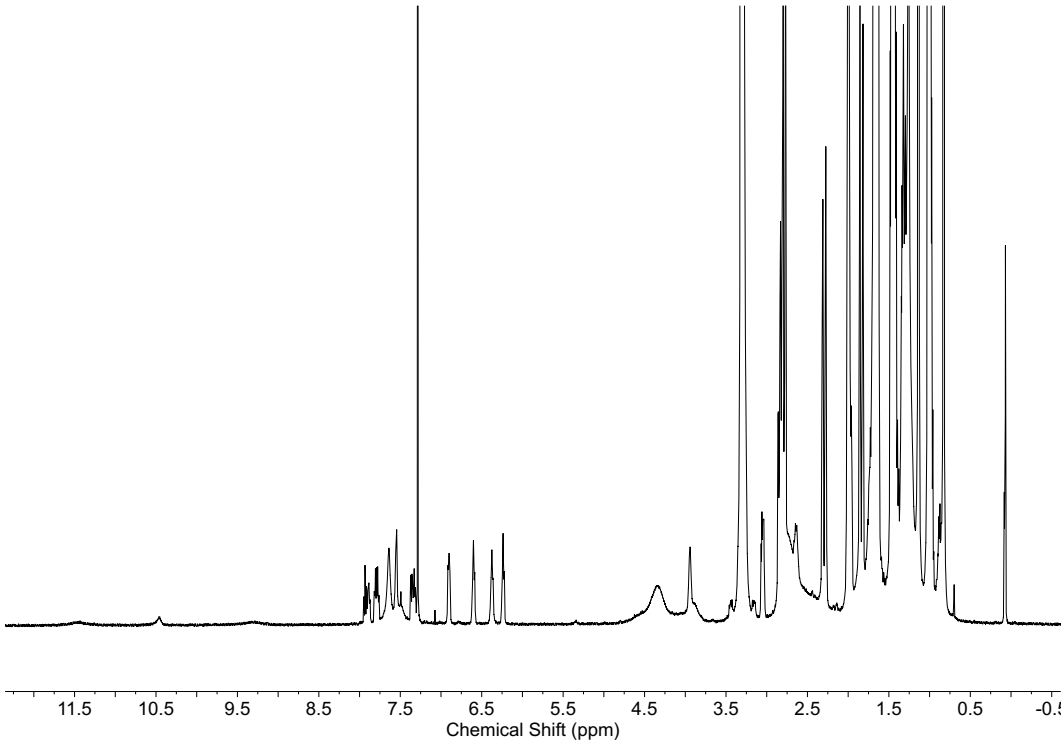

Figure 2.77 ^{1}H NMR (500 MHz, $CDCl_3$) of 1:10 **87**:**98** at 293 K.

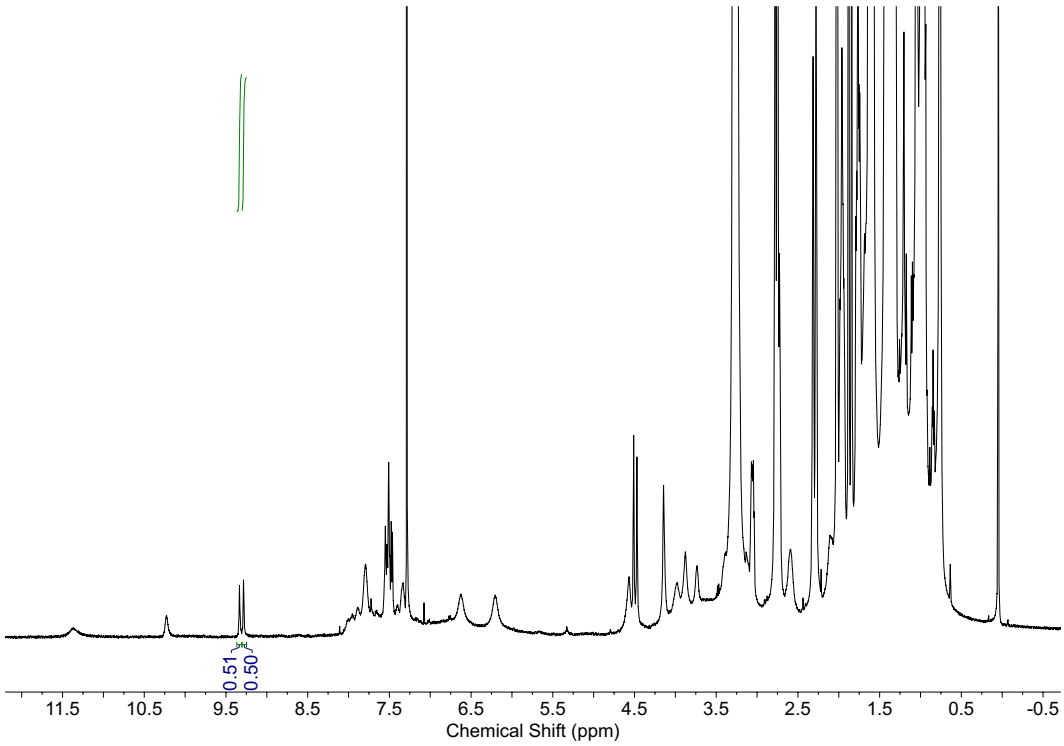

Figure 2.78 ^{1}H NMR (500 MHz, $CDCl_3$) of 1:10 **87**:**98** at 223 K.

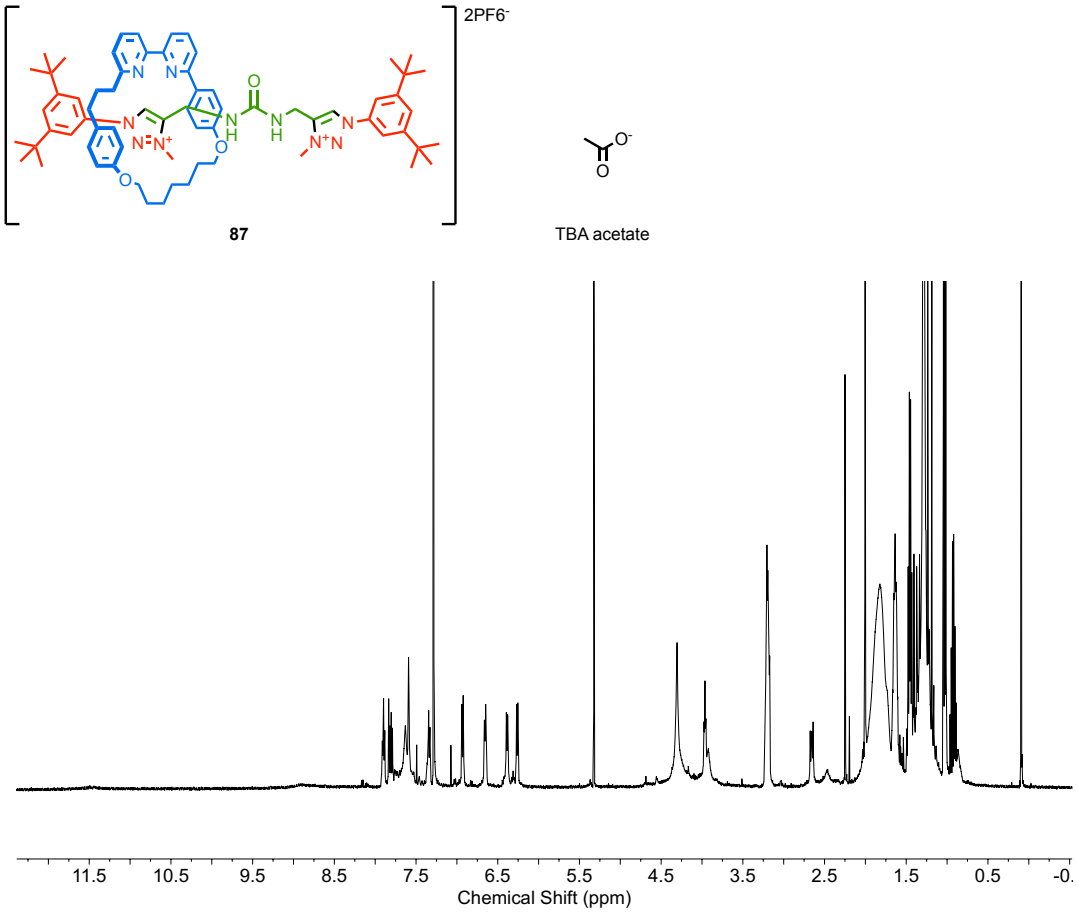

Figure 2.79 ^{1}H NMR (500 MHz, $CDCl_3$) of 1:1 **87**:Acetate at 293 K.

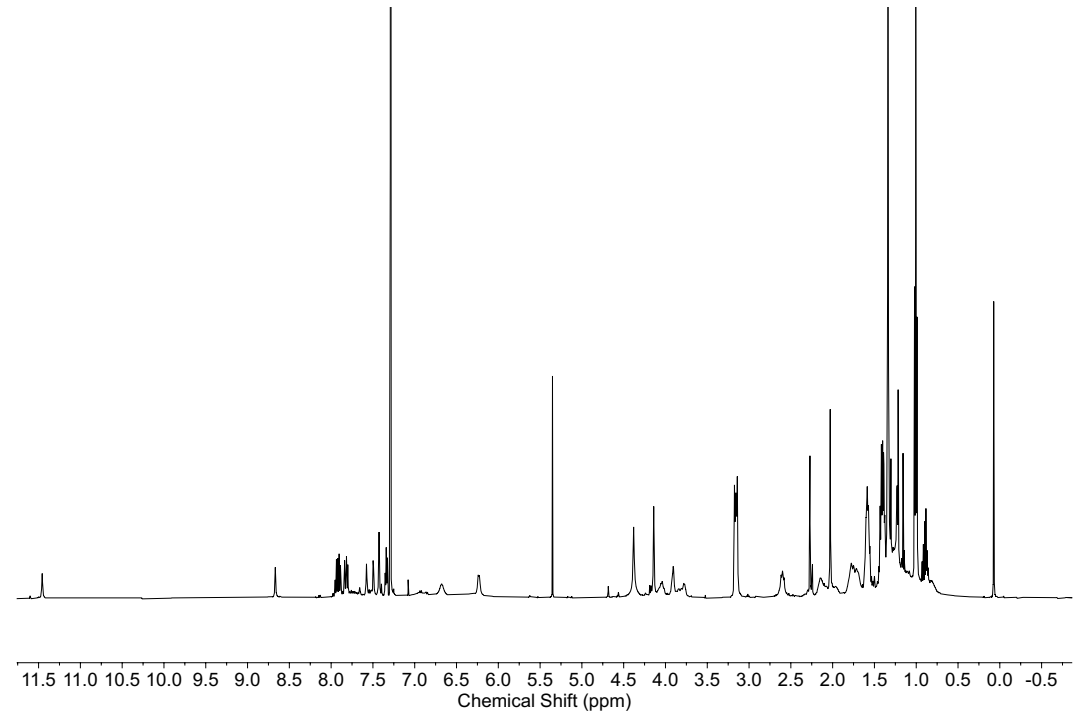

Figure 2.80 ^{1}H NMR (500 MHz, $CDCl_3$) of 1:1 **87**:Acetate at 223 K.

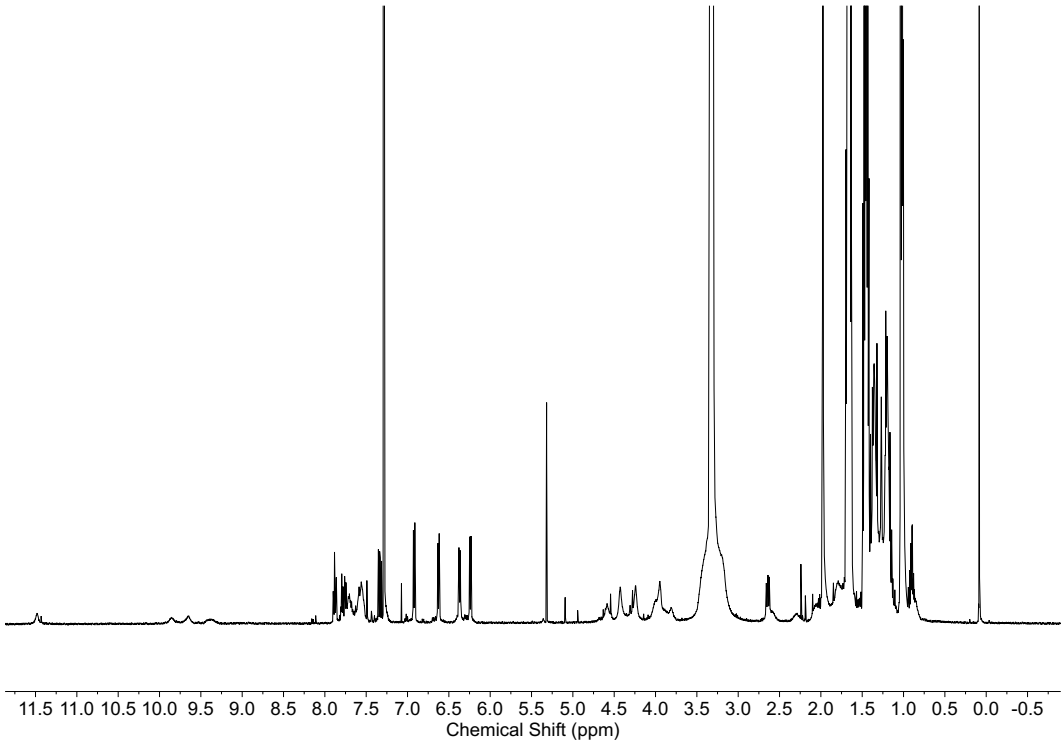

Figure 2.81 ^{1}H NMR (500 MHz, $CDCl_3$) of 1:10 **87**:Acetate at 293 K.

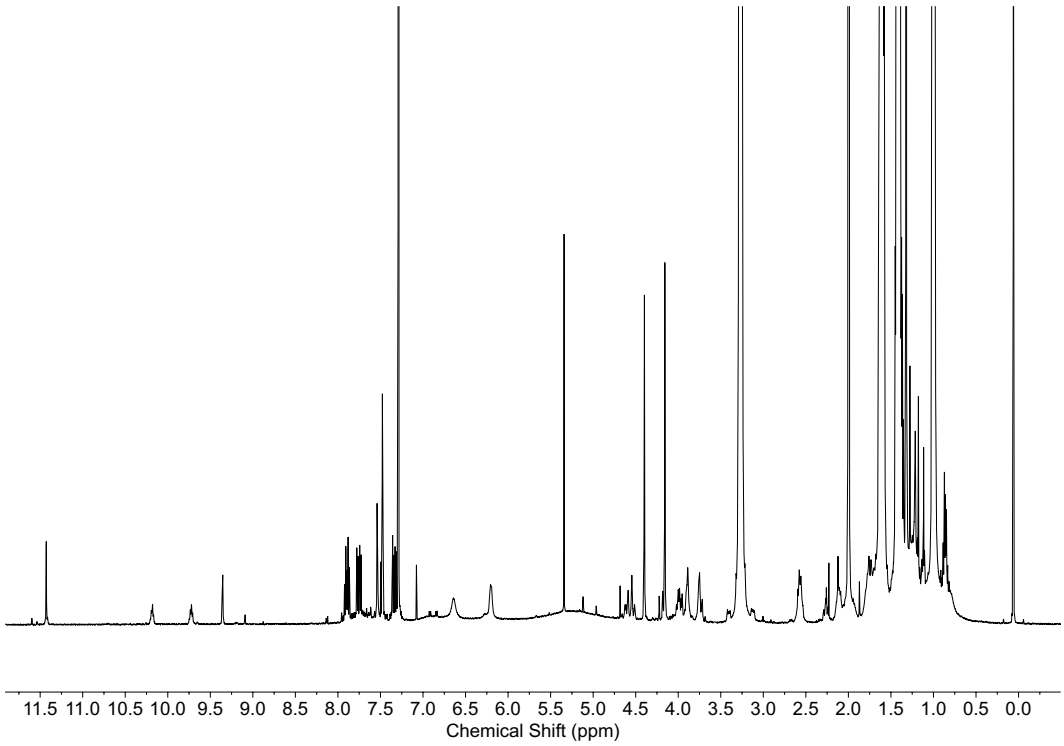

Figure 2.82 ^{1}H NMR (500 MHz, $CDCl_3$) of 1:10 **87**:Acetate at 223 K.

CD Spectroscopy

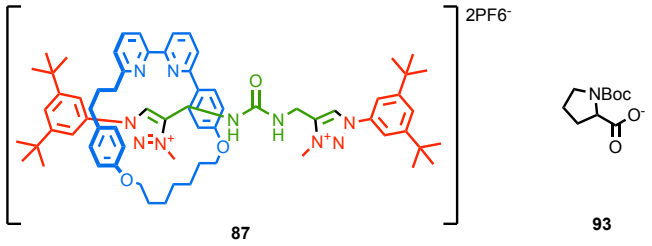

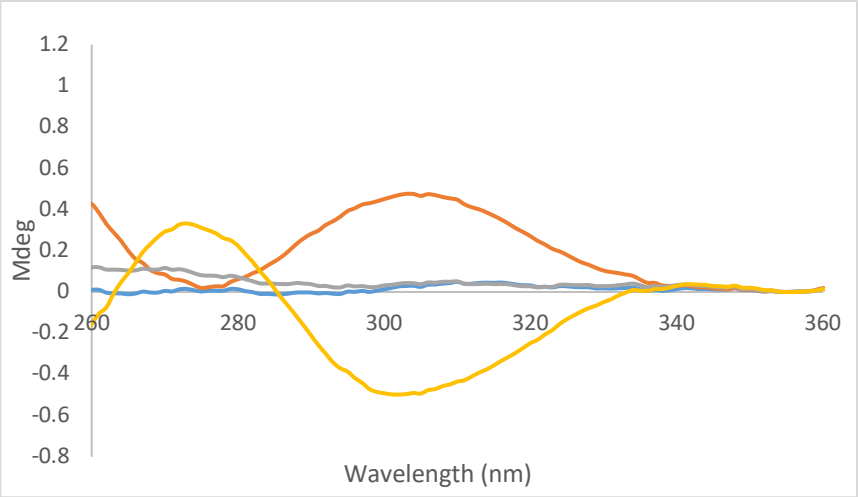

Figure 2. 83 CD spectra ($CHCl_3$, 293 K, C = 2.5 x 10^{-5}) of **87•**(*R*)-**93 1:1** (orange), (*R*)-**93** (blue), **87•**(*S*)-93 **1:1** (yellow), (*S*)-93 (grey). Spectra are normalized to 0 at λ = 355 nm and Savitzky-Golay smoothing data smoothing has been applied.

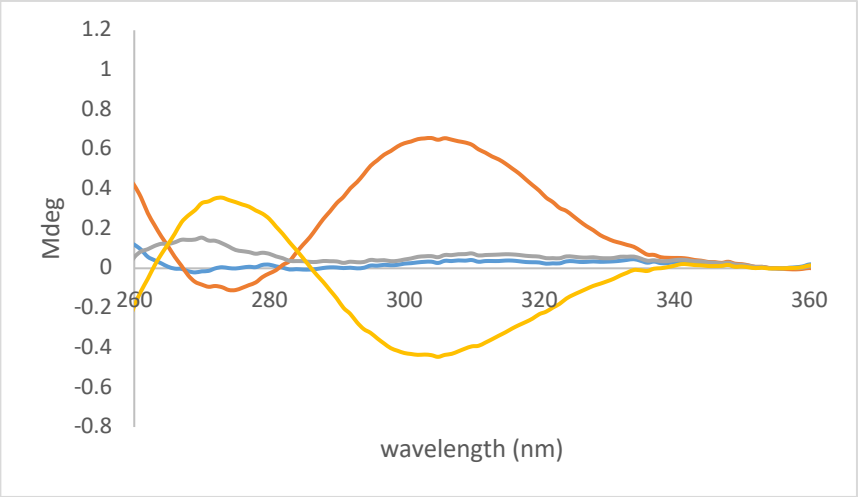

Figure 2.84 CD spectra ($CHCl_3$, 293 K, **93** C = 2.5 x 10^{-4}, **87** C = 2.5 x 10^{-5}) of **87•**(*S*)-93 **1:10** (orange), (*R*)-93 (blue), **87•**(*S*)-93 **1:10** (ywllow), (*S*)-93 (grey). Spectra are normalized to 0 at λ = 355 nm and Savitzky-Golay data smoothing has been applied.

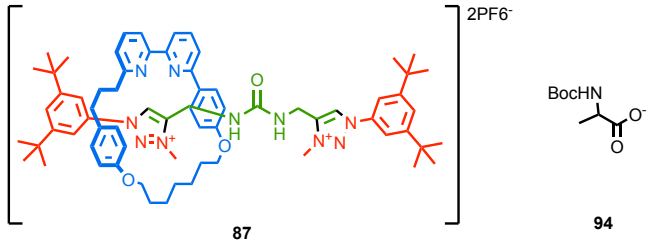

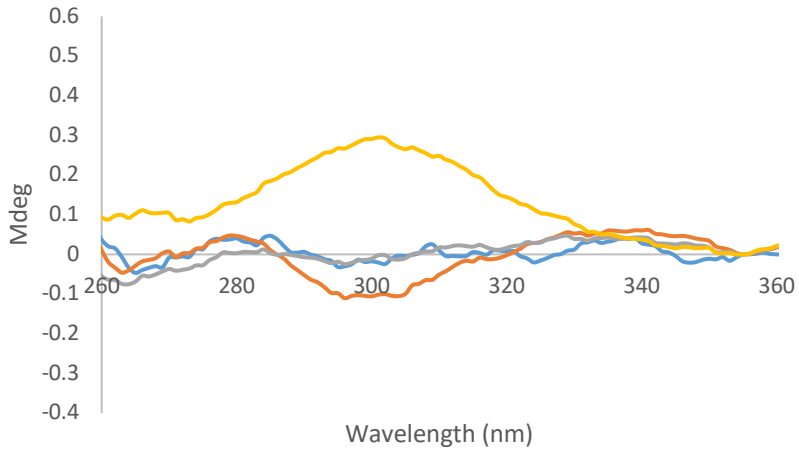

Figure 2.85 CD spectra ($CHCl_3$, 293 K, C = 2.5 x 10^{-5}) of **87**•(*R*)-94 **1:1** (orange), (*R*)-94 (blue), **87**•(*S*)-94 **1:1** (yellow), (*S*)-94 (grey). Spectra are normalized to 0 at λ = 355 nm and Savitzky-Golay data smoothing has been applied.

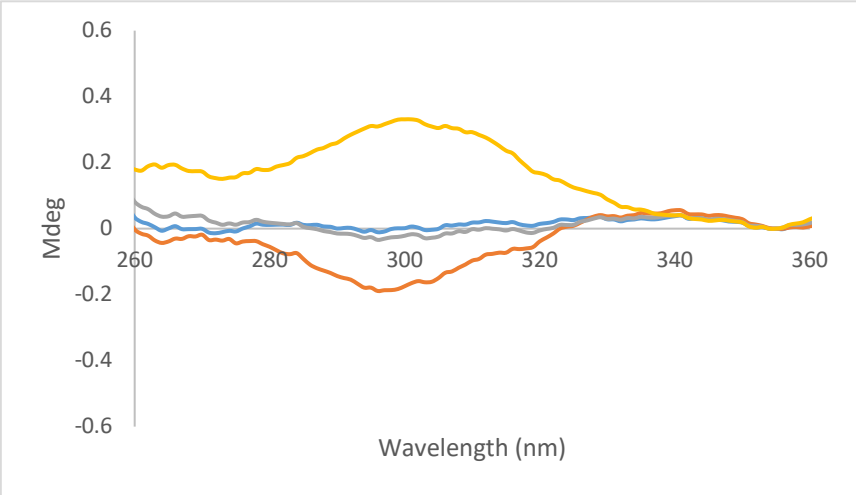

Figure 2.86 CD spectra ($CHCl_3$, 293 K, **94** C = 2.5 x 10^{-4}, **87** C = 2.5 x 10^{-5}) of **87**•(*R*)-94 **1:1** (orange), (*R*)-94 (blue), **87**•(*S*)-94 **1:1** (yellow), (*S*)-94 (grey). Spectra are normalized to 0 at λ = 355 nm and Savitzky-Golay data smoothing has been applied.

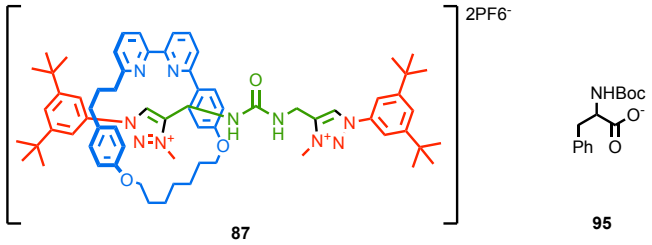

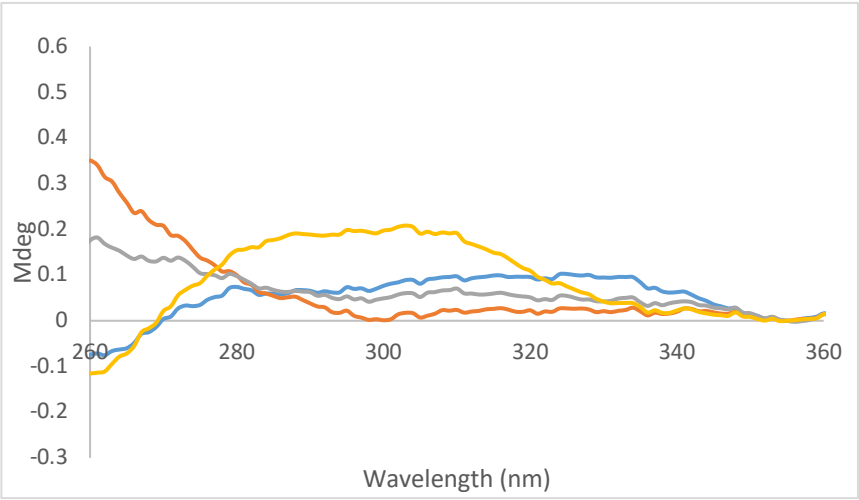

Figure 2.87 CD spectra ($CHCl_3$, 293 K, C = 2.5 x 10^{-5}) of **87**•(*R*)-94 **1:1** (orange), (*R*)-94 (blue), **87**•(*S*)-94 **1:1** (yellow), (*S*)-94 (grey). Spectra are normalized to 0 at λ = 355 nm and Savitzky-Golay data smoothing has been applied.

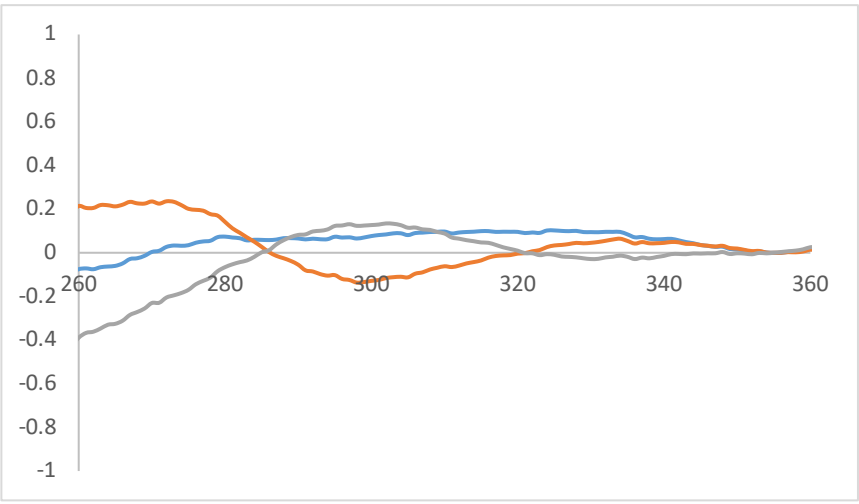

Figure 2.88 CD spectra ($CHCl_3$, 293 K, **95** C = 2.5 x 10^{-4}, **87** C = 2.5 x 10^{-5}) of **87**•(*R*)-95 **1:1** (orange), (*R*)-95 (blue), **87**•(*S*)-95 **1:1** (grey). Spectra are normalized to 0 at λ = 355 nm and Savitzky-Golay data smoothing has been applied.

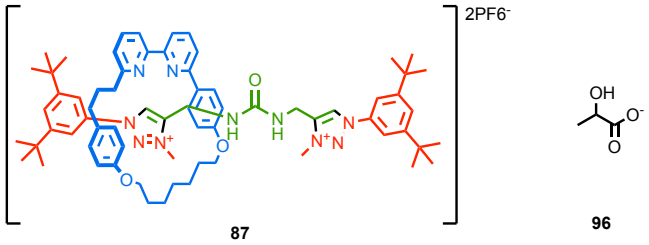

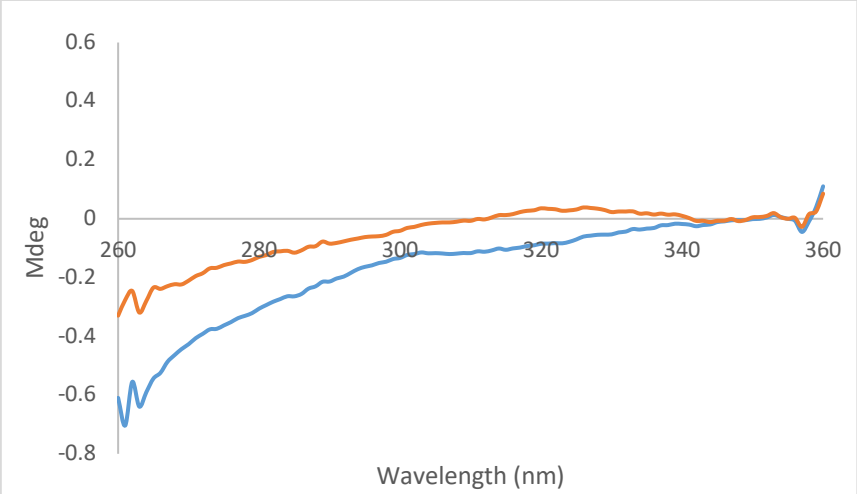

Figure 2.89 CD spectra ($CHCl_3$, 273 K, C = 2.5 x 10^{-5}) of **87**•(*S*)-96 **1:1** (orange) and (*S*)-96 (blue). Spectra are normalized to 0 at λ = 355 nm and Savitzky-Golay data smoothing has been applied.

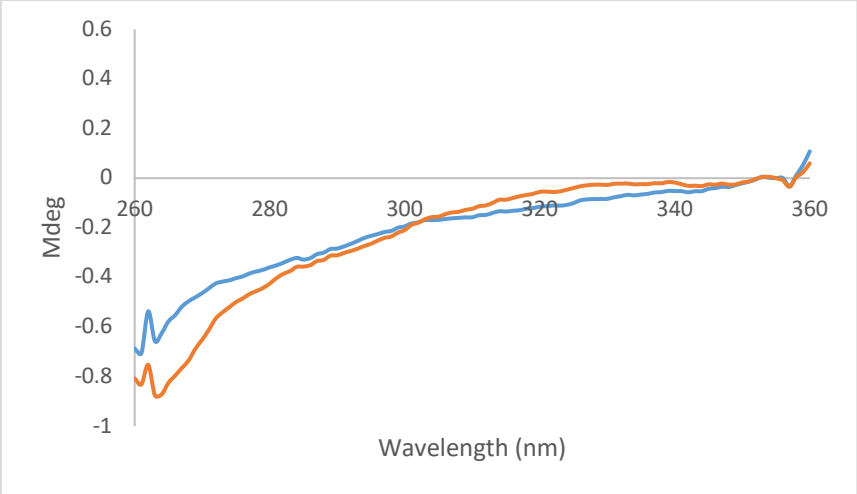

Figure 2.90 CD spectra ($CHCl_3$, 273 K, **96** C = 2.5 x 10^{-4}, **87** C = 2.5 x 10^{-5}) of **87**•(*S*)-96 **1:1** (orange), (*S*)-96 (blue). Spectra are normalized to 0 at λ = 355 nm and Savitzky-Golay data smoothing has been applied.

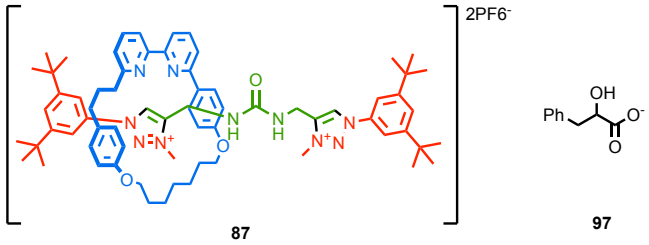

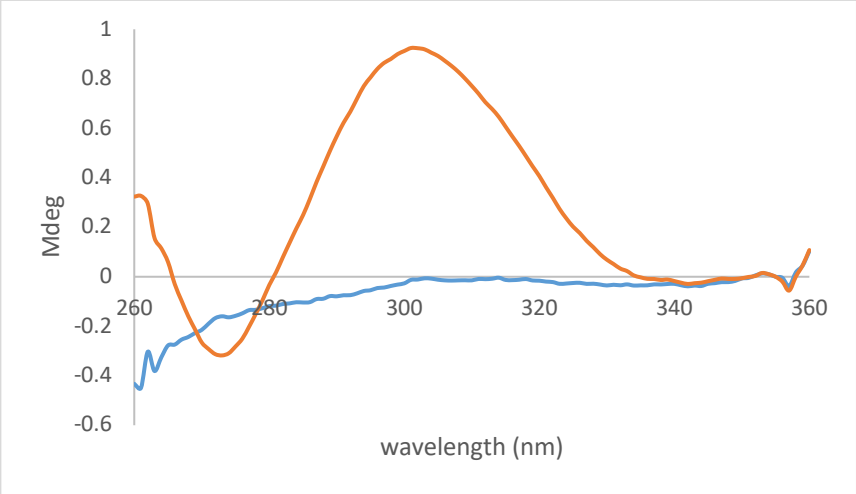

Figure 2.91 CD spectra ($CHCl_3$, 273 K, C = 2.5 x 10^{-5}) of **87•**(*R*)-97 **1:1** (orange) and (*R*)-97 (blue). Spectra are normalized to 0 at λ = 355 nm and Savitzky-Golay data smoothing has been applied.

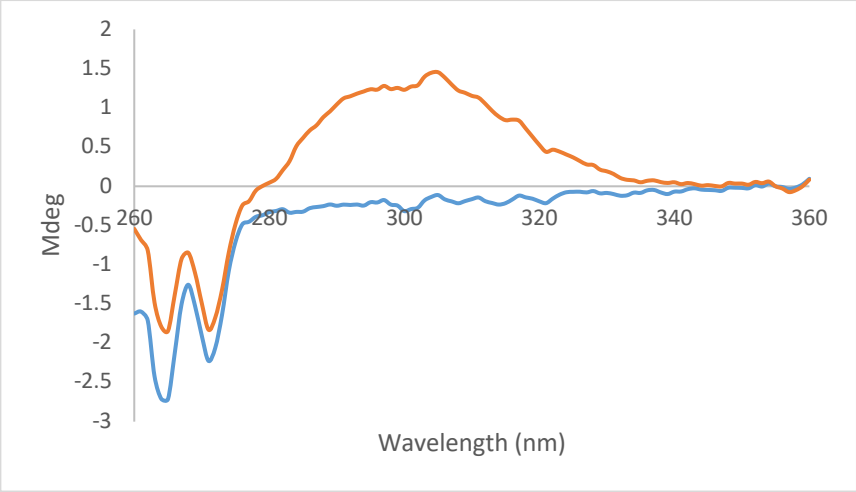

Figure 2.92 CD spectra ($CHCl_3$, 273 K, **97** C = 2.5 x10^{-4}, **87** C = 2.5 x 10^{-5}) of **87•**(*R*)-97 **1:10** (orange) and (*R*)-97 (blue). Spectra are normalized to 0 at λ = 355 nm. Savitzky-Golay data smoothing has been applied, to a lesser extent with **87•97 1:10** and **97** C = 2.5 x10^{-4} as it resulted in heavy alteration of the feature at 270 nm.

*Scalemic **93** CD spectra*

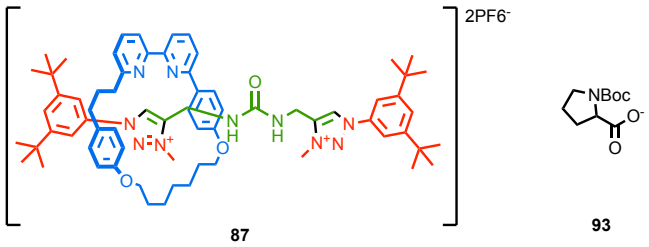

A 10 mM stock of the **87** was prepared as previously in HPLC grade $CHCl_3$. 100 mM stock solutions of (*R*)-**93 and** (*S*)-**93** were then prepared in HPLC grade $CHCl_3$. A 1500 µL sample of **87** was then was taken, and was mixed with 1500 µL of the desired ratio of (1-X)(*S*)-93/(X)(*R*)-93. This was performed for X = 0, 0.1, 0.2, 0.3, 0.4 and 0.5.

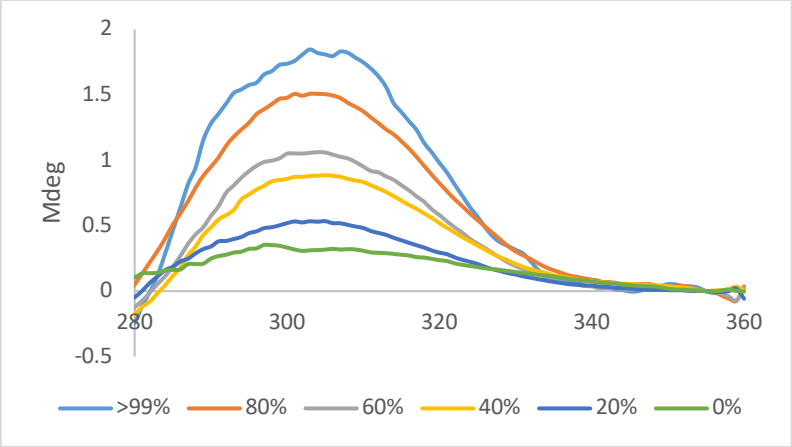

Figure 2.93 CD spectra ($CHCl_3$, 293 K, **93** C = 5.0 x 10^{-4}, **87** C = 5.0 x 10^{-5}) of **87•**(*S*)-93 **1:10** with varying enantiopurities. Spectra are normalized to 0 at λ = 355 nm and Savitzky-Golay data smoothing has been applied.

In order to maximise the relative intensity of the peak the concentration was increased, which lead to signal swamping below 280 nm, so this data was not collected.

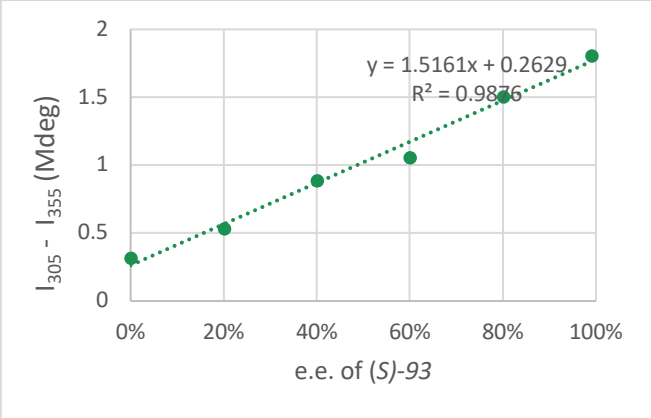

Figure 2. 94 Calibration plot of CD intenstiy (Mdeg) at 305 nm relative to 355 nm, against e.e. of sample.

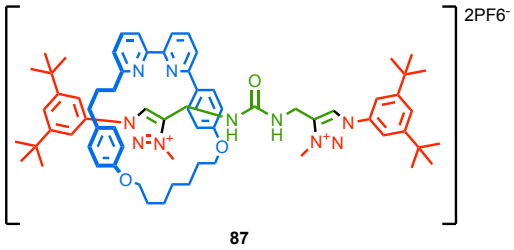

87

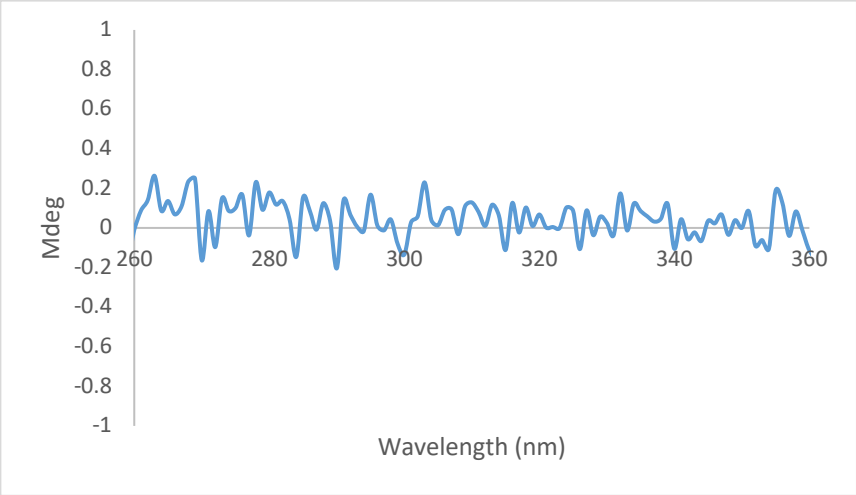

Figure 2.95 CD spectra ($CHCl_3$, 293 K, C = 2.5 x 10^{-5}) of **87**. Spectra are normalized to 0 at λ = 350 nm.

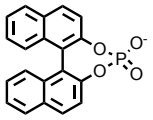

92

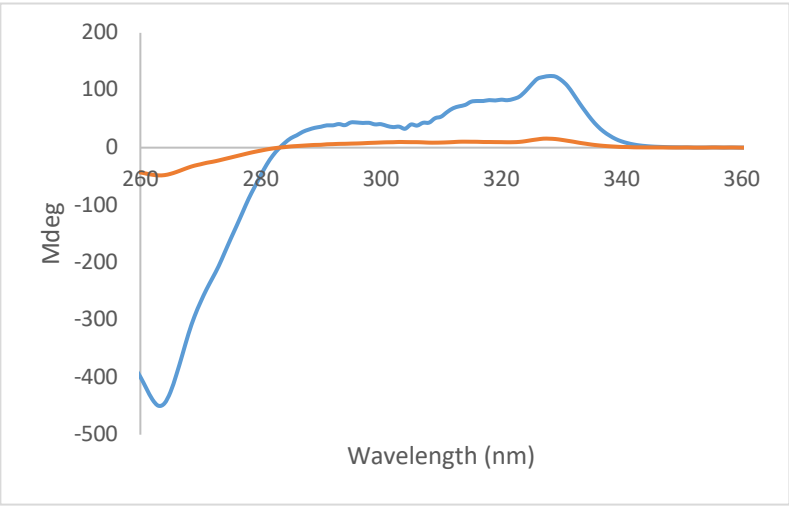

Figure 2.96 CD spectra ($CHCl_3$, 293 K, C = 2.5 x 10^{-5}, (orange) and C = 2.5 x 10^{-4}, (blue)) of **92**.

2.5. Bibliography

1 J. Y. C. Lim, I. Marques, A. L. Thompson, K. E. Christensen, V. Félix and P. D. Beer, *J. Am. Chem. Soc.*, 2017, **139**, 3122–3133.

2 M. J. Langton and P. D. Beer, *Acc. Chem. Res.*, 2014, **47**, 1935–1949.

3 J. Y. C. Lim, I. Marques, V. Félix and P. D. Beer, *Angew. Chem. Int. Ed.*, 2018, **57**, 584–588.

4 J. A. Wisner, P. D. Beer, M. G. B. Drew and M. R. Sambrook, *J. Am. Chem. Soc.*, 2002, **124**, 12469–12476.

5 M. K. Chae, J. M. Suk and K. S. Jeong, *Tetrahedron Lett.*, 2010, **51**, 4240–4242.

6 D. Curiel and P. D. Beer, *Chem. Commun.*, 2005, **10**, 1909–1911.

7 M. Denis, L. Qin, P. Turner, K. A. Jolliffe and S. M. Goldup, *Angew. Chem. Int. Ed.*, 2018, 2–7.

8 E. M. G. Jamieson, F. Modicom and S. M. Goldup, *Chem. Soc. Rev.*, 2018, **47**, 5266–5311.

9 M. M. Wiedmann, Y. S. Tan, Y. Wu, S. Aibara, W. Xu, H. F. Sore, C. S. Verma, L. Itzhaki, M. Stewart, J. D. Brenton and D. R. Spring, *Angew. Chem. Int. Ed.*, 2017, **56**, 524–529.

10 J. E. M. Lewis, R. J. Bordoli, M. Denis, C. J. Fletcher, M. Galli, E. A. Neal, E. M. Rochette and S. M. Goldup, *Chem. Sci.*, 2016, **7**, 3154–3161.

11 W. Zhu and D. Ma, *Chem. Commun.*, 2004, 888–889.

12 P. Thordarson, *Chem. Soc. Rev.*, 2011, **40**, 1305–1323.

13 M. A. Jinks, A. de Juan, M. Denis, C. J. Fletcher, M. Galli, E. M. G. Jamieson, F. Modicom, Z. Zhang and S. M. Goldup, *Angew. Chem. Int. Ed.*, 2018, **57**, 14806–14810.

14 M. Denis, J. E. M. Lewis, F. Modicom and S. M. Goldup, *Chem.*, 2019, **5**, 1512–1520.

15 J. E. M. Lewis, R. J. Bordoli, M. Denis, E. A. Neal, C. Fletcher, M. Galli, E. Rochette and S. M. Goldup, *Chem. Sci.*, 2016, **7**, 3154–3161.

16 J. Y. C. Lim, I. Marques, L. Ferreira, V. Félix and P. D. Beer, *Chem. Commun.*, 2016, **52**, 5527–5530.

17 F. Portier, J. Solier and S. Halila, *Eur. J. Org. Chem.*, 2019, **2019**, 6158–6162.

Chapter 3. Novel Rearrangement Due to the Mechanical Bond

Abstract: During preliminary investigations into a new rotaxane design with the goal of investigating small mechanically chiral sensor molecules, an unknown side product was observed. This was investigated and determined to be due to a novel rearrangement of a triazolide functionality. This chapter details the discovery and subsequent investigation of this novel rearangement, which yielded an acrylamide functionalised rotaxane instead of the exptected triazole product. Ultimately, these studies led to conditions that selectively produce the rearranged product, and the scope of the reaction investigated. Although it was found that selectivity for the rearrangement pathway decreased with decreasing steric bulk around the triazole group, limiting the reaction scope, this prompted further mechanistic studies which helped us to propose a reaction mechanism the accounts for all of the experimental observations.

Acknowledgements: This project was performed, and the results from sections **3.3.1** up to and including **3.3.4**, were obtained in equal collaboration with Florian Modicom.

Computational experiments in sections **3.2.5** and **3.4.** were performed by S. M. Goldup.

Prior publication: The majority of the results in chapter were previously published as part of: F. Modicom, E. M. G. Jamieson, E. Rochette and S. M. Goldup, "*Chemical consequences of mechanical bonding in catenanes and rotaxanes: isomerism, modification, catalysis and molecular machines for synthesis*", *Angew. Chem. Int. Ed.*, 2019, **58**, 3875–3879.

Compound **109** was previously published in: Michael A. Jinks, Alberto de Juan, Mathieu Denis, Catherine J. Fletcher, Marzia Galli, Ellen M. G. Jamieson, Florian Modicom, Zhihui Zhang, and Stephen M. Goldup, *Angew. Chem. Int. Ed.* 2018, **57**, 14806–14810.

3.1. Introduction

3.1.1. Rearrangement of 1,2,3-triazoles

In 2002 Sharpless and co-workers[1], and Meldal and co-workers[2], independently reported the copper catalysed 'click' reaction of alkynes with azides (CuAAC) to produce 4-substituted 1,2,3-triazoles. This reaction allows the reliable synthesis of 1,2,3-triazoles under mild conditions, unlike the thermally activated, non-specific Huisgen 1,3-dipolar cycloaddition,[3] that results in a mixture of 4 and 5 substituted products.

Considering the high ratio of N:C, triazoles are remarkably stable functional groups. However, very early reports on this functional group recognised that they can rearrange under certain conditions. The earliest example of this is the Dimroth rearrangement discovered in 1909.[4] The Dimroth rearrangement is a base catalyzed rearrangement of a triazole where an endocyclic and exocyclic nitrogen can exchange places as demonstrated with triazoles **100** and **101** (**Scheme 3.1**). This rearrangement is not limited to only triazoles, but can also occur in other 5- and 6-membered heterocyclic compounds.[5]

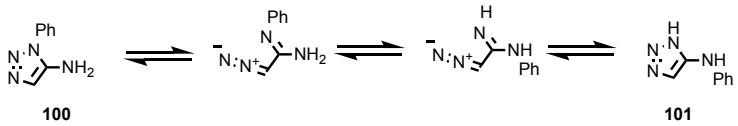

Scheme 3.1 Dimroth rearangement in the presence of base of 1,2,3-triazole molecules.

More recently, Fokin and co-workers reported a Cu^{I}-cascade reaction in which the Cu^{I} – triazolide intermediate, **103,** of the CuAAC reaction rearranges to yield a sulfonylazetidin-2-imine **104**, that subsequently undergoes dimerization to yield **105** (**Scheme 3.2**).[6] The direct loss of di-nitrogen (pathway a) has been proposed for lithiated triazoles previously,[7] which provides support for this mechanism. Pathway b invokes a Dimroth-like Cu^{I}-triazolide ring-opening step.[8] The authors do not provide direct evidence for which route is more likely to proceed. While the reaction was found to be relatively wide in scope with regards to the alkyne, tosyl-azide was necessary for the rearrangement to occur. This rearrangement process represents a simple method of synthesis of these densely functionalised azetidine compounds, which can be readily functionalized.

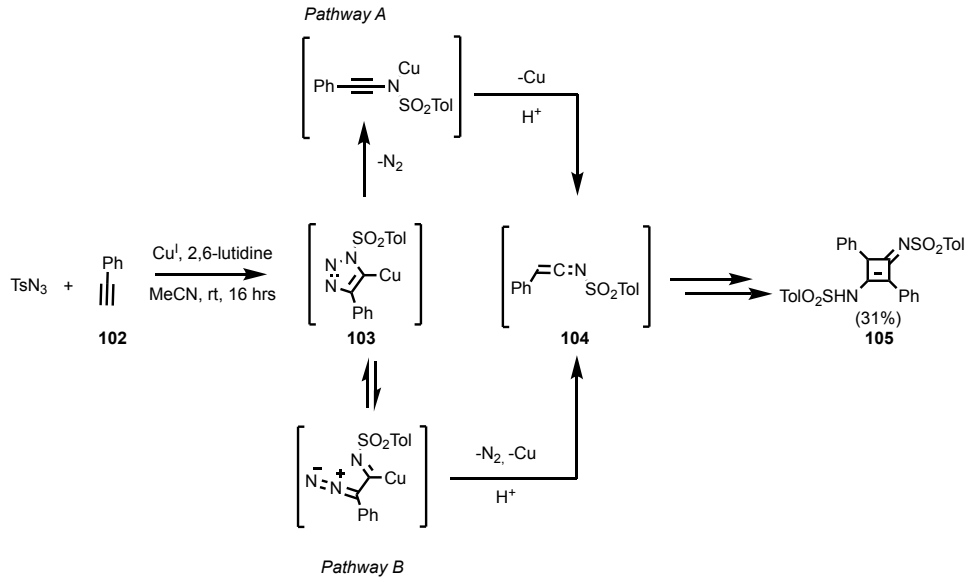

Scheme 3.2 Postulated mechanisms for the rearrangement reaction reported by Fokin and co-workers.

Subsequently, Fokin, Chang and co-workers disclosed a more detailed mechanistic study of the sulfonyl-1,2,3-triazolide rearrangement, including detailed computational studies of the N-N bond cleavage step. They found that the activation barrier for the sulfonyl functionalised triazole **106b** was significantly lower than methyl-triazole **106a** (**Scheme 3.3**). This study provides strong evidence that this rearrangement occurs via a ring opening mechanism for these sulfonyl substituted triazolides and that loss of N_2 from species **107b** proceeded 5 orders of magnitude faster than the proto-triazole alternative, showing how vital the copper is to this rearrangement.

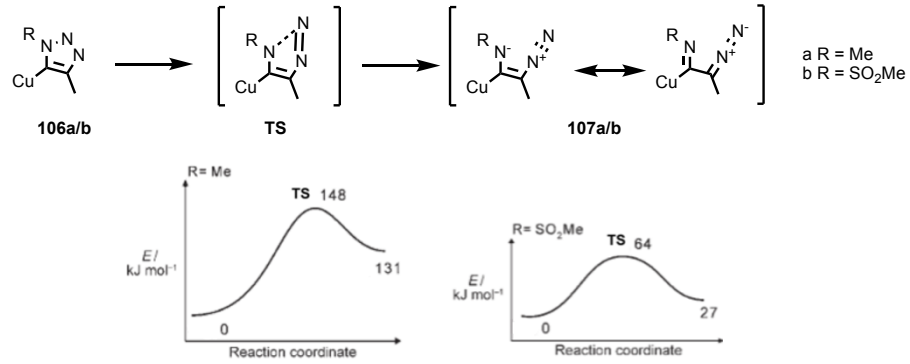

Scheme 3.3 Fokin and co-workers' computational study into ring opening of Cu^{I} triazolides. a) The reaction scheme studied. b) Reaction energy profile (DFT) for the key C-N bond cleaving step showing the difference in transition state energies depending on the nature of R.

3.1.2. Aims and Objectives

Alkyne **108** was designed as a new chiral auxiliary for the synthesis of MPC rotaxanes. The initial aim was to use alkyne, **108**, with azide **11** and macrocycle **51** to yield Rotaxane **109** (**Scheme 3.4**).

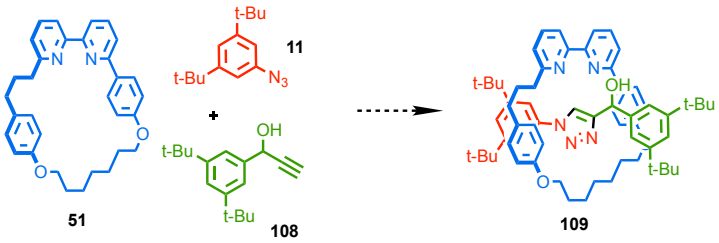

Scheme 3.4 Proposed synthesis of MPC diasterioisomeric rotaxane **109.**

Due to the covalent stereocentre present in **108**, rotaxane **109** was expected to be formed as a mixture of diastereoisomers. The diaselectivity of the reaction was to be investigated, then, pending diastereoisomer separation, **109** was to be oxidised to yield **110**. This ketone would be a "handle" for further functionalization, such as imine condensation to give **111**. Our intention was to investigate **110** as a selective host for chiral guests (**Scheme 3.4**).

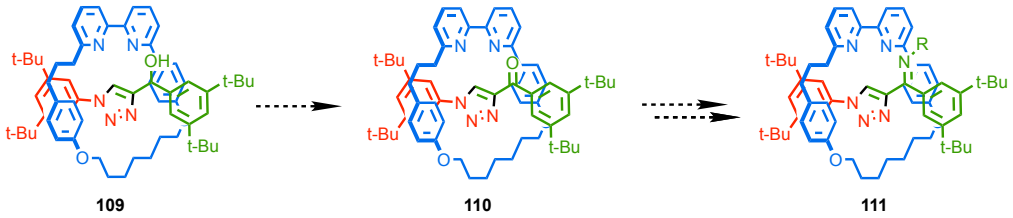

Scheme 3.5 Proposed route to MPC rotaxane with imine functionality, **111.**

However, during initial experiments with auxiliary **108**, a previous member of the group, (Dr. Elise Rochette) observed an unexpected interlocked side product in place of **109** (**Scheme 3.6**). LCMS analysis confirmed that the mystery product was a single component with m/z = 926.6199, corresponding to [**109** - N_2 + H]$^+$.

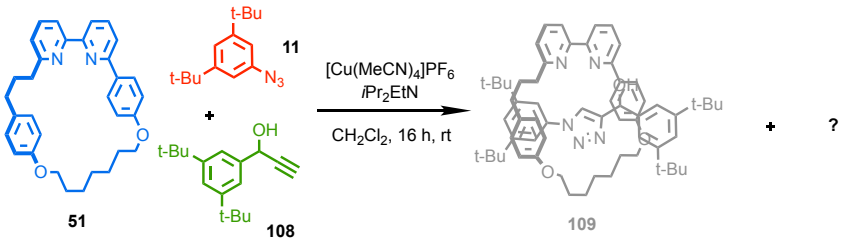

Scheme 3.6 Attempted synthesis of rotaxane **109.**

Based on these results, the initial aim of the project was to isolate and characterise the unknown product and selectively synthesise the intended rotaxane, **109**. Depending on the results of this first phase, we then aimed to investigate the mechanism for the formation of this unknown product, investigate the reaction scope, and if possible determine a selective route to synthesis of it.

3.2. Results and Discussion

3.2.1. Starting Material Synthesis

The study of the rearrangement reaction required a number of simple starting materials. To allow the reader to focus on the mechanistic study in the following sections, the synthesis of these starting materials is briefly discussed below. All other reagents (**11**,[9] **20**,[10] **124**,[11] **51**, [12] **131**,[12] **14**,[12] **12**[12] and **133**[12]) were prepared as previously reported.

The synthesis of **108** originally utilised a Bouveault reaction to yield aldehyde **113**, which could then give **108** by reaction with magnesium acetylide. This route proceeded in high yield (**Scheme 3.7**).

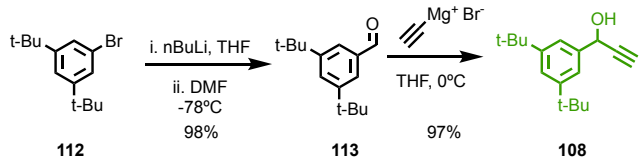

Scheme 3.7 Synthesis of **108**, via aldehyde **113**.

However, a different route to **113** was devised to combat scalability issues involved with butylithium reagents, which also pleasingly utilised less expensive starting materials than **112**. This route was based on a modified literature procedure,[13] and was very successful with a yield of 77% (**Scheme 3.8**). While the yield of **113** is lower, the use of **114** in place of **112** reduces the economic cost of the process, even taking into account the lower efficiency, and this reaction could be scaled to 30 mmol with ease.

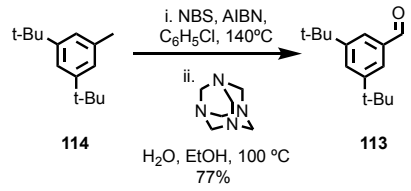

Scheme 3.8 Alternative synthesis of **113**.

Alkyne **116** was synthesised in an analogous manner to **108** starting from previously reported aldehyde **115** (**Scheme 3.9**).[14]

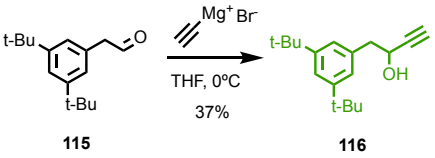

Scheme 3.9 Synthesis of alkyne **116**.

Alkyne **117** was produced by methylation of **108** in excellent yield (**Scheme 3.10**).

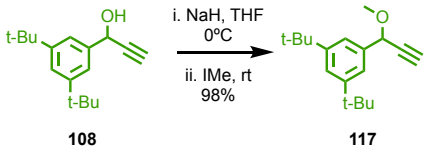

Scheme 3.10 Synthesis of alkyne **117**.

An alkyne stopper without the alcohol functionality was also required. Accordingly, **118** was synthesised from **115** using the Bestmann-Ohira reagent (**Scheme 3.11**).

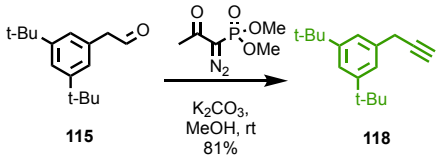

Scheme 3.11 Synthesis of alkyne **118.**

Quaternary alcohol analogue of **108**, alkyne **121**, was synthesised (**Scheme 3.12**). Benzoic acid **119**, was treated with methyl lithium to yield ketone **120** in an excellent yield. Subsequent reaction with magnesium acetylide yielded alkyne **121** in a reasonable yield of 48%. (**Scheme 3.12**)

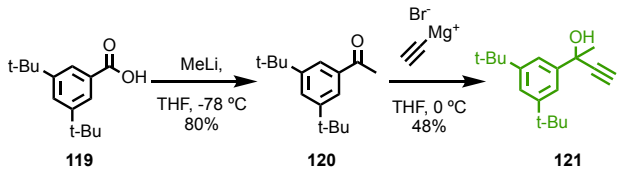

Scheme 3.12 Synthesis of alkyne **121.**

3.2.2. Isolation of a Mystery Product

As discussed above, the initial observation was that an unknown interlocked product was formed under standard AT-CuAAC conditions.[15] However when this reaction was repeated with under rigorous conditions (exclusion of air and moisture), the mystery product was not observed (**Scheme 3.13**). The diminished isolated yield of **109** is due to purification issues rather than a competing side reaction. Analysis of the crude reaction product by ^{1}H NMR revealed that **109** is the only interlocked product.

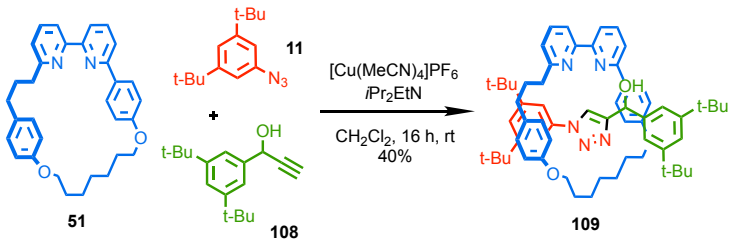

Scheme 3.13 Synthesis of rotaxane **109** under rigorously anaerobic and anhydrous AT-CuAAC conditions.

These conflicting results piqued our interest and we set out to try and understand how, in one case, the mystery product was observed as the major interlocked species but was completely absent when the reaction was repeated. Although the original project aim, the synthesis of a new MPC rotaxane, required the use of an oriented macrocycle such as **51**, for the sake of simplicity, the reaction was repeated with more readily available macrocycle **14**. Once again, under rigorously controlled conditions, only the expected 'simple' triazole rotaxane, **122**, was observed (**Scheme 3.14**).

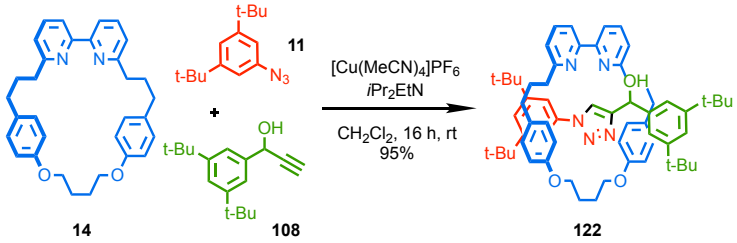

Scheme 3.14 Synthesis of rotaxane **122** under rigorously anaerobic and anhydrous AT-CuAAC conditions.

An obvious source of variation between the reactions performed here and those carried out by Dr Rochette was thought to be the presence of adventitious water. Pleasingly, when water was added (10% v/v) to the reaction between **108**, **11** and **14**, a significant proportion of a new mystery product was observed, allowing its isolation and characterisation (**Scheme 3.15**).

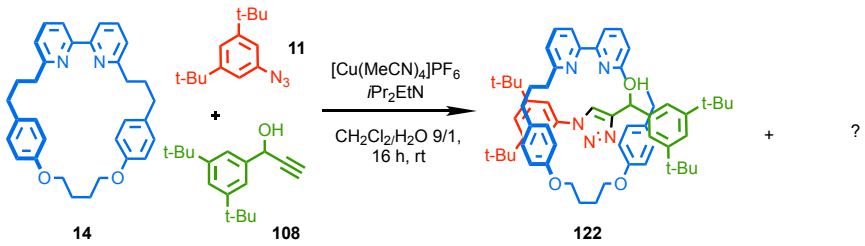

Scheme 3.15 Synthesis of rotaxane **122** and a mystery interlocked product in the presence of water.

Isolation of the mystery product allowed it to be characterised fully. LR MS analysis revealed confirmed that it was a single species and that it's mass corresponded to that of **122** – 27,

suggesting that the structures are related by loss of N_2 and addition of a proton. The ^{1}H NMR spectrum of the mystery product (**Figure 3.1**) showed signals characteristic of a *E*-disubstituted alkene; two coupled doublets with J = 15.5 Hz were observed at 6.85 ppm and 6.29 ppm. A broadened singlet at 9.91 ppm that had no correlated ^{13}C signals by HSQC analysis was also observed. Signals in this range for rotaxanes produced using the AT-CuAAC reaction are usually characteristic of the triazole proton, which appears at high ppm due to hydrogen bonding to the macrocyclic bipyridine. However, the triazole C-H resonance usually shows a cross peak in the HSQC to a ^{13}C signal at around 125 ppm. The mystery product also produces a smaller number of signals corresponding to macrocycle protons compared to triazole-containing rotaxane **122**. The bilateral symmetry of the macrocycle component is lifted in triazole rotaxane **122** due to the stereogenic centre on the axle and so, for instance, two sets of aromatic signals corresponding to the phenolic ether are observed.

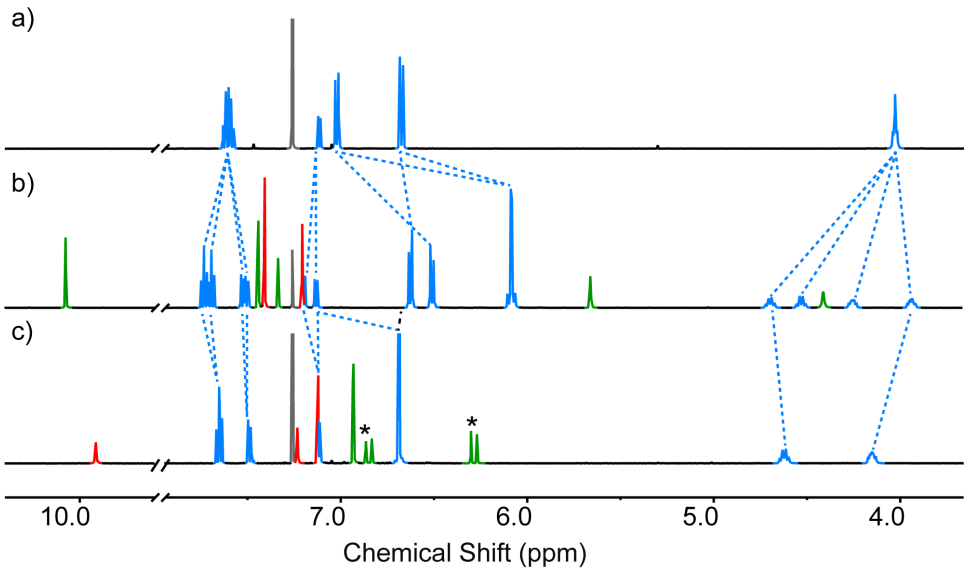

Figure 3. 1 Partial stacked ^{1}H NMR spectra ($CDCl_3$, 500 MHz) of a) **14,** b) triazole rotaxane **122**, and c) mystery interlocked product. Colour coding of signals as in Sch**eme 3.14.** Signals attributed to vinyl protons are marked with "*".

The MS and ^{1}H NMR data suggest that the mystery product is related to **122** by loss of N_2, indicating that the triazole is no longer present, that the axle no longer contains a stereogenic centre and that the axle contains an alkene with *E* geometry. Crystals suitable for diffraction were grown by slow diffusion of Et_2O into CH_2Cl_2. The solid-state structure revealed the unknown compound to be **123** in which the triazole ring appears to have been replaced by an acrylamide functionality (**Figure 3.2**).

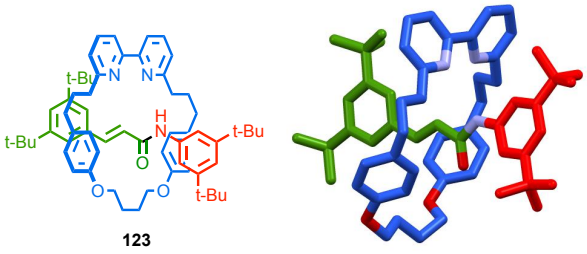

Figure 3.2 Structure of **123**, and its solid-state structure

The solid-state structure of **123** is entirely unexpected but is consistent with the solution-state data discussed above. Given the novelty of this result it was felt that the reaction required further investigation.

3.2.3. Reaction Optimization

Although the inclusion of water in the standard AT-CuAAC conditions allowed us to isolate and determine the structure of **123**, these conditions were capricious and the proportion of **122:123** varied run to run. Initially it was thought that variations in ambient light intensity could be the reason for the inconsistent reaction outcomes. However, excluding light during the reaction (**Scheme 3.16**, **Table 3.1**) led to similar variations in the reaction outcome. Once again, when water was excluded and the reaction was protected from ambient light, **123** was not observed.

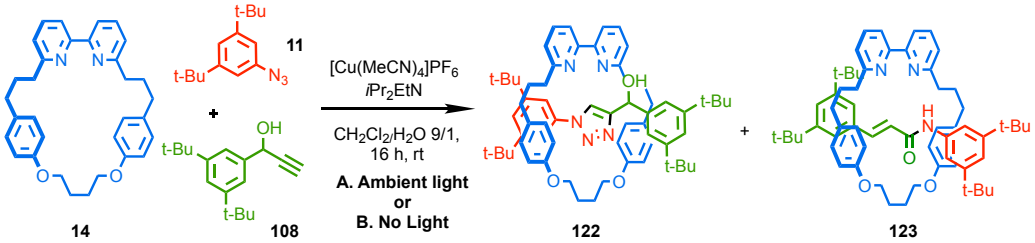

Scheme 3. 16 Effect of ambient light on the outcome of the reaction of **108**, **11** and **14**.

Entry	Conditions	123 (%)	122 (%)
1.	A. Ambient light	9	91
2.	B. No light	27	73
3.	B. No light (repeat)	11	89
4.	B. No light/No Water	0	100

Table 3.1 Ratio of **123**:**122** under various light conditions as shown in **Scheme 3.16**.

Next, we probed the role of the base. Reactions were conducted with 4 equivalents of NaH, 1,8-Bis(dimethylamino)naphthalene, DBU or $^{i}Pr_2EtN$, and one reaction in which h the base omitted entirely (**Scheme 3.17**, **Table 3.2**). In all cases, in the presence of added base,

selective formation of **122** was observed. However, in the absence of added base there was a significant increase in the proportion of **123**.

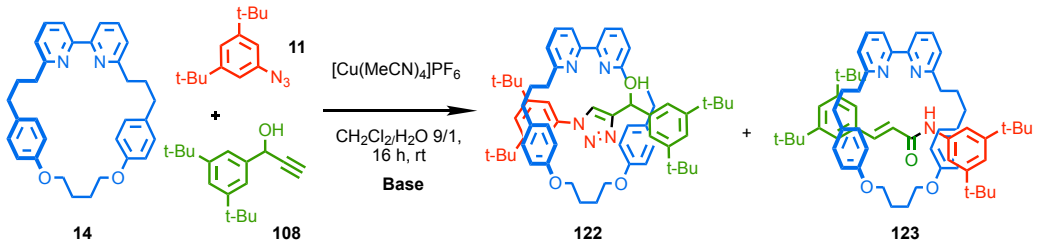

Scheme 3. 17 Effect of added base on the outcome of the reaction of **108**, **11** and **14**.

Entry	Base	123 (%)	122 (%)
1.	DBU	0	100
2.	Proton sponge™	0	100
3.	NaOH	0	100
4.	NaH	0	100
5.	$^{i}Pr_2EtN$	9	91
6	-	58	42

Table 3. 2 Ratio of **123:122** with various bases as shown in **Scheme 3.17**.

The results discussed above shed some light on the capricious nature of the reaction and suggest how the initial discovery of the reaction took place. It seems that the original observations of the rearranged product was due to errors in the addition of the base, which is typically a very small volume (16 µL for a 0.025 mM scale reaction), combined with a failure to ensure that the reaction conditions were anhydrous. This could also explain the significant differences observed in reaction outcomes in our screening reactions (e.g. table **Table 3.1**).

In order to verify this hypothesis, the reaction was repeated in the presence of varying equivalents of DIPEA (**Scheme 3.18**, **Table 3.3**). The results clearly show a relationship occurs between the equivalents of DIPEA added and the conversion to **123**.

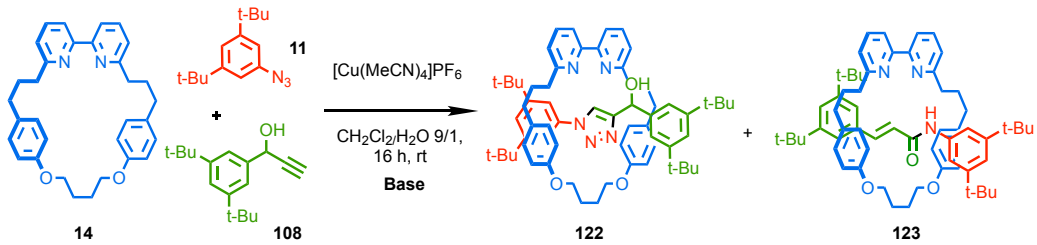

Scheme 3.18 Effect of equivalents of DIPEA on the outcome of the reaction of **108**, **11** and **14**.

Entry	Eq. of DIPEA	123 (%)	122 (%)
1.	3	10	90
2.	2	11	89
3.	1	21	79
4.	0	35	65

Table 3.3 Ratio of **123:122** with different equivalents of DIPEA as shown in **Scheme 3.18**.

While the general trend was promising, the exact conversion to **123** still varied between runs (**Tables 3.2:** entry 6 and **Table 3.3:** entry 4). It was thought this may be due to the immiscibility of CH_2Cl_2 and H_2O so the reaction was repeated replacing CH_2Cl_2 with THF as the reaction solvent (**Scheme 3.19**).

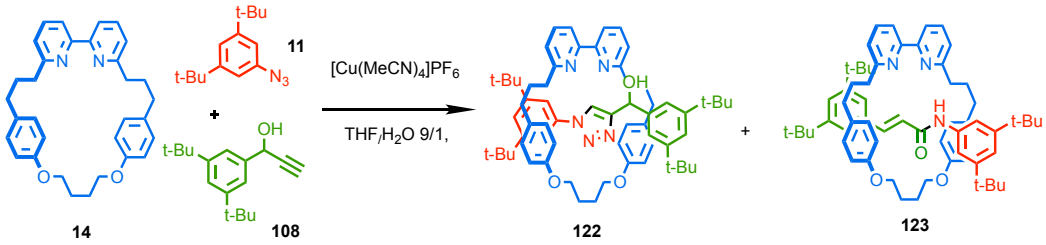

Scheme 3.19 Selective synthesis of **123** in THF/H_2O 9:1.

Pleasingly this solvent switch yielded complete selectivity for rotaxane **123** after 48 h reaction time. However, the conversion of **14** varied dramatically from run to run, although the selectivity remained consistently excellent. In order to gain more information, the reaction was repeated in deuterated solvents and monitored over the course of 48 h (**Figures 3.3, 3.4**).

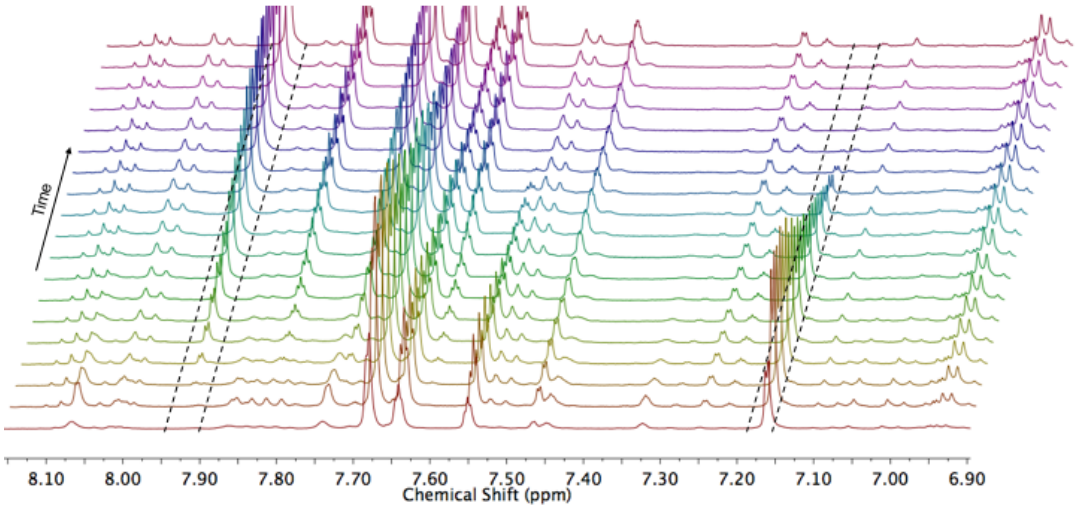

Figure 3.3 Stacked partial ^{1}H NMR spectra (400 MHz, $CDCl_3$) following the formation of **123** and consumption of starting material **14** (highlighted signals).

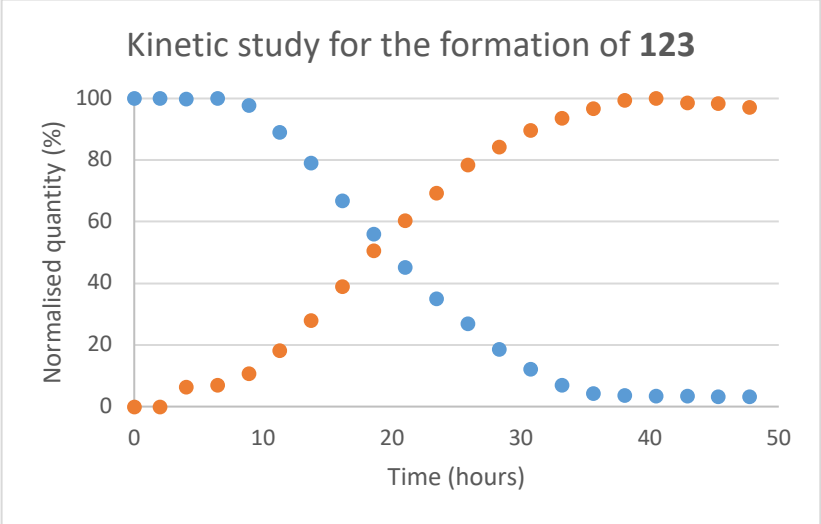

Figure 3.4 Graph of formation of **123** vs consumption of starting material with respect to time. with values normalised to the residual solvent.

Analysis of the data revealed a lag period of approximately 6-8 h before the reaction began, along with the absence of any persistent intermediate species that could give clues as to the possible mechanism for this reaction. The lag phase, combined with the previous observation of inconsistent reaction times, suggested that something was building up at the start of the reaction that was triggering formation of **123**.

From this observation, it was tentatively suggested that the PF_6 ion could be breaking down *in situ* to release F^-. Accordingly, we repeated the reaction in the presence of $KF_{(aq)}$ and compared the outcome with H_2O alone. To shorten the reaction time, both experiments were to 80ºC. Although both reactions displayed the same selectivity for **123** over **122**, the

conversion of the reaction with KF solution was significantly higher than that of the pure H_2O and also consistent (**Scheme 3.20, Table 3.4**).

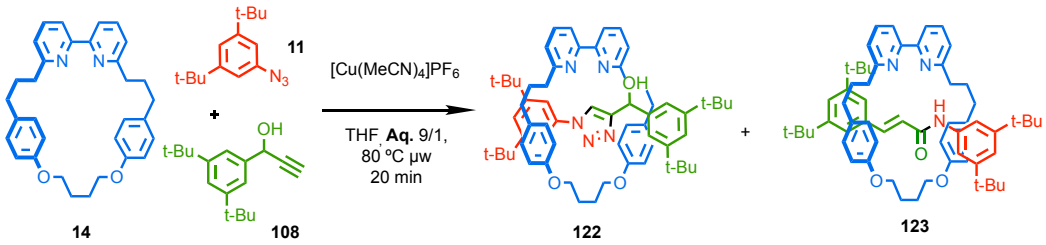

Scheme 3. 20 Reaction comparing selectivity and conversion given **Aq.** =. $KF_{(aq)}$ or = H_2O

Entry	Aqueous phases	123 (%)	122 (%)	Conversion of 14(%)
1.	KF	96	4	100
2.	H_2O	96	4	66-80*

Table 3.4 Ratio of **123:122** with differing aqueous additives as shown in Scheme **3.20**. *over various runs

To increase the selectivity, the reaction was repeated at 70 °C with the KF additive. This gave >99% selectivity for rotaxane **123**, with >99% conversion of macrocycle **14** in 1 h (**Scheme 3.21**). Under these conditions the reaction outcome was consistent between runs. Microwave heating was used for convenience, but the same outcome could be achieved using an oil bath.

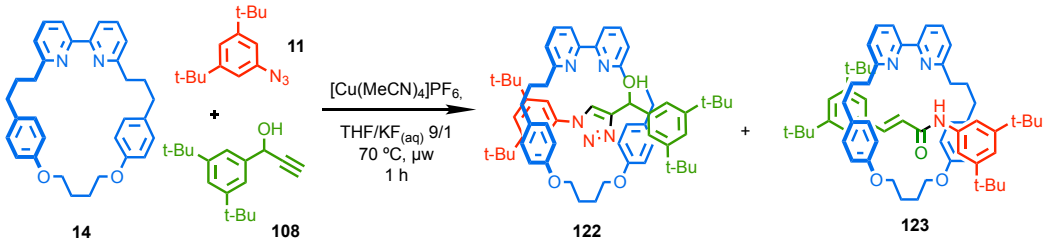

Scheme 3.21 Scheme for selective synthesis of **123**

Although KF clearly improves the rate of reaction and its reproducibility, the role of KF remains unclear. Indeed, replacing KF with other salts (**Scheme 3.22**, **Table 3.5**) failed to yield a clear picture; neither KNO_3 or TBAF produce the same selectivity for **123** as KF, suggesting the reaction outcome cannot be attributed to either the cation or anion alone. Even more intriguing perhaps is the switch in selectivity from KF to NO_3 when the reaction is performed with CuSO4/Na-ascorbate. It is obvious that this is a complex system and the reasons for this switch remain unclear.

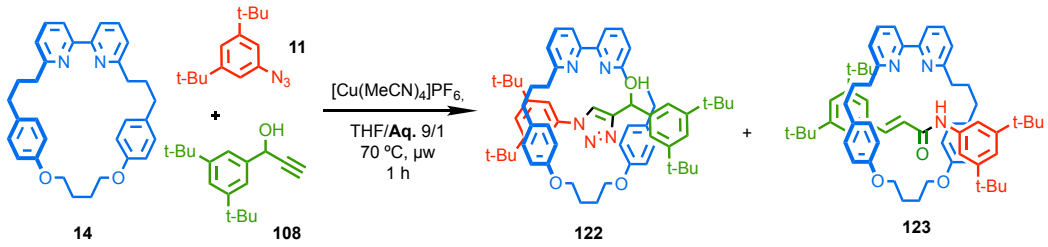

Scheme 3. 22 Reaction comparing selectivity given various aqueous salts, and differing copper sources

Entry	Aqueous phases	Cu	123 (%)	122 (%)
1.	KF	$Cu(MeCN)_4PF_6$	>99	1
2.	KNO_3	$Cu(MeCN)_4PF_6$	93	7
3.	TBAF	$Cu(MeCN)_4PF_6$	92	8
4.	KF	$CuSO_4$/NaAsc.	72	28
5.	KNO_3	$CuSO_4$/NaAsc.	>99	1

Table 3.5 Results for **Scheme 3.22**, showing selectivity of reaction with differing aqueous salts.

The exact role of the aqueous salt remains unclear, the results above demonstrate that we have developed conditions selective for either acrylamide rotaxane **123**, or the expected triazole rotaxane **122**. With these results in hand, we went on to explore the scope of these conditions.

3.2.4. Reaction Scope

We first investigated the reactions of azides **20** and **124** under conditions optimised for the rearrangement process (**Scheme 3.23**), both of which present a less sterically hindered reactive azide moiety than **11**. Both produced the corresponding rearrangement products in lower selectivity, with benzylic azide **20** presenting a slightly reduced selectivity, and **124**, a much less sterically hindered azide presenting a dramatically reduced selectivity for rotaxane **127** to just 20%.

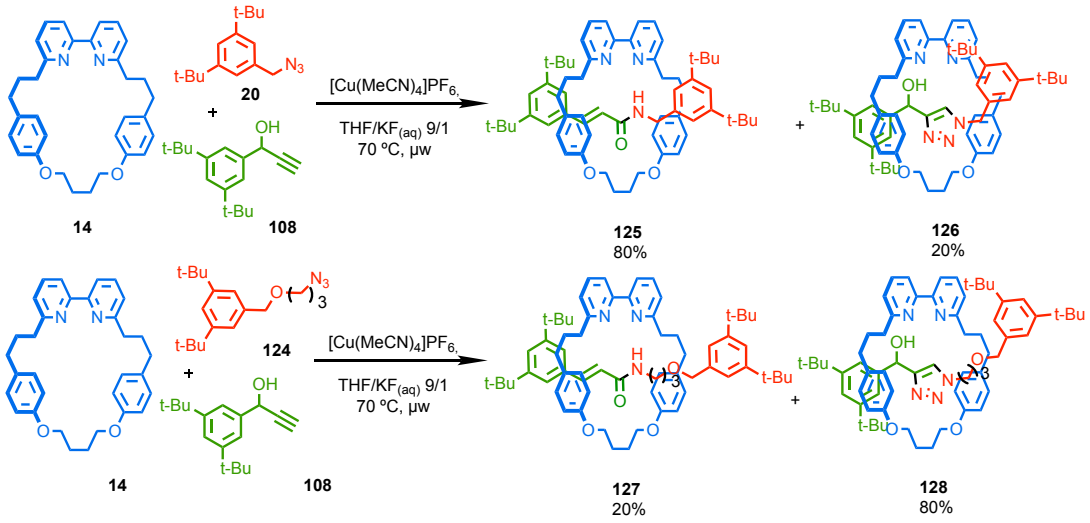

Scheme 3.23 Reaction of alkyne **108** with azides **20** and **124**. Selectivity is presented as percentage of interlocked products, as judged by ^{1}H NMR.

Replacing alkyne **108** with alkyne **116** resulted in a dramatic reduction in selectivity for the rearrangement reaction (**Scheme 3.24**). Again, this is consistent with steric hindrance around the reacting function groups being key to the reaction outcome. It should be noted that the reaction appears to be more sensitive to alkyne structure; alkyne **116** differs from **108** by a single methylene but results in a larger change in reaction outcome than **11** vs **20**, which also differ by a single methylene unit.

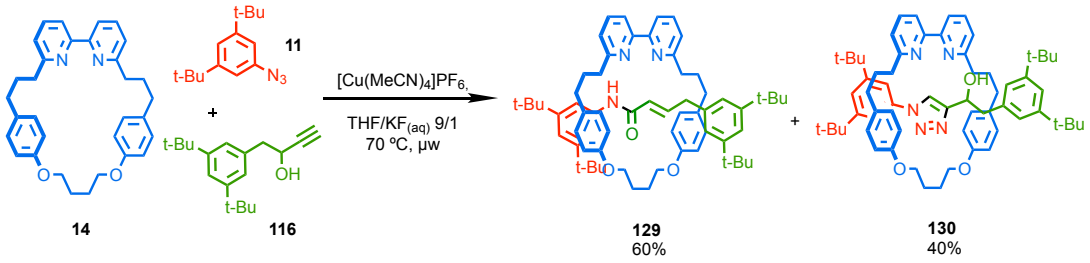

Scheme 3.24 Reaction of alkyne **119** with **11** under rearrangement conditions. Percentages relate to crude conversion taken from ^{1}H NMR.

The reaction was then performed with macrocycle **131**. **131** was chosen as it is too large to be retained by stoppers **108** and **11** and, although it presents the same metal binding unit, it does not present a confined cavity for the reaction to take place in. **132** was the only observed product, with no sign of the acrylamide functionalised axle, suggesting mechanical bond formation is essential for the rearrangement reaction to take place.

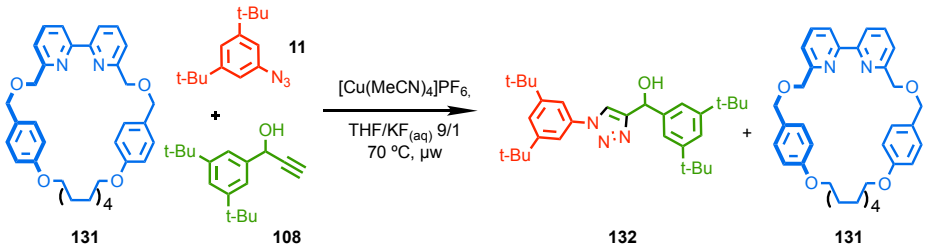

Scheme 3.25 Reaction of **108** and **11** with macrocycle **131** to yield triazole functionalised axle **132** as the sole product.

Finally, we investigated the scope with respect to the macrocycle used. Macrocycles **12** and **133** were used as they are of a similar size to macrocycle to **14** (**Scheme 3.25**). Macrocycle **12** behaved identically to **14**. However, the reaction conditions had to be altered to increase the macrocyclic conversion in the case of **133**, presumably due to increased steric hindrance around the bipyridine ligand. At this higher temperature the selectivity of the reaction is decreased in comparison to **12** and **14** but it is hard to determine if this is due to the change in macrocycle structure or simply due to the higher reaction temperature.

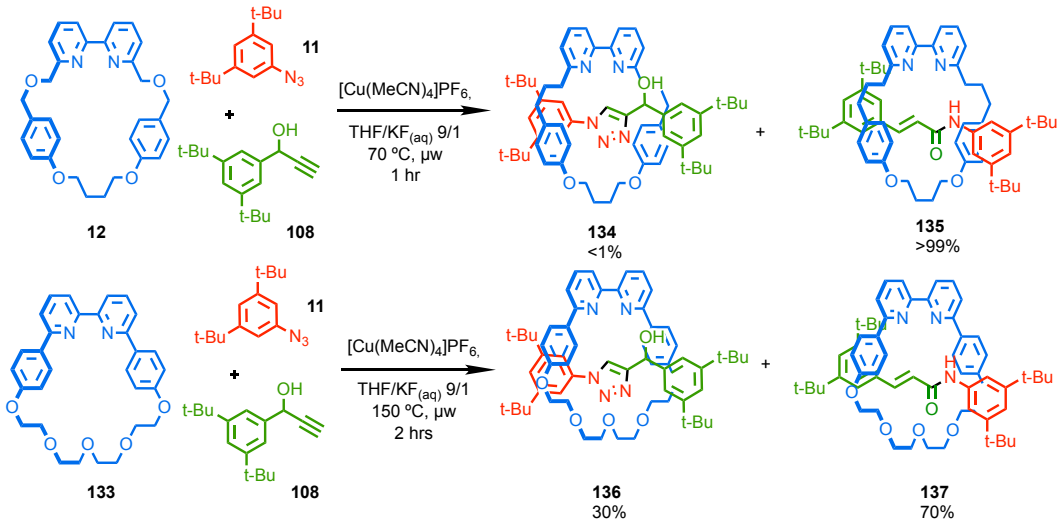

Scheme 3.26 Reaction with macrocycles **12** and **133**. Percentages relate to crude conversion taken from ^{1}H NMR.

The results above suggest the scope of the rearrangement reaction is somewhat limited. However the dependence of the reaction selectivity on the steric hinderance of the reaction partners provides information about the underlying mechanism of the process.

3.2.5. Mechanistic Investigations

Despite the AT-CuAAC reaction being reported many years ago, acrylamide products had never been reported. The obvious difference between the substrates described here and those previously investigated is the presence of the propargylic hydroxyl group. Thus, the

reaction was repeated replacing alkyne **108** with alkyne **118** to confirm if the hydroxy group was required (**Scheme 3.26**). The only observed product was triazole rotaxane **138** with no sign of the acrylamide rotaxane.

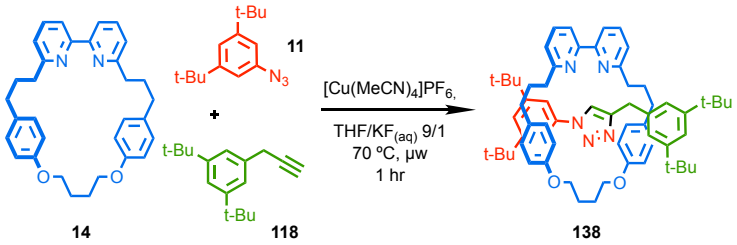

Scheme 3.27 Reaction of **11** and **14** with alkyne **118** to yield triazole rotaxane **138**.

In contrast, the reaction of alkyne **117**, in which a methyl ether group replaces the hydroxyl group of alkyne **108** gave rotaxane **123**, the same product as **108** (**Scheme 3.27**). Previously it had been unclear if the carbonyl oxygen of **123** was derived from the hydroxyl group of **108**. These results together suggest that the carbonyl oxygen does not originate from the hydroxyl/methoxy group directly, but rather that the rearrangement occurs via loss of this group, and that the carbonyl oxygen is derived from the water present in the reaction mixture.

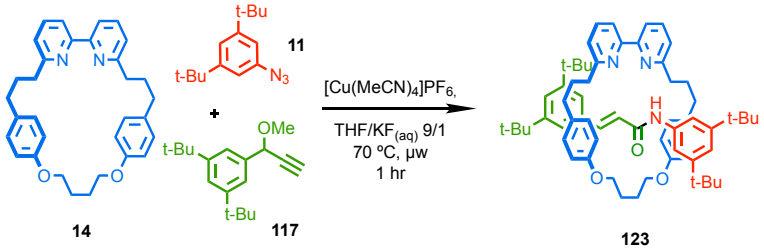

Scheme 3. 28 Reaction of **14** and **11** with alkyne **117** to yield rotaxane **123**.

Having established that the hydroxyl group is not derived directly from the starting material, we designed a substrate to allow us to determine if the carbon atom connectivity remained unchanged between starting materials and product. The reaction of quaternary propargyl alcohol, **121**, under the optimised conditions for the rearrangement gave the expected product, **139**, with completed selectivity for the acrylamide product (**Scheme 3.28**).

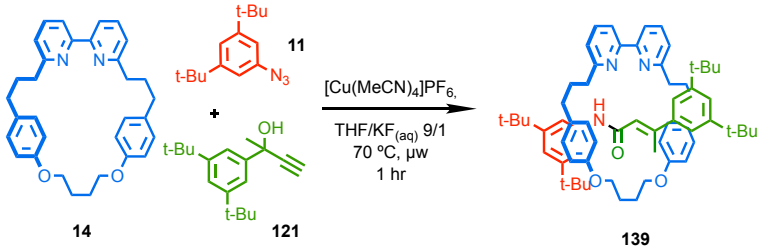

Scheme 3.29 Reaction of **11** and **14** with quaternary alkyne **121** to yield acrylamide rotaxane **139**.

As previously noted, during the AT-CuAAC reaction, the Cu^{I} triazolide intermediate can be rendered incredibly stable due to the sterically hinderance nature of the mechanical bond.[16] Considering that loss of selectivity for the acrylamide product appears to be linked to the lower steric bulk around the reaction centres, this would suggest that the Cu^{I} triazolide could be a common intermediate in the formation of the acrylamide and triazole rotaxanes.

3.2.6. Reactions of Triazolide 140

Whereas during synthesis of **122**, the Cu^{I}-triazolide was not observed post-workup, when attempting the formation of triazole rotaxane **141**, Cu^{I}-triazolide rotaxane **140** proved remarkably stable, as judged by ^{1}H NMR and confirmed by LCMS analysis. Indeed, treatment with KCN did not remove the copper and ultimately, Bu_4NCN was required to completely remove the copper over 5 days. While this was slightly troublesome for the synthesis of rotaxane **141**, this allowed us to access a sample of a triazolide and assess its potential an intermediate in the rearrangement pathway, (**Scheme 3.30**).

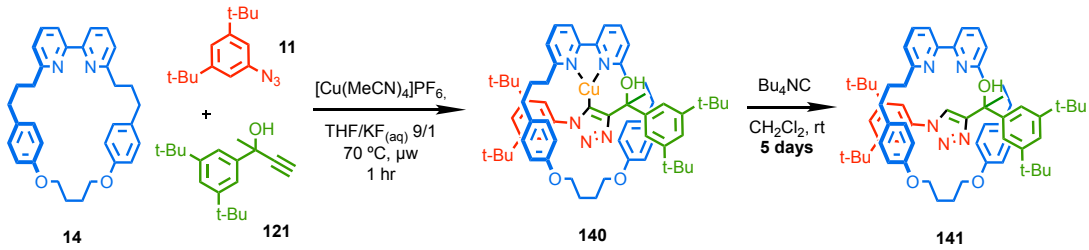

Scheme 3.30 Reaction scheme for rotaxane **141.**

With a sample of **140** in hand, the first test performed was to submit this triazolide to the optimised rearrangement conditions. This led to the appearance of some of **139** in the crude NMR spectra although a lot of triazolide **140** was still present (**Scheme 3.31**, **Figure 3.6**). The exact ratio of **140**:**139** could not be calculated due to the appearance of other signals in the aromatic region and the broad nature of the signals due to **140**.

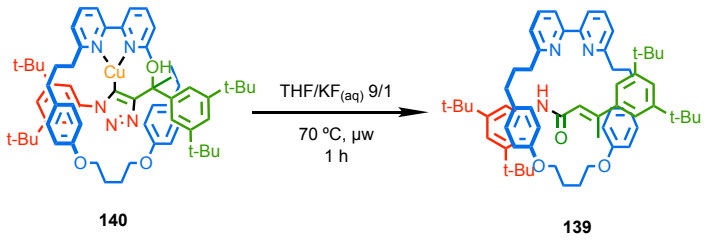

Scheme 3.31 Conversion of triazolide **140** to rotaxane **139** under the optimised rearrangement conditions.

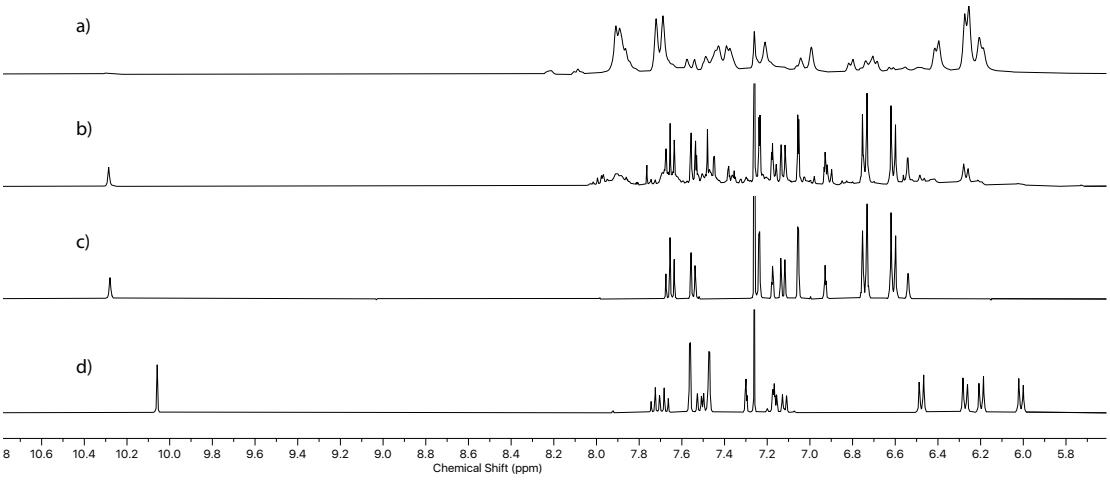

Figure 3.5 Partial stacked ^{1}H NMR spectra ($CDCl_3$, 400 MHz) of a) triazolide **140**, b) shows **140** after treatment shown in **Scheme 3.31**, c) acrylamide rotaxane **139** and d) triazole rotaxane **141** which are shown for comparison.

The appearance of **140** in the ^{1}H NMR spectrum of the crude reaction mixture is not consistent with outcome of the direct reaction of **121**, **11** and **14**. While this result was initially disappointing, upon further reflection it was realised that submitting **140** to the same reaction conditions that were used for the synthesis of **139** was not a direct model of the conditions of the reaction. The reaction of **121**, **11**, and **14** generates **140** alongside an equivalent of acid which is not present in our test reaction starting from **140**.

Accordingly, **140** was submitted to the same reaction conditions but with one equivalent of added HPF_6 (**Scheme 3.32**, **Table 3.6**, **Figure 3.6**). This pleasingly gave full conversion to acrylamide rotaxane **139**, suggesting that acid is involved, or at least accelerates the rearrangement of triazolide **140**. The same outcome was achieved when KF was omitted, and even when the reaction was carried out at room temperature. Both reactions showed complete conversion of triazolide **140** to acrylamide **139**.

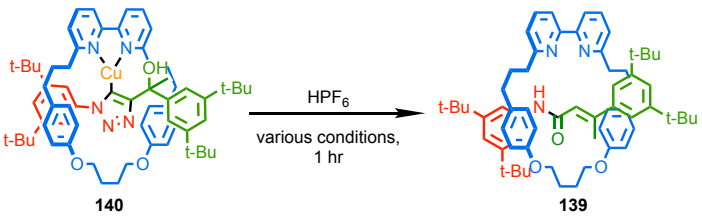

Scheme 3. 32 Conversion of triazolide 140 to rotaxane 139 in the presence of acid.

Entry	Solvent	Temp. (°C)	Conversion
1.	THF/$KF_{(aq)}$ 9:1	70	Full
2.	THF/H_2O 9:1	70	Full
3.	THF/H_2O 9:1	rt	Full

Table 3. 6 Conditions for **Scheme 3.32**.

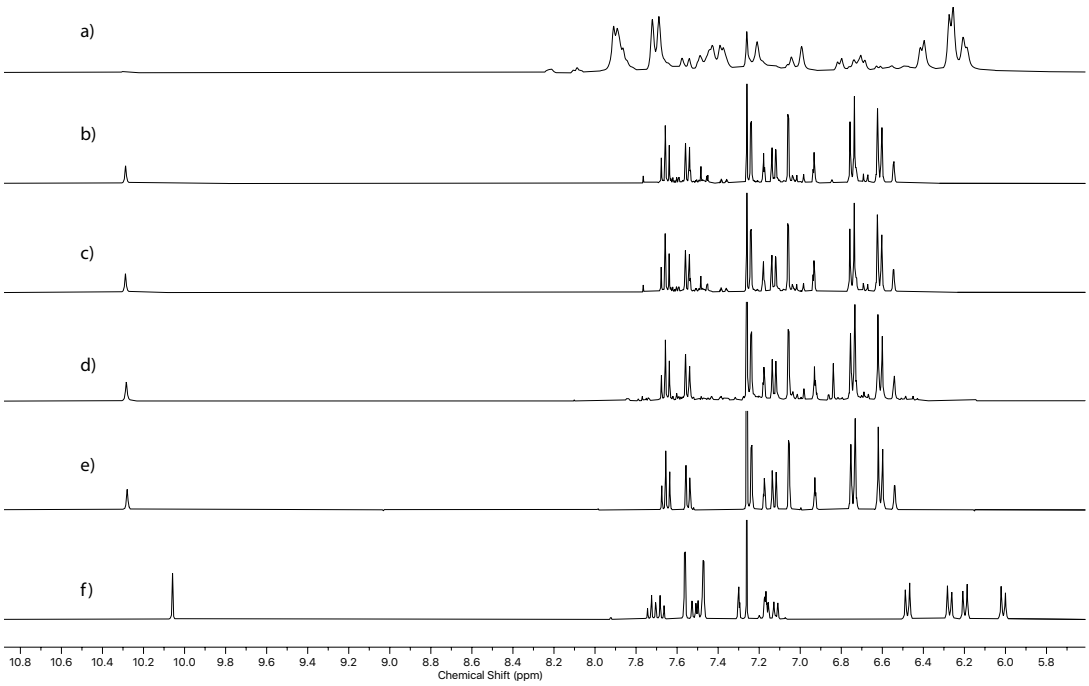

Figure 3. 6 Partial stacked ^{1}H NMR spectra ($CDCl_3$, 400 MHz) of a) triazolide **140**, and reactions **b)**, **c)**, and **d),** (**Scheme 3.32**). e) Acrylamide rotaxane **139** and f) triazole rotaxane **141** are shown for comparison.

These reactions demonstrate the acrylamide rotaxane **139** can arise directly from a rearrangement of Cu^I-triazolide intermediate **140** and not from any alternative reaction of half axles or decomposition of the alkyne or azide functionalities. It was shown previously that treatment of **140** with Bu_4NC to remove the copper ion produces **141**. This clearly demonstrates that the triazolide intermediate is involved in both pathways.

To confirm the importance of the triazolide intermediate, rotaxane **141** was subjected to the conditions under which triazolide **140** is efficiently rearranged (**Scheme 3.33**). Both in the presence and or absence of added Cu^I, no conversion to **139** was observed, confirming that this rearrangement does not occur under these conditions once the Cu^I-C bond of the triazolide has been removed. This final test confirms that the rearrangement occurs from the triazolide, which is stable as a consequence of the mechanical bond.

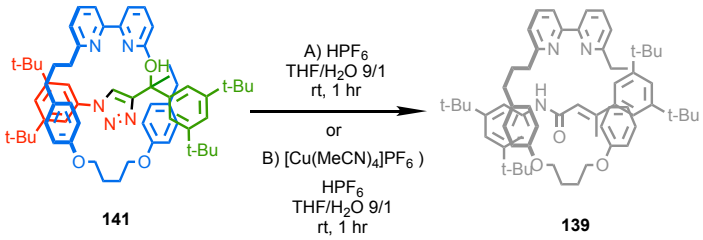

Scheme 3.33 Rotaxane **140** submitted to rearrangement conditions either in A) the absence of Cu^{I} or B) the presence of Cu^{I} gave no reaction.

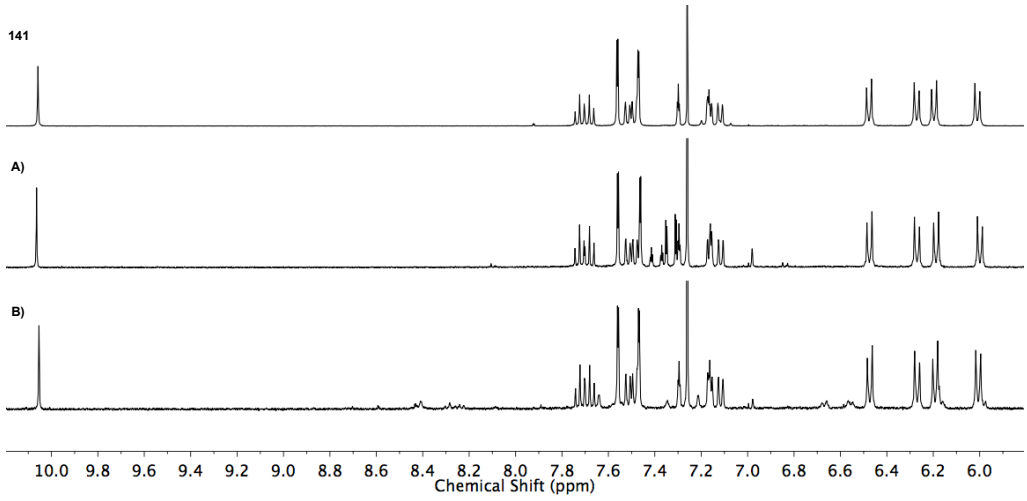

Figure 3.7 Partial stacked ^{1}H NMR spectra ($CDCl_3$, 400 MHz) of triazole **141**, and the crude reaction product of conditions A) and B) (**Scheme 3.32**).

3.2.7. Proposed Mechanism of the Rearrangement Reaction

The results above suggest that the rearrangement proceeds via protonation of the triazolide intermediate of the AT-CuAAC reaction. Typically, treatment of a Cu^{I}-triazolide wth acid results in protonation of the Cu-C bond, ultimately yielding the demetallated rotaxane species.[16] In this case, it appears that the Cu^{I}-Carbon bond must remain intact long enough for the rearrangement to occur. This, suggests that the steric hindrance enforced by the mechanical bond results in selective protonation of the propargylic hydroxyl group rather than organometallic centre as the first step in the route from triazolide to acrylamide. A computational study was performed, the results of which allowed us to postulate a detailed reaction mechanism (**Scheme 3.34**).

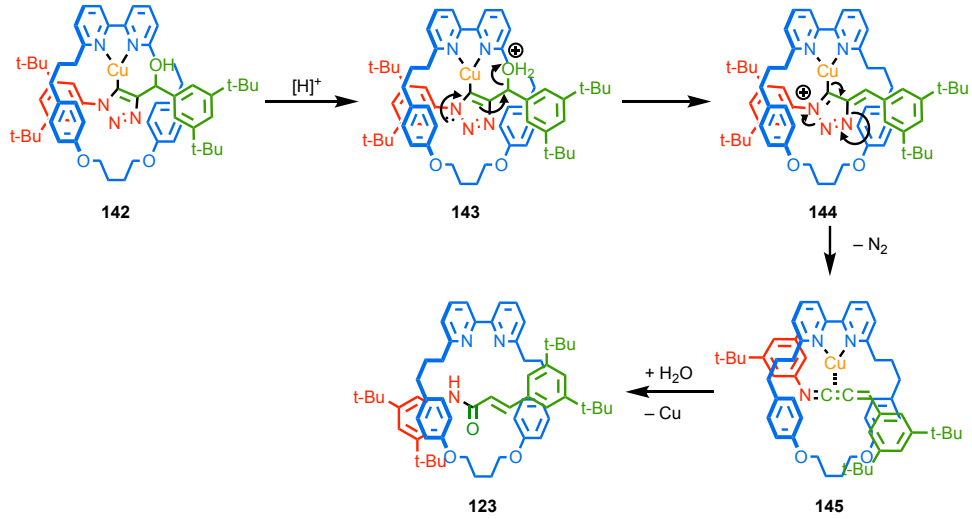

Scheme 3.34 Postulated reaction mechanism for rearrangement from Cu^{I}-Triazolide.

DFT calculations showed that protonation of the hydroxy led to rapid loss of water to give **144**, 'locking' the molecule into the rearrangement pathway. The subsequent loss of nitrogen to give proposed cumulated ketenimine intermediate **145** was predicted to be exergonic by ~44 kJ mol^{-1} and proceed with a barrier of about 78 kJ mol^{-1}. Calculations also suggested that loss of nitrogen happened simultaneously, as we were unable to locate a transition state for the stepwise intermediate, which was shown to have an energy 140 kJ mol^{-1} greater than cation **143** almost double the barrier for the concerted loss of N_2 shown. Cumulated ketenimine intermediate **145** was shown to interact with the Cu^{I} ion in the final structure prior to hydrolysis, and the C-C-C-N unit was not linear. This indicated that the true structure lies somewhere between the limiting resonance structures in which the Cu^{I}-ion engages the ketamine through a π-metal interaction (shown), and a σ-metal interaction.

3.2.8. Rearrangements Triggered by Triflic Anhydride

As shown previously, replacing the α-hydroxy group of **108** with a methyl ether (**118**) resulted in the same reaction product, suggesting that both OH and OMe act as leaving groups in this mechanism. Further to these experiments, it was decided to react the hydroxyl leaving group with triflic anhydride to convert it to a better leaving group without the requirement of aqueous acid.

140 was generated in situ under strictly anhydrous conditions in deuterated solvents in the presence of 4 equivalents of DIPEA to ensure the reaction could be monitored at each step (**Scheme 3.35**, **Figure 3.8**). This mixture was then treated with triflic anhydride and the ^{1}H NMR spectrum of the mixture collected. The spectrum of the mixture changed dramatically upon treatment with triflic anhydride. In particular, a distinctive doublet and triplet appeared

at high ppm (8.3 ppm and 8.1 ppm respectively). These signals were tentatively assigned to two of the three the macrocycle pyridine protons. That these appear as single environments suggests the axle stereogenic unit has been lost in this intermediate, consistent with the structure of cumulated ketenimine **147**. This assignment was supported by LCMS analysis of a portion of the reaction mixture; the major species observed has *m/z* =984.8 which is consistent with **147** (calc. for $109_4H_{79}CuN_3O_2$ = 984.6).

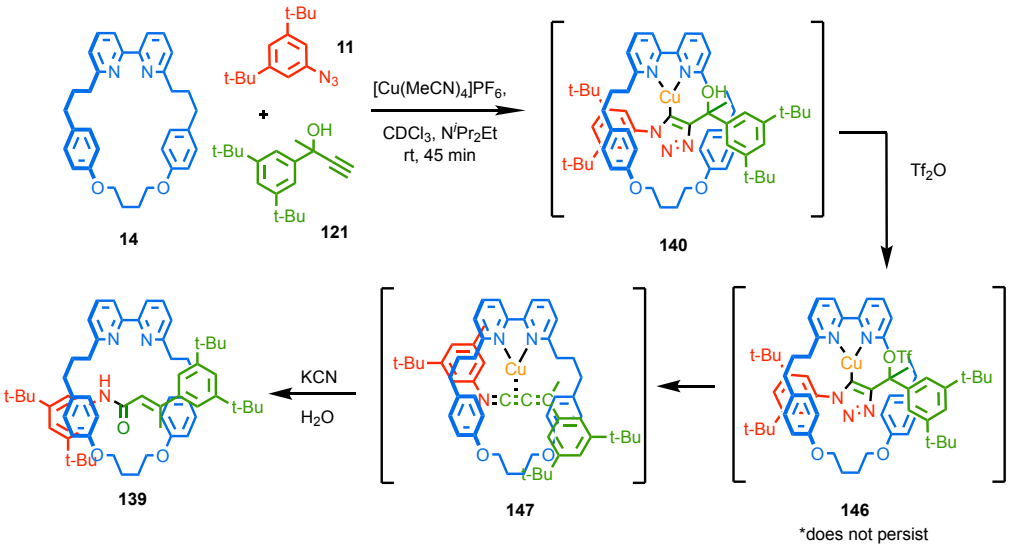

Scheme 3.35 *In situ* generation of triazolide **140**, treatment with triflic anhydride and subsequent rearrangement to cumulated ketenimine **147**.

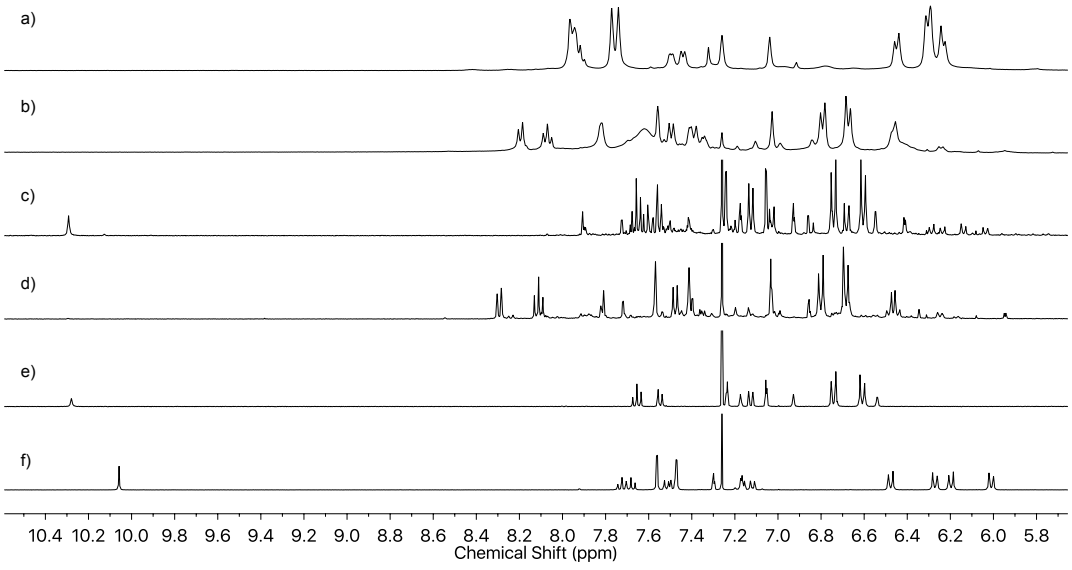

Figure 3.8 Partial stacked ^{1}H NMR spectra ($CDCl_3$, 400 MHz) of a) triazolide **140**, b) the product of the reaction of **140** with Tf_2O (cumulated ketenimine **147**), c) **147** after treatment with $KCN_{(aq)}$), d) **147** after treatment with water. ^{1}H NMR data for e) acrylamide rotaxane **139** and f) triazole rotaxane **141** are shown for comparison.

The sample presumed to be cumulene **147** was then split into two portions. One portion (**Figure 3.8c**) was treated with $KCN_{(aq)}$ whereas the other (**Figure 3.8d**) was treated with H_2O. The ^1H NMR spectrum of the sample treated with KCN showed conversion to **139** and minimal formation of **141**. The ^1H NMR spectrum of the sample treated with H_2O remained remarkably similar to that of **147**, suggesting that in the absence of KCN the cumulene persists in solution.

The 4 equivalents of DIPEA present in the reaction should prevent any protonation of the hydroxyl group under these conditions. However, to confirm that the rearrangement process was triggered by formation of triflate **146** rather than due to decomposition of Tf_2O to give TfOH, a separate sample of **140** was prepared and treated directly with TfOH (**Scheme 3.36**, **Figure 3.9**). As expected, negligible changes were observed. Treatment of this sample with $KCN_{(aq)}$ led to a sharpening of the spectra for but the major species remained triazolide **140** alongside trace amounts of **139** and **141**. These results confirm that conversion of **140** to **139** upon reaction with Tf_2O was indeed the result of triflate formation.

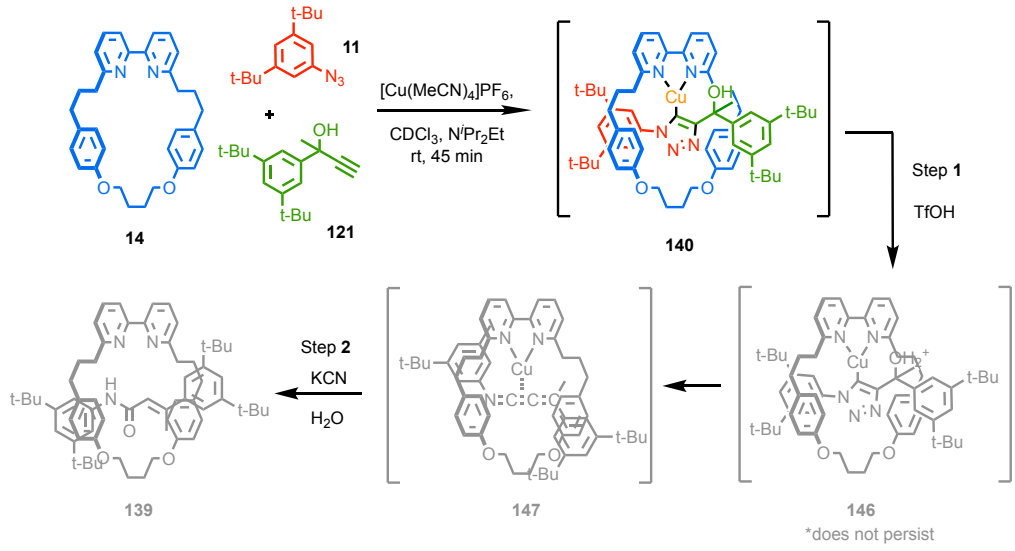

Scheme 3.36 *In situ* generation of triazolide **140** and its subsequent reaction with triflic acid.

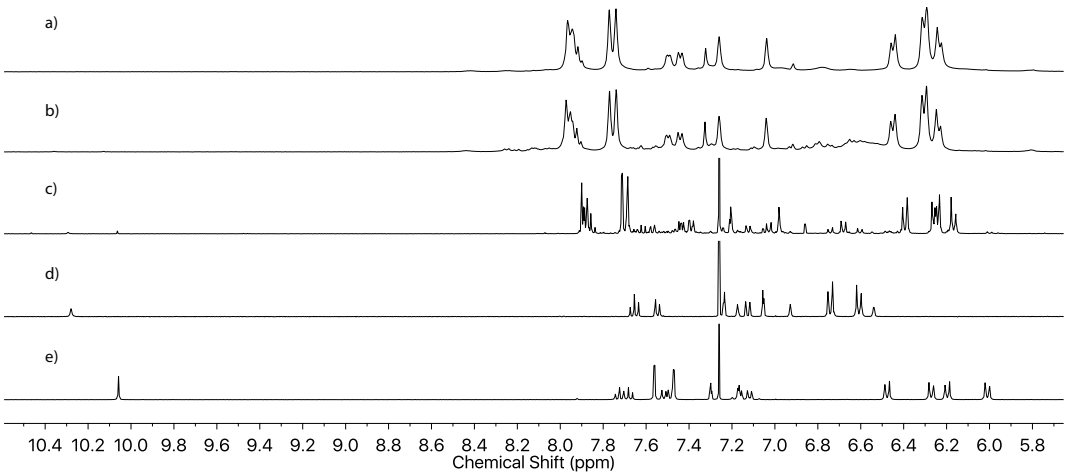

Figure 3.9 Partial stacked ^{1}H NMR spectra ($CDCl_3$, 400 MHz) of triazolide a) **140**, b) Step 1: **140**, after treatment with TfOH, and c) Step 2: **140** after treatment with KCN. The spectra of acrylamide rotaxane **139** and triazole rotaxane **141** are shown for comparison**.**

Following from this success, it was decided to test triflate formation as an alternative route to rotaxane **123**. Although triazolide **142** had not been observed previously, it was hoped that it could be generated *in situ* under anhydrous conditions and converted on the product (**Scheme 3.37**, **Figure 3.10**). Reaction of **108**, **11** and **14** produced a product mixture consistent with the formation of triazolide **142**. When this mixture was treated with Tf_2O this species was largely converted to a new species consistent with **144**, although the reaction appeared incomplete. Treatment of half of this mixture with $KCN_{(aq)}$ gave acrylamide **132** as the major product alongside 10% of triazole rotaxane **122**. Alternatively, treatment of the solution of **142** with H_2O gave incomplete conversion of **142** to a mixture containing 9:1 **123:122** alongside residual cumulene **145** and triazolide **142**.

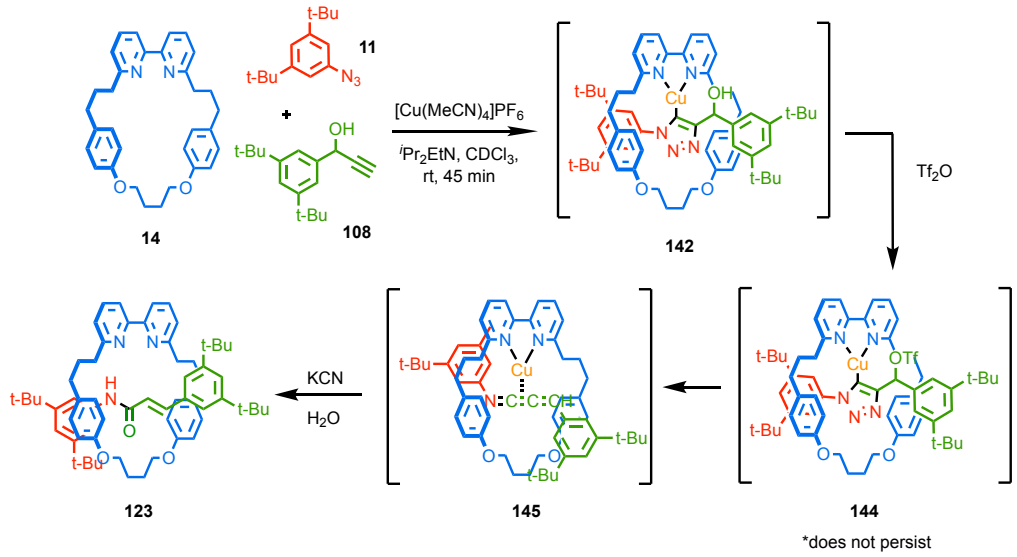

Scheme 3.37 *In situ* generation of triazolide **142**, treatment with triflic anhydride and subsequent rearrangement to cumulated ketenimine **145.**

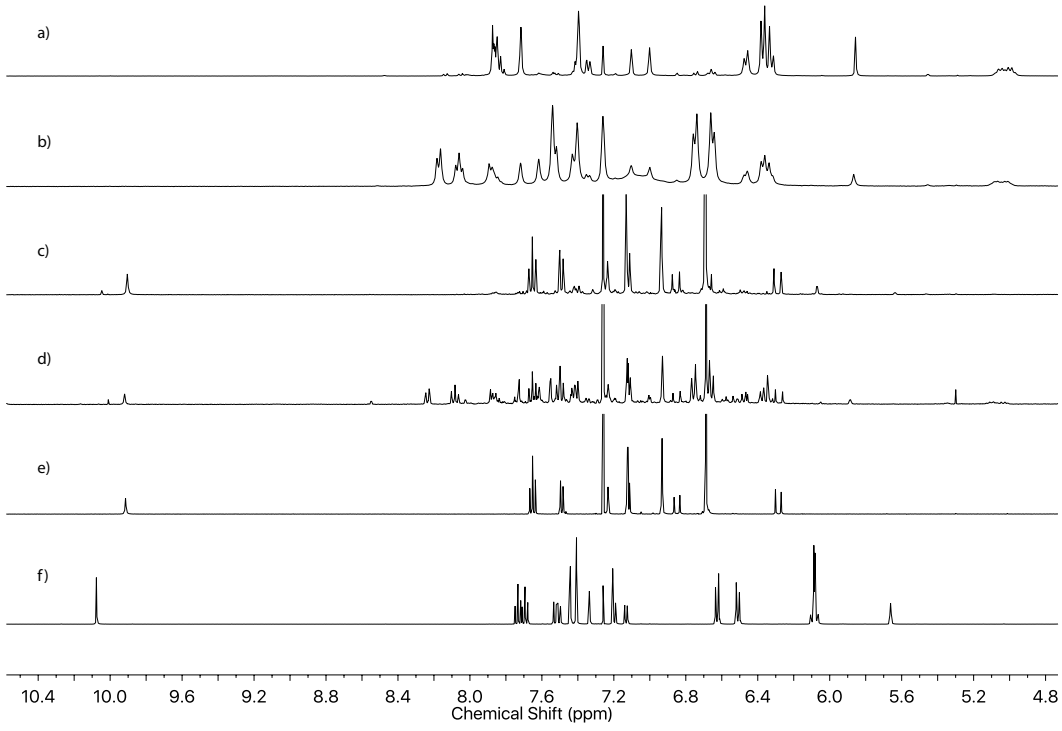

Figure 3. 10 Partial stacked ^{1}H NMR spectra ($CDCl_3$, 400 MHz) of a) triazolide **142**, b) the reaction mixture formed by reaction of **142** with Tf_2O, presumed to be cumulene **145**, c) the mixture after treatment with $KCN_{(aq)}$, and d) H_2O. The spectra of e) Acrylamide rotaxane **123** and f) triazole rotaxane **122** are shown for comparison**.**

The slight difference in reactivity between triazolides **142** and **140** is presumed to be due to the reduced steric protection of the Cu^{I}-carbon bond in the case of **142**. This test however

still clearly shows that triazolide **142** can be generated in situ, and then converted to acrylamide 123 by reaction with triflic anhydride.

3.2.9. Imine Synthesis

With a reproducible and reliable synthesis route to α-hydroxy-triazole functionalised rotaxanes in hand, we returned to the original aim of the project. Firstly, the reaction of **108**, **11** and **51** under conditions optimised for triazole formation was conducted to determine if any diastereoselectivity in the formation of **109** could be observed (**Scheme 3.39**). Pleasingly, in CH_2Cl_2 **109** was formed as a 2:1 mixture of diastereoisomers. Switching the solvent to THF improved the diastereoselectivity to 3:1.

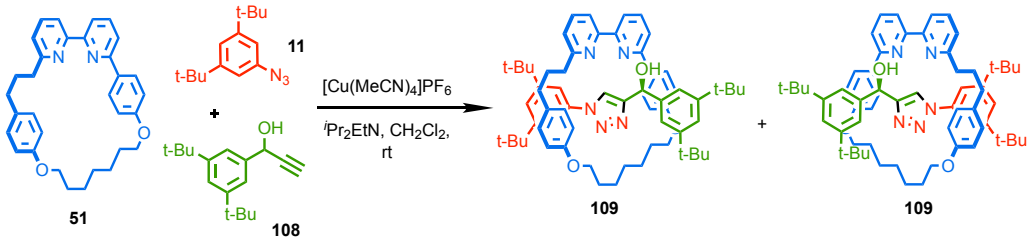

Scheme 3. 38 Synthesis of rotaxane **109** from racemic **108**. Diastereomers based on one enantiomer of **109** are shown. Their enantiomers are omitted for clarity.

Having demonstrated that it was possible to form rotaxane **109** stereoselectively, assuming enantiopure **108** could be produced, we decided to investigate the next steps, oxidation to give a ketone and imine formation, using readily available rotaxane **122**. Oxidation of rotaxane **122** with PCC, a strong chromium based oxidizing reagent, led to decomposition of the starting material (**Scheme 3.39**).

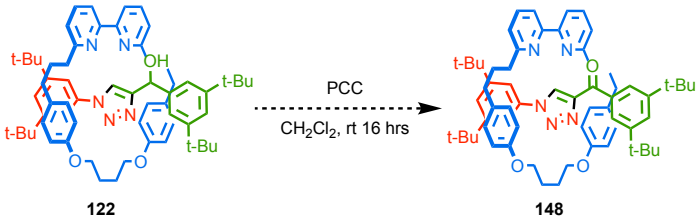

Scheme 3. 39 Attempted synthesis of **148** using PCC.

Replacing PCC with the Dess-Martin periodinane yielded rotaxane ketone **148** (**Scheme 3.40**).

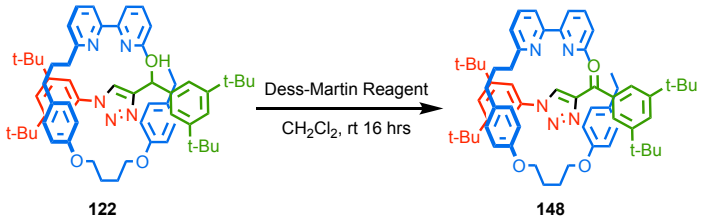

122 148

Scheme 3.40 Synthesis of **148** using Dess-Martin reagent.

With **148** in hand, the synthesis of imine functionalised rotaxanes could then be attempted (**Scheme 3.41**). Unfortunately, although forcing conditions were used, neither benzylic amine **149** or aliphatic amine **151** reacted with rotaxane **148** to produce an imine, as judged by ^{1}H NMR analysis of their crude reaction mixtures. **148** was the only observed interlocked species.

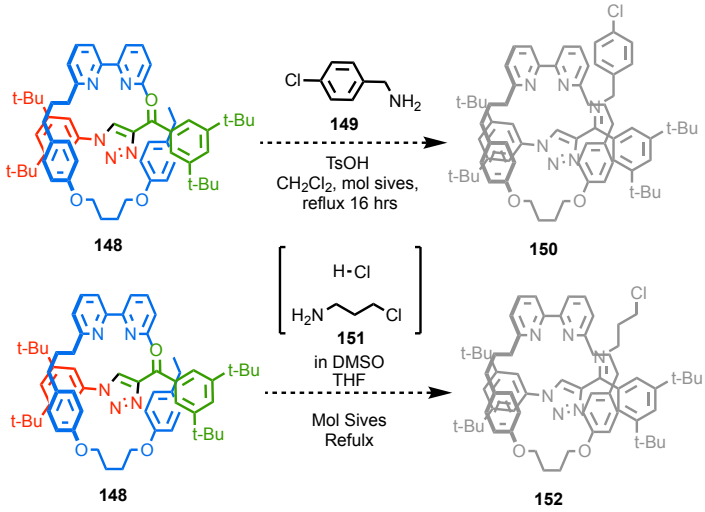

148 150 148 152

Scheme 3.41 Attempted condensation of **513** with amines a) **150** and b) **152** in under forcing conditions.

It is unclear if **148** is simply unreactive, or if the imine products are so unstable that they could not be observed due to hydrolysis on workup. To address this, we attempted formation of semicarbazide **154** as such hydrazones are generally more stable than imines (**Scheme 3.42**). This reaction unfortunately also failed, with no conversion of **148** observed.

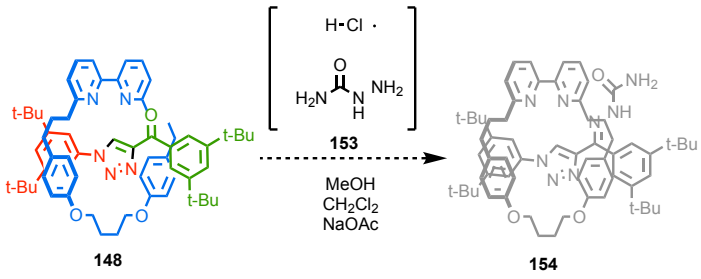

148 154

Scheme 3.42 Attempted synthesis of hydrazone rotaxane **155**.

Why **148** remains intact through all these reactions is not clear. It could be partially down to steric hinderance in this small rotaxane disfavouring these transformations. Given that imine and hydrazone functionalities exist in an equilibrium with the starting materials, it may be that they are simply strongly disfavoured, although the use of molecular sieves would be expected to drive the reaction to completion. Given the obvious issues with further functionalisation of **148** it is obvious that this is not a good platform for developing sensors based on imine formation.

3.3. Conclusions and Future Work

The first and most pressing aim of this project was to be able to control the novel rearrangement that had been observed, and selectively synthesise the intended α-hydroxy triazole rotaxane. These objectives were accomplished. We now have not only a selective and reliable route to synthesise the intended product, but also a selective route to the acrylamide functionalised rotaxane. Along the way, we successfully identified the structure of the mystery product and explored the scope of this rearrangement. Although it was not found to be very general, the requirement for steric hinderance around the triazolide moiety prompted an investigation into the mechanism of this reaction. Through a series of carefully designed reactions and experiments, we were able to determine this rearrangement occurs due to a selective protonation of a *less* basic site, due to the steric hinderance of the mechanical bond protecting the Cu^{I}-triazolide copper-carbon bond. This rearrangement is the first of its kind, and the first report of the AT-CuAAC yielding a rotaxane which is not triazole functionalised.

Although we demonstrated the use of propargylic alcohol **108** as a chiral auxiliary, its applications remain relatively unexplored as, in model system **149**, we were unable to transform the ketone functionality to an imine, possible due to steric hindrance. Future work could focus on different methods of imine functionalization, or possibly, a slightly less sterically hindered rotaxane to try and improve upon these problematic steps.

3.4. Experimental

General Experimental

Synthesis: Unless otherwise stated, all reagents, including anhydrous solvents, were purchased from commercial sources and used without further purification. All reactions were carried out under an atmosphere of N_2 using anhydrous solvents unless otherwise stated. Petrol refers to the fraction of petroleum ether boiling in the range 40–60 °C. EDTA-NH_3 solution refers to an aqueous solution of NH_3 (17% w/w) with 0.1 M sodium-ethylenediaminetetraacetate. Flash column chromatography was performed using Biotage Isolera-4 or Biotage Isolera-1 automated chromatography system, employing Biotage SNAP or ZIP cartridges. Analytical TLC was performed on precoated silica gel plates (0.25 mm thick, 60F254, Merck, Darmstadt, Germany) and observed under UV light or with potassium permanganate solution. Microwave heating of reactions was achieved using a Biotage Initiator+ microwave system. Reactions were run at a maximum power level of 400 W in crimp-cap sealed vials (CEM Ltd.). The temperature was monitored automatically and maintained at the set level throughout the reaction after an initial ramp period, typically ~ 1 minute.

Analysis: NMR spectra were recorded on Bruker AV400, AV3-400 or AV500 instrument, at a constant temperature of 298 K. Chemical shifts are reported in parts per million from low to high field and referenced to residual solvent. Coupling constants (*J*) are reported in Hertz (Hz). Standard abbreviations indicating multiplicity were used as follows: m = multiplet, quint = quintet, q = quartet, t = triplet, d = doublet, s = singlet, app. = apparent, br = broad. Signal assignment was carried out using 2D NMR methods (HSQC, HMBC, COSY, NOESY) where necessary. All melting points were determined using a Griffin apparatus. Low resolution mass spectrometry was carried out by the mass spectrometry services at the University of Southampton (Waters TQD mass spectrometer equipped with a triple quadrupole analyser with UHPLC injection [BEH C18 column; MeCN-hexane gradient {0.2% formic acid}]). High resolution mass spectrometry was carried out by the mass spectrometry services at the University of Southampton (MaXis, Bruker Daltonics, with a Time of Flight (TOF) analyser; samples were introduced to the mass spectrometer via a Dionex Ultimate 3000 autosampler and uHPLC pump in a gradient of 20% acetonitrile in hexane to 100% acetonitrile (0.2% formic acid) over 5 min at 0.6 mL min; column: Acquity UPLC BEH C18 (Waters) 1.7 micron 50 × 2.1mm).

The following compounds were synthesised according to literature procedures:

2-(3,5-di-*tert*-butylphenyl)acetaldehyde **115**,[14] 1-azido-3,5-di-*tert*-butylbenzene **11**,[9] 1-(azidomethyl)-3,5-di-*tert*-butylbenzene **20**,[10] 1-((3-azidopropoxy)methyl)-3,5-di-*tert*-butylbenzene **124**,[11] macrocycles **12**, **14**, **51**, **131**, and **133**. [12]

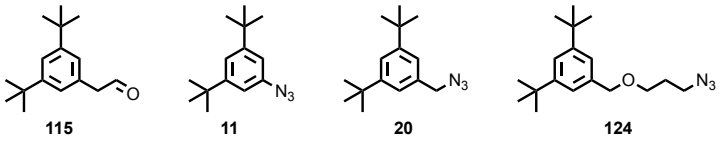

115 11 20 124

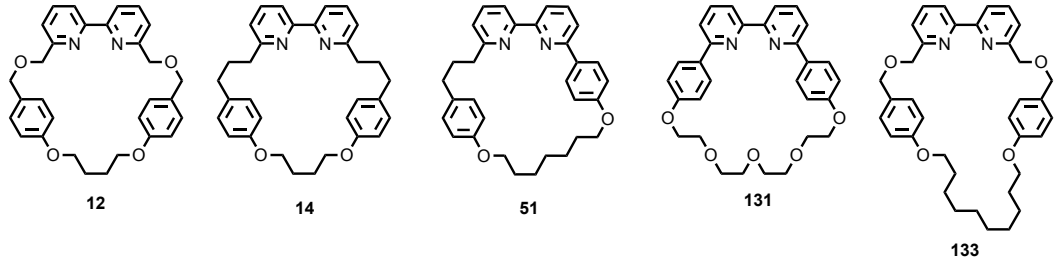

12 14 51 131 133

1-(3,5-Di-tert-butylphenyl)prop-2-yn-1-ol ***108***

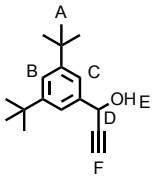

113 (1.4 g, 6.4 mmol) was dissolved in THF (20 mL) at 0 °C under N_2. Ethynylmagnesium chloride (0.6 M in THF, 10 mmol, 16 mL) was added dropwise. The mixture was stirred for 20 h at rt. Saturated $NH_4Cl_{(aq)}$ (10 mL) was added and the solvent removed *in vacuo*. The residue was extracted with Et_2O (3 × 20 mL). The combined organic layers were washed with brine (10 mL), dried ($MgSO_4$), filtered and the solvent removed *in vacuo.* Chromatography (petrol/ethyl acetate 9:1) gave **108** as a light-yellow oil (1.5 g, 97%). ^{1}H NMR (400 MHz, $CDCl_3$) δ: 7.44-7.39 (m, 3H, H_B, H_C), 5.46 (d, *J* =2.2, 1H, H_D), 2.67 (d, *J* =2.2, 1H, H_F), 2.14 (br. s, 1H, H_E), 1.34 (s, 18H, H_A). ^{13}C NMR (101 MHz, $CDCl_3$) δ: 151.2, 139.3, 122.7, 121.0, 84.1, 74.7, 65.1, 35.0, 31.6. HR-EI-MS *m/z* = 244.18118 $M^{+\cdot}$ (calc. for $C_{17}H_{24}O$ 244.18217).

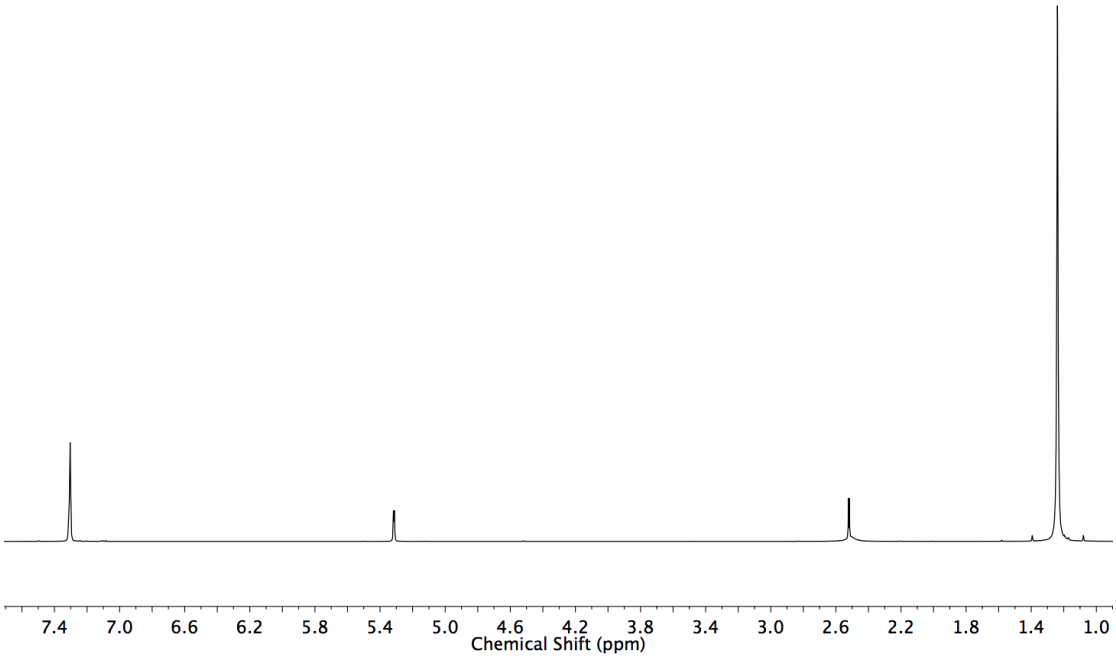

Figure 3.11 ^{1}H NMR ($CDCl_3$, 400 MHz) of **108**

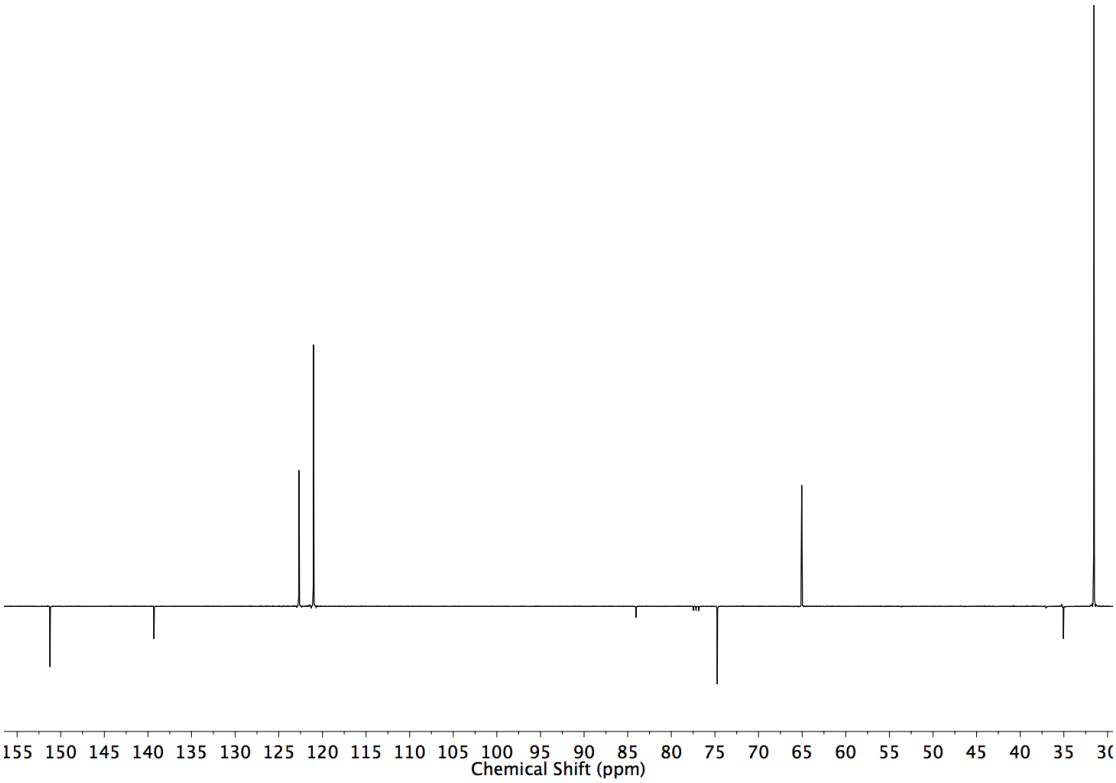

Figure 3.12 JMOD NMR ($CDCl_3$, 101 MHz) of **108**.

3,5-Di-tert-butylbenzaldehyde ***113***

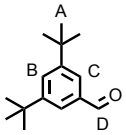

3,5-Di-tert-butyltoluene (6.1 g, 29.9 mmol) was treated with NBS (11.0 g, 62.0 mmol) and AIBN (33.8 mg, 0.2 mmol) in PhCl (150 mL), and stirred for 16 h at 140 °C. The mixture was cooled to rt and passed through a Celite plug. The solvent was removed *in vacuo.* The residue was slurried in 20 mL of 1:1 water/ethanol. Hexamethylenetetramine (12.2 g, 86.9 mmol) was added, and the mixture was heated to reflux for 4 h, cooled to rt, diluted with PhMe-Et_2O (1:1, 130 mL) and the phases separated. The organic phase was washed with brine (50 mL), dried ($MgSO_4$), filtered and the solvent removed *in vacuo.* Chromatography (petrol/Et_2O 95:5) gave **113** as a white solid (5.0 g, 77%). M.p. 84 - 86 °C. Spectra were consistent with those previously reported.[17] ^{1}H NMR (400 MHz, $CDCl_3$) δ: 10.01 (s, 1H, H_D), 7.75-7.68 (m, 3H, H_B and H_C), 1.37 (s, 18H, H_A). ^{13}C NMR (101 MHz, $CDCl_3$) δ: 193.3, 152.0, 136.3, 129.9, 124.2, 35.2, 31.3.

Alternative ^{n}BuLi method;

3,5-di-tertbutyl-1-bromobenzene (538.1 mg, 2.0 mmol) was dissolved in THF (19.5 mL) at -78 ºC. nBuLi (1.4 mL, 2.5 M, 3.5 mmol) was added dropwise and the reaction stirred for 1 h. DMF (0.45 mL) in THF (5.55 mL). The reaction was stirred for a further 1 h at -78 ºC, then stirred at rt for 3 h. Reaction was quenched with ammonium chloride (20 mL), and extracted with ether (3 x 20 mL). Organic phases were washed with water (2 x 20 mL) then brine (10 mL), dried ($MgSO_4$) filtered and the solvent removed in *vacuo,* yielding **23** as a white solid. (420 mg, 98%)

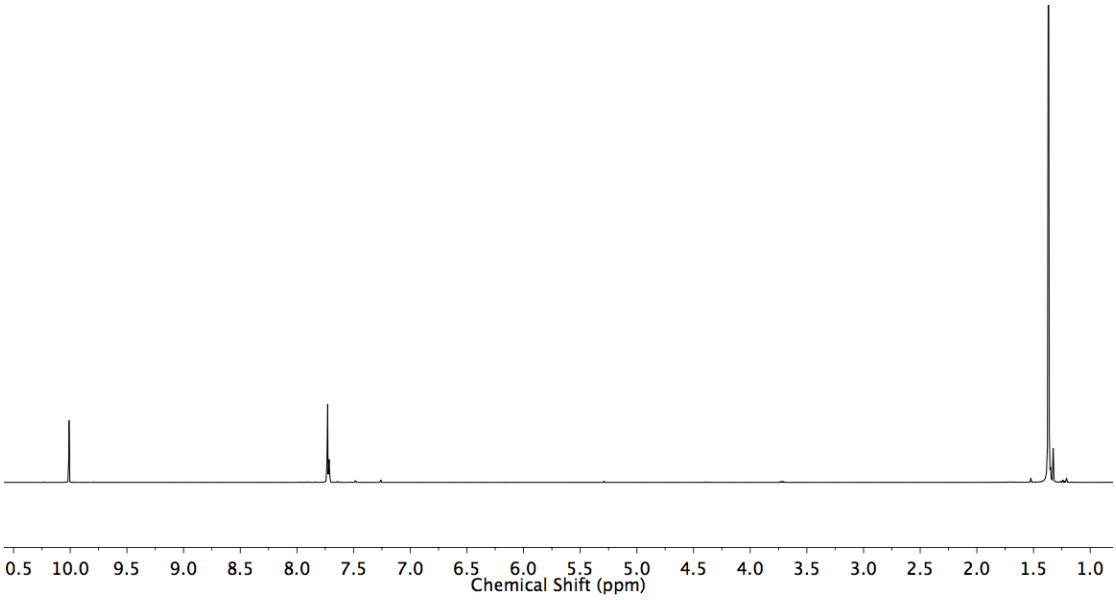

Figure 3.13 ^{1}H NMR ($CDCl_3$, 400 MHz) of **113**.

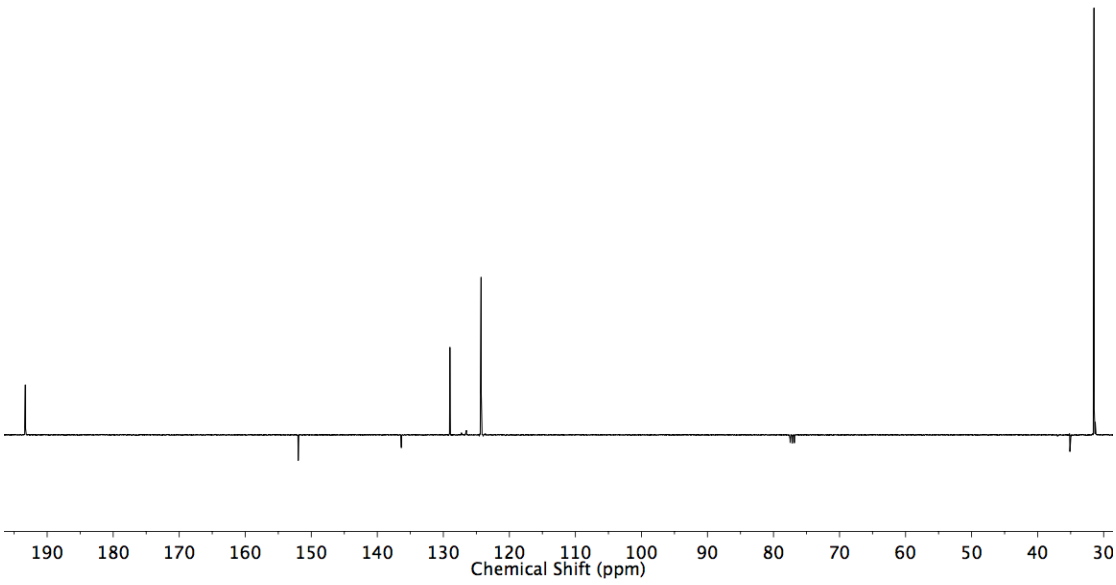

Figure 3.14 JMOD NMR ($CDCl_3$, 101 MHz) of **113**.

1-(3,5-Di-tert-butylphenyl)but-3-yn-2-ol ***116***

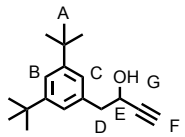

115 (400 mg, 1.7 mmol) was dissolved in THF (3 mL) at 0 °C under N_2. Ethynylmagnesium bromide (0.5 M in THF, 2.0 mmol, 4.0 mL) was added dropwise. The reaction mixture was stirred for 20 h at rt. Saturated $NH_4Cl_{(aq)}$ (5 mL) was added and the solvent was removed *in vacuo*. The residue was extracted with Et_2O (3 × 20 mL). The combined organic layers were washed with brine (10 mL), dried ($MgSO_4$), filtered and the solvent removed *in vacuo.* Chromatography (petrol/Et_2O 95:5) gave **116** as a colourless oil (160 mg, 36 %). ^{1}H NMR (400 MHz, $CDCl_3$) δ: 7.33 (t, *J* =1.9, 1H, H_B), 7.13 (d, *J* =1.9, 2H, H_C), 4.58 (app. qd, *J* =6.1, 2.0, 1H, H_E), 3.03 (qd, *J* =16.3, 6.5, 2H, H_D), 2.50 (d, *J* =2.1, 1H, H_F), 1.88 (d, *J* =6.1, 1H, H_G), 1.33 (s, 18H, H_A). ^{13}C NMR (101 MHz, $CDCl_3$) δ: 151.0, 135.1, 124.2, 121.2, 84.6, 73.7, 63.2, 44.6, 34.9, 31.6. HR-EI-MS *m/z* = 258.19765 M^+ (calc. for $C_{18}H_{26}O$ 258.19782).

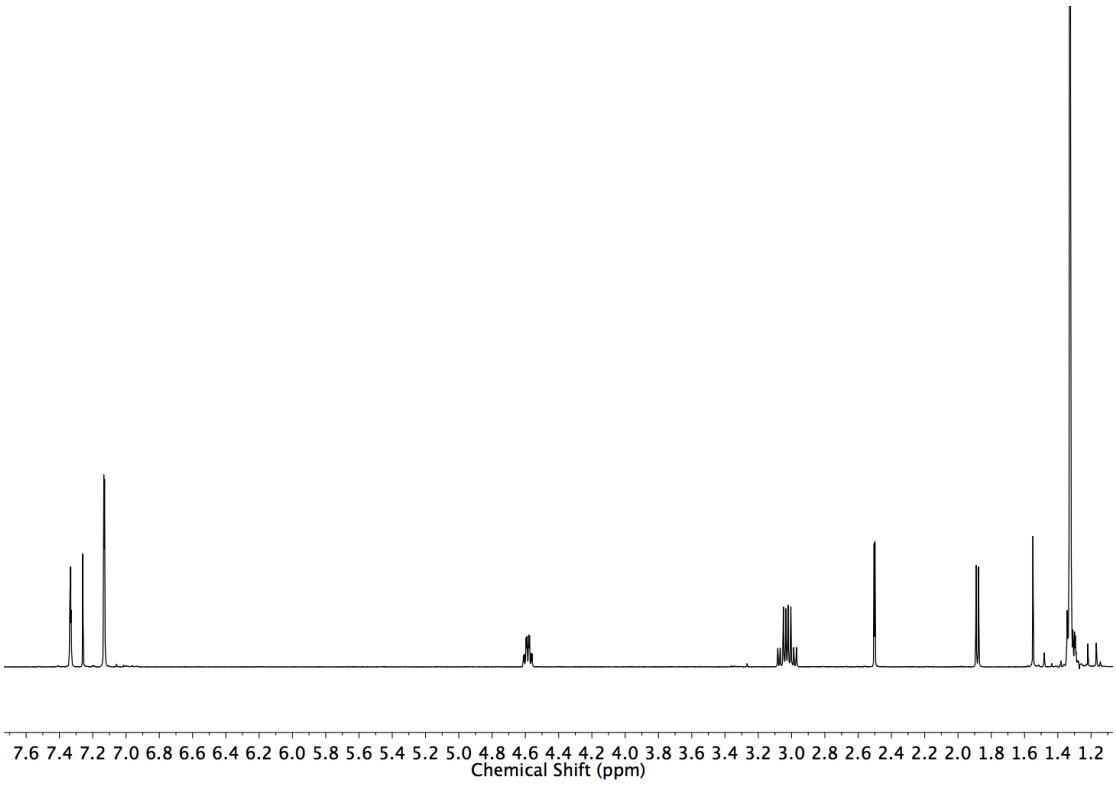

Figure 3.15 1H NMR (CDCl3, 400 MHz) of **116**.

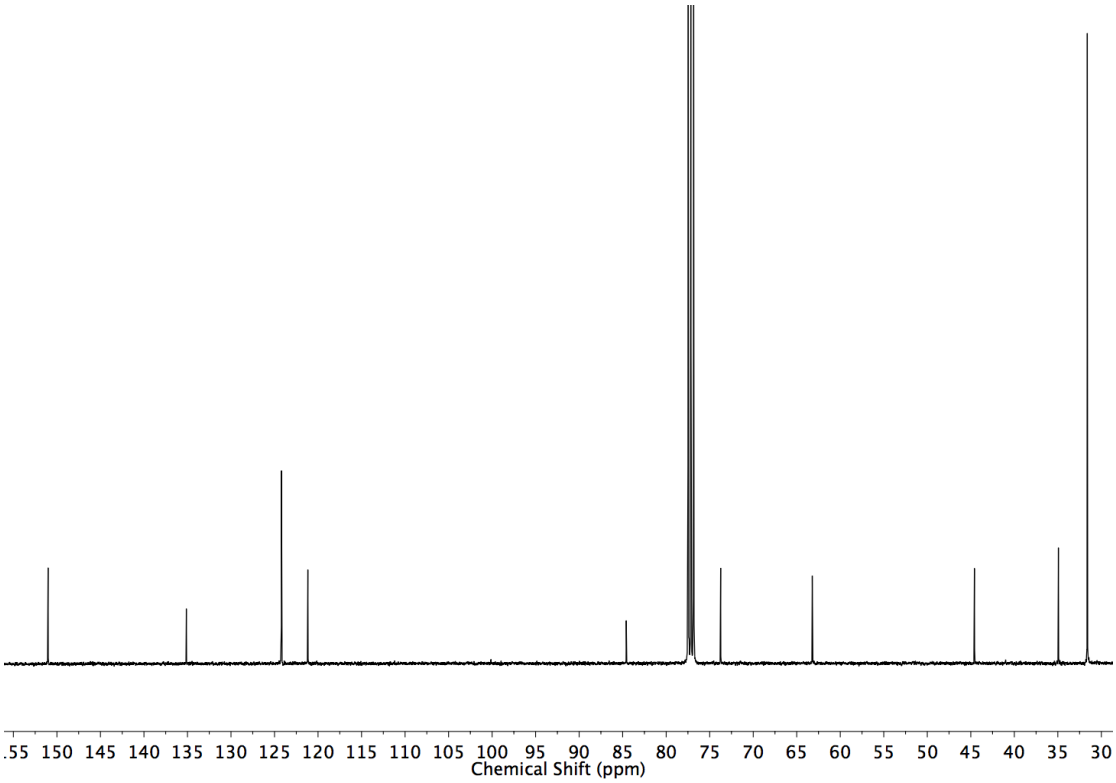

Figure 3. 16 ^{13}C NMR ($CDCl_3$, 101 MHz) of **116**.

1,3-Di-tert-butyl-5-(1-methoxyprop-2-yn-1-yl)benzene ***117***

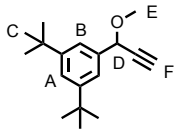

108 (50 mg, 0.2 mmol) was dissolved in THF (1 mL) at 0 °C under N_2. NaH (12 mg, 0.3 mmol) was added in one portion. The mixture was stirred for 10 minutes and MeI (26 µL, 0.4 mmol) was added. The mixture was stirred for 3 h at rt. Saturated $NH_4Cl_{(aq)}$ (5 mL) was added and the mixture extracted with Et_2O (3 × 10 mL). The combined organic layers were washed with brine (5 mL), dried ($MgSO_4$), filtered and the solvent removed *in vacuo*. Chromatography (petrol/Et_2O 95:5) gave **117** as a yellow oil (52 mg, 98%). ^1H NMR (400 MHz, $CDCl_3$) δ: 7.40 (t, *J* =1.8, 1H, H_A), 7.34 (d, *J* =1.8, 2H, H_B), 5.05 (d, *J* =2.2, 1H, H_D), 3.47 (s, 3H, H_E), 2.65 (d, *J* =2.2, 1H, H_F), 1.33 (s, 18H, H_C). ^{13}C NMR (101 MHz, $CDCl_3$) δ: 151.1, 137.1, 122.9, 121.8, 81.9, 75.7, 73.7, 56.3, 35.1, 31.6. HR-EI-MS *m/z* = 258.19835 M^+ (calc. for $C_{18}H_{26}O$ 258.19782).

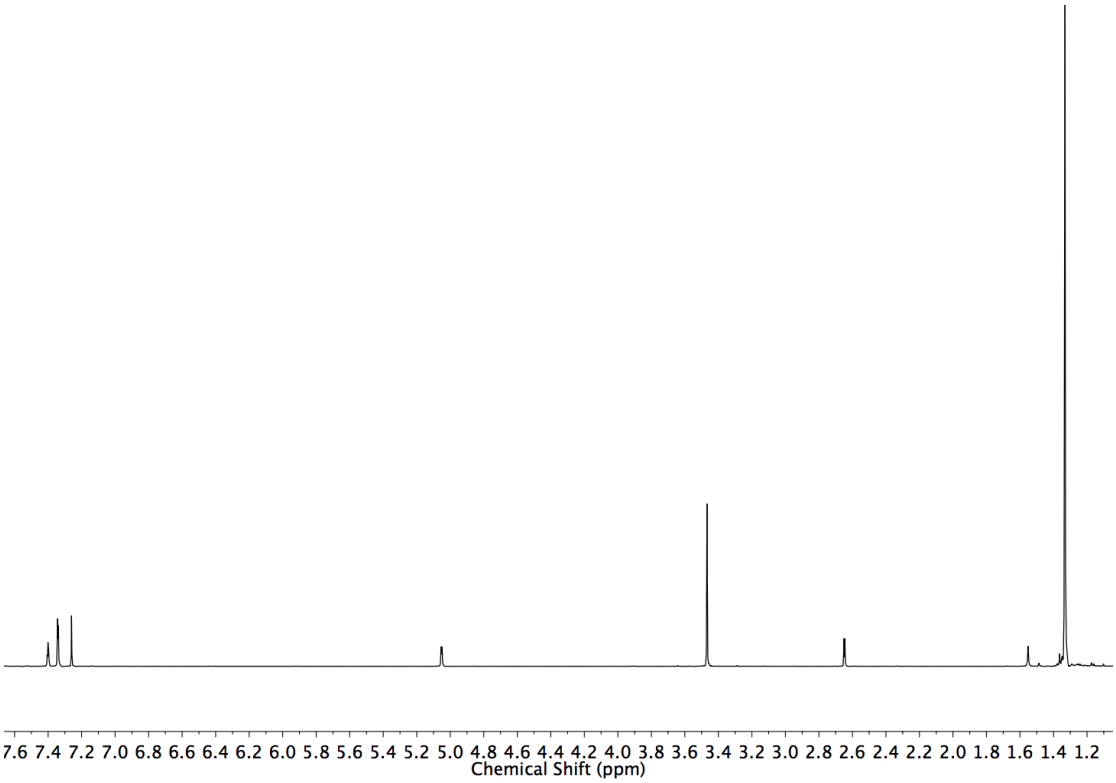

Figure 3.17 ^{1}H NMR ($CDCl_3$, 400 MHz) of **117**.

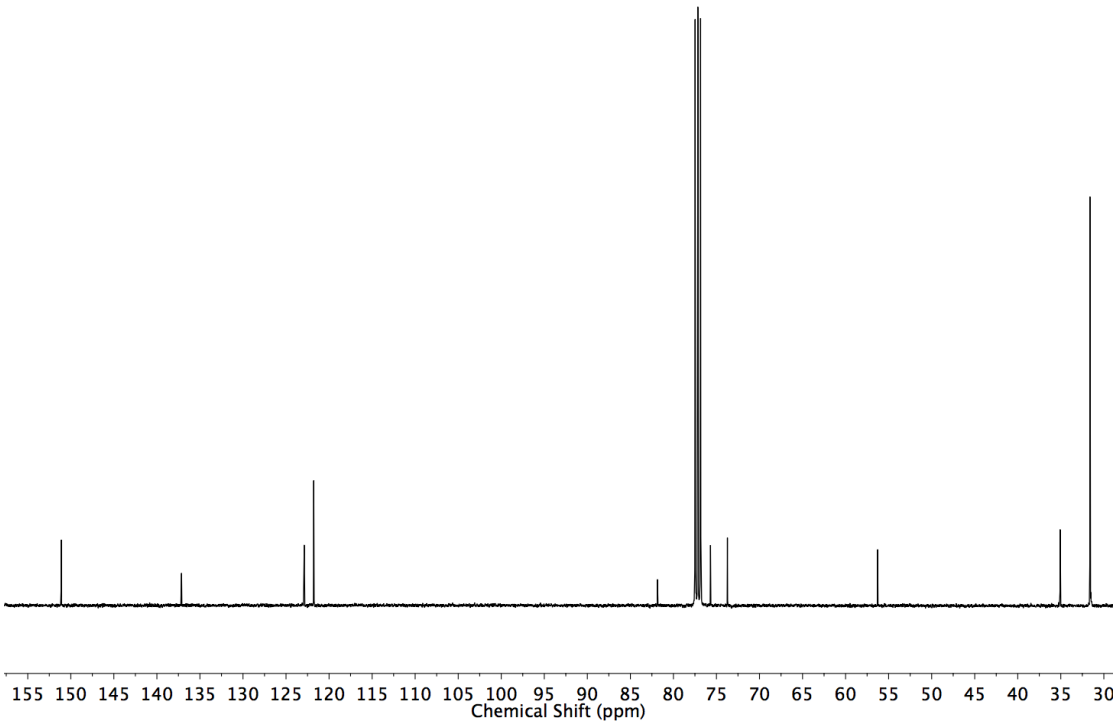

Figure 3.18 ^{13}C NMR ($CDCl_3$, 101 MHz) of **117**.

1,3-Di-tert-butyl-5-(prop-2-yn-1-yl)benzene ***118***

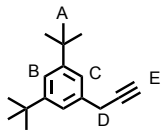

115 (200 mg, 0.86 mmol), dimethyl(1-diazo-2-oxo-propyl)phosphonate (192 mg, 1.00 mmol), and K_2CO_3 (235 mg, 1.7 mmol) were stirred in MeOH (2 mL) for 19 h at rt. The mixture was diluted with CH_2Cl_2 (10 mL), filtered and the filtrate washed with H_2O (5 mL) and brine (5 mL). The combined aqueous layers were extracted with CH_2Cl_2 (10 mL). The combined organic layers were dried ($MgSO_4$), filtered and the solvent removed *in vacuo.* Chromatography (petrol) gave **118** as a colorless oil (160 mg, 81%). ^{1}H NMR (400 MHz, $CDCl_3$) δ: 7.31 (t, *J* =1.8, 1H, H_B), 7.20 (d, *J* =1.8, 2H, H_C), 3.60 (d, *J* =2.6, 2H, H_D), 2.18 (t, *J* =2.6, 1H, H_E), 1.33 (s, 18H, H_A). ^{13}C NMR (101 MHz, $CDCl_3$) δ: 151.2, 135.2, 122.3, 120.9, 82.6, 70.4, 35.0, 31.6, 25.3. HR-EI-MS *m/z* = 228.18696 M^+ (calc. for $C_{17}H_{24}$ 228.18725).

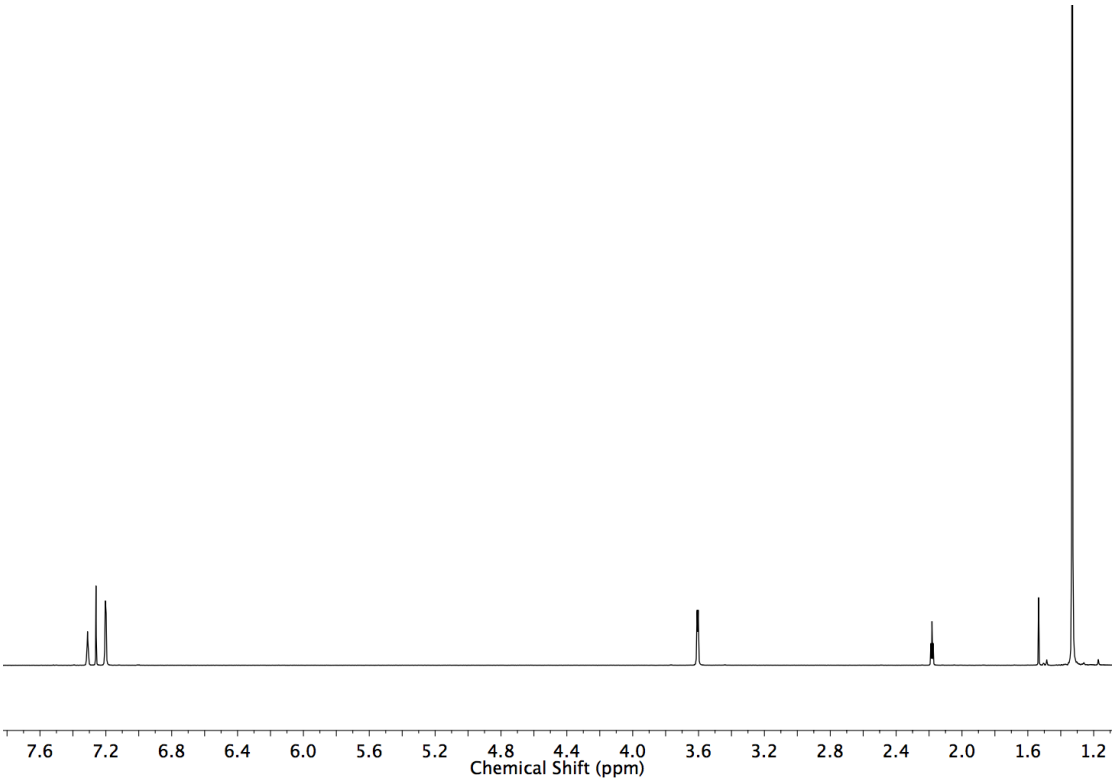

Figure 3.19 ^{1}H NMR ($CDCl_3$, 400 MHz) of **118**.

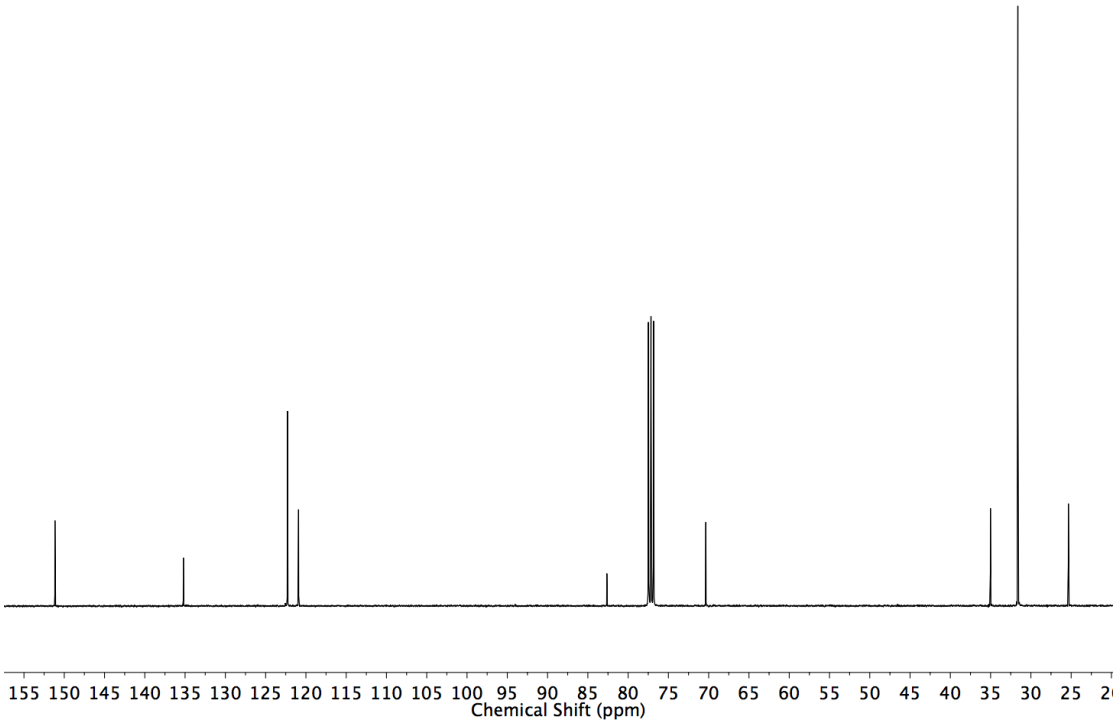

Figure 3.20 ^{13}C NMR ($CDCl_3$, 101 MHz) of **118**.

1-(3,5-Di-tert-butylphenyl)ethan-1-one ***120***

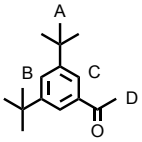

3,5-Di-tert-butylbenzoic acid (470 mg, 2 mmol) was dissolved in THF (5 mL) at –78 °C under N_2. MeLi (1.6 M in Et_2O, 2.75 mL, 4.4 mmol) was added dropwise. The mixture was slowly warmed to rt and stirred for 30 minutes then saturated $NH_4Cl_{(aq)}$ (10 mL) was added and the mixture extracted with petrol (3 × 20 mL), dried ($MgSO_4$), filtered and the solvent removed *in vacuo*. Chromatography (petrol/ethyl acetate 95:5) gave **120** as a colourless oil (370 mg, 80%). Spectra were consistent with those previously reported.[18] ^1H NMR (400 MHz, $CDCl_3$) δ: 7.81 (t, *J* =1.8, 1H, H_B), 7.65 (d, *J* =1.8, 2H, H_C), 2.61 (s, 3H, H_D), 1.36 (s, 18H, H_A). ^{13}C NMR (101 MHz, $CDCl_3$) δ: 199.1, 151.4, 137.0, 127.5, 122.7, 35.1, 31.5, 29.9.

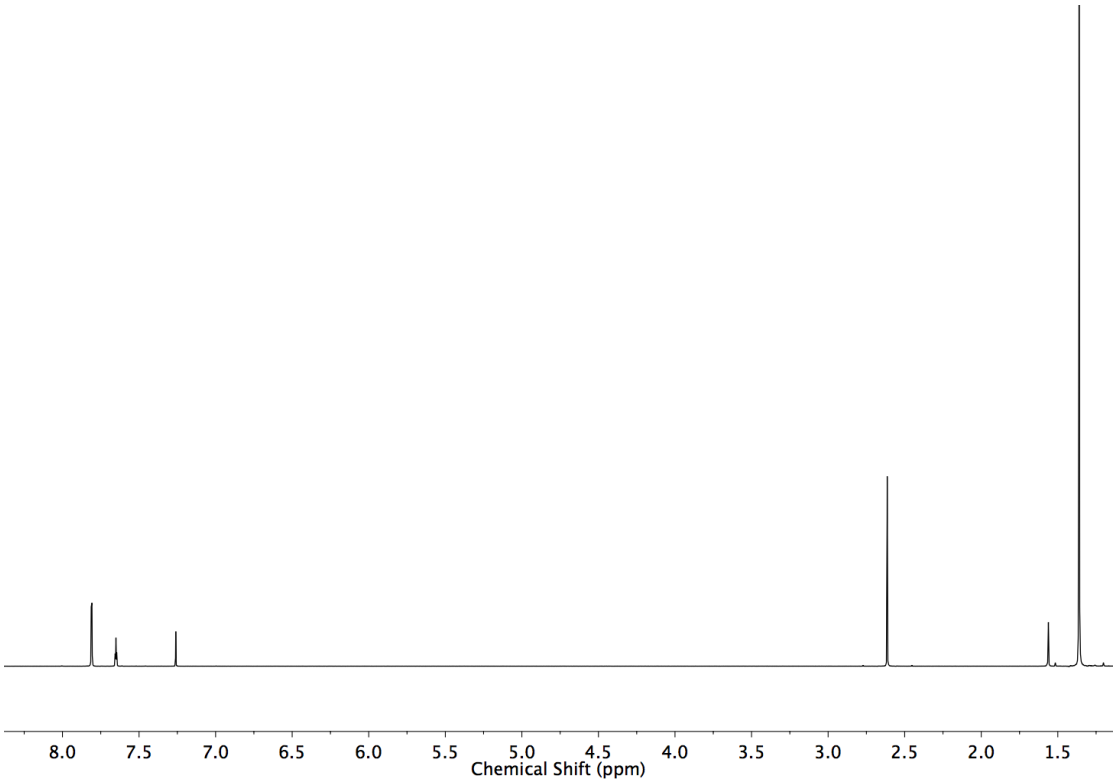

Figure 3.21 ^{1}H NMR ($CDCl_3$, 400 MHz) of **120**

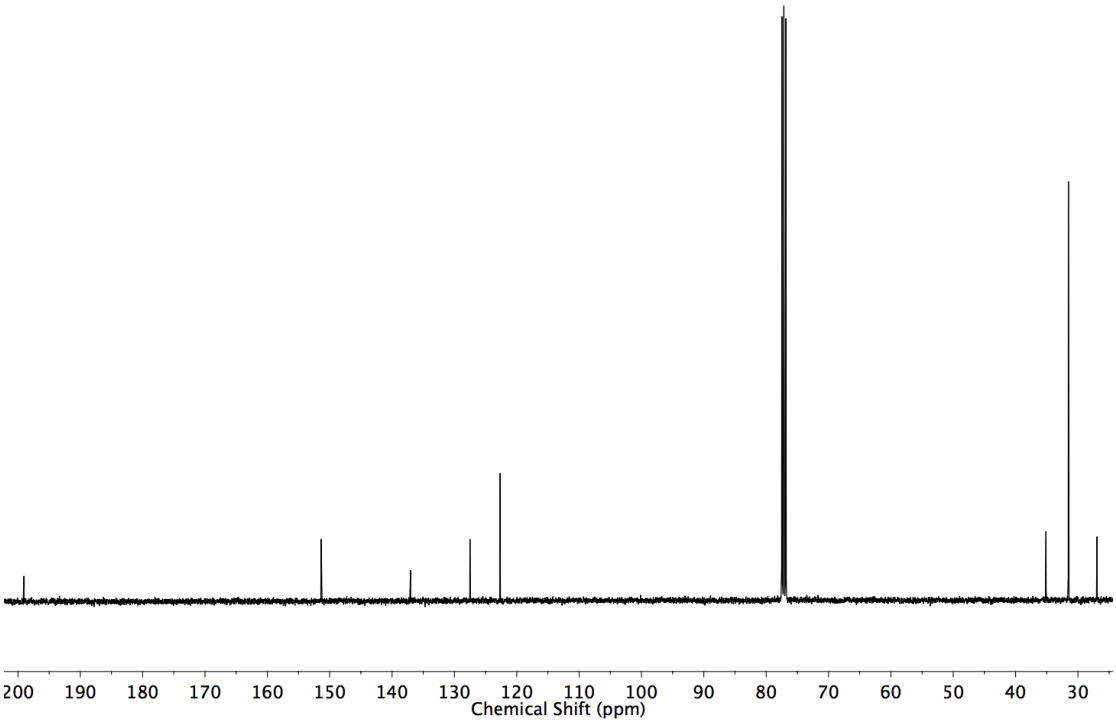

Figure 3. 22 ^{13}C NMR ($CDCl_3$, 101 MHz) of **120**.

2-(3,5-Di-tert-butylphenyl)but-3-yn-2-ol ***121***

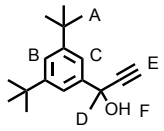

120 (370 mg, 1.6 mmol) was dissolved in THF (3 mL) at 0 °C under N_2. Ethynylmagnesium chloride (0.6 M in THF, 2.4 mmol, 4 mL) was added dropwise. The mixture was stirred for 16 h at rt. Saturated $NH_4Cl_{(aq)}$ (5 mL) was added and the solvent removed *in vacuo*. The residue was extracted with Et_2O (3 × 20 mL). The combined organic layers were washed with brine (10 mL), dried ($MgSO_4$), filtered and the solvent removed *in vacuo*. Chromatography (petrol/ethyl acetate 9:1) gave **121** as a colorless oil (200 mg, 48%). ^{1}H NMR (400 MHz, $CDCl_3$) δ: 7.53 (d, *J* =1.8, 2H, H_C), 7.38 (t, *J* =1.8, 1H, H_B), 2.68 (s, 1H, H_E), 2.37 (br. s, 1H, H_F), 1.81 (s, 3H, H_D), 1.35 (s, 18H, H_A). ^{13}C NMR (101 MHz, $CDCl_3$) δ: 150.9, 144.3, 122.1, 119.2, 87.8, 73.0, 70.6, 35.2, 33.3, 31.6. HR-EI-MS *m/z* = 258.19876 M^+ (calc. for $C_{18}H_{26}O$ 258.19782).

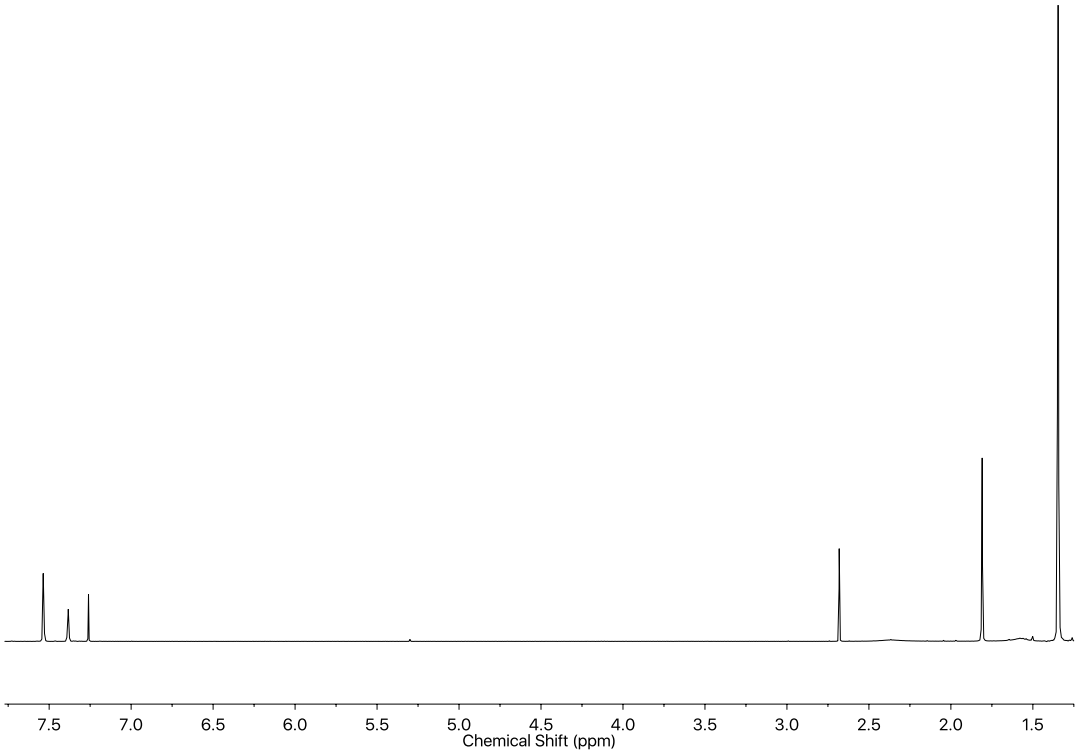

Figure 3.23 ^{1}H NMR ($CDCl_3$, 400 MHz) of **121**.

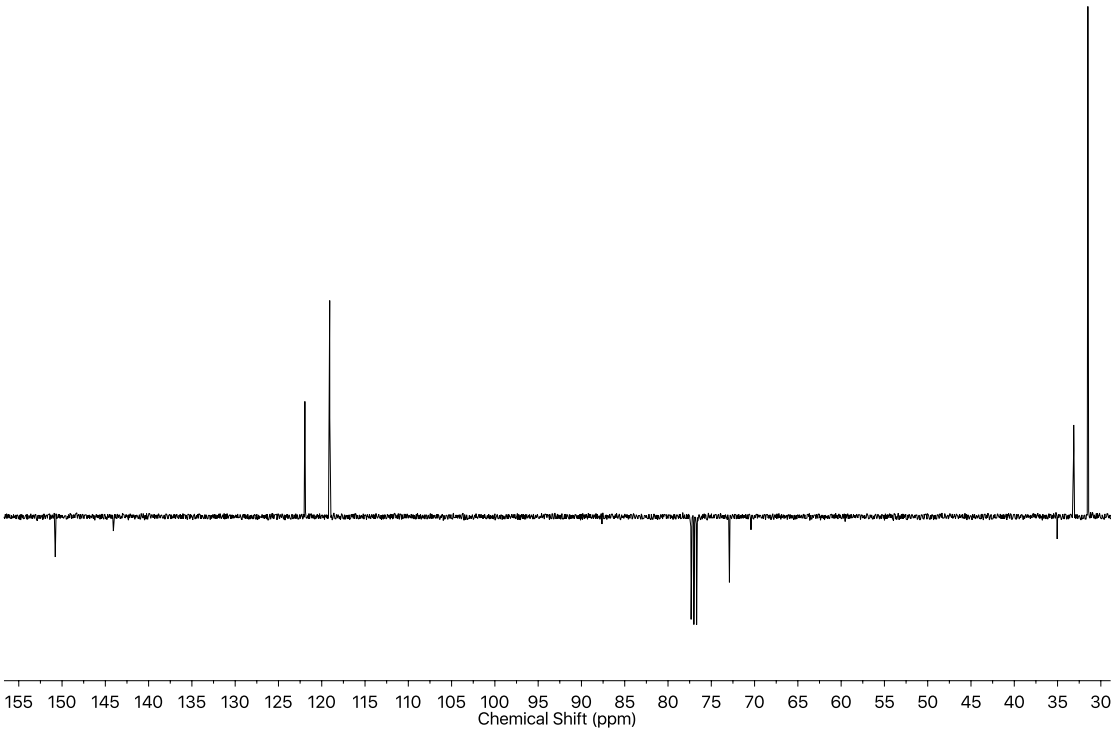

Figure 3.24 JMOD NMR ($CDCl_3$, 101 MHz) of **121**.

Synthesis of Acrylamide Rotaxanes

General Procedure A

$KF_{(aq)}$ (0.1 M, 0.8 eq.) was added to a solution of **alkyne** (1.2 eq.), **azide** (1.2 eq.), **macrocycle** (1 eq.) and $[Cu(MeCN)_4]PF_6$ (0.96 eq.) in THF (72 mL/mmol) in a microwave vial (CEM Ltd.) and the vial sealed. The orange mixture was stirred at 70 °C under microwave irradiation for 1 hour. The reaction mixgture was diluted with CH_2Cl_2 (200 mL/mmol), washed with EDTA-NH_3 solution (100 mL/mmol). The aqueous layer was extracted with CH_2Cl_2 (2 × 100 mL/mmol). The combined organic extracts were washed with brine (100 mL/mmol), dried ($MgSO_4$), filtered and the solvent removed *in vacuo*.

*Rotaxane **123***

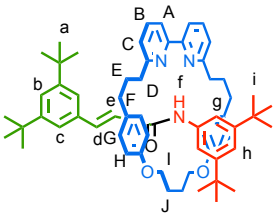

Prepared according to **general procedure A** with **14** (24.0 mg, 0.05 mmol), $[Cu(MeCN)_4]PF_6$ (17.9 mg, 0.048 mmol), **11** (13.8 mg, 0.06 mmol), and **108** (14.6 mg, 0.06 mmol). Chromatography (petrol with a gradient of 0 to 20% Et_2O) gave **123** as a white foam (44.0 mg, 95%). ^{1}H NMR (500 MHz, $CDCl_3$) δ: 9.91 (S, 1H, H_f), 7.65 (t, *J* =7.8, 2H, H_B), 7.49 (dd, *J* =7.8, 1.0, 2H, H_A), 7.23 (t, *J* = 1.8, 1H, H_h), 7.14 – 7.10 (m, 4H, H_g, H_C), 6.94 – 6.92 (m, 3H, H_b, H_c), 6.85 (d, *J* =15.5, 1H, H_d), 6.69 (s, 8H, H_G, H_H), 6.29 (d, *J* =15.5, 1H, H_e), 4.70 - 4.55 (m, 2H, H_I), 4.21 - 4.10 (m, 2H, $H_{I'}$), 2.62 – 2.42 (m, 8H, H_D, H_F), 2.40 – 2.30 (m, 2H, H_J), 2.11 – 2.00 (m, 2H, $H_{J'}$), 1.88 – 1.64 (m, 4H, H_E), 1.23 (s, 18H, H_a), 1.17 (s, 18H, H_i). ^{13}C NMR (126 MHz, $CDCl_3$) δ: 163.8, 163.5, 157.4, 156.8, 150.3, 150.1, 139.6, 139.0, 137.0, 135.9, 132.4, 129.1, 123.3, 122.2, 122.0, 121.8, 119.6, 116.2, 115.0, 114.2, 66.3, 36.6, 35.2, 34.8, 34.8, 31.5, 31.5, 31.3, 25.0. HR-ESI-MS *m/z* = 926.6199 $[M+H]^+$ (calc. for $C_{63}H_{80}N_3O_3$ 926.6194).

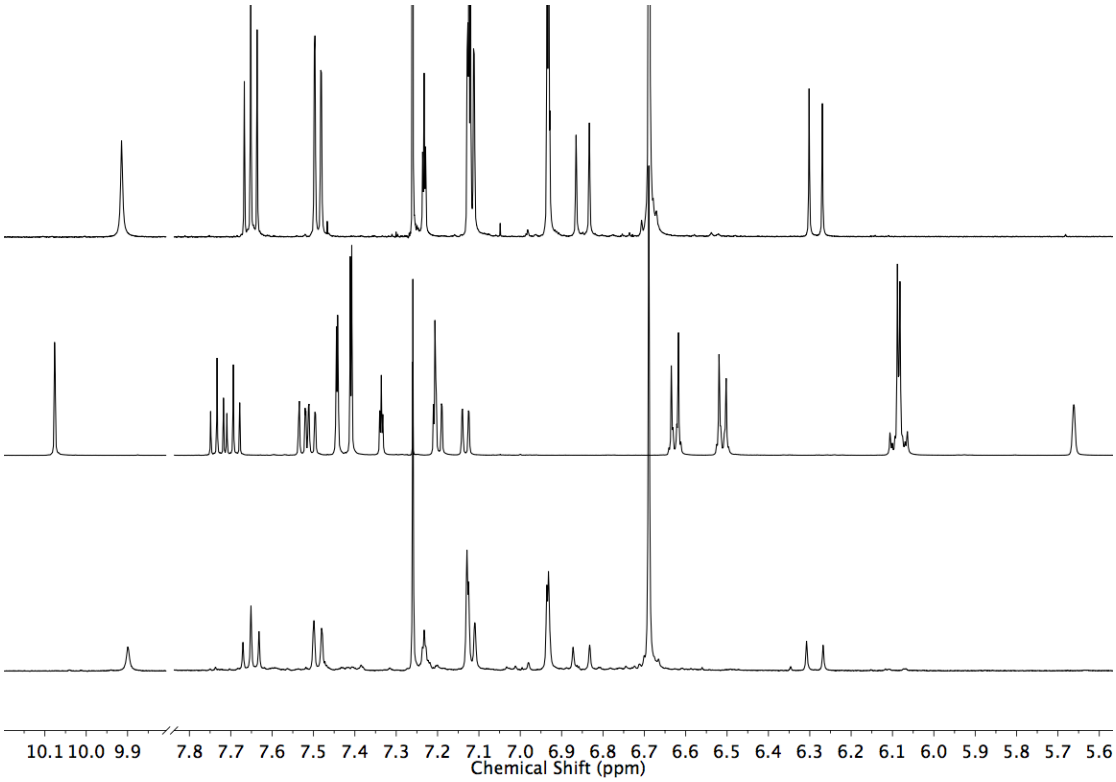

Figure 3.25 Stacked partial ^{1}H NMR (400 MHz, $CDCl_3$) spectra of **123** (top), **122.**(middle) and the crude reaction product before chromatography (bottom). Ratio of **123**:**122** = 100:0.

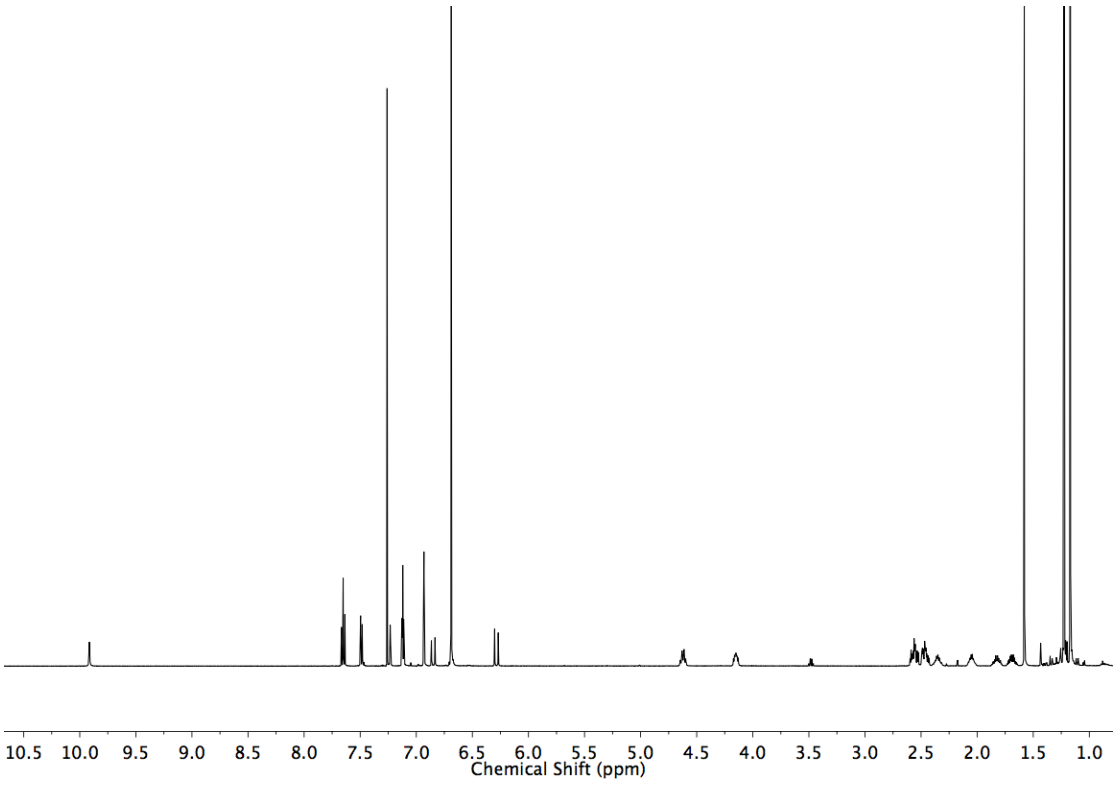

Figure 3.26 ^{1}H NMR ($CDCl_3$, 500 MHz) of **123**

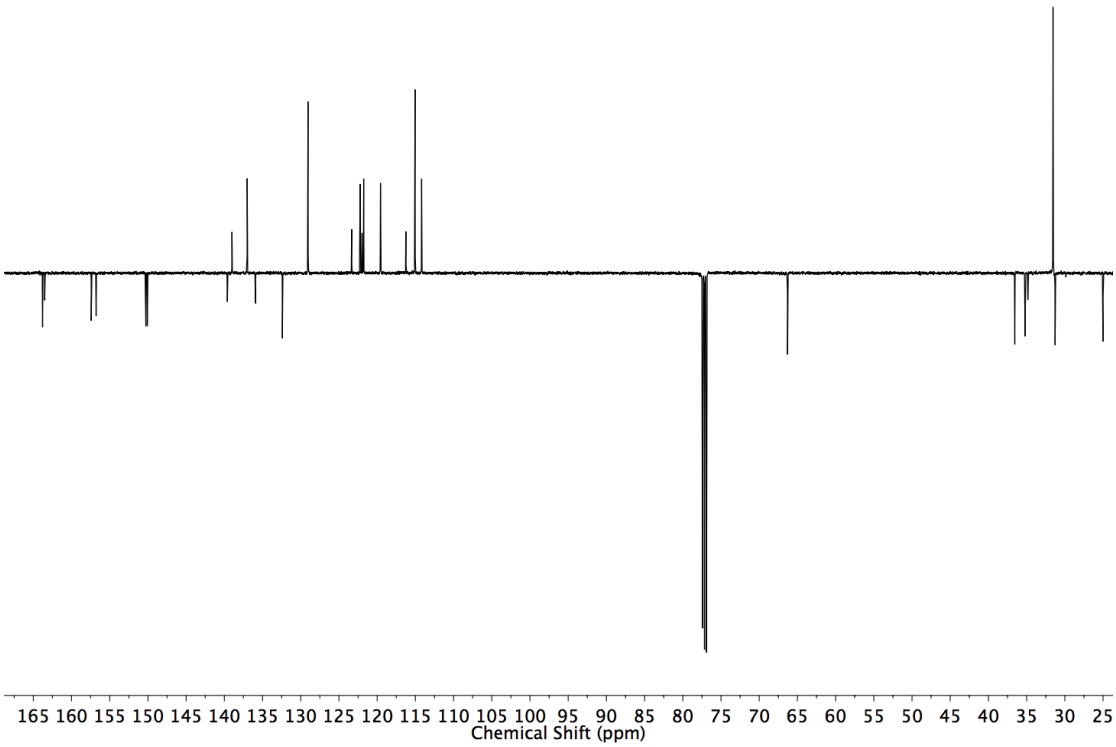

Figure 3.27 JMOD NMR ($CDCl_3$, 126 MHz) of **123**

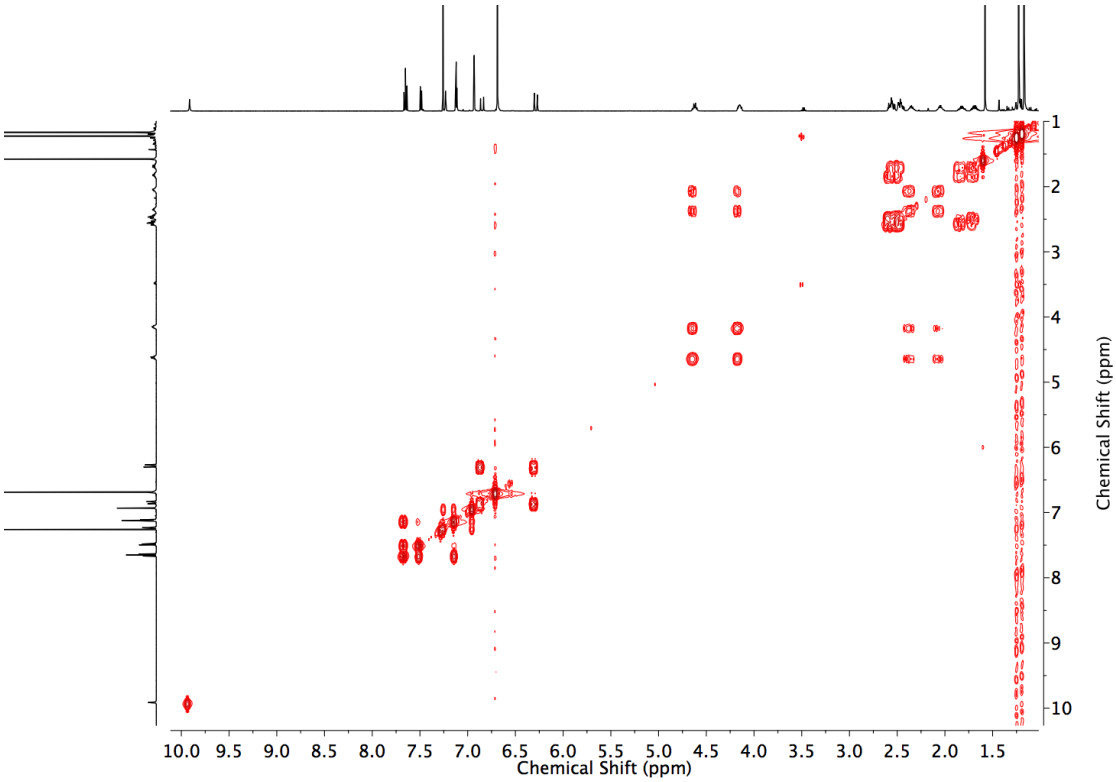

Figure 3.28 COSY NMR ($CDCl_3$) of **123**

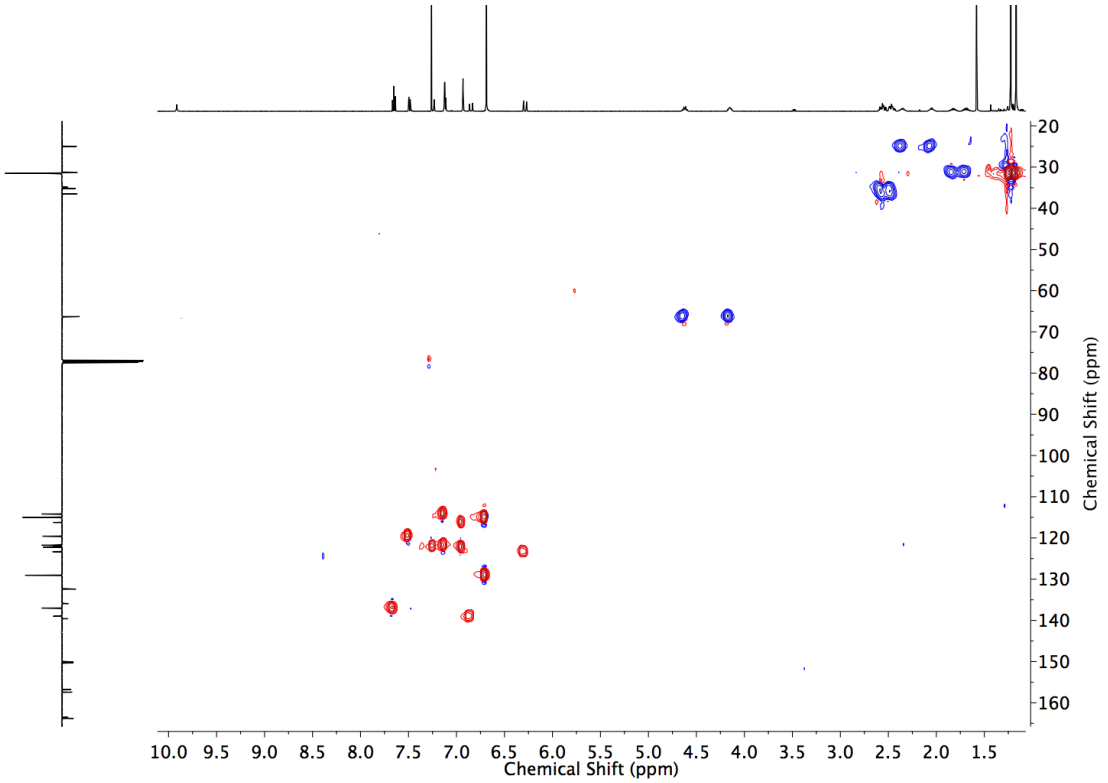

Figure 3.29 HSQC NMR ($CDCl_3$) of **123**.

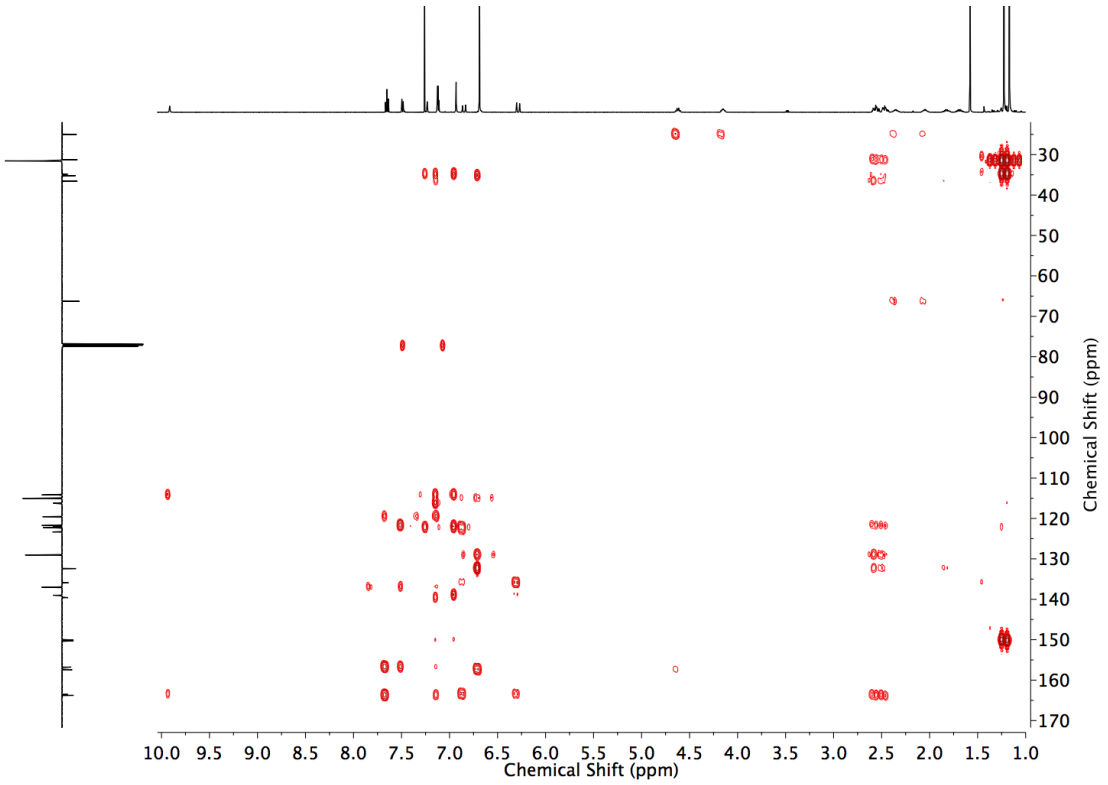

Figure 3.30 HMBC NMR ($CDCl_3$) of **123**.

*Rotaxane **125***

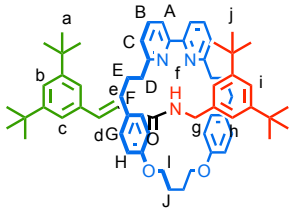

Prepared according to **general procedure A** with **14** (12.0 mg, 0.025 mmol), $[Cu(MeCN)_4]PF_6$ (8.9 mg, 0.024 mmol), **20** (7.3 mg, 0.03 mmol), and **108** (7.3 mg, 0.03 mmol). Chromatography (petrol with a gradient of 0 to 20% Et_2O) gave **125** as a white foam (16.0 mg, 68 %). ^{1}H NMR (500 MHz, $CDCl_3$) δ: 8.77 (t, *J* =4.8, 1H, H_f), 7.60 (t, *J* =7.8, 2H, H_B), 7.44 (dd, *J* =7.8, 1.0, 2H, H_A), 7.21 (t, *J* =1.8, 1H,H_b), 7.19 (d, *J* =16.0, 1H, H_d), 7.07 (dd, *J* =7.8, 1.0, 2H, H_C), 7.04 (j, *J* =1.9, 1H, H_i), 6.88 (d, *J* =1.9, 2H, H_c), 6.79 (s, 8H, H_G, H_H), 6.77 (d, *J* =1.8, 2H, H_h), 6.35 (d, *J* =16.0, 1H, H_e), 4.33 – 4.23 (m, 4H, H_I), 3.41 (d, *J* =4.8, 2H, H_g), 2.61 – 2.47 (m, 4H, H_F), 2.46 – 2.34 (m, 4H, H_D), 2.17 – 2.10 (m, 4H, H_J), 1.83 – 1.70 (m, 4H, H_E), 1.16 (s, 18H, H_a), 1.06 (s, 18H, H_j). ^{13}C NMR (126 MHz, $CDCl_3$) δ: 165.4, 163.6, 157.3, 156.5, 150.4, 149.8, 137.6, 137.2, 136.9, 135.7, 132.6, 129.4, 123.2, 122.9, 122.3, 121.9, 121.9, 120.5, 119.5, 115.2, 66.6, 44.2, 36.5, 35.2, 34.8, 34.7, 31.5, 31.4, 31.4, 25.0; HR-ESI-MS *m/z* = 940.6351 $[M+H]^+$ (calc. for $C_{64}H_{82}N_3O_3$ 940.6351).

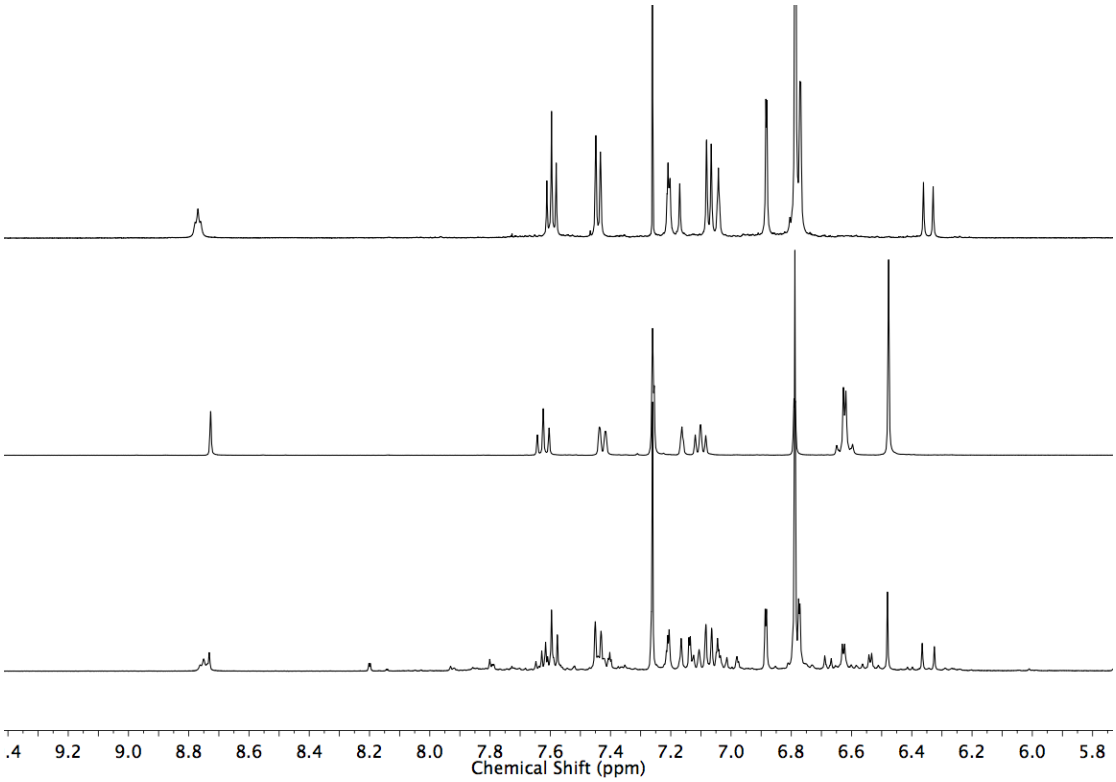

Figure 3.31 Stacked partial ^{1}H NMR (400 MHz, $CDCl_3$) spectra of **125** (top), **126** (middle) and the crude reaction product before chromatography (bottom). Ratio of **125**:**126** = 75:25.

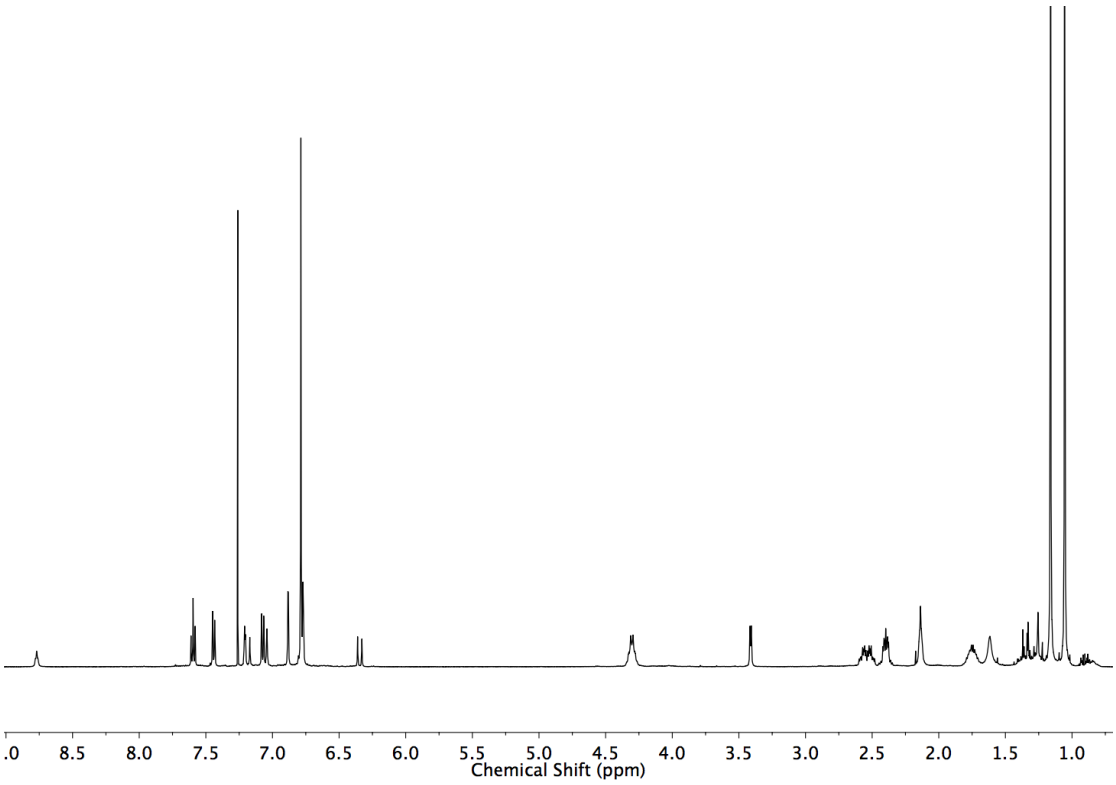

Figure 3.32 ^{1}H NMR ($CDCl_3$, 500 MHz) of **125**

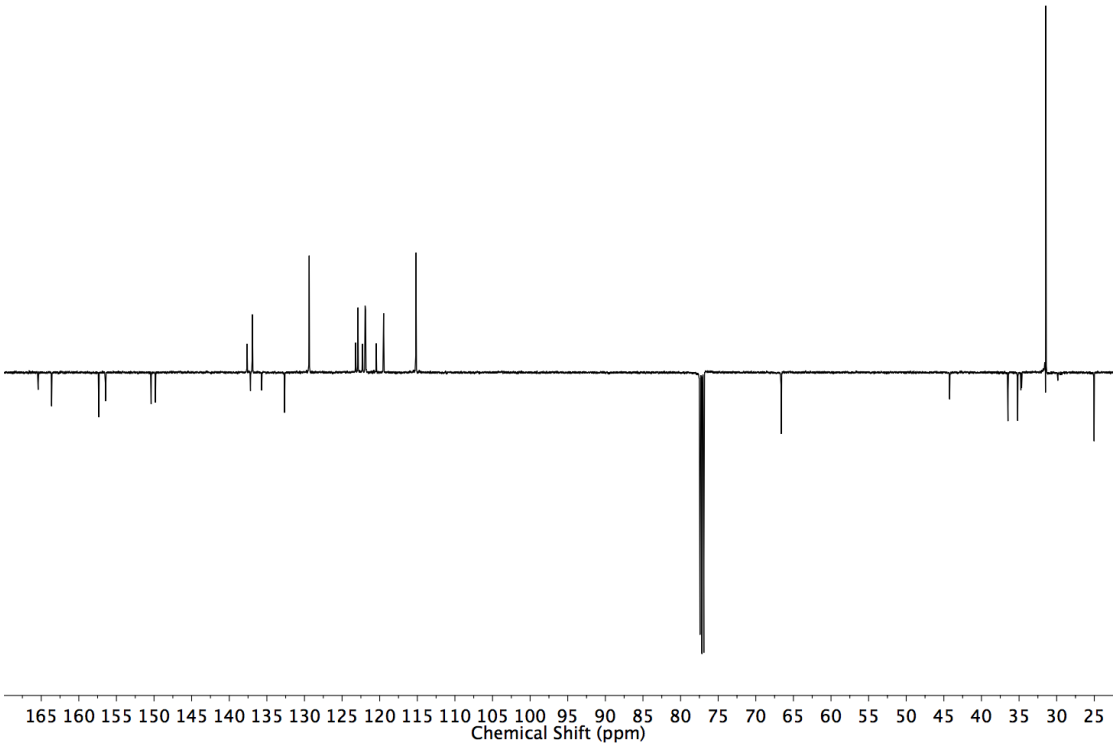

Figure 3.33 JMOD NMR ($CDCl_3$, 126 MHz) of **125**

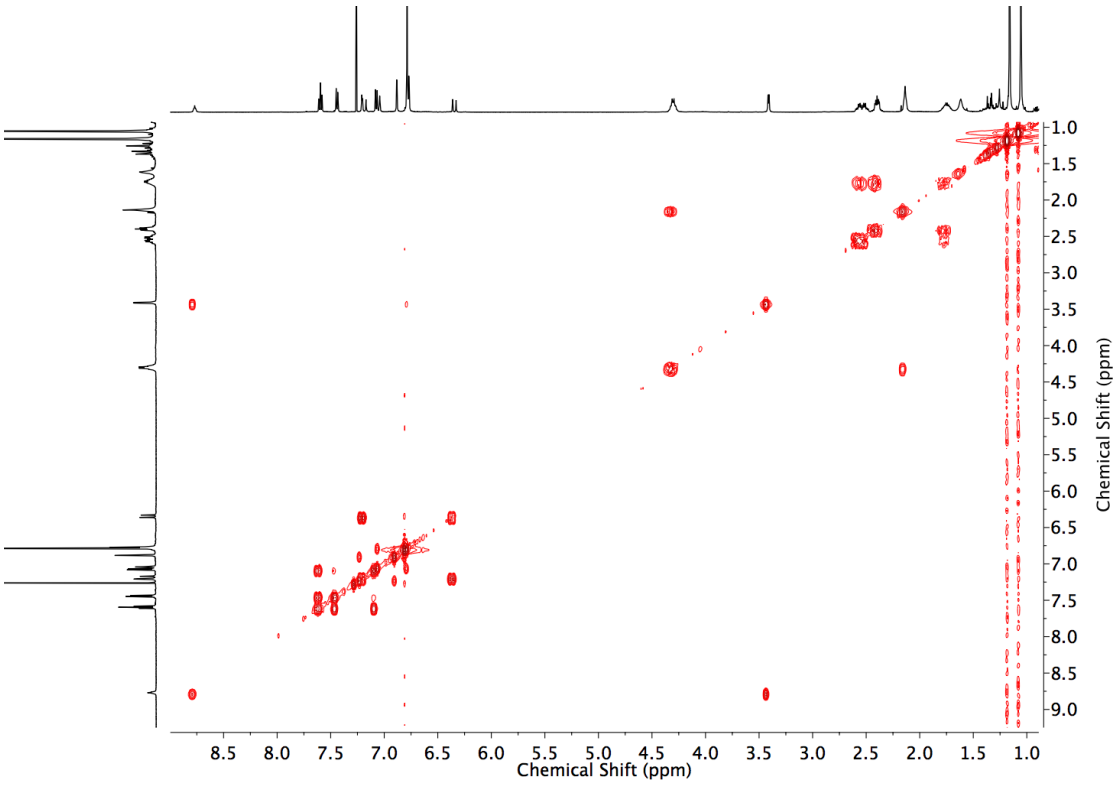

Figure 3.34 COSY NMR ($CDCl_3$) of **125**.

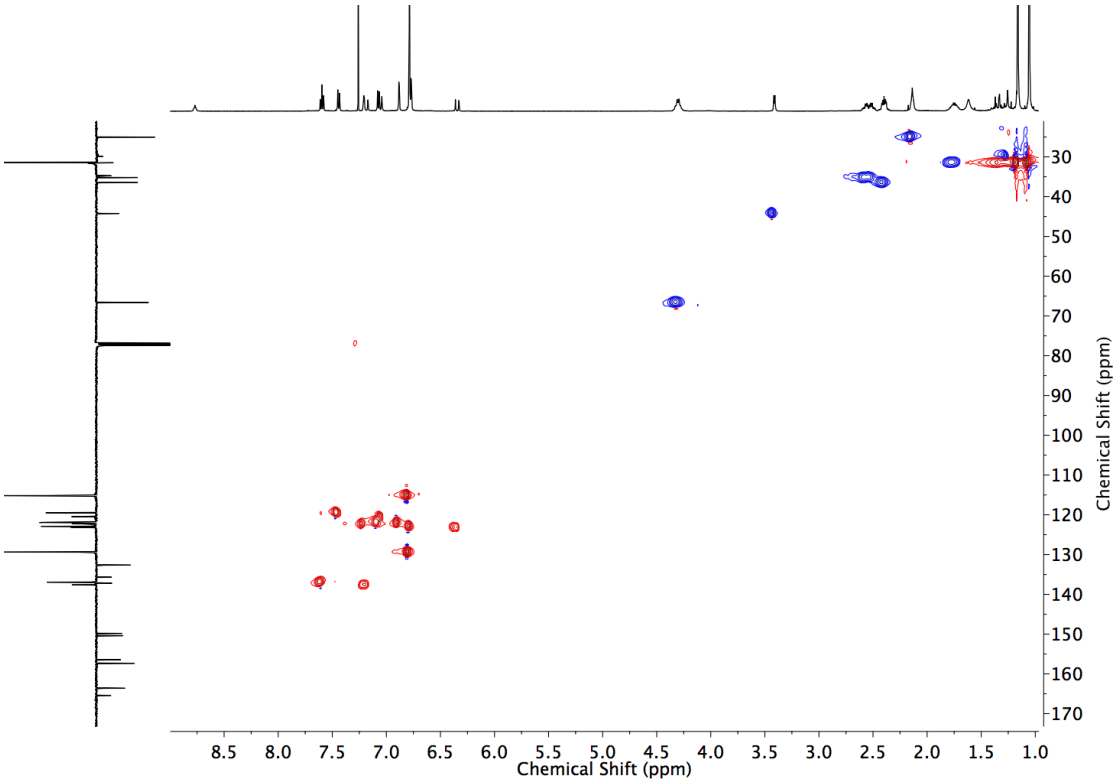

Figure 3.35 HSQC NMR ($CDCl_3$) of **125**.

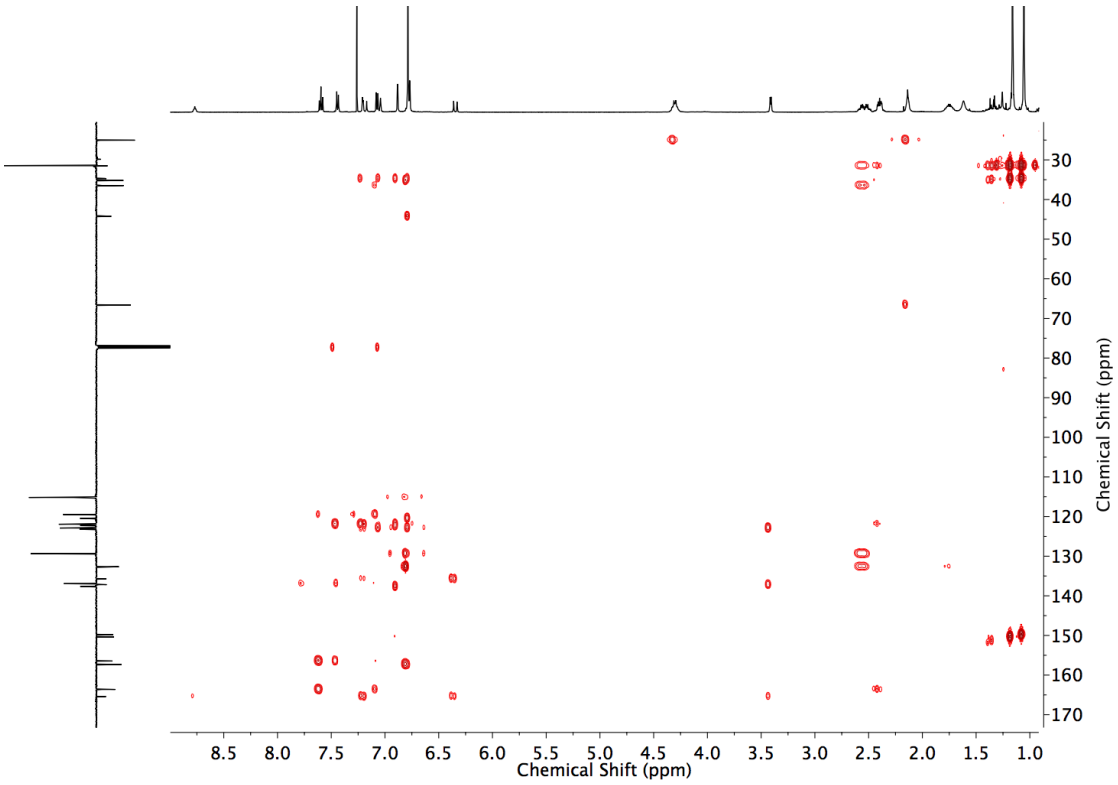

Figure 3.36 HMBC NMR ($CDCl_3$) of **125**.

Rotaxane ***127***

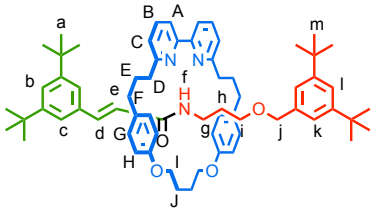

Prepared according to **general procedure A** with **14** (12.0 mg, 0.025 mmol), $[Cu(MeCN)_4]PF_6$ (8.9 mg, 0.024 mmol), **124** (9.1 mg, 0.03 mmol), and **108** (7.3 mg, 0.03 mmol). Chromatography (petrol with a gradient of 0 to 50% Et_2O) gave **127** as a colourless oil (4.0 mg, 16 %). ^{1}H NMR (500 MHz, $CDCl_3$) δ: 8.43 (t, *J* =5.4, 1H, H_f), 7.65 (t, *J* =7.8, 2H, H_B), 7.48 (dd, *J* =7.8, 0.9, 2H, H_A), 7.31 (t, *J* =1.9, 1H, H_l), 7.27 (d, *J* =16.0, 1H, H_d), 7.23 (t, *J* =1.9, 1H, H_b), 7.18 (dd, *J* =7.8, 0.9, 2H, H_C), 7.02 (d, *J* =1.9, 2H, H_k), 6.92 (d, *J* =1.9, 2H, H_c), 6.90 (d, *J* =8.5, 4H, H_G), 6.82 (d, *J* =8.5, 4H, H_F), 6.32 (d, *J* =16.0, 1H, H_e), 4.29 – 4.13 (m, 4H, H_I), 4.08 (s, 2H, H_j), 3.02 (t, *J* =7.2, 2H, H_i), 2.70 – 2.53 (m, 8H, H_D, H_F), 2.29 – 2.23 (m, 2H, H_g), 2.18 – 1.99 (m, 4H, H_J), 1.97 – 1.75 (m, 4H, H_E), 1.30 (s, 18H, H_a), 1.16 (s, 18H, H_m), 0.97 (t, *J* =7.8, 2H, H_h). ^{13}C NMR (126 MHz, $CDCl_3$) δ: 165.4, 163.5, 157.5, 156.6, 150.7, 150.6, 137.9, 137.8, 137.1, 135.5, 132.8, 129.6, 123.2, 122.6, 122.1, 121.9, 121.9, 121.7, 119.8, 115.1, 73.5, 68.8, 66.5, 36.6, 35.5, 35.3, 34.9, 34.8, 31.6, 31.5, 31.4, 28.8, 25.0. HR-ESI-MS *m/z* = 998.6749 $[M+H]^+$ (calc. for $C_{64}H_{82}N_3O_3$ 998.6769).

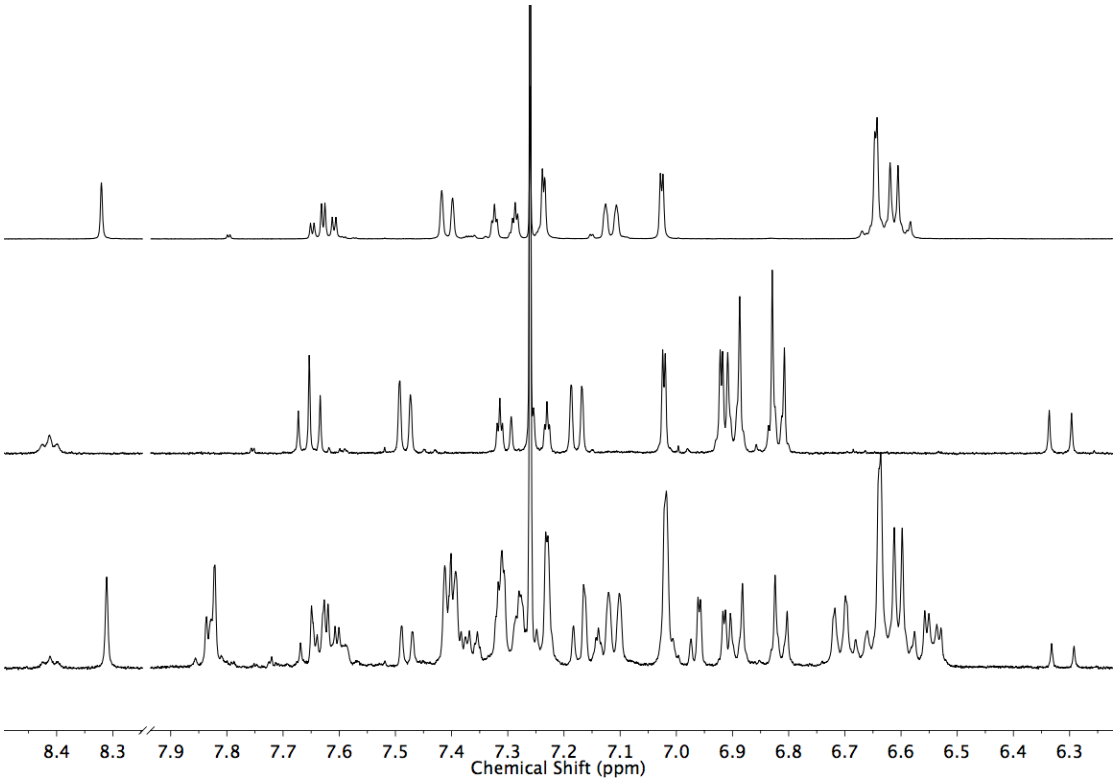

Figure 3.37 Stacked partial ^{1}H NMR (400 MHz, $CDCl_3$) spectra of **128** (top), **127** (middle) and the crude reaction product before chromatography (bottom). Ratio of **127**:**128** = 35:65.

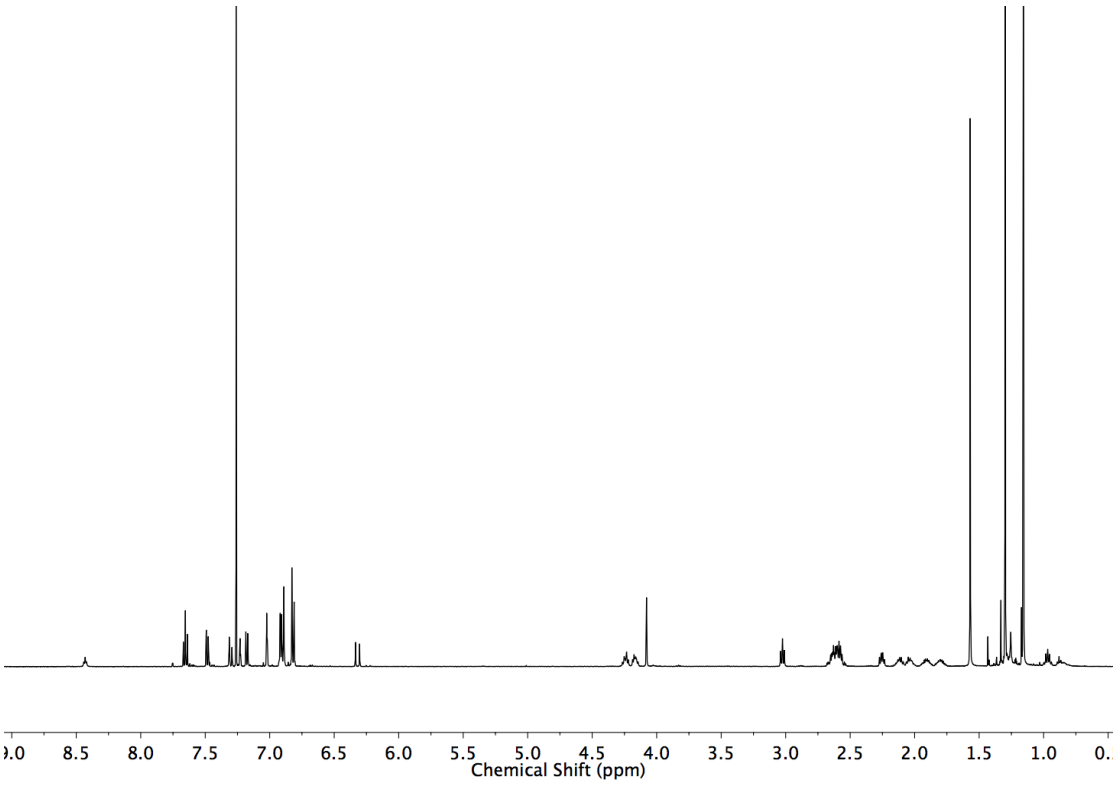

Figure 3.38 ^{1}H NMR ($CDCl_3$, 500 MHz) of **127**.

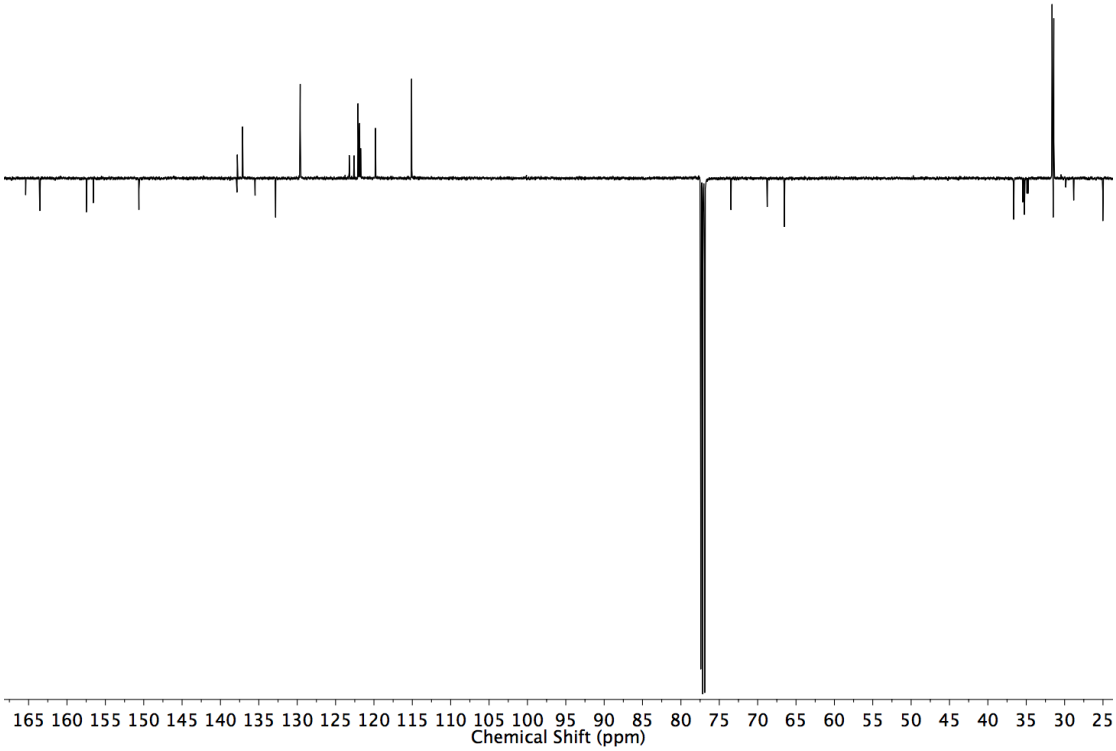

Figure 3.39 JMOD NMR ($CDCl_3$, 126 MHz) of **127**.

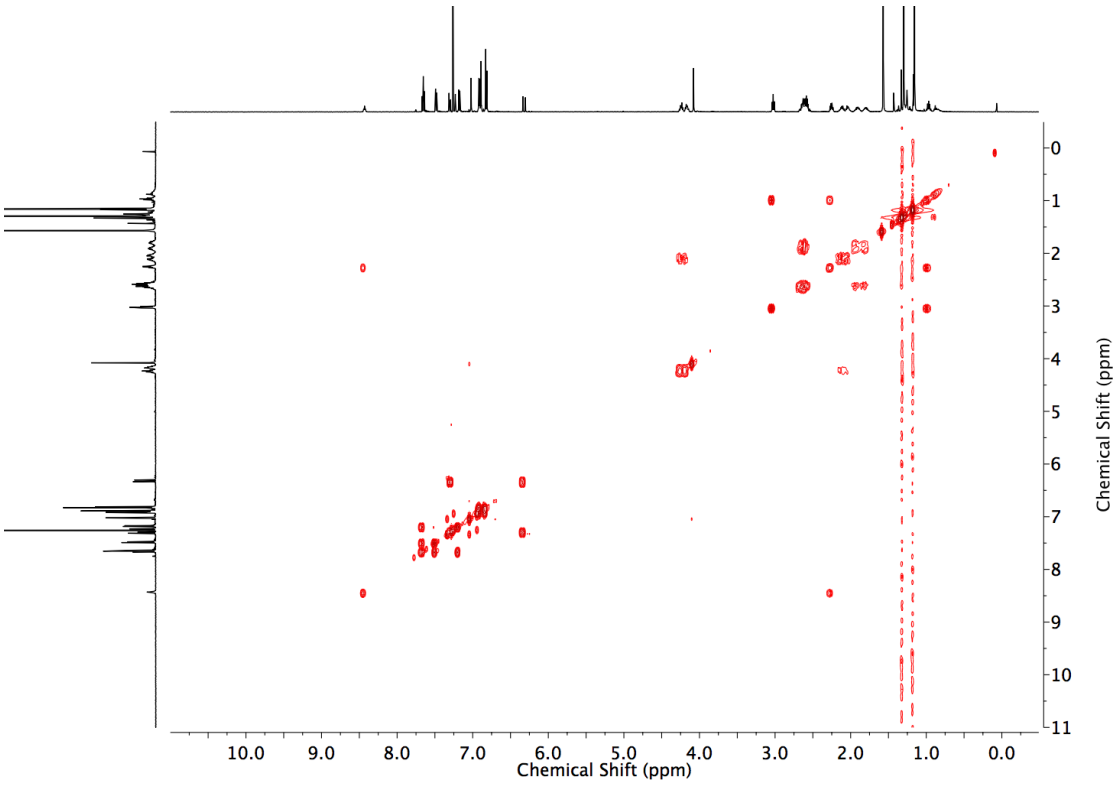

Figure 3.40 COSY NMR ($CDCl_3$) of **127**.

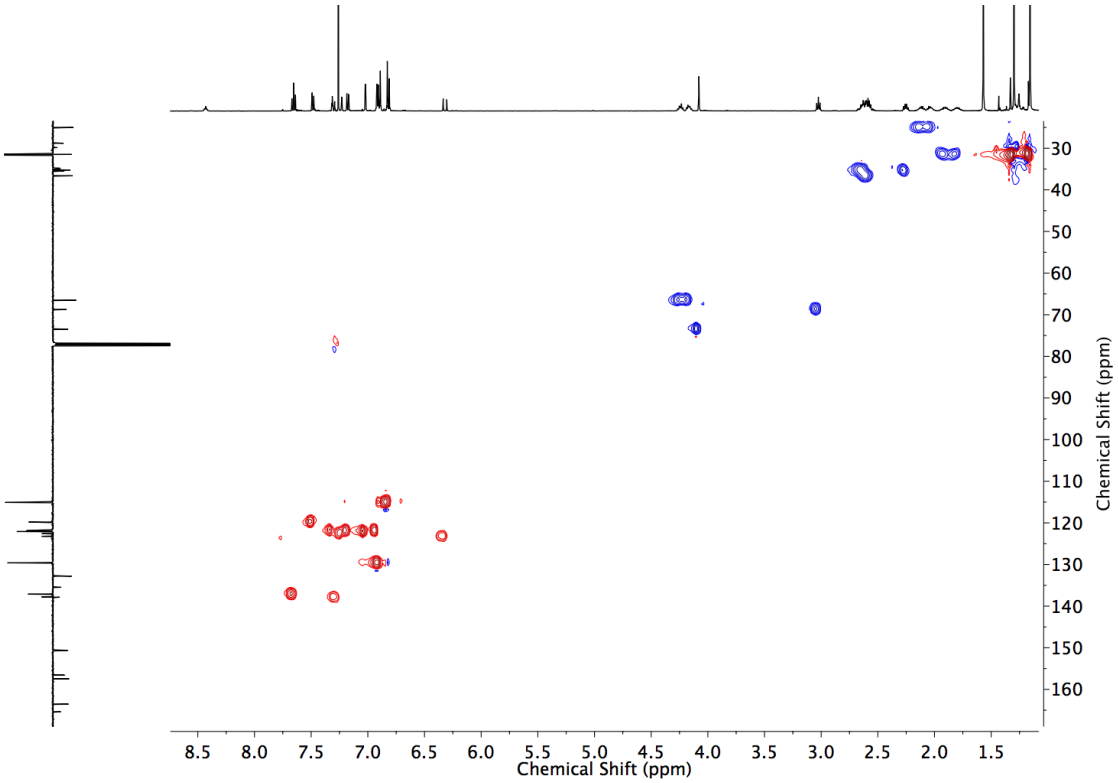

Figure 3.41 HSQC NMR ($CDCl_3$) of **127**.

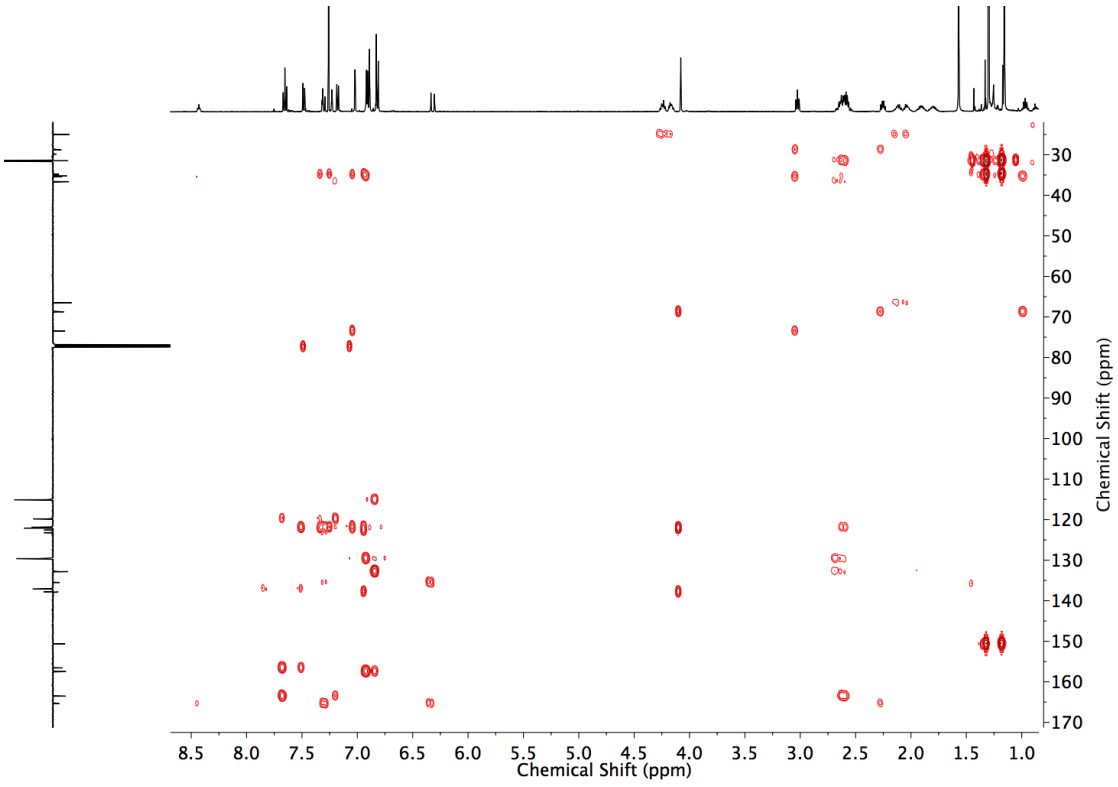

Figure 3.42 HMBC NMR ($CDCl_3$) of **127**.

*Rotaxane **129***

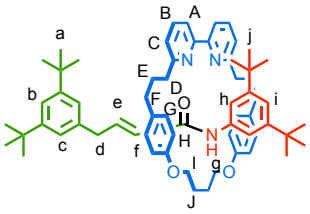

Prepared according to **general procedure A** with **14** (12.0 mg, 0.025 mmol), $[Cu(MeCN)_4]PF_6$ (8.9 mg, 0.024 mmol), **11** (6.9 mg, 0.03 mmol), and **116** (7.8 mg, 0.03 mmol). Chromatography (petrol with a gradient of 0 to 20% Et_2O) gave **129** as a colourless oil (10.0 mg, 43%). ^{1}H NMR (400 MHz, $CDCl_3$) δ: 9.92 (s, 1H, H_g), 7.62 (t, *J* =7.9, 2H, H_B), 7.48 (dd, *J* =7.9, 0.9, 2H, H_A), 7.15 (t, *J* =1.9, 1H, H_b), 7.10 (dd, *J* =7.9, 0.9, 2H, H_C), 6.97 (d, *J* =1.9, 2H, H_h), 6.85 (t, *J* =1.9, 1H, H_i), 6.82 (d, *J* =1.9, 2H, H_c), 6.77 (d, *J* =8.5, 4H, H_G), 6.70 (d, *J* =8.5, 4H, H_H), 6.42 (dt, *J* =15.5, 6.8, 1H, H_e), 5.46 (dt, *J* =15.5, 1.6, 1H, H_f), 4.50 – 4.38 (m, 2H, 2 of H_I), 4.17 – 4.06 (m, 2H, 2 of H_I), 2.93 (d, *J* =6.8, 2H, H_d), 2.63 – 2.41 (m, 8H, H_D, H_F), 2.29 – 2.16 (m, 2H, 2 of H_J), 2.07 – 1.95 (m, 2H, 2 of H_J), 1.90 – 1.67 (m, 4H, H_E), 1.21 (s, 18H, H_a or H_j), 1.10 (s, 18H, H_a or H_j). ^{13}C NMR (101 MHz, $CDCl_3$) δ: 163.6, 163.3, 157.6, 156.3, 150.4, 150.0, 141.3, 139.4, 138.5, 137.0, 132.6, 129.2, 125.6, 122.9, 121.9, 120.2, 119.6, 116.0, 115.1, 114.3, 66.5, 39.4, 36.6, 35.2, 34.8 (×2), 31.6, 31.5, 31.1, 25.2. HR-ESI-MS *m/z* = 940.6367 $[M+H]^+$ (calc. for $C_{64}H_{82}N_3O_3$ 940.6351).

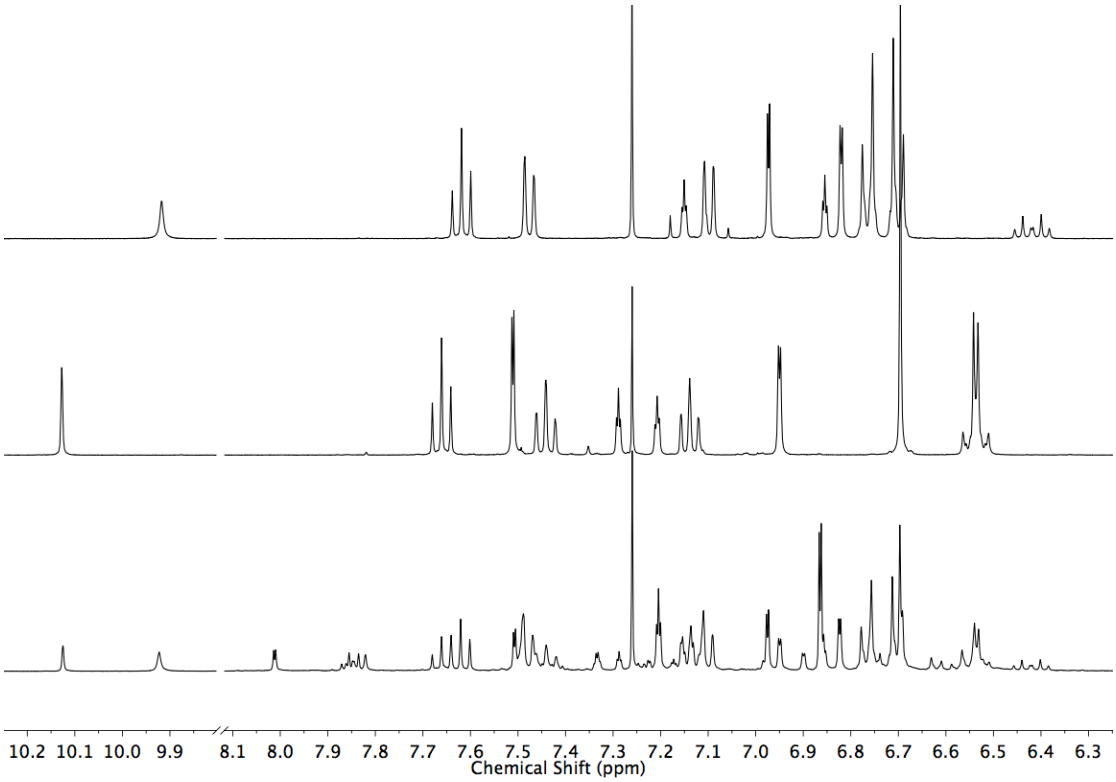

Figure 3.43 Stacked partial ^{1}H NMR (400 MHz, $CDCl_3$) spectra of **129** (top), **130** (middle) and the crude reaction product before chromatography (bottom). Ratio of **129**:**130** = 60:40.

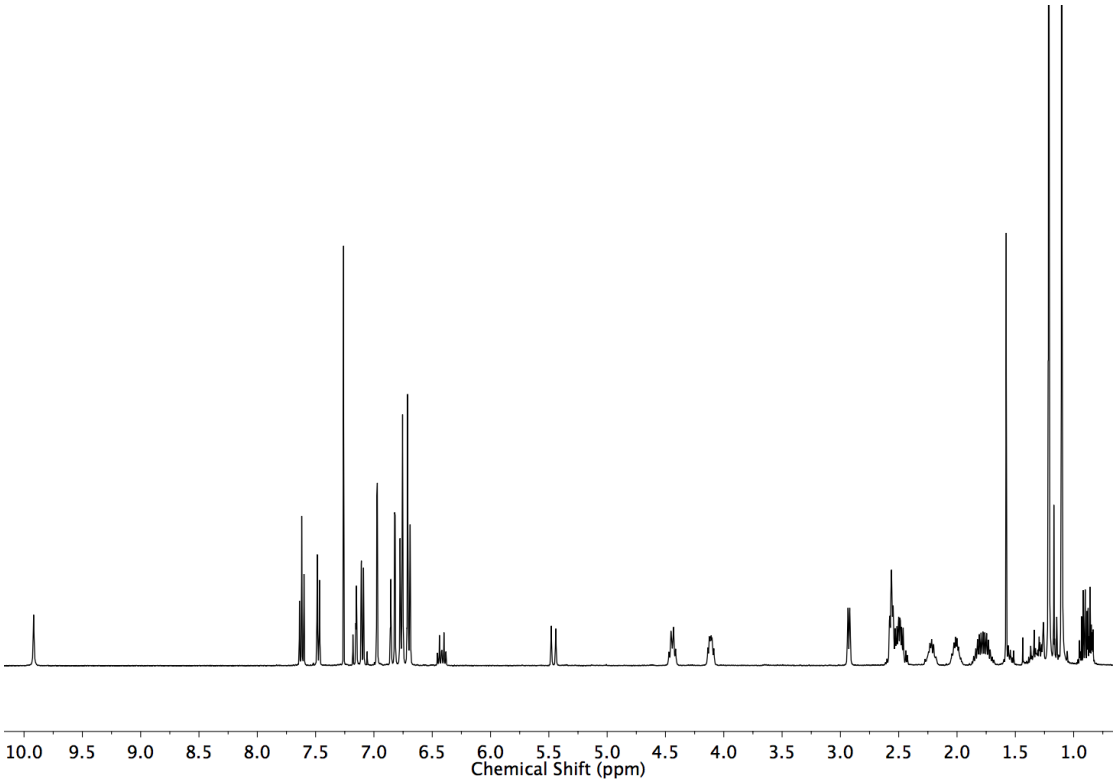

Figure 3.44 ^{1}H NMR ($CDCl_3$, 400 MHz) of **129**.

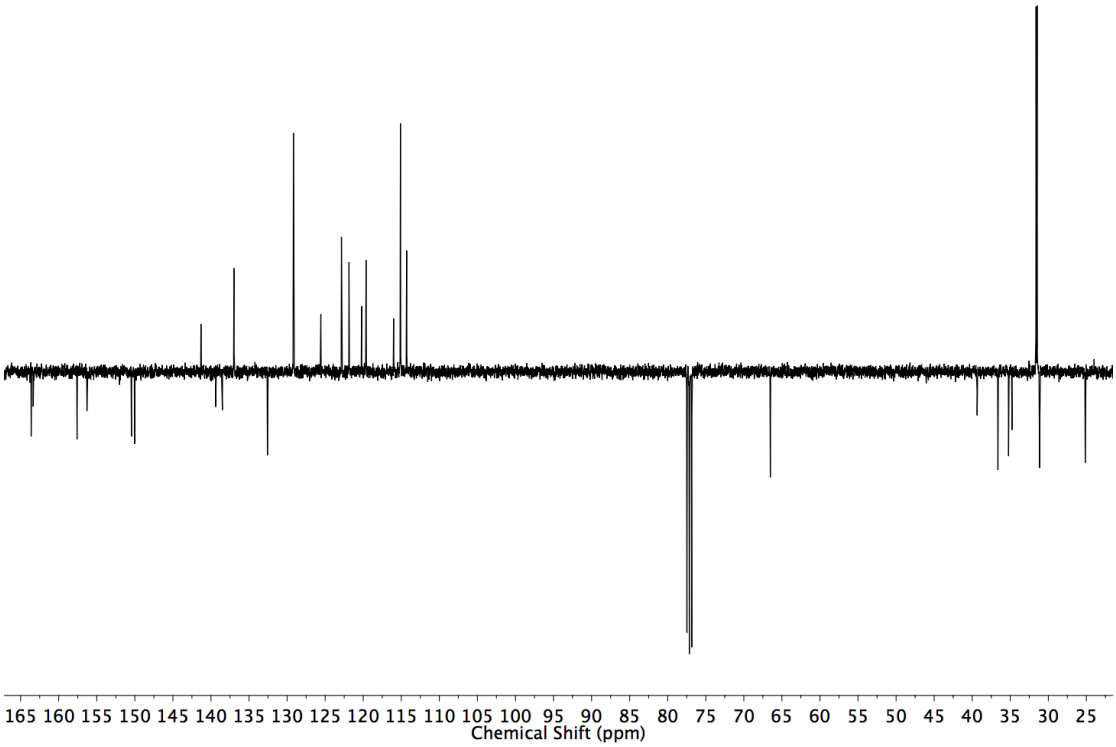

Figure 3.45 JMOD NMR ($CDCl_3$, 101 MHz) of **129**.

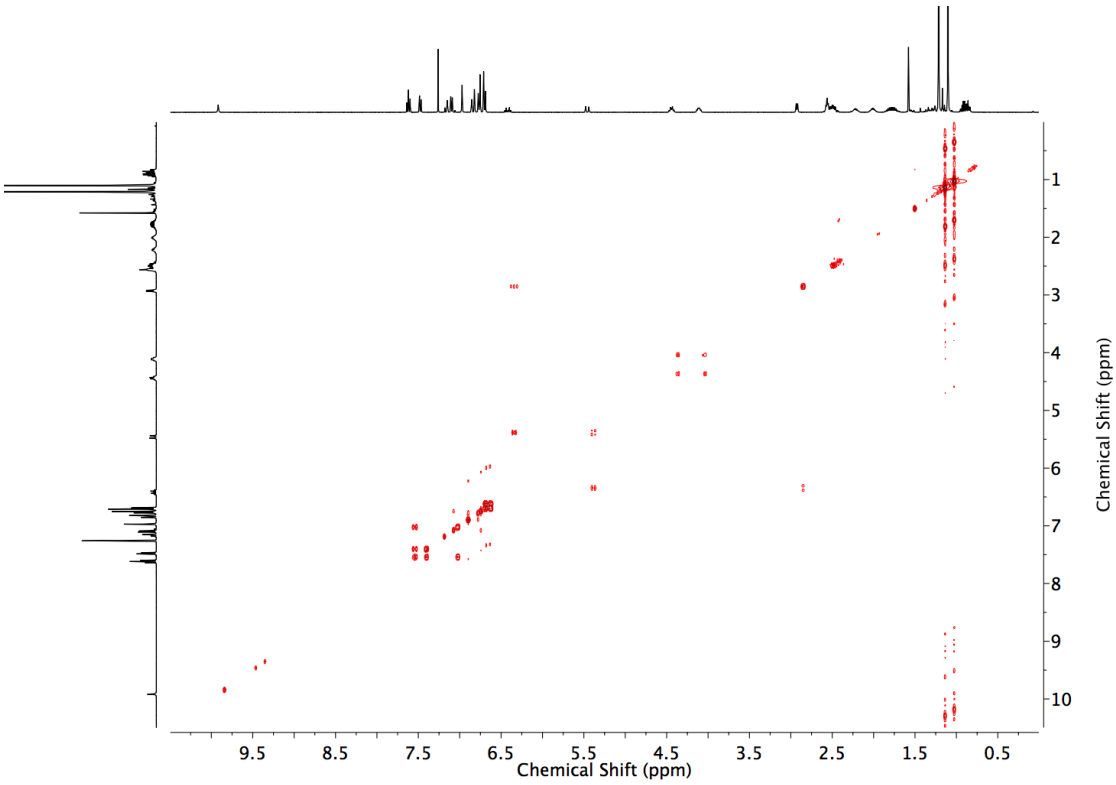

Figure 3.46 COSY NMR ($CDCl_3$) of **129**.

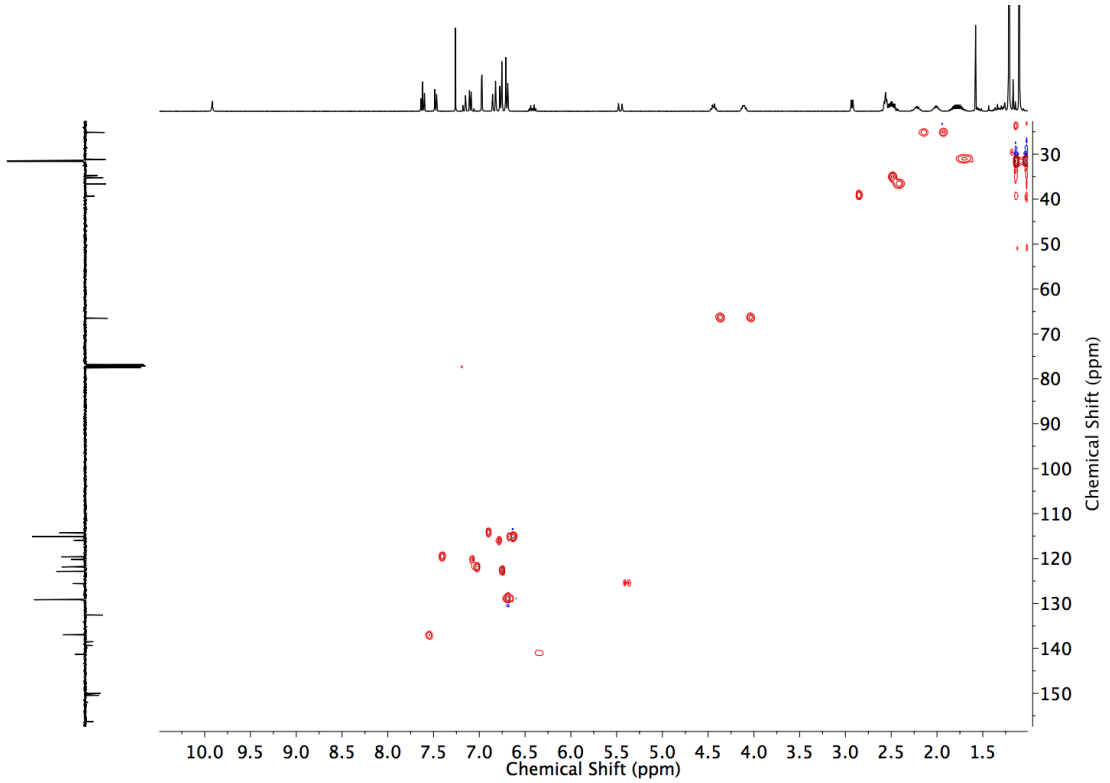

Figure 3.47 HSQC NMR ($CDCl_3$) of **129**.

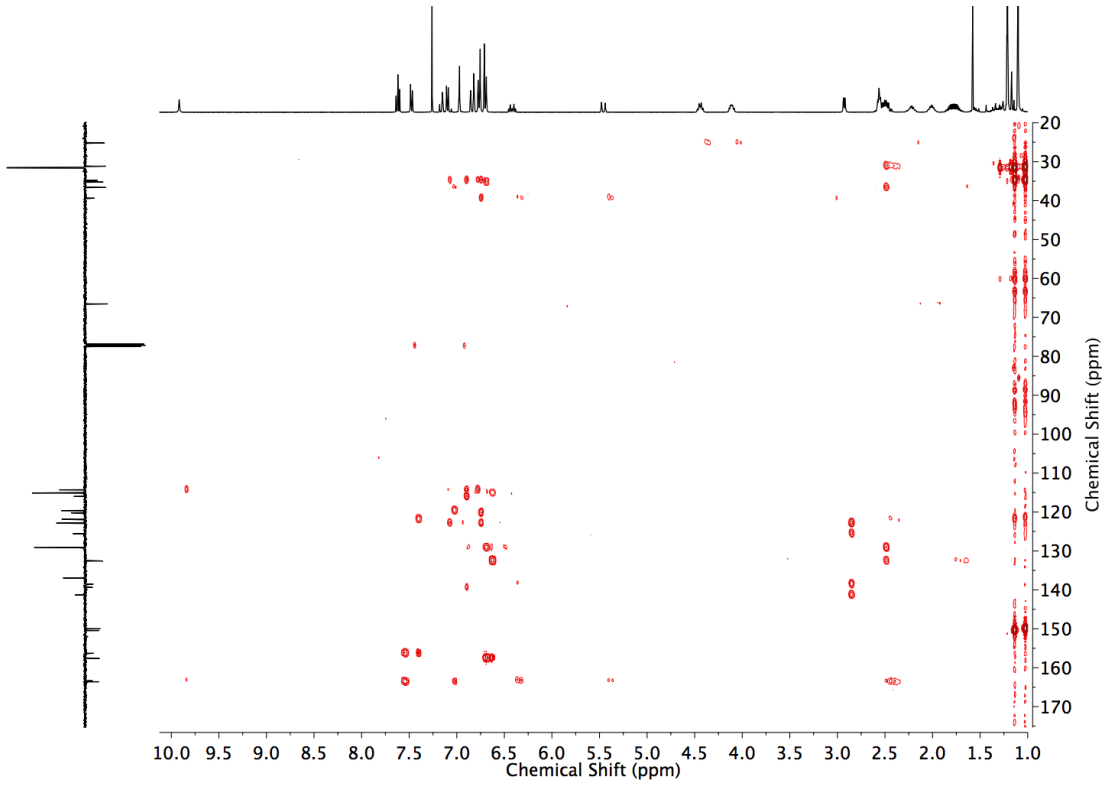

Figure 3.48 HMBC NMR ($CDCl_3$) of **129**.

*Rotaxane **135***

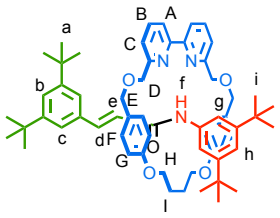

Prepared according to **general procedure A** with **12** (48.3 mg, 0.1 mmol), $[Cu(MeCN)_4]PF_6$ (35.8 mg, 0.096 mmol), **11** (29.3 mg, 0.12 mmol), **108** (27.8 mg, 0.12 mmol). Chromatography (petrol with a gradient of 0 to 20% Et_2O) gave **135** as a white foam (90.0 mg, 97%). ^{1}H NMR (400 MHz, $CDCl_3$) δ: 9.94 (s, 1H, H_f), 7.77 (t, *J* =7.7, 2H, H_B), 7.67 (dd, *J* =7.7, 1.0, 2H, H_A), 7.50 (dd, *J* =7.7, 1.0, 2H, H_C), 7.27 (d, *J* =1.8, 2H, H_g), 7.23 (t, *J* =1.8, 1H, H_b), 6.98 (t, *J* =1.8, 1H, H_h), 6.91 (d, *J* =8.5, 4H, H_F), 6.81 (d, *J* =16.0, 1H, H_d), 6.79 (d, *J* =1.8, 2H, H_c), 6.70 (d, *J* =8.5, 4H, H_G), 5.92 (d, *J* =16.0, 1H, H_e), 4.77 – 4.70 (m, 2H, 2 of H_H), 4.69 (d, *J* =12.0, 2H, 2 of H_D), 4.31 (d, *J* =12.0, 2H, 2 of H_D), 4.19 (d, *J* =13.8, 2H, 2 of H_E), 4.18 – 4.12 (m, 2H, 2 of H_H), 4.02 (d, *J* =13.8, 2H, 2 of H_E), 2.46 – 2.33 (m, 2H, 2 of H_I), 2.11 – 1.99 (m, 2H, 2 of H_I), 1.21 (s, 18H, H_a or H_i), 1.19 (s 18H, H_a or H_i). ^{13}C NMR (101 MHz, $CDCl_3$) δ: 163.3, 160.1, 159.2, 154.9, 150.5, 150.3, 139.6, 139.4, 127.5, 135.6, 129.9, 128.2, 122.9, 122.3, 122.1, 120.8, 119.9, 116.4, 115.1, 114.1, 72.9, 69.5, 66.1, 34.9, 34.8, 31.5, 25.0, 24.8. HR-ESI-MS *m/z* = 930.5763 $[M+H]^+$ (calc. for $C_{63}H_{76}N_3O_5$ 930.5779).

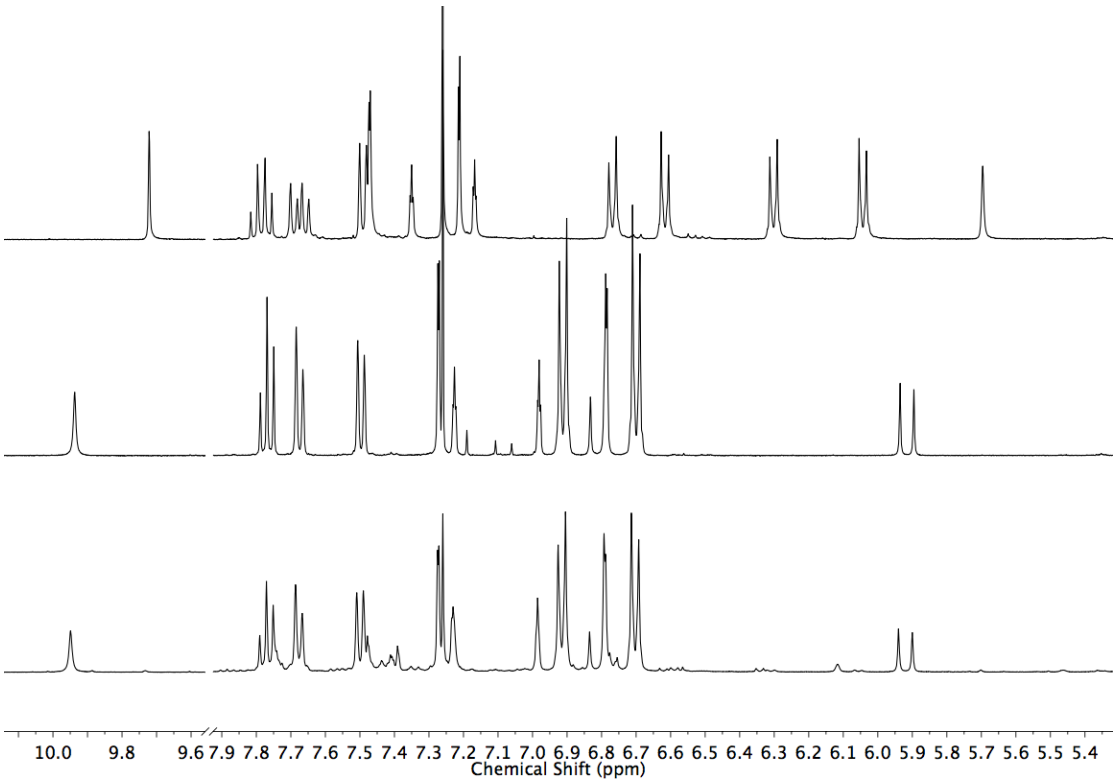

Figure 3.49 Stacked partial ^{1}H NMR (400 MHz, $CDCl_3$) spectra of **134** (top), **135** (middle), the crude reaction product before chromatography (bottom). Ratio of **135**:**134** = 100:0.

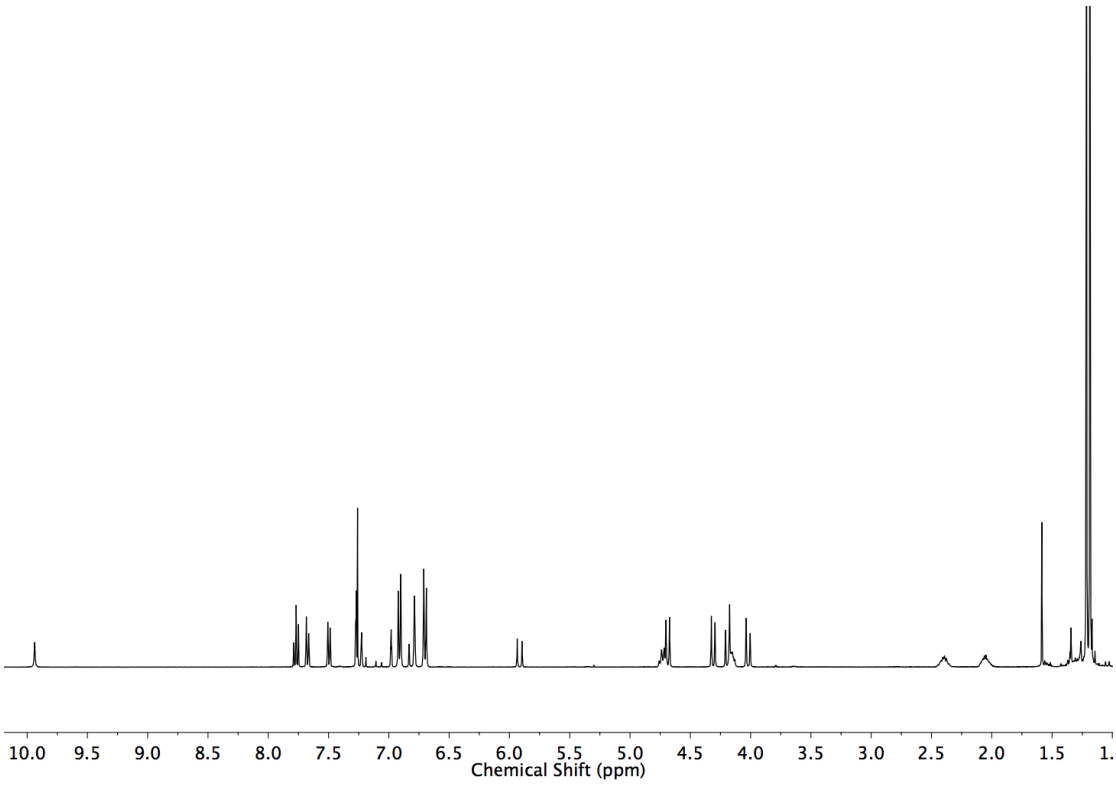

Figure 3.50 ^{1}H NMR ($CDCl_3$, 400 MHz) of **135**.

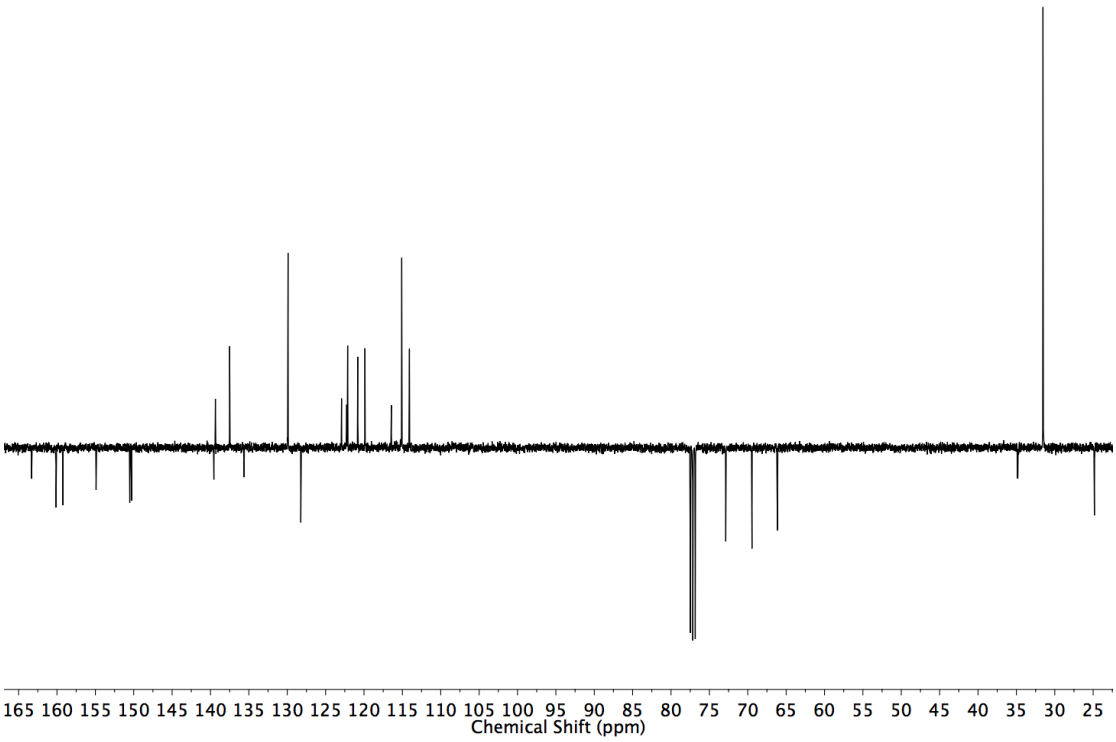

Figure 3.51 JMOD NMR ($CDCl_3$, 101 MHz) of **135**.

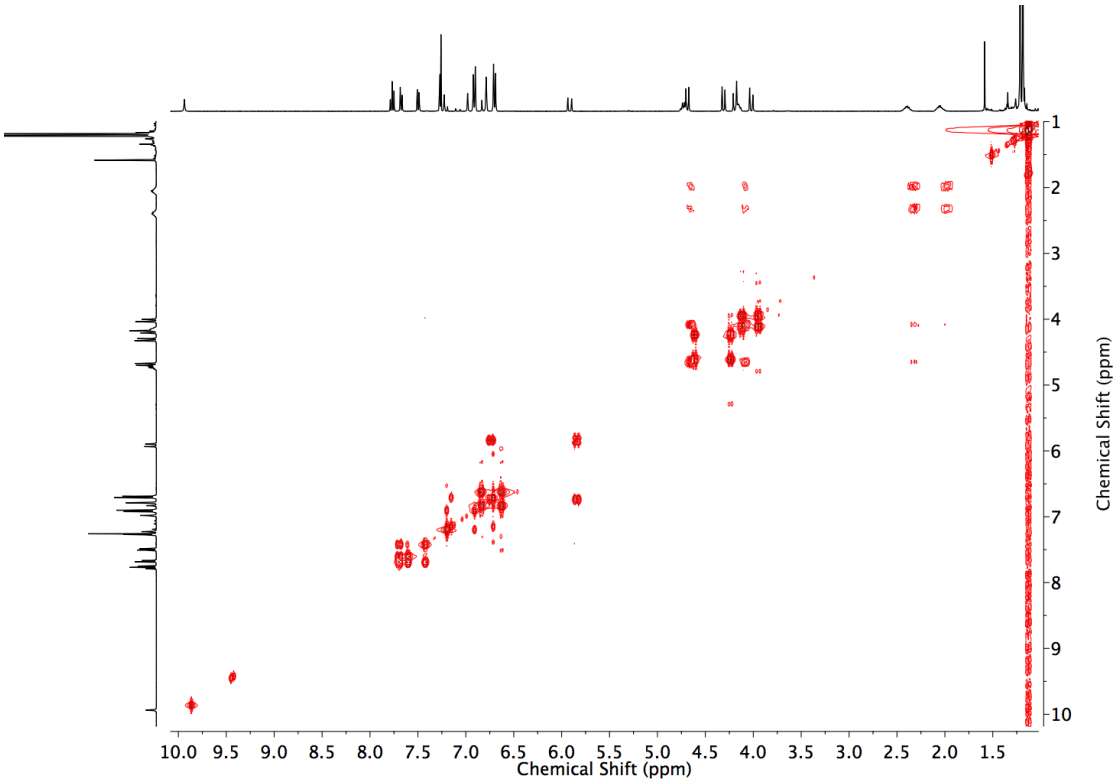

Figure 3.52 COSY NMR ($CDCl_3$) of **135**.

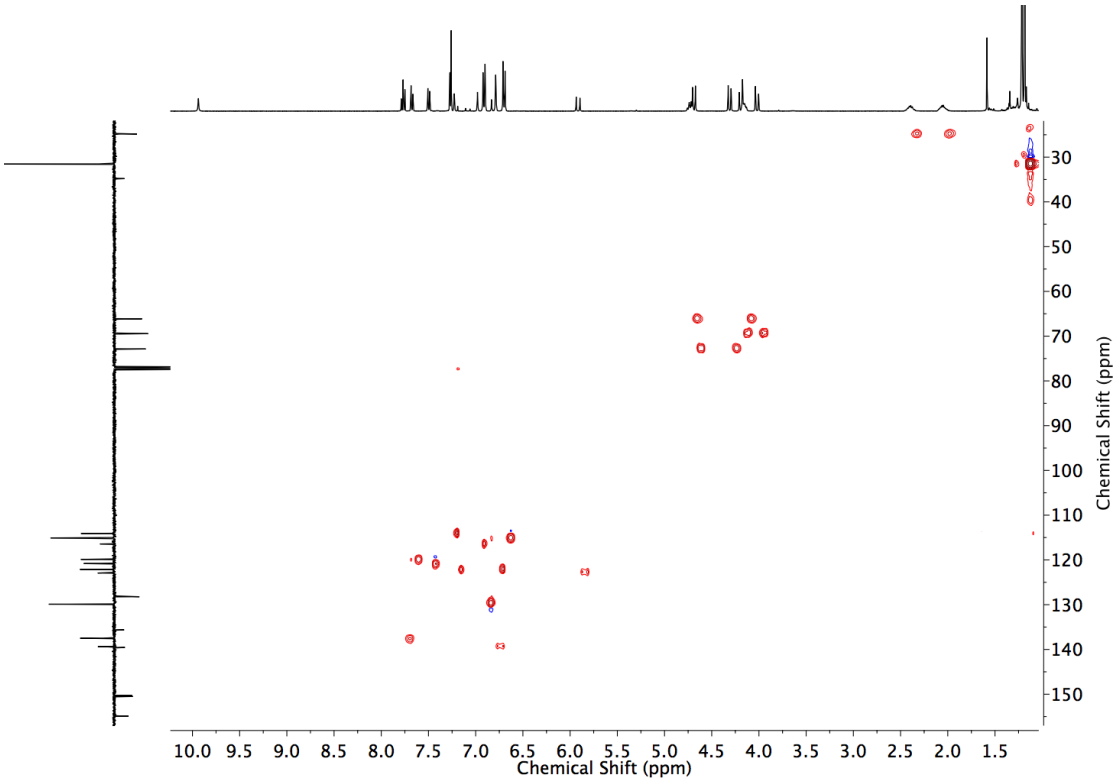

Figure 3.53 HSQC NMR ($CDCl_3$) of **135**.

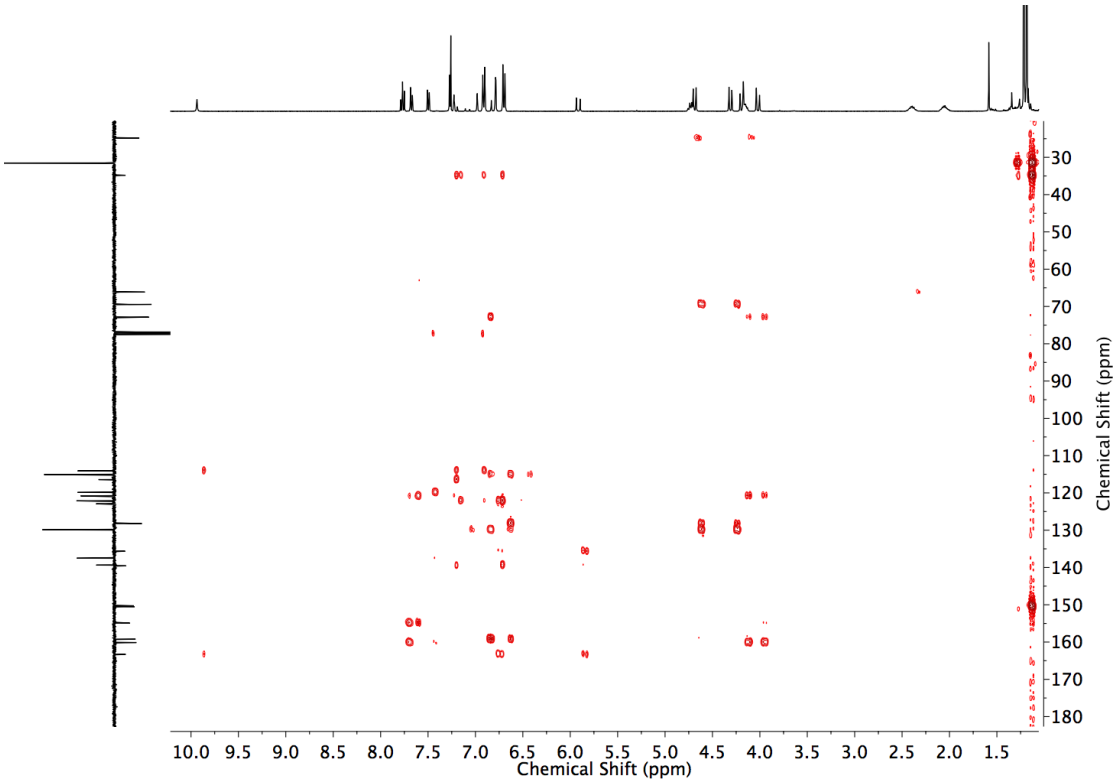

Figure 3.54 HMBC NMR ($CDCl_3$) of **135**.

Rotaxane ***137***

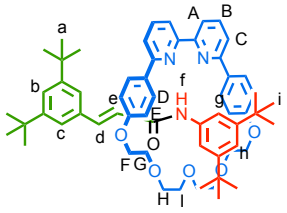

Prepared according to modified **general procedure A** (T = 150 °C, t = 2 h) with **133** (12.5 mg, 0.025 mmol), $[Cu(MeCN)_4]PF_6$ (8.9 mg, 0.024 mmol), **11** (6.9 mg, 0.03 mmol), and **108** (7.3 mg, 0.03 mmol). Chromatography (petrol with a gradient of 0 to 50% Et_2O) gave **137** as a white foam (11.8 mg, 50%). ^{1}H NMR (500 MHz, $CDCl_3$) δ: 9.78 (s, 1H, H_f), 7.90 (t, t, *J* =7.8, 2H, H_B), 7.80 (dd, *J* =7.8, 0.9, 2H, H_A), 7.57 (dd, *J* =7.8, 0.9, 2H, H_C), 7.42 (d, *J* =8.5, 4H, H_D), 7.30 (t, *J* =1.8, 1H, H_b), 7.27 (d, *J* =16.0, H_d), 7.06 (d, *J* =1.8, 2H, Hc), 6.90 (apps, 3H, H_g, H_h), 6.63 (d, *J* =8.5, 4H, H_E), 6.46 (d, *J* =16.0, 1H, H_e), 4.26 – 4.14 (m, 4H, H_F), 3.96 – 3.64 (m, 12H, H_G, H_H, H_I), 1.33 (s, 18H, H_a), 1.12 (s, 18H, H_h). ^{13}C NMR (126 MHz, $CDCl_3$) δ: 163.6, 159.9, 158.9, 157.2, 150.6, 150.2, 138.7, 138.5, 137.7, 135.5, 132.4, 129.4, 124.3, 122.8, 122.1, 120.5, 119.6, 116.7, 115.1, 113.6, 70.3, 70.1, 68.3, 66.9, 34.9, 34.7, 31.5 (×2). HR-ESI-MS *m/z* = 946.5712 $[M+H]^+$ (calc. for $C_{61}H_{76}N_3O_6$ 946.5729).

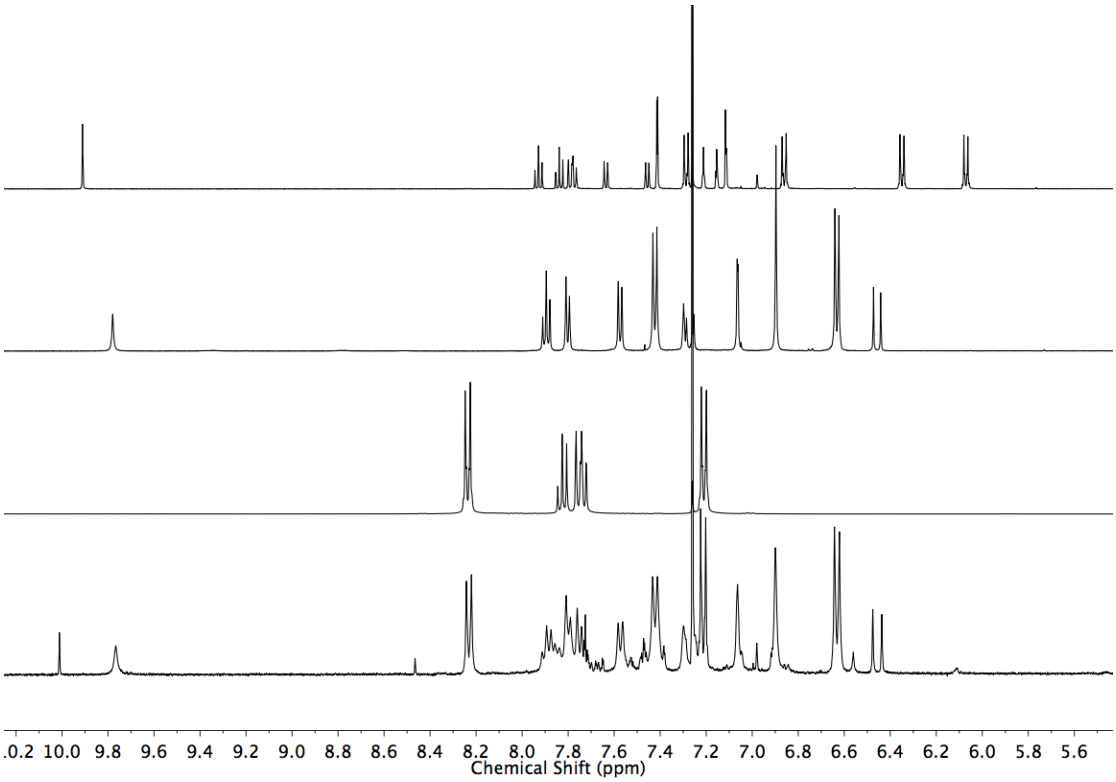

Figure 3.55 Stacked partial ^{1}H NMR (400 MHz, $CDCl_3$) spectra of (top), **137** (upper middle), macrocycle **133** (lower middle) and the crude reaction product before chromatography (bottom). Ratio of **137**: oxidised product of **136** = 80:20 (under these conditions the triazole derived rotaxane was observed to spontaneously oxidise to the ketone).

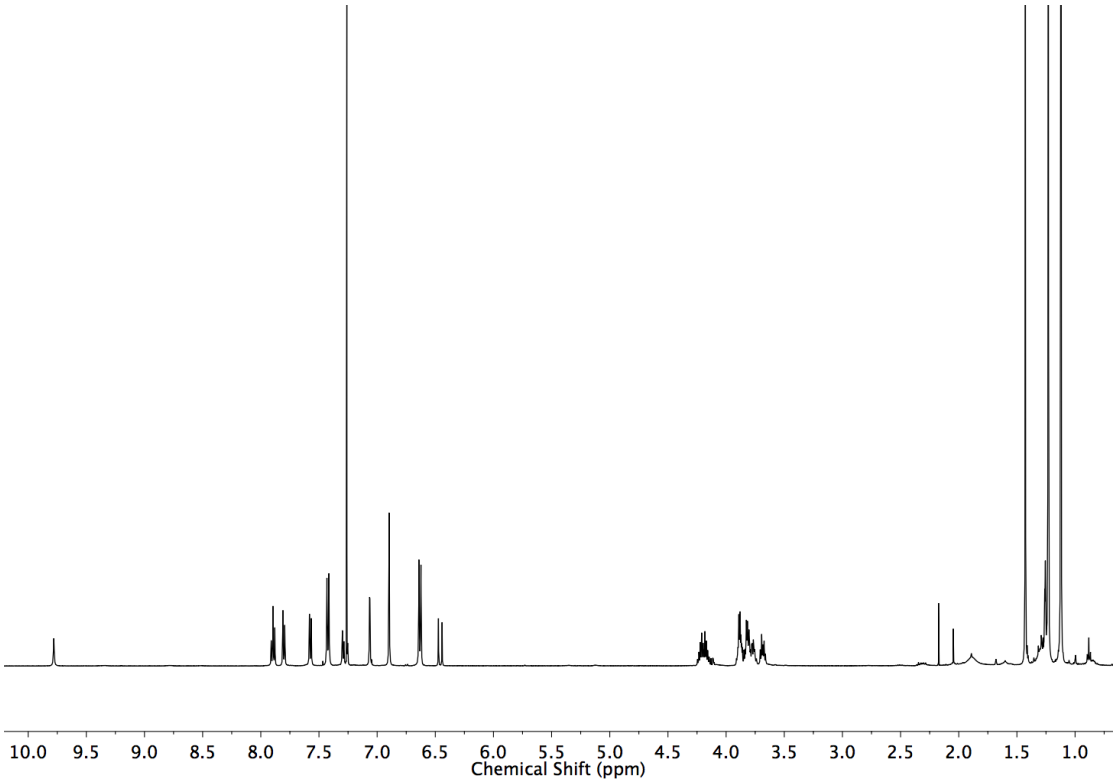

Figure 3.56 ^{1}H NMR ($CDCl_3$, 500 MHz) of **137**.

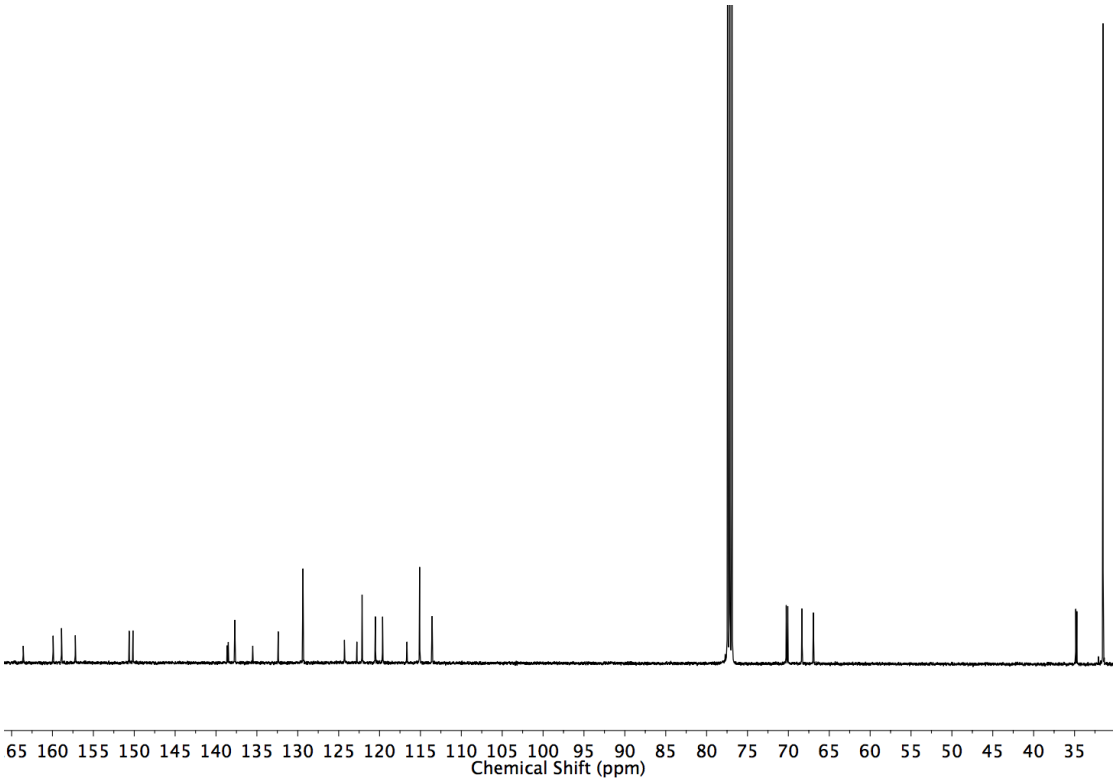

Figure 3.57 ^{13}C NMR ($CDCl_3$, 126 MHz) of **137**

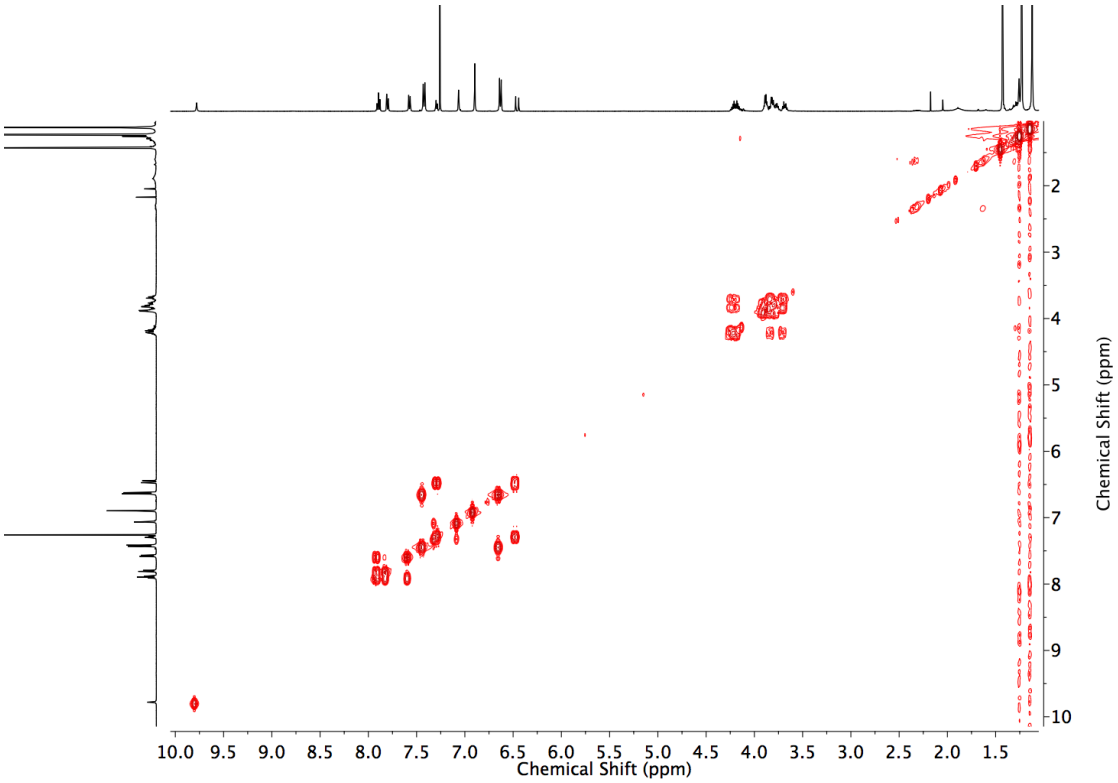

Figure S1 COSY NMR ($CDCl_3$) of **137**.

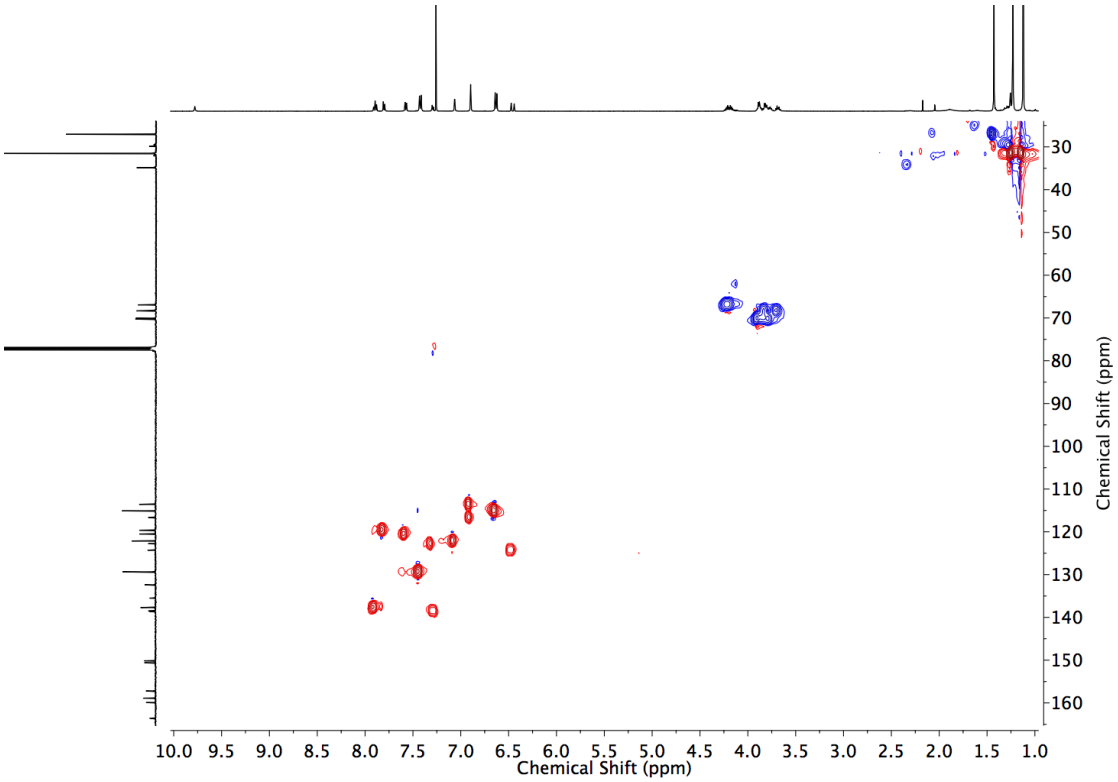

Figure 3.58 HSQC NMR ($CDCl_3$) of **137**.

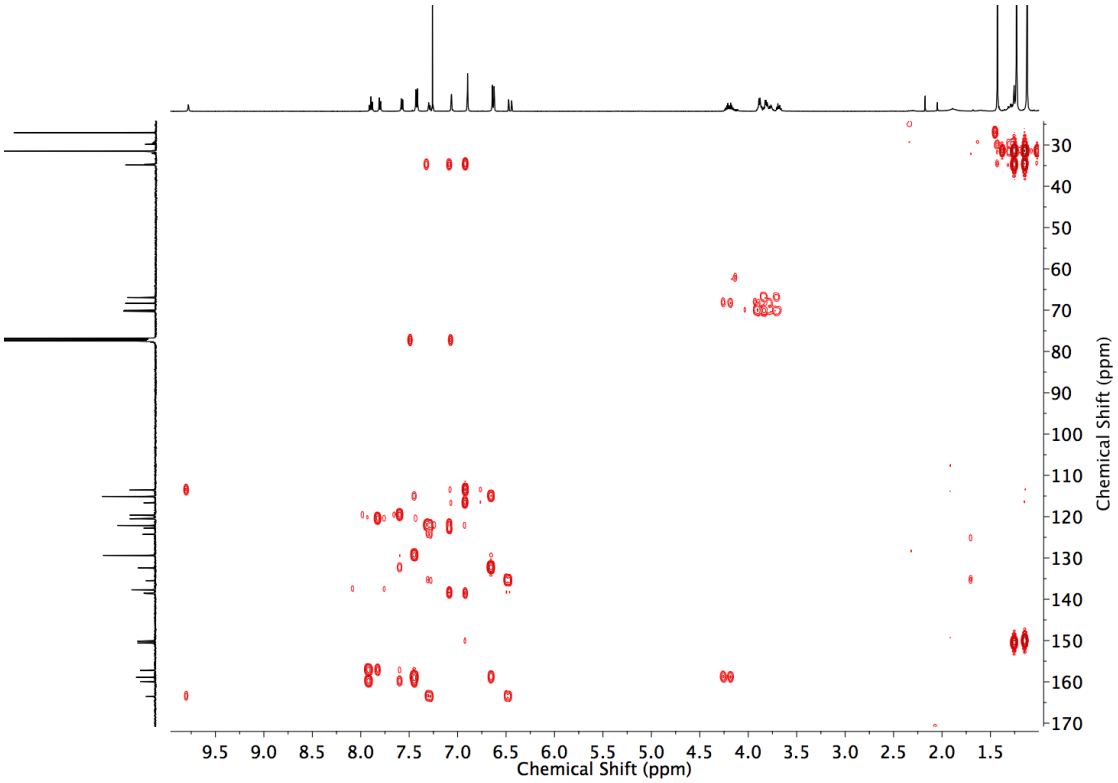

Figure 3.59 HMBC NMR ($CDCl_3$) of **137**.

*Rotaxane **139***

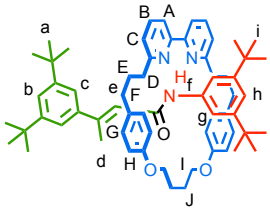

Prepared according to **general procedure A** with **14** (12.0 mg, 0.025 mmol), $[Cu(MeCN)_4]PF_6$ (8.9 mg, 0.024 mmol), **11** (6.9 mg, 0.03 mmol), and **121** (7.7 mg, 0.03 mmol). Chromatography (petrol with a gradient of 0 to 30% Et_2O) gave **139** as a colourless oil (19.9 mg, 85 %). ^{1}H NMR (500 MHz, $CDCl_3$) δ: 10.29 (s, 1H, H_f), 7.66 (t, *J* =7.8, 2H, H_B), 7.55 (dd, *J* =7.8, 0.9, 2H, H_A), 7.24 (d, *J* =1.9, 2H, H_g), 7.17 (t, *J* =1.9, 1H, H_b), 7.13 (dd, *J* =7.8, 0.9, 2H, H_C), 7.05 (d, *J* =1.9, 2H, H_c), 6.93 (t, *J* =1.9, 1H, H_h), 7.74 (d, *J* =8.5, 4H, H_G), 6.61 (d, *J* =8.5, 4H, H_H), 6.54 (q, *J* =1.2, 1H, H_e), 4.72 – 4.64 (m, 2H, 2 of H_I), 4.21 – 4.15 (m, 2H, 2 of H_I), 2.59 – 2.43 (m, 8H, H_D, H_F), 2.35 – 2.25 (m, 2H, 2 of H_J), 2.12 (d, *J* =1.2, 3H, Hd), 2.09 – 1.98 (m, 2H, 2 oh H_J), 1.82 – 1.60 (m, 4H, H_E), 1.19 (s, 18H, H_a), 1.08 (s, 18H, H_i). ^{13}C NMR (126 MHz, $CDCl_3$) δ: 164.0, 163.2, 157.7, 156.5, 150.0, 149.9, 147.5, 142.8, 140.6, 137.0, 132.1, 128.9, 122.2, 122.1, 121.3, 120.5, 119.4, 115.3, 115.2, 113.3, 66.4, 36.8, 35.4, 34.9, 34.8, 31.6, 31.6, 31.4, 25.0, 17.0. HR-ESI-MS *m/z* = 940.6343 $[M+H]^+$ (calc. for $C_{64}H_{82}N_3O_3$ 940.6351).

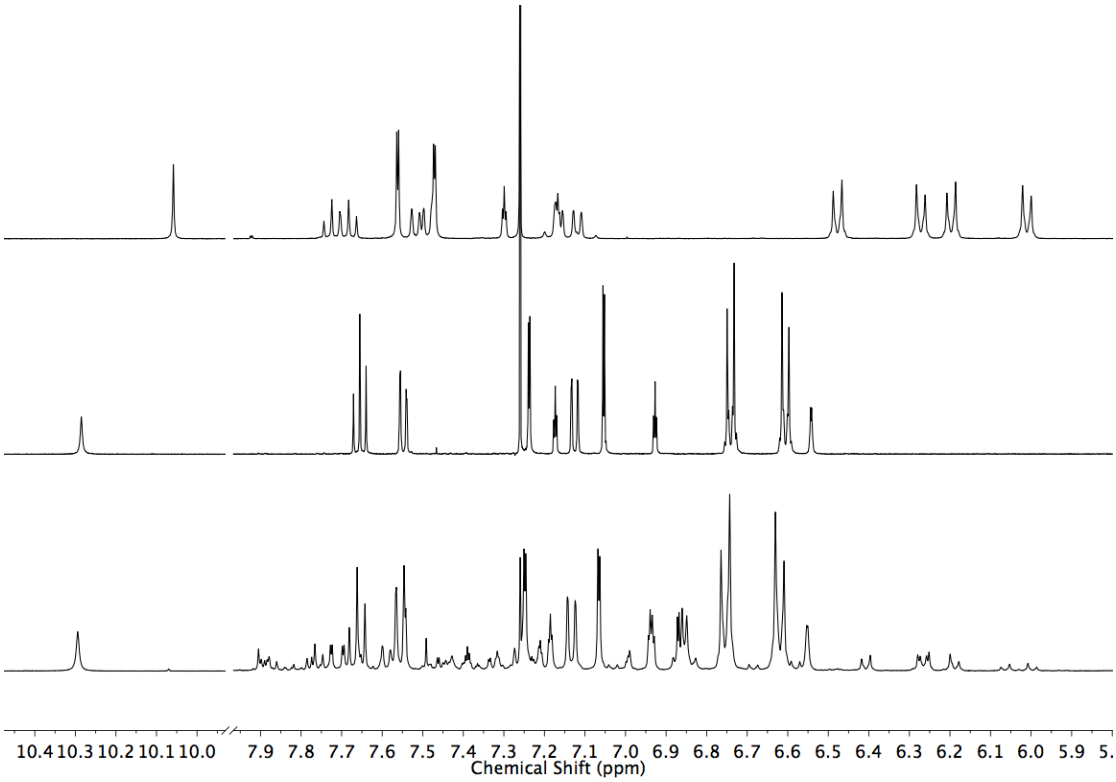

Figure 3.60 Stacked partial ^{1}H NMR (400 MHz, $CDCl_3$) spectra of **141** (top), **139** (middle) and the crude reaction product before chromatography (bottom). Ratio of **139**:**141** = 95:5.

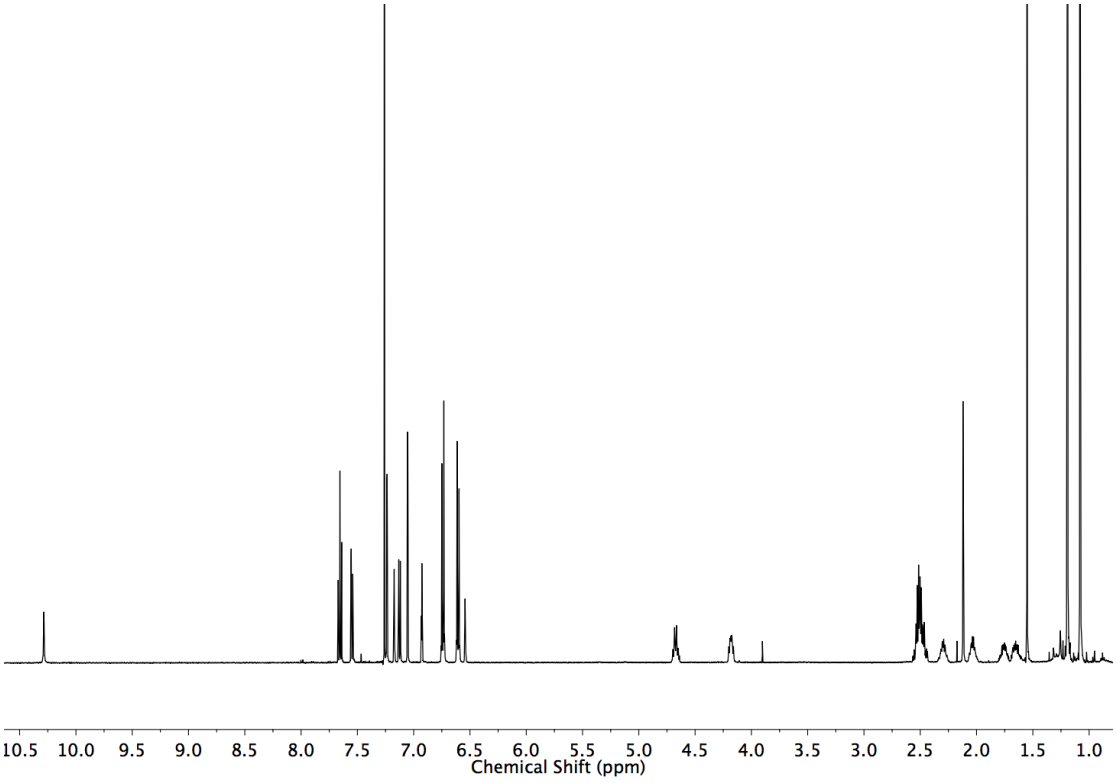

Figure 3.61 ^{1}H NMR ($CDCl_3$, 500 MHz) of **139**.

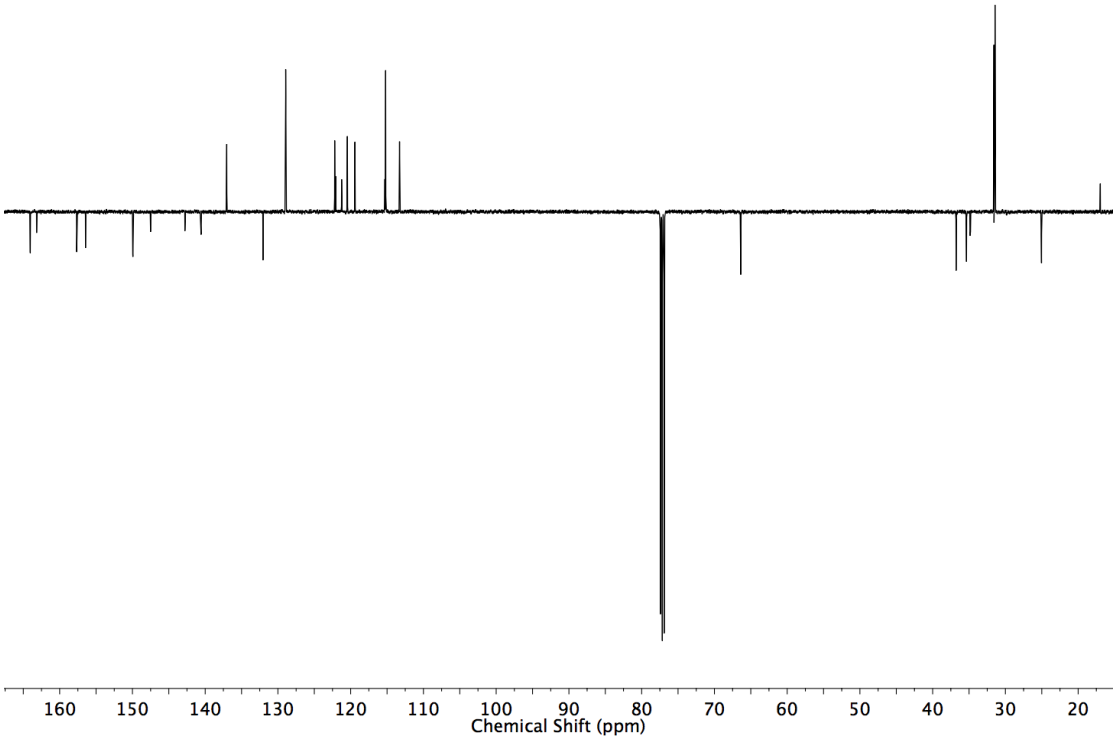

Figure 3.62 JMOD NMR ($CDCl_3$, 126 MHz) of **139**.

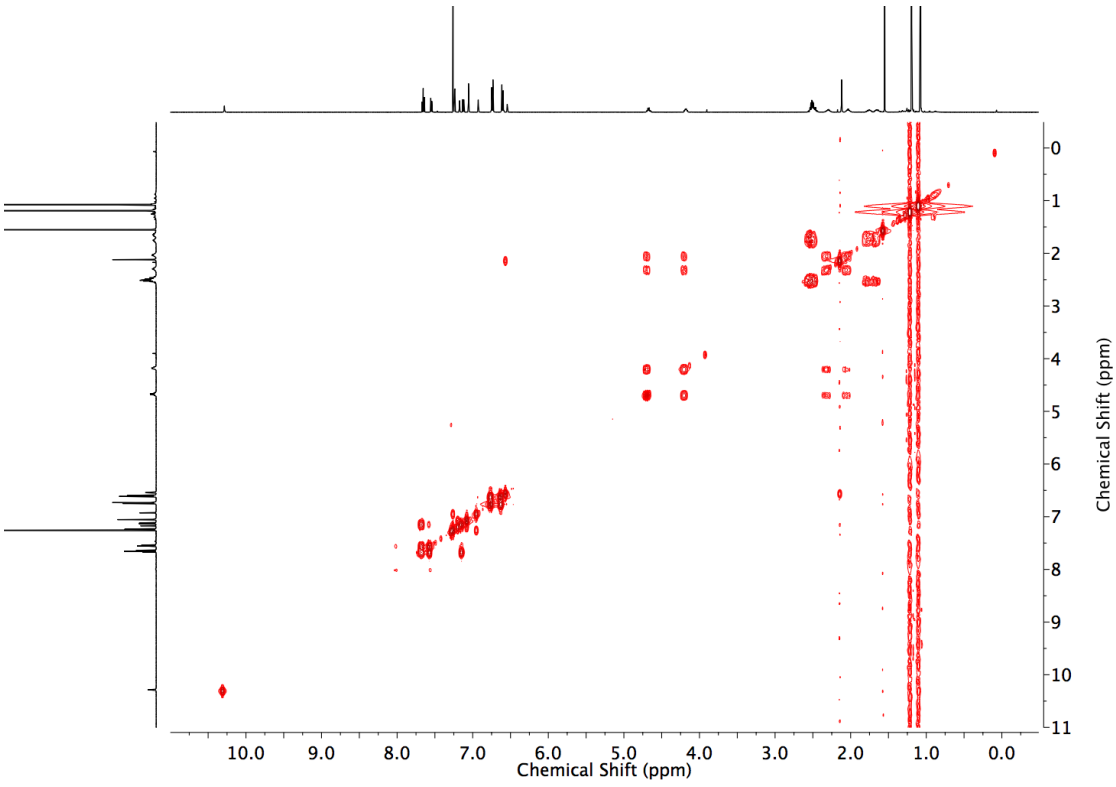

Figure 3.63 COSY NMR ($CDCl_3$) of **139**.

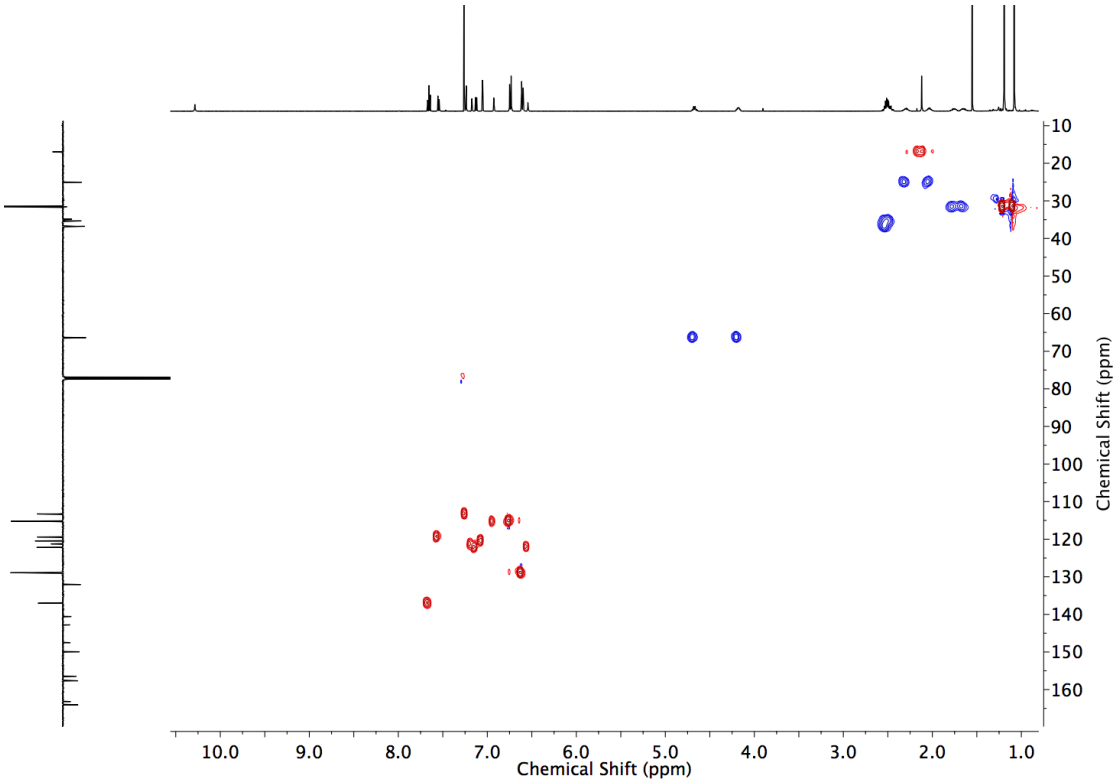

Figure 3.64 HSQC NMR ($CDCl_3$) of **139**.

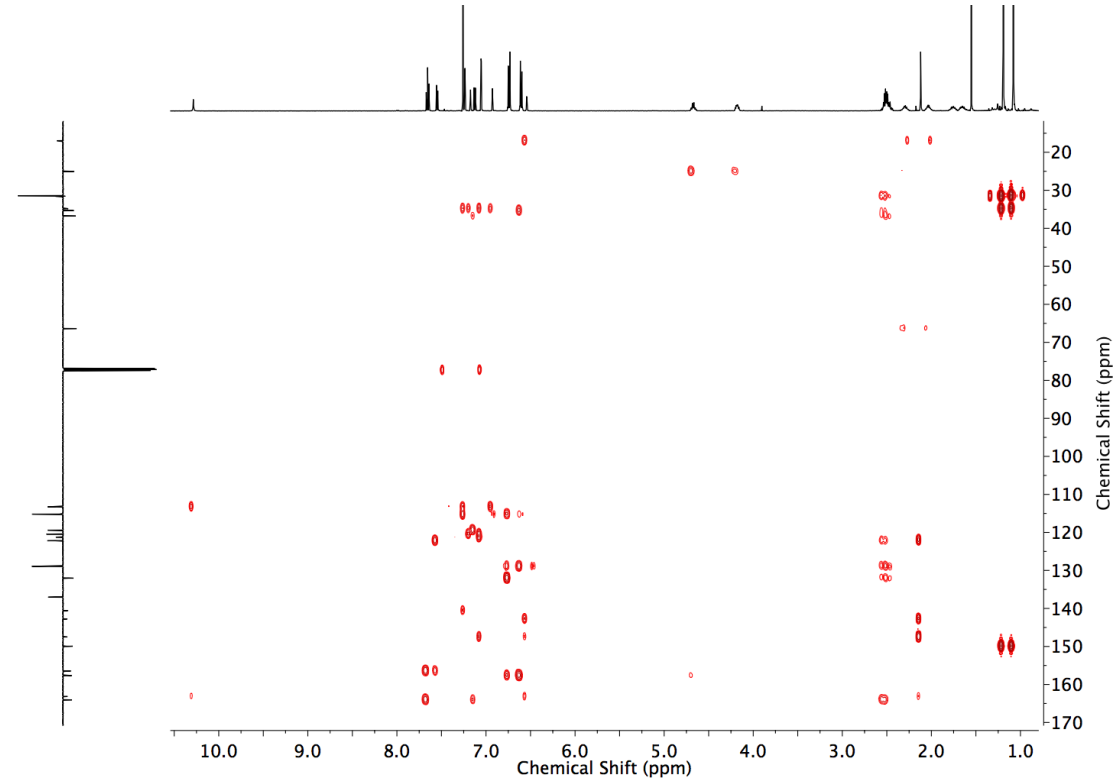

Figure 3.65 HMBC NMR ($CDCl_3$) of **139**.

Synthesis of triazole rotaxanes

General Procedure B

N^iPr_2Et (2 eq.) was added to a solution of **alkyne** (1.2 eq.), **azide** (1.2 eq.), **macrocycle** (1 eq.) and $[Cu(MeCN)_4]PF_6$ (0.96 eq.) in CH_2Cl_2 (80 mL/mmol) in a sealed microwave vial (CEM Ltd.). The deep red mixture was stirred at rt for 16 hours. The reaction mixture was diluted with CH_2Cl_2 (200 mL/mmol) and washed with EDTA-NH_3 solution (100 mL/mmol). The aqueous layer was extracted with CH_2Cl_2 (2 × 100 mL/mmol). Combined organic extracts were washed with brine (100 mL/mmol), dried ($MgSO_4$), filtered and the solvent removed *in vacuo*.

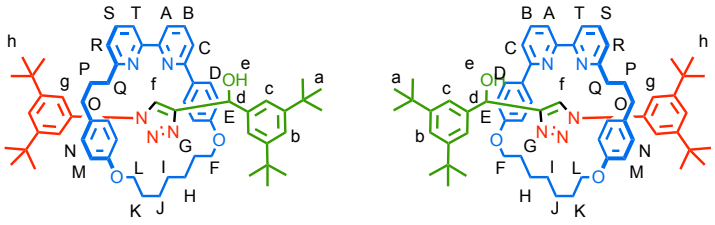

N^iPr_2Et (2 eq.) was added to a solution of **108** (6.1 mg, 0.025 mmol), **11** (5.8 mg, 0.025 mmol), **53** (12.0 mg, 0.025 mmol) and $[Cu(MeCN)_4]PF_6$ (8.9 mg, 0.024 mmol) in CH_2Cl_2 (2 mL) in a sealed microwave vial (CEM Ltd.). The reaction mixture was stirred at rt for 16 h, protected by a nitrogen atmosphere. KCN (20.0 mg, 0.307 mmol) was added and the reaction mixture was stirred for an additional 16 h. Air was bubbled though the reaction to remove the solvent and the residue was re-dissolved in CH_2Cl_2 (20 mL) and had H_2O (10 mL) added. The aqueous layer was extracted with CH_2Cl_2 (2 × 10 mL), washed with brine (10 mL), dried ($MgSO_4$) filtered, and had the solvent removed *in vacuo*. Chromatography (1:1 CH_2Cl_2-petrol with a gradient of 0 to 20% MeCN) gave **122** as a yellow foam (9.3 mg, 40%, 0.57:0.43 diastereoisomeric ratio after purification); ^{1}H NMR (400 MHz, $CDCl_3$, 298 K)* δ 9.88 (s, 1H, H_f (*major*)), 9.79 (s, 1H, H_f (*minor*)), 7.80 (app. q, 1H, *J* = 7.6, H_S), 7.74-7.67 (m, 1H, H_B), 7.65 (d, 1H, *J* = 7.8, H_T), 7.59-7.55 (m, 1H, H_A), 7.47 (d, 2H, *J* = 1.7, H_c (*major*)), 7.41 (d, 2H, *J* = 1.7, H_c (*minor*)), 7.36-7.21 (m, 5H, H_h (*major*), H_g, H_C, and H_R), 7.21 (t, 1H, *J* = 1.8, H_h (*minor*)), 7.15-7.13 (m, 1H, H_b), 6.79 (d, 2H, *J* = 8.7, H_E (*major*)), 6.61 (d, 2H, *J* = 8.7, H_E (*minor*)), 6.28 (d, 2H, *J* = 8.5, H_M (*minor*)), 6.16-6.09 (m, 4H, H_D and H_M (*major*)), 5.98-5.92 (m, 2H, H_N), 5.52 (br s, 1H, H_d (*minor*)), 5.42 (d, 1H, *J* = 3.1, H_d (*major*)), 4.23-4.07 (m, 2H, one of H_F and one of H_L) 3.99-3.90 (m, 1H, one of H_F or one of H_L), 3.81-3.71 (m, 1H, one of H_F or one of H_L), 3.10 (m, 1H, H_e (*minor*)), 2.92-2.46 (m, 3H, H_e (*major*) and H_Q) 2.45-2.18 (m, 3H, one of H_I and H_O), 2.08-1.15, (m, 11H, H_G, H_H, one of H_I, H_J, H_K and H_P), 1.18 (m, 18H, H_a or H_i), 1.14 (m, 18H, H_a (*minor*) or H_i (*minor*)), 1.13 (m, 18H, H_a (*major*) or H_i (*major*)); ^{13}C NMR (101 MHz, $CDCl_3$, 298 K) δ 2 × 163.7, 159.8, 159.7, 159.1, 159.0, 157.8, 2 × 157.7, 157.6, 2 × 156.8, 150.9, 150.8, 150.4, 150.2, 2 × 149.5, 148.9, 142.4, 2 × 137.3, 137.1, 2 × 137.0, 2 × 131.5, 131.3, 131.2, 128.7, 128.6, 128.1, 128.0, 122.8, 122.7, 122.0, 121.6, 120.6, 120.5, 120.4, 120.2, 120.1, 2 × 119.9, 2 × 119.8, 114.5, 114.4, 113.8, 113.6, 113.6, 113.5, 70.9, 70.3, 70.2 67.6, 65.6, 65.5, 37.7, 37.6, 35.2, 35.1, 35.0, 34.9, 33.4, 33.3, 31.6, 2 × 31.5, 29.9, 2 × 29.4, 29.2, 28.2, 25.8, 2 × 25.7; HR-ESI-MS (+ve) *m/z* = 954.6258 $[M+H]^+$ calc. 954.6256.

*As stereochemistry could not be unambiguously assigned, the signals are simply designated (*major*) or (*minor*). Proton counts are provided for each signal and represent the

expected integration of that environment. Where the major and minor diastereoisomer signals are coincident, no (*major*)/(*minor*) label is provided and the proton count indicated refers the expected integration of that signal in each of the stereoisomers that contributes to the multiplet.

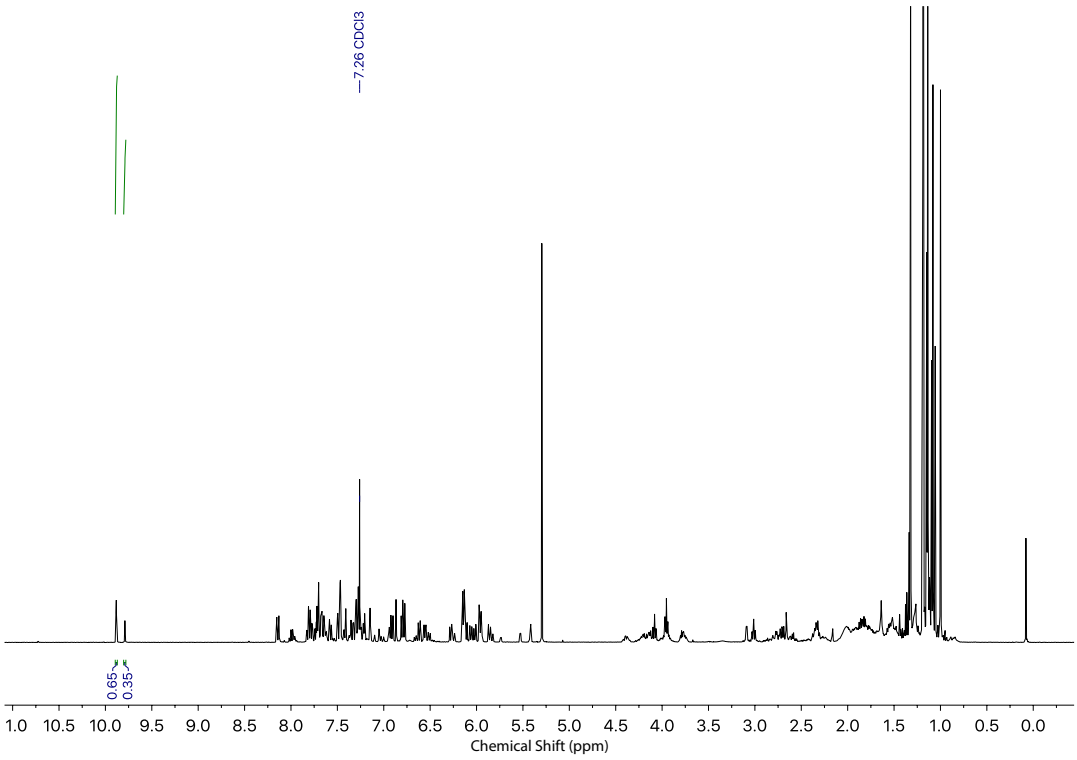

Figure 3.66 Crude ^{1}H NMR ($CDCl_3$, 400 MHz) of **109**.

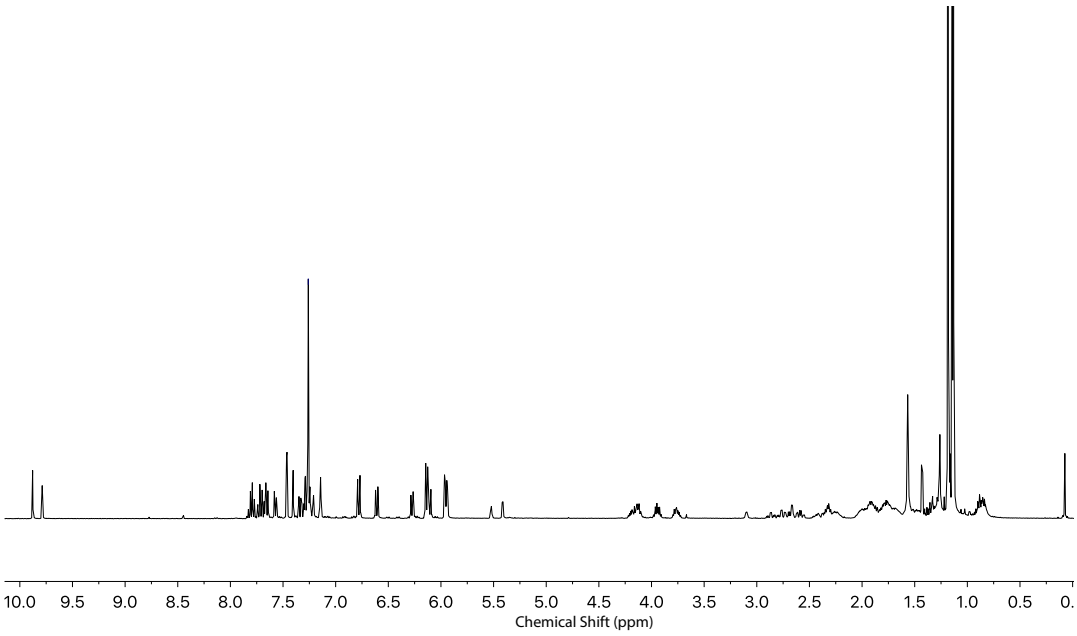

Figure 3.67 ^{1}H NMR ($CDCl_3$, 400 MHz) of **109**.

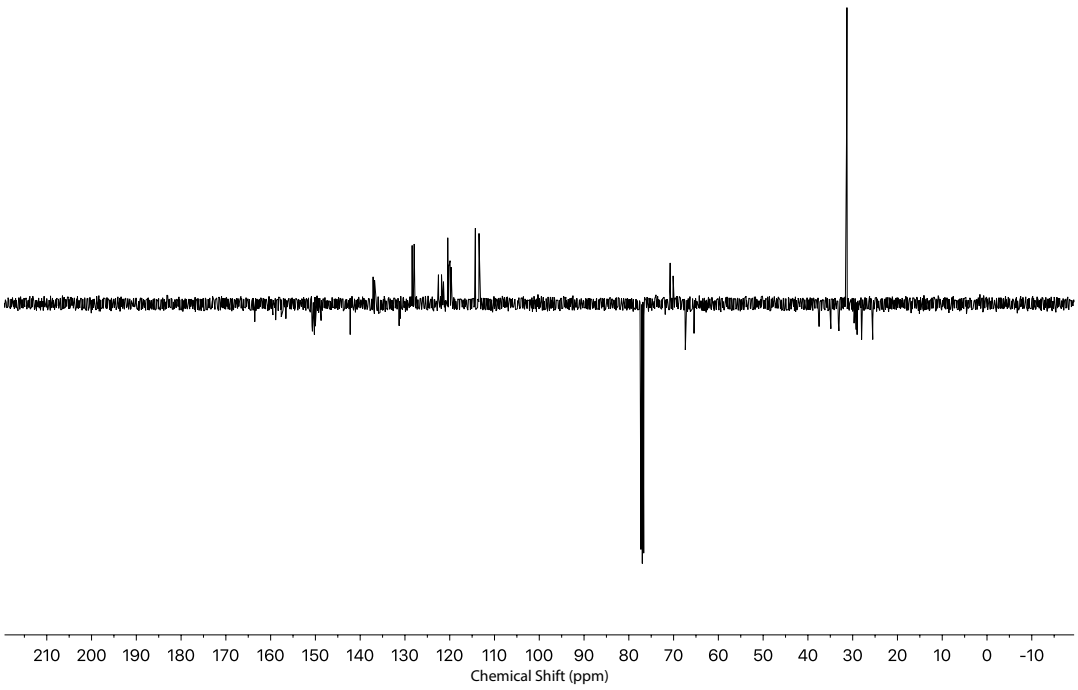

Figure 3.68 JMOD NMR ($CDCl_3$, 101 MHz) of **109**.

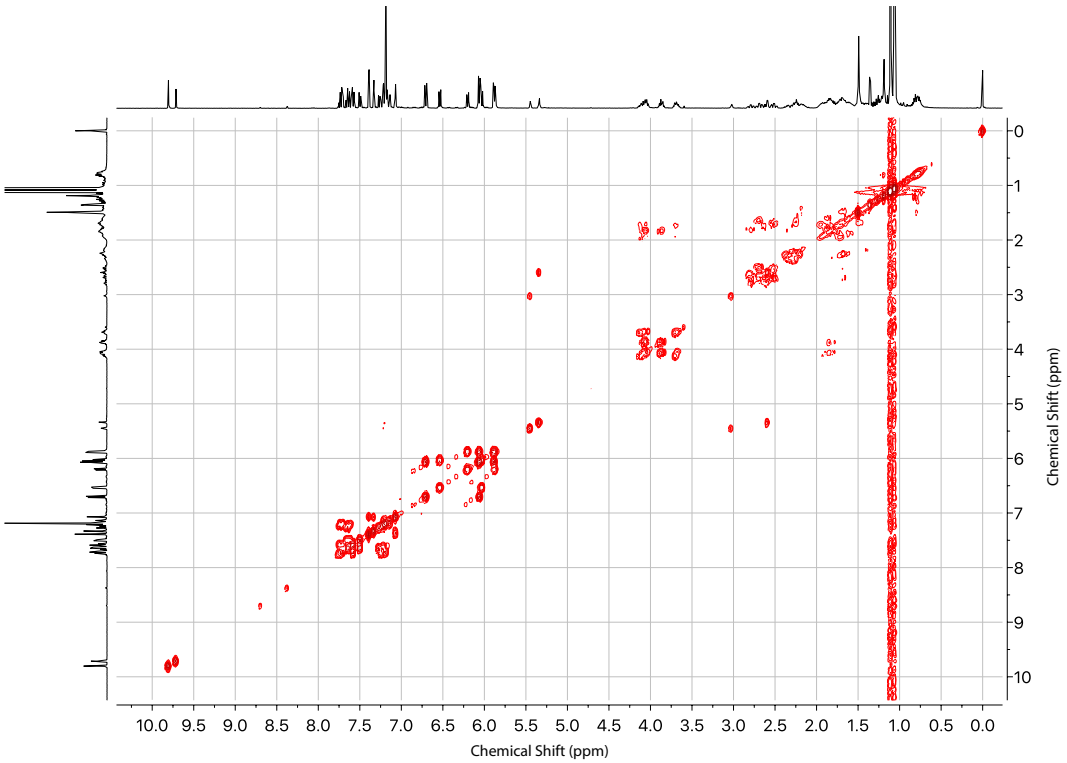

Figure 3.69 COSY NMR ($CDCl_3$) of **109**.

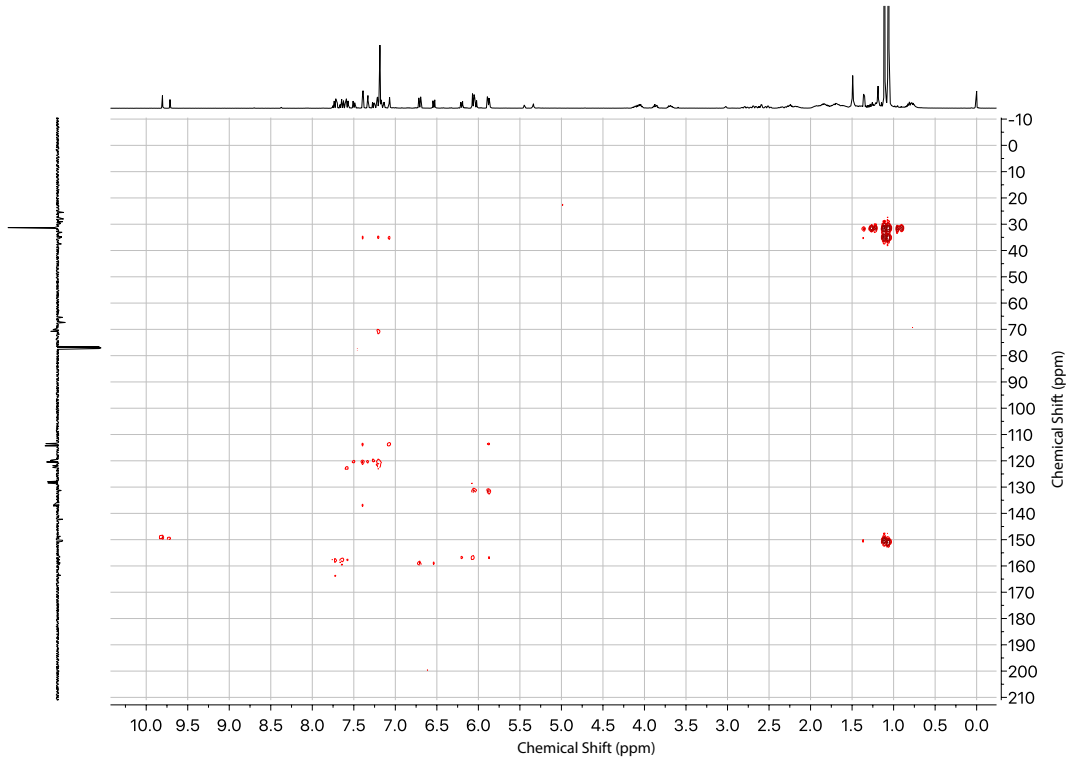

Figure 3.70 HMBC NMR ($CDCl_3$) of **109**.

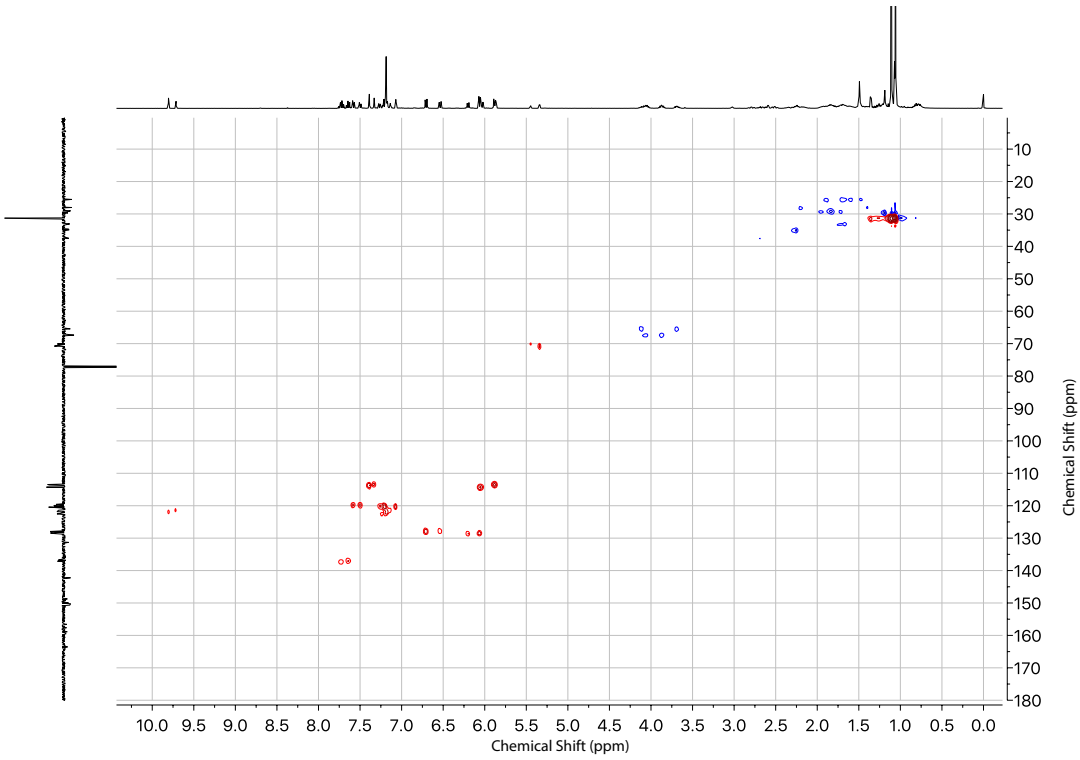

Figure 3.71 HSQc NMR ($CDCl_3$) of **109**.

Rotaxane ***122***

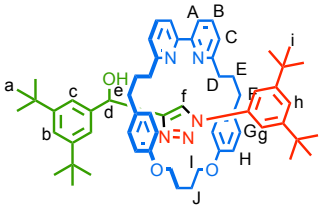

Prepared according to **general procedure B** with **14** (12.0 mg, 0.025 mmol), $[Cu(MeCN)_4]PF_6$ (8.9 mg, 0.024 mmol), **11** (7.0 mg, 0.03 mmol), and **108** (7.3 mg, 0.03 mmol). Chromatography (petrol with a gradient of 0 to 50% Et_2O) gave **122** as a white foam (18.0 mg, 76%). ^{1}H NMR (500 MHz, $CDCl_3$): δ 10.08 (d, *J* =0.8, 1H, H_f), 7.73 (t, *J* =7.8 1H, 1 of H_B), 7.69 (t, *J* =7.8, 1H, 1 of H_B), 7.53 (dd, *J* =7.8, 1.0, 1H, 1 of H_A), 7.50 (dd, *J* =7.8, 1.0, 1H, 1 of H_A), 7.44 (dd, *J* =1.9, 0.6, 2H, H_c), 7.41 (d, *J* =1.8, 2H, H_g), 7.34 (t, *J* =1.9, 1H, H_b), 7.18 – 7.21 (m, 2H, 1 of H_C, H_h), 7.13 (dd, *J* =7.8, 0.8, 1H, 1 of H_C), 6.63 (d, *J* =8.6, 2H, 1 of H_H), 6.51 (d, *J* =8.6, 2H, 1 of H_G), 6.05 – 6.11 (m, 4H, 1 of H_G, 1 of H_H), 5.66 (br s, 1H, H_d), 4.64 – 4.77 (m, 1H, 1 of H_I), 4.49 – 4.60 (m, 1H, 1 of H_I), 4.41 (s, 1H, H_e), 4.21 – 4.30 (m, 1H, 1 of H_I), 3.91 – 4.00 (m, 1H, 1 of H_I), 2.12 – 2.60 (m, 10H, H_D, 2 of H_J, H_F), 1.96 – 2.07 (m, 2H, 2 of H_J), 1.53 – 1.79 (m, 4H, H_E), 1.32 (s, 18H, H_a), 1.19 (s, 18H, H_i). ^{13}C NMR (126 MHz, $CDCl_3$): δ 163.4, 163.1, 157.9, 157.1, 157.1, 156.9, 151.1, 150.0, 149.9, 142.6, 137.3, 137.1, 137.1, 131.7, 151.5, 128.3, 128.2, 122.4, 121.6, 121.5, 121.4, 120.6, 120.2, 120.1, 120.1, 115.4, 114.4, 114.3, 69.9, 66.8, 66.3, 36.9, 36.1, 35.1, 35.1, 35.0, 34.7, 32.3, 31.7, 31.4, 30.0, 25.1, 24.9. HR-ESI-MS *m/z* = 954.6257 $[M+H]^+$ (calc. for $C_{63}H_{80}N_5O_3$ 954.6256).

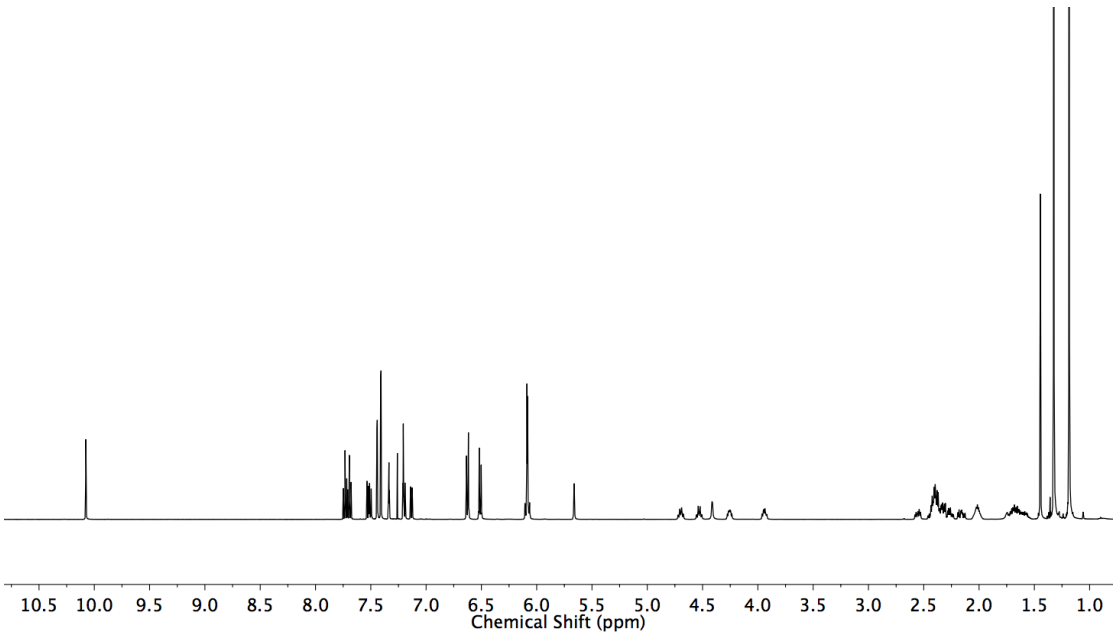

Figure 3.72 ^{1}H NMR ($CDCl_3$, 500 MHz) of **122**.

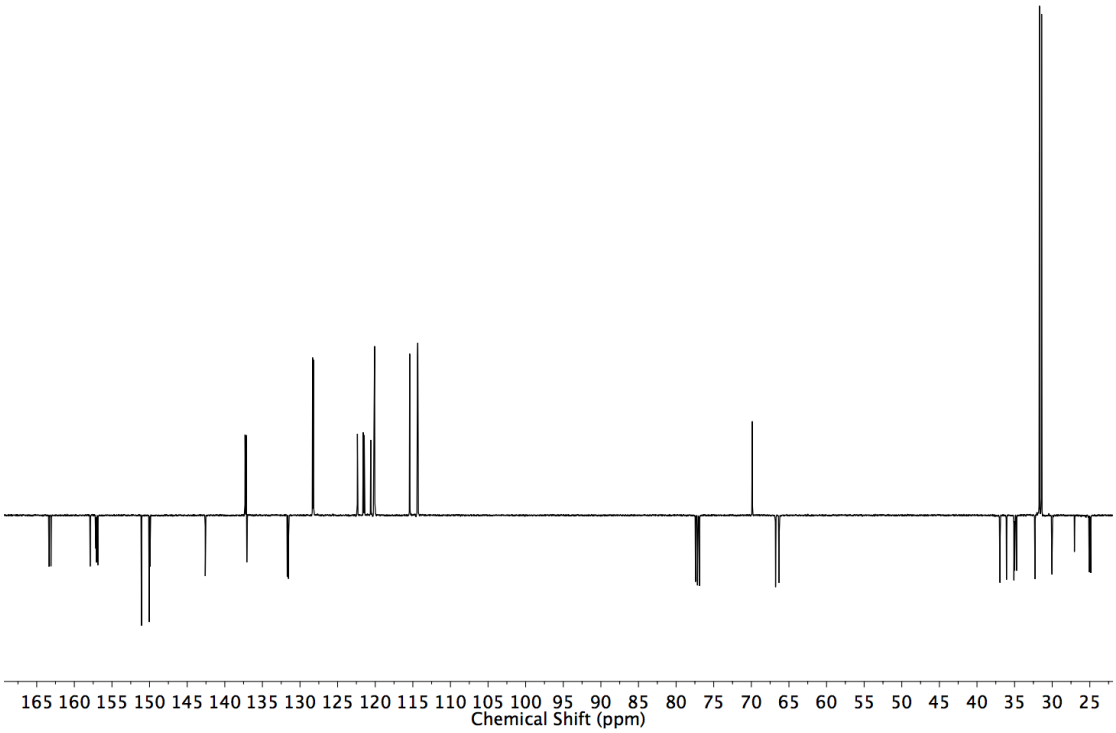

Figure 3.73 JMOD NMR ($CDCl_3$, 126 MHz) of **122**.

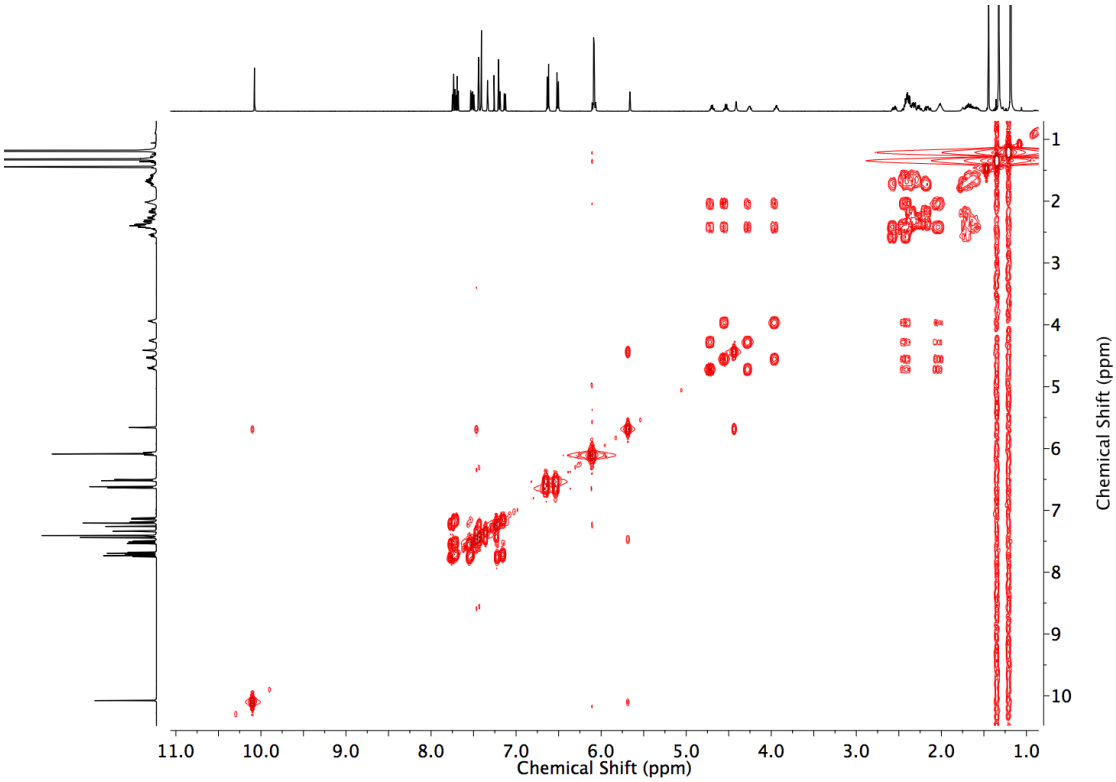

Figure 3.74 COSY NMR ($CDCl_3$) of **122**.

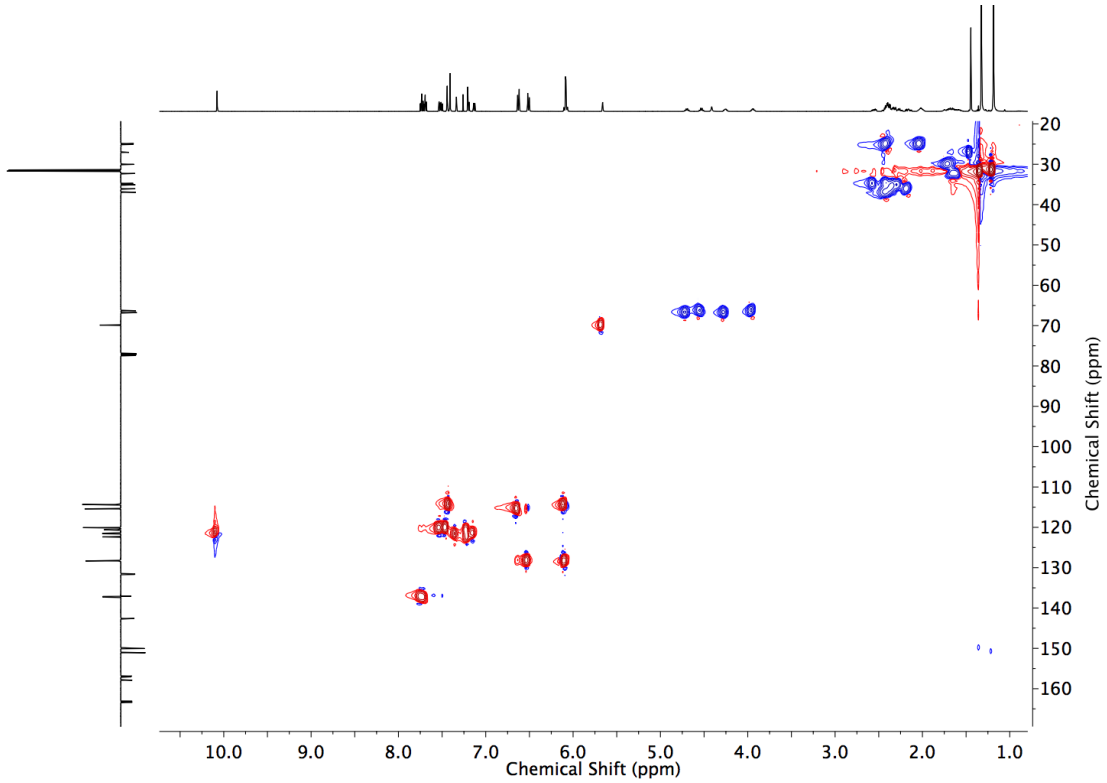

Figure 3.75 HSQC NMR ($CDCl_3$) of **122**.

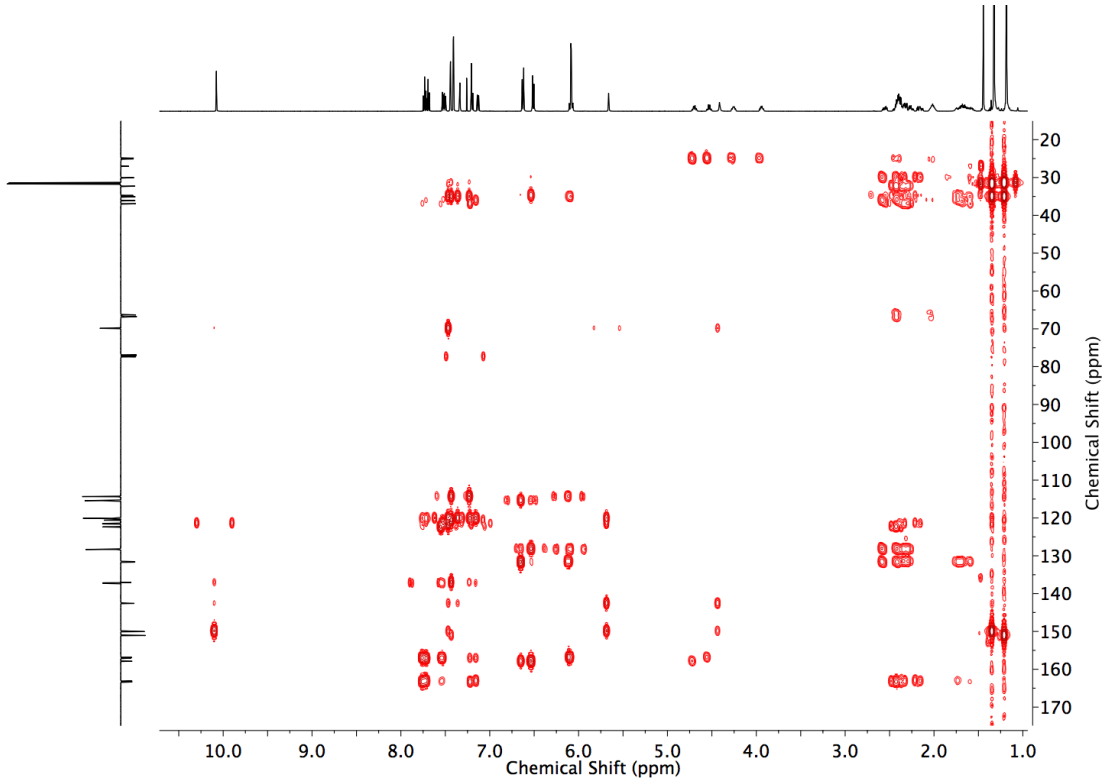

Figure 3.76 HMBC NMR ($CDCl_3$) of **122**.

Rotaxane ***126***

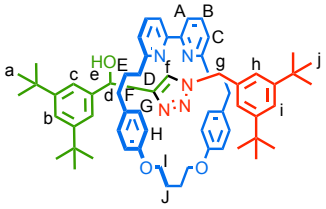

Prepared according to **general procedure B** with **14** (12.0 mg, 0.025 mmol), $[Cu(MeCN)_4]PF_6$ (8.9 mg, 0.024 mmol), **20** (7.3 mg, 0.03 mmol), and **108** (7.3 mg, 0.03 mmol). Chromatography (petrol with a gradient of 0 to 50% Et_2O) gave **126** as a white foam (17.0 mg, 70%). ^{1}H NMR (400 MHz, $CDCl_3$): δ 8.73 (s, 1H, H_f), 7.62 (t, *J* =7.8, 2H, H_B), 7.26 (app. s, 3H, H_b, H_c), 7.16 (t, *J* =1.8, 1H, H_i), 7.10 (app. t, *J* =7.7, 2H, H_C) 6.79 (d, *J* =1.8, 2H, H_h), 6.68 – 6.57 (m, 4H, 2 of H_G, 2 of H_H), 6.48 (s, 4H, 2 of H_G, 2 of H_H), 5.38 (br. s, 1H, H_d), 4.67 (d, *J* =3.7, 1H, H_e), 4.65 – 4.52 (m, 2H, 2 of H_I), 4.49 (d, *J* =13.9, 1H, 1 of H_g), 4.25 (d, *J* =13.9, 1H, 1 of H_g), 4.18 – 4.00 (m. 2H, 2 of H_I), 2.68 – 2.15 (m, 10H, H_D, H_F, 2 of H_J), 2.03 – 1.95 (m, 2H, 2 of H_J), 1.85 – 1.49 (m, 4H, H_E), 1.26 (s, 18H, H_a or H_j), 1.11 (s, 18H, H_a or H_j). ^{13}C NMR (101 MHz, $CDCl_3$): δ 162.8, 162.8, 157.6, 157.4, 156.9, 156.7, 150.7, 149.9, 149.2, 142.4, 137.1, 136.9, 133.2, 132.4, 132.3, 128.9, 128.7, 124.2, 123.3, 122.8, 121.7, 121.6, 121.5, 120.7, 120.0, 119.9, 115.2, 114.9, 69.8, 66.7, 66.5, 53.4, 36.6, 36.3, 34.9, 34.9, 34.7, 34.7, 31.7, 31.5, 31.1, 30.5, 25.1, 25.0. HR-ESI-MS *m/z* = 968.6402 $[M+H]^+$ (calc. for $C_{64}H_{82}N_5O_3$ 968.6412).

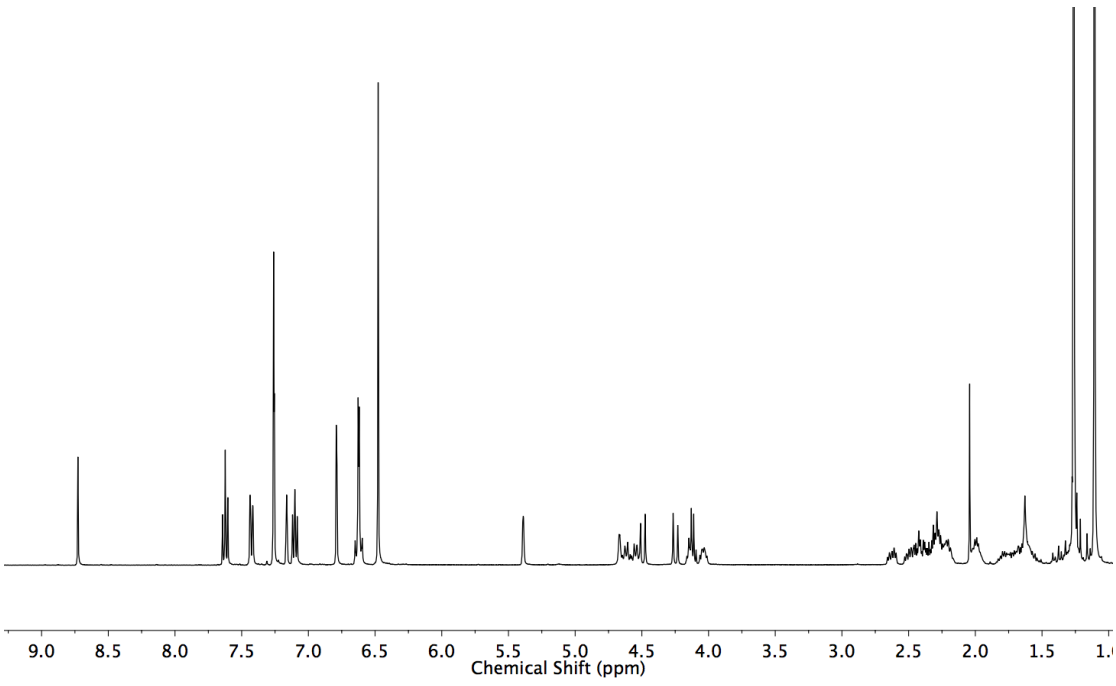

Figure 3.77 ^{1}H NMR ($CDCl_3$, 400 MHz) of **126**.

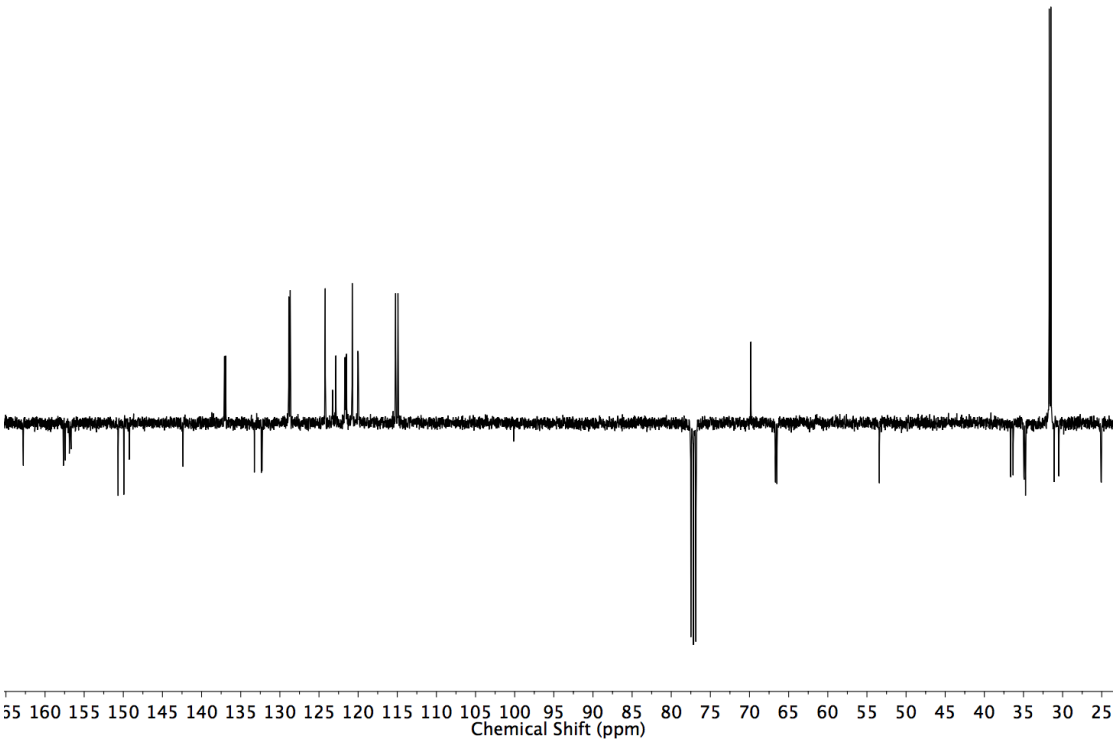

Figure 3.78 JMOD NMR ($CDCl_3$, 101 MHz) of **126**.

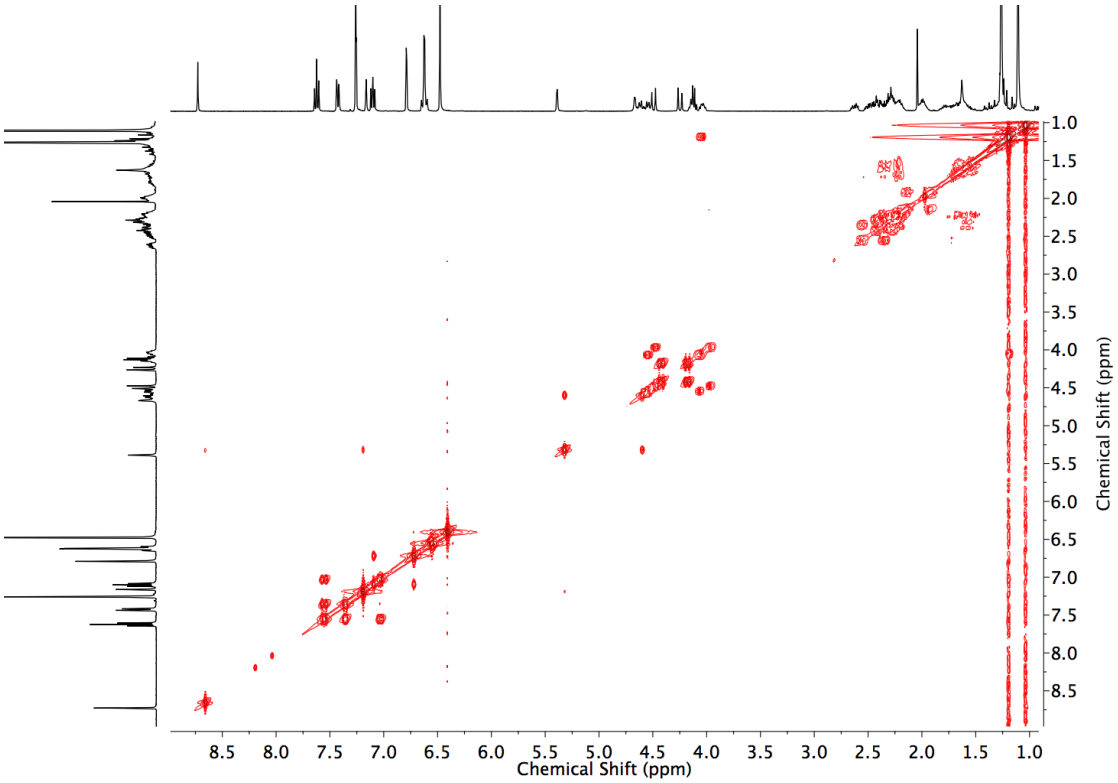

Figure 3.79 COSY NMR ($CDCl_3$) of **126**.

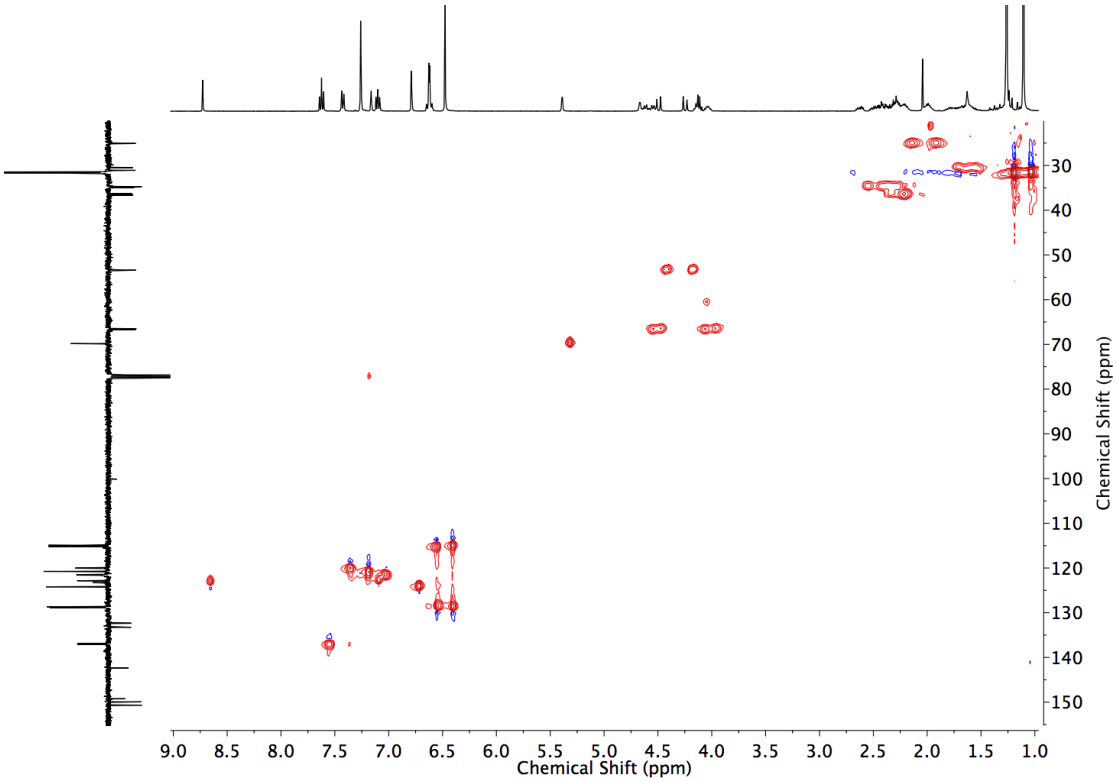

Figure 3.80 HSQC NMR ($CDCl_3$) of **126**.

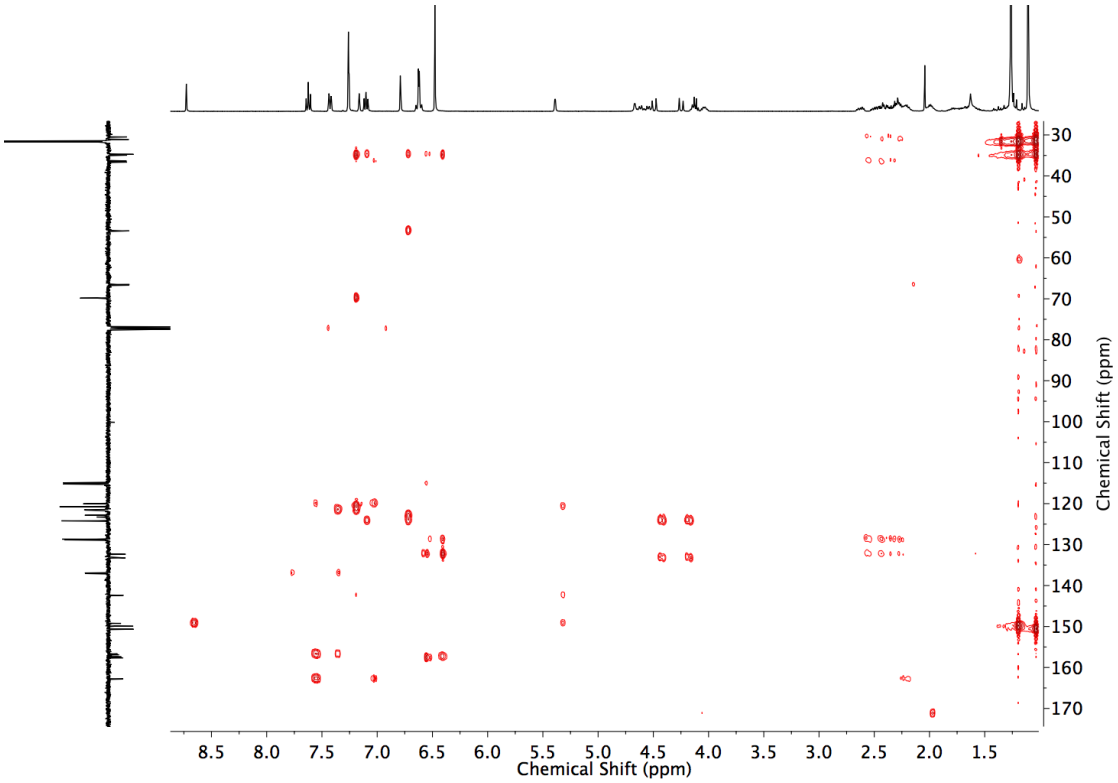

Figure 3.81 HMBC NMR ($CDCl_3$) of **126**.

Rotaxane ***128***

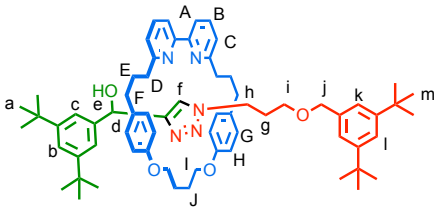

Prepared according to **general procedure B** with **14** (12.0 mg, 0.025 mmol), $[Cu(MeCN)_4]PF_6$ (8.9 mg, 0.024 mmol), **124** (9.1 mg, 0.03 mmol), and **108** (7.3 mg, 0.03 mmol). After purification by column chromatography on silica (petrol with a gradient of 0 to 50% Et_2O) **128** was obtained as a white foam (20.0 mg, 77%). ^{1}H NMR (400 MHz, $CDCl_3$): δ 8.32 (s, 1H, H_f), 7.63 (td, *J* =7.8, 2.6, 2H, H_B), 7.51 (d, *J* =7.7, 2H, H_A), 7.32 (t, *J* =1.9, 1H, H_l), 7.29 (t, *J* =1.9, 1H, H_b), 7.24 (t, *J* =1.9, 2H, H_c), 7.12 (d, *J* =7.7, H_C), 7.03 (d, *J* =1.9, 2H, H_k), 6.68 – 6.57 (m, 8H, H_G, H_H), 5.74 (d, *J* =4.5, 1H, H_d), 4.42 – 4.30 (m, 2H, 2 of H_I), 4.04 (s, 2H, H_j), 4.02 – 3.94 (m, 2H, 2 of H_J), 3.24 (d, *J* =4.7, 1H, H_e), 2.89 (t, *J* =6.7, 2H, H_i), 2.63 – 2.51 (m, 2H, H_g), 2.21 – 2.03 (m, 2H, 2 of H_J), 1.99 – 1.84 (m, 2H, 2 of H_J), 1.77 – 1.64 (m, 4H, H_E), 1.31 (s, 18H, H_a or H_m), 1.23 (s, 18H, H_a or H_m), 1.04 – 0.88 (m, 2H, H_h). ^{13}C NMR (101 MHz, $CDCl_3$) δ 162.8, 162.8, 157.6, 157.6, 157.5 (×2), 150.7, 150.7, 149.8, 142.2, 137.9, 137.0, 136.9, 133.0, 133.0, 129.4 (×2), 123.0, 122.0, 122.0, 121.7, 121.6, 121.6, 120.4, 120.4, 120.4, 115.1, 115.0, 73.0, 70.4, 67.6, 66.5 (×2), 46.7, 37.0 (×2), 36.8 (×2), 34.9, 34.9, 31.8, 31.7, 31.6, 28.8, 24.9, 24.9 (×2). LR-ESI-MS *m/z* = 1026.68 $[M+H]^+$ (calc. for $C_{67}H_{88}N_5O_4$ 1026.68).

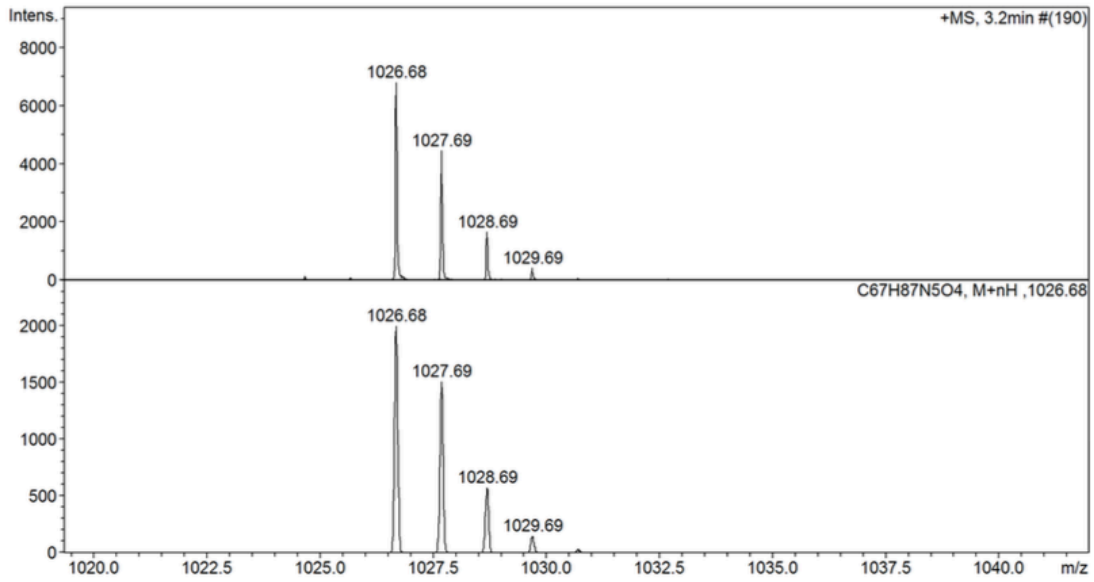

Figure 3.82 Observed (top) and calculated (bottom) isotopic patterns for $[M+H]^+$ of **128**.

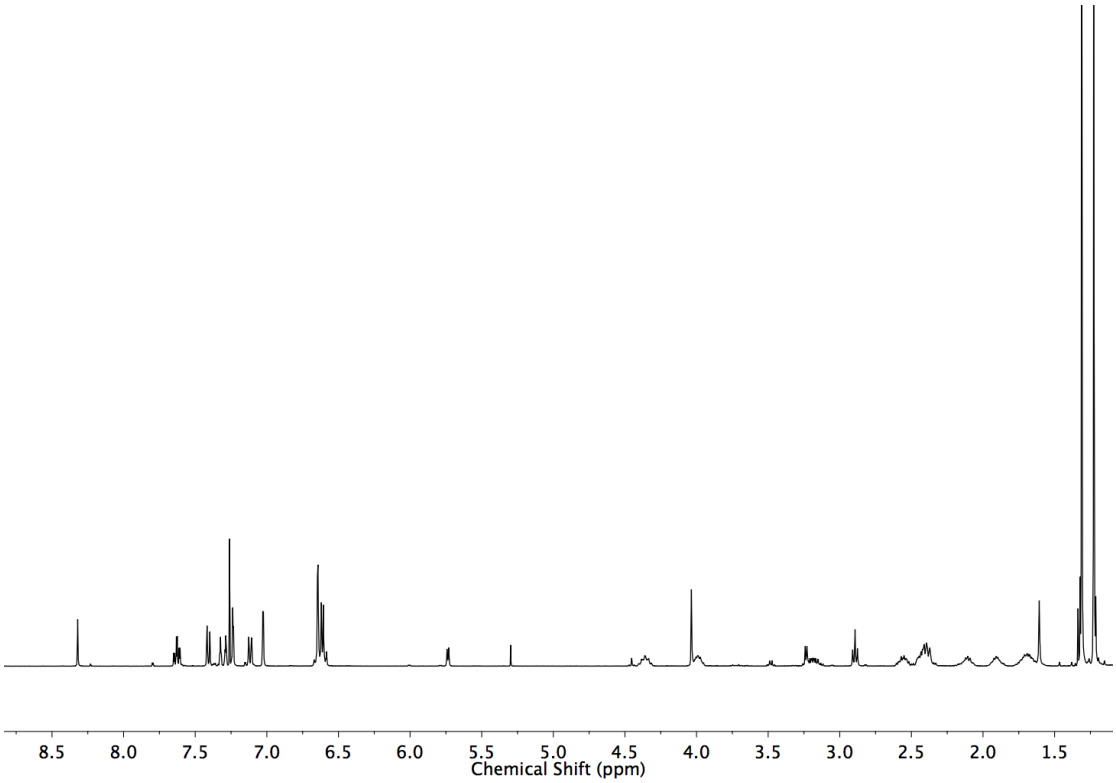

Figure 3.83 ^{1}H NMR ($CDCl_3$, 400 MHz) of **128**.

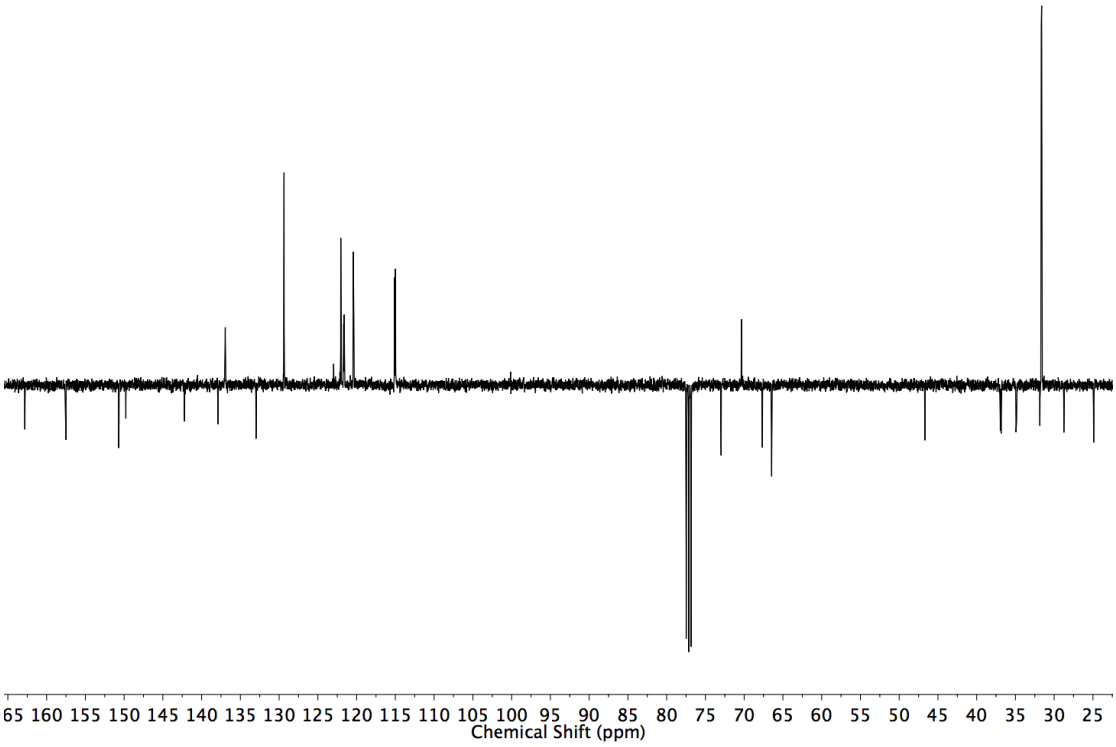

Figure 3.84 JMOD NMR ($CDCl_3$, 101 MHz) of **128**.

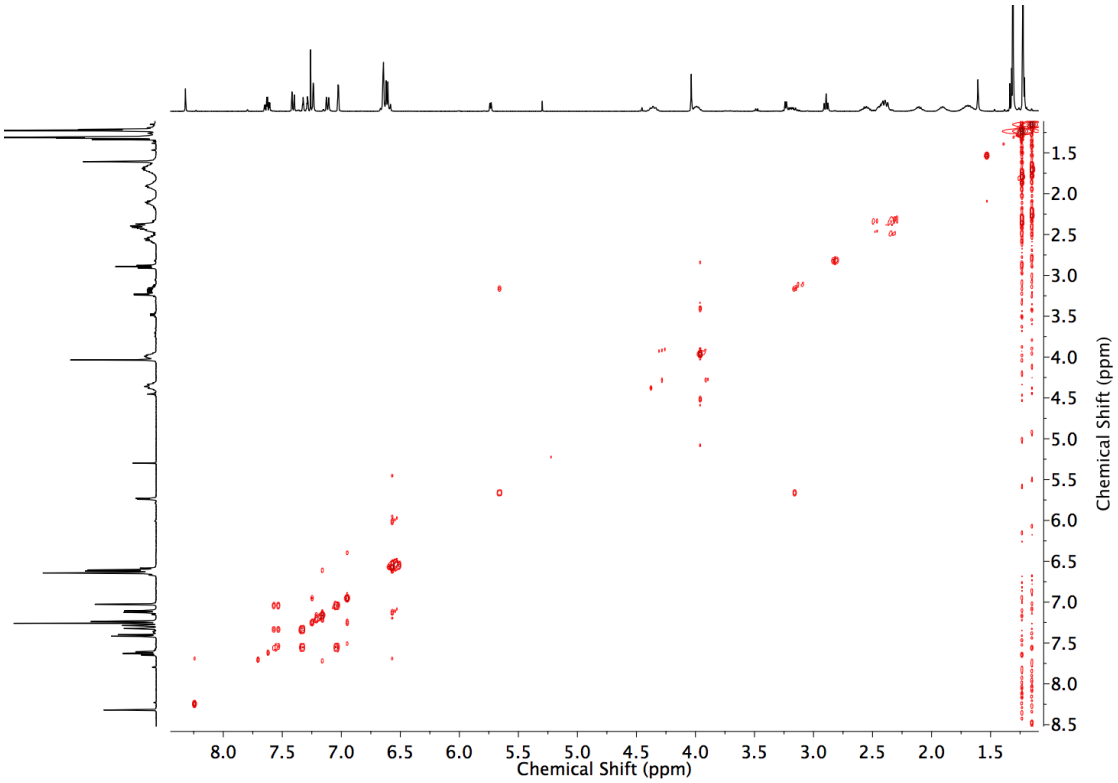

Figure 3.85 COSY NMR ($CDCl_3$) of **128**.

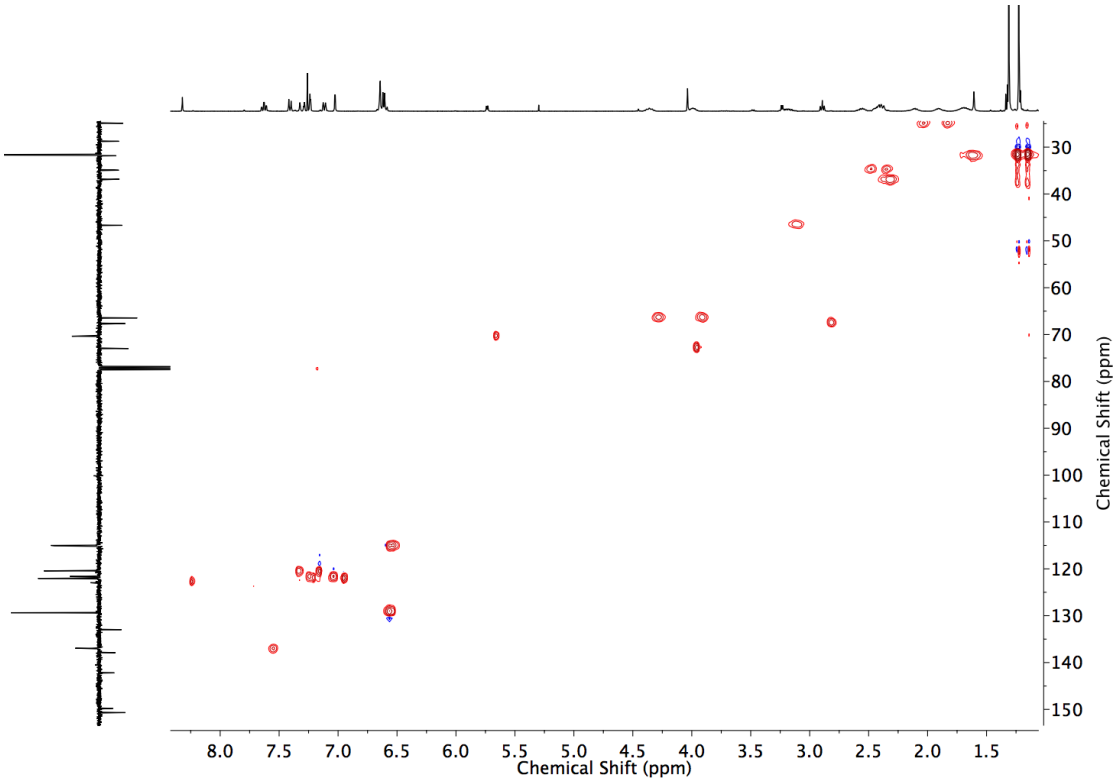

Figure 3.86 HSQC NMR ($CDCl_3$) of **128**.

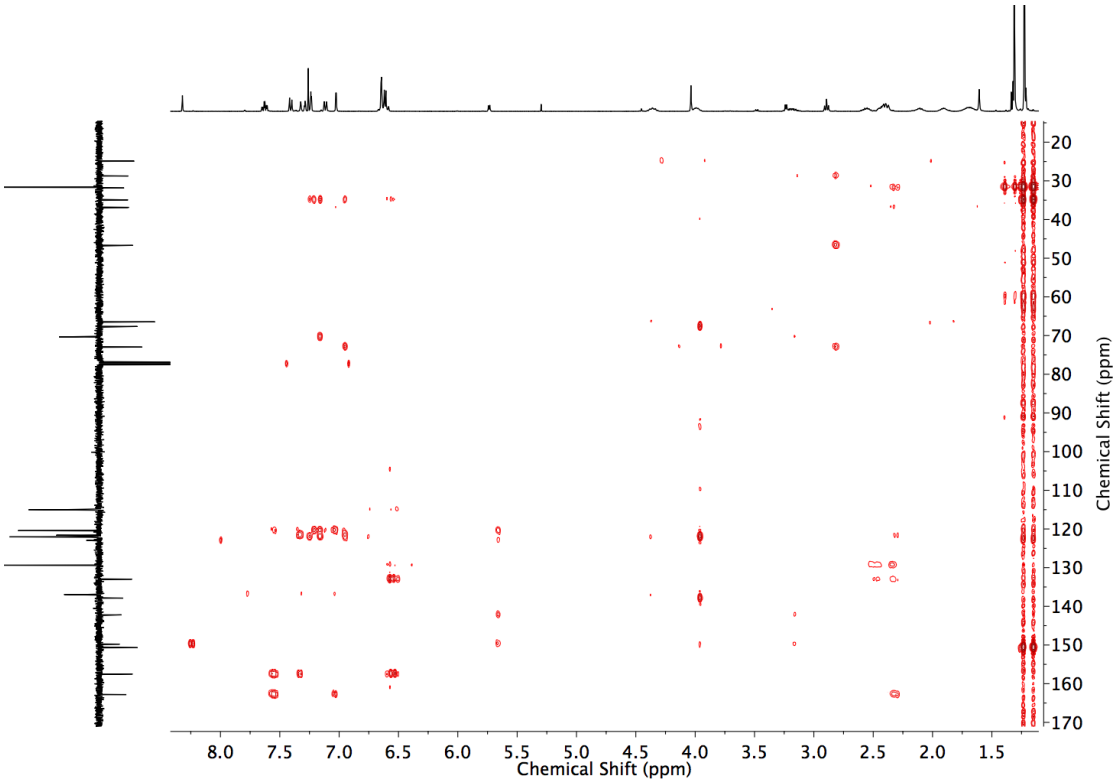

Figure 3.87 HMBC NMR ($CDCl_3$) of **128**.

*Rotaxane **130***

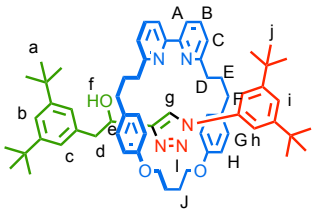

Prepared according to **general procedure B** with **14** (19.1 mg, 0.04 mmol), $[Cu(MeCN)_4]PF_6$ (14.1 mg, 0.038 mmol), **11** (10.4 mg, 0.045 mmol), and **116** (11.6 mg, 0.045 mmol). Chromatography (petrol with a gradient of 0 to 30% Et_2O) gave **130** as a white foam (31.0 mg, 80%). ^{1}H NMR (400 MHz, $CDCl_3$) δ: 10.13 (s, 1H, H_g), 7.66 (t, *J* =7.8, 2H, H_B), 7.51 (d, *J* =1.9, 2H, H_c), 7.44 (td, *J* =8.0, 0.9, 2H, H_A), 7.29 (t, *J* =1.9, 1H, H_i), 7.21 (t, *J* =1.9, 1H, H_b), 7.14 (dt, *J* =8.0, 0.9, 2H, H_C), 6.95 (d, *J* =1.9, 2H, H_c), 6.70 (s, 4H, 2 of H_G, 2 of H_H), 6.58 – 6.48 (m, 4H, 2 of H_G, 2 of H_H), 4.63 – 4.23 (m, 5H, H_I, H_e), 3.78 (s, 1H, H_f), 2.70 – 2.63 (m, 1H, 1 of H_d), 2.63 – 2.26 (m, 8H, H_D, H_F), 2.26 – 2.10 (m, 4H, H_J), 1.98 (dd, *J* =14.6, 11.2, 1H, 1 of H_d), 1.90 – 1.64 (m, 4H, H_E), 1.32 (s,18H, H_a), 1.21 (s, 18H, H_j). ^{13}C NMR (101 MHz, $CDCl_3$) δ 163.4, 163.4, 157.7, 157.7, 157.1, 157.1, 151.9, 149.8 (×2), 138.7 (×2), 137.4, 137.2, 137.1, 132.1, 128.8, 128.7, 123.7, 122.7, 122.0, 122.0, 121.0, 120.1, 120.0, 119.9, 115.4, 114.8, 114.4, 66.6, 66.6, 66.5, 43.6, 36.8 (×2), 35.4, 35.4, 35.2, 34.9, 32.0, 31.8, 31.4, 31.3, 25.1, 24.9. HR-ESI-MS *m/z* = 968.6392 $[M+H]^+$ (calc. for $C_{64}H_{82}N_5O_3$ 968.6412).

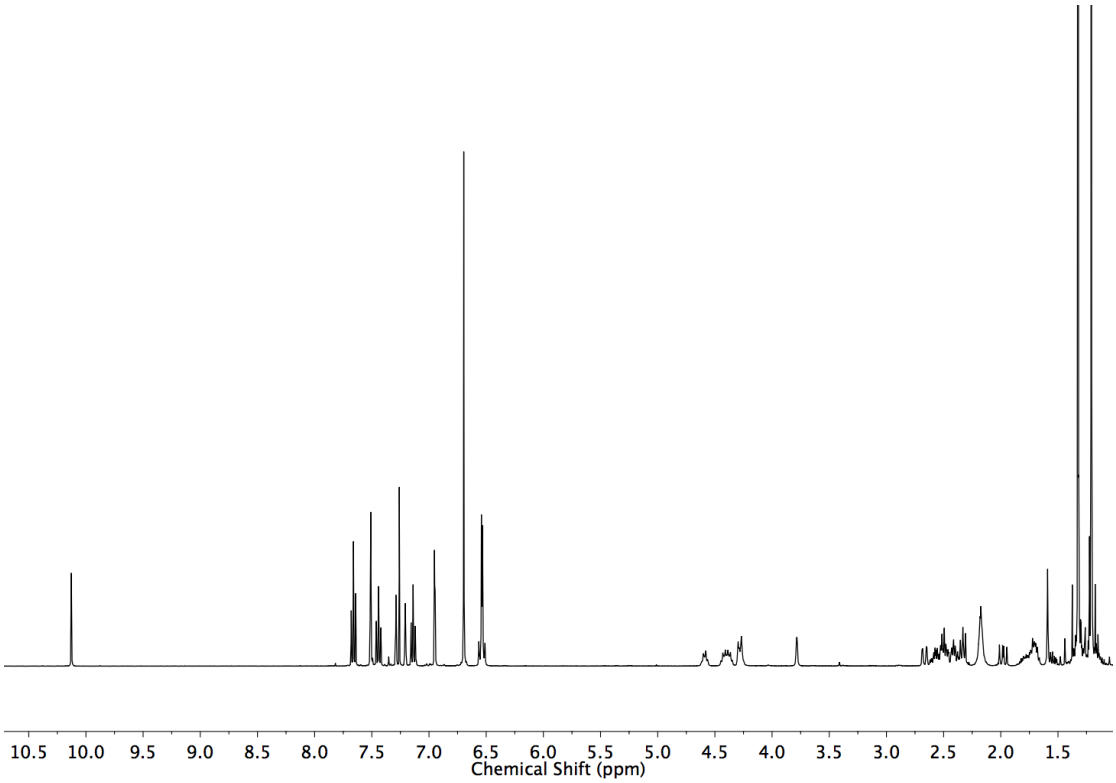

Figure 3.88 ^{1}H NMR ($CDCl_3$, 400 MHz) of **130**.

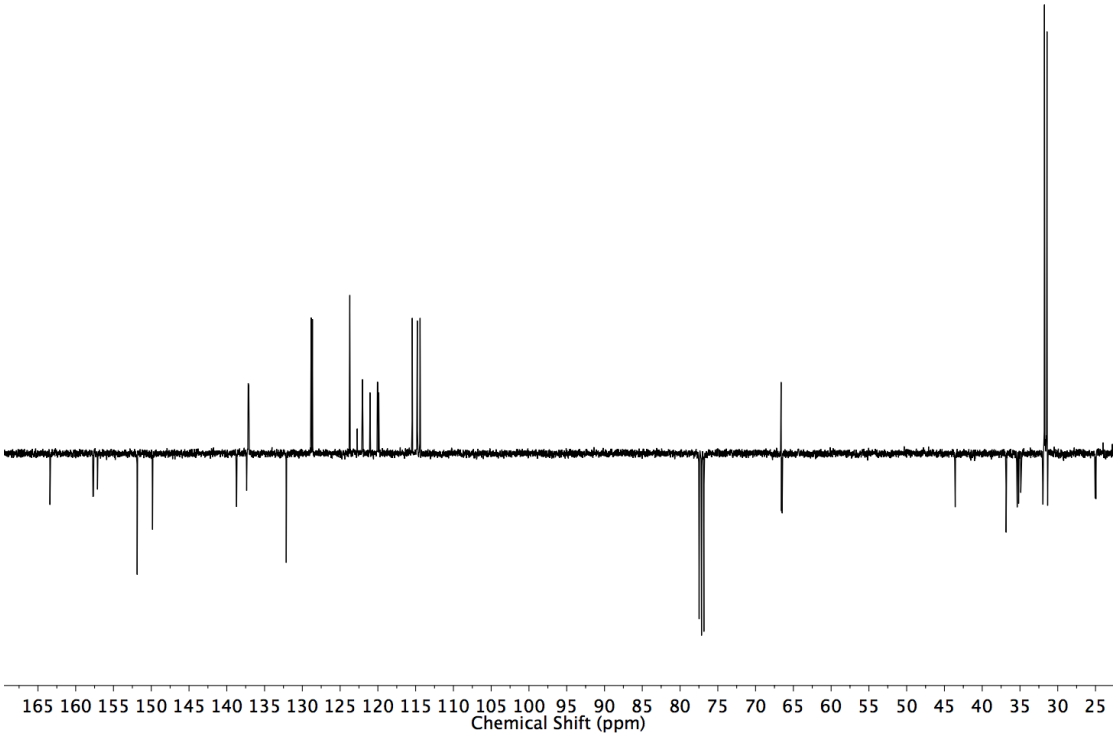

Figure 3.89 JMOD NMR ($CDCl_3$, 101 MHz) of **130**.

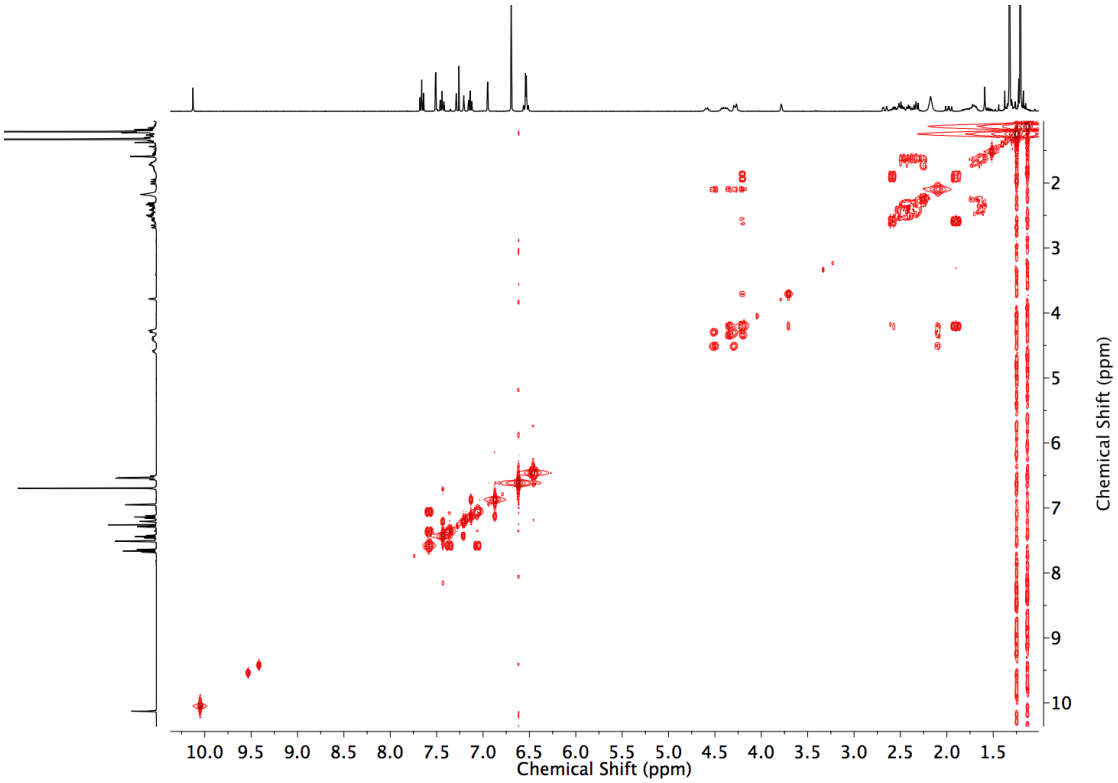

Figure 3.90 COSY NMR ($CDCl_3$) of **130**.

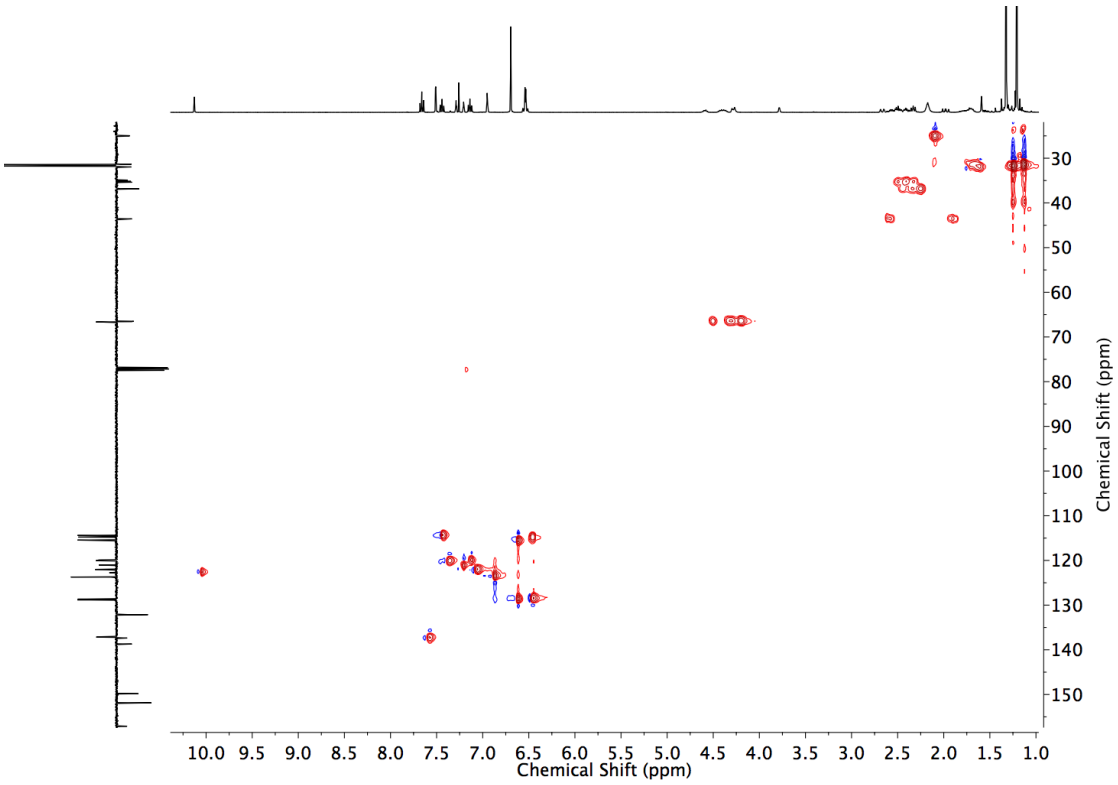

Figure 3.91 HSQC NMR ($CDCl_3$) of **130**.

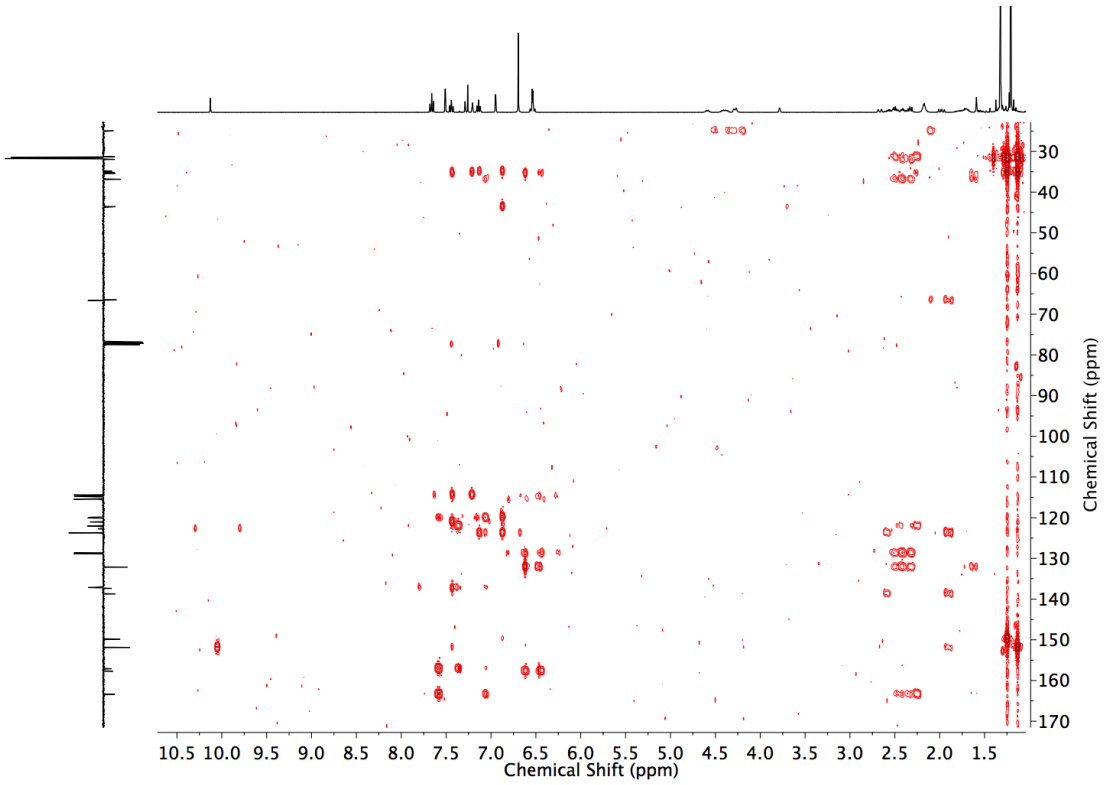

Figure 3.92 HMBC NMR ($CDCl_3$) of **130**.

Axle ***132***

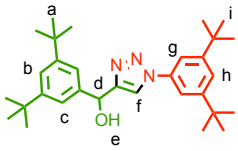

11 (24.4 mg, 0.1 mmol), **108** (23.1 mg, 0.1 mmol), $CuSO_4.5H_2O$ (12.5 mg, 0.05 mmol), and sodium ascorbate (19.8 mg, 0.1 mmol) were placed in a round bottom flask. DMF (2mL) was added and the mixture was stirred for 16 h. The crude reaction mixture was diluted with Et_2O (10 mL), washed with H_2O (2 × 10 mL), brine (5 mL), dried ($MgSO_4$), filtered and the solvent removed *in vacuo*. Chromatography (petrol with 0 to 50% Et_2O) gave **132** as a white foam (37.0 mg, 78%). ^{1}H NMR (400 MHz, $CDCl_3$): δ 7.74 (s, 1H, H_e), 7.48 (t, *J* =1.7, 1H, H_h), 7.47 (d, *J* =1.7, 2H, H_g) 7.40 (t, *J* =1.7, 1H, H_b), 7.38 (d, *J* =1.7, 2H, H_c), 6.11 (d, *J* =3.7, 1H, H_d), 2.85 (d, *J* =3.7, 1H, H_e), 1.35 (s, 18H, H_i), 1.33 (s, 18H, H_a). ^{13}C NMR (101 MHz, $CDCl_3$): δ 152.9, 151.9, 151.3, 141.2, 136.9, 123.1, 122.4, 121.0, 120.0, 115.7, 70.3, 35.3, 35.1, 31.6, 31.6. HR-ESI-MS *m/z* = 476.3624 $[M+H]^+$ (calc. for $C_{31}H_{46}N_3O$ 476.3635).

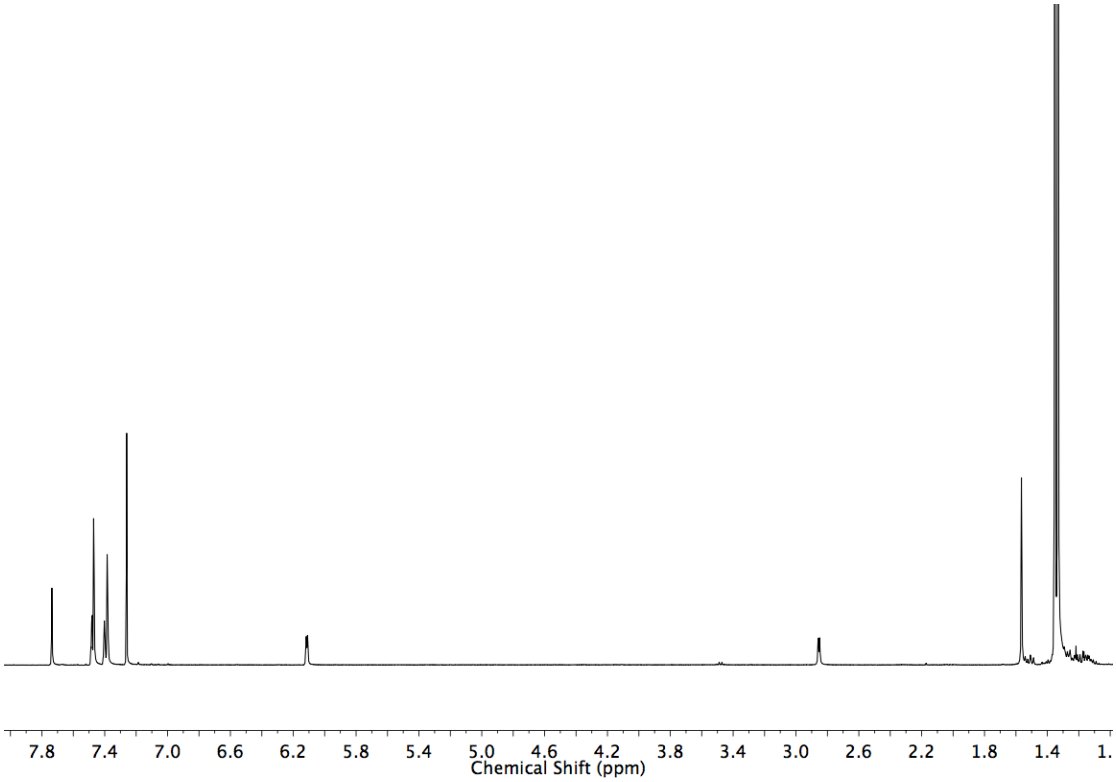

Figure 3.93 ^{1}H NMR ($CDCl_3$, 400 MHz) of **132**.

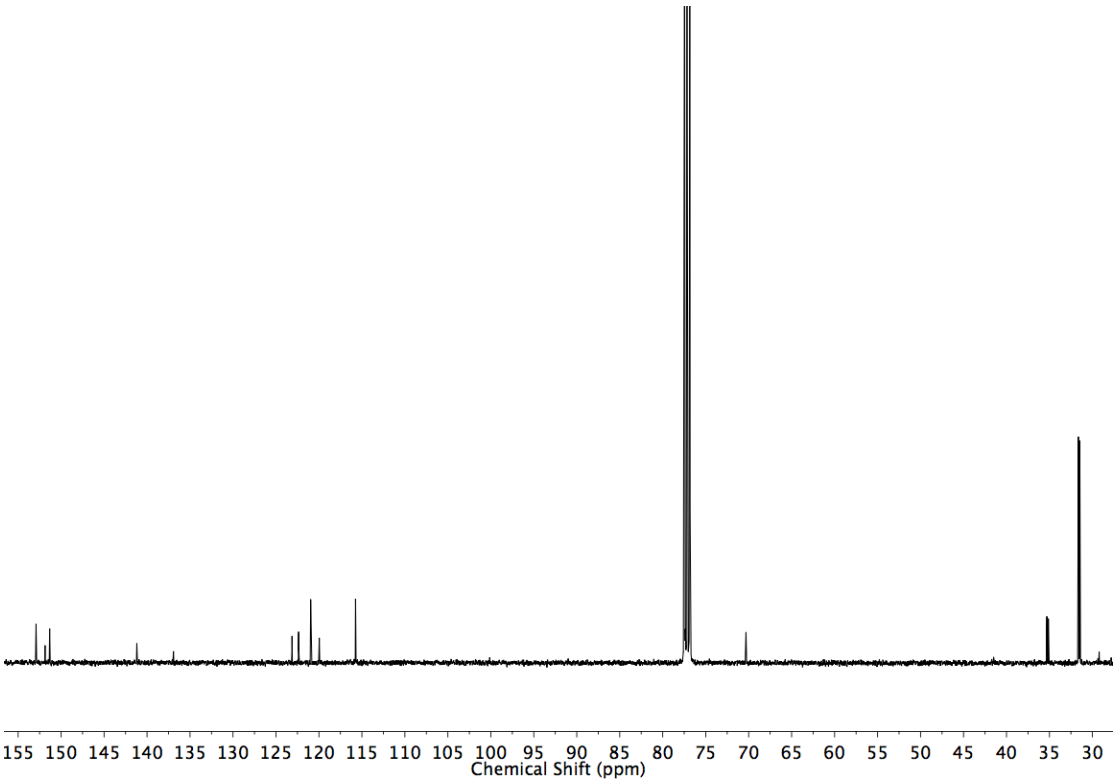

Figure 3.94 ^{13}C NMR ($CDCl_3$, 101 MHz) of **132**.

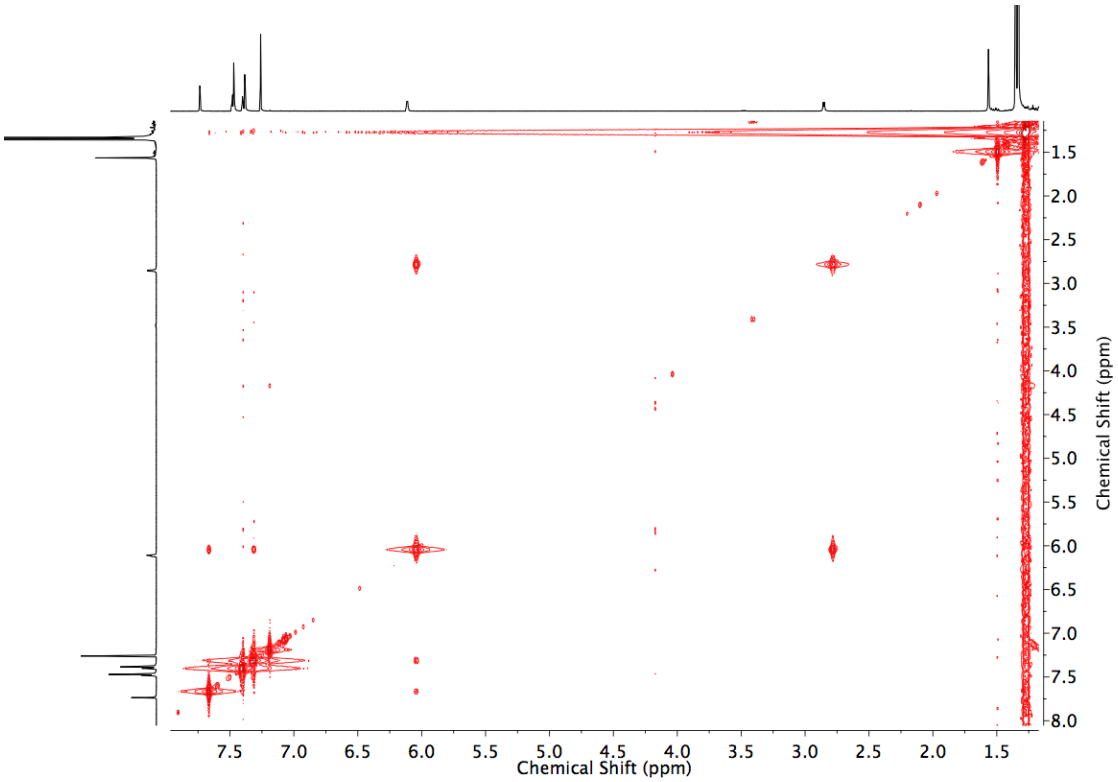

Figure 3.95 COSY NMR ($CDCl_3$) of **132**.

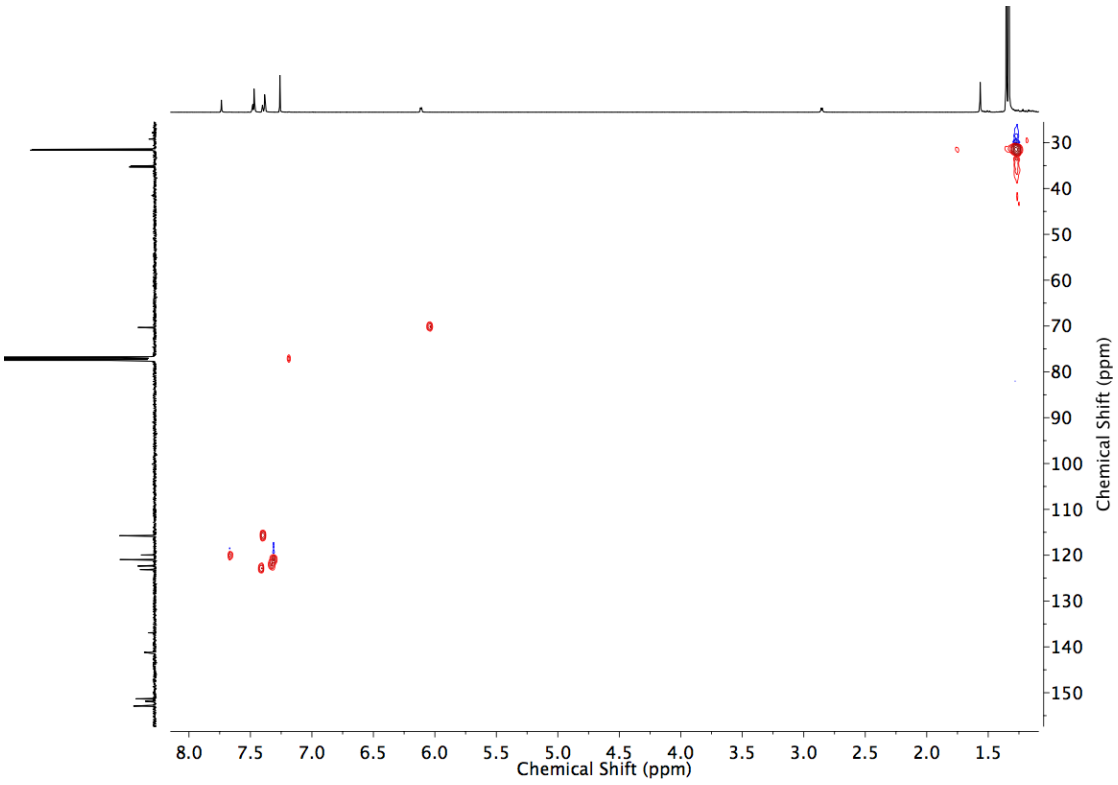

Figure 3.96 HSQC NMR ($CDCl_3$) of **132**.

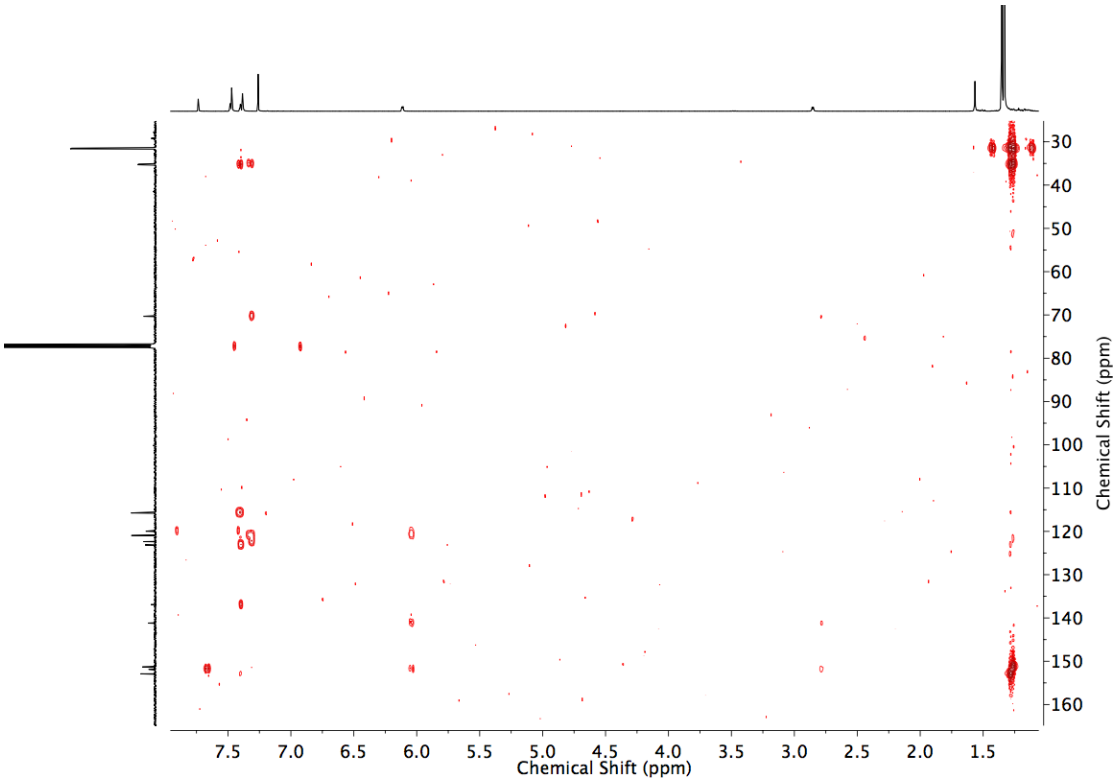

Figure 3.97 HMBC NMR ($CDCl_3$) of **132**.

*Rotaxane **134***

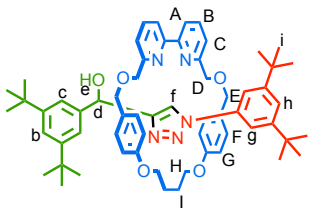

Prepared according to **general procedure B** with **11** (48.3 mg, 0.1 mmol), $[Cu(MeCN)_4]PF_6$ (35.8 mg, 0.096 mmol), **11** (29.3 mg, 0.12 mmol), and **108** (27.8 mg, 0.12 mmol). Chromatography (petrol with a gradient of 0 to 50% Et_2O) gave **134** as a white foam (90.0 mg, 97%). ^{1}H NMR (400 MHz, $CDCl_3$): δ 9.65 (s, 1H, H_f), 7.75 – 7.68 (m, 2H, H_B), 7.62 (dd, *J* =7.8, 1.0, 1H, 1 of H_A), 7.58 (dd, *J* =7.8, 1.0, 1H, 1 of H_A), 7.42 (dd, *J* =7.8, 1.0, 2H, H_C), 7.40 (d, *J* =1.9, 2.H, H_c), 7.28 (t, *J* =1.9, 1H, H_b), 7.14 (d, *J* =1.9, 2H, H_g), 7.10 (t, *J* =1.9, 1H, H_h), 6.70 (d, *J* =8.5, 2H, 2 of H_F), 6.54 (*J* =8.5, 2H, 2 of H_G), 6.23 (d, *J* =8.5, 2H, 2 of H_F), 5.97 (d, *J* =8.5, 2H, 2 of H_G), 5.62 (s, 1H, H_d), 4.68 (q, *J* =7.8, 1H, 1 of H_H), 4.57 (d, *J* =12.2, 1H, 1 of H_E), 4.48 (q, *J* =7.8, 1H, 1 of H_H), 4.36 (d, *J* =12.2, 1H, 1 of H_E), 4.21 (d, *J* =12.2, 1H, 1 of H_E), 4.16 (q, *J* =7.8, 1H, 1 of H_I), 4.02 (t, *J* =12.2, 2H, 1 of H_D, 1 of H_E), 3.95 (q, *J* =12.2, 2H, 2 of H_D), 3.83 (q, *J* =7.8, 1H, 1 of H_I), 3.77 (d, *J* =12.2, 1H, H_D), 2.40 – 2.33 (m, 2H, 2 of H_I), 2.00 – 1.83 (m, 2H, 2 of H_I), 1.27 (s, 18H, H_a or H_h), 1.09 (s, 18H, H_a or H_h). ^{13}C NMR (101 MHz, $CDCl_3$): δ 159.6, 159.6, 159.3, 158.6, 155.2, 155.1, 151.2, 147.9, 149.7, 142.3, 137.6, 137.4, 136.8, 129.4, 128.9, 127.9, 127.2, 121.8, 121.5, 120.9, 120.7, 120.4, 120.2, 120.2, 120.1, 115.3, 114.2, 114.0, 73.0, 72.9, 70.5, 70.0, 69.8, 66.7, 66.0, 34.9, 34.9, 31.6, 31.3, 24.8, 24.7. HR-ESI-MS *m/z* = 958.5843 $[M+H]^+$ (calc. for $C_{61}H_{76}H_5N_5$ 958.5841).

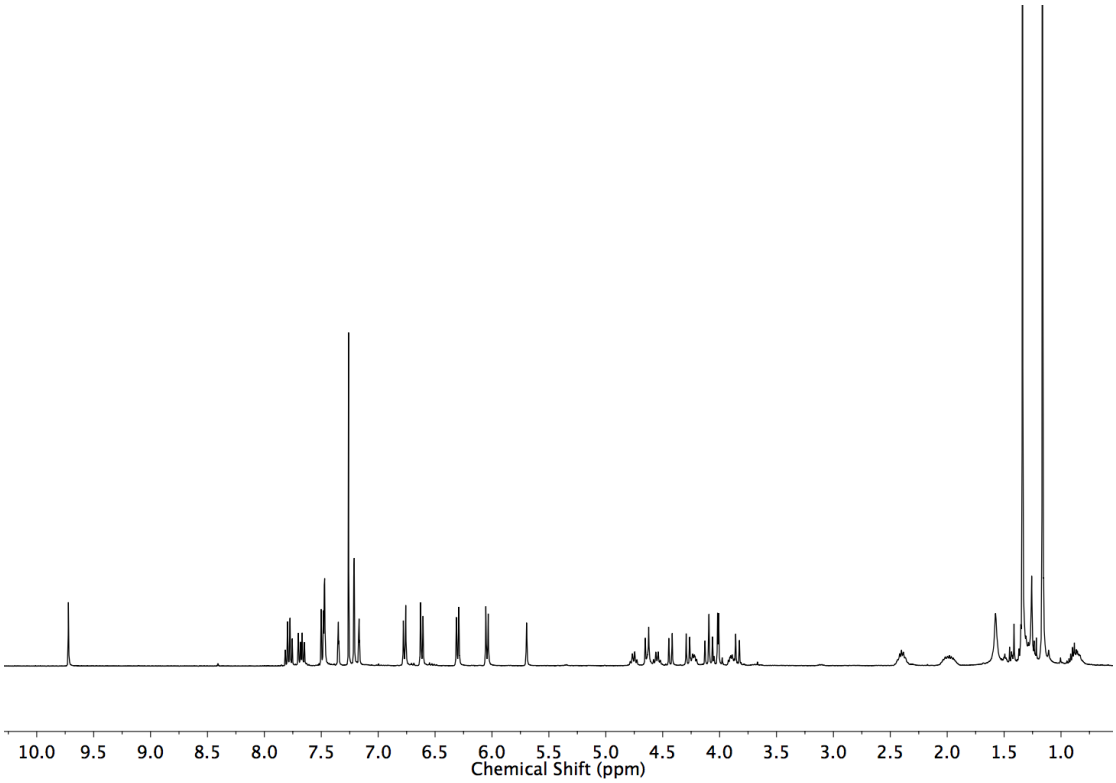

Figure 3.98 ^{1}H NMR ($CDCl_3$, 400 MHz) of **134**.

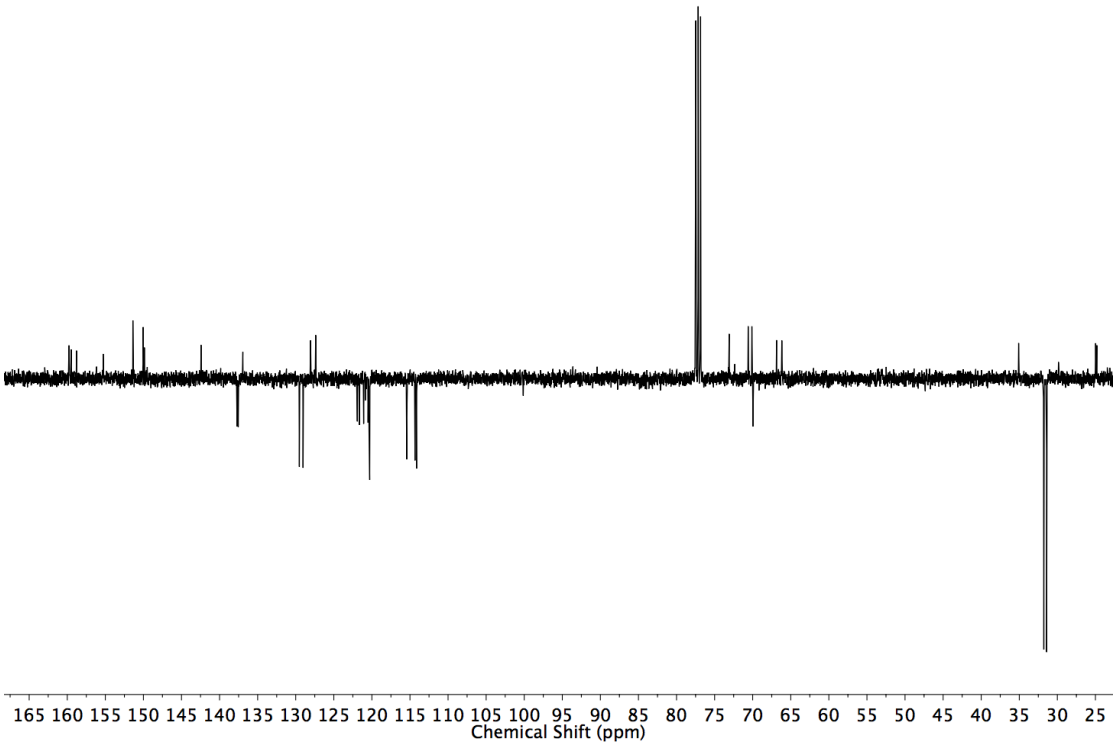

Figure 3.99 JMOD NMR ($CDCl_3$, 101 MHz) of **134**.

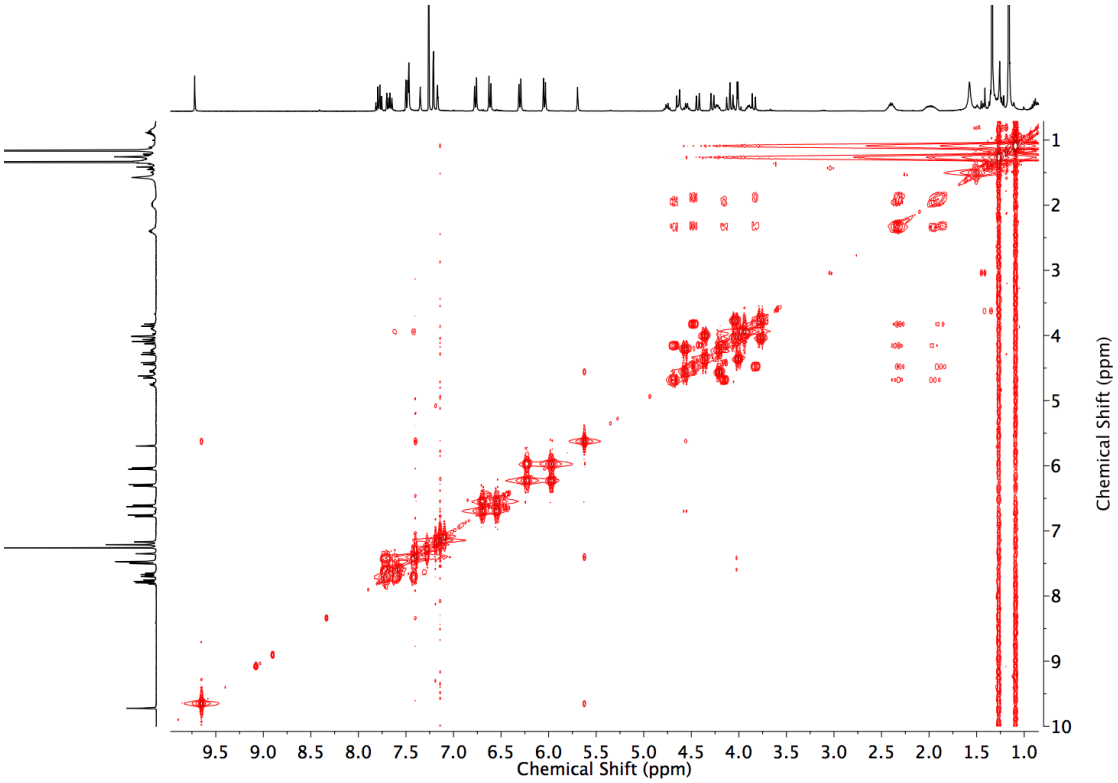

Figure 3.100 COSY NMR ($CDCl_3$) of **134**.

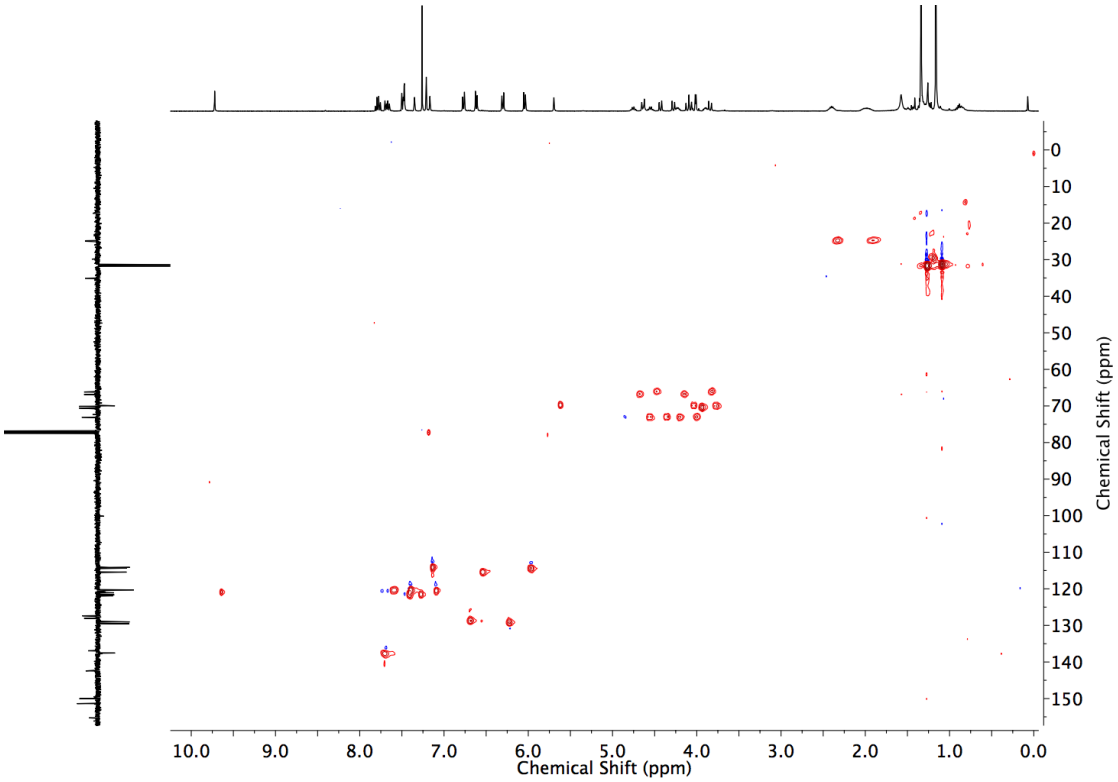

Figure 3.101 HSQC NMR ($CDCl_3$) of **134**.

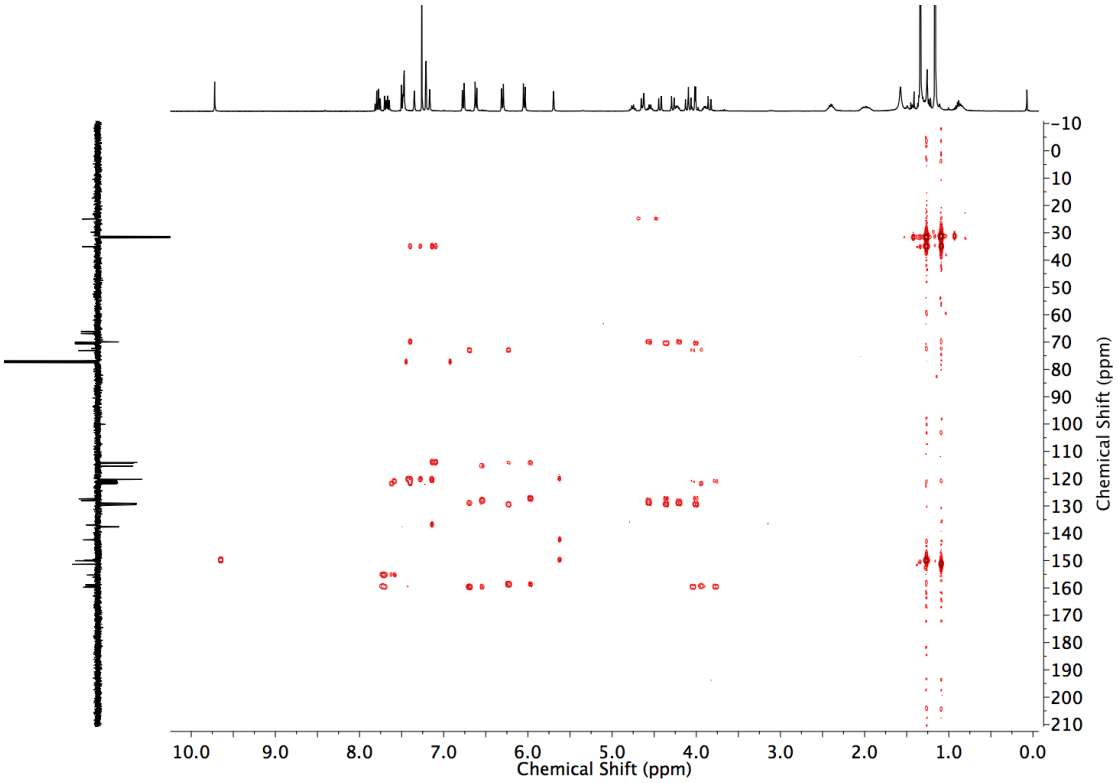

Figure 3.102 HMBC NMR ($CDCl_3$) of **134**.

Rotaxane ***136***

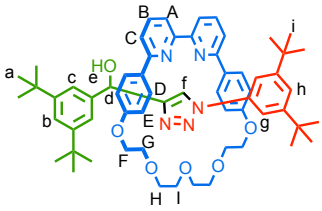

Prepared according to **general procedure B** with **133** (12.0 mg, 0.025 mmol), $[Cu(MeCN)_4]PF_6$ (8.9 mg, 0.024 mmol), **11** (6.9 mg, 0.03 mmol), and **108** (7.3 mg, 0.03 mmol). Chromatography (petrol with a gradient of 0 to 50% Et_2O) gave **136** as a white foam (9.0 mg, 37%). ^{1}H NMR (500 MHz, $CDCl_3$) δ: 9.91 (s, 1H, H_f), 7.93 (t, J = 7.8, 1H, 1 of H_B), 7.84 (t, J = 7.8, 1H, 1 of H_B), 7.79 (dd, J = 7.8, 0.9, 1H, 1 of H_A), 7.77 (dd, J = 7.8, 0.9, 1H, 1 of H_A), 7.64 (dd, J = 7.8, 0.9, 1H 1 of H_C), 7.46 (dd, J = 7.8, 0.9, 1H, 1 of H_C), 7.41 (d, J = 1.8, 2H, H_g), 7.29 (d, J = 8.7, 2H, 2 of H_E), 7.21 (t, J =1.8, 1H, H_h), 7.15 (t, J = 1.8, 1H, H_b), 7.11 (d, J = 1.8, 2H, H_c), 6.86 (d, J = 8.7, 2H, 2 of H_E), 6.35 (d, J = 8.7, 2H, 2 of H_D), 6.07 (d, J = 8.7, 2H, 2 of H_D), 5.00 (d, J = 2.3, 1H, H_d), 4.07 – 3.51 (m, 16H, H_F, H_G, H_H, H_I), 2.99 (d, J = 2.3, 1H, H_e), 1.12 (s, 18H, H_i), 1.09 (s, 18H, H_a). ^{13}C NMR (126 MHz, $CDCl_3$) δ 160.07, 159.47, 159.12, 158.45, 157.67, 157.40, 151.48, 150.44, 149.46, 142.21, 137.60, 137.53, 136.71, 132.80, 132.08, 129.54, 129.13, 125.67, 123.99, 121.90, 121.64, 120.64, 120.35, 120.15, 119.93, 119.62, 114.67, 114.33, 114.15, 70.14, 70.01, 69.91, 69.79, 69.64, 68.85, 68.22, 67.17, 66.09, 34.98, 34.79, 31.47, 31.33. HR-ESI-MS *m/z* = 974.5783 $[M+H]^+$ (calc. for $C_{61}H_{76}N_5O_6$ 974.5790).

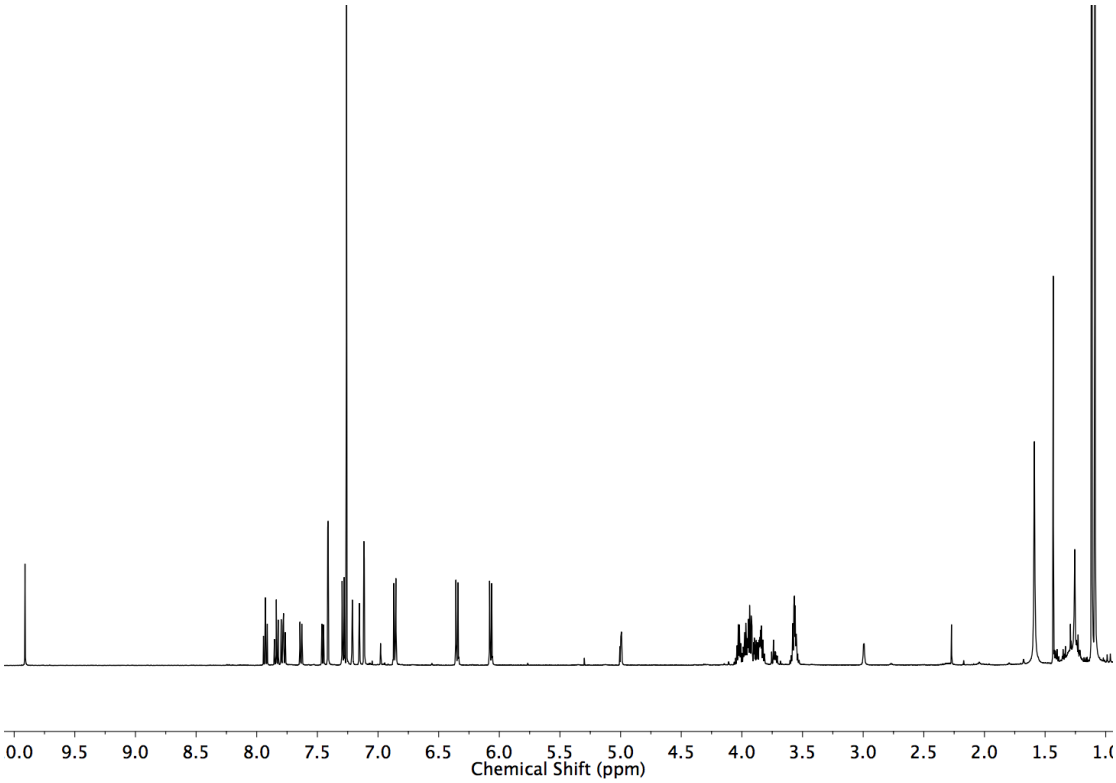

Figure 3.103 ^{1}H NMR ($CDCl_3$, 500 MHz) of **136**.

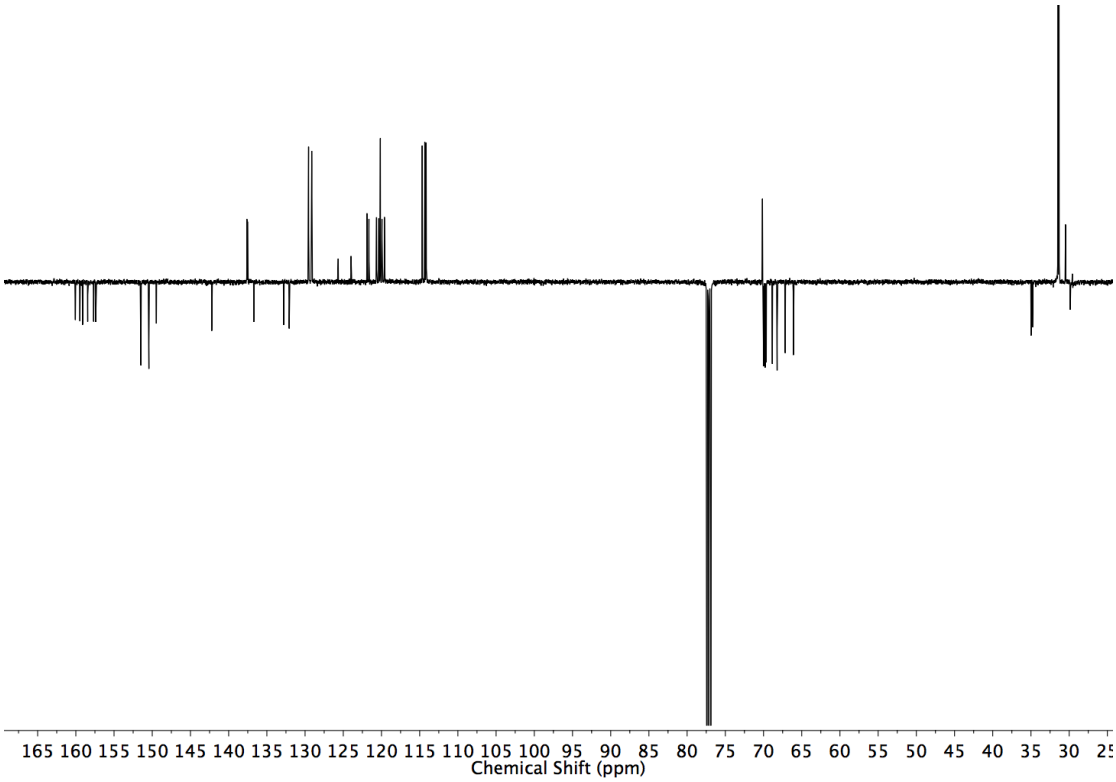

Figure 3.104 JMOD NMR ($CDCl_3$, 126 MHz) of **136**.

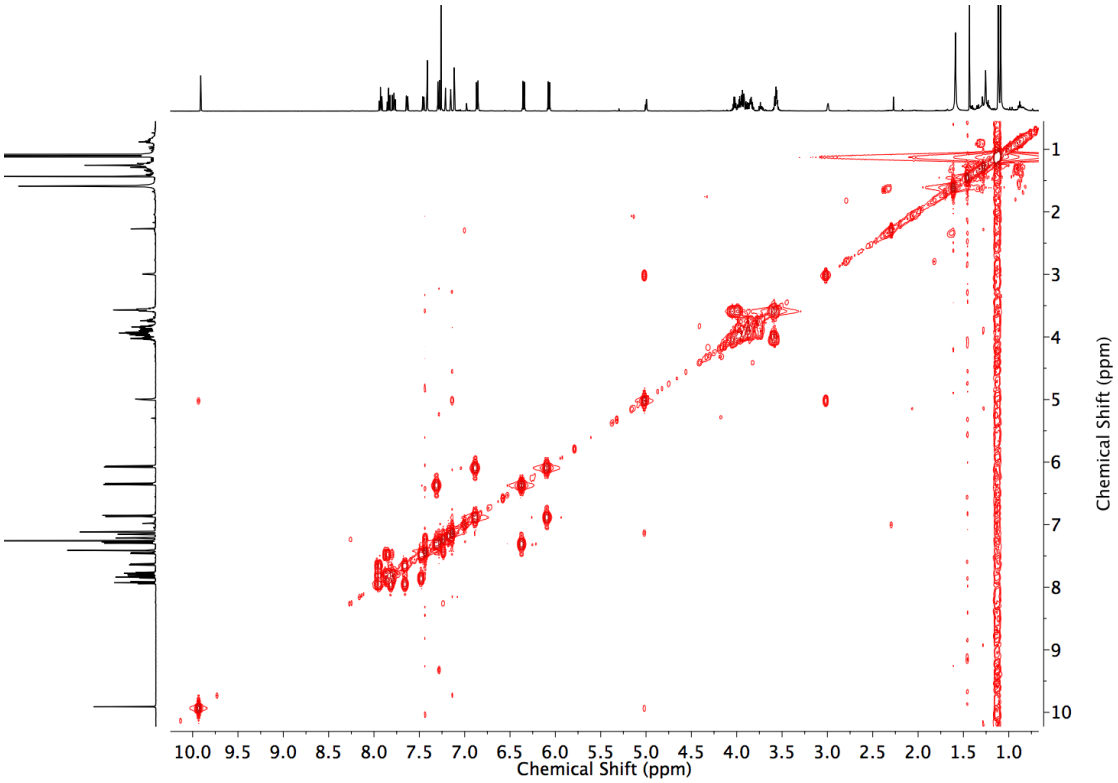

Figure 3.105 COSY NMR ($CDCl_3$) of **136**.

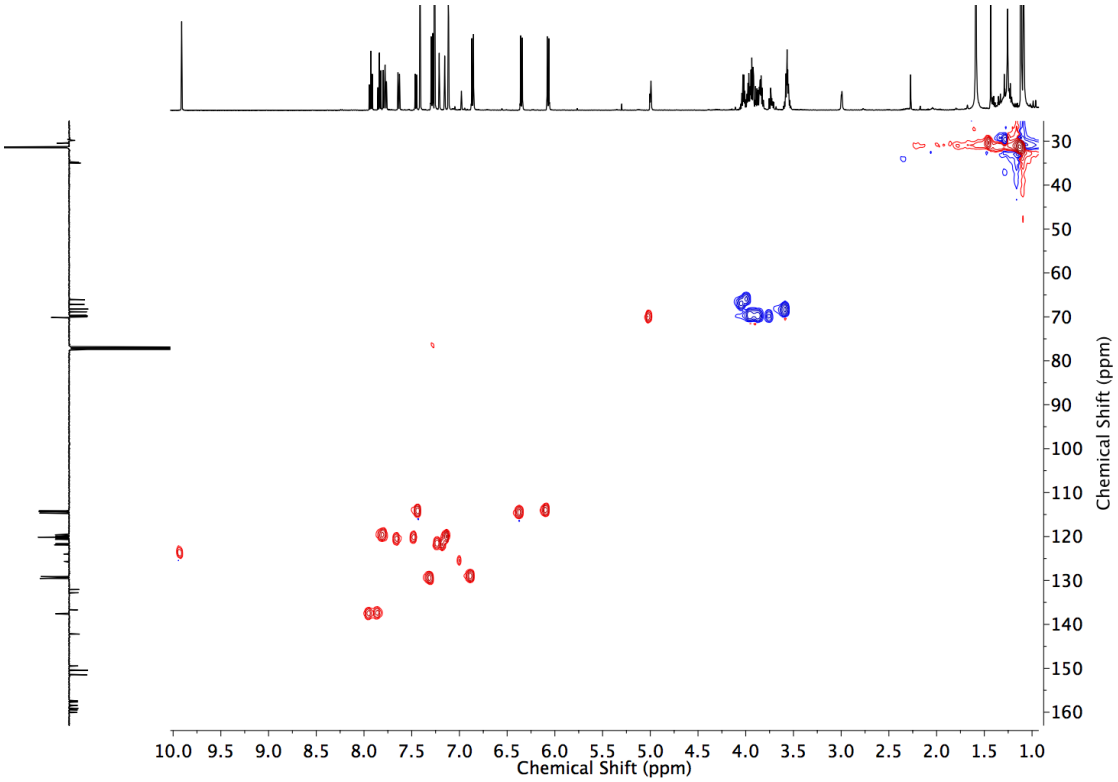

Figure 3.106 HSQC NMR ($CDCl_3$) of **136**.

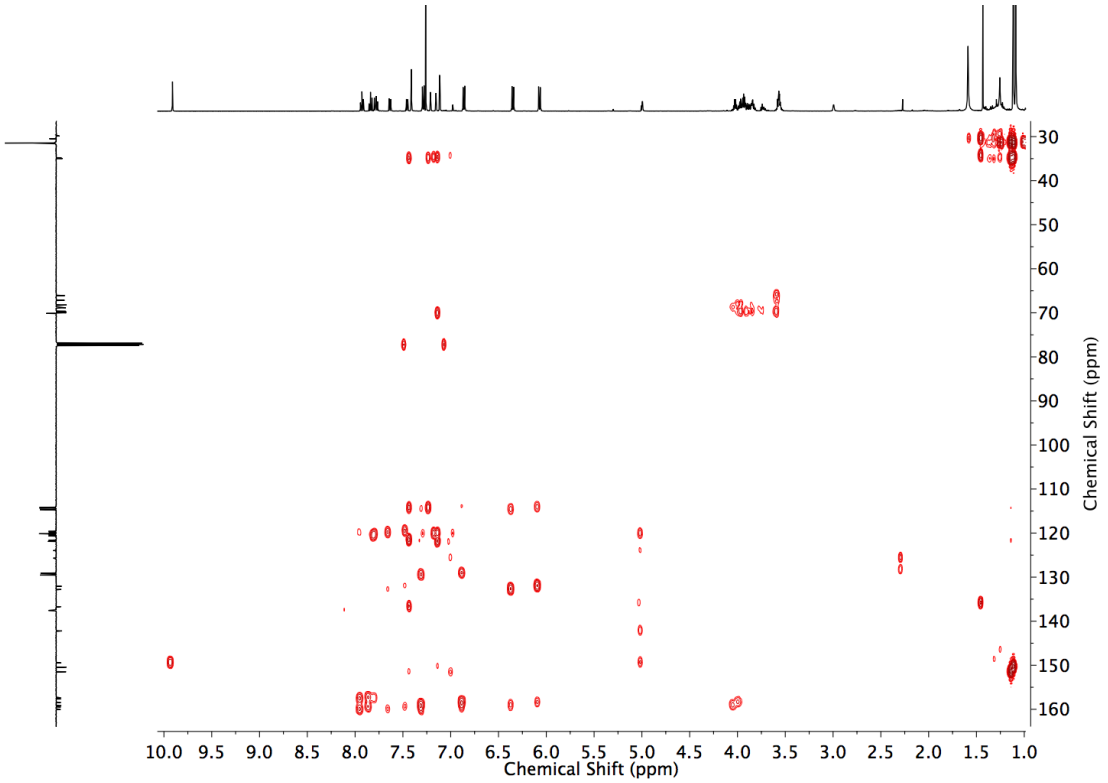

Figure 3.107 HMBC NMR ($CDCl_3$) of **136**.

Rotaxane ***138***

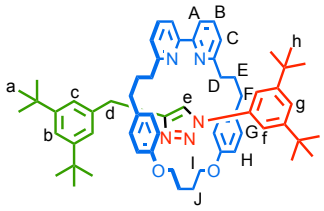

Prepared according to **general procedure B** with **14** (12.0 mg, 0.025 mmol), $[Cu(MeCN)_4]PF_6$ (8.9 mg, 0.024 mmol), **11** (7.0 mg, 0.03 mmol), and **118** (7.0 mg, 0.03 mmol). Chromatography (petrol with a gradient of 0 to 40% Et_2O) gave **138** as a white foam (17.0 mg, 72%). ^{1}H NMR (400 MHz, $CDCl_3$) δ: 10.09 (s, 1H, H_e), 7.69 (t, *J* =7.7, 2H, H_B), 7.51 (dd, *J* =7.8, 0.9, 2H, H_A), 7.45 (d, *J* =1.7, 2H, H_f), 7.18 (t, *J* =1.7, 1H, H_g), 7.16 (t, *J* =1.7, 1H, H_b), 7.09 (dd, *J* =7.8, 0.9, 2H, H_C), 6.95 (d, *J* =1.8, 2H, H_c), 6.40 (d, *J* =8.5, 4H, H_H), 6.16 (d, *J* =8.5, 54H, H_G), 4.72 (q, *J* =7.8, 2H, H_I), 4.26-4.09 (m, 2H, H_I), 3.45 (s, 2H, H_d), 2.45 – 1.98 (m, 12H, H_D, H_F, H_I), 1.57 – 1.29 (m, 4H, H_E), 1.16 (s, 18H, H_h), 1.12 (s, 18H, H_a). ^{13}C NMR (101 MHz, $CDCl_3$) δ: 163.5, 157.6, 157.3, 150.7, 150.5, 145.3, 139.6, 137.3, 136.9, 131.8, 128.2, 123.8, 123.1, 122.0, 120.8, 120.6, 119.7, 115.4, 115.1, 68.8, 37.0, 35.2, 35.1, 34.7, 33.2, 32.2, 31.5, 31.5, 25.0. HR-ESI-MS *m/z* = 938.6307 $[M+H]^+$ (calc. for $C_{63}H_{80}N_5O_2$ 938.6307).

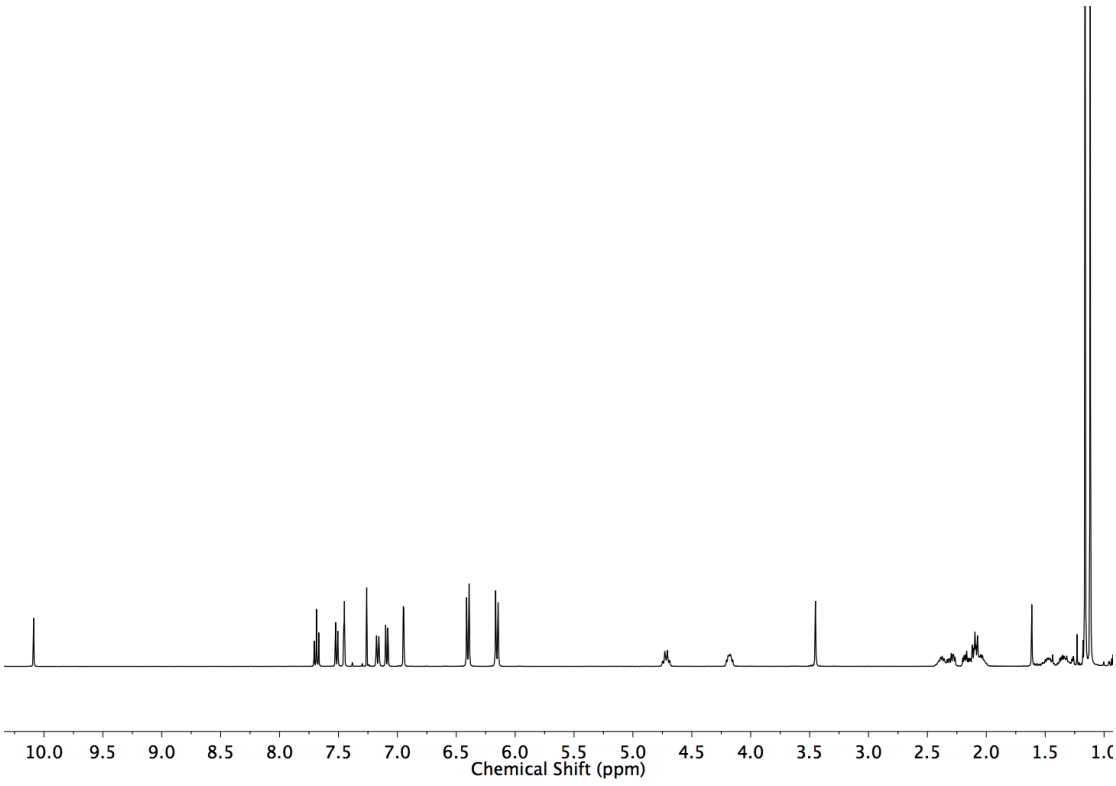

Figure 3.108 ^{1}H NMR ($CDCl_3$, 400 MHz) of **138.**

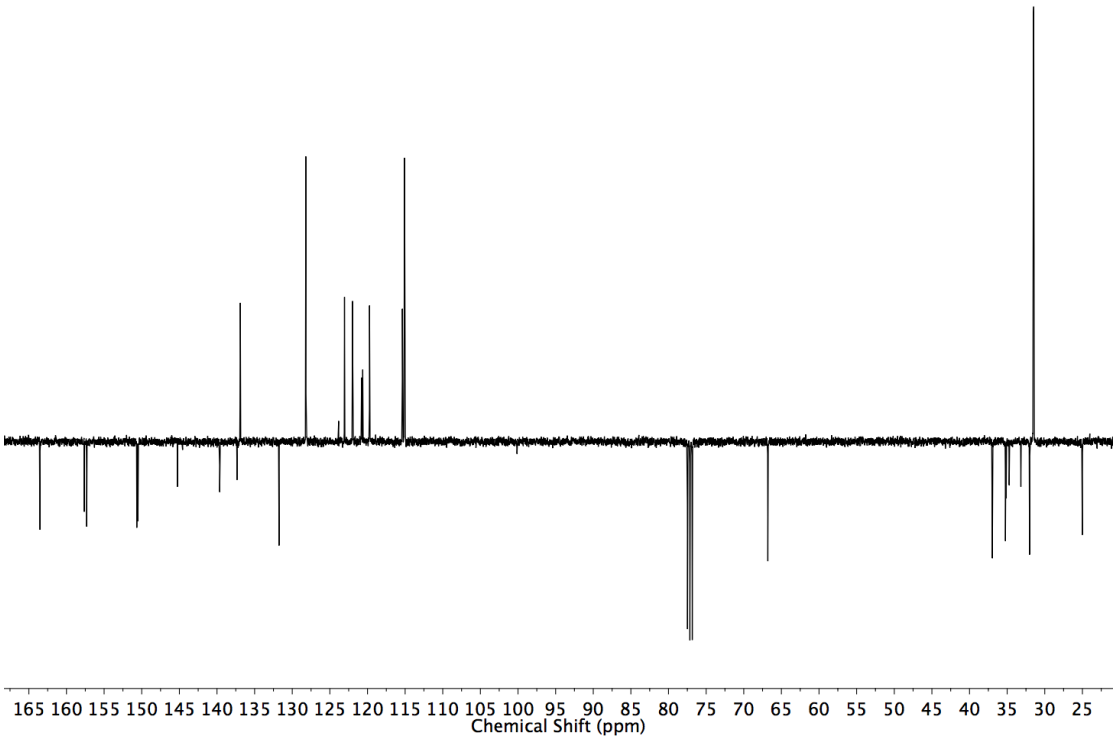

Figure 3.109 JMOD NMR ($CDCl_3$, 101 MHz) of **138.**

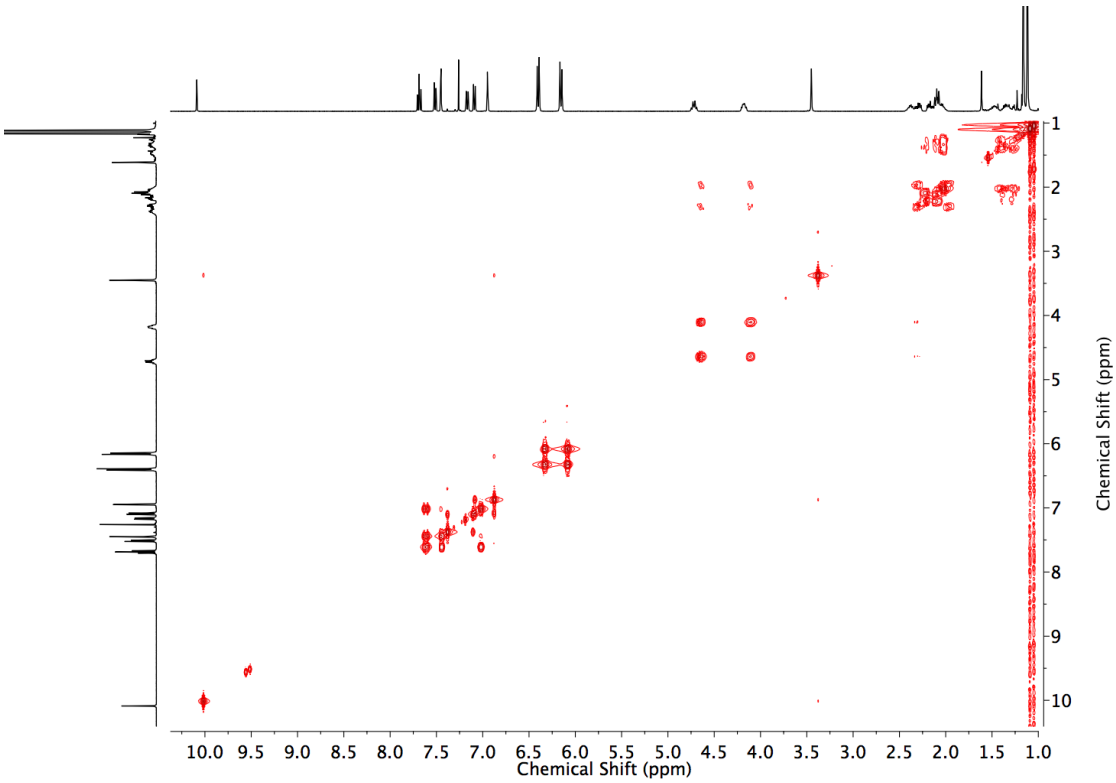

Figure 3.110 COSY NMR ($CDCl_3$) of **138.**

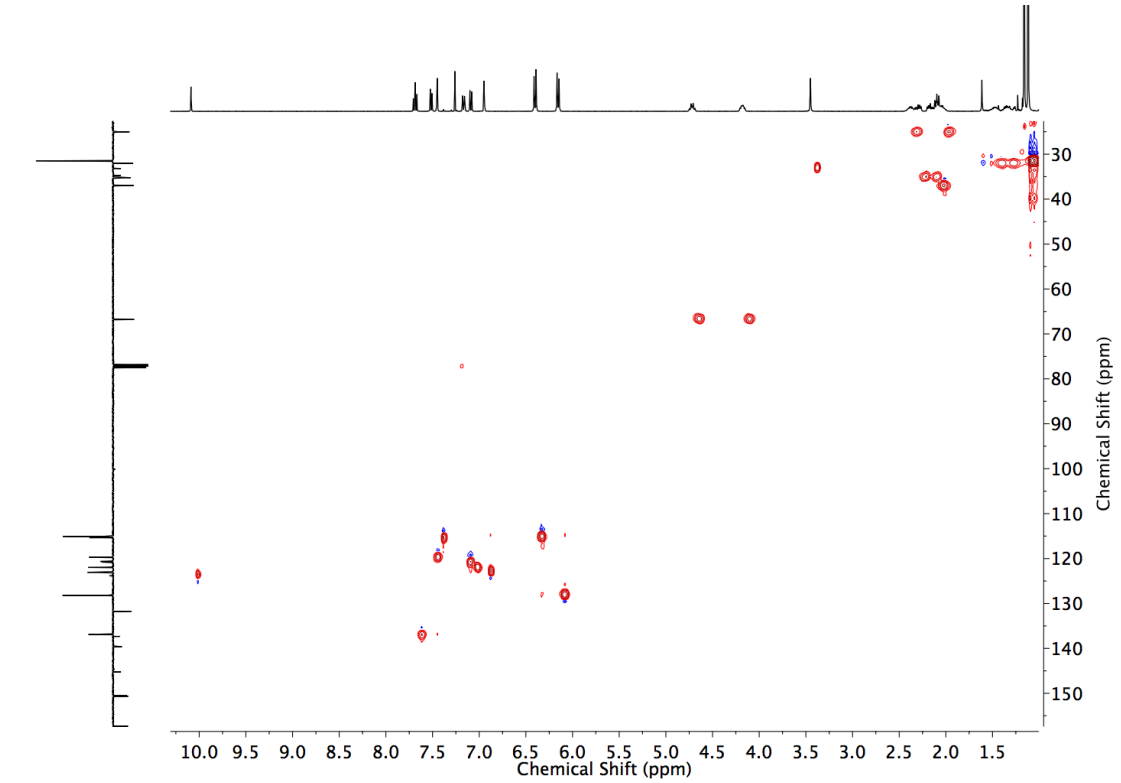

Figure 3.111 HSQC NMR ($CDCl_3$) of **138.**

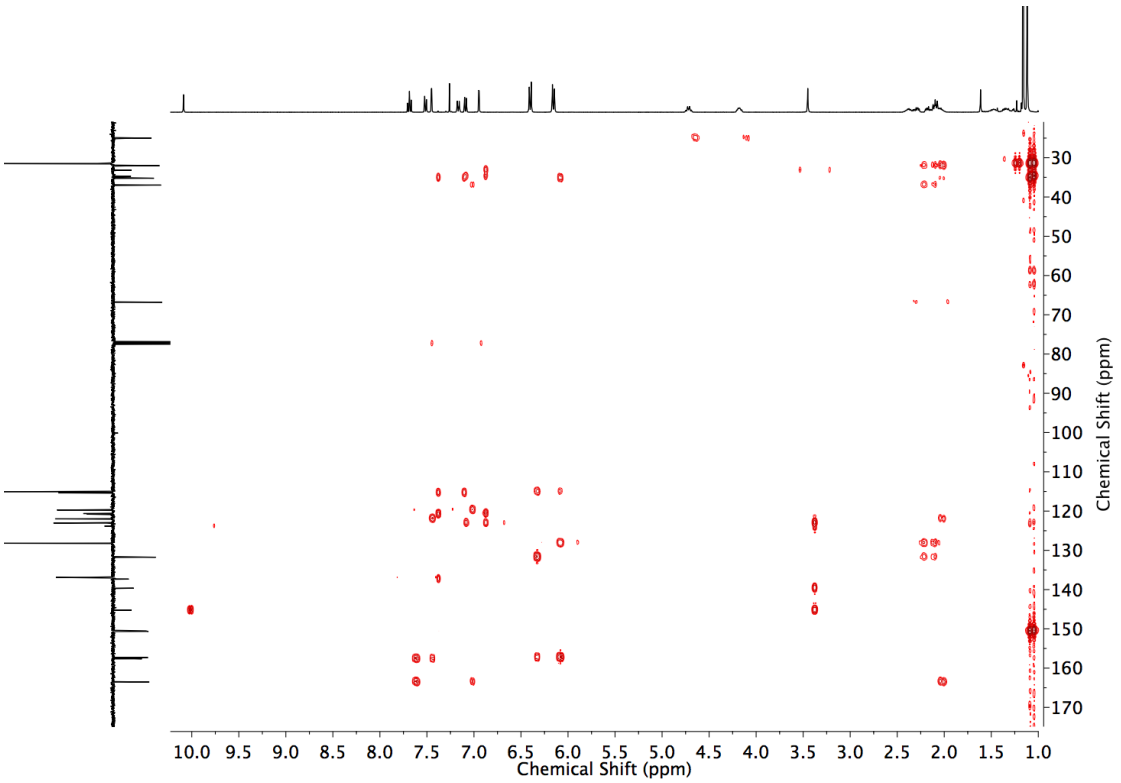

Figure 3.112 HMBC NMR ($CDCl_3$) of **138.**

Rotaxane ***141***

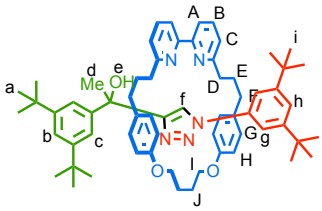

$^{i}Pr_2NEt$ (9.0 µl, 0.05 mmol) was added to a solution of **121** (6.5 mg, 0.025 mmol), **11** (5.8mg, 0.025 mmol), **14** (12.0 mg, 0.025 mmol) and $[Cu(MeCN)_4]PF_6$ (8.9 mg, 0.024 mmol) in CH_2Cl_2 (2.0 mL) in a microwave vial. The deep red mixture was stirred at rt for 16 h. TBACN (26.0 mg, 0.097 mmol) in CH_2Cl_2 was added to the mixture and stirred for five days at rt until the solution turned black. N_2 was bubbled through the reaction mixture to remove the solvent. The residue was diluted with CH_2Cl_2 (20 mL), and washed with H_2O (10 mL). The aqueous layer was extracted with CH_2Cl_2 (2 × 10 mL). The combined organic extracts were washed with brine (10 mL), dried ($MgSO_4$), filtered and the solvent removed *in vacuo*. Chromatography (petrol:CH_2Cl_2 1:1, with a gradient of 0 to 5% acetonitrile) gave **141** as a white foam (20.0 mg, 84%).^{1}H NMR (400 MHz, $CDCl_3$) δ: 10.06 (s, 1H, H_f), 7.72 (app t, *J* = 7.8 1H, 1 of H_B), 7.68 (app t, *J* =7.7, 1H, one of H_B), 7.56 (d, *J* = 1.8, 2H, H_c), 7.52 (dd, *J* = 7.8, 0.9, 1H, one of H_A), 7.50 – 7.46 (m, 3H, H_g, one of H_A,), 7.30 (t, *J* = 1.8, 1H, H_b), 7.18-7.10 (m, 3H, H_h, H_C), 6.48 (d, *J* = 8.6, 2H, 2 of H_G), 6.27 (d, *J* = 8.6, 2H, 2 of H_G) 6.20 (d, *J* = 8.6, 2H, 2 of H_H) 6.01 (d, *J* = 8.6, 2H, 2 of H_H), 4.81 (q, *J* = 7.9, 1H, 1 of H_I), 4.66 (q, *J* = 7.9, 1H, 1 of H_I), 4.19 – 4.10 (m, 1H, 1 of H_I) 4.03 – 3.81 (m, 2H, H_e, 1 of H_I), 2.52 – 1.92 (m, 12H, H_D, H_F, H_J), 1.70-1.50 (m, 7H, H_d, H_E), 1.24 (s, 18H, H_a), 1.09 (s, 18H, H_i). ^{13}C NMR (101 MHz, $CDCl_3$) δ 163.4, 163.4, 157.5, 157.3, 156.9, 153.4, 150.9, 150.9, 149.7, 137.1, 137.1, 137.0, 131.6, 131.5, 128.2, 122.1, 121.8, 121.1, 120.7, 120.4, 120.2,120.0, 129.4, 115.2, 113.6, 114.4, 72.3, 66.3, 66.3, 37.0, 36.8, 35.2, 35.1, 35.1, 31.8, 31.5, 31.4, 31.0, 25.0, 24.3. HR-ESI-MS *m/z* =968.6397 $[M+H]^+$ (calc. for $C_{64}H_{82}N_5O_3$ 968.6412).

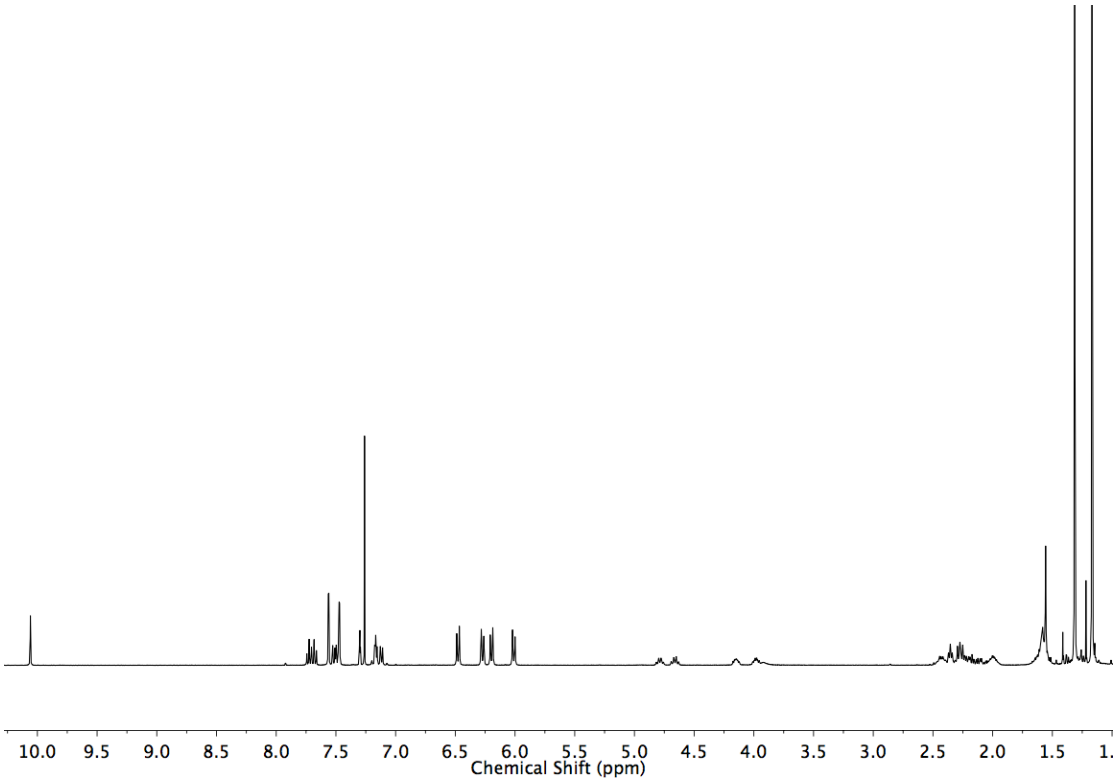

Figure 3.113 ^{1}H NMR ($CDCl_3$, 400 MHz) of **141**.

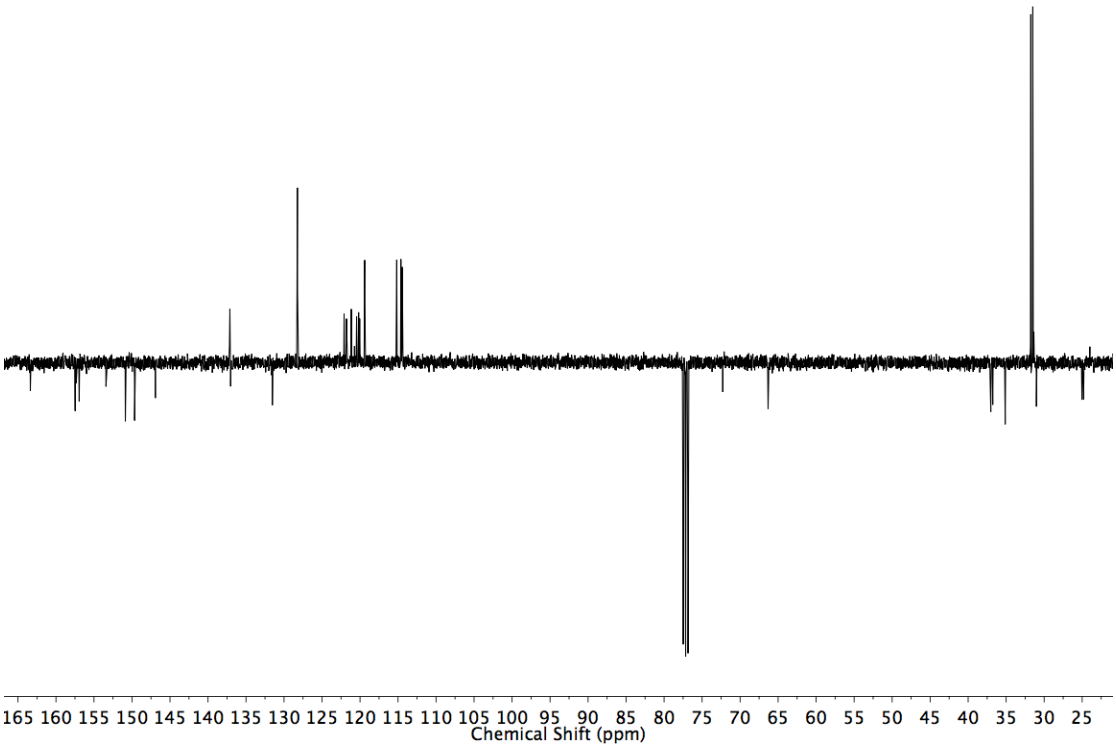

Figure 3.114 ^{13}C NMR ($CDCl_3$, 101 MHz) of **141**.

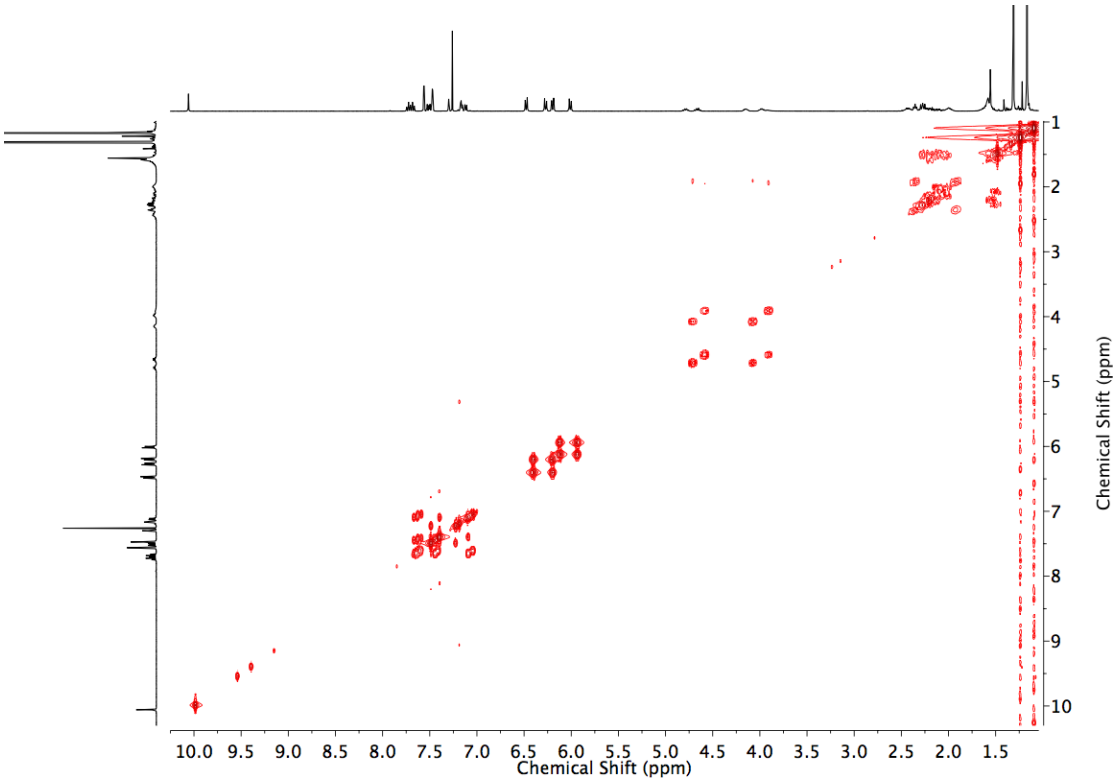

Figure 3.115 COSY NMR ($CDCl_3$) of **141**.

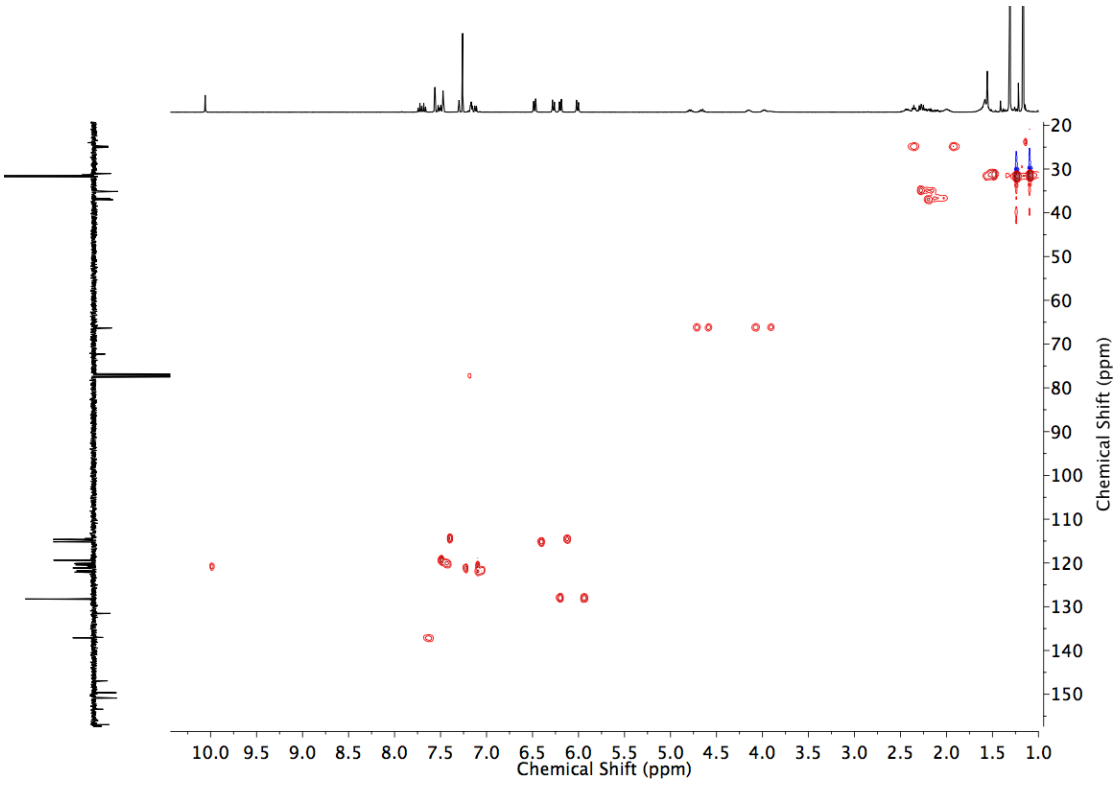

Figure 3.116 HSQC NMR ($CDCl_3$) of **141**.

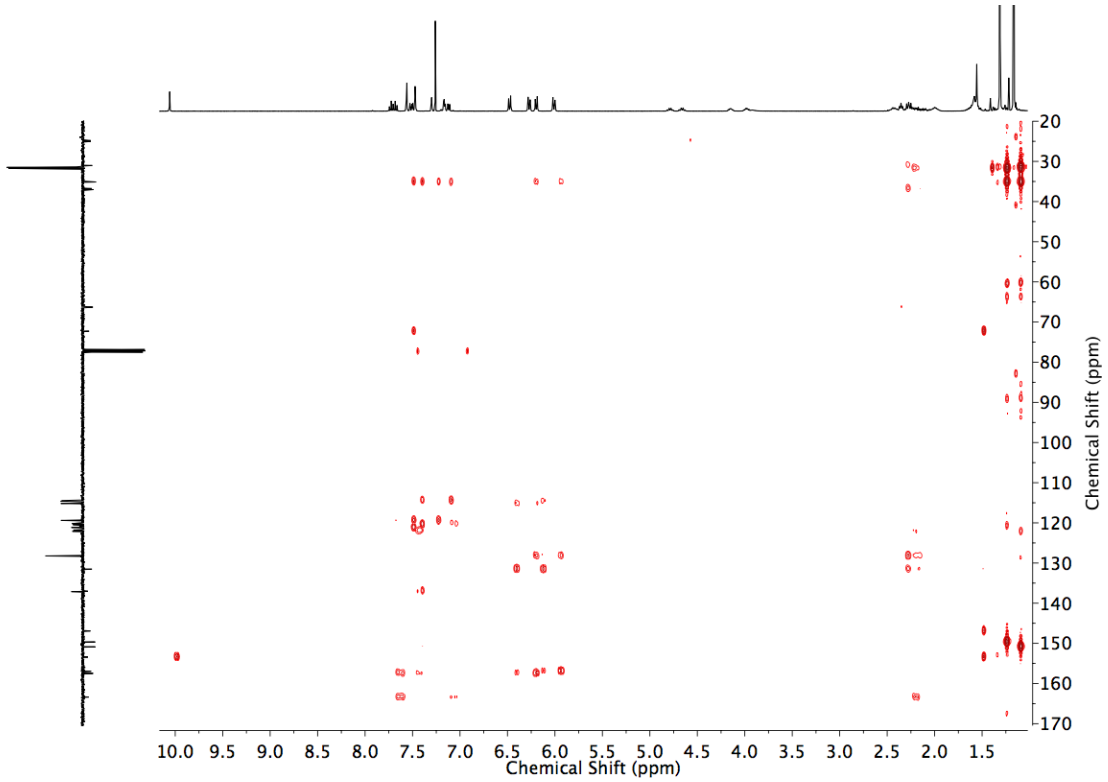

Figure 3.117 HMBC NMR ($CDCl_3$) of **141**.

Rotaxane ***148***

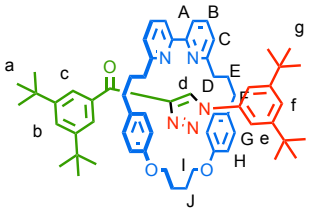

N^{i}Pr$_2$Et (20 µL, 4 eq.) was added to a solution of **108** (15.0 mg, 0.06 mmol), **11** (14.2 mg, 0.06 mmol), **14** (24.5 mg, 0.05 mmol) and [Cu(MeCN)$_4$]PF$_6$ (17.8 mg, 0.048 mmol) in CH_2Cl_2 (2 mL) in a sealed microwave vial (CEM Ltd.). The deep red mixture was stirred at rt for 16 hours. The reaction mixture was diluted with MeOH and treated with KCN (12 mg, 0.184 mmol) until it turned to a pale yellow. Air was bubbled through the reaction mixture to remove the solvent. Mixture was then redissolved in CH_2Cl_2, and organic extracts were washed with H_2O (3 x 2 mL), dried ($MgSO_4$), filtered and the solvent removed *in vacuo*. Chromatography (petrol, with a gradient of 0 to 5% EtOAc) gave **148** as a white film (10.2 mg, 21%).^{1}H NMR (400 MHz, $CDCl_3$) δ: 11.10, (s, 1H, H_d) 8.45 (d, *J* = 1.9, 2H, H_c), 7.77 (d, *J* = 1.7, 2H, H_e), 7.67 (t, *J* = 1.9, 1H, H_b), 7.62, (app. t, *J* = 7.7, H_B), 7.48 (d, *J* = 6.9, H_C), 7.28, (t, *J* = 1.7, 1H, H_f), 7.03 (d, *J* = 8.7, 2H, H_A) 6.48 (d, *J* = 8.6, H_G) 6.41 (d, *J* = 8.6, H_H), 4.67 (q, *J* = 7.7, 2H, 2 of H_I) 4.15-4.12 (m, 2H, 2 of H_I), 2.50 - 2.33 (m, 4H, 2 of H_J, 2 of H_F), 2.31 – 2.24 (m, 2H, 2 of H_F), 2.18-1.98 (m, 6H, H_D, 2 of H_J), 1.73-1.58 (m, 4H, H_E),1.45 (s, 18H, Ha or g), 1.19 (s, 18 H, Ha or g). ^{13}C NMR (101 MHz, $CDCl_3$) δ 185.2, 163.0, 157.3, 150.9, 150.3, 146.6, 137.1 136.7, 136.6, 132.1, 128.9, 128.3, 126.3, 125.2, 121.8, 121.5, 119.8, 115.8, 114.9, 100.0, 66.5, 37.0, 35.3, 35.1, 35.1, 32.0, 31.5, 31.3, 24.8. HR-ESI-MS m/z = 952.6118 $[M+H]^+$ (calc. for $C_{63}H_{78}N_5O_3$ 952.6099).

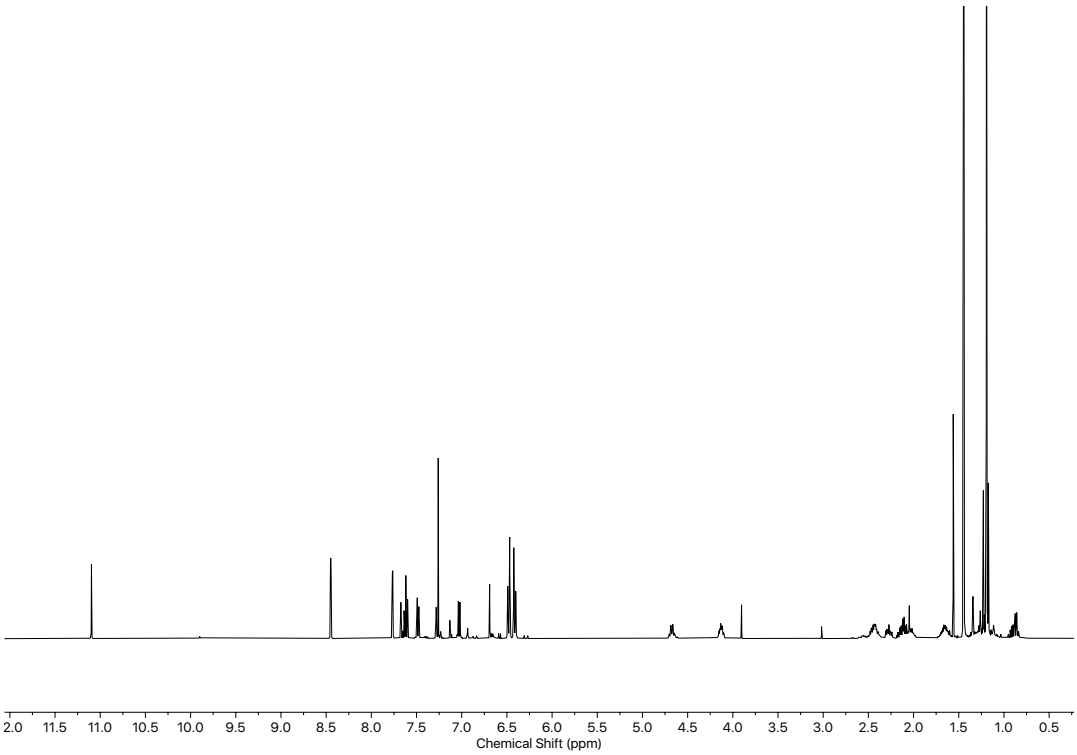

Figure 3.118 ^{1}H NMR ($CDCl_3$, 400 MHz) of **148**

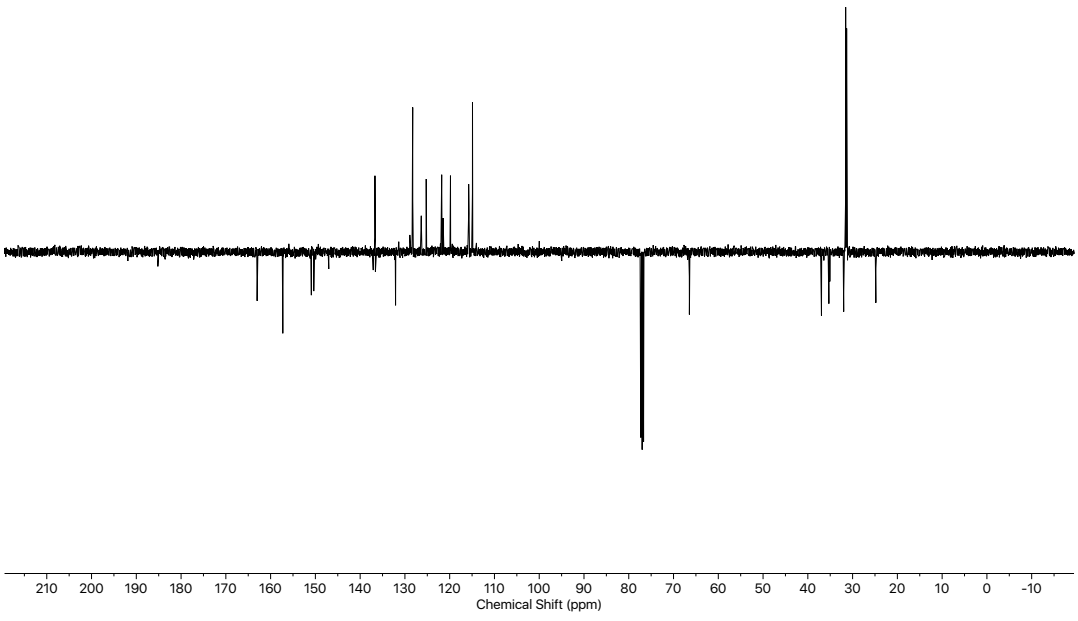

Figure 3.119 JMOD NMR ($CDCl_3$, 101 MHz) of **149**.

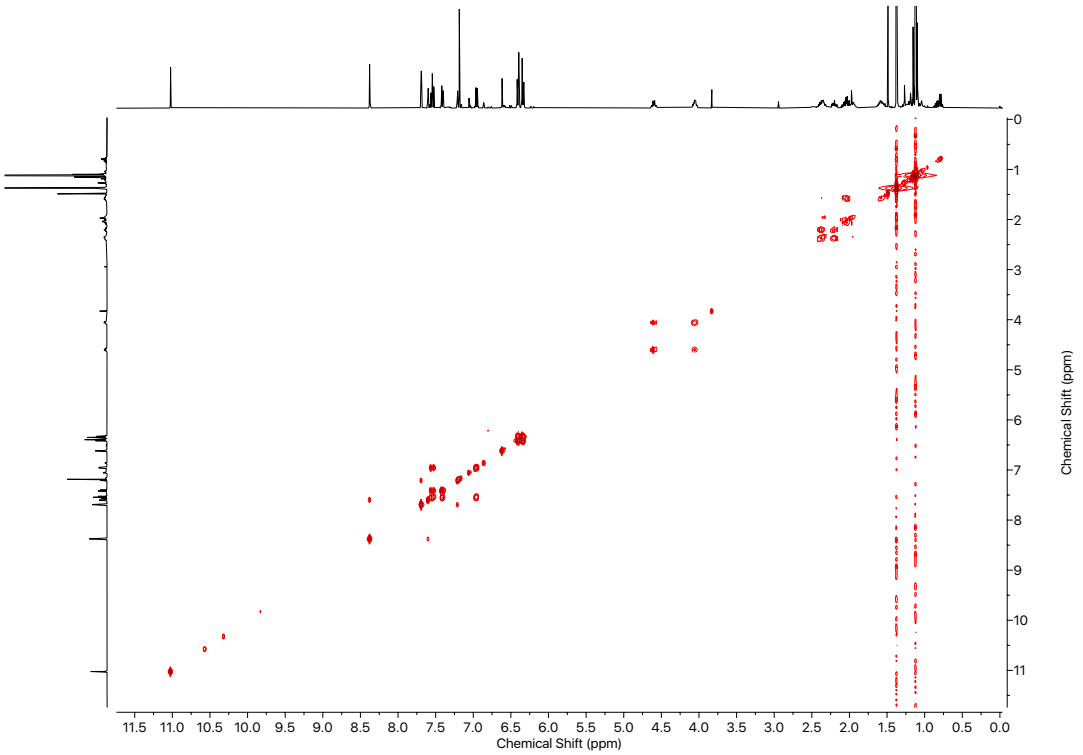

Figure 3.120 COSY NMR ($CDCl_3$) of **149**.

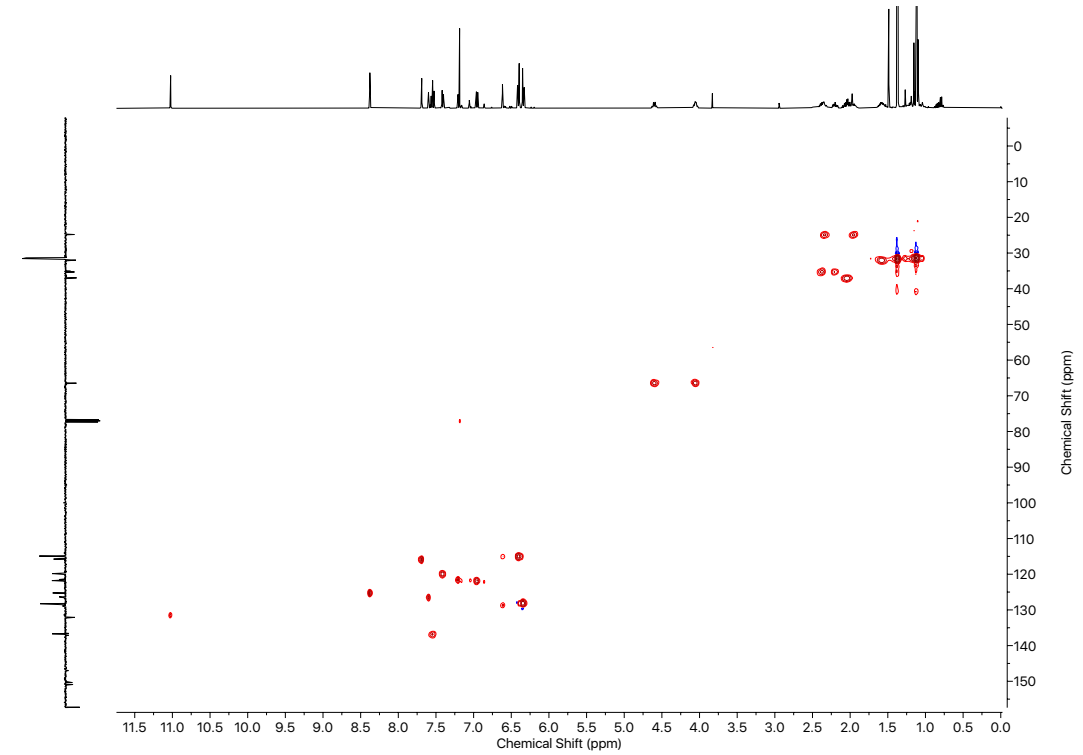

Figure 3.121 HSQC NMR ($CDCl_3$) of **149**.

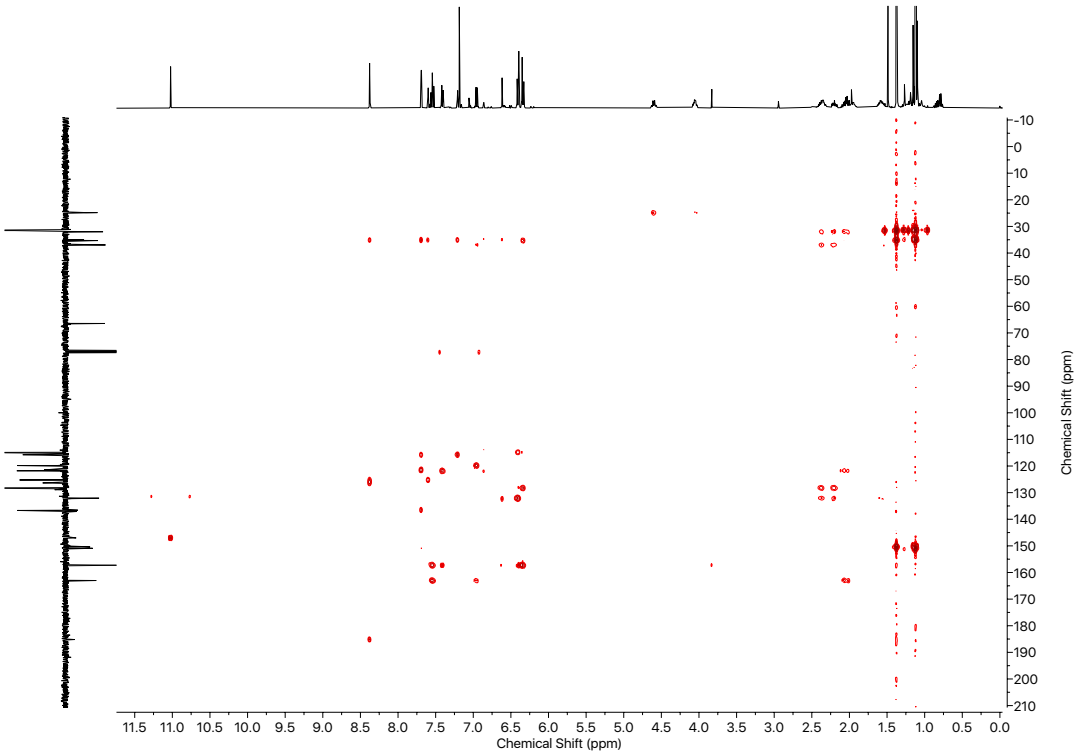

Figure 3.122 HMBC NMR ($CDCl_3$) of **149**.

Rotaxane ***S1***

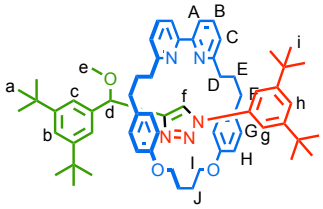

$^{i}Pr_2NEt$ (9.0 µl, 0.05 mmol) was added to a solution of **117** (6.5 mg, 0.025 mmol), **11** (5.8mg, 0.025 mmol),**14** (12.0 mg, 0.025 mmol), and $[Cu(MeCN)_4]PF_6$ (8.9 mg, 0.024 mmol), in CH_2Cl_2 (2.0 mL) in a sealed microwave vial (CEM Ltd.). The deep red mixture was stirred at rt for 16 h. KCN (10.0 mg, 0.153 mmol) in MeOH was added and the reaction mixture and stirred for two days at rt until the solution turned black. N_2 was bubbled through the reaction mixture to remove the solvent. The residue was diluted with CH_2Cl_2 (20 mL) and washed with H_2O (10 mL). The aqueous layer was extracted with CH_2Cl_2 (2 × 10 mL). The combined organic extracts were washed with brine (10 mL), dried ($MgSO_4$), filtered and the solvent removed *in vacuo*. Chromatography (petrol with a gradient of 0 to 50% EtOAc) gave **S1** as a white foam (4.7 mg, 19%). Decomposition to unidentified species was observed during purification, accounting for the low isolated yield. ^{1}H NMR (500 MHz, $CDCl_3$) δ: 10.24 (s, 1H, H_f), 7.73 (t, *J* =7.8, 1H, 1 of H_B), 7.69 (t, *J* = 7.8, 1H, 1 of H_B), 7.60 (d, *J* = 1.7, 2H, H_c), 7.54 (ddd, *J* = 7.8, 2.7, 0.9, 2H, H_A), 7.25 (t, *J* = 2.7, 1H, H_h), 7.21 (d, *J* = 2.7, 2H, H_g), 7.18 (t, *J* = 2.7, 1H, H_b), 7.12 (dd, *J* = 7.8, 1.0, 1H, 1 of H_C), 7.07 (dd, *J* = 7.8, 1.0, 1H, 1 of H_C), 6.44 (d, *J* = 8.6, 2H, 2H, 2 of H_H), 6.28 (d, *J* = 8.6, 2H, 2 of H_H), 6.18 (d, *J* = 8.6, 2H, 2 of H_G), 5.97 (d, *J* = 8.6, 2H, H_G), 4.91 (s, 1H, H_d), 4.89 – 4.81 (m, 1H, 1 of H_I), 4.81 – 4.73 (m, 1H, 1 of H_I), 4.19 – 4.11 (m, 1H, 1 of H_I), 4.10 – 4.06 (m, 1H, 1 of H_I), 3.00 (s, 3H , H_e), 2.48 – 1.95 (m, 2H, 2 of H_J), 2.36 – 2.25 (m, 14H, H_D, H_E, H_F, 2 of H_J), 1.17 (s, 36H, H_a, H_i). ^{13}C NMR (126 MHz, $CDCl_3$) δ 163.5, 163.5, 157.6, 157.5, 157.3, 157.1, 150.6, 150.4, 146.3, 141.0, 137.1, 137.0, 136.9, 131.5, 131.5, 128.2, 128.1, 124.2, 122.3, 121.9, 121.8, 121.0, 120.9, 119.9, 119.8, 115.21, 115.1, 114.9, 79.8, 66.7, 66.5, 56.7, 37.2, 37.0, 35.2, 35.2, 35.2, 34.9, 31.9, 31.5, 31.5, 31.4, 24.9, 24.9. HR-ESI-MS *m/z* =968.6402 $[M+H]^+$ (calc. for $C_{64}H_{82}N_5O_3$ 968.6412).

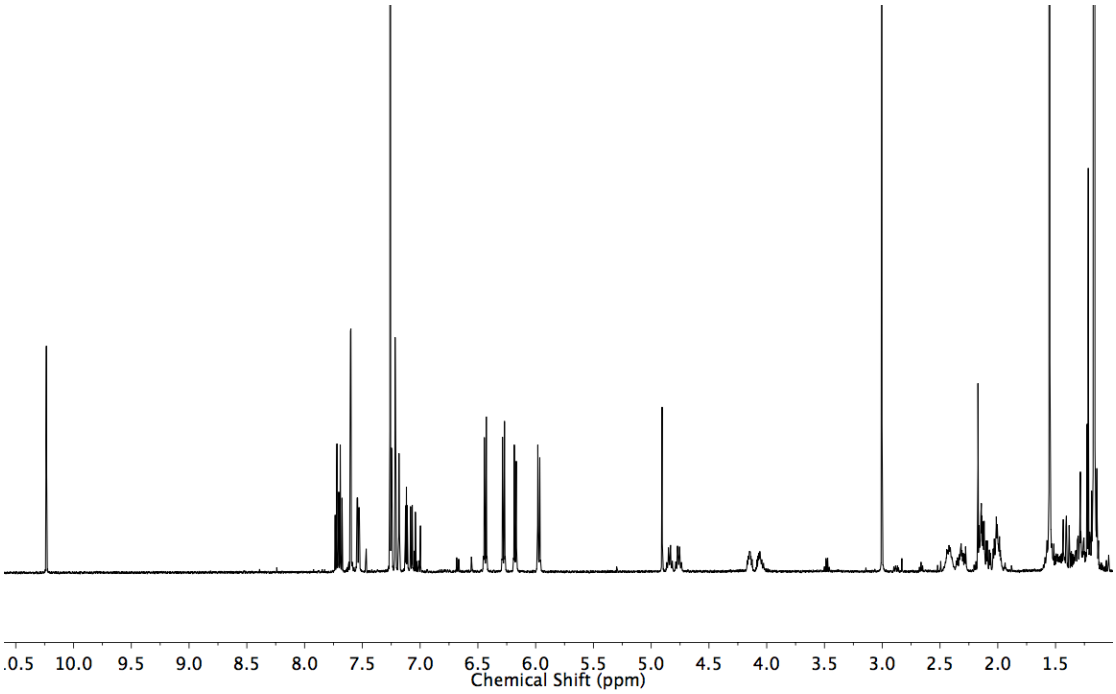

Figure 3.123 ^{1}H NMR ($CDCl_3$, 500 MHz) of **S1**.

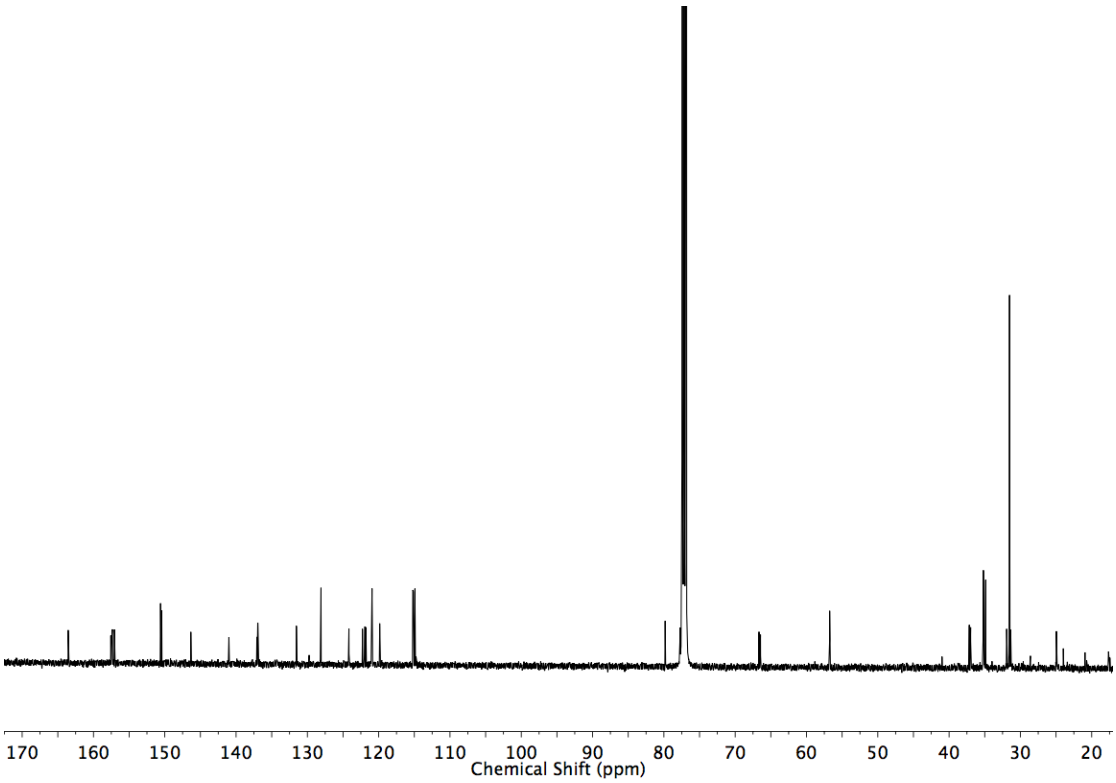

Figure 3.124 ^{13}C NMR ($CDCl_3$, 126 MHz) of **S1**.

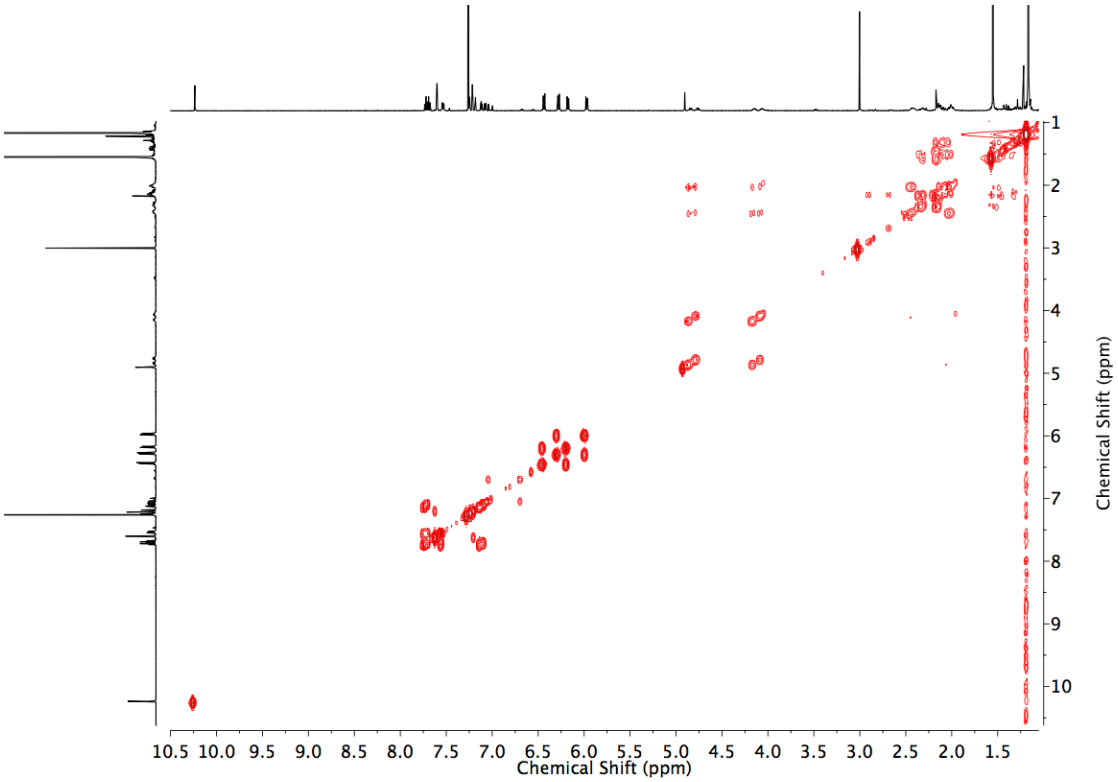

Figure 3.125 COSY NMR ($CDCl_3$) of **S1**.

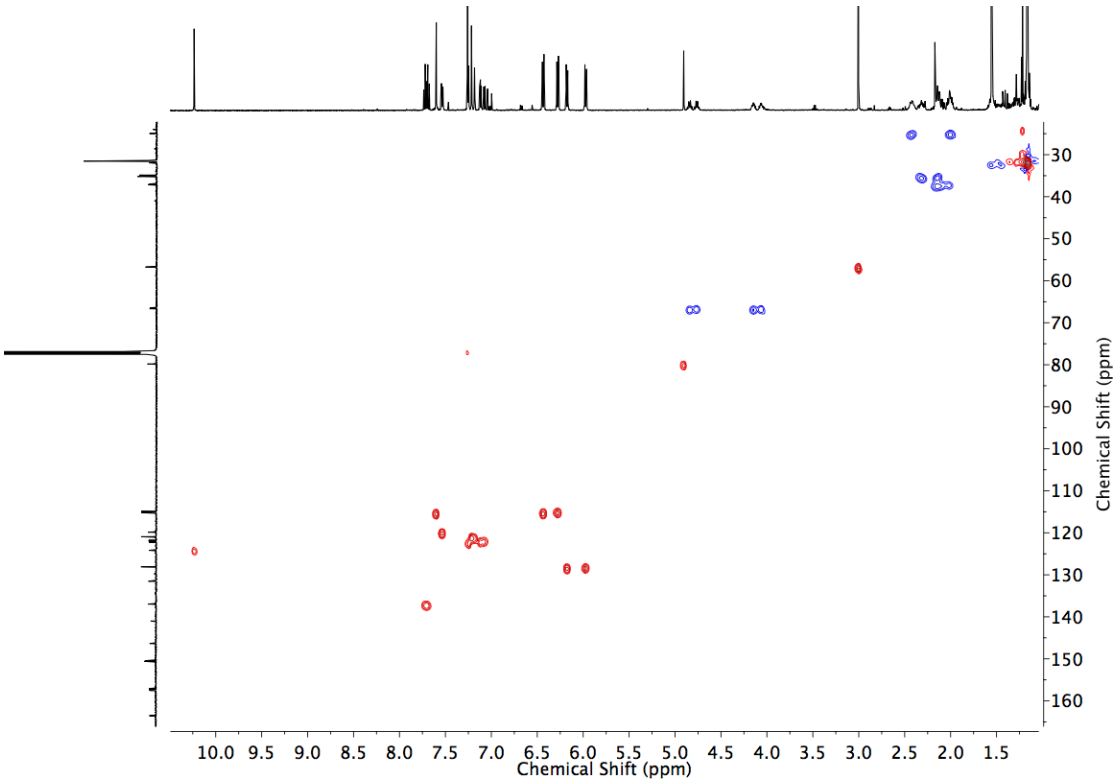

Figure 3.126 HSQC NMR ($CDCl_3$) of **S1**.

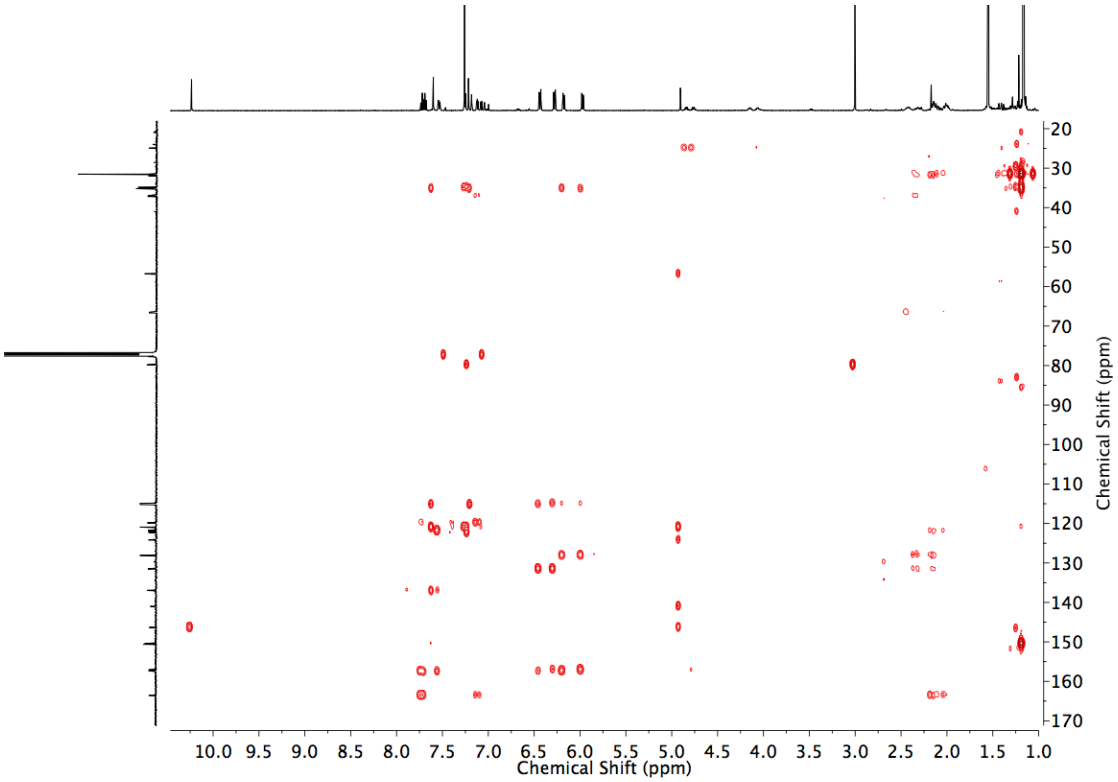

Figure 3.127 HMBC NMR ($CDCl_3$) of **S1**.

3.5. Thread **S2**

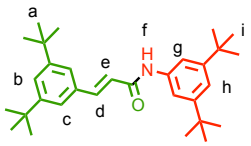

Rotaxane **134** (30.0 mg, 0.03 mmol) was dissolved in CH_2Cl_2 (1.0 mL). CF_3CO_2H (0.5 mL) was added and the mixture was stirred for 16 h at rt. The reaction mixture was diluted with CH_2Cl_2 (10 mL), washed with saturated $NaHCO_{3(aq)}$ (5 mL), brine (5 mL), dried ($MgSO_4$), filtered and the solvent removed *in vacuo*. Chromatography (petrol and 0 to 10% Et_2O) gave **134** as a white foam (11.0 mg, 82%). ^{1}H NMR (400 MHz, $CDCl_3$): δ 7.79 (d, *J* = 15.5, 1H, H_d), 7.51 (br. s, 2H, H_g), 7.46 (t, *J* =1.7, 1H, H_b) 7.39 (d, *J* =1.7, 2H, H_c), 7.34 (br. s, 1H, H_f), 7.21 (br. s, 1H, H_h), 6.57 (d, *J* = 15.5, 1H, H_e), 1.35 (s, 18H, H_i), 1.34 (s, 18H, H_a). ^{13}C NMR (126 MHz, $CDCl_3$) δ 164.1, 151.7, 151.4, 143.3, 137.5, 134.0, 124.4, 122.3, 120.3, 118.6, 114.5, 35.0, 34.9, 31.4, 31.4. HR-ESI-MS *m/z* = 448.3570 $[M+H]^+$ (calc. for $C_{31}H_{46}NO$ 448.3574).

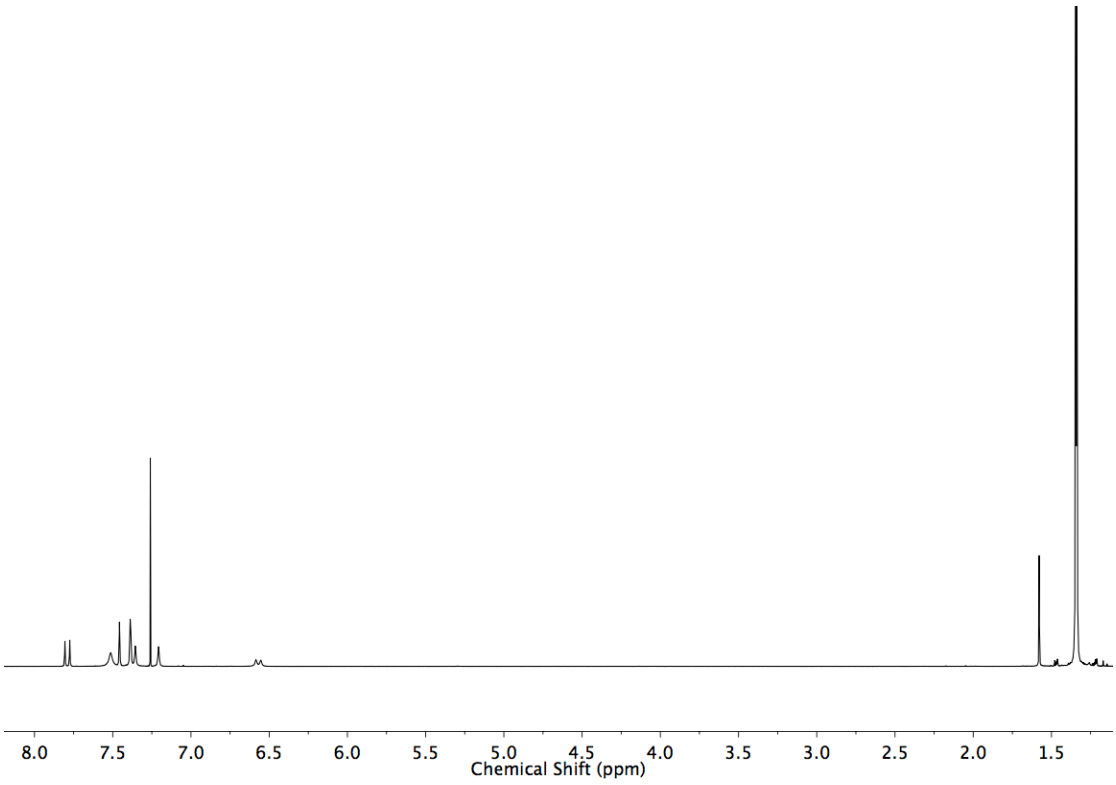

Figure 3.128 ^{1}H NMR ($CDCl_3$, 500 MHz) of **S2**.

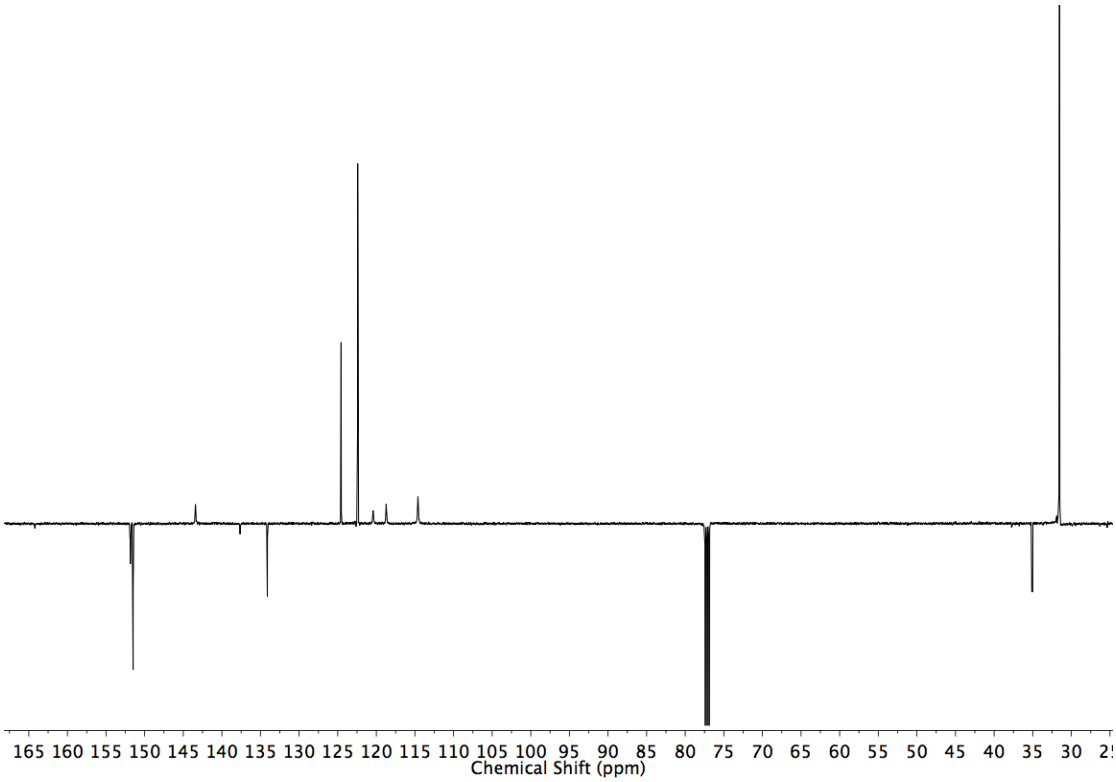

Figure 3.129 JMOD NMR ($CDCl_3$, 126 MHz) of **S2**.

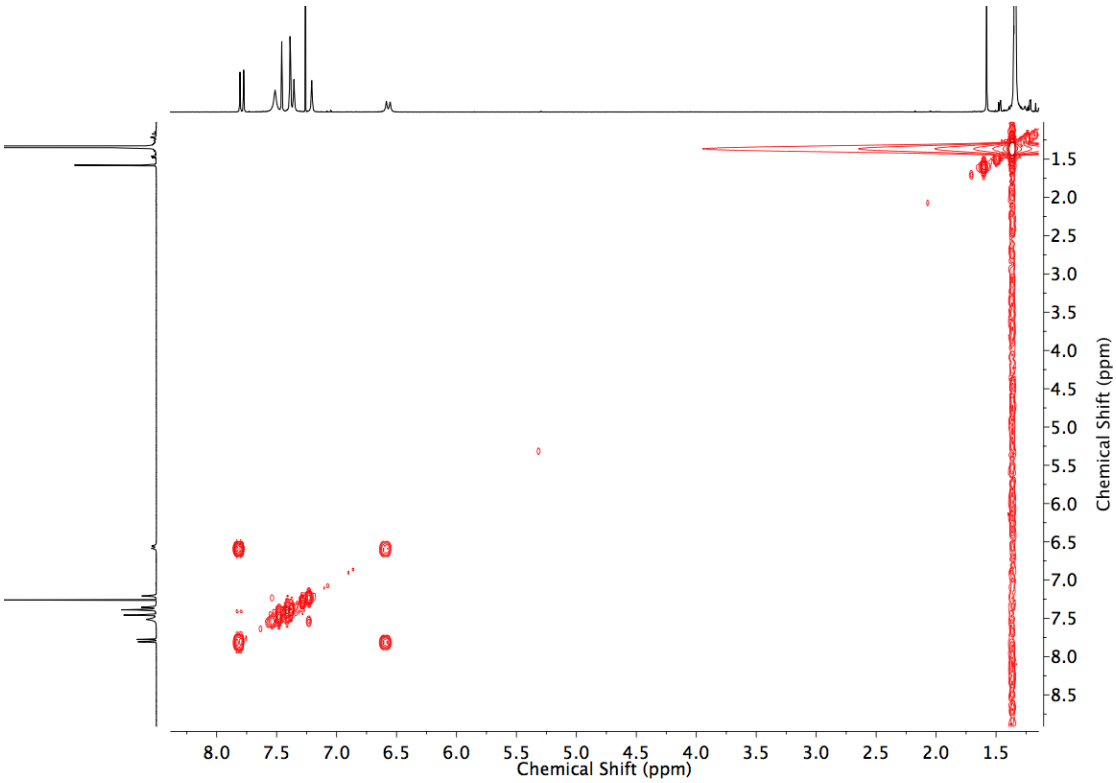

Figure 3.130 COSY NMR ($CDCl_3$) of **S2**.

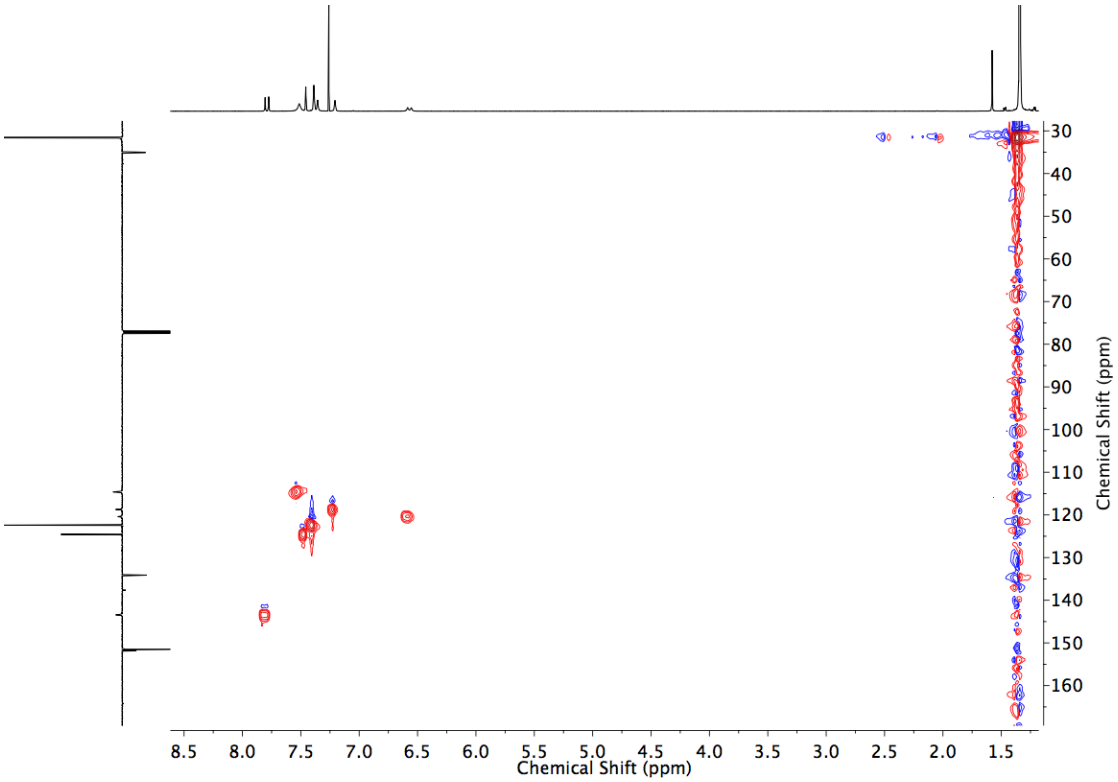

Figure 3.131 HSQC NMR ($CDCl_3$) of **S2**.

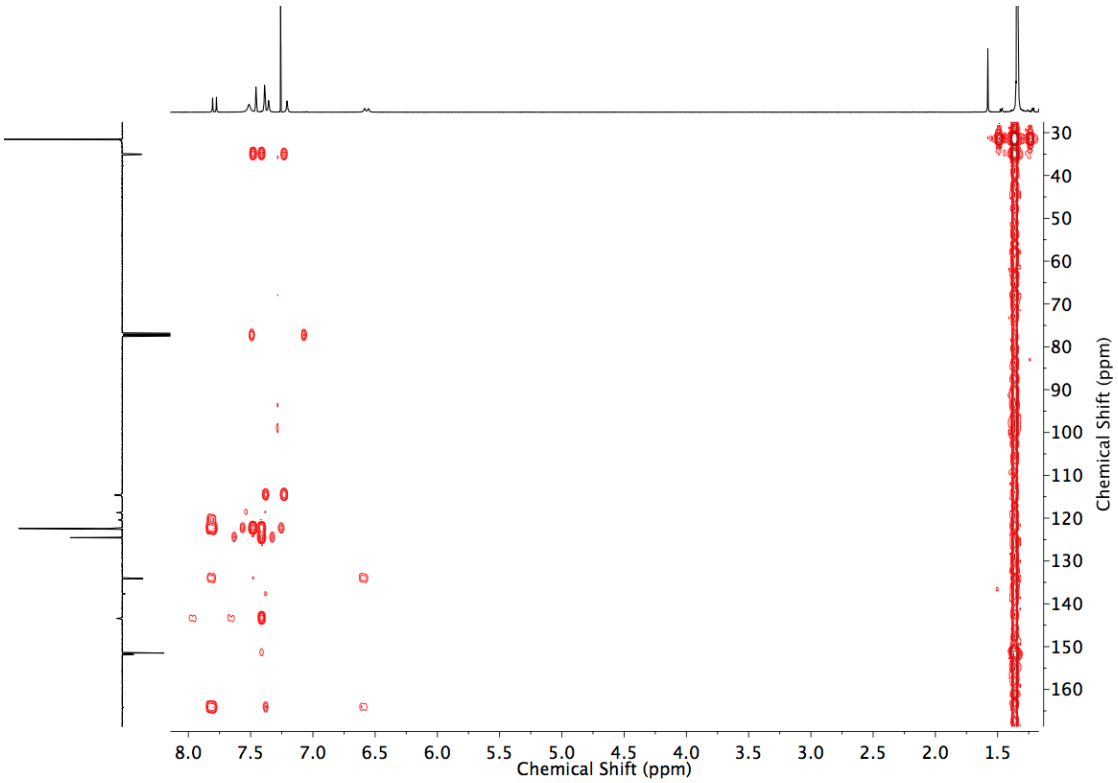

Figure 3.132 HMBC NMR ($CDCl_3$) of **S2**.

Single crystal X-ray analysis of rotaxanes **122**, **123**, **125** and **134**.

Crystals of **122** were grown by vapour diffusion of Et_2O into a CH_2Cl_2 solution. Crystals of **123**, **125** and **134** were grown by vapour diffusion of pentane into a Et_2O solution.

Data were collected at 100 K using a FRE+ HF diffractometer equipped with a Saturn 724+ enhanced sensitivity detector. Cell determination, data collection, data reduction, cell refinement and absorption correction were performed with CrysalisPro. The structures **122** and **125** were solved using SUPERFLIP,[19,20] **123** was solved using ShelXT,[21] and **134** was solved using ShelXS.[22] All structures were refined against F_2 using anisotropic thermal displacement parameters for all non-hydrogen atoms using ShelXL[23] and software packages within. Hydrogen atoms were placed in calculated positions, except structure **123** H(1) which was located in the difference map, and all were refined using a riding model.

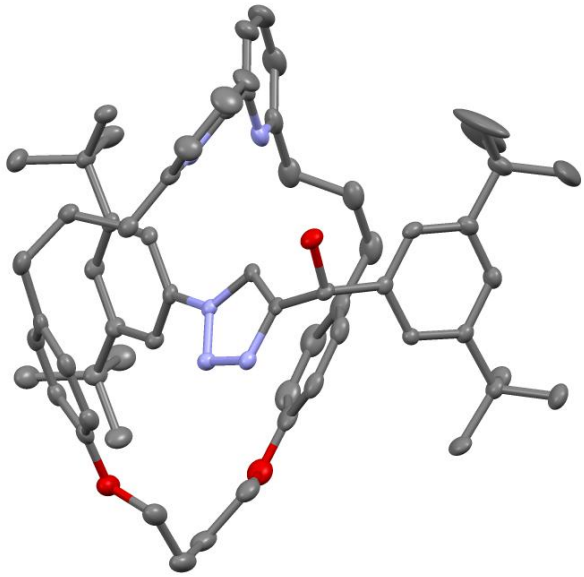

Figure 3.133 Ellipsoid plot of the asymmetric unit of **122** (ellipsoids shown at 50% probability). Hydrogen atoms omitted for clarity.

Compound	**122**
CCDC	1890755
Empirical formula	$C_{63}H_{79}N_5O_3$
Formula weight	954.31
Temperature/K	293(2)
Crystal system	monoclinic
Space group	$P2_1/n$
a/Å	13.8964(7)
b/Å	21.8200(10)
c/Å	18.2565(9)
α/°	90
β/°	94.479(5)
γ/°	90
Volume/Å^3	5518.8(5)
Z	4
ρ_{calc}g/cm^3	1.149
μ/mm^{-1}	0.070
F(000)	2064.0
Crystal size/mm^3	0.055 × 0.05 × 0.015
Radiation	MoKα (λ = 0.71075)
2Θ range for data collection/°	4.752 to 52.744
Index ranges	-17 ≤ h ≤ 17, -27 ≤ k ≤ 27, -22 ≤ l ≤ 22

Reflections collected	63066
Independent reflections	11291 [R_{int} = 0.0677, R_{sigma} = 0.0463]
Data/restraints/parameters	11291/0/656
Goodness-of-fit on F^2	1.004
Final R indexes [I>=2σ (I)]	R_1 = 0.0543, wR_2 = 0.1189
Final R indexes [all data]	R_1 = 0.0731, wR_2 = 0.1284
Largest diff. peak/hole / e Ă$^{-3}$	0.54/-0.25

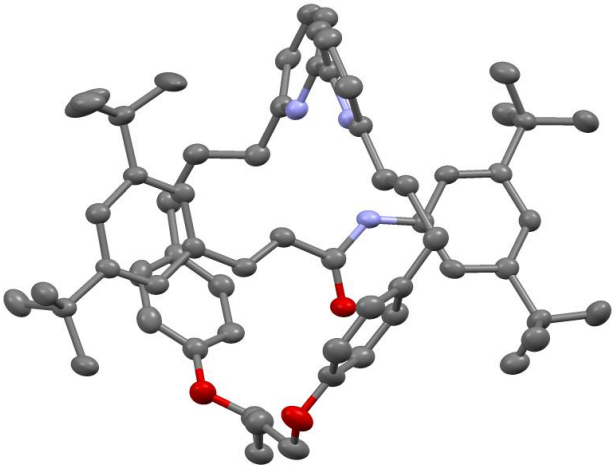

Figure 3.134 Ellipsoid plot of the asymmetric unit of **123** (ellipsoids shown at 50% probability). Hydrogen atoms omitted for clarity.

Compound	**123**
CCDC	1890756
Empirical formula	$C_{63}H_{79}N_3O_3$
Formula weight	926.29
Temperature/K	100(2)
Crystal system	orthorhombic
Space group	$Pca2_1$
a/Å	17.0247(4)
b/Ă	26.2343(10)
c/Å	12.4688(4)
α/°	90
β/°	90
γ/°	90
Volume/Å^3	5569.0(3)
Z	4

ρ_{calc}g/cm^3	1.105
μ/mm^{-1}	0.067
F(000)	2008.0
Crystal size/mm^3	0.2 × 0.07 × 0.035
Radiation	MoKα (λ = 0.71075)
2Θ range for data collection/°	3.92 to 52.746
Index ranges	-11 ≤ h ≤ 21, -18 ≤ k ≤ 32, -15 ≤ l ≤ 15
Reflections collected	21233
Independent reflections	11078 [R_{int} = 0.0474, R_{sigma} = 0.0902]
Data/restraints/parameters	11078/1/637
Goodness-of-fit on F^2	1.026
Final R indexes [I>=2σ (I)]	R_1 = 0.0738, wR_2 = 0.1496
Final R indexes [all data]	R_1 = 0.1213, wR_2 = 0.1810
Largest diff. peak/hole / e Å^{-3}	0.31/-0.24

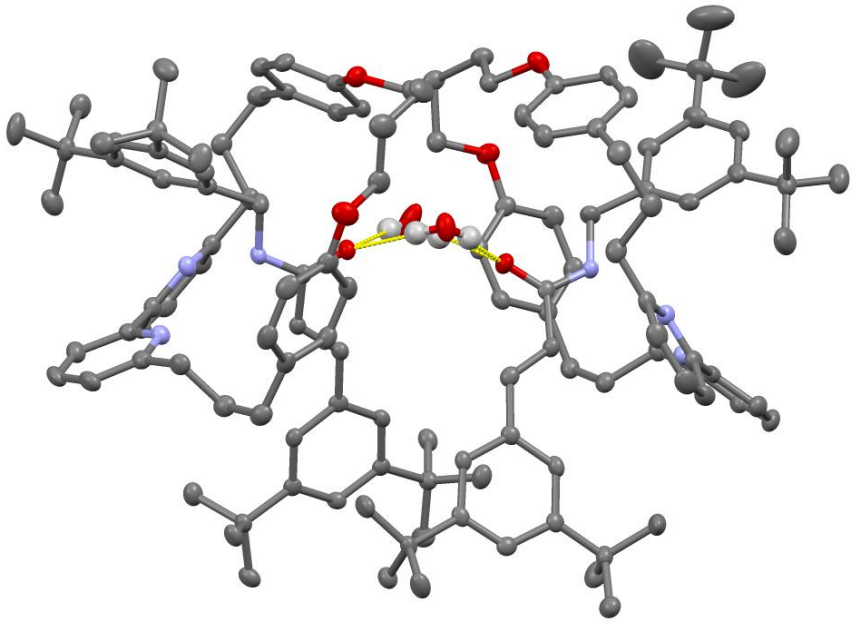

Figure 3.135 Ellipsoid plot of the asymmetric unit of **125** (ellipsoids shown at 50% probability). Hydrogen atoms omitted for clarity, except for H11C, H11D, H15L and H15M.

Compound	**125**
CCDC	1890758
Empirical formula	$C_{64}H_{83}N_3O_4$
Formula weight	958.33
Temperature/K	100(2)
Crystal system	triclinic

Space group	P-1
a/Ă	15.5175(6)
b/Ă	16.9490(5)
c/Ă	23.3325(6)
α/°	105.257(2)
β/°	100.079(3)
γ/°	93.338(3)
Volume/Ă^3	5793.7(3)
Z	4
ρ_{calc}g/cm^3	1.099
μ/mm^{-1}	0.067
F(000)	2080.0
Crystal size/mm^3	0.1 × 0.05 × 0.01
Radiation	MoKα (λ = 0.71075)
2Θ range for data collection/°	5.804 to 52.744
Index ranges	-19 ≤ h ≤ 17, -20 ≤ k ≤ 21, -29 ≤ l ≤ 25
Reflections collected	51024
Independent reflections	22793 [R_{int} = 0.0432, R_{sigma} = 0.0799]
Data/restraints/parameters	22793/0/1309
Goodness-of-fit on F^2	1.155
Final R indexes [I>=2σ (I)]	R_1 = 0.0877, wR_2 = 0.1845
Final R indexes [all data]	R_1 = 0.1236, wR_2 = 0.1990
Largest diff. peak/hole / e Å^{-3}	0.89/-0.50

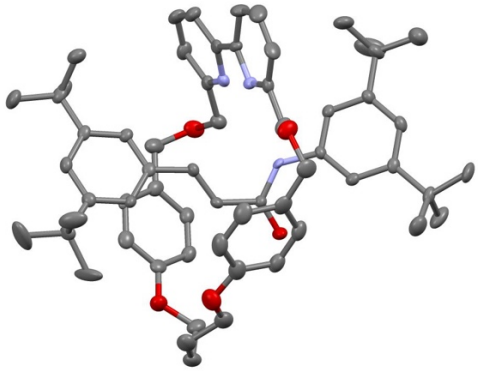

Figure 3.136 Ellipsoid plot of the asymmetric unit of **134** (ellipsoids shown at 50% probability). Hydrogen atoms omitted for clarity.

A “B–level” alert was detected using the IUCR checkcif algorithm. This was determined to be due to the geometry of the acrylamide combined with the macrocycle orientation which forces the amide proton and one of the alkene protons into close proximity. Thus, this alert is not a crystallographic error but an unusual feature of the interlocked structure which sterically constrains the covalent subcomponents in an otherwise energetically disfavoured arrangement.

Compound	**134**
CCDC	1890757
Empirical formula	$C_{61}H_{75}N_3O_5$
Formula weight	930.24
Temperature/K	100(2)
Crystal system	monoclinic
Space group	$P2_1$
a/Ă	10.8046(5)
b/Å	16.8432(5)
c/Ă	15.2219(6)
α/°	90
β/°	105.545(4)
γ/°	90
Volume/Å^3	2668.80(19)
Z	2
ρ_{calc}g/cm^3	1.158
μ/mm^{-1}	0.073
F(000)	1004.0
Crystal size/mm^3	0.1 × 0.05 × 0.02
Radiation	MoKα (λ = 0.71075)
2Θ range for data collection/°	5.876 to 52.744
Index ranges	-13 ≤ h ≤ 13, -20 ≤ k ≤ 21, -19 ≤ l ≤ 19
Reflections collected	25741
Independent reflections	10822 [R_{int} = 0.0558, R_{sigma} = 0.0948]
Data/restraints/parameters	10822/1/634
Goodness-of-fit on F^2	1.042
Final R indexes [I>=2σ (I)]	R_1 = 0.0718, wR_2 = 0.1599
Final R indexes [all data]	R_1 = 0.1045, wR_2 = 0.1737
Largest diff. peak/hole / e Ă$^{-3}$	0.47/-0.21

Optimisation of reaction conditions for the rearrangement reaction

Table S1 Optimisation of the formation of **123** with respect to solvent, temp. and additive.

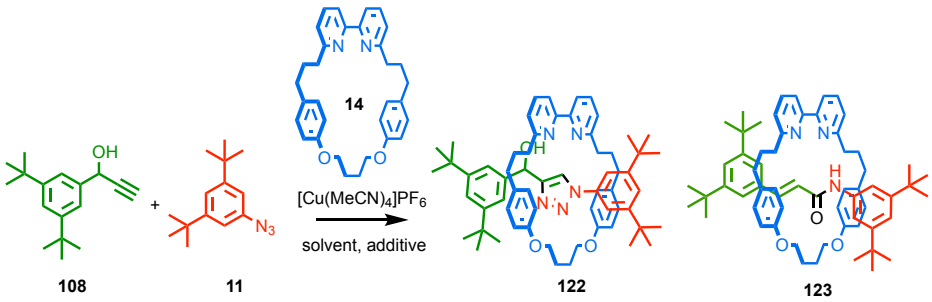

Entry	Time	Solvent	Temp	Additive	Conversion[a]	Ratio 122:123[a]
1	**16 h**	**CH_2Cl_2**	**RT**	**N^{i}Pr$_2$Et (2 eq.)**	**100%**	**>99:<1**
2	16 h	CH_2Cl_2 + 10% H_2O	RT	N^{i}Pr$_2$Et (2 eq.)	100%	90:10
3	16 h	CH_2Cl_2 + 10% H_2O	RT	-	trace - 100%*	60:40
4	24 h	CH_2Cl_2	RT	-	0	-
5	24 h	THF	RT	-	0	-
6	48 h	THF + 10% H_2O	RT	-	24 - 100%*	<1:>99
7	48 h	THF + 10% H_2O	RT	KF (0.9 eq.)	100%	<1:>99
8	48 h	THF + 10% H_2O	RT	TBAF (0.9 eq.)	100%±	50:50
9[b]	20 min	THF + 10% H_2O	80 °C	-	66 - 80%*	<1:>99
10[b]	20 min	THF + 10% H_2O	80 °C	KF (0.9 eq)	>99%	4:96
11[b]	20 min	THF + 10% H_2O	80 °C	TBAF (0.9 eq)	100%	57:43
12[b]	**1 h**	**THF + 10% H_2O**	**70 °C**	**KF (0.9 eq)**	**100%**	**<1:>99**
13[c]	**1 h**	**THF + 10% H_2O**	**70 °C**	**KF (0.9 eq)**	**100%**	**<1:>99**
14[b]	1 h	THF + 10% H_2O	70 °C	KNO_3 (0.9 eq)	100%	7: 93
15[b]	1 h	THF + 10% H_2O	70 °C	TBAF (0.9 eq)	100%	8:92
16[b,d]	1 h	THF + 10% H_2O	70 °C	KF (0.9 eq)	100%	72:28
17[b,d]	1 h	THF + 10% H_2O	70 °C	KNO_3 (0.9 eq)	100%	>99:<1

[a]Determined by ^{1}H NMR, [b]Performed in a microwave reactor. [c]Performed under thermal conditions in an oil bath. [d]$[Cu(MeCN)_4]PF_6$ was replaced by $CuSO_4$/NaAsc. *Conversion varied run-to-run. ±Decomposition to an unknown product was also observed.

The role of KF remains unclear; neither TBAF (entries 8, 11 and 15) nor KNO_3 (entries 14 and 17) produce the same outcome as KF under the same conditions, suggesting that both the cation and anion play a role. Interestingly at 70 °C, TBAF and KF appear more comparable (entry 12 vs 15). (note: at 80 °C [Entry 11] the lower selectivity of TBAF may be due to fluoride-mediated decomposition of the tetrabutyl ammonium cation)[1] Interestingly, when $[Cu(MeCN)_4]PF_6$ is replaced by $CuSO_4$/Na-ascorbate, KNO_3 outperforms KF, suggesting that the role of the inorganic salt is quite complex.

Kinetic Study of the reaction of **14**, **11** and **108**.

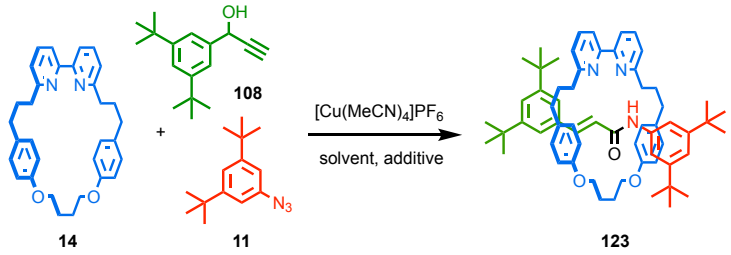

14 (7.3 mg, 0.0153 mmol), $[Cu(MeCN)_4]PF_6$ (5.5mg, 0.0147 mmol), **11** (4.3mg, 0.0184 mmol), and **108** (4.5 mg, 0.0184 mmol) were dissolved in D_2O-THF-d_8 (1:9, 1.2 mL). The solution was passed through a Celite plug and 0.6 ml was transferred into a NMR tube and analysed by ^1H NMR at 2 h intervals. The disappearance of the peak at 7.16 ppm (d, *J* = 1.7, 2H) and the appearance of the peak at 7.91 (d, *J* = 1.7 Hz, 1H) was monitored.

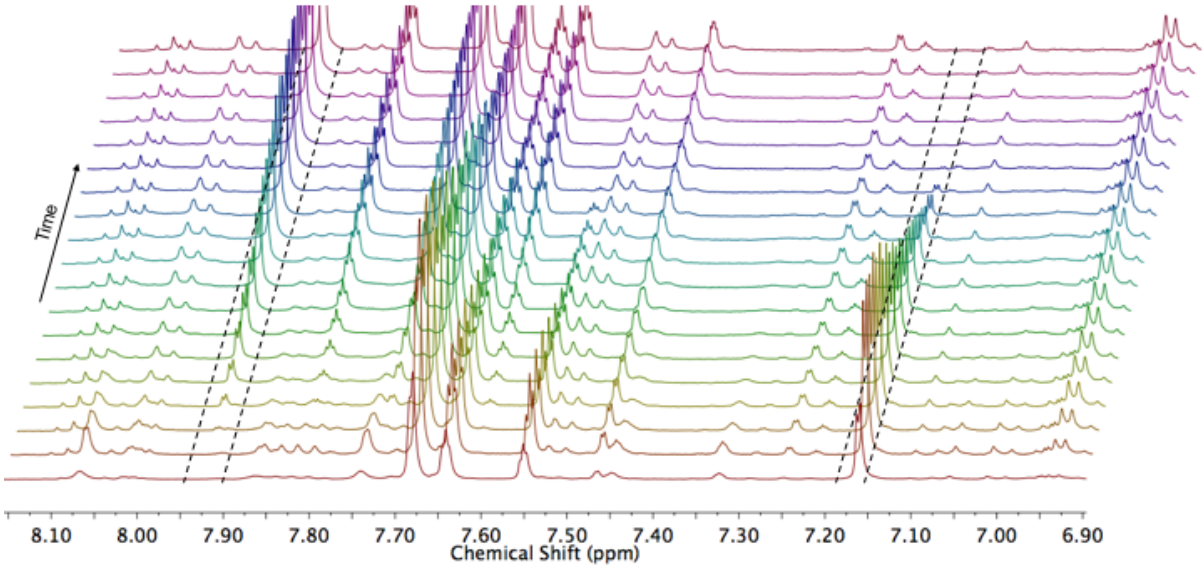

Figure 3.137 Stacked partial ^1H NMRs (400 MHz, THF-d_8/D_2O 9:1) showing formation of **123** and consumption of **11**.

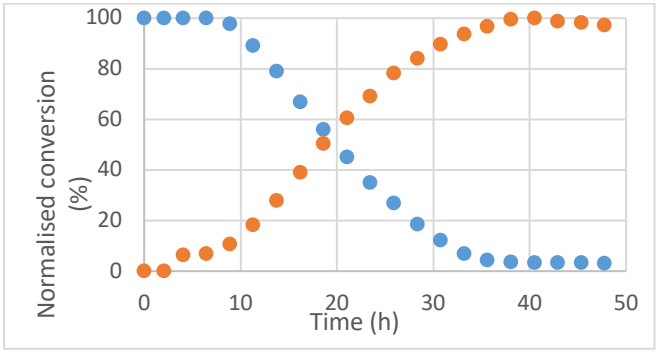

Figure 3.138 Consumption of **11** (blue) and formation of **123** (orange) based on their normalised integrals with respect to the residual protonated THF signal (3.62 ppm).

Control experiments: axle formation under conditions optimised for the formation of acrylamide rotaxane **123**

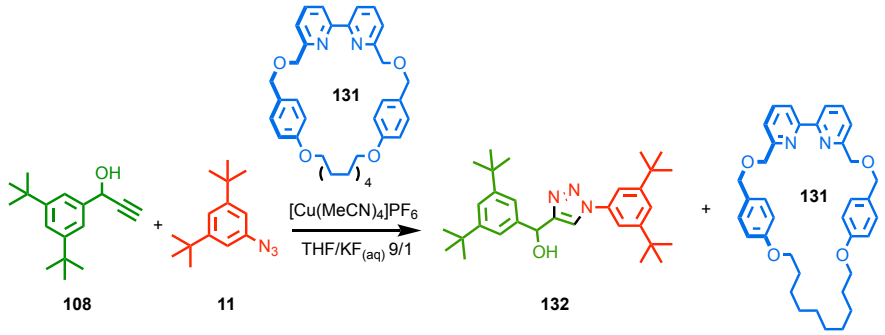

$KF_{(aq)}$ (0.2 mL, 0.1 M), was added to a solution of **108** (7.3 mg, 0.030 mmol), **11** (6.9 mg, 0.030 mmol) **131** (14.3 mg, 0.025 mmol) and $[Cu(MeCN)_4]PF_6$ (8.9 mg, 0.024 mmol) in THF (1.8 mL) in a microwave vial. The orange mixture was stirred at 70 °C (μW) for 1 h. The reaction mixture was diluted with CH_2Cl_2 (10 mL) and washed with EDTA-NH_3 solution (10 mL). The aqueous layer extracted with CH_2Cl_2 (2 × 50 mL). The combined organic extracts were washed with brine (50 mL), dried ($MgSO_4$), filtered and the solvent removed *in vacuo*. Analysis by ^{1}H NMR revealed **132** to be the sole product.

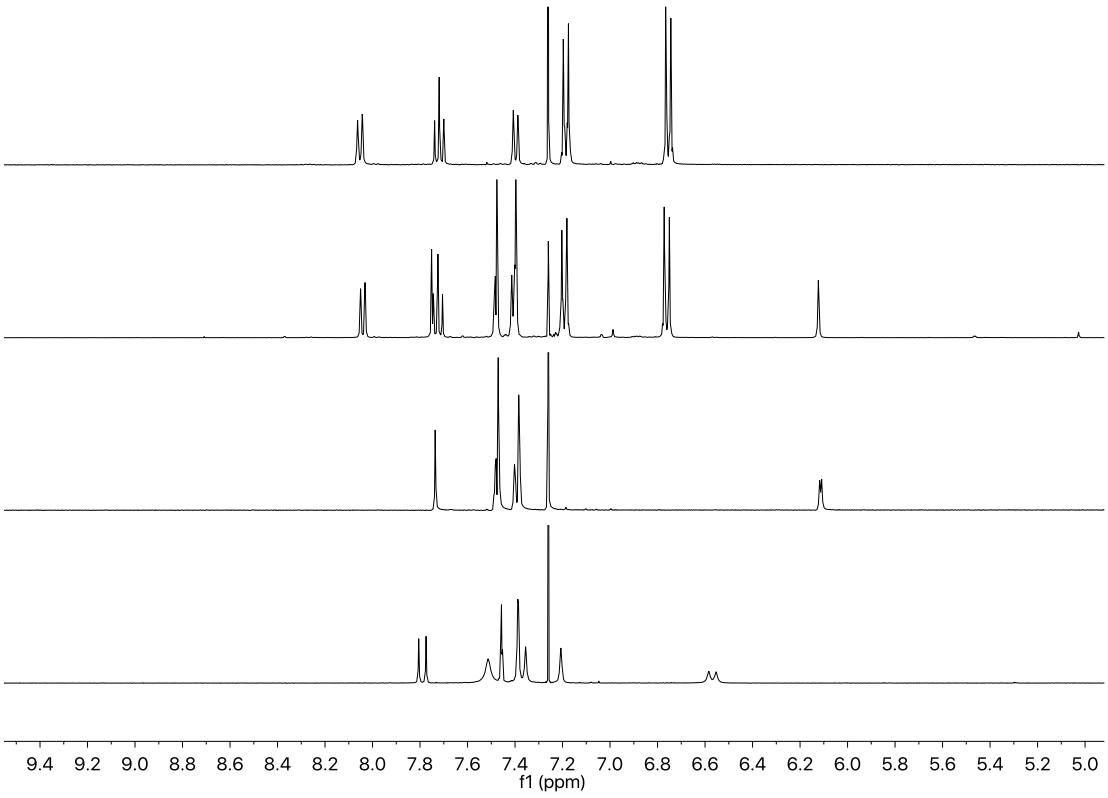

Figure 3.139 Stacked partial ^{1}H NMR (400 MHz, $CDCl_3$) spectra of (from top to bottom) **1c**, the crude reaction mixture, triazole axle **132** and acrylamide **S2**.

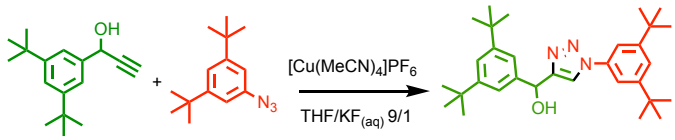

108 **11** **132**

$KF_{(aq)}$ (0.2 mL, 0.1M), was added to a solution of **108** (7.3 mg, 0.030 mmol), **11** (6.9 mg, 0.030 mmol) and $[Cu(MeCN)_4]PF_6$ (8.9 mg, 0.024 mmol) in THF (1.8 mL) in a microwave vial. The yellow mixture was stirred at 70 °C (μW) for 1 h. The crude reaction mixture was diluted with CH_2Cl_2 (10 mL) and washed with EDTA-NH_3 solution (10 mL). The aqueous layer was extracted with CH_2Cl_2 (2 × 50 mL). The combined organic extracts were washed with brine (50 mL), dried ($MgSO_4$), filtered and the solvent removed *in vacuo*. Analysis by ^{1}H NMR revealed **S12** to be the sole product.

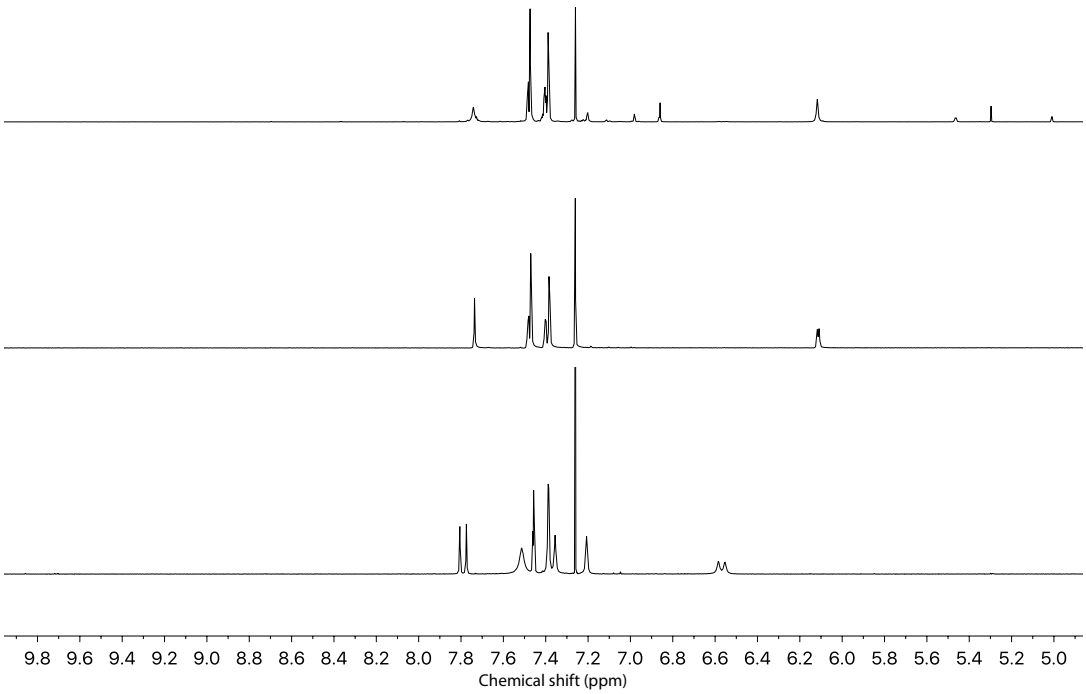

Figure 3.140 Stacked partial ^{1}H NMR (400 MHz, $CDCl_3$) of (from top to bottom) the crude reaction mixture, triazole axle **108** and acrylamide **S2**.

Mechanistic studies: rearrangement of triazolide 12 under aqueous conditions

To investigate whether triazolide **140** was an intermediate *en route* to acrylamide rotaxane **139** we explored the reaction of **140** under various conditions and analysed the results by ^{1}H NMR:

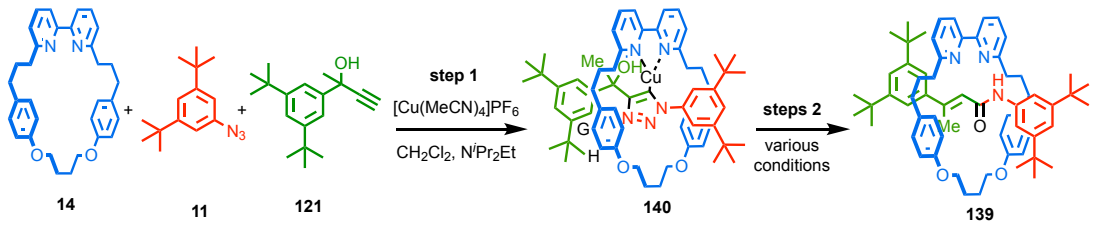

Step 1: ^{i}Pr$_2$NEt (40.0 µl, 0.23 mmol) was added to a solution of **121** (25.6 mg, 0.10 mmol), **11** (23.1 mg, 0.10 mmol), **14** (48.0 mg, 0.10 mmol) and [Cu(MeCN)$_4$]PF$_6$ (36.6 mg, 0.098 mmol) in CH_2Cl_2 (8.0 mL). The deep-red solution was washed with H_2O (10 mL), brine (10 mL), dried ($MgSO_4$) and the solvent removed *in vacuo*. ^{1}H NMR analysis of the residue confirmed that the starting materials had been consumed to produce a new species whose ^{1}H NMR resonances are consistent with triazolide **140**; four signals are observed for macrocycle protons H_G and H_H (~ 6.2 ppm) due to the presence of the axle stereogenic centre, no triazole resonance was observed, and the spectrum is distinct from that of the [Cu(**141**)]$^+$. MS analysis of a portion of the solution supports this assignment (*m/z* =1030.9 [M+H]$^+$; calc. for $C_{64}H_{80}CuN_5O_3$ = 1030.9).

Step 2A: The residue from **step 1** was dissolved in a mixture of $KF_{(aq)}$ (0.1 M, 0.1 mL) and THF (0.9 mL). The orange mixture was stirred at 70 °C (µW) for 1 h. The reaction mixture was diluted with CH_2Cl_2 (20 mL) and washed with EDTA-NH_3 solution (10 mL). The aqueous layer was extracted with CH_2Cl_2 (2 × 10 mL). The combined organic extracts were washed with brine (10 mL), dried ($MgSO_4$) and the residue analysed by ^{1}H NMR.

Step 2B: The residue from **step 1** was dissolved in a mixture of $KF_{(aq)}$ (0.2 M, 0.05 mL), $HPF_{6(aq)}$ (0.2 M, 0.05 mL) and THF (0.9 mL). The orange mixture was stirred at 70 °C (µW) for 1 h. The reaction mixture was diluted with CH_2Cl_2 (20 mL) and washed with EDTA-NH_3 solution (10 mL). The aqueous layer was extracted with CH_2Cl_2 (2 × 10 mL). The combined organic extracts were washed with brine (10 mL), dried ($MgSO_4$) and the residue analysed by ^{1}H NMR.

Step 2C: The residue from **step 1** was dissolved in a mixture of $HPF_{6(aq)}$ (0.13 M, 0.1 mL, 1 eq,) and THF (0.9 mL). The orange mixture was stirred at 70 °C (µW) for 1 h. The reaction mixture was diluted with CH_2Cl_2 (20 mL) and washed with EDTA-NH_3 solution (10 mL). The aqueous layer was extracted with CH_2Cl_2 (2 × 10 mL). The combined organic extracts were washed with brine (10 mL), dried ($MgSO_4$) and the residue analysed by ^{1}H NMR.

Step 2D: The residue from **step 1** was dissolved in a mixture of $HPF_{6(aq)}$ (0.13 M, 0.1 mL, 1 eq,) and THF (0.9 mL). The orange mixture was stirred for 1 h at rt. The reaction mixture was diluted with CH_2Cl_2 (20 mL) and washed with EDTA-NH_3 solution (10 mL). The aqueous layer was extracted with CH_2Cl_2 (2 × 10 mL). The combined organic extracts were washed with brine (10 mL), dried ($MgSO_4$) and the solvent removed *in vacuo*. The residue was analysed by ^{1}H NMR.

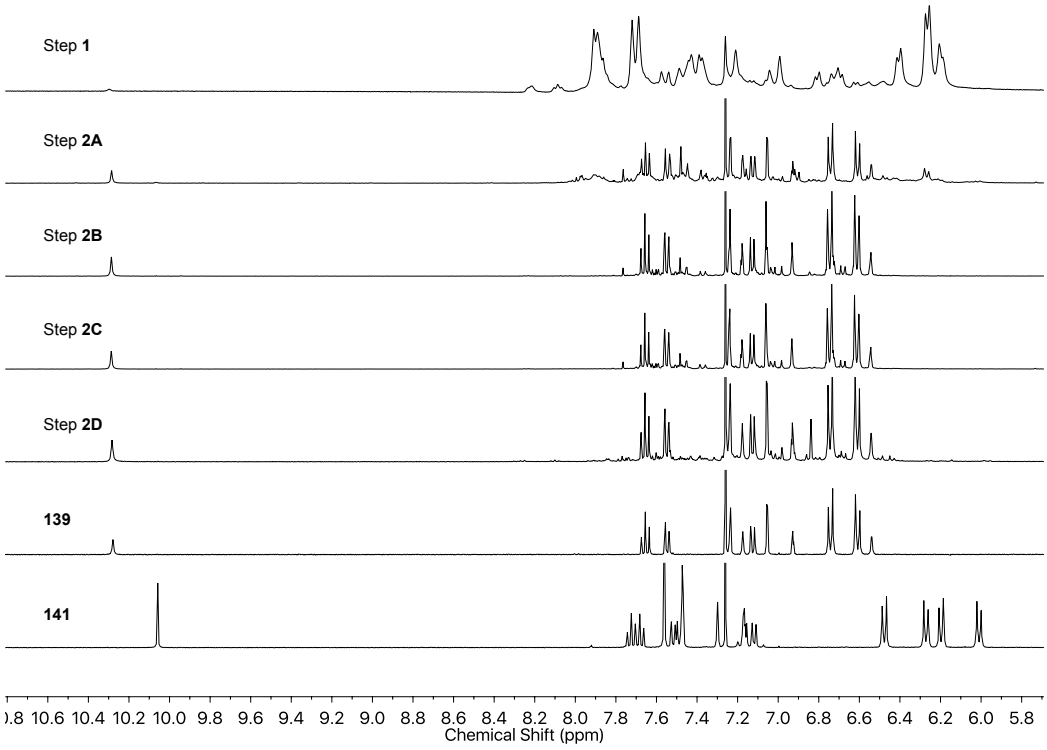

Figure 3.141 Stacked partial ^{1}H NMR (400 MHz, $CDCl_3$) of the products of **step 1** and **steps 2** alongside **139** and **141** for comparison.

Production of **139** was confirmed by ^{1}H NMR. In all cases, triazole rotaxane **141** was not observed. Due to broadening of the signals corresponding to triazolide **12**, conversion could not be quantified in the case of **step 2b**. However, the presence of the doublet at 6.21 ppm which is assigned to **140**, indicates that consumption of **140** is incomplete.

Control experiments

To rule out the conversion of **12** to rotaxane **141** followed by reaction to produce **11**, control experiments with rotaxane **141** were performed under the same conditions:

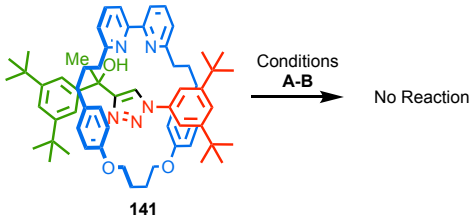

141

Conditions A: Triazole rotaxane **141** (1.6 mg, 0.0017 mmol) in THF (200 µL) was treated with a solution of $HPF_{6(aq)}$ (20 µL, 0.08 M, 0.0017 mmol) in a sealed microwave vial. The mixture was stirred at 70 °C (µW) for 1 h. The reaction was diluted with CH_2Cl_2 (10 mL) and washed with EDTA-$NH_{3(aq)}$ (5 mL). The aqueous layer was extracted with CH_2Cl_2 (2 × 10 mL). The combined organic extracts were washed with brine (10 mL), dried ($MgSO_4$), filtered and the solvent removed *in vacuo*. Analysis of the residue by ^{1}H NMR showed some decomposition but no formation of **139**.

Conditions B: Triazole rotaxane **141** (1.6 mg, 0.0017 mmol) and $[Cu(MeCN)_4]PF_6$ (0.6 mg, 0.0016 mmol) were dissolved in THF (200 µL) and treated with a solution of $HPF_{6(aq)}$ (20 µL, 0.08 M, 0.0017 mmol), in a sealed microwave vial. The mixture was stirred at 70 °C (µW) for 1 h. The reaction mixture was diluted with CH_2Cl_2 (10 mL) and washed with EDTA-$NH_{3(aq)}$ (5 mL). The aqueous layer was extracted with CH_2Cl_2 (2 × 10 mL). The combined organic extracts were washed with brine (10 mL), dried ($MgSO_4$), filtered and the solvent removed *in vacuo*. Analysis of the residue by ^{1}H NMR showed a small amount of decomposition but no formation of **139**.

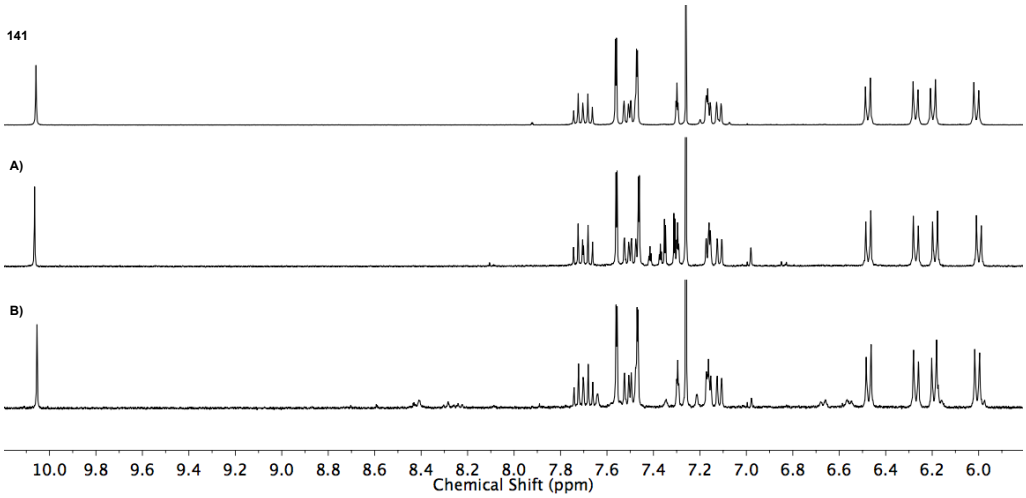

Figure 3.142 Stacked partial ^{1}H NMR (400 MHz, $CDCl_3$) of the product of **conditions A** and **B**, compared with triazole rotaxane **141**.

Mechanistic studies: rearrangements triggered by Tf_2O under anhydrous conditions

*In situ ^1H NMR analysis of the reaction of the product of **14**, **11** and **121** with Tf_2O*

To demonstrate the key role of the OH of triazolide **140** as a leaving group and to attempt to observe the proposed cumulene intermediate we explored the reaction of **12** with Tf_2O under anhydrous conditions and analysed the results by ^1H NMR:

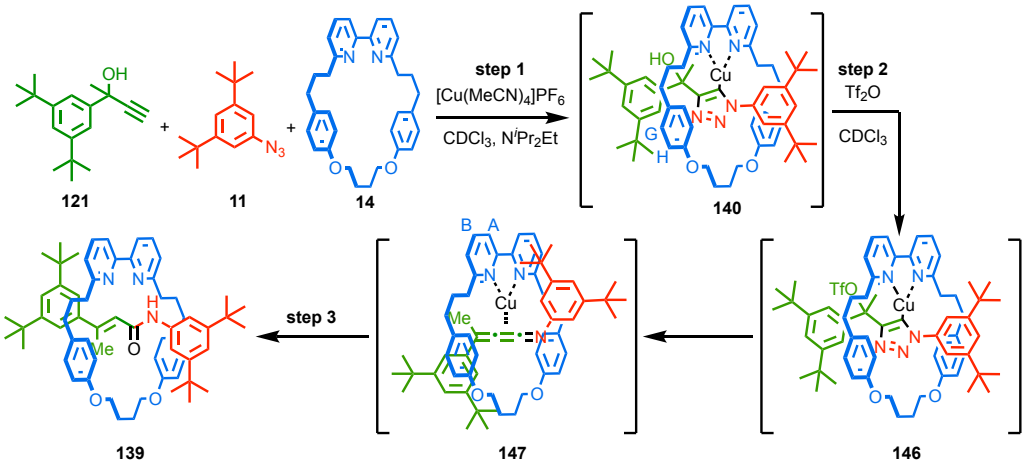

Step 1: $^iPr_2NEt$ (70 µl, 0.40 mmol) was added to a solution of **121** (25.8 mg, 0.10 mmol), **11** (23.1 mg, 0.10 mmol), **14** (47.8 mg, 0.10 mmol) and $[Cu(MeCN)_4]PF_6$ (36.8 mg, 0.099 mmol) in $CDCl_3$ (4.0 mL) in a sealed microwave vial, and the mixture stirred at rt for 45 min. ^1H NMR analysis of the reaction mixture confirmed that the starting materials had been consumed to produce a new species whose ^1H NMR resonances are consistent with triazolide **140**; four signals are observed for macrocycle protons H_G and H_H (~ 6.2 ppm) due to the presence of the axle stereogenic centre, no triazole resonance was observed, and the spectrum is distinct from that of the [Cu(**141**)]$^+$. MS analysis of a portion of the solution supports this assignment (*m/z* =1030.9 $[M+H]^+$, calc. for $C_{64}H_{80}CuN_5O_3$ = 1030.9).

Step 2: A portion (2.0 mL) was removed and treated with Tf_2O (0.1 M in $CDCl_3$, 0.05 mL, 0.05 mmol) and the reaction mixture was stirred at rt for 20 mins. ^1H NMR analysis of the reaction mixture reveals the species assigned as **140** has largely been consumed to produce a new major species whose ^1H NMR resonances are consistent with cumulene **147**; macrocycle protons H_A and H_B (8.3 ppm and 8.1 ppm respectively) appear as single environments suggesting the axle stereogenic unit has been lost. This assignment is supported by LCMS analysis of a portion of the reaction mixture; the major species observed has *m/z* =984.8 (retention time = 3.02 min) which is consistent with **147** (calc. for $C_{64}H_{79}CuN_3O_2$ = 984.6). Fractions were also observed corresponding to macrocycle **14** (2.14 min), rearranged product

139 and also **140**-OH, suggesting that **146** persists in the reaction mixture ([M-OTf]$^+$), or that the corresponding cation is a stable intermediate in the case of **140**.

Step 3a: A portion of the solution produced in **Step 2** (0.5 mL, 0.0125 mmol) was treated with KCN (7.2 mg, 0.110 mmol) in H_2O (1 mL) and the mixture stirred at rt for 16 h. The reaction mixture was diluted with CH_2Cl_2 (20 mL), washed with H_2O (3 × 3 mL), dried ($MgSO_4$) and the solvent removed *in vacuo*. The crude residue was analysed by ^{1}H NMR to reveal **139** as the major product (**139**:**141** ~ 95:5).

Step 3b: A portion of the solution produced in **Step 2** (0.5 mL, 0.0125 mmol) was treated with H_2O (1 mL) and the mixture stirred at rt for 16 h. The reaction mixture was diluted with CH_2Cl_2 (20 mL), washed with H_2O (3 × 3 mL), dried ($MgSO_4$) and the solvent removed *in vacuo*. The crude residue was analysed by ^{1}H NMR to reveal a spectrum remarkably similar to that at the end of step 2, albeit sharper resonances were observed. This suggests that **147** survives treatment with H_2O in the absence of KCN.

Control experiment: A portion of the solution produced in **step 1** (0.5 mL, 0.0125 mmol) was treated with TfOH (1.1 µL, 0.0125 mmol), and diluted with $CDCl_3$ (25 µL). No significant change was observed by ^{1}H NMR (**control i**). The solution was treated with KCN (7.1 mg, 0.110 mmol) in H_2O (1 mL) and stirred for 16 h . The reaction mixture was diluted with CH_2Cl_2 (20 mL), washed with H_2O (3 × 3 mL), dried ($MgSO_4$) and the solvent removed *in vacuo*. ^{1}H NMR analysis (**control ii**) revealed the major product to be triazolide **140** (**139** and **141** observed in trace amounts).

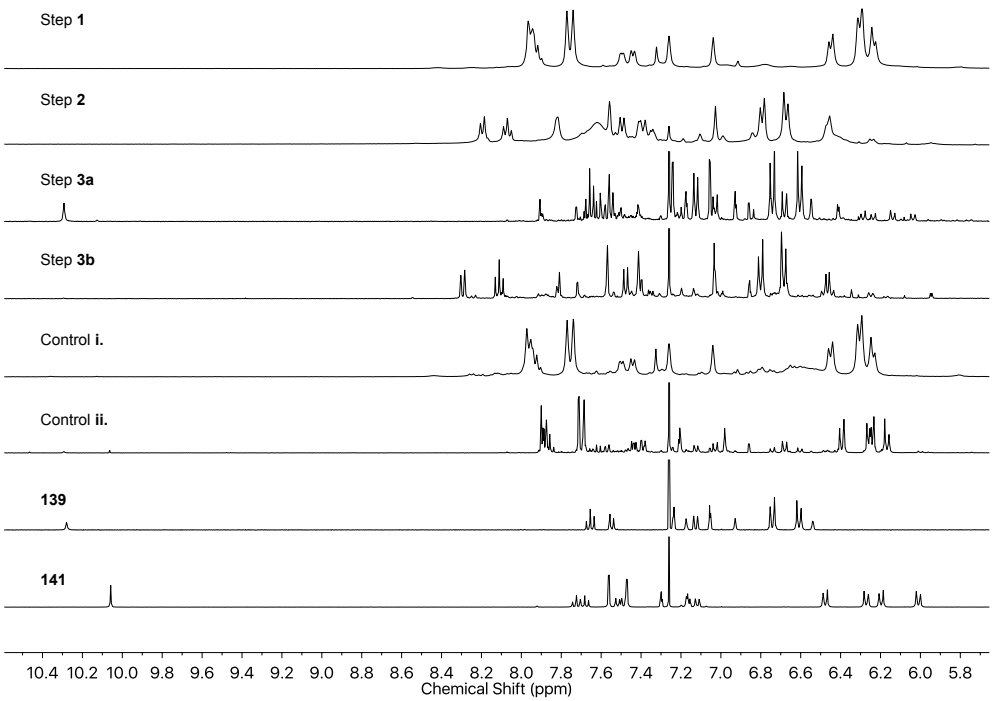

Figure 3.143 Stacked partial ^{1}H NMR (400 MHz, $CDCl_3$) of the products of **step 1**, **step 2**, **step 3a**, **step 3b**, **control i**, and **control ii**, compared with purified **11** and **S12**. At the end of **step 3a**, the ratio of **139**:**141** = 95:5.

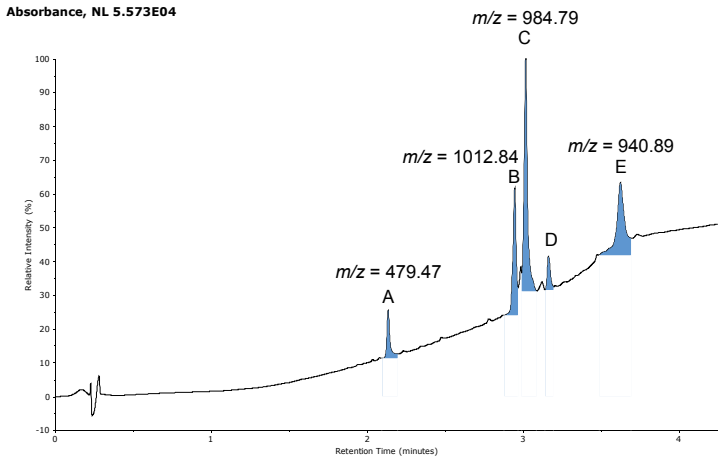

Figure 3.144 LCMS trace (UV = 254 nm, C18 column [1:4 MeCN-H_2O + 0.2% HCO_2H → MeCN + 0.2% HCO_2H), of the reaction mixture at the end of step 2. Note Peak **D** did not appear in the total ion count.

These experiments suggest that Tf_2O triggers the extrusion of N_2 from triazolide **140** and provide evidence that a cumulene of the form **147** is an intermediate in the reaction. The control experiment with TfOH rules out the *in situ* hydrolysis of Tf_2O to produce acid that then triggers the rearrangement. The slow reaction of **147** with H_2O in contrast with $KCN_{(aq)}$ suggests that the Cu^I ion stabilises the cumulene structure, although the lower pH of the KCN

solution may also play a role in accelerating the nucleophilic attack. These results also suggest that the hydrolysis of the cumulene intermediate under the optimised reaction conditions is accelerated by H^+, given that **140** rearranges to **139** rapidly at rt in the presence of HPF_6 without added KF.

*In situ ^{1}H NMR analysis of the reaction of **14**, **11** and **108** followed by Tf_2O*

To provide evidence that the same mechanism observed for **12** is in operation with other substrates we investigated the reaction of **14**, **11** and **108** under anhydrous conditions with Tf_2O and analysed the results by ^{1}H NMR:

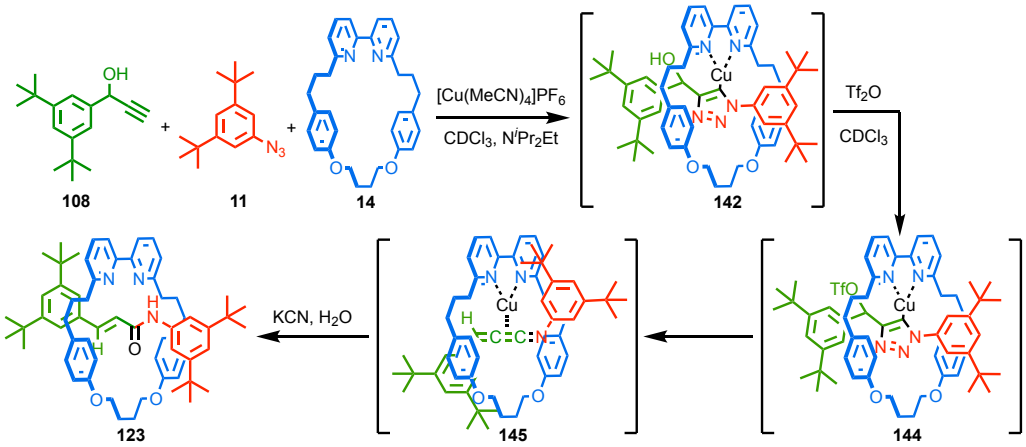

Following the same procedure as above with **14**, **11** and **108** gave a similar outcome as above. After **step 1** a new species was observed that was consistent with triazolide **142**. Treatment with Tf_2O (**step 2**) led to ~70% conversion of **142** to produce a species assigned as cumulene **145** (ratio of signals at ~5.0 ppm [2H of **142**] to doublet at ~8.2 ppm [2H of **145**] = 1:2.6). Treatment of this product with $KCN_{(aq)}$ (**step 108**) gave acrylamide **123** as the major product (**123**:**122** = 90:10). Conversely, treatment of a solution of cumulene **145** with H_2O (**step 3b**) resulted in incomplete consumption of **145** to produce **123** (**123**:**122** = 90:10).

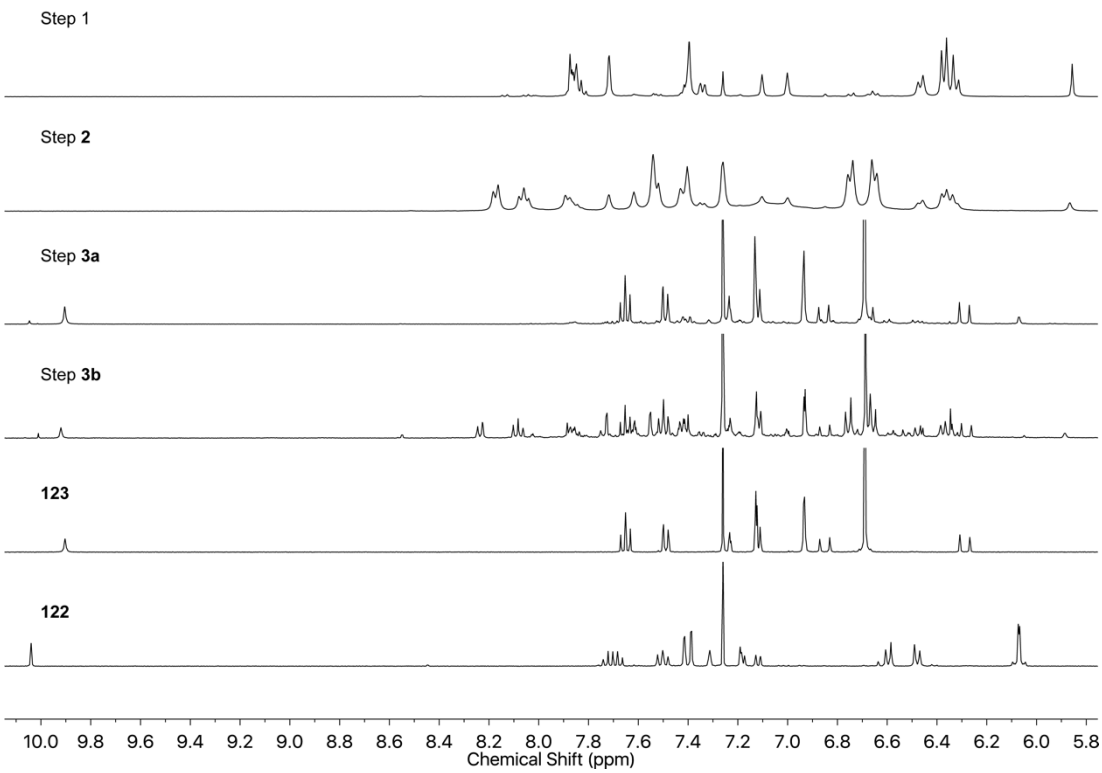

Figure 3.145 Stacked partial ^{1}H NMR (400 MHz, $CDCl_3$) of **step 1**, **step 2**, **step 3a** (**123**:**122** 90:10) and **step 3b** (incomplete, **123**:**122** 90:10), compared with spectra of isolated **123** and **122**.

Preliminary computational analysis of the mechanism of the rearrangement process

The experiments in the following section were performed solely by S. Goldup.

In order to provide further information on the pathway of the rearrangement process and in an attempt to identify the role of the Cu^{I} ion in the process, we carried out a preliminary computational investigation of the reaction pathway.

*Preparation of a truncated model **Ia** of triazolide **142***

Preliminary molecular modelling was carried out to assess the feasibility of the mechanism proposed. Due to the large size of the interlocked intermediates of the reaction a truncated model was used.

A model of triazolide **142** was prepared using Spartan '10 (Wavefunction Ltd.) and a conformation search performed using mechanics (MMFF, vacuum). The lowest energy structure identified was optimised using the PM6 semi-empirical method (vacuum). The model was then truncated to provide a starting point (**Ia**) for DFT calculations below

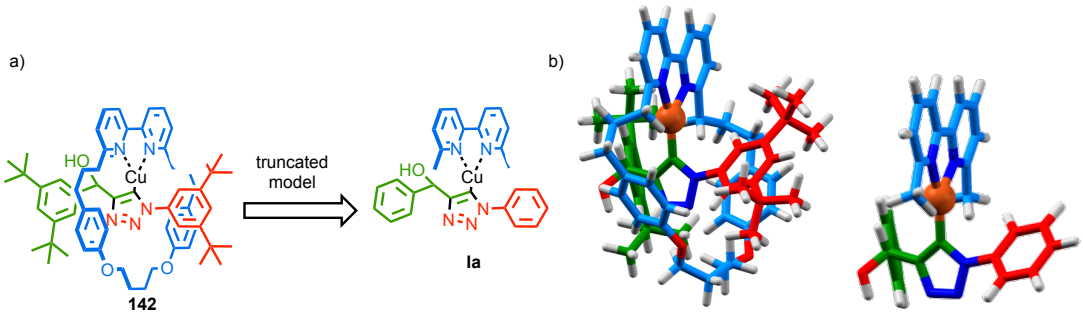

Figure 3.146 a) Structures and b) models of **142** and truncated triazolide model **Ia**

*DFT evaluation of the pathway of N_2 loss from truncated triazolide model **Ia***

Gaussian '09 (DFT-rB3LYP-631G) was used for subsequent calculations with the default H_2O solvation model.[26] The reaction pathway obtained, computed structures obtained and their relative energies are shown in **Figure 3.317** and **Figure 3.318**.

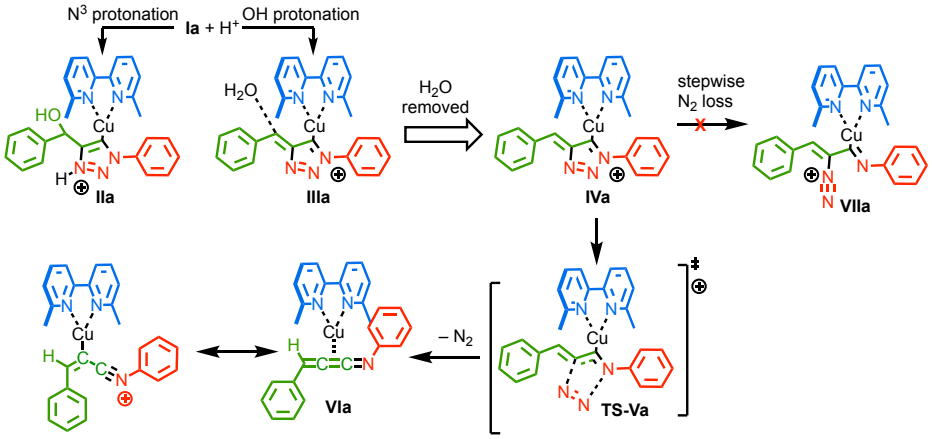

Figure 3.147 Intermediates in the calculated path from truncated axle **Ia** to cumulene **VI**.

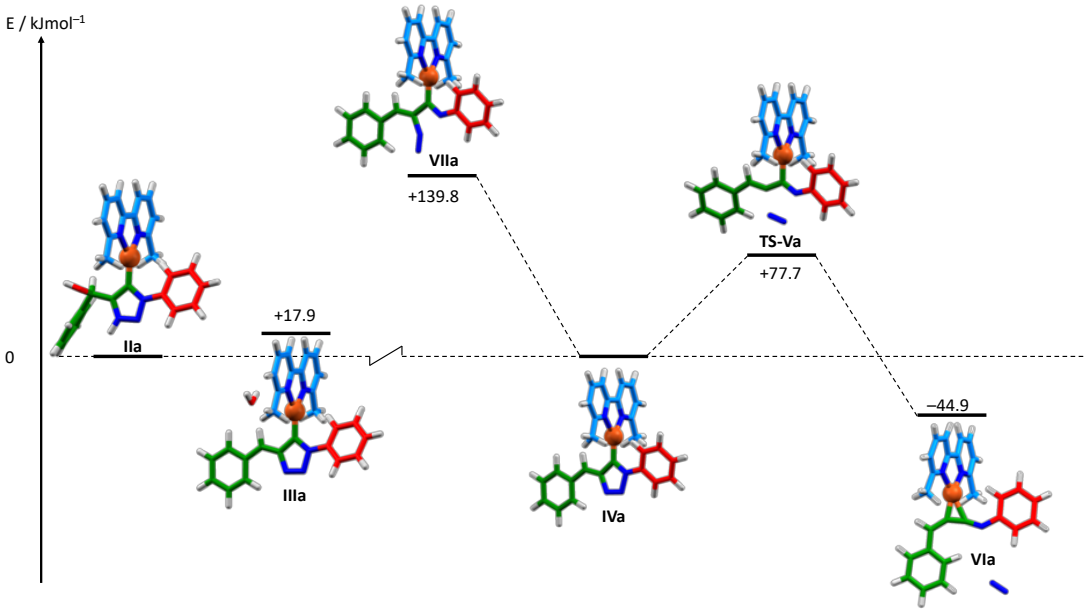

Figure 3.148 Calculated (Gaussian '09, rB3LYP-631G, default H_2O solvent model) structures and energies of intermediates **IIa** to **VIIa**

H^+ was added to either N^3 of the triazole or the OH of structure **Ia** and the geometry of these species was optimised. No stable structure could be identified for the O-protonated species in which the C-O bond was maintained. The energy difference between N-protonated (**IIa**) and O-protonated (**IIIa**) models was found to be 17.9 kJmol^{-1}.

The departed H_2O leaving group was removed from the model of the carbocation and the geometry was optimised again (**IVa**). This structure was used as a starting point for further calculations and its computed energy was used as the new baseline.

A scan (unrestricted, 10 steps of 0.1 Å) was performed using the C-N^3 bond length as the redundant coordinate. The outcome of this scan indicated that an energy maximum was reached with C-N^3 = 1.82276 Å (**Figure 3.139a**). A transition state calculation was performed

using the maximum energy structure found in this scan as a starting point. A species (**TS-Va**) with a single imaginary frequency was identified. An IRC calculation (20 steps forward and 20 steps reverse, final structures optimised, (**Figure 3.139b**) confirmed that this transition state connected the starting cation (**IV**) and a cumulene species (**VI**) in which N_2 had been extruded. The reaction is exergonic by 44.9 kJmol^{-1} and **TS-Va** lies 77.7 kJmol^{-1} above cation **Va**.

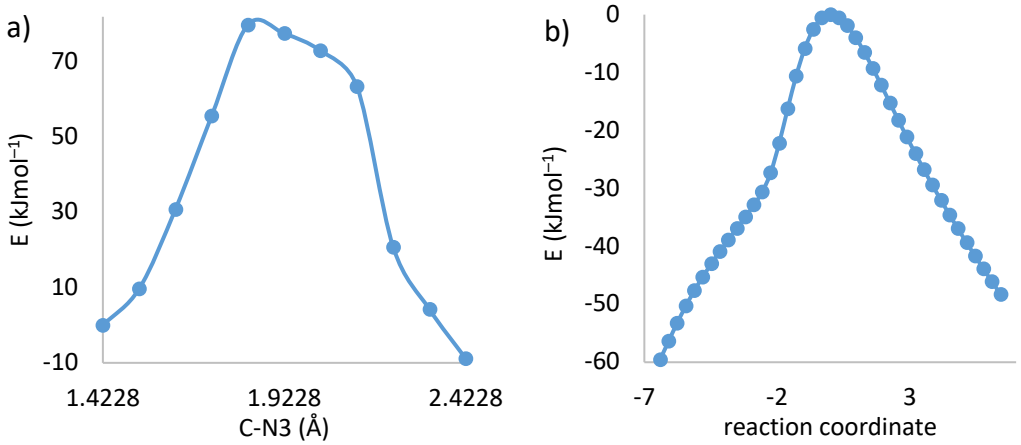

Figure 3.149 a) Plot of the scan (unrestricted with N^1-N^2 as redundant coordinate) of the N^1-N^2 length in 0.1 Å steps vs energy. b) Plot of the IRC scan for **TS-V**.

Examining the calculated structure of cumulene (**VI**), it is worth noting that a) the Cu^I-ion remains associated with the π-system and b) the C-C-C-N unit is not linear. This may indicate that the true structure lies somewhere between the limiting resonance structures in which the Cu^I-ion engages the cumulene through a π-metal interaction and a σ-metal interaction.

We were unable to locate a transition state for the stepwise opening of the triazole to give vinyl diazonium **VIIa**, the expected intermediate if N_2 loss were to proceed in a stepwise manner. This is unsurprising as this species was found to lie 139.8 kJmol^{-1} above that of cation **IVa** (i.e. 62.1 kJmol^{-1} above **TS-Va**) when prepared and optimised directly. The IRC plot shows an inflection before **TS-Va** and examining the computed structures, it is clear that whereas early in the process the reaction coordinate is primarily associated with the stretching of the N^1-N^2 bond, as would be expected en route to **VIIa**, the inflection point is associated with the stretching of the C-N^3 bond starting to contribute to the pathway.

DFT evaluation of the pathway of N_2 loss from truncated triazole model

Finally, for comparison, we repeated the above calculations for the corresponding reaction of triazole starting material **Ib** (pathway shown in **Figure 3.141**, calculated structures and energies shown in **Figure 3.140**.The reaction of **Ib** was found to proceed via a stepwise pathway in which vinyl diazonium **VIIb** is an intermediate lying in a shallow minimum ~1 kJmol^{-}

[1] below the transition state which is itself found 49.1 kJmol^{-1} above **IVb**. The transition state for loss of N_2 from **VIIb** was found to lie ~ 90.9 kJmol^{-1} above this intermediate and thus, including the pre-equilibrium between **IVb** and **VIIb**, the transition state of the rate limiting loss of N_2 lies 139 kJmol^{-1} above cation **IVb**. Furthermore, an IRC calculation suggests that the product of this pathway is best represented by limiting the limiting resonance structures shown rather than a cumulene structure analogous to **VIa** as migration of the C-H bond was not found to take place spontaneously during loss of N_2.

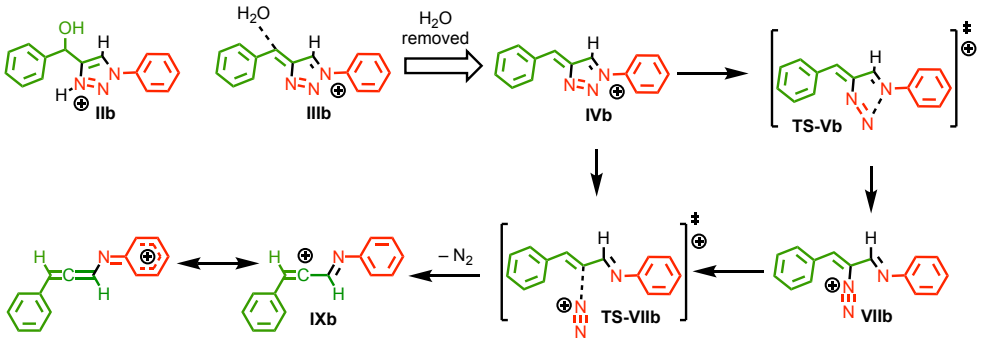

Figure 3.150 Intermediates in the calculated path from truncated axle **Ia** to cumulene **VI**.

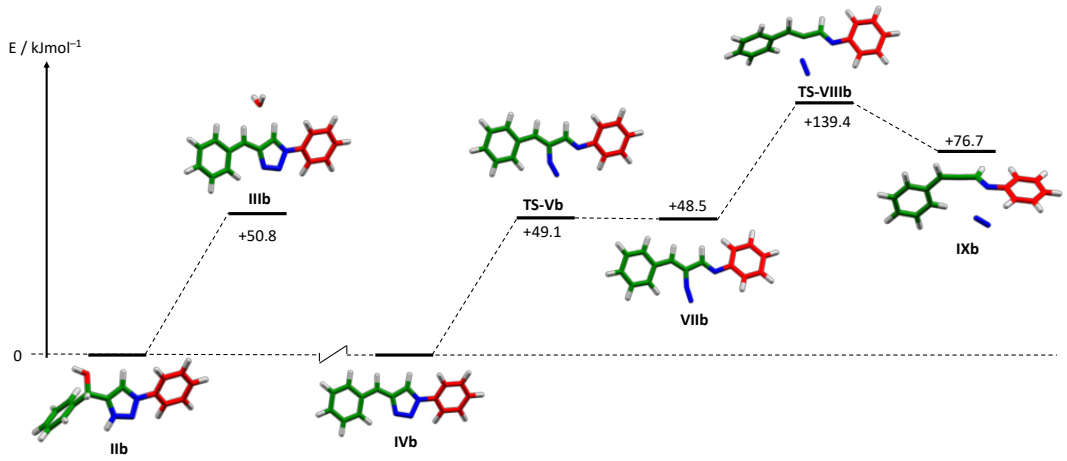

Figure 3.151 Calculated (Gaussian '09, rB3LYP-631G, default H_2O solvent model) structures and energies of intermediates **IIb** to **IXb**

3.5 Bibliography

1 V. V. Rostovtsev, L. G. Green, V. V Fokin and K. B. Sharpless, *Angew. Chemie. Int. Ed.*, 2002, **41**, 2596–2599.

2 C. W. Tornøe, C. Christensen and M. Meldal, *J. Org. Chem.*, 2002, **67**, 3057–3064.

3 R. Huisgen, *Angew. Chem.*, 1963, **13**, 604–637.

4 O. Dimroth, *Justus Liebigs Ann. Chemie.*, 1909, **364**, 183–226.

5 W. Zerong, *Comprehensive Organic Name Reactions and Reagents*, John Wiley and Sons, Inc., 2010.

6 M. Whiting and V. V Fokin, *Angew. Chemie. Int. Ed*, 2006, **45**, 3157–3161.

7 R. Raap, *Can. J. Chem.*, 1971, **49**, 1792–1798.

8 W.-Q. Fan and A. R. Katritzky, *Comprehensive Heterocyclic Chemistry II*, Pergamon Press, Oxford, Volume 4., 1996.

9 W. Zhu and D. Ma, *Chem. Commun.*, 2004, **0**, 888–889.

10 J. J. Gassensmith, L. Barr, J. M. Baumes, A. Paek, A. Nguyen and B. D. Smith, *Org. Lett.*, 2008, **10**, 3343–3346.

11 E. A. Neal and S. M. Goldup, *Angew. Chemie. Int. Ed.*, 2016, **55**, 12488–12493.

12 J. E. M. Lewis, R. J. Bordoli, M. Denis, C. J. Fletcher, M. Galli, E. A. Neal, E. M. Rochette and S. M. Goldup, *Chem. Sci.*, 2016, **7**, 3154–3161.

13 I. Karamé, M. Jahjah, A. Messaoudi, M. L. Tommasino and M. Lemaire, *Tetrahedron Asymmetry*, 2004, **15**, 1569–1581.

14 J. Hornung, D. Fankhauser, L. D. Shirtcliff, A. Praetorius, W. B. Schweizer and F. Diederich, *Chem. A Eur. J.*, 2011, **17**, 12362–12371.

15 H. Lahlali, K. Jobe, M. Watkinson and S. M. Goldup, *Angew. Chemie. Int. Ed.*, 2011, **50**, 4151–4155.

16 J. Winn, A. Pinczewska and S. M. Goldup, *J. Am. Chem. Soc.*, 2013, **135**, 13318–13321.

17 L. M. Urner, M. Sekita, N. Trapp, W. B. Schweizer, M. Wörle, J.-P. Gisselbrecht, C. Boudon, D. M. Guldi and F. Diederich, *Eur. J. Org. Chem.*, 2015, **2015**, 91–108.

18 Y. Itoh, R. Kitaguchi, M. Ishikawa, M. Naito and Y. Hashimoto, *Bioorg. Med. Chem.*, 2011, **19**, 6768–6778.

19 L. Palatinus, S. J. Prathapa and S. van Smaalen, *J. Appl. Crystallogr.*, 2012, **45**, 575–580.

20 L. Palatinus and G. Chapuis, *J. Appl. Crystallogr.*, 2007, **40**, 786–790.

21 G. M. Sheldrick, *Acta Crystallogr. Sect. C Struct. Chem.*, 2015, **71**, 3–8.

22 G. M. Sheldrick, *Acta Crystallogr. Sect. A Found. Crystallogr.*, 2008, **64**, 112–122.

23 Ramesh K Sharma and James L Fry, *J. Org. Chem.*, 1983, **48**, 2112–2114.

24 J. E. Green, J. W. Choi, A. Boukai, Y. Bunimovich, E. Johnston-Halperin, E. DeIonno, Y. Luo, B. a Sheriff, K. Xu, Y. S. Shin, H.-R. Tseng, J. F. Stoddart and J. R. Heath, *Nature*, 2007, **445**, 414–7.

25 R. K. Sharma and J. L. Fry, *J. Org. Chem.*, 1983, **48**, 2112–2114.

26 M. J. Frisch, G. W. Trucks, H. B. Schlegel, G. E. Scuseria, M. A. Robb, J. R. Cheeseman, G. Scalmani, V. Barone, B. Mennucci, G. A. Petersson, H. Nakatsuji, M. Caricato, X. Li, H. P. Hratchian, A. F. Izmaylov, J. Bloino, G. Zheng, J. L. Sonnenberg, M. Hada, M. Ehara, K. Toyota, R. Fukuda, J. Hasegawa, M. Ishida, T. Nakajima, Y. Honda, O. Kitao, H. Nakai, T. Vreven, J. A. Montgomery, Jr., J. E. Peralta, F. Ogliaro, M. Bearpark, J. J. Heyd, E. Brothers, K. N. Kudin, V. N. Staroverov, R. Kobayashi, J. Normand, K. Raghavachari, A. Rendell, J. C. Burant, S. S. Iyengar, J. Tomasi, M. Cossi, N. Rega, J. M. Millam, M. Klene, J. E. Knox, J. B. Cross, V. Bakken, C. Adamo, J. Jaramillo, R. Gomperts, R. E. Stratmann, O. Yazyev, A. J. Austin, R. Cammi, C. Pomelli, J. W. Ochterski, R. L. Martin, K. Morokuma, V. G. Zakrzewski, G. A. Voth, P. Salvador, J. J. Dannenberg, S. Dapprich, A. D. Daniels, Ö. Farkas, J. B. Foresman, J. V. Ortiz, J. Cioslowski, and D. J. Fox, *Gaussian 09* (Gaussian, Inc., Wallingford CT, 2009).